

AD 658372
#67-62866

FOREIGN TECHNOLOGY DIVISION



PHYSICAL PRINCIPLES OF THE WORKING PROCESS IN COMBUSTION CHAMBERS OF JET ENGINES

By

B. V. Raushenbakh, S. A. Belyy, et al.



Distribution of this document
is unlimited. It may be
released to the clearinghouse,
Department of Commerce, for
sale to the general public.

Reproduced by the
CLEARINGHOUSE
for Federal Scientific & Technical
Information Springfield Va. 22151

503

EDITED MACHINE TRANSLATION

PHYSICAL PRINCIPLES OF THE WORKING PROCESS IN
COMBUSTION CHAMBERS OF JET ENGINES

By: B. V. Raushenbakh, S. A. Belyy, et al.

English Pages: 491

TM7500243

THIS TRANSLATION IS A RENDITION OF THE ORIGINAL FOREIGN TEXT WITHOUT ANY ANALYTICAL OR EDITORIAL COMMENT. STATEMENTS OR THEORIES ADVOCATED OR IMPLIED ARE THOSE OF THE SOURCE AND DO NOT NECESSARILY REFLECT THE POSITION OR OPINION OF THE FOREIGN TECHNOLOGY DIVISION.

PREPARED BY:

TRANSLATION DIVISION
FOREIGN TECHNOLOGY DIVISION
WP-AFB, OHIO.

1	
2	
3	
4	
5	
6	
7	
8	
9	
10	
11	
12	
13	
14	
15	
16	
17	
18	
19	
20	
21	
22	
23	
24	
25	
26	
27	
28	
29	
30	
31	
32	
33	
34	
35	
36	
37	
38	
39	
40	
41	
42	
43	
44	
45	
46	
47	
48	
49	
50	
51	
52	
53	
54	
55	
56	
57	
58	
59	
60	
61	
62	
63	
64	
65	
66	
67	
68	
69	
70	
71	
72	
73	
74	
75	
76	
77	
78	
79	
80	
81	
82	
83	
84	
85	
86	
87	
88	
89	
90	
91	
92	
93	
94	
95	
96	
97	
98	
99	
100	

This document is a machine translation of Russian text which has been processed by the AN/GSQ-16(XW-2) Machine Translator, owned and operated by the United States Air Force. The machine output has been post-edited to correct for major ambiguities of meaning, words missing from the machine's dictionary, and words out of the context of meaning. The sentence word order has been partially rearranged for readability. The content of this translation does not indicate editorial accuracy, nor does it indicate USAF approval or disapproval of the material translated.

B. V. Raushenbakh, S. A. Belyy, I. V. Bespalov,
V. Ya. Borodachev, M. S. Volynskiy, A. G. Prudnikov

FIZICHESKIYE OSNOVY RABOCHEGO PROTSESSA V KAMERAKH
SGORANIYA VOZDUSHNO-REAKTIVNYKH DVIGATELEY

Izdatel'stvo
"Mashinostroyeniye"

Moskva - 1964

Page 1-526

CIRC ABSTRACT WORK SHEET

(01) Acc No. TM7500243	(65) SIS Ass No. BX5007778	(40) Country of Info UR	(41) Translation No. MT6500078
(42) Author RAUSHENBAKH, B.V.; BELYY, S.A.; BESPALOV, I.V.; BORODACHEV, V.YA.; VOLYNSKIY, M.S.		Priority II	Distribution STD
(43) Source FIZICHESKIYE OSNOVY RABOCHEGO PROTSESSA V KAMERAKH SGORANIYA VOZDUSHNOREAKTIVNYKH DVIGATELEY			
(02) Cny UR	(03) Ref 0000	(04) Yr 64	(05) Vol 000
(06) Iss 000	(07) S. Pg 0001	(45) E. Pg 0526	(73) Date NONE
(47) Subject Code 20, 21			
Language RUSS	N/A	MOSKVA	IZD-VO MASHINOSTROYENIYE
(59) Topic combustion gas dynamics, thermodynamic analysis, ramjet engine, fuel combustion, fuel stability, industrial furnace, hydraulic resistance, exhaust gas wake			
(66) Foreign Title SEE TITLE ABOVE			
(09) English Title PHYSICAL PRINCIPLES OF THE WORKING PROCESS IN COMBUSTION CHAMBERS OF JET ENGINES			
(97) Header Clas 0		(63) Clas 00	(64) Rel 0
(60) Release Expansion			

ABSTRACT: This book is a monograph devoted to one of the important questions of modern aviation and rocket techniques - the theory of the working process taking place in the combustion chambers of air-jet engines. The book deals in detail with the working process of combustion chambers of straight-flow air-jet engines. Various questions treated in the book refer to combustion chambers of turbo-jet engines and to boiler furnaces. This book is one of the first scientific monographs on this question in the USSR. The book consists of nine chapters in which the most important questions of the physical principles and the calculation of the working process of the combustion chambers are elaborated. In the brief introduction a schematic description of the working process is given for a simplified combustion chamber of a straight-flow engine. Chapter 1 is devoted to the general thermodynamic analysis of the combustion chamber. Here we must bear in mind the consideration of questions of the supply of heat to a moving gas in tubes of constant and variable cross section, the analysis of the effect of the various parameters on the characteristics of the combustion chamber, the calculation of the temperature and composition of the products of combustion, and questions of the hydraulic resistance of the straight-flow chamber and its elements. In Chapter 2, which takes up 121 pages of text, authors consider questions of the preparation of the combustion mixture

0898 1563

(questions of forming a mixture). Unlike the first chapter, the material of Chapter 2, which is richer in content, is based to a large extent on the work of Soviet researchers, in particular on the investigations of the authors themselves. After a general analysis of the processes of forming the mixture, the elementary processes are considered which constitute the process of mixing in chambers into which the fuel is fed in liquid form and is atomized in a stream of air. In the analysis of the processes of atomization of the liquid, a general physical picture is given of the breakdown processes of films and drops, and quantitative characteristics of these processes are quoted (criterial formulas, distribution curves of the drops with respect to size). Unfortunately there are no data for jet injectors, for which only the theory of deformation of a jet injected into the flow at some angle is developed. The material on an atomization torch in a supersonic flow of air is of especial interest. At the end of the chapter, some material is cited on the distribution of the liquid phase of fuel in the airstream, and also on questions of the vaporization of drops and clusters of drops. In Chapter 3 a beginning is made on the consideration of the processes of ignition and combustion. In this chapter are studied forced ignitions and the combustion of homogeneous mixtures, i.e. this chapter is a preparation for the study of subsequent material. The size of the chapter, evidently, is not very large (34 pp), since the material is, generally speaking, known from other sources. In Chapter 4, which is also of a preparatory nature, questions of the turbulence of flows of air are studied. In spite of the fact that the material of this chapter is, generally speaking, known from other sources, the analysis in the chapter is sufficiently clear and at a modern level. Data are cited which relate directly to the elements of the working process taking place in the combustion chamber (turbulence of a flow beyond cascades, turbulence in the case of deformation of the flow, etc). Chapter 5 gives further material on the combustion of homogeneous mixtures in a turbulent flow. These occupy a good deal of space (90 pp). Here authors consider existing theories of turbulent combustion and also the experimental data of many researchers. The treatment of turbulent combustion proposed by the authors occupies a good deal of space (analysis of the one-dimensional combustion zone, of a turbulent torch in an open channel and in a tube, analysis of the statistical distribution of the scales of temperature, nonhomogeneities in the macrozone). A separate paragraph contains a consideration of the hydrodynamic peculiarities of turbulent combustion in the wake behind a stabilizer. In the last paragraph, data are given on the dependence of the velocity of turbulent combustion on various parameters. In Chapter 6, which is small in bulk but important in significance,

c898 1564

authors consider questions of vibrational combustion in the chambers of air-jet engines. Here the general physical mechanism of the phenomenon is explained, and a scheme is given for the theoretical analysis. The possible special feedback mechanisms are calculated. At the end of the chapter there are some general recommendations about how to overcome vibrational combustion. In Chapter 7, they consider the stabilization of a flame in a flow of fuel mixture. After studying the effect of the form of the stabilizer on the parameters of the wake, authors proceed to analyze the effect of the various parameters on the characteristics of stable combustion. At the end of the chapter the theory and calculation of the stabilization of a flame by a poorly streamlined body is given. Chapter 8 is devoted to questions of the combustion of a mixture in the wake behind a stabilizer. First of all the combustion in the wake of a homogeneous mixture is studied, taking into account the effect of the walls of the tube. The effect of the two-phase nature on the characteristics of combustion is then demonstrated. Finally, some material is given on the generalization of the data of the investigation of combustion in the wake behind a stabilizer. In Chapter 9 (the final chapter), the authors deal with questions of the cooling of the combustion chamber walls and of the nozzle of straight-flow air-jet engines. Some different methods of the air-cooling of combustion chambers are given, and formulas for calculating the external cooling of the walls are cited. The calculation of barrage and combined cooling is treated in fairly extensive detail. The limits of applicability of the air-cooling of the combustion chamber and the nozzle are indicated. At the end of each chapter there is a bibliography of the questions dealt with. The book contains a number of misprints, including some in the formulas. English translation; 490 pages.

TABLE OF CONTENTS

U. S. Board on Geographic Names Transliteration System.....	v
Preface.....	1
Symbols and Designations.....	5
Introduction.....	11
Chapter I. Certain Problems of Thermodynamics of the Combustion Chamber.....	15
§ 1. Thermodynamic Cycle of a Ramjet Engine.....	15
§ 2. Supply of Heat to Moving Gas in a Pipe at $F = \text{const.}$	20
§ 3. Heat Addition to a Moving Gas in a Pipe with Varying Cross Section.....	25
§ 4. Influence of Flow Velocity on Characteristics of the Combustion Chamber.....	29
§ 5. Dependence of Engine Characteristic on Combustion Efficiency of Fuel.....	31
§ 6. Peculiarities of Thermodynamic Processes at High Temperatures.....	32
§ 7. Calculation of Composition of Combustion Products at High Temperatures.....	35
§ 8. Losses of Pressure in Combustion Chambers.....	40
Literature.....	48
Chapter II. Carburetion.....	49
§ 1. General Characteristics of Carburation Processes.....	49
§ 2. Disintegration of a Jet of Liquid, Splitting up and Deformation of Drops in a Flow of Air.....	50
§ 3. Application of Similarity Theory to the Problem of Atomization of a Liquid by Swirl Injectors.....	61
§ 4. Formula of the Atomization Spectrum.....	69
§ 5. Scheme of Analysis of a Centrifugal Injector with Consideration of Coarseness of Atomization.....	76
§ 6. Direct-Spray Atomization.....	78
§ 7. Atomization Jet in a Supersonic Flow.....	85
§ 8. Motion of a Single Drop in a Gas Flow.....	91
§ 9. Motion of Drops in a Fuel Jet.....	105

§ 10. Dispersion of Drops Relative to Trajectories of Ordered Motion.....	110
§ 11. Distribution of Liquid Phase of Fuel.....	115
§ 12. Distribution of Vapor Phase and Two-Phase Mixture During Atomization of Fuel in a Swirl Injector.....	121
§ 13. Distribution of Specific Fuel Rates During Atomization of Fuel by the Manifolds.....	127
§ 14. Heat-Mass Transfer of a Drop.....	128
§ 15. Influence of Pressure of Medium, Nonuniformity of Heating and Fractionation of Fuel on Rate of Vaporization of Drops...	138
§ 16. Evaporation of Drops in a Fuel Jet (Spray).....	142
§ 17. Comparison of Calculated and Experimental Data on Evaporation of a Fuel Jet.....	152
§ 18. Evaporation of Drops in the Combustion Zone.....	156
Literature.....	160
Chapter III. Forced Ignition and Burning of Uniform Fuel-Air Mixtures in a Laminar Flow.....	162
§ 1. Influence of Different Factors on Burning Velocity.....	162
§ 2. Forced Ignition.....	171
§ 3. Concentration Limits of Ignition of a Combustible Mixture.....	173
§ 4. Influence of Different Factors on Concentration Boundaries of Ignition.....	176
§ 5. Conditions of Forced Ignition (Influence of Thermal Power of Ignition Source).....	179
§ 6. Dependence of Minimum Ignition Source Power on Physicochemical Parameters of the Mixture.....	185
§ 7. Influence of Physicochemical Properties of a Mixture on Concentration Boundaries of Ignition.....	188
§ 8. Ignition Limits of Two-Phase (Heterogeneous) Mixtures.....	192
Literature.....	196
Chapter IV. Turbulence in Air Flows.....	199
§ 1. Description and Definition of Turbulent Motion Following Euler's Treatment.....	199
§ 2. Description of Turbulence According to the Lagrange Treatment.....	208

§ 3. Experimental Data on Turbulence.....	216
Literature.....	241
Chapter V. Burning of Homogeneous Fuel-Air Mixtures in a Turbulent Flow.....	244
§ 1. Probability Characteristics of a Turbulent Flame.....	244
§ 2. Equations of Hydrodynamics for a Turbulent Flame.....	248
§ 3. Stages of Development of the Turbulent Burning Zone.....	253
§ 4. Parameters of a Turbulent Flame.....	272
§ 5. Distribution of Average Parameters in the Turbulent Burning Zone.....	281
§ 6. Hydrodynamic Peculiarities of Turbulent Burning After Bluff Bodies (Flame-Holders).....	305
§ 7. Empirical Dependences of the Speed of Turbulent Combustion on Parameters of Turbulence; Composition of the Mixture and Pressure.....	319
Literature.....	334
Chapter VI. Vibrational Burning Regimes.....	337
§ 1. General Characteristic of Vibrational Burning.....	337
§ 2. Generation of Acoustic Energy by the Burning Process.....	340
§ 3. Idealization of a Perturbed Combustion Process.....	345
§ 4. Feedback Mechanisms.....	351
§ 5. Certain Recommendations for Overcoming Vibrational Burning.....	359
Literature.....	361
Chapter VII. Flame Stabilization in a Flow of Fuel Mixture.....	362
§ 1. Structure of the Flow and Mechanism of Flame Stabilization in the Wake after a Bluff Body.....	362
§ 2. Experimental Data on Flame Stabilization by Bluff Bodies.....	369
§ 3. Theory of Flame Stabilization by a Bluff Body.....	378
§ 4. Analysis of Flame Stabilization by a Bluff Body.....	384
Literature.....	388
Chapter VIII. Burning of Fuel-Air Mixtures in the Wake after a Bluff Body.....	389
§ 1. Burning of a Homogeneous Mixture in the Wake after a Single Stabilizer in a Half-Open Flow.....	389

§ 2. Certain Peculiarities of Burning of Homogeneous Gas Mixtures after a Grid of Flame-Holders in a Pipe.....	393
§ 3. Dependence of Angle of Expansion of Flames on Various Factors.....	396
§ 4. Influence of Various Factors on Fuel Depletion in the Plane of Symmetry Between the Flame-Holders.....	397
§ 5. Burning After a Grid of Flame-Holders, Located in the Same Plane and Echeloned Along the Length of the Combustion Chamber.....	401
§ 6. Characteristics of Burning of Two-Phase Mixtures in a Turbulent Flow.....	404
§ 7. Experimental Data on Burning of Two-Phase Mixtures After an Array of Flame-Holders in a Pipe.....	410
§ 8. Burning in Turbulent Flow Near Wall of Pipe.....	412
§ 9. Generalization of Experimental Data on Investigation of Burning in the Wake After Bluff Bodies.....	415
Literature.....	418
Chapter IX. Cooling of Walls of the Combustion Chamber and the Nozzle.....	420
§ 1. Different Methods of Air Cooling of a Ramjet Engine.....	420
§ 2. Basic Information from Heat Exchange.....	423
§ 3. External Cooling.....	430
§ 4. Convection Cooling.....	441
§ 5. Calculation of Flow in a Two-Loop Cylindrical Combustion Chamber with Consideration of Heat Release and Heat Transfer Through the Wall of the Flame Tube.....	458
§ 6. Boundary Cooling.....	464
§ 7. Combined Cooling.....	486
§ 8. The Limits of Applicability of Air Cooling of Combustion Chamber and Nozzle.....	489
Literature.....	490

U. S. BOARD ON GEOGRAPHIC NAMES TRANSLITERATION SYSTEM

Block	Italic	Transliteration	Block	Italic	Transliteration
А а	<i>А а</i>	A, a	Р р	<i>Р р</i>	R, r
Б б	<i>Б б</i>	B, b	С с	<i>С с</i>	S, s
В в	<i>В в</i>	V, v	Т т	<i>Т т</i>	T, t
Г г	<i>Г г</i>	G, g	У у	<i>У у</i>	U, u
Д д	<i>Д д</i>	D, d	Ф ф	<i>Ф ф</i>	F, f
Е е	<i>Е е</i>	Ye, ye; E, e*	Х х	<i>Х х</i>	Kh, kh
Ж ж	<i>Ж ж</i>	Zh, zh	Ц ц	<i>Ц ц</i>	Ts, ts
З з	<i>З з</i>	Z, z	Ч ч	<i>Ч ч</i>	Ch, ch
И и	<i>И и</i>	I, i	Ш ш	<i>Ш ш</i>	Sh, sh
Й й	<i>Й й</i>	Y, y	Щ щ	<i>Щ щ</i>	Shch, shch
К к	<i>К к</i>	K, k	Ъ ъ	<i>Ъ ъ</i>	"
Л л	<i>Л л</i>	L, l	Ы ы	<i>Ы ы</i>	Y, y
М м	<i>М м</i>	M, m	Ь ь	<i>Ь ь</i>	'
Н н	<i>Н н</i>	N, n	Э э	<i>Э э</i>	E, e
О о	<i>О о</i>	O, o	Ю ю	<i>Ю ю</i>	Yu, yu
П п	<i>П п</i>	P, p	Я я	<i>Я я</i>	Ya, ya

* ye initially, after vowels, and after ъ, ь; e elsewhere.
 When written as ѣ in Russian, transliterate as yě or ě.
 The use of diacritical marks is preferred, but such marks
 may be omitted when expediency dictates.

In this book there are expounded the physical principles of fuel combustion processes in air flows and methods of calculation of combustion chambers of jet engines.

There are considered thermodynamic and aerodynamic characteristics of combustion chambers, processes of atomization and carburetion of fuels, ignition and combustion of gas mixtures in laminar and turbulent flows, methods of flame stabilization, vibrational combustion, combustion in the wake behind a bluff body, processes of heat exchange and thermal protection of chambers.

This book is intended for scientists and engineers in aviation, as well as nonaviation specialists; furthermore, it will be useful for students of technical colleges.

PREFACE

In this book there are presented the physical principles of the working process of straight-through-flow combustion chambers.

In Chapter I there are considered certain questions of thermodynamics of combustion chambers. There is given a qualitative analysis of ideal and real thermodynamic cycles of an air-breathing jet engine. There is shown the influence of pressure and flow velocity in the combustion chamber and of hydraulic losses on the degree of conversion of heat fed into the chamber into effective work of the cycle (i.e., thermal efficiency of the cycle). There is given a method of approximate calculation of flow friction of the combustion chamber. In this same chapter, there is briefly discussed the known method of calculation of specific pressure losses caused by heat addition to a moving gas.

In Chapter II there are given criterial dependences for determination of the spectrum of atomization of fuel by swirl injectors, which were obtained on the basis of generalization of a large number of experimental data on atomization of liquids, the results of theoretical and experimental investigation of the motion of a liquid during its atomization into the flow of a direct-spray injector. There are presented certain experimental materials on atomization of liquid in a supersonic flow. There are given new materials on the distribution of vapor and liquid phases of fuel, on the influence of deformation of drops on the trajectory of their motion, on dispersion drops on area of section of fuel on the influence of preheating of fuel on the character of its distribution in the flow.

In Chapter III there are assembled the most interesting for practice experimental materials on ignition and laminar burning of homogeneous mixtures in reference

to straight-through-flow combustion chambers. These materials are especially important, since in works having an applied character, the physical essence of the influence of turbulence on the above mentioned processes still has not been considered.

Chapter IV is dedicated to fundamentals of the statistical theory of turbulence. Experimental material in this chapter is selected in reference to conditions of operation of a straight-through-flow combustion chamber.

In Chapter V there are considered processes of turbulent combustion of homogeneous mixtures. Until recently, in the technical literature there could not be found a clear account of a model of the process of turbulent combustion. The experimental investigation of N. V. Kokushkin and other investigators made it possible to deepen our concepts of the mechanism of turbulent burning, and at the same time confirmed the accuracy of the known model of surface combustion. On the basis of this model, it was possible to simplify hydrodynamic equations of flow in which burning occurs, and to solve them for a series of simple cases: for a turbulent flame jet after burners in open flow, after a linear burner in a pipe, and so forth. Analysis and generalization of extensive experimental material on the basis of the given theory show that burning is basically influenced by turbulent characteristics of the fresh mixture.

Fundamentals of the theory of vibrational combustion are presented in Chapter VI. Such burning is characterized by powerful regular oscillations of pressure and flow rate, which not infrequently lead to damage of the combustion chamber, strong vibrations of the construction and other undesirable phenomena (incomplete burning of fuel, etc.).

In distinction from the conventional theory of vibrational burning, which consists of composition of equations of acoustics taking into account boundary conditions, the authors applied the energy method, which made it possible to obtain all basic conclusions by use of a very simple mathematical apparatus.

Results obtained by this method at the same time permit us to give certain recommendations on methods of suppression of vibrational burning.

In Chapter VII there are considered hydrodynamics of flow in the wake after a bluff body and conditions of stability of burning in dependence on dimensions and relative location of stabilizers. In this chapter there is described a method of calculation of a stabilizer for assigned parameters of the fuel mixture.

Results of experimental investigations of burning of homogeneous and

heterogeneous mixtures in the wake after a single stabilizer and an array of stabilizers are discussed in Chapter VIII. In it there are given basic features of the process of burning and its dependence on physicochemical characteristics of the fuel mixture, dimensions, geometric shape and relative location of stabilizers.

The last chapter is dedicated to one of the important problems -- to the problem of thermal protection of a combustion chamber, on the successful solution of which the possibility of creation of a high-speed engine to a considerable degree depends. The authors describe diverse variants of the simplest (structurally) methods of air cooling (convection, barrage, combined) and consider the influence of radiation from combustion products on temperature of the chamber walls.

During writing of this book, the authors widely used Soviet and foreign literature. Examples of calculations given in the book are based on hypothetical data.

Chapters of book are written by: I, VII, VIII -- I. V. Besspalov; II (§ 1-8) -- M. S. Volynskiy; II (§ 8-18) -- S. A. Belyy; III, IV, V -- A. G. Prudnikov; VI -- B. V. Raushenbakh; IX -- V. Ya. Borodachev.

The authors are grateful to Corresponding Member of the Academy of Sciences of the USSR L. N. Khitrin for a series of useful suggestions on the contents of this monograph.

The authors also express gratitude to Comrades V. F. Donskiy, A. M. Gubertov, V. M. Iyevlev, K. I. Svetushkin, I. M. Kuptsov and V. Ya. Pereverzev for their help rendered during writing of this book.

All remarks and wishes concerning the contents of this book should be directed to the address: Moscow, I-51, Petrovka, 24, "Machine Building" Publishing House.

SYMBOLS AND DESIGNATIONS

1. DIMENSIONLESS NUMBERS

- c_f - coefficient of friction;
- c_x - drag coefficient;
- c_y - lift coefficient;
- c_R - thrust coefficient;
- M - Mach number;
- Nu - Nusselt number;
- Nu' - diffusion Nusselt number;
- Pr - Prandtl number;
- Pr' - diffusion Prandtl number;
- $P_1(x)$ - probability of appearance of fresh mixture at point x ;
- $P_2(x)$ - probability of appearance of combustion products at point x ;
- $R(\tau)$ - Lagrange correlation coefficient;
- Re - Reynolds number;
- St - Stanton number;
- $V(a)$ - volume fraction of drops in atomization spectrum with diameter less than a ;
- $\Delta V(a)$ - volume fraction of drops in the spectrum with diameter a ;
- Z - degree of vaporization of liquid;
- c - dimensionless concentration of fuel vapors;
- c_0 - on surface of drop;
- c_∞ - in the surrounding medium;
- f - relative area; f_{kp} - in nozzle throat;
- f_a - at nozzle edge; f_H - stream of air in front of the engine (at infinity);

q_1, r_1 — weight, volume component of i -th gas in a mixture;
 $q(\lambda), z(\lambda)$ — gas-dynamic function for determination of flow rate, momentum;
 m — ratio of velocities of mixing flows;
 k — adiabatic coefficient;
 n — polytropic coefficient;
 $p(x)$ — frequency distribution function;
 η_z — completeness of burning; η — softening coefficient of inlet;
 η_{xhm} — chemical completeness of burning; η_0 — total efficiency of engine;
 η_e — effective efficiency of engine;
 λ — reduced velocity; thermal conductivity coefficient;
 μ — discharge coefficient of injector; coefficient of dynamic viscosity;
 ϵ — intensity of turbulence of flow (in %); degree of blackness;
 ζ — temperature recovery factor;
 ξ — coefficient flow friction of the chamber;
 σ — pressure recovery factor.

2. GEOMETRIC DIMENSIONS IN m, TIME IN sec

D — diameter of pipe;
 $D_{\text{ЭКВ}}$ — equivalent diameter;
 D_{HP} — throat diameter of nozzle;
 F — area in m^2 ;
 L — length of plate, coordinate of drop in relative motion (see Chapter III);
 Y_0 — characteristic width of the zone of molecular mixing of two chemically inactive media;
 Y_T — characteristic width of zone of turbulent mixing of two chemically inactive media;
 a — diameter of drop; a_0 — initial; a_M — median diameter in atomization spectrum; coefficient of thermal diffusivity;
 b — width of zone of turbulent mixing;
 h — height of cooling channel;
 l — length of pipe, heat of evaporation of liquid;
 l_E — Euler scale of turbulence;
 l_L — Lagrange scale of turbulence;
 r_c — radius of nozzle;
 x, y, z — coordinates in orthogonal system;

δ — thickness of hydrodynamic boundary layer;
 ε — thickness of vortex sheet of liquid flowing from injector;
 σ_0 — characteristic width of burning front during turbulent mixing of two chemically active media;
 σ_0 — characteristic width of laminar flame front;
 σ_T — characteristic width of zone of turbulent burning (zone of mixing of two chemically active media);
 δ — momentum thickness;
 α — half of atomization angle of injector;
 β — angle at vertex of stabilizer;
 γ_0 — angle of slope of relative velocity of blowoff of drops to axis Ox;
 T_E — Euler time scale;
 T_L — Lagrange time scale;
 τ — time, degree of preheating of working substance (air).

3. PARAMETERS OF WORKING SUBSTANCE

G — flow rate of gas in kg/sec;
 G_T — fuel flow rate through injector in kg/sec;
 Q — heat flux in kcal/sec;
 $L_{ad, p}$ — work of adiabatic expansion of gases in the nozzle in kg-m;
 $L_{ad, c\pi}$ — work of adiabatic compression in kg-m;
 L_e — effective work of cycle in kg-m;
 L_t — network of cycle in kg-m;
 J — specific impulse of engine in sec;
 T — absolute temperature in $^{\circ}K$;
 T_0 — stagnation temperature in $^{\circ}K$;
 T_w — wall temperature in $^{\circ}K$;
 T_e — equilibrium temperature in $^{\circ}K$;
 T_1 — temperature at nozzle exit in $^{\circ}K$;
 T_2 — temperature of wake in $^{\circ}K$;
 U, V — speed of flight in m/sec;
 a — speed of sound in m/sec;
 a_{kp} — speed of sound in water in m/sec;
 c — mass concentration in kg/m³;
 c_T — specific flow of fuel in g/cm²·sec; c_{π} — specific flow of liquid phase; c_v — specific flow of vaporized fuel;

q - impact pressure $\left(\frac{\rho v^2}{2}\right)$ in kg/m^2 ;
 p - static pressure in kg/m^2 ;
 p_0 - stagnation pressure in kg/m^2 ;
 Δp_T - fuel feed pressure in kg/m^2 ;
 p_H - saturated vapor pressure of fuel in kg/m^2 ;
 t - temperature of drop in $^{\circ}\text{C}$; t_0 - initial; t_p - equilibrium vaporization temperature of drop; t_g - air temperature;
 u - component of flow velocity along the axis Ox ; air velocity relative to the drop in m/sec ;
 u_1 - velocity of main flow in m/sec ;
 u_2 - speed of barrage flow in m/sec ;
 w - flow velocity in m/sec ;
 w' - pulsational flow velocity in m/sec ;
 v - velocity of drop in m/sec ;
 α - heat transfer coefficient in $\text{kcal/m}^2 \cdot \text{hr} \cdot \text{deg}$;
 β - coefficient of mass transfer in m/sec ;
 τ_w - coefficient of friction in kg/m^2 .

4. PHYSICAL PROPERTIES OF MATERIALS

A - thermal equivalent of work (426.4 kg-m/kcal);
 D - coefficient of molecular diffusion in m^2/sec ;
 D_T - coefficient of turbulent diffusion in m^2/sec ;
 $D_{M,T}$ - coefficient of accelerated molecular diffusion in m^2/sec ;
 E - heat of reaction in $\text{kcal/kg} \cdot \text{mole}$;
 E_{00p} - heat of formation in $\text{kcal/kg} \cdot \text{mole}$;
 H_u - calorific value of fuel (lowest) in kcal/kg ;
 H_B - highest calorific value of fuel in kcal/kg ;
 L_0 - stoichiometric coefficient, theoretically the quantity of air necessary for burning 1 kg of fuel;
 a - coefficient of thermal diffusivity in m^2/hr ;
 c_p - heat capacity of gas at constant pressure in $\text{kcal/kg} \cdot \text{deg}$;
 g - gravitational constant (9.81 m/sec^2);
 i - enthalpy in kcal/kg ;
 s - entropy in $\text{kcal/kg} \cdot \text{deg}$;
 l - heat of vaporization in kcal/kg ;

γ — specific gravity in kg/m^3 ;
 μ — dynamic coefficient of viscosity in $\text{kg}\cdot\text{sec}/\text{m}^2$;
 ν — kinematic coefficient of viscosity in m^2/sec ;
 ε — degree of blackness;
 ρ — density in $\text{kg}\cdot\text{sec}^2/\text{m}^2$;
 λ — coefficient of thermal conductivity in $\text{kcal}/\text{m}\cdot\text{hr}\cdot\text{deg}$;
 σ — coefficient of surface tension of liquid in kg/m ;
 ξ — heating efficiency of a hot mixture in kcal/kg .

5. SUBSCRIPTS

B — air;
 kp — critical;
 ж — liquid;
 п — vapor;
 т — fuel, turbulently;
 p — equilibrium;
 н — normal;
 л — laminar;
 O — initial value;
 r — (products of) combustion;*
 x — cold (fresh) mixture;*
 д — deformed.

*In certain chapters, instead of subscripts "x" and "r" there are used respectively subscripts "1" and "2."

INTRODUCTION

In spite of the structural variety of combustion chambers, processes occurring in them have many common features and frequently obey the same laws. Therefore, the authors limited their account to investigations of one of the simplest chambers. This monograph is dedicated to the study of physics of processes in combustion chambers of ramjet engines.

A number of elementary processes common to many chambers occur in the ramjet chamber under relatively simple conditions, which allows us to conduct necessary observations and measurements. These processes (carburetion, flame stabilization, etc.) in chambers of turbojet engines with swirling flow are more complicated and difficult to observe.

It is necessary to note that the method and many results of investigations of these processes in ramjet chambers can be applied in industrial boiler installations and furnaces, in internal-combustion engines, apparatuses of chemical technology, etc. At present, considerable attention is allotted in the power and fuel industry of our country to combustion processes of petroleum, black oil and natural gas. Due to this, there appears the necessity of rational organization of the process of combustion of gas in boiler furnaces of thermoelectric power stations, of achievement of stability of the burning process, carburetion and several other processes.

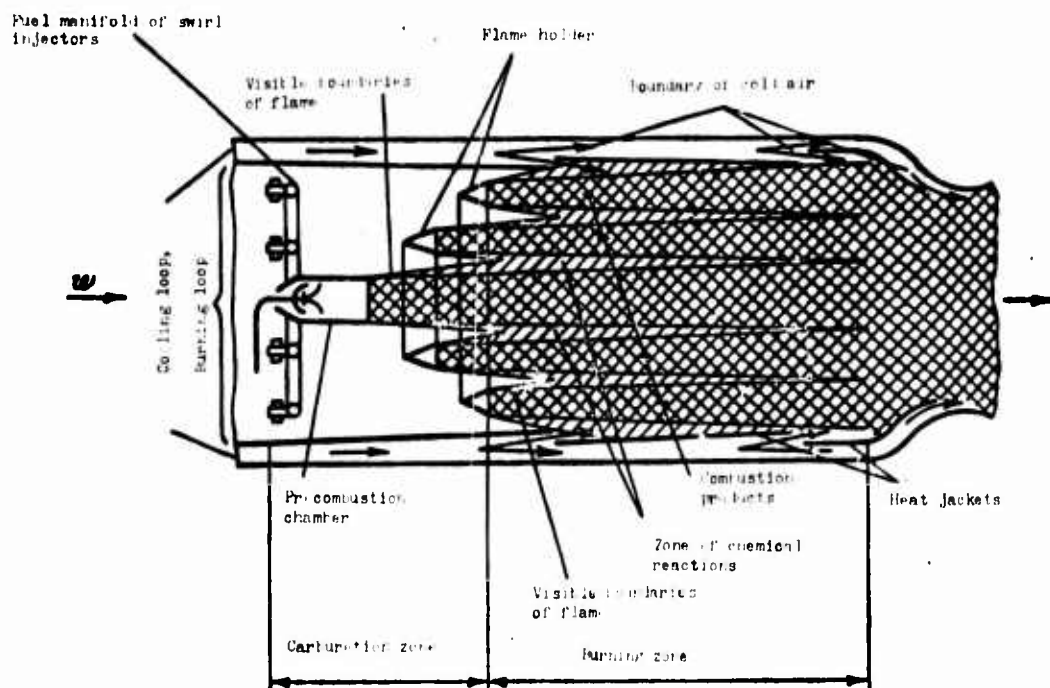
From the history of development of many branches of technology, it is known that at the initial stage of their development theory insufficiently reinforces the rapidly developing practical activity of the designer. In the beginning designers developing new systems can use an idea only in its most general thermodynamic or aerodynamic formulation. Concrete development, for instance of a system of organization of combustion in the chamber, estimate of its main dimensions, etc., is conducted

with the help of so-called "general physical concepts."

Now the requirement of high efficiency, and also use of rational and fast methods of creation of combustion chambers has advanced to first place. This poses the problem of deeper study of physics of the working process. Results of efforts of numerous investigations permit us to proceed to creation of a scientifically proven method of development of chambers and design of its elements, source of ignition, stabilizers, cooling system, etc.

The authors have tried to describe the working process of preparation and combustion of fuel on the whole, and to breakdown into separate elementary processes according to their internal nature. Where possible and expedient, they have constructed a graphic model of the phenomenon and given theoretical or experimental dependences determining its basic parameters. These dependences serve as the foundation of the method or system of methods of approximate calculation of elementary processes.

We will briefly consider stages of the working process in a chamber of straight-flow-through type (see the diagram). Thus for clarity we will follow along the chain of interconnected elementary processes occurring in the flow of air from the inlet section of the chamber to its outlet. Immediately let us note that such a sequence is more methodological than space-time. In reality separate processes overlap one another and flow simultaneously.



Typical scheme of organization of working process in the combustor of a ramjet engine.

The initial process which is developed in the inlet section of the chamber is carburetion. Its purpose is to create a fuel mixture with appropriate distribution of liquid and vapor phases over the cross section of the chamber. For this purpose there is usually used a system of collectors with swirler or direct-spray injectors, which atomize the liquid fuel in the air flow and create a set of mutually intersecting flames.

Drops entrained in the flow should insofar as possible be uniformly distributed over the given volume of the chamber (sometimes it is attempted to create higher enrichment or impoverishment of fuel of individual zones of the flow). Processes of carburetion are developed in the "cold" section of the chamber, which has an extent of 100-600 mm (for various systems of organization of combustion). The time the mixture remains in the "cold" section usually is small (5-20 msec) and insufficient for completion of full vaporization of the drops and mixing of fuel with air.

Further on the two-phase mixture enters the zone of ignition and stabilization, where carburetion and burning flow in parallel. Here the mixture is ignited by an electrical spark in a special device — a precombustion chamber, and the appearing flame front is held in a steady state with the help of stabilizers [flame-holders] (see the diagram). Hence there begins the "hot" section of the chamber.

The precombustion chamber is a miniature cylindrical or annular chamber with a "pinched" inlet, which creates inside its vortex flow with low velocities (10 to 15 m/sec). This ensures inside the precombustion chamber favorable conditions for ignition and burning of the mixture with high completeness and a stable "pilot flame" at its outlet independently of variation of parameters of the basic flow in the chamber.

The fuel mixture moves along the chamber with sufficiently high speed (60 to 200 m/sec). For stabilization of the flame front with respect to walls of the chamber it is necessary to satisfy a series of conditions which have an aerodynamic and thermal nature and basically reduce to observance of equality between velocity of flame propagation and the component of velocity of the incident flow along the normal to the flame front.

For creation of these conditions there are applied stabilizers, which consist of a body of bluff form (cone, ring with V-shaped radial cross section, etc.). In the stern region of the stabilizer there appears a vortex zone with counter currents. The fuel mixture entering this zone is ignited by the precombustion chamber flame,

burns with high completeness, and combustion products ignite the mixture after the nearest stabilizer. Thus there are created conditions for stabilization of the flame front over the entire cross section of the chamber.

Fresh fuel mixture passing through the flame front ignites, but does not completely burn it; the extent of the combustion zone after the front can be considerable. Individual combustion zones of separate stabilizers (which are echeloned in the chamber) overlap, forming a common combustion zone, where combustion of the fuel is completed. In the "hot" section of the chamber processes of carburetion (vaporization and mixing) of vaporized fuel with air, chemical combustion reactions, and turbulent diffusion and mixing of fuel mixture with combustion products occur in complicated interaction.

The presence of very high temperature of combustion products leads to the necessity of creation of systems of thermal protection and cooling of elements of the engine. These systems must provide heat resistance and thermal stability of the construction during the entire time of operation of the engine.

With air cooling, part of the air not participating in burning is used for cooling of the combustion chamber and nozzle. Air coolant is removed into the external loop of the chamber, and then through slots flows into the combustion chamber, forming an air curtain between combustion products and chamber walls. Thus, the stagnation temperature of air used for cooling should be less than the maximum permissible temperature of the material which the basic elements of the engine are made.

Such basically is the division of the working process in the chamber into elements. According to this arbitrary division, the material of the following chapters is presented.

CHAPTER I

CERTAIN PROBLEMS OF THERMODYNAMICS OF THE COMBUSTION CHAMBER

§ 1. THERMODYNAMIC CYCLE OF A RAMJET ENGINE

The complexity of working process in an air-breathing jet engine (БРД) hampers its general analysis with the help of the usual equations and formulas of engineering thermodynamics. For analysis and graphic description of the most important factors determining the basic quality indices of the cycle of an air-breathing jet engine, there is usually considered the thermodynamic cycle of an ideal engine.

By an ideal air-breathing engine there is understood an engine in which internal losses are absent; the working substance is air; heat capacity of air is constant, i.e., does not depend on temperature; the flow is completely decelerated in the diffuser and completely expanded in the exit nozzle.

Thus, the ideal cycle consists of a simplified (arbitrary) scheme of combination of real processes occurring in a real engine. All parameters of the working substance determining the operation of the engine cycle take limiting values in the

in the ideal, and the degree of approximation of parameters of a real engine to them characterizes the degree of perfection of the real engine.

As an example we will consider the thermodynamic cycle of a ramjet engine (ПБРД). At the basis of the working process of a ramjet engine there lies an ideal thermodynamic cycle with adiabatic compression and expansion of air and heat addition at constant pressure.

Variation of parameters of the gas along the length of the ideal ramjet engine is shown in Fig. 1.1. Change

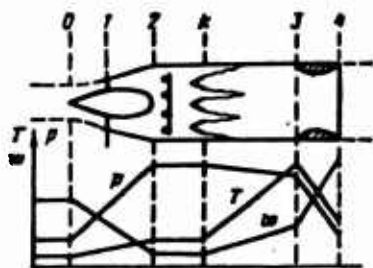


Fig. 1.1. Variation of parameters of gas along the length of a ramjet engine.

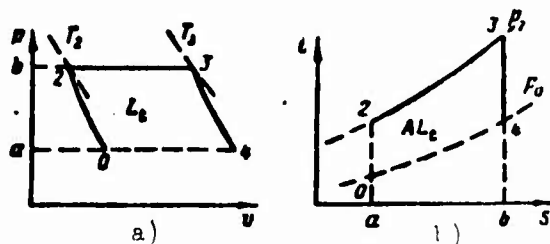


Fig. 1.2. Ideal gas cycle of a ramjet engine during nonshock compression of air.

of heat removal 4-0 represents the arbitrary process which closes the cycle; in reality it occurs outside the engine.

The total work of expansion of gases in the nozzle (referred to 1 kg of air) $L_{вд.г}$ and p-V-diagram is depicted by the area of 2-3-4; work expended in adiabatic compression of air in the diffuser $L_{ад.сж}$ is depicted by the area a-b-0; net work of the cycle is determined by the difference $L_t = L_{ад.г} - L_{ад.сж}$ and area 0-2-3-4.

In a ramjet engine, net work of the cycle is used for increase of kinetic energy of the flow of air passing through the engine:

$$L_t = \frac{w_4^2 - V^2}{2g}, \quad (1.1)$$

where w_4 — exhaust velocity of gases from the nozzle in m/sec;

V — velocity of flight in m/sec.

The basic characteristic of the thermodynamic cycle is thermal efficiency, i.e., the degree of conversion of supplied heat Q into useful work of the cycle. Thermal efficiency η_t is equal to the ratio of heat converted into useful work L_t to the heat Q supplied from without:

$$\eta_t = \frac{A \cdot L_t}{Q} = \frac{Q_1 - Q_2}{Q_1}, \quad (1.2)$$

where Q_1 — heat supplied on the section 1-2 (area a-1-2-b on the i-s diagram);

Q_2 — heat removed in the cycle on the section 4-0 (area a-0-4-b).

Referring heats Q_1 and Q_2 to 1 kg of air, it is possible to write

$$\left. \begin{aligned} Q_1 &= c_p (T_{03} - T_{02}), \\ Q_2 &= c_p (T_4 - T_0). \end{aligned} \right\} \quad (1.3)$$

Then*

$$\eta_t = 1 - \frac{T_4 - T_0}{T_{03} - T_{02}} = 1 - \frac{T_0}{T_{02}} \frac{\frac{T_4}{T_0} - 1}{\frac{T_{03}}{T_{02}} - 1}. \quad (1.4)$$

*Subscript "0" denotes temperature of the medium before flow.

From the equations of adiabats 3-4 and 0-2 we have

$$\frac{T_{02}}{T_4} = \left(\frac{p_{02}}{p_4}\right)^{\frac{k-1}{k}} \text{ and } \frac{T_{02}}{T_0} = \left(\frac{p_{02}}{p_0}\right)^{\frac{k-1}{k}}. \quad (1.5)$$

Since

$$p_4 = p_0 \text{ and } p_{02} = p_{02}$$

then

Whence

$$\frac{T_{02}}{T_4} = \frac{T_{02}}{T_0} \text{ or } \frac{T_{02}}{T_{02}} = \frac{T_4}{T_0}.$$

$$\eta_t = 1 - \frac{T_4}{T_{02}} = 1 - \frac{1}{\left(\frac{p_{02}}{p_0}\right)^{\frac{k-1}{k}}}. \quad (1.6)$$

The degree of increase of pressure at the end of the diffuser for an ideal engine (without losses) can be expressed in terms of velocity of flight M_H . With complete adiabatic deceleration

$$\left(\frac{p_{02}}{p_0}\right)^{\frac{k-1}{k}} = 1 + \frac{k-1}{k} M_H^2.$$

For air $k = 1.4$, and then

$$\eta_t = \frac{1}{\frac{3.5}{M_H^2} + 1}. \quad (1.7)$$

Expressions (1.6) and (1.7) show that thermal efficiency of an ideal engine depends only on the degree of increase of pressure at the end of the diffuser and continuously increases with increase of velocity of flight (Fig. 1.3). This is explained by the fact that with increase of the degree of pressure increase there occurs higher expansion of air when heat Q_1 is supplied to it; a larger quantity of this heat is used for increase of kinetic energy of gases exhausted from the engine, which leads to decrease of the heat Q_2 lost from the cycle into the atmosphere.

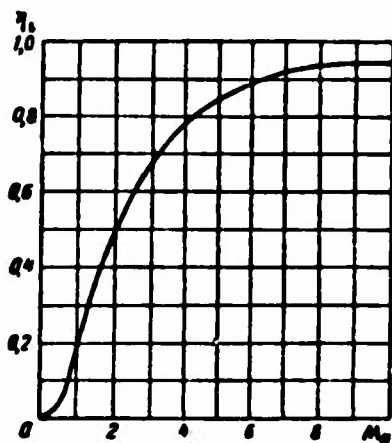


Fig. 1.3. Change of thermal efficiency depending upon M_H , during nonshock compression of air.

If with increase of velocity of flight Q_1 is kept constant, then net work of the cycle will continuously increase, since

$$L_t = \frac{Q_1}{A} \eta_t.$$

The obtained relationships (1.6) and (1.7) are valid for an engine with nonshock compression of air. Shock compression, due to losses in shock waves, leads to decrease of pressure p_{02} and to worsening of all parameters of the engine. In

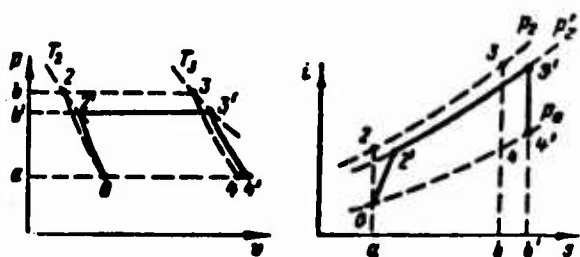


Fig. 1.4. Ideal cycle of a ramjet engine with shock compression of air.

the flow of air in shock waves at the same speed of flight M_H , shock compression leads to lower pressure (p_{02}' at the end of the diffuser and consequently to decrease of thermal efficiency, and with constant heat addition Q_1 also to decrease of net work L_t as compared to the case of nonshock compression.

Change of state of gas in a real engine, taking into account losses existing in it, is illustrated in Fig. 1.5. For comparison, on these graphs the dotted lines

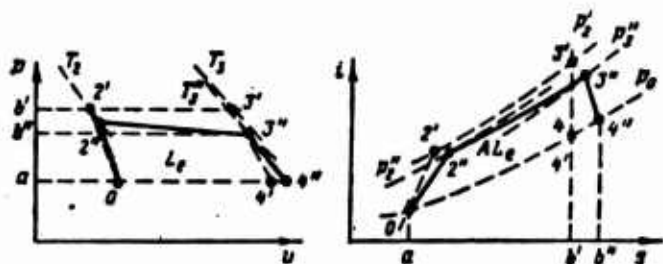


Fig. 1.5. Real cycle of ramjet engine.

denote curves corresponding to an ideal engine with shock compression of air. In Fig. 1.4 it is clear that at the end of compression, the air has lower pressure ($p_{02}'' < p_{02}'$) and somewhat lower thermodynamic temperature ($T_{02}'' < T_{02}'$), than in the ideal case. Pressure at point 2 decreases as a result of hydraulic losses in the diffuser and the presence of residual velocity at the beginning of the combustion chamber ($w_1 \neq 0$). Temperature decreases also due to the fact that $w_2 \neq 0$, since the following relationship is always valid:

$$T_2 = T_{02} - \frac{Aw_2^2}{2gc_p}.$$

Pressure on the line of heat addition 2''-3'' drops due to flow friction in the combustion chamber, and due to heat addition to the moving air during combustion of the fuel. The higher the flow friction of the combustion chamber and the higher the flow velocity are, the bigger the drop of pressure is on section 2''-3''.

Gas is expanded along the line 3''-4'', which due to hydraulic losses in the nozzle is more gently sloping than adiabatic curve 3'-4'.

Work of the real cycle on the p-v-diagram is determined by area 0-2''-3''-4''. This work is called the net work and in a ramjet engine is wholly expended in increase of

the kinetic energy of gases, i.e., in creation of jet thrust. For the same supply of heat Q_1 net work L_e decreases with decrease of pressure on the line 2"-3".

Efficiency of the ramjet engine as a heat engine is equal to the ratio of heat converted into net work AL_e to the heat introduced into the engine in the form of chemical energy of the fuel $G_T \cdot H_u$:

$$\eta_e = \frac{AL_e}{G_T H_u} = \frac{A(G_{\text{ex}}^2 - G_{\text{in}}^2)}{2g \cdot G_T \cdot H_u}, \quad (1.8)$$

where G_T - flow rate of gas (flow rate of air G_{a} + flow rate of fuel G_{f}) through the engine in kg/sec;

w_4 and V - flow velocity of gases at the nozzle edge and velocity of flight of the engine in m/sec;

H_u - lowest calorific value of fuel in kcal/kg;

$A = \frac{1}{427}$ - thermal equivalent of work in kcal/kg-m;

$g = 9.81$ - acceleration due to gravity in m/sec².

Expression (1.8) shows that other conditions being equal, the net efficiency of the engine depends on w_4 - the exhaust velocity of gases from the nozzle, which depends on temperature T_{03} and pressure p_{03} of the gas before the nozzle, since with full expansion, without taking into account losses in the nozzle,

$$w_4 = a_{\text{ex}} \lambda_4 = \sqrt{\frac{2k}{k-1} gRT_{03} \left[1 - \left(\frac{p_4}{p_{03}} \right)^{\frac{k-1}{k}} \right]}. \quad (1.9)$$

In turn, temperature of gases before the nozzle, other conditions being equal, depends on combustion efficiency of the fuel

$$\eta_c = \frac{Q_1}{G_T \cdot H_u}, \quad (1.10)$$

where Q_1 - quantity of actually released heat during combustion of fuel and expended in heating the gases:

$$Q_1 \approx G_T c_p T_{03} - G_{\text{f}} c_{p\text{f}} T_{02}. \quad (1.11)$$

Thus, net efficiency of the engine depends on combustion efficiency of the fuel η_c (i.e., on the perfection of the process of burning of fuel in the combustion chamber) and on flow friction in the combustion chamber, with increase of which pressure before the nozzle p_{03} decreases.

§ 2. SUPPLY OF HEAT TO MOVING GAS IN A PIPE AT $F = \text{const}$

Heat addition to a moving gas in pipe of uniform cross section (Fig. 1.6) is typical for combustion chambers of the ramjet engine and afterburners of turbojet engines (ТРД).

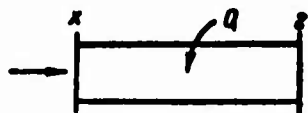


Fig. 1.6. For calculation of flow during heat addition to a moving gas in a pipe of uniform cross section.

The problem of thermodynamic analysis of a combustion chamber is reduced to determination of:

- a) parameters of flow along the length of the combustion chamber, if parameters of flow at the inlet p_x, w_x, ρ_x, T_x and the law of heat addition are known;
- b) maximum heating of the work substance (air).

Parameters of flow at the inlet into the chamber are determined during calculation of optimum thrust and efficiency characteristics of the engine, taking into account its arrangement in the aircraft, and are taken initial data for designing.

Following [1], we will consider variation of parameters of gas along the length of the combustion chamber. From the equation of continuity

$$\rho_x w_x = \rho_r w_r \quad (1.12)$$

it is easy to note that during heat addition to moving air in a pipe of uniform cross section, its velocity increases, consequently static pressure drops.

According to the momentum equation,

$$p_x - p_r = \rho_r w_r (w_r - w_x) \quad (1.13)$$

increase of velocity causes a drop of pressure. From the equation of state we have

$$\frac{p_r}{\rho_r T_r} = \frac{p_x}{\rho_x T_x} \quad (1.14)$$

But since $p_r < p_x$, density of gas along the length of the pipe drops somewhat faster than $1/T$; therefore, gas velocity is increased faster than temperature. Speed of sound, which is proportional to the square root of absolute temperature, is increased along the pipe considerably more slowly than flow velocity. Therefore, Mach number $M = w/a$ along the length of the pipe increases consequently, with appropriate heating, a flow having any initial velocity can be accelerated to critical velocity ($M_r = 1.0$).

But no heating can cause the flow of gas in a cylindrical pipe to reach supersonic speed. This phenomenon is called thermal crisis.

The enthalpy equation of the flow can be written in the following way:

$$Q = c_{p,r} T_{0r} - c_{p,x} T_{0x} = c_{p,r} T_r - c_{p,x} T_x + \frac{\lambda}{2g} (w_r^2 - w_x^2). \quad (1.15)$$

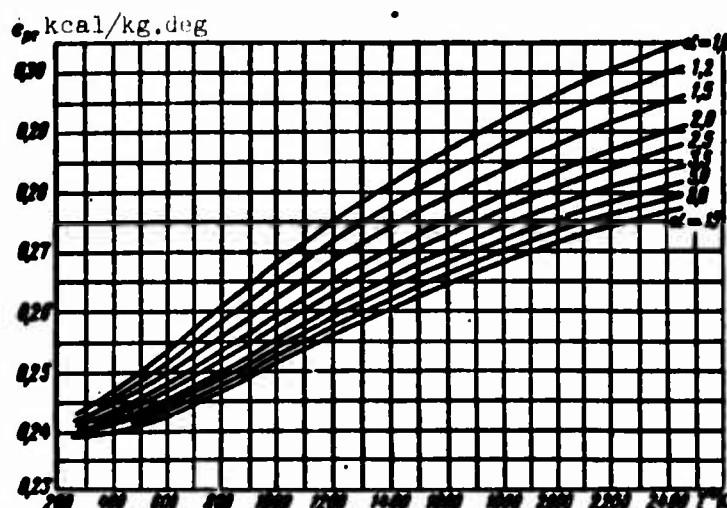


Fig. 1.7. Average heat capacity of combustion products of kerosene in air.

where Q is the heat, introduced into the gas. Values of c_{pr} are given in Fig. 1.7.

With help of four equations (1.12)-(1.15), we can determine four parameters of the gas at the end of the pipe p_r , ρ_r , T_r and w_1 , if there are known the same parameters at the beginning of the pipe. The considered system of four equations with four unknowns is reduced to one quadratic equation.

The momentum equation (1.13) can be rewritten as

$$p_r \left(\frac{p_x}{p_r} - 1 \right) = p_r w_r (w_r - w_x).$$

We will substitute in this equation the value of p_x/p_r from the equation of state (1.14):

$$\frac{p_x}{p_r} \cdot \frac{T_x}{T_r} - 1 = \frac{p_r}{p_r} \cdot \alpha_r \left(1 - \frac{p_r}{p_x} \right). \quad (1.16)$$

But

$$\frac{p_r}{p_r} = \frac{p_r}{p_r g R T_r} \quad \text{and} \quad \alpha_r = \sqrt{k g R T_r},$$

whence

$$\frac{p_r}{p_r} = \frac{k}{\alpha_r^2}.$$

Consequently, formula (1.16) will take the form

$$\frac{p_x}{p_r} \cdot \frac{T_x}{T_r} - 1 = k M_r^2 \left(1 - \frac{p_r}{p_x} \right). \quad (1.17)$$

Values of k are given in Fig. 1.8. Ratio of temperature in the flow

$$\frac{T_x}{T_r} = \frac{T_{0x} - \left(\frac{A w_x^2}{2 g c_{px}} \right)}{T_{0r} - \left(\frac{A w_r^2}{2 g c_{pr}} \right)} = \frac{\frac{T_{0x}}{T_{0r}} - \left(\frac{A w_x^2}{2 g c_{px} T_{0r}} \right)}{1 - \left(\frac{A w_r^2}{2 g c_{pr} T_{0r}} \right)}.$$

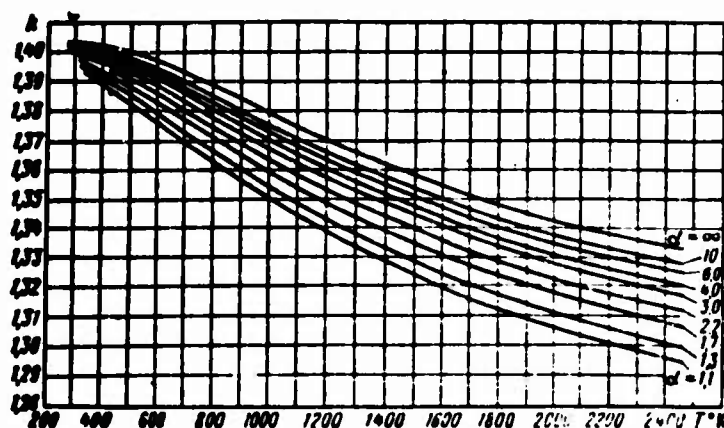


Fig. 1.8. Average adiabatic index of combustion products of kerosene in air.

Introducing the critical speed

$$a_{cr} = \sqrt{\frac{2k}{k+1} gRT_{cr}}$$

and using the continuity equation (1.12) and dimensionless coefficient of velocity

$\lambda_r = \frac{w_r}{a_{cr}}$, we will obtain

$$\frac{T_x}{T_r} = \frac{\frac{T_{cr}}{T_r} - \frac{k_r - 1}{k_r + 1} \left(\frac{p_r}{p_x} \right)^2 \lambda_r^2}{1 - \frac{k_r - 1}{k_r + 1} \lambda_r^2}.$$

Using the known relationship of gas dynamics

$$M_r^2 = \frac{\frac{2}{k_r + 1} \lambda_r^2}{1 - \frac{k_r - 1}{k_r + 1} \lambda_r^2}$$

and substituting values of M_r^2 and T_x/T_r in equation (1.17), we will obtain the sought quadratic equation

$$\left(\frac{p_r}{p_x} \right)^2 \frac{\lambda_r^2}{1 + \lambda_r^2} - \frac{p_r}{p_x} + \frac{T_{cr}}{T_{cr}} \cdot \frac{1}{1 + \lambda_r^2} = 0,$$

by solving which, we will find

$$\frac{p_r}{p_x} = \frac{1 + \lambda_r^2}{2\lambda_r^2} \left[1 - \sqrt{1 - \frac{4\lambda_r^2}{(1 + \lambda_r^2)^2} \cdot \frac{T_{cr}}{T_{cr}}} \right]. \quad (1.18)$$

Analogously we will obtain

$$\frac{p_x}{p_r} = \frac{1 + \lambda_x^2}{2\lambda_x^2} \left[1 - \sqrt{1 - \frac{4\lambda_x^2}{(1 + \lambda_x^2)^2} \cdot \frac{T_{cr}}{T_{cr}}} \right]. \quad (1.18')$$

With the help of equations (1.14), (1.15) and (1.18), we will determine parameters of the gas at the end of the combustion chamber.

If at the end of the pipe there occurs thermal crisis ($\lambda_r = 1$), then equation (1.18) will take the form

$$\frac{p_r}{p_x} = \frac{w_r}{w_x} = 1 - \sqrt{1 - \frac{T_{ox}}{T_{or}}} \quad (1.19)$$

or in dimensions form

$$\lambda_x = \frac{\lambda_r \cdot a_{pr}}{a_{px}} \left(1 - \sqrt{1 - \frac{T_{ox}}{T_{or}}} \right).$$

But $\lambda_r = 1.0$, and the ratio

$$\frac{a_{pr}}{a_{px}} = \sqrt{\frac{T_{or}}{T_{ox}}}.$$

whence

$$\lambda_x = \sqrt{\frac{T_{or}}{T_{ox}}} \left(1 - \sqrt{1 - \frac{T_{ox}}{T_{or}}} \right) = \sqrt{\frac{T_{or}}{T_{ox}}} - \sqrt{\frac{T_{or}}{T_{ox}} - 1}. \quad (1.20)$$

This equation shows that at thermal crisis, a completely determined value of λ_x at the beginning of the combustion chamber corresponds to a given quantity of supplied heat. At $T_{or}/T_{ox} = 1$, the coefficient of velocity at the beginning of the pipe also is equal to unity; for infinitely large heating $\lambda_x = 0$.

Critical heating of gas is possible with appropriate pressure at the beginning of the pipe — more correctly, with appropriate pressure ration p_x/p_r .

According to the momentum equation, pressure drop in the pipe us equal to

$$\frac{p_x}{p_r} - 1 = \frac{p_r w_r^2}{p_r} \left(1 - \frac{w_x}{w_r} \right).$$

But

$$\frac{p_r}{p_r} = \frac{a_r^2}{k} = \frac{1}{k} \frac{1 - \frac{k-1}{k+1} \lambda_r^2}{\frac{2}{k+1}} a_{pr}^2$$

therefore,

$$\frac{p_x}{p_r} = 1 + \frac{\frac{2k}{k+1} \lambda_r^2}{1 - \frac{k-1}{k+1} \lambda_r^2} \left(1 - \frac{w_x}{w_r} \right). \quad (1.21)$$

Consequently, to every value of flow velocity at the beginning of the pipe and degree of heating, there corresponds a definite value of pressure drop p_x/p_r .

The limiting value of pressure drop is obtained upon achievement of thermal crisis ($\lambda_r = 1$). In this case, on the basis of (1.19)

$$\left| \frac{p_x}{p_r} \right|_{\max} = 1 + k \sqrt{1 - \frac{T_{ox}}{T_{or}}}. \quad (1.22)$$

With very strong heating ($\frac{T_{ox}}{T_{or}} \rightarrow 0$) pressure drop can reach the largest magnitude:

$$\left| \frac{p_x}{p_r} \right|_{\max} = k + 1.$$

If pressure drop is less than required according to formula (1.22), then for the given preheating T_{Or}/T_{Ox} through the combustion chamber air will pass with lower flow rate, coefficient of velocity λ_r will be less than unity, and the ratio of velocities w_x/w_r will be established to be such, that it satisfies equality (1.21).

By increasing pressure at the beginning of the pipe, we will increase flow rate of air and speed w_x until, for the given preheating T_{Or}/T_{Ox} , λ_r becomes equal to 1. With further increase of pressure p_x flow rate of air through the pipe will be accordingly increased, and the ratio of speeds and pressures at the beginning

and at the end of the pipe will remain constant.

Let us determine the drop of total pressure in a cylindrical pipe. According to the equations of gas dynamics, we have accordingly

$$\frac{p_x}{p_{\max}} = \left(1 - \frac{k-1}{k+1} \lambda_x^2 \right)^{\frac{k}{k-1}},$$

$$\frac{p_r}{p_{\max}} = \left(1 - \frac{k-1}{k+1} \lambda_r^2 \right)^{\frac{k}{k-1}}.$$

Dividing the first equation by the

second, we will obtain

$$\sigma_{\text{R.C.}} = \frac{p_{\text{or}}}{p_{\text{ox}}} = \frac{p_r}{p_x} \left(\frac{1 - \frac{k-1}{k+1} \lambda_x^2}{1 - \frac{k-1}{k+1} \lambda_r^2} \right)^{\frac{k}{k-1}}. \quad (1.23)$$

Pressure coefficient $\sigma_{\text{R.C.}}$ decreases with increase of λ_x for constant degrees of preheating, and with increase of preheating at constant velocity at the inlet. This situation is graphically illustrated by the curve $\sigma_{\text{R.C.}} = f\left(\lambda_x, \frac{T_{\text{or}}}{T_{\text{ox}}}\right)$ in Fig. 1.9, which was calculated on the basis of equations (1.18'), (1.21) and (1.23) on the assumption of constant value of $k = 1.4$.

The biggest drop of total pressure is obtained under the conditions of thermal crisis ($\lambda_r = 1$). Substituting expressions (1.20) and (1.22) into equality (1.23), we will express the total drop of total pressure as a function of the ratio of stagnation temperatures

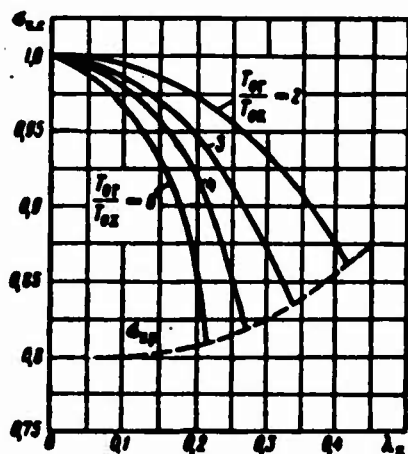


Fig. 1.9. Pitot losses in a combustion chamber during heat addition ($F = \text{const}$, $k = 1.4$).

$$\epsilon_{tp} = \frac{\left[k - (k-1) \left(1 - \sqrt{1 - \frac{T_{0x}}{T_{0r}}} \right) \frac{T_{0r}}{T_{0x}} \right]^{\frac{k}{k-1}}}{1 + k \sqrt{1 - \frac{T_{0x}}{T_{0r}}}}. \quad (1.24)$$

The dependence of ϵ_R on the ratio of stagnation temperatures during thermal crisis, calculated for $k = 1.4$, by formula (1.24), is given in Table 1.1.

Table 1.1

T_{0r}/T_{0x}	1	1.5	2.0	4	6	8	∞
ϵ_{tp}	1	0.89	0.86	0.82	0.81	0.80	0.79

Consequently, for preheating $T_{0r}/T_{0x} \approx 4.0$, Pitot losses almost attain their maximum magnitude and compose ~20% of the total pressure at the beginning of the combustion chamber. Pressure drop on the heat addition line, as follows from analysis of the thermodynamic cycle, leads to decrease of net work (thrust) and net efficiency of the engine. Thermal losses can be lowered by means of decrease of the coefficient of flow velocity at the beginning of the combustion chamber λ_x , but this leads to increase of dimensions of the engine, its weight and external drag.

§ 3. HEAT ADDITION TO A MOVING GAS IN A PIPE WITH VARYING CROSS SECTION

Heat Addition at $p = \text{const}$

Such a process can be realized in a divergent pipe, the area of cross section of which is selected in accordance with the law of heat addition, so that pressure in the flow remains constant along the length of the pipe.

Let us consider the variation of parameters of the gas along the length of the pipe when heat added to the moving gas at $p = \text{const}$.

From the Bernoulli equation written in differential form

$$w dw + \frac{dp}{\rho} = 0,$$

we have

$$w_r - w_x + \int_{p_x}^{p_r} \frac{dp}{\rho} = 0. \quad (1.25)$$

But since $p_r = p_x$, then $w_r = w_x$, i.e., flow velocity along pipe remain constant. Total pressure of flow at the end of the pipe

$$p_{0x} = \frac{p_x}{\left(1 - \frac{k-1}{k+1} \lambda_x^2\right)^{\frac{k}{k-1}}}. \quad (1.26)$$

Let us express λ_T in terms of λ_x . Since $w_T = w_x$, then

and

$$a_{0T} \lambda_T = a_{0x} \lambda_x$$

$$\lambda_T = \lambda_x \sqrt{\frac{T_{0x}}{T_{0T}}}. \quad (1.27)$$

Placing value λ_T from (1.16) in (1.26), we will obtain

$$p_{0x} = \frac{p_x}{\left(1 - \frac{k-1}{k+1} \lambda_x^2 \frac{T_{0x}}{T_{0T}}\right)^{\frac{k}{k-1}}}. \quad (1.28)$$

Ratio of temperatures of decelerated flow T_{0x}/T_{0T} is found by means of equation of enthalpy (1.15).

Replacing in (1.28) magnitude p_x by pressure of decelerated flow

$$p_x = p_{0x} \left(1 - \frac{k-1}{k+1} \lambda_x^2\right)^{\frac{k}{k-1}},$$

at constant value of k , we will have

$$\frac{a_{0x}}{a_{0T}} = \frac{p_{0x}}{p_{0T}} = \left[\frac{1 - \frac{k-1}{k+1} \lambda_x^2}{1 - \frac{k-1}{k+1} \lambda_x^2 \frac{T_{0x}}{T_{0T}}} \right]^{\frac{k}{k-1}}. \quad (1.29)$$

Thus, during heat addition to moving gas at $p = \text{const}$, total pressure in flow also drops, and more, the higher λ_x and degree of preheating of gas T_{0T}/T_{0x} , are.

Change of cross section of pipe, necessary for heat addition to moving gas at $p = \text{const}$, on the assumption of absence of hydraulic losses, is determined only by the law of heat addition. From continuity equation

$$\rho_1 w_1 F_1 = \rho_2 w_2 F_2$$

taking into account the fact that pressure and speed along length of pipe remain constant, we will obtain

$$\frac{F_2}{F_1} = \frac{T_2}{T_1}. \quad (1.30)$$

Here subscript "1" denotes values in the considered cross section.

Heat Addition to a Moving Gas in a Pipe with Arbitrarily Varying Area of Cross Section

Flow of gas with heat addition in a pipe with arbitrarily varying area of cross section can be calculated approximately by the method of numerical integration proposed by V. S. Zuyev.

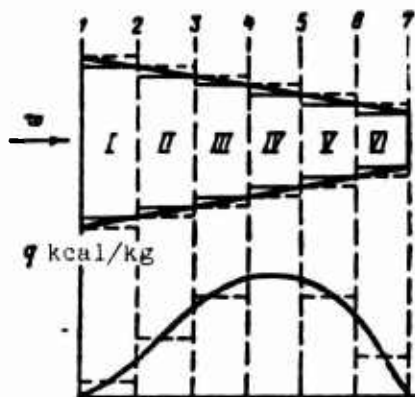


Fig. 1.10. Analysis of flow during heat addition to a moving gas in a conical convergent pipe.

posed by V. S. Zuyev.

Let us assume that the gas flows through a pipe of arbitrary cross section with a given law of heat addition (Fig. 1.10). Let us replace this channel by circumscribed and inscribed step contours consisting of n cylindrical sections.

Calculation of parameters of flow is conducted consecutively from first to subsequent sections along both contours, with use of relationships obtained in § 2 of the present chapter for the case of heat addition to a moving gas at $F = \text{const.}$

Transition from one cylindrical step to another is considered to be adiabatic. Results obtained along both contours are averaged, and the arithmetic mean is taken as the true result. The larger the number of sections n into which the channel is divided, the higher the accuracy of the calculation.

The method expounded below is useful for analysis of flow in a channel of any arbitrary geometric form, but two cases may be of practical interest — heat addition to a moving gas in divergent and convergent conical channels. As an example we will consider the latter case. Parameters of the gas at the channel inlet w_1, ρ_1, T_1, p_1 , areas of inlet and outlet cross sections and the law of heat addition along the length of the channel are given.

It is required to determine: parameters of flow at the end of the channel, pressure coefficient $\sigma_{k.c.}$, permissible (critical) heating of the gas for which λ will be equal to 1.0 at the end of the channel.

The formulated problem is solved in the following way. We divide the channel into n (in Fig. 1.10, into six) sections and perform successive calculation of change of parameters of the flow along the outer (circumscribed) step contour.

The quantity of heat added in each section will be

$$Q_i = \int_{l_{i-1}}^{l_i} q dl \quad (1.31)$$

We will determine the temperature of the flow at the end of each i -th section by the heat balance equation

$$Q_i = c_{p,i} T_{0i} - c_{p,i-1} T_{0(i-1)} = c_{p,i} T_i - c_{p,i-1} T_{(i-1)} + \frac{A}{2g} (w_i^2 - w_{(i-1)}^2). \quad (1.32)$$

Flow velocity at the end of the first section of the outer step contour will be found according to the relationships

$$\frac{w_{\text{max}}}{w_i} = \frac{F_1}{F_i} = \frac{1 + \lambda_i^2}{2\lambda_i^2} \left[1 - \sqrt{1 - \frac{4\lambda_i^2}{(1 + \lambda_i^2)^2} \frac{T_{0i}}{T_{01}}} \right] \quad (1.33)$$

and

$$\lambda_{\text{max}} = \frac{w_{\text{max}}}{a_{01}}. \quad (1.34)$$

With transition to second section, coefficient of velocity is determined by the formula

$$\lambda_2 \left(1 - \frac{k-1}{k+1} \lambda_2^2 \right)^{\frac{1}{k-1}} = \frac{F_1}{F_2} \lambda_{\text{max}} \left(1 - \frac{k-1}{k+1} \lambda_{\text{max}}^2 \right)^{\frac{1}{k-1}}. \quad (1.35)$$

Ratio of velocities at the end and at the beginning of i -th section will be obtained by means of an expression analogous to (1.33):

$$\frac{w_{\text{max}}}{w_{(i-1)}} = \frac{F_{(i-1)}}{F_{\text{max}}} = \frac{1 + \lambda_{(i-1)}^2}{2\lambda_{(i-1)}^2} \left[1 - \sqrt{1 - \frac{4\lambda_{(i-1)}^2}{(1 + \lambda_{(i-1)}^2)^2} \frac{T_{0i}}{T_{0(i-1)}}} \right].$$

Then we make adiabatic recalculation of velocity at the end of this section:

$$\lambda_i \left(1 - \frac{k-1}{k+1} \lambda_i^2 \right)^{\frac{1}{k-1}} = \frac{F_{(i-1)}}{F_i} \lambda_{\text{max}} \left(1 - \frac{k-1}{k+1} \lambda_{\text{max}}^2 \right)^{\frac{1}{k-1}}.$$

We will take λ_1 as velocity at the beginning of the section, etc., up to the last section. We will complete calculation of the outer step contour by adiabatic recalculation of velocity $\lambda_{6\text{Hap}}$ for the ratio of areas F_5/F_6 by means of the formula (1.35), and will determine $\lambda_{6\text{Hap}}$.

We will start calculation of flow along outer contour with determination of coefficient of velocity at beginning of first section by means of relationship analogous to (1.35):

$$\lambda_{1\text{max}} \left[1 - \frac{k-1}{k+1} (\lambda_{1\text{max}})^2 \right]^{\frac{1}{k-1}} = \frac{F_1}{F_2} \lambda_1 \left(1 - \frac{k-1}{k+1} \lambda_1^2 \right)^{\frac{1}{k-1}}.$$

Then we will find coefficient of velocity at the end of the first section of inner countour λ_2 , recalculate velocity at beginning of second, third sections, etc., until determination of $\lambda_{6\text{BH}}$; this is analogous to calculation according to the outer contour.

Coefficient of velocity at the end of the channel will be determined by the relationship

$$\lambda_6 = \frac{1}{2} (\lambda_{\text{sup}} + \lambda_{\text{son}}). \quad (1.36)$$

Pressure at the end of channel will be found by means of expression (1.21)

$$\frac{p_1}{p_6} = 1 + \frac{\frac{2k}{k+1} \lambda_6^2}{1 - \frac{k-1}{k+1} \lambda_6^2} \left(1 - \frac{u_1}{u_6} \right)$$

and pressure coefficient - by (1.23)

$$c_{x,c} = \frac{p_6}{p_1} \left(\frac{1 - \frac{k-1}{k+1} \lambda_1^2}{1 - \frac{k-1}{k+1} \lambda_6^2} \right)^{\frac{k}{k-1}}.$$

If $\lambda_6 < 1.0$, then this completes solution of the first problem - determination of parameters of flow at the end of the channel and the pressure coefficient. If at the end of some section (including the last one), as a result of calculation coefficient of velocity is obtained to be larger than unity, then the given heat addition is above limiting.

Limiting heating can be determined by the above method, by successively taking total value of supplied heat Q until there is obtained convergence, i.e., until given quantity of heat corresponds to transonic speed at the end of the channel.

Calculation of flow of gas with heat addition in a channel of variable cross section by method of numerical integration is cumbersome and labor-consuming, but division of channel into a sufficiently large number of sections gives very high accuracy. It is necessary to indicate, however, that in motors heat addition along the length of combustion chamber (i.e., burnup) depends on many factors - organization of carburetion and burning of fuel, parameters of flow of air, geometric form of chamber, etc. Therefore, during calculation of flow in combustion chamber of variable cross section, it is impossible practically to assign in advance a law of heat addition, although total amount of supplied heat is usually known.

§ 4. Influence of Flow Velocity on Characteristics of the Combustion Chamber

Above it was indicated that thermal efficiency of the engine is increased with increase of air pressure at the end of compression. For increase of p_2 (see Fig. 1.2) at given speed of flight, it is necessary to try to decelerate air at the end of the

diffuser as much as possible - w_2 . Decrease of speed w_2 is possible by means of increase of area ratio F_2/F_0 , i.e., the cross-sectional area of the combustion chamber F_2 . However, considerable increase of area ratio F_2/F_0 leads to impermissible increase of dimensions, weight and external drag of the engine.

In a ramjet engine, total pressure of air at the end of compression p_{02} depends on work of the diffuser and is determined by the relationship

$$p_{02} = \sigma_D p_{00}$$

where σ_D - pressure recovery factor in diffuser;

p_{00} - total pressure during adiabatic deceleration of flow.

In engines of usual design, flow velocity at the end of the diffuser is always subsonic ($\lambda_2 \ll 1.0$) and usually is equal to $\lambda_2 = 0.15$ to 0.25 , in rare cases attaining $\lambda_2 = 0.4$ to 0.5 . With such values of λ_2 , the ratio of static pressure at the end of the diffuser to total pressure of the decelerated flow p_2/p_{02} is accordingly equal to 0.985 to 0.855 . Thus, change of flow velocity at the beginning of the combustion chamber, even within such a wide range as $\lambda_2 = 0.15$ to 0.5 , does not in practice directly affect the magnitude of thermal efficiency of the cycle.

Increase of velocity at the beginning of the combustion chamber is not desirable for other reasons: with increase of λ_2 proportionally to the square of velocity, hydraulic losses increase and, furthermore, thermal losses are increased.

Decrease of the ratio of total pressure at the end of the chamber p_{03} to total pressure at the beginning of the chamber for p_{02} , which is caused only by hydraulic losses, is shown in Fig. 1.11 in dependence upon coefficient of flow friction $\xi_{K.C}$ and velocity and coefficient at the end of the diffuser λ_2 . From this graph it is clear that if, for instance, $\xi_{K.C} = 3.0$, then with change of λ_2 from 0.15 to 0.5 losses of total pressure at the end of the combustion chamber as a result of hydraulic losses will compose accordingly in first case only $\sim 4\%$, and in the second will increase to 40% of the total pressure at the beginning of the combustion chamber. Due to this, at $\lambda_2 = 0.5$ net efficiency and thrust of the engine will worse.

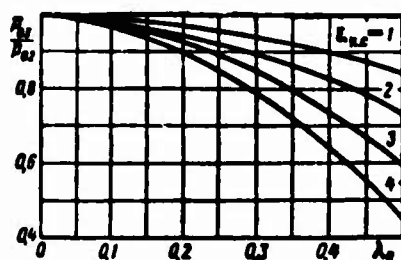


Fig. 1.11. Change of total pressure at the end of the combustion chamber, depending on $\xi_{K.C}$ and λ_2 .

The discussed example shows how important it is during creation of a combustion chamber to try to its flow friction as much as possible, especially for high flow velocities at the end of the diffuser. High flow velocities at the beginning of the combustion chamber are also not desirable from the point of view of organization of

the process of burning of fuel, since they cause stabilization of the flame to become worse, and for ensuring stable burning it is necessary to increase dimensions of the flame-holders; but this, in turn, leads to increase of flow friction of the flame front devices with all of the above-indicated negative consequences.

Furthermore, with increase of flow velocity, burning of two-phase fuel-air mixture becomes worse, since time of stay of fuel in the combustion chamber decreases, as a result of which in a number of cases (at relatively low temperatures of flow for insufficiently fine atomizing of liquid fuel, during burning of solid fuel, etc.) combustion efficiency of the fuel η_z decreases. For increase of combustion efficiency in this case, it is necessary to increase length of combustion chamber, and consequently also weight of the engine.

§ 5. Dependence of Engine Characteristic on Combustion Efficiency of Fuel

Combustion efficiency of fuel η_z is one of the basic parameters characterizing perfection of the combustion chamber.

Analysis of thermodynamic cycle of an air-breathing jet engine shows that at constant net efficiency, net work, and consequently also engine thrust are proportional to the quantity of heat Q_1 added to the gas. Heat is introduced into the combustion chamber in the form of chemical energy of fuel. In the process of burning there is not released all chemical energy of the fuel, but only part of it:

$$\eta_z = \frac{Q_1}{G_T \cdot H_u}, \quad (1.57)$$

where G_T — fuel consumption in kg/sec;

H_u — lowest calorific value of fuel in kcal/kg.

It is obvious that at a given value of Q_1 , which provides a given engine thrust, fuel consumption G_T will be greater, than less η_z is. Consequently, fuel combustion efficiency in all cases directly affects magnitude of engine specific impulses: specific impulse J is changed proportionally to η_z .

In turn magnitude of engine specific impulse determines range of powered flight of an aircraft with engine working. By the formula of Tsiolkovsky

$$L = kJV \ln \frac{1}{1-\theta},$$

where k — lift-drag ratio of the aircraft;

J — engine specific impulse;

V — speed of flight in m/sec;

\bar{G} — relative fuel weight.

At constant fuel consumption, engine thrust naturally decreases with decrease of η_z . However, at certain values of $\alpha > 1.0$ and not very low combustion efficiency, decrease of η_z as compared to its design value can be compensated by increase of fuel consumption.

On the basis of (1.37), total quantity of heat added to gas, will be

$$Q_1 = G_1 H_z \eta_z. \quad (1.38)$$

Quantity of heat added to 1 kg of gas:

$$q_1 = \frac{Q_1}{G_s + G_r} = \frac{G_r}{G_s + G_r} \cdot H_z \eta_z. \quad (1.39)$$

But fuel consumption is equal to

$$G_r = \frac{G_s}{\alpha L_0}, \quad (1.40)$$

where α — excess air ratio;

L_0 — stoichiometric coefficient — theoretically necessary quantity of air for full combustion of 1 kg of fuel.

Consequently, it is possible to write

$$q_1 = H_z \frac{\eta_z}{1 + \alpha L_0}. \quad (1.41)$$

To provide the given thrust it is required that for any values of η_z , magnitude of q_1 be constant. It follows from this (if we disregard the insignificant change of mass of combustion products during small change of α) that the magnitude of $\eta_z / (1 + \alpha L_0)$ must be constant. Compensation for incompleteness of combustion of fuel by increase of its flow rate is possible as long as $\alpha \approx 0.9-1.0$. With further decrease of α , temperature of gas, and consequently also engine thrust will decrease.

§ 6. Peculiarities of Thermodynamic Processes at High Temperatures*

At high speeds of flight of aircraft or use of high energy propellants, temperature in engine combustion chamber can be higher than 2000-2500°K. At such high temperatures, there starts to noticeably appear dissociation of combustion products. Since the dissociation reactions are accompanied by absorption of heat, then as a result gas temperature will be considerably lower than in the absence of dissociation.

*§§ 6 and 7 were written jointly with V. A. Chernov.

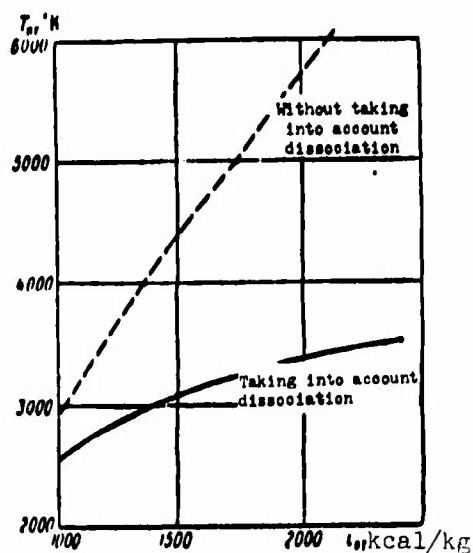


Fig. 1.12. Theoretical temperature of combustion products of kerosene in air both without taking into account, and taking into account dissociation ($\alpha = 1.1$; $p = \text{atm (abs.)}$).

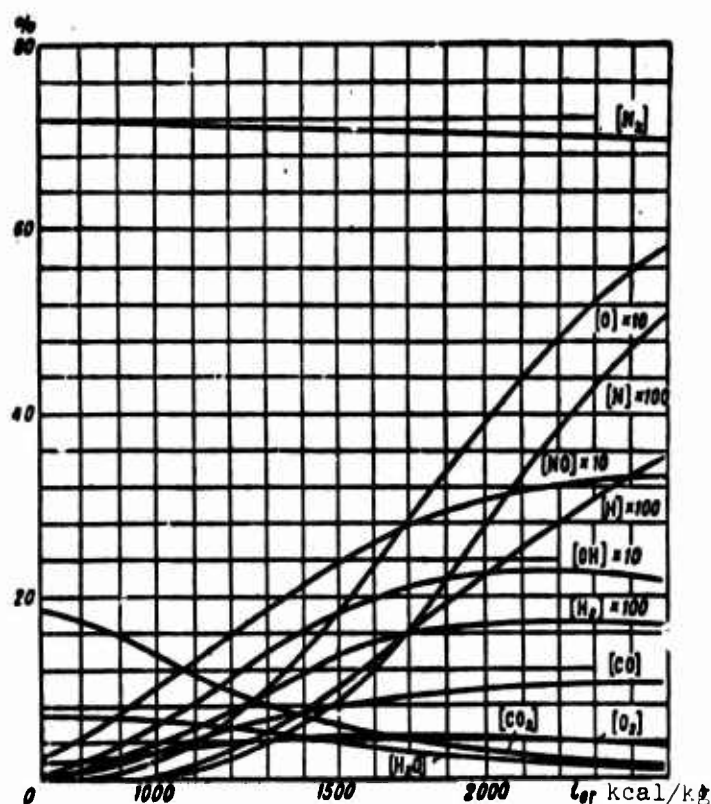


Fig. 1.13. Change of composition of combustion products of kerosene in air depending upon enthalpy of mixture ($\alpha = 1.1$; $p = 1.0 \text{ atm (abs.)}$).

In Figs. 1.12 and 1.13 there are given graphs of change of temperature of combustion products of kerosene in air at $\alpha = 1.1$ and weight fractions of components depending upon magnitude of enthalpy of the mixture i_{OT} . In Fig. 1.12 the dotted line illustrates the temperature change curve in the case of absence of dissociation. From the graphs it is clear that process of dissociation starts to noticeably show up approximately at $T = 2000^\circ\text{K}$. To a temperature of 2500°K the influence of dissociation is weak, and in certain approximate calculations it is possible to disregard it. At $T > 2500^\circ\text{K}$ in all calculations we should consider influence of dissociation on thermodynamic properties of components of combustion products.

Errors appearing when influence of dissociation reactions is disregarded can be estimated by examining Fig. 1.14. Curve a on this figure corresponds to process of isentropic compression of air to full deceleration in the absence of dissociation of the air components. Curve b corresponds to the same process, but taking into account influence of dissociation; curve c corresponds to the process of combustion of hydrocarbon fuel in "decelerated" air in the absence of dissociation of combustion products, and curve d — to the process of combustion taking into account dissociation.

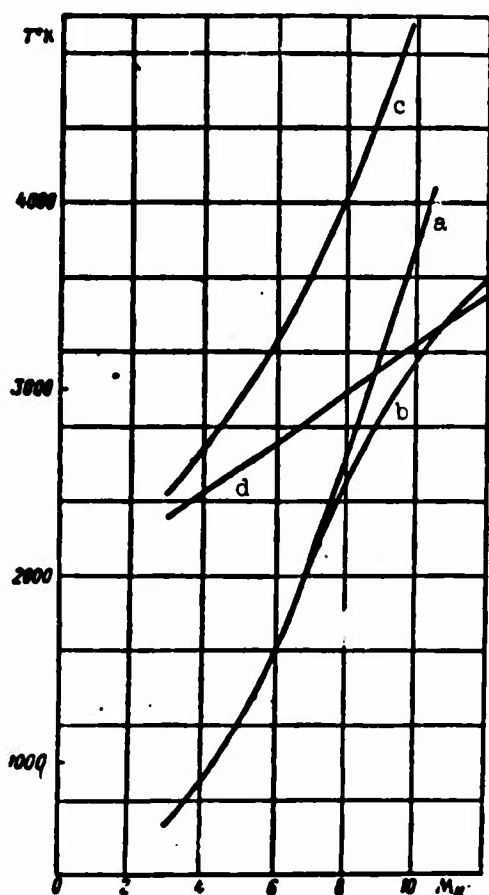


Fig. 1.14. Theoretical change of air temperature and combustion products of kerosene burned in air both taking into account and without taking into account dissociation, depending upon Mach number of flight ($\alpha = 1.1$; $p = 1.0$ atm (abs.)). a, b) air; c, d) combustion products.

Thus, curves b and d correspond to real processes. At very high speeds of flight, temperature of gases after "combustion" of fuel can be even less than initial temperature of air. This is explained by great expenditure of heat on dissociation.

At high temperatures, the value of temperature itself cannot completely characterize energy state of system. Really, in the last example temperature of combustion products turned out to be lower than temperature of air in which the fuel burned, but enthalpy, the total energy of the system, will of course be much higher than the enthalpy of the air. This energy can be realized in the supersonic nozzle of the engine, where during expansion of gas its temperature will decrease and there will occur a recombination reaction with liberation of heat. It is true that the quantity of returned energy will depend on degree of equilibrium of the process of recombination occurring in time, i.e., on to what degree the recombination reaction will have time to occur during flow of the gas in the nozzle.

To avoid impermissibly large errors during calculations of processes accompanying noticeable dissociation of components, it is impossible to use thermodynamic relationships for a gas of constant composition. For instance, Mayer's equation for reacting mixtures takes the form

$$c_p - c_v = A \left[R + T \left(\frac{\partial R}{\partial T} \right)_p \right].$$

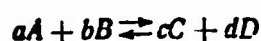
In this expression the term $T \left(\frac{\partial R}{\partial T} \right)_p$ under certain conditions becomes close in order of magnitude to R .

Chemical processes also influence adiabatic index k , which in the case when composition of the gases varies during the given process is determined by the ratio

$$k = \frac{1 + \left(\frac{\partial \ln R}{\partial \ln p} \right)_T}{1 - \frac{AR}{\left(\frac{\partial}{\partial T} \right)_T}}.$$

§ 7. Calculation of Composition of Combustion Products at High Temperatures

The rate of chemical reactions is measured by change of concentration of reactants per unit of time. On the basis of the law of mass action, the proof of which is given in courses in chemical thermodynamics, rate of reaction at every given moment is proportional to the product of concentrations of reactants at this given time. For reactions of the type



reaction rate is equal to

$$V = kc_A^a \cdot c_B^b,$$

where k — rate constant of the reaction;

c_A and c_B — are respectively concentrations of substances A and B.

They are expressed usually either by the number of moles or the number of molecules per unit volume (usually per 1 cm³).

For instance, for the reaction $H_2 + 0.5O_2 = H_2O$, rate of water formation

$$V_1 = k_1 c_{H_2} \cdot c_{O_2}^{1/2}.$$

All reactions are chemically reversible, i.e., they can go forward as well as in the opposite direction. For instance, for the reaction $H_2 + 0.5O_2 \rightleftharpoons H_2O$ the resultant rate of formation of water is

$$V = V_1 - V_2 = k_1 c_{H_2} \cdot c_{O_2}^{1/2} - k_2 c_{H_2O}.$$

Upon the expiration of a certain time, rate of formation of water V and rate of its decomposition V_2 will be equal to each other. Then there will exist chemical equilibrium of the system, which for the considered example gives

$$k_1 c_{H_2} \cdot c_{O_2}^{1/2} - k_2 c_{H_2O} = 0$$

or

$$k_{p, H_2O} = \frac{k_1}{k_2} = \frac{c_{H_2} c_{O_2}^{1/2}}{c_{H_2O}}. \quad (1.4)$$

The quantity k_{p, H_2O} is called the chemical equilibrium constant for formation of water from oxygen and hydrogen. Equilibrium constant are determined by

experimental means, are functions of only temperature and do not depend either on pressure at which the mixture is reacting or on the presence of other impurities.

According to the Avogadro's law, partial pressure of every component of gas mixture is proportional to the number of gram molecules of considered substance in the given volume. Consequently, equilibrium constant can be expressed in terms of partial pressures:

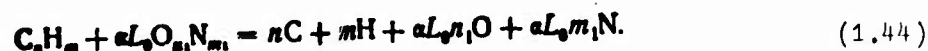
$$k'_{p, H_2O} = \frac{p_{H_2} \cdot p_{O_2}^{1/2}}{p_{H_2O}} \quad (1.43)$$

Let us note that the numerical values of the equilibrium constant expressed in terms of concentrations and in terms of partial pressures are different ($k_p' \neq k_p$). They turn out to be identical only in that case when concentrations are expressed in moles, and the number of moles before and after the reaction remains identical.

Depending upon temperature, equilibrium shifts in one direction or another. At a temperature below 1700°C, dissociation of H₂O, CO₂ and other combustion products is insignificantly small; the reaction of formation of these substances is practically irreversible; at a temperature over 4000°C combustion products are practically completely dissociated. Degree of dissociation increases with decrease of pressure.

Dissociated combustion products of hydrocarbon fuels in air contain CO₂, CO, H₂O, OH, H₂, H, O₂, O, N₂, NO, N. Analysis of the composition of dissociated combustion products is carried out by means of simultaneous solution of equations of equilibrium and material balance.

Equation of material balance during burning of hydrocarbons in air can be written in the following form:



This equation shows that the number of atoms of each of the four elements (C, H, O and N) is not changed during burning. Ratios of weight fractions of these elements will also remain constant:

$$\left. \begin{aligned} \frac{g_H}{g_C} &= \frac{r_H \cdot m}{r_C n} = a, \\ \frac{g_O}{g_C} &= \frac{r_O a L_0 n}{r_C n} = \delta, \\ \frac{g_N}{g_C} &= \frac{r_N a L_0 m_1}{r_C n} = b, \end{aligned} \right\} \quad (1.45)$$

where n — molecular weight of components.

On the other hand, ratios of weight fractions of elements can be expressed in terms of partial pressures of substances containing the given elements. Thus, carbon is contained in CO_2 and CO ; hydrogen — in H_2O , OH , H_2 , H ; oxygen — in CO_2 , CO , H_2O , OH , O_2 , O , NO ; nitrogen in N_2 , NO , N .

In one gram mole CO_2 contains 12 g of carbon; the same quantity of carbon is contained in one gram mole of CO . The total amount of carbon will be equal to

$$\frac{1}{1000} (12M_{\text{CO}_2} + 12M_{\text{CO}}) \text{ kg},$$

where M — number of moles of the given substance or combustion products. But according to Avogadro's law partial pressure of the given substance is proportional to the number of gram moles in this substance in the given volume. Then the last expression can be rewritten in the following form:

$$\frac{12}{1000} \frac{M_{\Sigma}}{P_{\Sigma}} (p_{\text{CO}_2} + p_{\text{CO}}) \text{ kg},$$

where M_{Σ} — number of gram moles of all substances composing combustion products;

P_{Σ} — total pressure in combustion products;

p_{CO_2} and p_{CO} — partial pressures of CO_2 and CO .

Analogously to this, the quantity of hydrogen in 1 kg of combustion products is equal to

$$\frac{1}{1000} \frac{M_{\Sigma}}{P_{\Sigma}} (2p_{\text{H}_2\text{O}} + 2p_{\text{H}_2} + p_{\text{H}} + p_{\text{OH}}) \text{ (kg)}.$$

Then equation (1.45) can be written in the following form:

$$\left. \begin{aligned} a &= \frac{g_{\text{H}}}{g_{\text{C}}} = \frac{P_{\text{H}}}{P_{\text{C}}} \frac{2p_{\text{H}_2\text{O}} + 2p_{\text{H}_2} + p_{\text{H}} + p_{\text{OH}}}{p_{\text{CO}_2} + p_{\text{CO}}}, \\ b &= \frac{g_{\text{O}}}{g_{\text{C}}} = \frac{P_{\text{O}}}{P_{\text{C}}} \frac{2p_{\text{CO}_2} + p_{\text{CO}} + p_{\text{H}_2\text{O}} + p_{\text{OH}} + 2p_{\text{O}_2} + p_{\text{O}} + p_{\text{NO}}}{p_{\text{CO}_2} + p_{\text{CO}}}, \\ c &= \frac{g_{\text{N}}}{g_{\text{C}}} = \frac{P_{\text{N}}}{P_{\text{C}}} \frac{2p_{\text{N}_2} + p_{\text{NO}} + p_{\text{N}}}{p_{\text{CO}_2} + p_{\text{CO}}}. \end{aligned} \right\} \quad (1.46)$$

The fourth will be equation

$$P_{\Sigma} = \sum_i^i P_i \quad (1.47)$$

which shows that the sum of all partial pressures is equal to the pressure in the chamber.

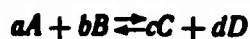
But in dissociated combustion products there can be contained eleven substances. The total number of equations should be equal to the number of unknowns. Therefore, we will write seven more equations of chemical equilibrium:

$$\left. \begin{aligned} k_p &= \frac{P_{O_2}^{1/2} \cdot P_{CO}}{P_{CO_2}}, \\ k_p &= \frac{P_H}{P_{H_2}^{1/2}}, \\ k_p &= \frac{P_O}{P_{O_2}^{1/2}}, \\ k_p &= \frac{P_N}{P_{N_2}^{1/2}}, \\ k_p &= \frac{P_{OH} \cdot P_{H_2}^{1/2}}{P_{H_2O}}, \\ k_p &= \frac{P_{H_2} \cdot P_{CO_2}}{P_{H_2O} \cdot P_{CO}}, \\ k_p &= \frac{P_{NO}}{P_{N_2}^{1/2} \cdot P_{O_2}^{1/2}} \end{aligned} \right\} \quad (1.48)$$

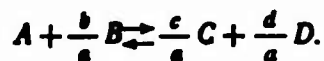
By solving this system of eleven equations and determining partial pressures of every component of the mixture, we find the weight and volume fractions of these components, and then by the same relationships as for undissociated gases we find thermodynamic parameters of the dissociated combustion products of $-u$, R , i , s , c_p , c_v , k .

There exist many methods of solution of this system of equations based on the method of successive approximations. Let us consider the most convenient method, proposed by Vanichev [2].

We will consider the chemical reaction equation



or



We will find the time derivative of concentration of the first substance $d[c_A]/dt$. Let us assume that with the appearance of substances in the right side, they are removed; i.e., the formation reaction flows irreversibly, and the reverse reaction does not occur. Then change of concentration of first substance A depends on number of collisions of its molecules with molecules of substance B per unit of time, which decreases with consumption of substances A and B. According to the law of mass action,

$$\frac{d[c_A]}{dt} = -k_1[c_A]_t \cdot [c_B]_t^{1/2}.$$

Under real conditions, along with the forward reaction of formation there also occurs the reverse reaction, which increases concentration of substances A and B. Thus, total rate of reaction will be

$$\frac{d[c_A]}{dt} = -k_1[c_A]_t \cdot [c_B]_t^{1/2} + k_2[c_C]_t^{1/2} \cdot [c_D]_t^{1/2}.$$

Expressing concentrations in terms of partial pressures, we will obtain

$$\frac{dp_1}{dt} = -k'_1 p_{1t} \cdot p_{2t}^{1/2} + k'_2 p_{3t}^{1/2} \cdot p_{4t}^{1/2}.$$

Replacing the derivative by the ratio of finite differences, we will obtain

$$\frac{p_{1(t+\Delta t)} - p_{1t}}{\Delta t} = -k'_1 p_{1t} \cdot p_{2t}^{1/2} + k'_2 p_{3t}^{1/2} \cdot p_{4t}^{1/2},$$

whence

$$p_{1(t+\Delta t)} = p_{1t} + k'_1 \Delta t \left[\frac{k'_2}{k'_1} p_{3t}^{1/2} \cdot p_{4t}^{1/2} - p_{1t} \cdot p_{2t}^{1/2} \right].$$

Inasmuch as the magnitude of Δt is arbitrarily chosen, we will replace $k'_1 \Delta t$ by an arbitrarily selected magnitude ξ . Then, taking into account (1.42) it is possible to represent system of equations (1.48) in the following form:

$$\left. \begin{aligned} p_{CO} &= p'_{CO} + \xi \left[k_p \frac{p_{CO_2}}{p_{O_2}^{1/2}} - p'_{CO} \right], \\ p_H &= p'_H + \xi [k_p p_{H_2}^{1/2} - p'_H], \\ p_O &= p'_O + \xi [k_p p_{O_2}^{1/2} - p'_O], \\ p_N &= p'_N + \xi [k_p p_{N_2}^{1/2} - p'_N], \\ p_{OH} &= p'_{OH} + \xi \left[k_p \frac{p_{H_2O}}{p_{H_2}^{1/2}} - p'_{OH} \right], \\ p_{H_2} &= p'_{H_2} + \xi \left[k_p \frac{p_{H_2O} p_{CO}}{p_{CO_2}} - p'_{H_2} \right], \\ p_{NO} &= p'_{NO} + \xi [k_p p_{N_2}^{1/2} p_{O_2}^{1/2} - p'_{NO}]. \end{aligned} \right\} \quad (1.49)$$

Usually there is taken the magnitude $\xi < 0.5$. Let us note that with increase of ξ , the necessary number of approximations decreases; at the same time this can lead to divergence of the equations. The obtained system of equations can be conveniently solved in the following way:

First approximation. Take partial pressures (usually zeroes) of substances expressed in terms of chemical equilibrium constants, i.e., p_{CO} , p_H , p_O , p_N , p_{OH} ,

p_{H_2} , p_{NO} . We put these values in equations (1.46) and (1.47) and solve them explicitly for the remaining partial pressures p_{CO_2} , p_{H_2O} , p_{O_2} , p_{N_2} . These four found values of partial pressures we put in equations (1.49), replace in these equations the partial pressures marked with primes (p'_{CO} , p'_H , etc.) by the initially given values (usually zeroes), and find new values of the seven partial pressures p_{CO} , p_H , p_O , etc.

Second approximation. The new found values of seven partial pressures we put in equations (1.46) and (1.47), find new values of p_{CO_2} , p_{H_2O} , p_{O_2} and p_{N_2} , put them in (1.49) and find new values of p_{CO} , p_H , p_{OH} , etc. Calculation is continued until results of the last two approximations differ by a magnitude less than the given one.

Thus, calculation of composition of dissociated combustion products is a very labor-consuming task. At present these calculations are conducted on high speed electronic computers. By the obtained data there are constructed diagrams for the given mixture ratio α and fuel combustion efficiency η_z , which are used during analysis of thermodynamic processes.

§ 8. LOSSES OF PRESSURE IN COMBUSTION CHAMBERS

Flow of air through the combustion chamber is accompanied by losses of energy and losses of total pressure of flow [Pitot losses]. These losses appear due to flow friction of the gas-air channel and due to heat addition to the moving gas.

Hydraulic losses and heat addition cause variation of parameters of the flow — pressure, density, velocity — along the length of the combustion chamber and a corresponding distribution of flow rates of air along its contours.

Hydraulic losses are composed of losses due to friction of air against walls of the combustion chamber and local losses — losses due to eddy formation, appearing during flow around the flame-holders, fuel manifold, precombustion chamber and other bodies installed in the chamber, and also from losses appearing during mixing of air coolant with combustion products during air-boundary cooling of walls of the combustion chamber.

FLOW FRICTION OF BLUFF BODIES (FLAME-HOLDERS)

Losses of pressure due to eddy formation appear mainly during flow around flame front devices — fuel manifold, precombustion chamber, flame-holders, mounts of these elements to walls of the chamber, etc. Drop of total pressure by the formula

$$\Delta p_0 = \xi \frac{\rho v^2}{2},$$

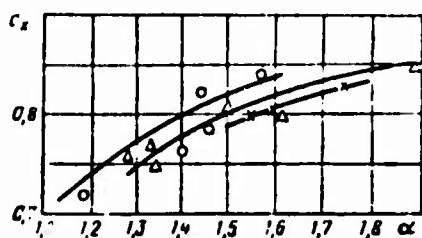


Fig. 1.15. Dependence of drag coefficient on α and Re for V-shaped flame-holder with vortex angle $\beta = 60^\circ$ in half-open flow. \circ - $Re = 6 \cdot 10^4$; Δ - $Re = 9 \cdot 10^4$; \times - $Re = 13 \cdot 10^4$.

where ξ - coefficient of local flow friction;

w - flow velocity to which coefficient of local friction is referred.

To the investigation of flow friction of bluff bodies in fluid flow are dedicated many theoretical and experimental works; however up to now this question has not been finally solved.

It is known [3] that during turbulent flow of a real liquid, drag coefficient of a bluff body c_x depends on its geometric form, the degree of obstruction

of the pipe by bluff bodies, relative location of bluff bodies to one another and to the wall of the pipe.

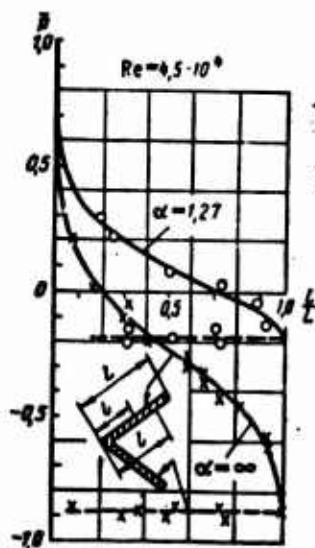
Under conditions of infinite or half-open flow (bounded by two walls), drag coefficient of a bluff body with combustion in the wake behind it considerably decreases as compared to flow without combustion and depends on air-fuel ratio α . Thus, according

to experimental data obtained in half-open isothermal flow at $Re = 5 \cdot 10^4$ to $11 \cdot 10^4$, drag coefficient of a V-shaped flame-holder with vertex angle $\beta = 60^\circ$ is equal to ~ 1.12 , and with combustion in the range $\alpha = 1.15$ to 2.0 is correspondingly lowered to 0.75 to 0.85 (Fig. 1.15), and thus decreases somewhat with increase of Reynolds number.

Decrease of drag of flame-holder during burning in its wake in an infinite or half-open flow is explained by the fact that due to heat emission there is increased pressure in the stern region, the flame-holder to be considerable degree loses the properties of "bluffness" and expenditures of energy of the flow on eddy formation decrease.

In Fig. 1.16 there is shown the pressure distribution of front and rear surfaces of a stabilizer placed in an isothermal flow, and during combustion. In this figure

Fig. 1.16. Change of dimensionless pressure $\bar{P} = (p - p_\infty)/q_\infty$ on front and rear surface of a flame-holder during combustion and without combustion in half-open flow.



along the axis of abscissas there is plotted the dimensionless length of the generatrix of the stabilizer

$$l = \frac{l}{L}.$$

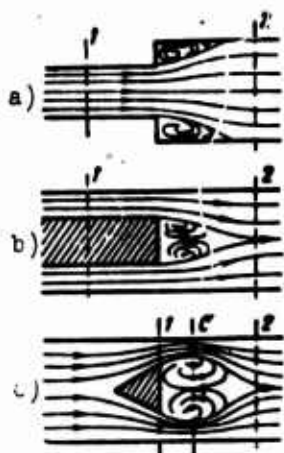


Fig. 1.17. Determination of flow friction coefficient of flame-holders.

and along the axis of ordinates - the dimensionless pressure

$$\bar{p} = \frac{p - p_{\infty}}{q_{\infty}},$$

where p and p_{∞} - static pressure on surface of a flame-holder at a given point l and in an undisturbed flow in kg/m^2 ;

q_{∞} - impact pressure of undisturbed flow in kg/m^2 .

In pipes, drag of bluff bodies during combustion and without combustion depends on degree of obstruction of the area of cross section of the pipe by these bodies $\bar{F} =$

$$= \frac{F_{\text{CT}}}{F_{\text{TP}}}. \text{ With increase of degree of obstruction of the pipe}$$

there is increased drag of the flame-holders in a cold flow, and, to still a higher degree, their drag during combustion. Thus drag during combustion can become equal to or even higher than drag in the cold flow. There are known experimental data, according to which drag coefficient of a flat disk $d = 47 \text{ mm}$, fixed in a pipe $d = 57 \text{ mm}$, during flow around it by a cold flow, is equal to ~ 1.5 , and during combustion ($\alpha = 1.7$) increases to 3.0 .

During flow in closed channels of uniform cross section, the relation between drag coefficient of the bluff body

$$c_x = \frac{2R}{\rho w^2 F_{\text{TP}}}, \quad (1.50)$$

where R - drag force in kg/m^2 , and the local flow friction coefficient

$$\xi = \frac{2\Delta p}{\rho w^2}$$

can be found from consideration of the momentum equation and Bernoulli's equation.

According to the momentum equation, the resultant of aerodynamic forces, acting on the bluff body (Fig. 1.17c) is

$$R = \Delta p F_{\text{TP}} - \rho_1 w_1 (w_2 - w_1) F_{\text{TP}}, \quad (1.51)$$

where $\Delta p = p_1 - p_2$ - drop of static pressures caused by local friction, in kg/m^2 ;

w_1 and w_2 - respectively average flow velocity in cross sections 1 and 2 - before and after the bluff body - in m/sec ;

ρ_1 - air density in cross section 1-1 in $\text{kg}\cdot\text{sec}^2/\text{m}^4$;

F_{TP} - area of transverse cross section of the pipe in m^2 .

According to the Bernoulli equation, for sections 1-1 and 2-2 it is possible to write

$$\Delta p = p_1 - p_2 = \Delta p_0 + \frac{\rho_2 w_2^2}{2} - \frac{\rho_1 w_1^2}{2}. \quad (1.52)$$

Placing in (1.51) the value of R from (1.50) and of Δp from (1.52), we obtain

$$c_x \frac{\rho_1 w_1^2}{2} \cdot \frac{F_{cv}}{F_{np}} = \Delta p_0 + \frac{\rho_2 w_2^2}{2} - \frac{\rho_1 w_1^2}{2} - \rho_1 w_1 (w_2 - w_1)$$

or after certain transformations with the use of the continuity equation

$$c_x \frac{F_{cv}}{F_{np}} = \frac{\Delta p_0}{\frac{\rho_1 w_1^2}{2}} + 1 - \frac{\rho_1}{\rho_2},$$

whence

$$\xi = c_x \bar{f}_{np} + 1 - \frac{\rho_1}{\rho_2}. \quad (1.53)$$

For an incompressible liquid ($\rho_1 = \rho_2$) we will have

$$\xi = c_x \bar{f}_{np}. \quad (1.54)$$

As Kuptsov showed, losses of total pressure during flow around flame-holders in a pipe can be considered as losses due to sudden expansion. During flow of an incompressible liquid in a channel with sudden expansion (Fig. 1.17a), losses of pressure are determined by the formula of Borda

$$\Delta p_0 = \frac{\rho (w_1 - w_2)^2}{2}. \quad (1.55)$$

It is obvious that the relationship will also be valid in the case of the flow shown in Fig. 1.17b. For this case F_1 is the area of the ring between walls of the pipe and the central body. It is possible to expect that such a relationship will also determine losses of pressure and during flow around a flame-holder fixed in the center of a pipe (Fig. 1.17c), but in formula (1.55) instead of velocity w_0 — in the narrowest section of the stream, which is located at a certain distance from the flame-holder. Magnitude of compression of the stream, which we will estimate by contraction coefficient of the stream

$$\alpha = \frac{F_c}{F_1},$$

basically depends on geometric form of the body in the flow. If the front part of the body ends in a section whose walls are parallel to the walls of the pipe, then the fluid flow is not subjected to additional compression and $\alpha = 1.0$. During flow around a flat obstacle (disk or plate fixed perpendicularly to the axis of the pipe), there occurs maximum compression of the stream and coefficient α has maximum value.

In work [3] it is shown that during flow through a hole in a diaphragm from one channel into another or into free space, the contraction coefficient of the stream is determined by the formula

$$\alpha = \frac{1}{1 + \sqrt{1 - \frac{F_1}{F_2}}} \quad (1.56)$$

where η — damping coefficient of the inlet depends on viscosity of the liquid, geometric form of the body, rounding of edges of the hole in the diaphragm, etc.

Thus, during flow around a flame-holder, expression (1.55) will be written in the following form:

$$\Delta p_0 = \frac{\rho (u_1 - u_2)^2}{2}.$$

Whence, referring loss factor to impact pressure in section 1-1 and disregarding change of density on section 1-2, we will have

$$\xi = \left(\frac{F_1}{F_2} \right)^2 \left(1 - \frac{u_2}{u_1} \right)^2. \quad (1.57)$$

For an incompressible liquid, in (1.57) the velocity ratio can be replaced by the area ratio; then

$$\xi = \left(\frac{F_1}{F_2} - \frac{F_1}{F_2} \right)^2.$$

If we take into account (1.56), we can write the last expression in the following form:

$$\xi = \left(\sqrt{1 - \frac{F_1}{F_2}} + \frac{F_1}{F_2} \right)^2$$

or finally

$$\xi = \left(\sqrt{1 - \frac{F_1}{F_2}} - \frac{F_1}{F_2} \right)^2. \quad (1.58)$$

If the drag coefficient is referred not to impact pressure in section 1-1, but to impact pressure of the incident flow, then for incompressible liquid we will have

$$\xi = \left(\sqrt{1 - \frac{F_1}{F_2}} - \frac{F_1}{F_2} \right)^2 \frac{1}{(1 - \frac{F_1}{F_2})^2}. \quad (1.59)$$

For V-shaped and conical flame-holders located in an air flow, damping coefficient of the inlet depends only on the vertex angle of these flame-holders β° . Experimental dependences $\eta = f(\beta)$ are shown in Fig. 1.18.

Relationships (1.58) and (1.59) may also be used for calculation of flow friction of an array of flame-holders located in one plane or echeloned along the length

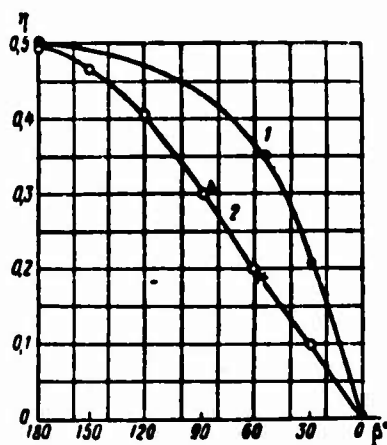


Fig. 1.18. Damping coefficient of inlet $\eta = f(\beta)$ for flame-holders: 1 - conical, 2 - V-shaped.

of the combustion chamber. In the first case T_{Tp} is determined by the total area of all flame-holders, but ξ is calculated by (1.59). With echeloned placement of flame-holders in the pipe, if the distance between them (along axis of pipe) is equal to or larger than length of the zone of counter currents (with cold flows the length of the zone of counter currents is equal to 1.5-2.0 heights of the flame-holders), drag coefficient of the array will be equal to the sum of drag coefficients of each flame-holder. If axial distance between flame-holders is less than length of zone of counter currents, drag of the array will be increased.

As was shown, flow friction of stabilizers during combustion can be smaller than, equal to or larger than friction flow during cold flow due to change of the contraction coefficient of the stream, which depends basically on degree of blockage of the pipe and, to a smaller degree on relative increase of the temperature of the flow $\tau = T_{Or}/T_{Cx}$. Functional dependence of ξ on T_{Tp} and τ at present has not been established. However, experience shows that at $T_{Tp} \leq 0.5$, coefficient of flow friction of flame-holders during cold flow and during combustion remains practically the same.

Flow Friction of Fuel Manifold and Mounting Elements Flame Front Devices to Walls of Combustion Chamber

In combustion chambers of ramjet engines and afterburners of turbojet engines, fuel manifold is usually made from pipes of round or elliptic shape, which in the form of rings or radial branches are located in the same plane or echeloned along the length of the combustion chamber at certain distances ahead of the flame-holders. Precombustion chamber, flame-holders and fuel manifold are fastened to walls of combustion chamber with help of braces or pylons.


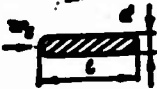
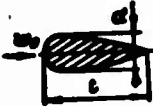


It is possible to calculate losses of pressure on these elements by means of the formula

$$\Delta p_0 = \xi \frac{\rho v^2}{2}.$$

Resistance of such bodies during external flowing around them is usually estimated by the drag coefficient c_x . The relation between ξ and c_x is established by

relationships (1.53) or (1.54). Values of c_x for certain bodies are given in Table 1.2 (plane-parallel flow) [4].

Table 1.2. Values of Drag Coefficients for Different Bodies

Type	Diagram	Re	c_x	Parameters
Circular cylinder		$> 5 \cdot 10^4$	0,3—0,4	—
Wire		$< 5 \cdot 10^4$	1,2	
Plate with edges rounded along the arc of a circle.		$5 \cdot 10^3$ $2 \cdot 10^4$	0,78 0,65	$\frac{d}{l} = 0,0333$
Profiles of different thickness		$1 \cdot 10^4$	0,193	$\frac{d}{l} = 0,053$
			0,086	$\frac{d}{l} = 0,125$
			0,080	$\frac{d}{l} = 0,197$
Profiled wire, pipe, and so forth		$3 \cdot 10^3 + 10^4$	0,3—0,4	
Profiled steel pipe (drop-shaped profile).		$5 \cdot 10^4$	0,2	$\frac{d}{l} = 0,5$
			0,1	$\frac{d}{l} = 0,33$

Taking into account (1.54), it is possible to estimate hydraulic losses on fuel manifold, mounting braces, and so forth, by the formula

$$\Delta p_0 = c_x \bar{l} \eta \frac{\rho v^2}{2}.$$

Total Pressure Losses in Combustion Chamber

Total coefficient of flow friction of combustion chamber

$$\xi_z = \frac{\sum \Delta p_{0, \text{расп}}}{\frac{\rho_1 v_1^2}{2}}.$$

where $\Sigma \Delta p_{\text{гидр}}$ - sum of all hydraulic losses on friction of gas against walls and local losses on flame-holders, precombustion chamber, fuel manifold, etc.; $\frac{\rho_1 w_1^2}{2}$ - average impact pressure of flow of air at entrance to combustion chamber.

The "specific weights" of different components in the total sum of hydraulic losses are unequal.

The main fraction of the total hydraulic losses is composed of losses on the flame-holders. Friction losses, local losses on the fuel manifold and structural elements are so insignificant that in engineering calculations it is possible to disregard them. However, we should emphasize that losses due to friction of air against the walls in an annular channel, in spite of their relatively small magnitude in the total balance of losses, very significantly affect the distribution of flow rates of air along the contours of the combustion chambers when they are referred to the entire flow rate of air through the chamber, and therefore have to be carefully determined.

Pitot losses in the combustion chamber are expressed by the pressure coefficient $\sigma_{\text{к.с.}}$. Pitot losses caused by flow friction of the combustion chamber are determined by the relationship

$$\sigma_{\text{к.с. рас}} = 1 - \frac{p_{\text{к.с.}}}{p_{\text{к.с.}}}$$

In § 2, Chapter I, it was shown that heat addition to a moving gas is also accompanied by Pitot losses, which are increased with increase of flow velocity and degree of preheating of the gas. These losses are determined by the formula

$$\sigma_{\text{к.с. теп}} = \frac{p_r}{p_k} \left(\frac{1 - \frac{k-1}{k+1} \lambda_r^2}{1 - \frac{k-1}{k+1} \lambda_k^2} \right)^{\frac{k}{k-1}}$$

Overall hydraulic and thermal losses of total pressure can be evaluated by the total pressure coefficient

$$\sigma_{\text{к.с. в}} = \sigma_{\text{к.с. рас}} \cdot \sigma_{\text{к.с. теп}}$$

LITERATURE

1. G. N. Abramovich. Applied gas dynamics. State Press for Technical and Theoretical Literature, 1953.
2. A. V. Kvasnikov. Theory of liquid-propellant rocket engines, Part I. Sudpromgiz, 1959.
3. I. Ye. Idel'chik. Flow friction during entrance of a flow into channels and flow through holes. "Industrial Aerodynamics," Oborongiz, 1954.
4. S. S. Kutateladze and V. M. Borishanskiy. Reference book on heat transfer. State power engineering publishing house, 1958.

CHAPTER II

CARBURETION

§ 1. GENERAL CHARACTERISTICS OF CARBURETION PROCESSES

Carburetion is the primary preparatory process in combustion chambers in air-breathing jet engines (БРД). As a result of this process liquid and vapor fuel are distributed over a given volume of the chamber in definite concentrations, which are able to support the chemical reaction of burning. Range of stable operation of the chamber and rate of combustion, as well as other factors (temperature of the medium, turbulence in the flow and others), depend on the quality of the mixture on local air-fuel ratios, relationship between vapor and liquid phase, dimensions and velocity of the drops, etc. Atomization by injectors is the most wide-spread method of introduction of fuel into the chamber. Along with swirl injectors, which give a comparatively wide cone of fuel, there are successfully applied direct-spray atomizers, the axis of which is set at a certain angle to the flow.

Carburetion represents a complicated complex of separate elementary processes interacting with each other. Let us trace the sequence of these processes in the jet of a single atomizer.

Fuel in the form of cylindrical stream or the sheet of a swirl injector enters the flow passing through the chamber. Usually at a small distance from the place of injection (0.5-10 mm) disintegration of the stream is completed. From this moment, drops start to move along definite trajectories as a system of separate material particles. Simultaneously with entrainment of drops by the flow, they are heated by the heat of the surrounding medium (or are cooled, for instance, for heated fuel) and are vaporized.

The system of moving particles determines the profile of concentrations or

specific flows of liquid fuel, and vapor mixed with air creates a distribution of concentrations of gaseous fuel mixture. Vaporized drops upon approach to the flame-holders partially settle on their surfaces, and partially penetrate into the zone of burning.

Experience shows that a stable and intense process of burning in the chamber of an air-breathing jet engine must be organized for a mixture which is close to homogeneous (with small contents or complete absence of liquid phase), as well as for a mixture proceeding into the flame zone with a large percentage of vaporized fuel (30 to 60%). In the latter case there appear local regions of fuel concentrations, and drops in the flame are quickly vaporized, supporting the process of combustion. When speeds of the drops are low and the level of turbulence of the flow is low, sometimes diffusion burning of liquid particles or burning of vapor in the stern zone after the drop is possible. In the flame front and behind it, liquid particles, already losing their relative speed, again fall into the zone of high relative speeds (flow of hot gases is accelerated with combustion of the mixture) and can be subjected to a further process of splitting.

The method of calculation proposed in the present work permits rational choice of type and location of injectors in the chamber, type of fuel and its initial temperature and also allows estimation of necessary length of the section of preparation of the mixture. Certain results on analysis of elementary processes (as already has been said) can appear useful in other regions of technology (boiler and gas turbine installations, devices for cooling of hot flows of gas, apparatus of the chemical industry and others).

§ 2. DISINTEGRATION OF A JET OF LIQUID, SPLITTING UP AND DEFORMATION OF DROPS IN A FLOW OF AIR

The task of atomization is distribution of fuel by a certain method in the volume of a combustion chamber and increase of the surface area of liquid for the purpose of intensification of vaporization. The process of disintegration of liquid streams is very complicated. In spite of numerous works, there still is absent a theory of atomization useful for determination of the spectrum of drops in the combustion chamber of an air-breathing jet engine. However, observation and theoretical analysis permit representation of this phenomenon in broad terms. Disintegration of a stream in its initial phase occurs due to instability of motion of the liquid due to the influence of small perturbations. As their source serves

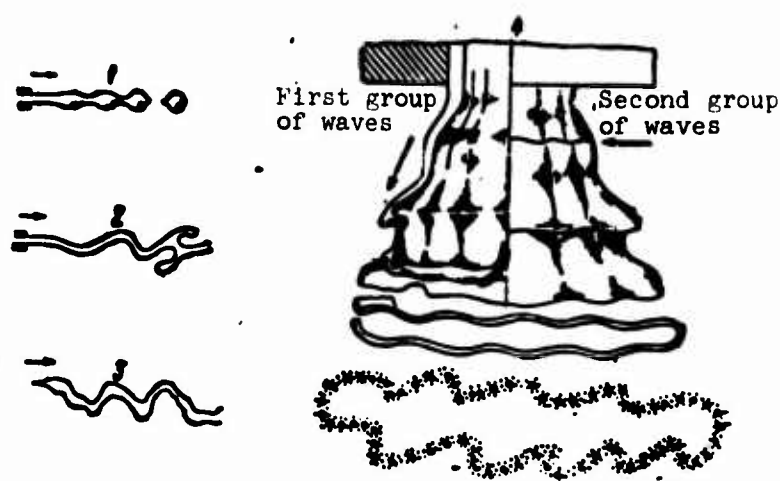


Fig. 2.1. Diagram of disintegration during outflow of a liquid jet. 1 - development of symmetric perturbations; 2 - development of antisymmetric perturbations; 3 - cylindrical jet, superposition of symmetric and antisymmetric perturbations; antisymmetric perturbations increase faster, $\Delta p = 7 \text{ atm (abs.)}$; 4 - liquid sheet (long-wave perturbations).

roughness of the nozzle surface, deviation of the outlet contour from a perfect circle, vibrations, turbulent pulsation in the liquid and environment, etc.

Amplitudes of waves of small oscillations appearing in the liquid rapidly increase, causing considerable deflection of flow lines of perturbed motion from initial flow lines. This causes sharp change of the configuration of the stream and disintegration of it into separate parts. The initial phase of the process has certain features in common with the phenomenon of the arising of turbulent flow from laminar flow. Intermediate formations and drops obtained after disintegration can be subjected to further disintegration and splitting.

For explanation of the mechanism of the process of atomization, we will at first consider the case of a cylindrical jet.

For the first time the problem of disintegration of a motionless infinitely extended liquid cylinder without the influence of an external medium was solved by Rayleigh in 1878 [1]. Let us give the basic physical premises of this solution:

1) wave of increasing amplitude constitutes a future drop, i.e., the developing wave is separated from the stream in the form of a particle (Fig. 2.1); thus, the order of magnitude of the drop is determined by the wavelength of the unstable oscillation;

2) of all possible waves of perturbations superimposed on the stream, there is developed only one, the rate of increase of perturbations of which has a maximum

(maximum of increment of increase). Such a wave of length λ_{OPT} is called "optimum;"

3) during solution of the problem (by the method of small perturbations), the optimum wave λ_{OPT} is in the linear region corresponding to the initial moment of motion, when amplitudes of oscillations are still small as compared to diameter of the stream. Further, it is assumed that in the nonlinear region, where developing amplitudes of oscillations no longer can be considered to be small, length of the optimum wave is retained. This assumption sometimes is called the Rayleigh hypothesis. It is used in hydrodynamics during solution of analogous problems of stability.

Rayleigh found that long-wave oscillations $\lambda \geq 2\pi a_0$ (a_0 - radius of the stream) are unstable, and $\lambda_{\text{OPT}} = 4.508 \cdot 2a_0$.

Results of further theoretical analysis [2] and investigation with the help of spark photography showed that the form of development of instability is changed with increase of outflow velocity relative to the surrounding medium.




Fig. 2.2. Form of surface of stream near the nozzle of a swirl injector. Water. $\Delta p = 3$ atm (gage).

Symmetric perturbations 1 (Fig. 2.1) are gradually replaced by antisymmetric perturbations 2 (deformations of stream axis). Then there appears an intermediate regime of flow 3, when there simultaneously exist both types of waves (there are developed more complicated forms, helically symmetric, tangential, etc.). Subsequently there occurs the atomization regime, in which perturbations of shorter and shorter waves become unstable and start to increase, their crests break off from the liquid surface in the form of a great number of tiny particles.

Thus there is created a whole spectrum of drops of different fineness. Optimum wavelength of oscillations characterizing the most probable dimension of drops in the spectrum shifts to the region of small waves (fineness of drops increases with increase of outflow velocity). Let us now turn to disintegration of the sheet of liquid ensuing for a swirl injector.* It is known that the boundaries of the liquid sheet after leaving the nozzle of the injector (Fig. 2.2) are close to the surfaces of hyperboloids of one sheet. In approximate consideration, they can be considered conical; their vertex angle is close to the angle of atomization (spray angle).

*Here there is not considered the mathematical solution of the problem of disintegration. It, as is known, consists of application of the method of small perturbations to hydrodynamic equations of motion of a stream or sheet (for instance, the Euler equation) and boundary conditions on the liquid - gas boundary (taking into account surface tension).

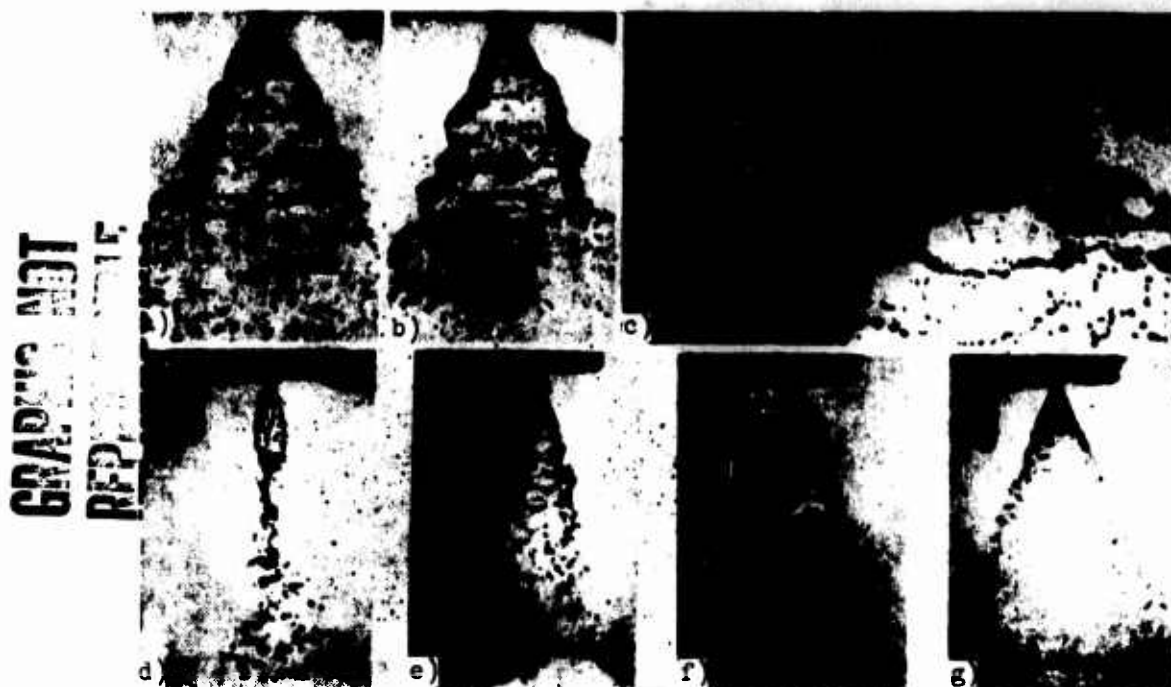


Fig. 2.3. Outflow from swirl injector (spark photographs). Water. a) $\Delta p = 2.8$ atm (gage); b) $\Delta p = 3.0$ atm (gage); c) $\Delta p = 10$ atm (gage) $\times 2$, $d_c = 3$ mm; d) $\Delta p = 1$ atm (gage); e) $\Delta p = 3$ atm (gage); f) $\Delta p = 5$ atm (gage); g) $\Delta p = 30$ atm (gage), $d_c = 0.83$ mm.

Numerous spark photographs show that there always exists a certain small initial section of nondisintegrated and little perturbed stream. With outflow, on the sheet there are developed waves of perturbations whose amplitudes rapidly increase (Fig. 2.3).

On the sheet, in general, it is possible to reveal two groups of waves (see Fig. 2.1). Contours of crests of the first group, travelling downstream, are seen on the external boundary of the stream. These waves tend to divide the sheet into a system of rings, as if strung on the axis of the injector. The second group of waves goes in the tangential direction, i.e., transverse motion of the stream (perpendicular to the first group); waves tend to divide the sheet into a sheet of streams diverging in a fan-like manner from the center of the nozzle. The tendency to formation of waves of both groups can be seen, for instance, in Fig. 2.3c; here there predominates the annular form of disintegration, i.e., rate of increase of amplitude of waves of the first group exceeds the rate of growth of the second.

In the place of disintegration of the sheet (there are excluded smallest feed pressures, at which the sheet after outflow is again closed, the so-called "bubble" regime - Fig. 2.3d), there are usually discovered liquid rings with a wavy outline,

surrounding the axis of the injector. Consequently, ring constitutes a separated crest of an annular wave of an antisymmetric perturbation (see Fig. 2.1). As it is known, a liquid ring, similarly to a liquid cylinder is an unstable form and is again broken up into drops.

With increase of relative outflow velocity (Fig. 2.3d and g), the wavelength of unstable perturbation (analogously to what was said for the cylindrical stream) decreases. This corresponds to decrease of thickness of the liquid ring and, consequently, of dimensions of the obtained drops.*

Finally, at sufficiently high speed, there occurs the atomization regime; from the surface of the stream break off crests of the smallest waves in the form of a swarm of drops, before the ring has time to be completely formed (Fig. 2.3g). This is especially characteristic during atomization in a flow of air. As already has been said, drops can then be formed during disintegration split up as a result of influence of the surrounding flow.

Let us consider separately the process of splitting up of an isolated drop. On the surface of the liquid particle with the flow passing around it, there is created a distribution of pressures (close to the distribution on a sphere) which deform the drop. For a definite relationship between parameters, external forces overcome the force of surface tension, causing splitting up of the drop. The process of disintegration of drops has been studied by a number of the authors. Experimentally there was established a simple criterial relationship [3], which determines the range of regimes corresponding to splitting up. It is valid for comparatively large drops ($a = 1.5$ to 2 mm) of different liquids (mercury, water, alcohol) in a flow of gas:

$$\frac{\rho_r w^2}{\sigma} = \text{const} = D, \quad (2.1)$$

where a and σ — diameter and coefficient of surface tension of the drop;

ρ_r — density of surrounding gas;

w — flow rate.

Parameter D is called the deformation criterion, splitting criterion or Weber number and constitutes the ratio of quantities proportional to the aerodynamic

*The considered scheme is, of course, ideal. In reality the sheet of the still incompletely separated ring are broken at the "weak" point, and there are frequently observed segments of distorted liquid filaments.

pressure of flow on the drop and pressure of surface tension.

Experiment has shown that at $D < 10.7$, the drop is deformed, but still does not disintegrate in the flow; at $D = 10.7$ there is attained the power limit of splitting and the drop is split (of the total number of particles 10-20% decay). With increase of D in the interval $10.7 \leq D < 14$, the drop divides into 3, 4, 5, etc., small drops, and the percentage of split-up drops increases. For D close to or equal to 14, there is attained the upper limit of splitting, 100% of the drops are split into a great number of small particles (regime of atomization of the drop). The formed spectrum of drops will be smaller, the larger the magnitude of D . The regime of splitting is maintained at all $D > 14$.

In the literature sometimes there are also given other values of the experimental constant D which are close in order of magnitude to the above-indicated values.

With cinematographic study of the process of disintegration of drops in a flow (with determination of the speed of entrainment of the drop), there is obtained a minimum value of $D \approx 9$. The physical cause of disintegration of the drop is that, its deformation attains a so-called critical phase [4], when the shape of the drop sharply changes and becomes unstable relative to small perturbations. A spherical drop under the action of pressures on its surface is turned into a body close to an ellipsoid (with major axis perpendicular to the flow), which is more and more flattened. At a definite critical ratio of semiaxis, the ellipsoid starts to be punched through in its center and rapidly becomes a liquid ring, which is, as it is known, an unstable form, which disintegrates into drops.

In Fig. 2.4 there are given consecutive phases of deformation of a drop, formation of the ring, and its disintegration. Thus, $D = D_{kp} = 10.7$; 14 corresponds to values of the

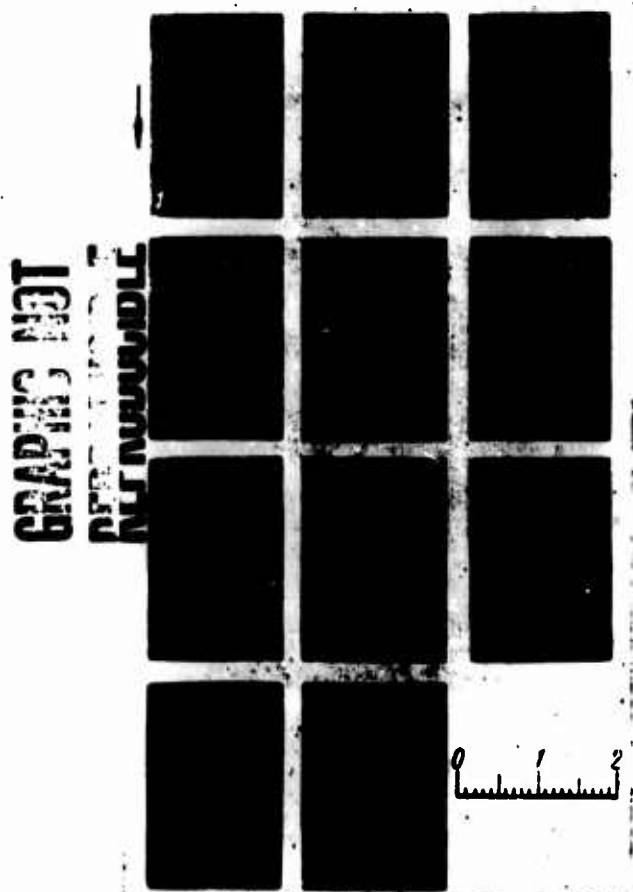


Fig. 2.4. Consecutive phases of destruction of a drop [28]. 1-11 - phases; the arrow indicates direction of flow.

critical phase of deformation at the lower and upper limits of stability.

When the drop falls into a flow, aerodynamic forces deform and simultaneously entrain it; relative speed and parameter D thus decrease. If time of achievement of the critical phase of deformation is less than the time of its entrainment to level D_{kp} , then there will occur splitting. If the time of achievement of critical phase is longer than the time of entrainment of the drop to level D_{kp} , deformation, after attaining a certain maximum, will start to gradually decrease and the drop will again, as relative speed decreases, near the shape of a sphere. Time of achievement of critical phase can be approximately estimated by the formula

$$\tau_{kp} \approx 1.65 \frac{a}{u_0} \sqrt{\frac{\gamma_{\pi}}{\gamma_r}}, \quad (2.2)$$

which is obtained on the assumption of small change of relative speed of the drop; γ_{π} ; γ_r are specific gravities of liquid and gas (u_0 - initial relative velocity of the drop).

Let us consider characteristics of splitting of a drop entrained in a gas flow [4]. We will determine speed of the uniform flow w around the drop, which does not have an initial velocity, and deforms it up to the phase of disintegration; if the drop possesses initial velocity V_0 along the flow, then it is necessary to determine the initial relative velocity $u_0 = (\bar{w} = V_0)$.

During flow around the drop drag coefficient c_x and its middle section f change due to deformation. We will replace these variable parameters by unknown average constants \bar{c} ; \bar{f} for simplification of the problem:

$$f = \frac{\pi a_{cp}^2}{4},$$

where a_{cp} - average middle diameter of deformed drop.

The equation of the motion of center of mass of the drop projected on the flow axis has the form

$$m \frac{dV}{dt} = \frac{\rho_r a^3}{2} \bar{c} \bar{f} \quad (2.3)$$

or

$$\rho_{\pi} \frac{\pi a^3}{6} \frac{dV}{dt} = \rho_r \frac{(w-V)^2}{2} \bar{c} e \frac{\pi a^3}{4},$$

where $e = \frac{\bar{f}}{\bar{f}} = \frac{a_{cp}^2}{a^2}$ - can be called the center section coefficient of the drop;

u - relative velocity.

Finally the equation of motion will be written in the form

$$\frac{dV}{dt} = \pi(w - V)^2, \quad (2.4)$$

$$\pi = \frac{3}{4} \frac{\bar{\sigma}}{a} \frac{R}{R_0}. \quad (2.5)$$

After integration of equation (2.4) for boundary conditions $\tau = 0$; $V = 0$ and $n = \text{const}$, we will obtain

$$V = \frac{\pi w^2}{\pi w + 1}. \quad (2.6)$$

We will compose an approximate expression for average rate of deformation of the drop. The drop in its critical phase of deformation takes a certain fully definite form, which depends on the diameter of the initial spherical drop.

Let us assume that γ is the displacement of some characteristic point of the surface of the deformed drop in fractions of its initial radius in the system of coordinates connected with the center of mass of the drop. As such a characteristic point it is possible to take, for instance, the stagnation point of the drop in the flow. If τ_1 — time from beginning motion of drop in the flow to the critical phase, then average rate of deformation will be

$$V_{\text{av}} = \frac{\gamma^2}{2\tau_1}, \quad (2.7)$$

where the unknown quantity γ lies within the interval

$$0 < \gamma < 1. \quad (2.8)$$

In this state the drop acquires the form of a body which is unstable with respect to small perturbations, as a result of development of which it disintegrates.

Let us write the system of equations for the critical phase of deformation:

$$\left. \begin{aligned} \frac{R^2 \sigma}{\sigma} &= D, * \\ w - u &= \frac{\pi_1 w^2}{\pi_1 w + 1}, \\ V_{\text{av}} &= \frac{\gamma^2}{2\tau_1}, \end{aligned} \right\} \quad (2.9)$$

where u — relative flow velocity in the critical stage of deformation. Eliminating from system (2.9) quantities τ_1 and u , we will obtain the following dependence for the unknown parameter:

*We assume that the particular relationship (2.1) turns out to be universal for the critical stage of deformation of any drop. In the case of large drops $u \approx w$.

$$w = u_0 = \frac{\sqrt{\frac{D_0}{\rho_r}}}{\sqrt{a} - \frac{3}{8} \sqrt{D} \frac{\rho_r}{\rho_m} \sqrt{\frac{c}{\rho_r} \frac{\sigma \gamma}{V_{\text{def}}}}} \quad (2.10)$$

In the formula there is contained the complex of unknown quantities $\bar{c} \bar{e} \bar{\gamma} / V_{\text{def}}$, which are difficult to determine within the framework of elementary theory.

In work [4] there is given a description of the method and results of experiments in determination of regimes of splitting up of quite small drops entrained in a flow of air. Comparison of expression (2.10) with the empirical curve $w = \varphi(a)$, given in work [4] shows that the unknown complex of quantities can be found and taken to be approximately constant for a given kind of liquid within quite a wide range of values of diameters a , $250 \leq a \leq 2500 \mu$. Consequently,

$$\frac{3}{8} \sqrt{D} \frac{\rho_r}{\rho_m} \sqrt{\frac{c}{\rho_r} \frac{\sigma \gamma}{V_{\text{def}}}} = \text{const.} \quad (2.11)$$

The obtained constant has two values for regimes of splitting and atomization. Let us designate the constant in expression (2.11) by $\sqrt{a_{\text{min}}}$; then as $a \rightarrow a_{\text{min}}$ $w \rightarrow \infty$. Thus, for every liquid there exists a particle of such small diameter a_{min} that a drop of equal or smaller dimension no longer can be split-up by any gas flow. It is natural that determination of a_{min} will be correct only insofar as formula (2.11) is valid for the entire region of small values of diameters of the drops. This means that the smaller the diameter of a drop landing in the flow, the greater its acceleration and the less its deformation under the influence of the flow. It is obvious that at $a \leq a_{\text{min}}$ the particle will be entrained in the flow before the critical phase of deformation can be attained. In this case, the time in which the drop entrained in the flow will lose its relative velocity will become less than the time passing before the phase of deformation.* Equation (2.10) in dimensionless parameters will take the form

$$\frac{\rho_r u_0}{c} = \frac{D}{\left(1 - \sqrt{\frac{a_{\text{min}}}{a}}\right)^2} \quad (2.12)$$

where $D = 10.7$ - at the lower limit of stability;

$D = 14$ - at the upper limit of stability.

*The assumption about the existence of a limiting small value of diameter of the drop a_{min} may, of course, be incorrect for the case of motion of a drop in a flow which is variable in velocity (for instance, in accelerated flows).



Fig. 2.5. Splitting up of a flow of air. Mercury, $a = 3.17$ mm. a) splitting is absent, $w = 35$ m/sec; b) regime of splitting, $w = 37$ m/sec; c) regime is of atomization, $w = 40$ m/sec; d) formation of lift, $w = 60$ m/sec.

At $a \approx 1.5-2$ mm, the denominator in the right side of the equation in practice is close to unity; therefore, we obtain a particular form of the relationship — formula (2.1), which is valid for large drops. For instance, for drops of alcohol in a flow of air $a_{\min} = 59; 10^4 \mu$ (respectively regimes of splitting and atomization). The quantity a_{\min} within itself does not determine minimum diameters in atomization spectra of liquids. In the process of splitting of a drop, besides the main secondary drops, there are formed very small particles — this is the result of disintegration of the liquid film appearing during destruction of the initial drop. Particles into which the drop is split-up in regimes lying above the upper boundary of stability (at $D > 14$) may also be less than a_{\min} .

In Fig. 2.5 there is shown disintegration of drops of mercury introduced into a flow of air. Photography was conducted in a darkened room with objective lens open and side illumination. A beam of light from the illuminator, reflected by the drop, passed through the objective and traced the trajectory of motion on a photographic plate, giving an image of the point of disintegration.*

For large drops, 1.5 to 3 mm, the velocity corresponding to critical phase and entering into criterion D, is close to the initial velocity of the flowing gas w , since deformation attains critical phase before the drop starts to be noticeably entrained by the flow. During investigation of splitting of the smaller particles with which it is necessary to deal in straight-through-flow combustion chambers, it is necessary to consider the process of entrainment of a drop by a flow (see formula 2.12).

In Fig. 2.6 there are compared maximum diameters of drops in atomization jets

*The unstable form of the drop appears a little before its disintegration is recorded on the photograph. By this moment, the drop is already carried slightly further along by the flow.

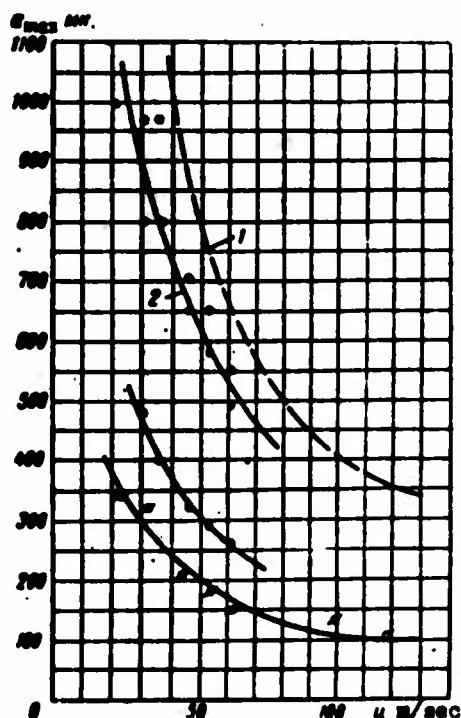


Fig. 2.6. Comparison of limiting diameters of drops with their maximum diameters in the atomization spectra. 1 - upper limit of stability; 2 - water, $\sigma - \epsilon = 0.072 \text{ mm}$, $\circ - \epsilon = 0.150 \text{ mm}$, $\bullet - \epsilon = 0.22 \text{ to } 0.25 \text{ mm}$.

of the injectors with different thickness of sheet ϵ with limiting diameters of drops according to the theory of splitting at $D = 14$ (taking into account entrainment of the drops). The graphs shows that limiting dimensions of drops noticeably exceed a_{\max} in spectra of injectors with comparatively low flow rate.

In the monograph [5], Longwell giving results of experiments of Lane, makes the assumption that a dependence of type (2.1) is valid within a wide range of small diameters of drops. On this basis there are estimated dimensions of small particles of hydrocarbon fuel, which retain their stability at flow velocities of the order of 60 m/sec.

In light of what has been said about the interaction of processes of entrainment and deformation of small drops [see formula (2.28)], it is clear that results of estimates of Longwell cannot be considered to be sufficiently well founded.

The entire process of deformation and motion of drops at $D = 10.7$ occurs in the following manner (see Figs. 2.28 and 2.29): the initial spherical drop is maximally deformed in a very short interval, corresponding to AC (as compared to the total time of its stay in the chamber):* This state depends on the initial value of the criterion $D_0 = \rho_r a_0 u_0^2 / \sigma$ and conditions of entrainment of the drop. Then there occurs slower decrease of deformation of the drop with its entrainment by the flow.

The given process can be considered as a quasi-static process, in which the drag coefficient of the deformed drop c_D and its middle F_D are simply determined by current values of the diminishing quantity D .

A more detailed description of motion of the drop during variable deformation will be given below. The influence of deformation of the drop on increase of its center section and drag coefficient should be considered subsequently introduction of the special function $\psi(D)$.

*The drop moving in the flow experiences oscillations due to attenuate separation of vortices from different sections of its surface (formation of a turbulent wake).

Let us expound briefly certain results of theoretical investigation of development of instability of a drop located in a flow.

The process of disintegration itself, without taking into account entrainment of the particle by a flow, is analytically discussed in work [6]. The liquid of the drop and the surrounding gas are taken to be ideal, and there are considered only perturbations which are axially symmetric relative to the flow axis. Solution by the method of small perturbations makes it possible to determine the critical value of the Weber number. At large magnitudes of this number there occurs instability and disintegration of the drop.

An important result of the work is the determination of forms of perturbations of the liquid surface corresponding to the equation of nodal lines. Nodal line is the locus of points on the drop at which the speed of rise of the surface is equal to 0. In sketching different pictures of deformation, it is possible to assume that independence upon values of the deformation or Weber numbers, disintegration of the initial drop will lead to formation of drops or tori.

In the particular case of equality of the Weber number to zero, (absence of flow around the drop), is obtained the well-known result of Rayleigh about stability of a spherical drop. General conclusions about the critical Weber number as needed, apparently, in subsequent refinement, since this solution was conducted with disregard of dissipation of energy and with replacement of the real distribution of pressures on the drop by pressures corresponding to ideal flow around it.

Probably, in the general case, development of the real process of instability leading to disintegration can start either on a spherical drop or on a deformed drop (for instance, an ellipsoid, a liquid ring with a film, etc.).

§ 3. APPLICATION OF SIMILARITY THEORY TO THE PROBLEM OF ATOMIZATION OF A LIQUID BY SWIRL INJECTORS

With the help of a series of well-known experimental methods (the capture method, method of paraffin separation, spark photography) there has been accumulated considerable material on the fineness of atomization by swirl injectors.

For the purpose of obtaining dependences, possessing certain generality, results of experiment have to be processed in dimensionless parameters. This problem can be solved either with the help of consideration of equations defining the process, or by means of general methods of the theory of similarity. For finding the number and structure of dimensionless criteria, we will use an alternate path based on the

GRAPHIC NOT
REPRODUCIBLE

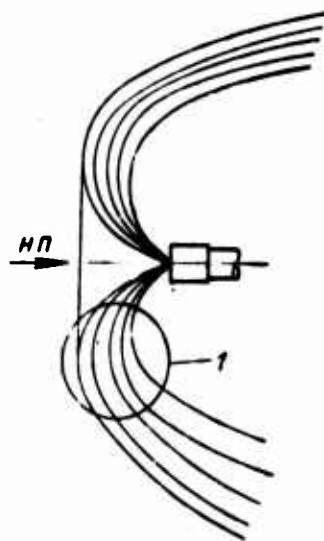
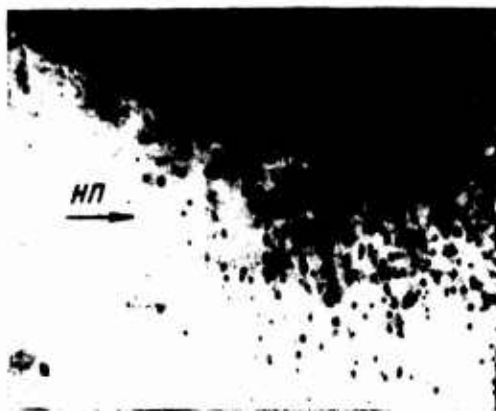


Fig. 2.7. Atomization jet from a swirl injector during fuel feed upstream. 1 - zone of photography; the arrow indicates direction of the flow.

well-known " Π -theorem" [7]. Use of equations of stability of a film of liquid (method of small perturbations) gives in principle the same result.

The system of basic dimensional parameters characterizing the process includes eight quantities: a , u , ϵ , σ , μ_{Γ} , ρ_{Γ} , μ_{κ} , ρ_{κ} . The quantity a is a definite average diameter, for instance the median diameter of the spectrum a_M , corresponding to the ordinate "0.5" on the statistical curve of total relative volumes. By maximum diameter a_{\max} we will understand the diameter corresponding to ordinate "0.95" on the curve of total relative volumes, i.e., the largest diameter for the mass of drops constituting 95% of the entire volume of atomized liquid (see more about curves of the spectrum below). Quantity u is the initial outflow velocity of liquid relative to the system of coordinates connected with the surround flow.

As theoretical and experimental investigations have shown, the process of atomization is determined by velocity of liquid relative to air at the place of disintegration of the stream. For the case of atomization in motionless air this speed coincides with outflow velocity. For an injector aimed upstream relative to the flow, it is equal to the geometric difference between velocity vectors of outflow velocity and the oncoming flow velocity.

In straight-through-flow chambers, there can be used this centraflow system of fuel supply, since it provides sufficient fineness of atomization and a good quality of carburetion. In Fig. 2.7 there is shown a spark photograph of a section of the atomization jet of a swirl injector set against the flow. Many (especially the large) drops on it are deformed and have ellipsoidal shape, with major axis oriented

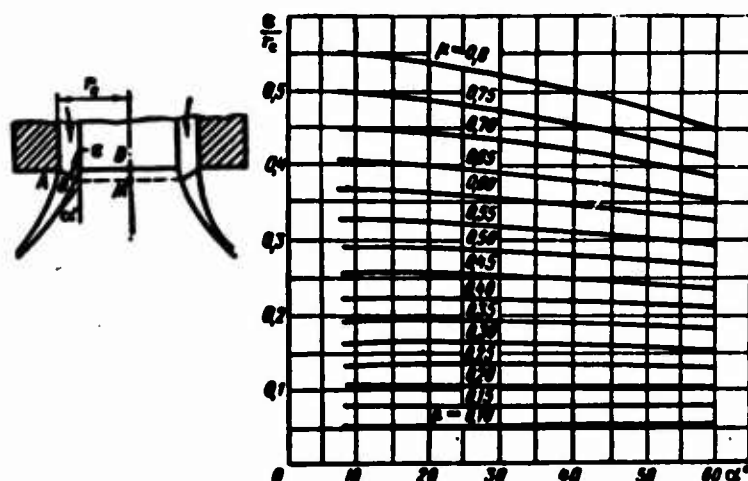


Fig. 2.8. Thickness of liquid sheet of swirl injector.

$$\frac{s}{r_c} = \frac{1 - \sqrt{1 - \mu \cos \alpha}}{\cos \alpha}.$$

perpendicularly to the oncoming flow velocity (in accordance with the character of distribution of pressure on the sphere located in the flow). For an injector aimed downstream, this relative velocity is close to the outflow velocity since the body of the injector protects the root section of the stream from the action of the flow.

Quantity s is the thickness of the sheet of liquid ensuing from the swirl injector, measured along the normal to the sheet (along the normal to the average velocity of the liquid V). This quantity characterizes the quality of the injector as an atomizer. The smaller the s of a given injector is, the smaller (other things being equal) are the drops which are formed. Using the expression of volumetric flow rate Q through the injector (Fig. 2.8), we can obtain a dependence for calculation of s :

$$Q = \mu \pi r_c^2 \sqrt{\frac{\Delta p}{2\rho}}; \quad (2.13)$$

$$Q = f \cdot v = \pi (2r_c - s \cos \alpha) s v \sqrt{\frac{\Delta p}{2\rho}}. \quad (2.14)$$

where f — area of normal cross section of liquid sheet with thickness s (surface area of frustum of a cone with generatrix AB);

v — average outflow speed through cross section f ;

μ — flow coefficient of injector, taking into account filling of the nozzle section by the stream, turn of the stream by the angle of atomization, losses of pressure and velocity profile in the liquid;

μ_v — coefficient taking into account losses of pressure and the velocity profile of the liquid;

Δp — pressure drop on liquid feed.

Equating the right sides of equations (2.13) and (2.14) and solving the quadratic equation, we find

$$\epsilon = r_0 \cos \alpha = \frac{r_c}{\cos \alpha} \left(1 \pm \sqrt{1 - \frac{\mu}{r_0} \cos \alpha} \right). \quad (2.15)$$

From Fig. 2.8 it follows that $\epsilon < r_0 / \cos \alpha$, and therefore the square root corresponding to the plus sign does not have physical meaning. At present in the literature there is not contained sufficiently complete materials for estimate of μ_v , which depends on regime of flow and type of injector. Order of magnitude of $\mu_v \approx 0.8$ to 0.9 . Omitting coefficient μ_v in the first approximation, we will write equation (2.15) in the form

$$\epsilon = \frac{r_c}{\cos \alpha} (1 - \sqrt{1 - \mu \cos \alpha}). \quad (2.16)$$

Curves expressing dependence of ϵ/r_0 on α and μ are shown in Fig. 2.8. Quantity μ is easy to determine experimentally after tests of the injector, or to calculate theoretically. The graph of the dependence for ϵ/r_0 shows that over a considerable interval of change, quantity ϵ depends little on angle of atomization α . Thus, during measurement of angle 2α (for determination of ϵ) there is not required high accuracy. This permits us to be limited to usual photography of the atomization jet. Quantity ϵ can be calculated the same way with the help of the theory of the swirl injector:*

$$\epsilon = (r_c - r_m) \cos \alpha, \quad (2.17)$$

where α and r_m — functions of parameter A ;

r_m — radius of air vortex of injector.

In Fig. 2.9 there is given a corresponding graph for function $\epsilon/r_0 = f(A)$ according to the theory of Abramovich [8]. Quantity σ is the capillary constant of liquid in air (or another medium) and is determined by the nature of the liquid and its temperature. Finally quantities ρ_l ; μ_l ; ρ_g ; μ_g are density and dynamic viscosity of the gas and liquid.

The majority of available experimental data for such liquids as water, gasoline, kerosene, alcohol, indicate the fact that the change of surface tension is more important during the process of disintegration of streams than change of other physical constants. Applying the "Π-theorem" of similarity theory to the considered

*The question about the form of the liquid sheet ensuing from the swirl injector is considered in more detail, for instance in work [9].

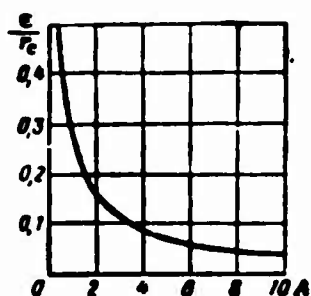


Fig. 2.9. Dependence of thickness of liquid sheet on the geometric characteristic of injector.

$A = \frac{r \cdot R}{r_{BX}^2 \cdot n}$ is the geometric characteristic of the injector according to data of Abramovich.

problem, we will write a dependence between 5 dimensionless parameters (8 dimensional magnitudes and 3 basic units of measure - kg, m, sec) in the following form

$$\frac{\epsilon}{\epsilon_0} = F_1 \left(\frac{\rho_T u^2}{\mu_T}; \frac{\rho_T u^2}{\rho_T^2}; \frac{\mu_T}{\mu_T}; \frac{\mu_T}{\mu_T} \right). \quad (2.18)$$

In the right side, the first complex is Reynolds number for the liquid sheet (i.e., a quantity proportional to the ratio of forces of dynamic pressure during flow of the sheet to viscosity forces. The second complex is a ratio of the form

$$\frac{\rho_T u^2}{\rho_T^2} = \left(\frac{\rho_T u^2}{\mu_T} \right)^2 : \frac{\rho_T u^2}{\epsilon};$$

sometimes in the literature it is called the Onezorge number. This number is obtained as the ratio of the square of Reynolds number to the Weber number $\rho_T u^2 \epsilon / \sigma$. As already was said, the Weber number has a simple physical meaning and is a magnitude proportional to the ratio of dynamic pressure of the air flow to pressure of surface tension.

It is also possible to consider other dimensionless combinations, but equation (2.18) is more convenient in the processing and analysis of experimental materials. However, it is quite complicated, since it contains four independent parameters. For decrease of their number we will introduce certain simplifying assumptions. We will consider that the influence of change of number μ_T / μ_T on the process of atomization is small compared with other factors. This is indicated by experimental data. Theoretical solution of Weber [2] for disintegration of acylindrical stream of viscous liquid and experiments on splitting of drops show the comparatively small influence of change of μ_T on the process of atomization.

Thus, it is possible to expect that the stipulation which was made will be valid for the not very viscous liquids enumerated above (at temperatures of the liquid not too much differing from room temperature). Viscosity affects thickness of the sheet ϵ (fineness of drops) due to influence on the flow coefficient and angle of atomization of the injector. This is taken into account by formula (2.16).

Let us consider at first the case of the small influence of ratio of densities of liquid and gas ($\rho_T / \rho_T \approx \text{const}$), for instance atomization under atmospheric conditions of the surrounding air.

After the above made assumptions, the dependence between numbers determining the

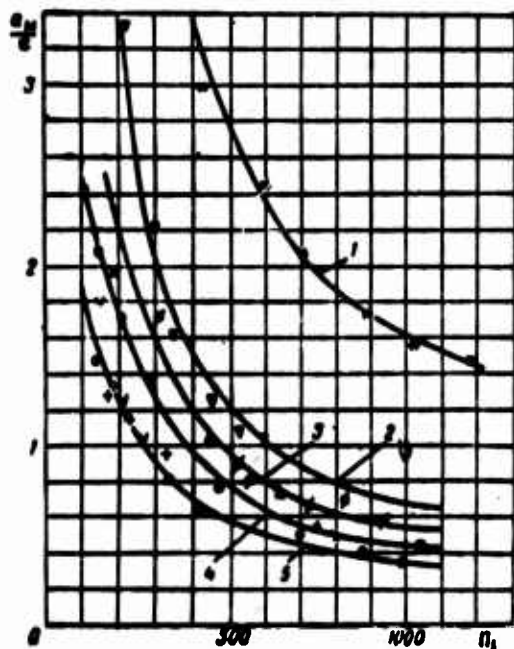


Fig. 2.10. Relation between dimensionless parameters for the process of atomization of liquid by swirl injector (a_M).

1 - $\pi_2 = 78\ 300$, 2 - $\pi_2 = 40\ 500$, 3 - $\pi_2 = 26\ 200$ (29 700-22 800), 4 - $\pi_2 = 20\ 300$ (21 700-19 400), 5 - $\pi_2 = 6000$ (8140-5140).

Liquid	Water	Kerosene	Gasoline
	● 78 300	△ 22 800	● 8140
	▽ 40 500	● 21 700	+ 5140
	⊙ 29 700	× 21 800	
	○ 19 400	■ 20 700	
		√ 7130	

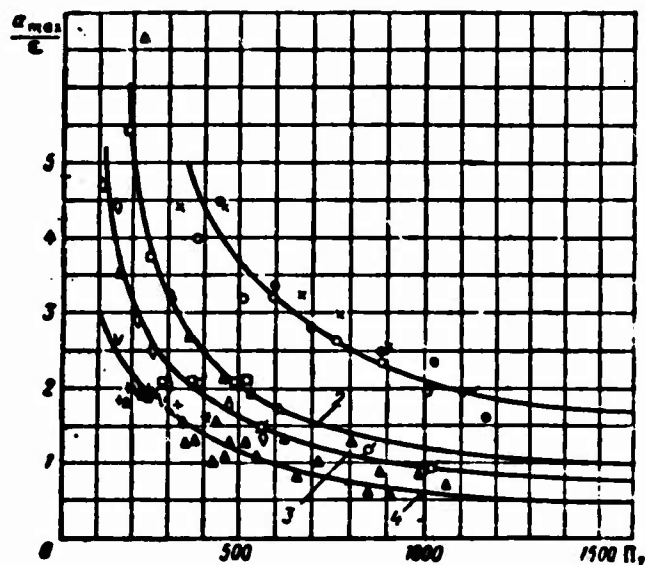


Fig. 2.11. Relation between dimensionless parameters for the process of atomization of liquid by swirl injectors (a_{max}).

1 - $\pi_2 = 68\ 000$ (78 300-38 400), 2 - $\pi_2 = 36\ 200$ (40 500-32 000), 3 - $\pi_2 = 1700$ (19 400-14 400), 4 - $\pi_2 = 6700$ (8400-5140).

Liquid	Water	Kerosene	Gasoline
	● 78 300	⊙ 16 800-14 400	△ 8140
	○ 47 500	× 7200	+ 5140
	× 59 400	√ 7130	
	△ 40 500		
	□ 32 000		
	◇ 19 400		

phenomenon of atomization will acquire the form

$$\frac{a}{\epsilon} = F\left(\frac{u \epsilon \rho_r}{\mu_r}; \frac{\epsilon \rho_r a}{\mu_r^2}\right). \quad (2.19)$$

For determination of the form of the functional dependence F , experimental data on atomization obtained by us and other researchers were processed in the corresponding dimensionless numbers.

Graphs shown in Figs. 2.10 and 2.11 illustrating results of this processing show that points are located approximately on a certain family of averaging curves. Number $\Pi_1 = u \epsilon \rho_r / \mu_r$ was taken as the argument, and $\Pi_2 = \epsilon \rho_r a / \mu_r^2$ was taken as the parameter of the curve. For convenience of review of results, every curve was

constructed not for one constant value of the parameter, but for points corresponding to a comparatively small interval of its change. Thus, every curve corresponds to a definite value of $\epsilon \rho_T \sigma / \mu_T^2$, equal to the average magnitude on the given interval of change (values of limits of change of this parameter are shown on the graphs).

Let us analyze the character of the obtained dependences. Experimental curves show that relative fineness is less, the larger the Reynolds number Re given at $\epsilon \rho_T \sigma / \mu_T^2$. Thus, for a given injector and liquid coarseness of drops is less, the larger the relative velocity of the liquid u . Starting at a definite value of $u \epsilon \rho_T / \mu_T$, further increase of the dimensionless number little affects decrease of coarseness. This value is attained faster, the less the corresponding magnitude of $\epsilon \rho_T \sigma / \mu_T^2$.

In every specific case, according to Figs. 2.10 and 2.11, it is possible for a given flow velocity w to determine the limiting value of u and the pressure drop Δp for the fuel feed which it is inexpedient to increase further for production of finer atomization. $u \epsilon \rho_T / \mu_T = \text{const}$, relative coarseness will be less, the less $\epsilon \rho_T \sigma / \mu_T^2$ is. At constant u for a given liquid, coarseness of atomization under standard atmospheric conditions will be less, the less the thickness of the liquid sheet ϵ .

Using logarithmic coordinates, we can obtain a form of function approximating the curves in Figs. 2.10 and 2.11. These functions will be written in the following way:

$$\frac{a_n}{\epsilon} = (135 + 3.67 \cdot 10^{-3} \pi_2) \pi_1^{-0.9}; \quad (2.20)$$

$$\frac{a_{max}}{\epsilon} = (67 + 3.44 \cdot 10^{-3} \pi_2) \pi_1^{-0.7}, \quad (2.21)$$

where

$$\pi_1 = \frac{u \rho_T}{\mu_T} \text{ and } \pi_2 = \frac{\epsilon \rho_T \sigma}{\mu_T^2}.$$

In experiments whose results are generalized by formulas (2.20) and (2.21), parameters u , ϵ and σ changed within the following limits:

$$\begin{aligned} 27 &< u < 120 \text{ m/sec;} \\ 70 &< \epsilon < 290 \text{ } \mu; \\ 0.002 &< \sigma < 0.0073 \text{ kg/m;} \\ 30 &< a_n < 700 \text{ } \mu; \\ 60 &< a_{max} < 1000 \text{ } \mu. \end{aligned}$$

In the given formulas, dimensionless parameters vary within the limits

$$120 < \pi_1 < 1200;$$

$$7000 < \pi_2 < 60000.$$

As the subsequent check* showed, formulas (2.20) and (2.21), in which parameters of the environment are taken at standard atmospheric conditions, give results satisfactory in practice for the following range of change of magnitudes of pressures p , temperature of the medium t_g ; and temperature of the liquid t :

$$0.8 < p < 3 \text{ atm (tech)}$$

$$10^\circ < t_g < 100^\circ \text{ C};$$

$$5^\circ < t < 40^\circ \text{ C}.$$

Further, based on dependences (2.20) and (2.21), it is possible to obtain formulas determining the atomization spectrum. In the literature, for problems of atomization and carburetion [10] there is widely used an empirical equation for representation of the curve of the volume (or mass) atomization spectrum in coordinates y , a and V_s , a (Rozin-Ramler formulas):

$$y = \frac{n}{\bar{a}} a^{n-1} e^{-\left(\frac{a}{\bar{a}}\right)^n}; \quad (2.22)$$

$$V_s = 1 - e^{-\left(\frac{a}{\bar{a}}\right)^n}, \quad (2.23)$$

where $y = \frac{\Delta V_1}{\Delta a_1 V_0}$ - relative volume of the drops, i.e., the volume of all drops ΔV_1 occurring on a given (small) interval of the spectrum which have dimensions $(a_1; a_1 + \Delta a_1)$, referred to the volume of all drops V_0 and the length of the interval Δa_1 ;

a_1 - diameter of drops in the atomization spectrum (diameter on small interval Δa_1);

V_s^1 - total relative volume, i.e., the sum of relative volumes of all drops with diameter smaller than or equal to the given drop a_1 ;

\bar{a} ; n - constants, called respectively dimension constant and distribution constant.

Equation (2.22) expresses the probability density curve for volumes of liquid with respect to dimensions of drops in the atomization spectra of swirl injectors.

Functions y , V_s are defined on the whole interval a ; at $a = \infty$, $V_s = 1$. Experience shows that their application for a finite interval $(a_{\min}; a_{\max})$ does not lead

*The check consisted of comparison of results of calculation of the distribution of concentrations of atomized liquid in a flow of air (see § 11, Chapter II) with data on experimental determination of these concentrations.

to large errors. As it was earlier agreed, $V_{s \max} = 0.95 \approx 1$ at $a = a_{\max}$.* It is easy to note that

$$\bar{a} = \frac{a_n}{\frac{1}{(\ln 2)^n}}. \quad (2.24)$$

The larger the dimension constant \bar{a} , the bigger the drop; the larger the distribution constant n (at given \bar{a}), the more uniformly they are distributed over dimensions, i.e., the steeper the slope of the curve constructed according to equation (2.22). Quantities n and \bar{a} change in dependence upon the injector and the regime of its operation; i.e., they depend on all measured parameters determining the process of atomization of the liquid.

§ 4. FORMULA OF THE ATOMIZATION SPECTRUM

Using the above materials, we can make an attempt to derive approximate dimensionless relationships for determination of parameters n and \bar{a} . From relationship (2.23) we find

$$a_{\max} = \bar{a} \left(\ln \frac{1}{1 - V_{s \max}} \right)^{\frac{1}{n}}. \quad (2.25)$$

Substituting \bar{a} from equation (2.24) into equation (2.25), we find the ratio a_{\max}/a_n :

$$\frac{a_{\max}}{a_n} = \frac{\left(\ln \frac{1}{1 - V_{s \max}} \right)^{\frac{1}{n}}}{\frac{1}{(\ln 2)^n}}. \quad (2.26)$$

Hence we determine quantity n :

$$n = \frac{\lg \left(\frac{\ln \frac{1}{1 - V_{s \max}}}{\ln 2} \right)}{\lg \frac{a_{\max}}{a_n}}. \quad (2.27)$$

Finding ratio a_{\max}/a_n with help of term by term division of equations (2.20) and (2.21), and remembering that $V_{s \max} = 0.95$, we derive from expression (2.27) a formula for calculation of n :

$$n = \frac{0.638}{\lg \left(\frac{1 + 5.4 \cdot 10^{-3} \Pi_2 \Pi_1^{0.104}}{2 + 5.4 \cdot 10^{-3} \Pi_2} \right)}. \quad (2.28)$$

* a_{\min} is usually a minute magnitude of the order of 1 to 3 μ ; the volume (or mass) of such drops turns out to be practically insignificant in the total spectrum.

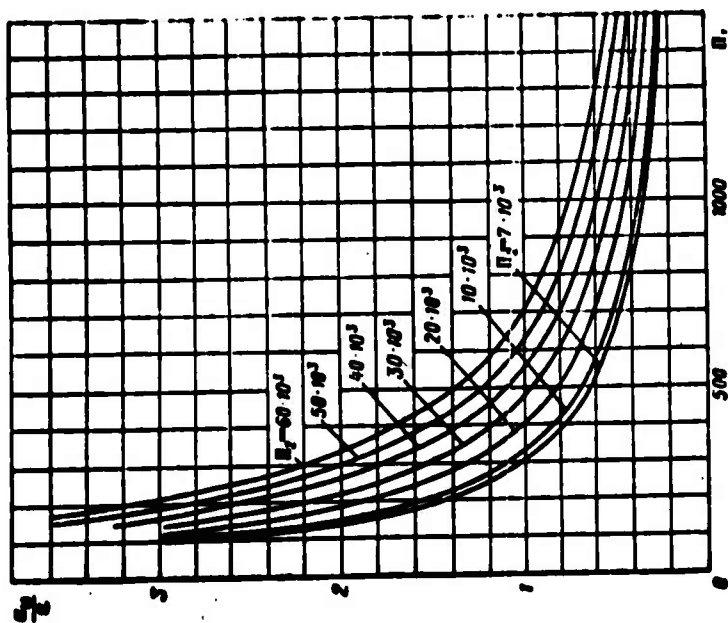


Fig. 2.12. Graph for determination of a_M according to similarity dimensionless numbers.

$$\frac{a_M}{a_{M0}} = \frac{135 + 3.67 \cdot 10^{-3} \left(\frac{w_2^2}{v_2^2} \right)}{\left(\frac{w_2^2}{v_2^2} \right)^{0.9}}$$

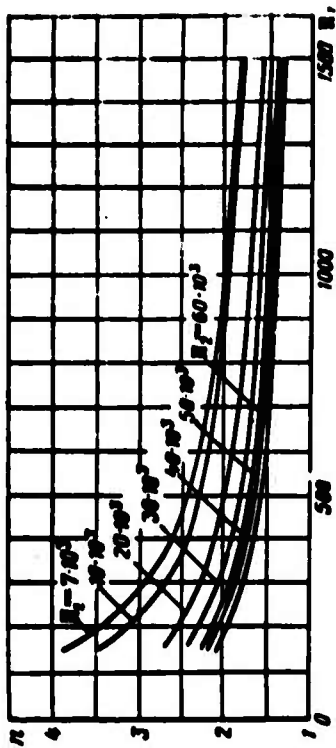


Fig. 2.13. Dependence of distribution constant on similarity criteria.

$$\frac{a_M}{a_{M0}} = \frac{0.436}{n}$$

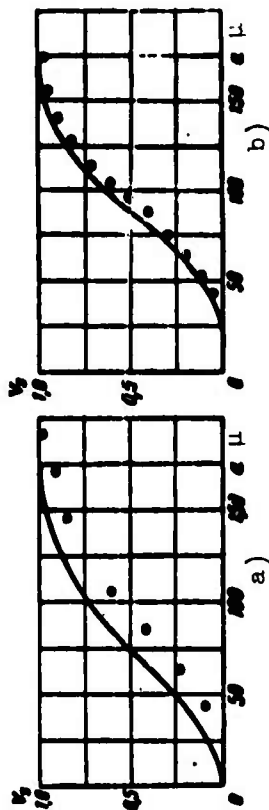


Fig. 2.14. Atomization spectra of swirl injector (fuel is kerosene). a) injector operating against the flow (upstream) $\Delta p = 5$ atm (gage); $w = 36$ m/sec; $\epsilon = 84$ μ ; \bullet — experiment; $-\cdot-$ — calculation; b) injector operating along the flow (downstream) $\Delta p = 10$ atm (gage); $w = 36$ m/sec; $\epsilon = 71$ μ ; \circ — experiment; $-\cdot-$ — calculation.

Substituting the value of a_M from (2.20) in equation (2.24), we will obtain a formula for calculation of \bar{a} :

$$\bar{a} = \frac{e(135 + 3.67 \cdot 10^{-3} \Pi_2) \Pi_1^{-0.9}}{(\ln 2)^{\frac{1}{a}}} \quad (2.29)$$

Thus, formulas (2.28) and (2.29) make it possible according to given parameters of the flow, feed pressure, dimensions of injector and parameters of liquid air, to construct the atomization spectrum. For convenience of calculation, these formulas can be represented in the form of the corresponding graphs shown in Figs. 2.12 and 2.13. For more exact description of the empirical curves of the atomization spectra, there can be constructed more complicated formulas, containing not two, but three or more constants.

In work [11], of the three constants of the distribution curve, there is considered the maximum diameter of a drop in the spectrum. Use of equations of form (2.23) is the first approximation in the solution of the complicated problem of the relation between distribution of drops in atomization spectra and regime parameters characterizing disintegration of the stream of liquid.

In Fig. 2.14, spectra obtained according to formulas (2.28) and (2.29) are compared with experimental spectra.

Calculations conducted for conditions of atomization in a flow of air show that distribution constant n usually varies within the limits $2 \leq n \leq 4$.

We will consider as an example the calculation of the distribution spectrum of drops for a specific regime of atomization by a swirl injector in a flow of air.

Initial Data of Calculation

1. Location of injector — against flow.
2. Fuel — kerosene.
3. Velocity of air flow $w = 86$ m/sec.
4. Temperature and pressure in flow of air $t_B = 20^\circ\text{C}$, $p_B = 1$ atm (abs.).
5. Pressure drop during fuel feed and fuel flow rate through injector $\Delta p_T = 2$ atm (gage); $G_T = 8.73$ g/sec.
6. Temperature, specific gravity and surface tension of fuel $t_T = 43^\circ\text{C}$; $\gamma_T = 806$ kg/m³; $\sigma_T = 2.48 \cdot 10^{-3}$ kg/m.
7. Diameter of nozzle opening and atomization angle of injector $d_0 = 1.2$ mm; $2\alpha = 82^\circ$.

Calculations start with determination of parameters of fuel supply, discharge (flow) coefficient of injector μ , thickness of liquid sheet δ and outflow velocity of liquid V .

Discharge coefficient through injector is equal to

$$\mu = \frac{G}{\pi c \sqrt{2\Delta p \cdot g \cdot \gamma_r}} = \frac{8.73 \cdot 10^{-3}}{3.14 \cdot (0.6 \cdot 10^{-3})^2 \sqrt{2 \cdot 2 \cdot 10^4 \cdot 9.81 \cdot 806}} = 0.434.$$

The formula for thickness of the liquid sheet gives

$$\delta = \frac{1 - \sqrt{1 - \mu \cos \alpha}}{\cos \alpha} r_c = \frac{1 - \sqrt{1 - 0.434 \cdot 0.755}}{0.755} \cdot 0.6 = 0.143 \text{ mm}.$$

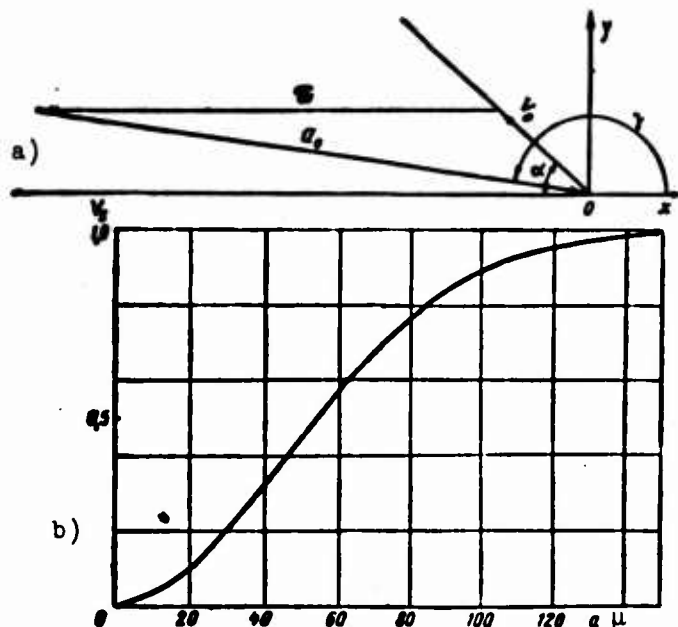


Fig. 2.15. Calculation of atomization spectrum.
a) graphic determination of u , b) atomization spectrum.

Outflow velocity (we will take velocity coefficient $\mu_v \approx 1$) is equal to

$$V = \sqrt{\frac{2g\Delta p}{\gamma_r}} = \sqrt{\frac{2 \cdot 9.81 \cdot 2 \cdot 10^4}{806}} = 22 \text{ m/sec.}$$

Knowing the quantities V , α , w , we find the value of initial relative velocity u_0 . For this, it is most convenient to use the graphic method of the velocity triangle (Fig. 2.15). It gives the value $u_0 = 103 \text{ m/sec}$.

Having at our disposal all necessary dimensional parameters, we calculate dimensionless numbers of the atomization process. Magnitudes of viscosity $\mu_r = \mu_B$ and density ρ_B are taken from tables for physical constants of air:

$$\Pi_1 = \frac{\mu_r \mu_B}{\rho_B} = \frac{143 \cdot 10^{-4} \cdot 0.12 \cdot 103}{1.79 \cdot 10^{-4}} = 990, \quad \Pi_2 = \frac{\mu_r \mu_B^2}{\rho_B^2} = \frac{143 \cdot 10^{-4} \cdot 0.12 \cdot 2.48 \cdot 10^{-3}}{(1.79 \cdot 10^{-4})^2} = 13300.$$

The median and maximum diameter of drops and characteristics of the atomization spectrum, we determine by the formulas given in §§ 3 and 4 of the present chapter:

$$a_m = (135 + 3,67 \cdot 10^{-2} \pi_1^{0.9}) \pi_1^{-0.9} = 57,5 \mu;$$

$$a_{max} = (67 + 3,44 \cdot 10^{-2} \pi_1^{0.9}) \pi_1^{-0.9} = 126 \mu.$$

Distribution constant

$$n = \frac{0,636}{\lg \left[1 - \frac{1}{2 + 5,4 \cdot 10^{-2} \pi_1^{0,184}} \right]} = 1,84.$$

Dimension constant

$$\bar{a} = \frac{a_m}{(\ln 2)^{1/n}} = 70 \mu.$$

Curve of the atomization spectrum

$$V_s = 1 - e^{-\left(\frac{a}{\bar{a}}\right)^n} = 1 - e^{-\left(\frac{a}{70}\right)^{1,84}}.$$

In Fig. 2.15 there is given the calculated curve of the atomization spectrum.

Magnitude of the ratio $\frac{a_{max}}{a_m} = \frac{a_{95\%}}{a_{50\%}} \approx 2$ is characteristic for the majority of types of swirl injectors. Coarseness of atomization obtained in the example may be acknowledged from the point of view of quality of carburetion in the air flow (volatility, etc.) to be fully satisfactory. Presence of an injector system in the combustion chamber (fuel manifold) will not change coarseness of atomization obtained above a single injector noticeably. The density of distribution of injectors in usual straight-through-flow chambers turns out to be not too great, and the mutual interference of atomization jets will not be very significant from this point of view.

We now touch the question of influence of parameters of the environment and liquid $\rho_r, \mu_r, \rho_{\pi}, \mu_{\pi}$ on the process of atomization. Materials available at present do not permit us to answer it with sufficient completeness. Here it is possible to give only individual experimental data.

Let us note systematically the obtained, but strange at first glance result: with fall of pressure and density of the surrounding medium, coarseness of atomization of the swirl injector decreases. This can be explained by the presence of two contradicting tendencies manifested in the process of atomization. With decrease of external forces acting on the liquid sheet, (decrease of density of the medium), the intensity of disintegration should decrease, i.e., the optimum wave of unstable

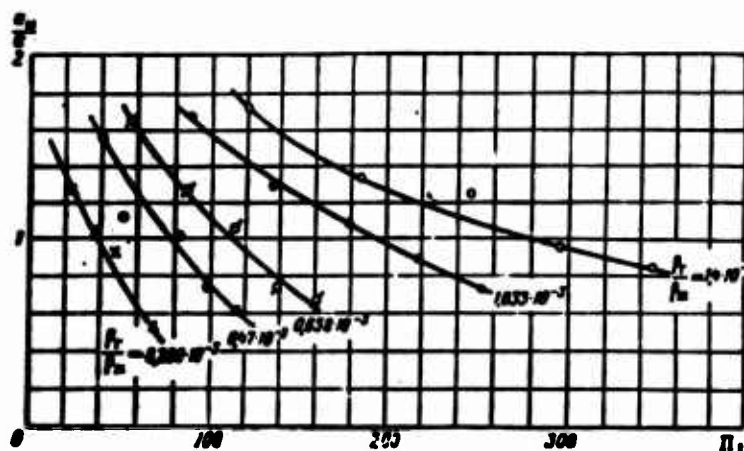


Fig. 2.16. Influence of density of medium on coarseness of atomization (the fuel is kerosene).

$$\frac{p_m^{0.5}}{p_r^2} = 7080 \cdot 10^3.$$

oscillation should increase (which is indicated by experiments with direct-spray injectors). Forces splitting up the already formed drops also decrease. Consequently, there can be formed and retained bigger drops which will not be subjected to splitting.

On the other hand, decrease of intensity of the process of disintegration leads to essential lengthening of the nondisintegrated section of the sheet and, consequently, to its thinning in the zone of disintegration (due to considerations of constancy of flow rate of liquid through the annular cross sections of the sheet). This should lead to considerable decrease of coarseness of the drops into which the thin sheet disintegrates.

As experiments show, (in the range of lowered pressures) the second tendency predominates, which explains the given result. Processing data for pressure of the medium $0.2 \leq P \leq 1$ atm (abs.) and temperature $t = 20^\circ\text{C}$ in the similarity criteria offered above and taking into account the parameter ρ_r/ρ_m , we can generalize the earlier obtained formula for the range of changing pressures of the surrounding medium. In Fig. 2.16 there is shown the influence of factor ρ_r/ρ_m on the coarseness of atomization.

Corresponding analysis shows that the sought dependence

$$\frac{d_m}{d_r} = F\left(\frac{p_r^{0.5}}{p_r}; \frac{p_m^{0.5}}{p_r^2} \frac{p_r}{p_m}\right) \quad (2.30)$$

has the form

$$\frac{a_n}{\varepsilon} = \frac{A \frac{p_r}{p_n}}{\varepsilon_1^n}, \quad (2.31)$$

where

$$A = A \left(\frac{p_r^{0.8}}{p_r^2} \right); \quad (2.32)$$

$$n = \text{const} \approx 0.83 \text{ to } 0.9.$$

On the basis of this there can be obtained the approximate formula

$$\frac{a_n}{\varepsilon} \approx 720 \frac{p_r}{p_n} \frac{135 + 5.2 \cdot 10^{-4} \frac{p_n^{0.8}}{p_r^2}}{\left(\frac{p_r^{0.8}}{p_r} \right)^{0.9}}, \quad (2.33)$$

which is valid in the same range of change of dimensional parameters as formula (2.20):

$$0.286 \cdot 10^{-3} < \frac{p_r}{p_n} < 1.4 \cdot 10^{-3}.$$

For the case of atmospheric conditions, equation (2.33) becomes (2.20). During rough estimate of magnitude of a_{\max} , it is possible to use relationship

$$\frac{a_{\max}}{a_n} \approx \frac{\left(\frac{p_r^{0.8}}{p_r} \right)^{0.35}}{0.23} \left(\frac{p_r}{p_n} \right)^{0.38}. \quad (2.34)$$

The question about the influence of parameters μ_r and μ_n on the process of atomization has been studied to a still lesser degree than the influence of factors ρ_r and ρ_n . However, the majority of data testify to their small influence. Consideration of change of μ_n may be needed when heated fuel is atomized.

According to data of Giffen and Murashov [10],

$$a_{cp} \approx \left(\frac{p_n}{p_r} \right)^{0.14}. \quad (2.35)$$

Thus, it is possible to consider approximately the influence of μ_n/μ_r for such liquids as water, gasoline, kerosene and alcohol, multiplying results obtained by the formulas (2.20), (2.21) and (2.33) by the factor $\left(\frac{\mu_n/\mu_n^0}{\mu_r/\mu_r^0} \right)^{0.14}$, where μ_r^0 ; μ_n^0 are data corresponding to the temperature 15°C.

According to data of Longwell [5], the influence of viscosity of liquid on coarseness of drops starts to appear at quite large values of $\mu_n \approx 0.13$ poise. This value is lower than parameters for conventional propellants of air-breathing jet engine under normal conditions.

§ 5. SCHEME OF ANALYSIS OF A CENTRIFUGAL INJECTOR WITH CONSIDERATION OF COARSENESS OF ATOMIZATION

Using the given formulas, it is possible to give a basic scheme of calculation of parameters of an injector providing a definite fuel flow rate at a given average

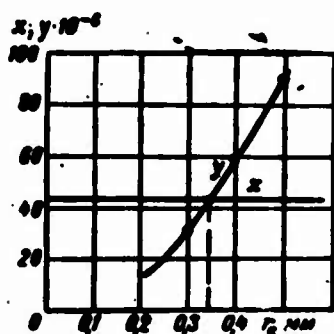


Fig. 2.17. Analysis of a swirl injector taking into account coarseness of atomization. For solution of the transcendental equation $x = y$; $x = \theta_3$; $y = (\theta_1 r_c + \theta_2) r_c^{0.9}$.

coarseness of atomization. For the purpose of simplification we will use the theory of a swirl injector developed by Abramovich [8] for an ideal liquid. Results of calculation will be nearer to reality, the less the viscosity of the given liquid.

The problem of calculation is formulated in the following way: There is given flow rate of liquid G which is atomized in a flow of air of velocity w , where average coarseness of drops should be equal to a_m . We want to determine basic structural parameters of such an injector r_c , R , r_{BX} , n^* and feed pressure Δp (see Figs. 2.9, 2.17 and 2.18).

Let us derive relationships for determination of such unknown magnitudes as

$$a_m = \left(135 + 3.67 \cdot 10^{-3} \frac{G^2 r_c^2}{\mu_r^2} \right) \left(\frac{\mu_r \Delta p}{\mu_r} \right)^{-0.9}, \quad (1)$$

flow rate of liquid through the injector

$$G = 13.92 \mu_r^2 \sqrt{\Delta p_{1x}}. \quad (2)$$

outflow velocity of liquid (for simplification we again take $\mu_v \approx 1$)

$$v = \sqrt{\frac{2 \Delta p}{\rho_m}}. \quad (3)$$

thickness of liquid sheet of swirl injector

$$\begin{aligned} \epsilon &= r_c \cdot f(A) = r_c \cdot f, \\ A &= \frac{r_c R}{n^2 r_{BX}}. \end{aligned} \quad (4)$$

Formula (4) determines thickness of liquid sheet of injector in terms of its geometric characteristic. Function $f(A)$ is more conveniently represented graphically (see Fig. 2.9). Further calculation can be conducted in the following way. Take the arbitrary quantity A according to which ϵ/r_c is determined, and also μ and α according

* n — number of feed channels of swirl injector.

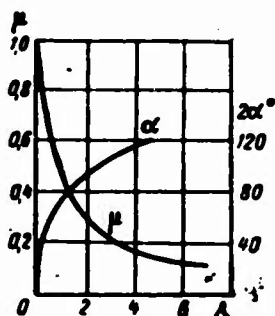


Fig. 2.18. Dependence of discharge coefficient and atomization angle on geometric characteristic of injector.

to the curves shown in Fig. 2.18. Selection of quantity A can be subjected to the additional requirement of obtaining the given atomization angle 2α . Let us express quantity u_0 in relationship (1) in terms of Δp and r_c . If the injector is directed along the flow, then $u_0 = v$ (according to what was stated above); for an injector directed against the flow, quantity u_0 is determined by \bar{w} , \bar{v} (for instance, with help of construction of a velocity triangle $u_0 = \bar{v} - \bar{w}$).

For simplicity we will assume that the injector is directed along the flow. We will substitute in formula (3)

the value of Δp from equation (2):

$$u = \sqrt{\frac{2}{g} \frac{G}{13.92 \mu r_c^2}}; \quad (5)$$

$$\rho_m = \frac{1\pi}{g}; \quad g = 9.81 \text{ m/sec}^2.$$

We will substitute in equation (1) values of u from relationship (5) and ϵ from relationship (4). After transformations, we will obtain an equation for determination of the value of r_c of the injector

$$\theta_1 r_c^{2.9} + \theta_2 r_c^{1.9} - \theta_3 = 0, \quad (6)$$

where

$$\theta_1 = \frac{\rho_r g}{\mu_r^2} \cdot f;$$

$$\theta_2 = 135;$$

$$\theta_3 = 0.046 \left(\frac{\rho_r G}{\rho_m \mu_r} \right)^{0.9} \frac{a_m}{f^{0.1}}.$$

Coefficients in formula (6) are calculated by the initial parameters given in the calculation. This equation is transcendental and must be solved graphically (see Fig 2.17). After determining r_c from formula (2), we find Δp .

Example of calculation.

Given: $G = 9 \text{ g/sec}$; $a_m = 60 \mu$; the fuel is gasoline; surround medium is air under normal conditions.

Constants of air and fuel are the following:

$$\rho_r = 0.12 \text{ kg} \cdot \text{sec}^2/\text{m}^4;$$

$$\rho_m = 77 \text{ kg} \cdot \text{sec}^2/\text{m}^4;$$

$$\mu_r = 1.79 \cdot 10^{-6} \text{ kg} \cdot \text{sec}/\text{m}^2;$$

$$\sigma = 0.002 \text{ kg/m}.$$

Determine: basic structural parameters of the injector and feed pressure of the fuel. We take quantity $A = 1$; then from the given graphs we will obtain $f = 0.24$, $\mu = 0.44$ (angle of atomization of the injector will be equal to 78°).

We calculate coefficients of equation (6)

$$\theta_1 = 6.61 \cdot 10^{-4} \text{ 1/m};$$

$$\theta_2 = 43.1 \cdot 10^{-4} \text{ m}^{1.9}.$$

For convenience of graphical solution, we write equation (6) in the form

$$(\theta_1 r_c + \theta_2) r_c^{2.9} = \theta_3, \quad (7)$$

$$y = (\theta_1 r_c + \theta_2) r_c^{1.9} \quad (8)$$

$$x = \theta_3. \quad (8)$$

In Fig. 2.17 there is shown the method of graphical solution of equation (6). Ordinate of the point of intersection of curves (x) and (y) gives the unknown value of $r_c \approx 0.35 \text{ mm}$. From structural considerations we will determine values of R , r_{BX} and n satisfying the relationship

$$\frac{R \cdot r_c}{r_{BX}^2 \cdot n} = A = 1.$$

By equation (2) we find $\Delta p = 18.2 \text{ atm (gage)}$; thickness of the liquid sheet of such an injector is equal to 84μ . According to calculation, parameters of the injector will be the following:

A	$\frac{a}{r_c} = f$	μ	$2\alpha^\circ$	$r_c \text{ mm}$	$\epsilon \text{ mm}$	$R \text{ mm}$	$r_{BX} \text{ mm}$	n	Δp atm (gage)
1	0.24	0.44	78	0.35	0.084	3.6	0.8	2	18.2

§ 6. DIRECT-SPRAY ATOMIZATION

As has already been said, along with the use of swirl injectors, in combustion chambers there can be used the simpler direct-spray fuel feed (Fig. 2.19). Usually the axis of fuel streams is set at an angle to the flow; this permits the obtaining of quite a wide atomization jet. Combustion chambers of direct-spray injector manifolds have shown fully satisfactory results.

On the surface of the still undisintegrated section of the cylindrical stream fed into the gas flow there act the aerodynamic forces of the gas flow. The stream is resisted by the external influence; this is expressed in increase of the internal pressure of the liquid. Pressure grows due to the appearance of centrifugal forces

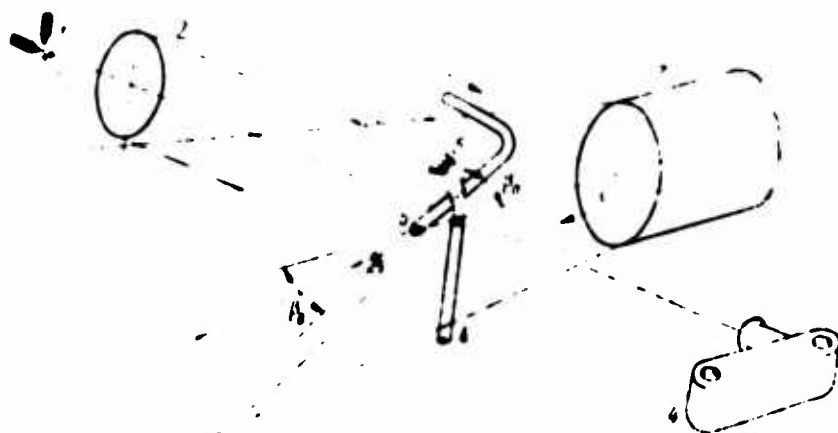


Fig. 2.19. Diagram of an experiment in photographing the jet of a direct-spray atomizer in an airflow. 1 - spark illuminator; 2 - condenser; 3 - air conduit; 4 - camera; 5, 6 - atomization jets (sprays) during photographing in profile and vertical projections.

in inertia during distortion of flow lines (bending of the stream), which remained rectilinear while the liquid was inside the channel of the atomizer. Simultaneously,



Fig. 2.20. Position of axis of deformed stream of liquid (white line) in a flow of air. Profile projection. Water. $d_c = 1.3 \text{ mm}$; $\rho_r = 0.12 \text{ kg} \cdot \text{sec}^2/\text{m}^4$; $\beta_0 = 90^\circ$; a) $w = 90 \text{ m/sec}$, $v = 11.7 \text{ m/sec}$; b) $w = 72 \text{ m/sec}$; $v = 11.7 \text{ m/sec}$; c) $w = 49.3 \text{ m/sec}$; $v = 12.4 \text{ m/sec}$.

external forces flatten the round stream, transforming it into a liquid sheet (Figs. 2.20 and 2.21).

Thus, not the stream disintegrates but the sheet, which is jet like an element of the sheet of a swirl injector. Corresponding calculations and experiments confirm the possibility of use of this analogy for approximate determination of coarseness of drops.

It turns out that coarseness of

the drops of a direct-spray atomizer has, other things being equal, the order of magnitude of drops of a swirl injector with thickness of sheet ϵ equal to the average thickness of the sheet δ_{cp} into which the cylindrical stream is flattened. This permits us to apply the formulas presented above for coarseness of atomization to the given case.

Let us briefly expound certain ideas of the elementary theory of deformation of a cylindrical stream of liquid in a flow of gas. The theory makes it possible to determine approximately the form of the stream and parameters influencing coarseness of atomization.

Basic assumptions on which the theory is based consist of the following:

At Reynolds numbers of the gas flow around the stream equal approximately to 1000 and larger, which are of practical interest, the role of tangents of frictional

The transition from liquid surface to solid surface will reflect mainly on the magnitude of tangential stresses. On a liquid surface, tangential stresses must be less due to the fact that tangential velocities on the interface due to circulation inside the liquid are not equal to zero.

ponding cases of data obtained for flow around a flat plate. Experiment confirms this assumption.

-80-

cross sections of the stream. This assumption also permits us not to consider non-uniformity of velocities in the initial section of the stream and decrease of speed along its axis.

4. Let us disregard weight of the stream, which is small compared to other acting forces.

Let us select the origin of coordinates of the absolute system to be in the center of the nozzle opening. Axis Ox will be directed parallel to vector \bar{w} , and axis Oy will be vertical. Outflow velocity of liquid \bar{v} will be directed at angle β_0 to axis Ox (Fig. 2.22). The modulus of vector \bar{v} , as already was said, in a certain range is taken to be constant. Experiment show that there exists a fully definite section of undisturbed stream where the process of disintegration has only begun. On this section the amplitude of perturbations waves is comparatively small, and the liquid surface can be considered to be smooth.

Considering the motions of the center of mass of an element of the sheet and applying to it D'Alembert's principle (in projections on the normal to the axis of the stream), we will obtain

$$c_n \frac{F v^2}{2} df = \frac{v^2}{R} dm, \quad (2.36)$$

where R is the radius of curvature of the trajectory of the center of mass of the element of the sheet.

In the left side of equation (2.36) there is written the expression for external force acting on the surface of element df (normal component); in the right side - force of inertia applied to center of mass of element dm.

Applying to the stream the "solidification principle," we take magnitude c_n as the drag coefficient of an inclined plate of small aspect ratio

$$c_n = c_{n0} \sin \beta, \quad (2.37)$$

where c_{n0} is the drag coefficient of an infinitely long plate installed transverse to the flow. Corresponding estimates for the conditions of our problem show that $1 < c_{n0} < 2$, and that it is possible to take approximately $c_{n0} = 1.2$.

The sine of angle β (angle of slope of the tangent to the axis of the distorted stream) is expressed in terms of derivatives of the trajectory of the center of mass

$$\sin \beta = \frac{y'}{\sqrt{1+y'^2}} = \frac{r'}{(1+r'^2)^{1/2}}. \quad (2.38)$$

For the radius of curvature R we use the well-known formula of differential geometry

$$R = \frac{|1+y'^2|^{3/2}}{y'}. \quad (2.39)$$

Putting the value of $\sin \beta$ and R from relation (2.38) and (2.39) into equality (2.36) and carrying out appropriate transformations, we will obtain

$$y'' = -k(y')^2 \sqrt{1+y'^2}, \quad (2.40)$$

where

$$k = \frac{p_x}{p_m} \left(\frac{u}{v} \right)^2 \frac{c_m}{\delta}. \quad (2.41)$$

Here δ is thickness of the liquid sheet into which the cylindrical stream is deformed.

Relation (2.40) is the differential equation of the axis of the liquid stream deformed by the flow $y = f(x)$. This curve will be called the liquid line (by analogy with an elastic line). Boundary conditions have the form

$$x = 0; y = 0; y' = \operatorname{tg} \beta_0.$$

Simplifying the problem, we will take the quantity δ , which varies with x , in the expression for parameter k as a certain average, constant thickness of the sheet δ_{cp} ; then $k = \text{const}$ and differential equation (2.40) can easily be integrated.

Solving the equation and using the boundary conditions, we will obtain the equation of the liquid line in the form

$$y = \frac{1}{k} \ln \left[\frac{1 + \sin \beta_0 \left(kx + \sqrt{k^2 x^2 + \frac{2kx}{\sin \beta_0} + \operatorname{ctg}^2 \beta_0} \right)}{1 + \cos \beta_0} \right]. \quad (2.42)$$

Expression (2.42) is the equation of a family of affine curves; i.e., for given β_0 all curves are obtained from one similarity transformation with coefficient k . The larger parameter k is, i.e., the higher the impact pressure of the gas and lower the impact pressure of the liquid, the smaller ordinate y is and the more strongly the stream will be deformed.

Radius of curvature of the stream can be expressed in terms of the instantaneous angle of slope of the liquid line

$$R = \frac{\operatorname{ctg}^3 \beta}{k}. \quad (2.43)$$

From the given relationship (2.43), it is clear that curvature of the stream decreases with its "deflection." In the particular case of supply of liquid transverse to the flow, initial angle β_0 is equal to 90° ; under this condition we will obtain a simpler expression for the equation of the liquid line:

$$y = \frac{1}{k} \ln [1 + kx + \sqrt{kx(kx + 2)}]. \quad (2.44)$$

Carrying out analysis of deformation of the stream under the influence of the force of the gas flow, it is possible to derive approximate formulas describing the process of its transition to a liquid sheet. They permit us to determine average thickness of the deformed stream δ_{cp} over the section from the nozzle opening of the channel to the zone of disintegration, and the average thickness $\bar{\delta}_{cp}$ of the liquid sheet itself, on coarseness of the drops formed during disintegration depends:

$$\delta_{cp} = \frac{d}{3} \left(1 + \frac{\pi}{2\sqrt{D_w A_{\beta_0}}} \right), \quad \pi = 3.14; \quad (2.45)$$

$$\bar{\delta}_{cp} = \frac{\pi d_c}{4\sqrt{D_w A_{\beta_0}}}; \quad (2.46)$$

$$D_w = \frac{\pi \pi d_c}{c}. \quad (2.47)$$

For the case $\beta_0 = 90^\circ$

$$A_{\beta_0} = 1.2 \sin^2 \beta_0. \quad (2.48)$$

Parameter D_w is the deformation criterion of the sheet. In the process of deformation, deforming forces of the external flow and resisting forces of surface tension oppose each other. The factor A_{β_0} expresses the influence of initial slope of the stream on thickness of the sheet.

In Fig. 2.20 there is shown a liquid stream ejected from a cylindrical atomizer into a flow of air at an angle $\beta_0 = 90^\circ$. Curves drawn on the photograph constitute liquid lines constructed according to the formula (2.44). Curves follow the axis of the deformed stream in the first approximation. The given conformity is maintained on a certain interval of the stream which is strongly disturbed and disintegrates into drops; i.e., the center of mass of the stream continues for a certain time to move by inertia along a curve, which is close to the liquid line. This can be explained by the fact that after disintegration, liquid particles form a quite dense cluster of drops, the main mass of which moves as a single whole. Results of experimental investigations also indicate the validity of the more complicated formula (2.42) for initial angle of the stream $\beta_0 = 45^\circ; 60^\circ$.

Applying the above-described method, we can construct an elementary theory of deformation for a cylindrical stream of diameter d_0 , which is not flattened, but is only bent in the flow, preserving circular shaped cross section (or little changing cross sections). Physically this corresponds to the case of outflow of a very viscous liquid, or of a liquid with high surface tension.

By corresponding reasoning and transformations, we will obtain the same differential equation as (2.40), but parameter k_1 contained in it will have the following form:

$$k_1 = \frac{p_r}{p_m} \left(\frac{w}{v} \right)^2 \frac{2c_x}{ad_c}, \quad (2.49)$$

where $c_x \approx 1$ to 1.13 (for usual regimes of flow in an engine combustion chamber).

Thus, during estimate of the upper boundary of possible positions of the real liquid line, which corresponds to a stream flattened by the gas flow, it is possible to use expression (2.42) or (2.44), which contain the complex k_1 . It is easier to find than the analogous parameter k , inasmuch as the latter is determined by the entire complicated process of deformation of the stream.

Example of determination of coarseness of atomization for a direct-spray system of fuel supply.

Initial data: diameter of atomizer opening

$$d_0 = 0.4 \text{ mm}; w = 54 \text{ m/sec}; \Delta p = 1.3 \text{ atm (gage)}; v_0 = 18 \text{ m/sec}; \beta_0 = 90^\circ.$$

Fuel is kerosene; surrounding medium is air under normal conditions.

Let us determine the average thickness of the sheet and the initial relative outflow velocity u . Let us find the diameter of the stream:

$d = d_0 \mu_v$, where μ_v is the contraction ratio of the stream, equal in our case to approximately 0.87; then, $d = 0.36 \text{ mm}$. The value of \bar{v}_{cp} according to formula (3.46) at $D_w = 16$ will be 0.073 mm; $\bar{v}_{cp} = 73 \mu$. The quantity u_0 after subtraction of vectors according to $\bar{u}_0 = \bar{v} - \bar{w}$ (rule of the velocity triangle) is obtained to be equal to 53 m/sec. Corresponding criteria in equations (2.20) and (2.21) will be

$$\frac{\bar{v}_{cp}^2}{p_r} = 357; \quad \frac{\bar{v}_{cp}^2}{p_r^2} = 7300.$$

After the calculations we will obtain $a_M = 63 \mu$ and 107μ . A specially conducted experiment in determination of the coarseness drops for this case gives values which are close in order of magnitude $a_M = 70 \mu$ and $a_{max} = 135 \mu$.

Results of this calculation show that a cylindrical stream during disintegration in a gas flow will form drops of considerably smaller dimensions than its diameter. Thus, during atomization of fuel by direct-spray injectors located at an angle to the flow, there can be obtained the same spectra drops as during the operation of swirl injectors.

During calculation of trajectories of motion of drops of an atomization jet,

it is necessary to determine the coordinates of the point of beginning of motion of the drops and the slope of the initial velocity vector V_0 . Corresponding formulas of elementary theory permit us to conduct the necessary calculations and to determine the rotation of the velocity vector during deformation of a cylindrical stream.

§ 7. ATOMIZATION JET IN A SUPERSONIC FLOW

Below we will consider certain questions connected with supply of liquid into a supersonic flow [12].

Let us assume that an aircraft moves with high supersonic speed. Then, as it is known, retardation of flow in the system of shocks of the intake diffuser to the level of subsonic velocities will lead to a very considerable increase of air temperature in the combustion chamber. In this case, along with a series of unfavorable factors (dissociation and others), the process of additional heat supply from combustion of fuel in the chamber will be little effective. Therefore, it is more expedient to create in the engine incomplete deceleration of flow, and to carry out the process of burning in supersonic flow. In work [13] it is assumed, for instance, that combustion of a preliminarily prepared mixture will occur in a stabilized detonation wave.

High temperature in the flow (or in the shockwave) will ensure small periods of induction and high chemical reaction rate. It is possible, therefore, to expect that development of the process of burning in a supersonic flow will be determined by the rate and quality of carburetion — atomization, vaporization and mixing. Processes of atomization and carburetion can be used for organization of combustion on stabilizing surfaces or control surfaces of aircraft for increase of forces acting along the normals to them (problem of increase of life and effectiveness of control, for instance, in rarefied air).

The low intensity of turbulent diffusion in a supersonic flow (concerning which there are definite data) may predetermine the use of liquid fuel, and not fuel in gaseous form. Since components of the mixture remain in the chamber with supersonic flow for an insignificant time, there is required rational organization of carburetion, which is capable of limiting the whole working process of the engine. First of all, it is necessary to establish the shape of the atomization jet and its external boundaries. It is further important to estimate wave losses connected with the fuel injection.

For the purpose of establishing basic physical characteristics of this little studied phenomenon and determination of the shape of the atomization jet, there have

been conducted corresponding experiments [12]. For carrying out basic experiments there was used an installation with supersonic flow. Air was fed from a pressure chamber into a supersonic nozzle adjoining to a rectangular chamber 120×120 mm, with windows. The atomizer was a cylindrical tube with conical tip, which ensured the absence of shocks on the atomizer tube. The tip of the atomizer and atomization cone were in the rhombus equal velocities. From a cylindrical channel in the wall of the tube at an angle of 90° to the axis of the chamber there was injected liquid (flow coefficient $\mu \approx 0.7$ to 0.75). Parameters of the incident flow changed within the following range: Mach number $M = 2.902$ to 2.0 , total pressure $p_0 = 15.5$ to 7.7 atm (abs.); stagnation temperature $T_0 = 253^\circ\text{K}$. Shapes of the atomization jet and shockwave were studied with the help of photography by the Toepler method and spark photography. Photographs were made in profile and vertical projections. Analysis of obtained photographs showed the following features of the studied phenomenon:

1. Before the atomization jet there appears a shockwave. The element of the wave adjoining the root of the fuel stream is obviously a shockwave which is close to normal (Fig. 2.23). On certain photographs, especially at small feed pressures, in this zone before the normal shock there is seen a small - shaped or oblique shock.

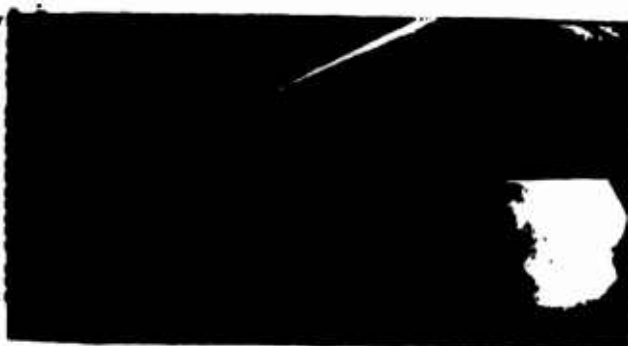


Fig. 2.23. Atomization jet in a supersonic flow. $M = 2.9$; $d_c = 1$ mm; $\Delta p = 40$ atm (gage); $p_0 = 16$ atm (abs.); $T_0 = 253^\circ\text{K}$. Alcohol.

2. The initial section of the shock wave has large slope, which rapidly decreases. For the most part the wave is quite gently sloping and has in both projections almost rectilinear outlines.

On this section the wave rapidly approaches the characteristic (Mach line).

3. The range of the atomization jet in the profile projection turns out to be greater, the higher the feed pressure of liquid Δp and the larger the diameter of the nozzle opening of the atomizer d_c other things being equal (Fig. 2.24). In vertical projection, the width of the jet changes little (although it also increases somewhat with increase of the indicated parameters).

4. The outer boundary of the atomization jet which over its initial section

*Data on coarseness of atomization in supersonic flow can be found, for instance, in the article of M. S. Volynskiy (News of Academy of Sciences of the USSR, Technical Sciences Branch, 1963, No. 2)

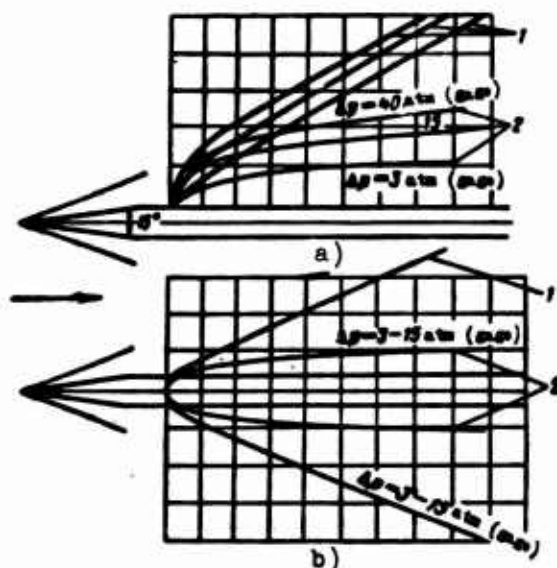


Fig. 2.24. Configuration of atomization jet and shock wave during feed of liquid into a supersonic flow. a) profile projection; b) vertical projection, $M = 2.9$, $T_0 = 253^\circ\text{K}$, $p_0 = 16 \text{ atm (abs.)}$, $d_c = 1 \text{ mm}$. Alcohol. 1 — shockwave; 2 — boundary of jets.

the question concerning shape of the initial section of the outer boundary of the jet (without taking into account processes of vaporization or burning).

On the basis of observations it is possible to assume that the liquid stream near its point of injection is blown by a flow whose parameter $p_r w'^2$ is close to parameters of the gas behind the normal shock wave. Then, according to formula (2.44), the equation of the liquid line on the interval of the undisintegrated stream will have the form

$$ky = \ln[1 + kx + \sqrt{kx(kx + 2)}], \quad (2.50)$$

at small values of kx and ky :

$$ky = \frac{p_r w'^2}{p_{cr}^2} \frac{c_m}{\delta} y; \quad (2.51)$$

$$kx = \frac{p_r w'^2}{p_{cr}^2} \frac{c_m}{\delta} x. \quad (2.52)$$

According to the well-known relationship of gas dynamics, it is possible to write

$$p_r w'^2 = \frac{p_{cr}^2}{\lambda^2}, \quad (2.53)$$

where $\lambda = \frac{w}{a_{cr}}$ — velocity coefficient (gas-dynamic parameter);

a_{cr} — critical velocity of gas.

has large slope, tends with increase of distance from the point of injector to approach a certain asymptote, which is parallel to the flow axis.

Photographs done according to the Toepler method make it possible to determine quite exactly the outer boundary of the jet for different flow engines. The zone of burning (and first of all its initial region) will be close to the zone of the atomization jet, since at high t^0 of the flow ignition apparently occurs before the moment of vaporization of the main mass of injected liquid.

Using equations of the liquid line (§ 6 of the present chapter), we will analyze the question concerning shape of the initial

According to the formulas of § 6, we will estimate the magnitude of δ at large values of D_w (large values of $\rho_r w'^2$):

$$\delta_{cp} \approx \frac{d}{3}. \quad (2.54)$$

Then for $c_{n0} \approx 1.3$ we will obtain expressions of ky and kx in terms of parameters of the incident flow:

$$ky \approx \frac{4}{\lambda d_c} \frac{p_r}{p_m} \left(\frac{w}{v} \right)^2 y, \quad (2.55)$$

$$kx \approx \frac{4}{\lambda d_c} \frac{p_r}{p_m} \left(\frac{w}{v} \right)^2 x. \quad (2.56)$$

Considering the region of small values of kx ($kx \ll 1$) and keeping in expression (2.50) only terms of the form \sqrt{kx} , we can write

$$ky \approx \ln[1 + \sqrt{2kx}]. \quad (2.57)$$

Expanding the right side of equation (2.57) in a power series and leaving the first term of the expansion, we will obtain

$$\frac{y}{d} \approx \sqrt{\frac{p_m}{p_r}} \frac{v}{w} \lambda \sqrt{\frac{x}{d}}. \quad (2.58)$$

Relationship (3.58) gives a rough approximate formula for the axis of the distorted stream. It is valid only under the condition that

$$\sqrt{kx} = \frac{2}{\lambda} \sqrt{\frac{p_r}{p_m}} \frac{w}{v} \sqrt{\frac{x}{d}} < 1, \quad (2.59)$$

i.e., at small x/d , high fuel feed pressures, large Mach number and high total pressures of flow p_0 .

Assuming that the front boundary of the stream is close in shape to (approximately equidistant from) the liquid line, we will write the equation of the initial segment of the boundary in the form

$$\frac{y}{d} \sim \sqrt{\frac{p_m}{p_r}} \frac{v}{w} \lambda \sqrt{\frac{x}{d}}. \quad (2.60)$$

The real proportionality factor in expression (2.60) should be, thus, close to but somewhat less than unity. This is explained by the circumstance that real local values of velocity heads $\rho_r w'^2/2$ of the flow around the liquid stream gradually increase (consequently, the value of y should decrease as compared to values corresponding to formula (2.58)) with departure of liquid from the zone of the normal shock.

Using results of measurement of the boundaries of jets by photographs obtained

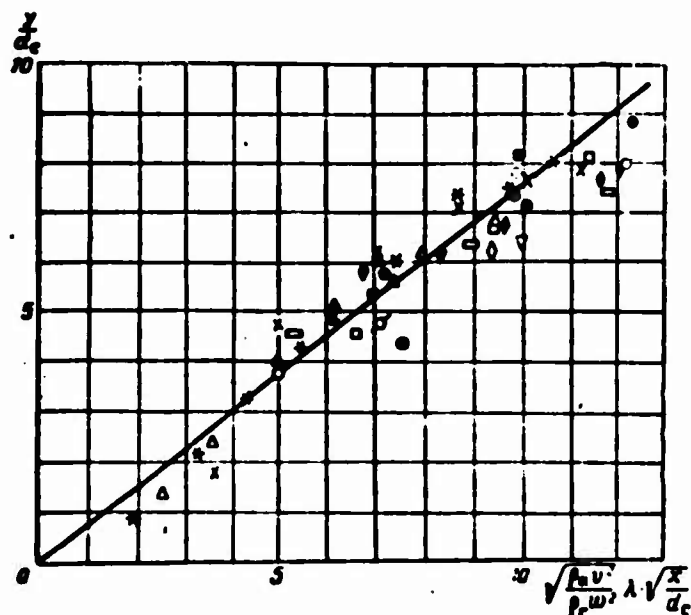


Fig. 2.25. Initial section of boundary of an atomization jet in a supersonic flow (approximate analytic formula).

Designation	Fuel	M	d_c , mm	ΔP , atm (gage)	P_0 , atm (abs.)	T_0 , K
□	Alcohol	2.003	1.0	40	16	253
•	"	2.003	1.0	3	16	253
•	"	2.003	0.7	45	16	253
◊	"	2.003	0.7	30	16	253
□	"	2.003	0.7	15	16	253
◊	"	2.003	0.4	40	16	253
■	"	2.003	0.4	20	16	253
•	"	2.00	1.0	40	12	253
•	"	2.00	1.0	20	12	253
•	"	2.00	1.0	10	12	253
•	Gasoline	2.003	1.0	40	7.7	253
•	"	2.003	1.0	20	7.7	253
•	"	2.003	1.0	10	7.7	253
•	"	2.003	1.0	5	7.7	253

by the Toepler method, and processing materials of the experiments in dimensionless parameters, we can check the accuracy of relationship (2.60). From the graph in Fig. 2.25, it follows that experimental points approach the line described by expression (2.60); its slope, in accordance with what has been said, indeed is close in order of magnitude to unity, and is equal to 0.75. Thus, the approximate relationship of the initial section of the boundary of the jet will have the form

$$\frac{y}{d} \approx 0.75 \sqrt{\frac{P_{\infty}}{P_r}} \frac{v}{u} \lambda \sqrt{\frac{x}{d}}. \quad (2.61)$$

Like the feature shown in § 6 for conditions of subsonic flow, in our case equation (2.62) also turns out to be approximately correct over a certain section

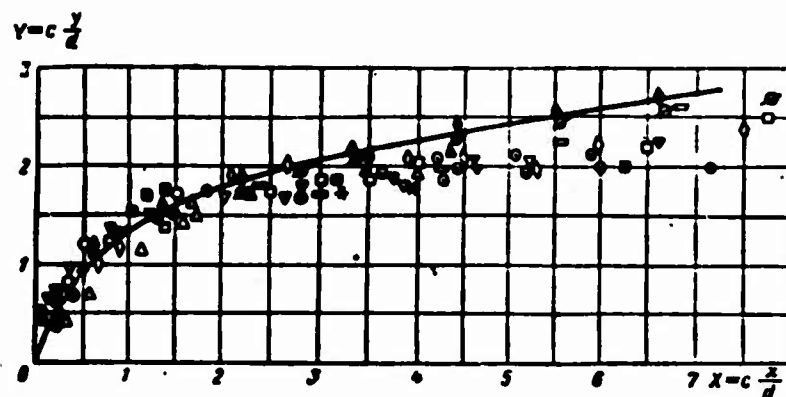


Fig. 2.26. Initial section of boundary of atomization jet in a supersonic flow.

Designation	Fuel	M	d_c mm	ΔP atm (mm Hg)	P_0 atm (mm Hg)	ρ kg-sec/m ⁴	T_0 °K
□	Alcohol	2.903	1.0	40	16	0.186	253
●	"	2.903	1.0	15-19	16	0.186	253
○	"	2.903	1.0	5	16	0.186	253
●	"	2.903	0.7	45	16	0.186	253
○	"	2.903	0.7	30	16	0.186	253
□	"	2.903	0.7	15	16	0.186	253
○	"	2.903	0.4	40	16	0.186	253
○	"	2.903	0.4	30	16	0.186	253
○	"	2.903	0.4	10	16	0.186	253
○	"	2.00	1.0	40	12	0.420	253
○	"	2.00	1.0	30	12	0.420	253
○	"	2.00	1.0	10	12	0.420	253
▽	Gasoline	2.903	1.0	40	7.7	0.093	253
▽	"	2.903	1.0	30	7.7	0.093	253
□	"	2.903	1.0	10	7.7	0.093	253
○	Kerosene	2.50	1.0	30	2.0	0.037	243

after disintegration of the stream into droplets where there moves a dense cluster of liquid particles. It is possible to note that expression

$$y \sim \sqrt{x}$$

for the boundary of the atomization jet in a supersonic flow was obtained by Malyuzhenets, proceeding from the motion of a separate element of the liquid of a disintegrating stream.

If we consider a longer interval of the initial section of the boundary, then results of experiment satisfactorily follow an empirical curve of the form shown in (Fig. 2.26).

$$y = \ln[1 + X + \sqrt{X(X+2)}]. \quad (2.62)$$

where

$$y = 0.412 \sqrt{\frac{P_0^2}{P_{\infty}^2} \frac{x}{d}}; \quad (2.63)$$

$$X = 0.412 \sqrt{\frac{p_{0H}}{p_{0O}}} \frac{x}{d}. \quad (2.64)$$

The structure of quantities X , Y in dependence upon (2.62) reflects the influence of variability of densities of velocities at different points of the flow behind the shock wave and several other factors.

An important circumstance determining the technical possibilities of using liquid fuel in a chamber of the considered type is wave losses from the actual injection. By determining photographs (made in two projections) the shape of the shock wave appearing before the atomization jet, we can estimate the magnitude of wave losses due to atomization of fuel in the supersonic flow.

The Pitot loss coefficient in the flow σ will be expressed by formula

$$\sigma = \frac{p_{0cp}}{p_{0H}} = \frac{\frac{1}{G} \int p_0' dG}{p_{0H}}, \quad (2.65)$$

where p_{0cp} , p_{0H} — the averages over flow rate of total pressures behind the shock-wave and in the incident flow;

p_0' ; p_0 — total pressure at different points behind the shockwave and in the incident flow;

G — flow rate of air through the cross section of the atomization jet.

Values of quantities p_0' can be determined in dependence upon the slope of the shock wave surface at different points.

Examples of calculations (with a certain exaggeration of losses) give for the value of a single atomizer at $M = 2.9$ the values 0.85 to 0.9, which apparently is acceptable from the point of view of permissible Pitot losses. However, if there is used a group of atomizers, the given value of losses for the chamber can noticeably increase. Let us note that the boundary of the jet is sensitive to the influence of the shock waves, which the jet can encounter in the chamber (shocks from the diffuser and others). In these cases liquid particles try to follow the flow lines behind the shock. Shocks can also cause separation of the boundary layer on the atomizer or chamber wall, which sharply changes the configuration of the jet and the magnitude of losses.

§ 8. MOTION OF A SINGLE DROP IN A GAS FLOW

Data on kinematics of motion of droplets (velocity, coordinates, time of stay in the flow) are required for analysis of vaporization and distribution of drops in a gas flow. After completion of disintegration of the stream, the appearing system of drops moves along definite trajectories, forming the fuel jet. During

investigation of the motion of the entire fuel jet from the injector, it is necessary to consider a series of complicated phenomena: perturbation of initial parameters of motion of the drops after disintegration of the stream, interaction of the air flow with the fuel jet, etc.

Let us consider at first the motion of an isolated drop. The obtained results will be initial data for construction of a method of analysis of motion of a system drops in a fuel jet. Furthermore, they will be used during calculations connected with heat and mass transfer of the drops.

For the purpose of simplification of the problem we will assume that

- temperature and velocity in the gas flow are constant;
- weight of the drop is negligible as compared to the other acting forces;
- different pulsations in the flow, for instance turbulence, do not render an essential perturbing influence of behavior of the liquid particle.

Study of motion of a drop in a medium exerting resistance is based on the equation of motion of the center of mass of a solid sphere, which is written in the form

$$\frac{G}{g} \frac{d\bar{u}}{dt} = -c_m \cdot F_m \phi(D) \rho_g \frac{a}{2} \bar{u} - \frac{1}{S} \int_S \frac{1}{g} \frac{dG}{dt} \bar{v}_n dS; \quad (2.66)$$

$$\bar{u} = \bar{v} - \bar{w}, \quad (2.67)$$

where \bar{u} - blowing velocity of the drop (see Fig. 2.15a);

\bar{v} - absolute velocity of the drop (of its center of mass);

v_n - flowoff velocity of vapor from the drop.

The second term in the right side of equation (2.66) represents the reaction force appearing due to nonuniform flowoff of vapor from different sections of the surface of the drop. It is possible to show that reaction forces appearing due to nonuniform flowoff from the drop can be disregarded. Thus, we take

$$\frac{1}{S} \int_S \frac{1}{g} \frac{dG}{dt} \bar{v}_n dS = 0.$$

At

$$\bar{w} = \text{const } d\bar{v} = d\bar{u}. \quad (2.68)$$

From comparison of equation (2.66), in which there is discarded the second term in the right side, with equation (2.68), it follows that $d\bar{u} \parallel \bar{u}$, i.e., the direction of relative velocity during entrainment of the drop by a uniform flow remains constant. Consequently, the trajectory of relative motion of the drop is a straight line located at an angle γ to the axis \overline{OX} , where $\gamma = \text{const}$.

The finding of function $c_m(\text{Re})$ for determination of the drag coefficient of the drop during its entrainment by the flow is the main job in the considered problem.

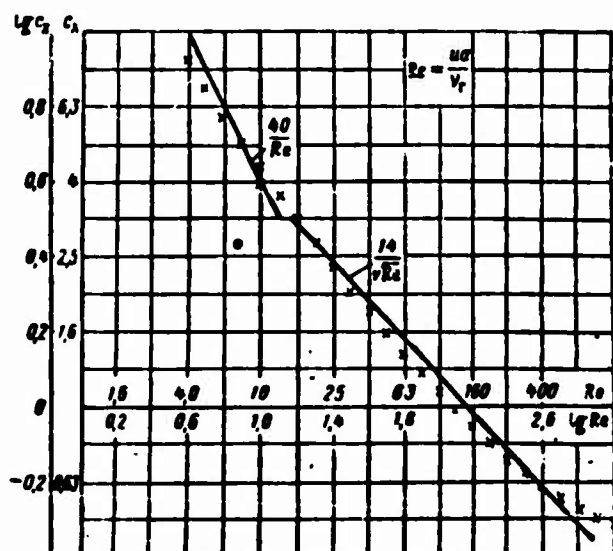


Fig. 2.27. Drag coefficient of a sphere.

Use of dependence $c_m = c_m(Re)$, according to Wieselsberger [7], as this is done in all practical calculations on carburetion, is equivalent to the assumption that around the drop at the time of its entrainment by the flow is quasi-static. In other words, it is assumed that flow near the drop passes through a series of steady states corresponding to flow at current values of Reynolds number Re . For the main mass of particles encountered in the spectra, this assumption is apparently close to reality, but is somewhat incorrect for the smallest drops [15].

In the literature there are offered a number of approximation formulas for determination of the drag coefficient of a solid sphere. In the region of small Reynolds numbers ($Re \leq 1$) Stokes theorem is valid:

$$c_m = \frac{24}{Re}.$$

A formula which sufficiently accurate and applied in a wide range of Reynolds number Re [16], has the form

$$c_m = \frac{24}{Re} + \frac{4.4}{\sqrt{Re}} + 0.32 \quad \text{at } 10^{-3} < Re < 6 \cdot 10^2.$$

However, use of this dependence leads to complicated expressions, and in practical calculations there is usually applied the formula proposed by Vyrubov [17]

(Fig. 2.27):

$$c_m = \frac{n}{\sqrt{Re}}. \quad (2.69)$$

where $n = 12.5$ ($10 \leq Re \leq 1000$) and $n = 14$ ($10 \leq Re \leq 500$).

Mean deviation of results obtained by formula (2.69) at $n = 14$ from experimental data is 3 to 5%. In calculations concerning carburetion, we will use formula (2.69) at $n = 14$.

Let us note that subsequently the influence of vaporization of the drop and drag coefficient will be disregarded. The influence of deformation on change

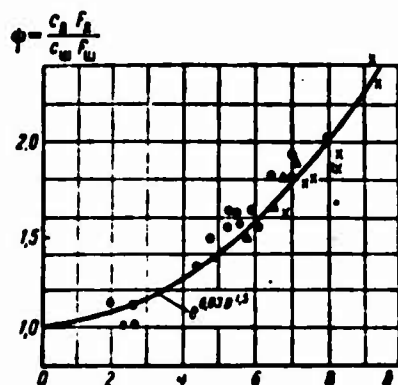


Fig. 2.28. Dependence of function ψ on the deformation criterion of the drop ($Re = 719-1750$). ● — water, × — ethyl alcohol, ▲ — alcohol-soap solution.

of center section and drag coefficient of the drop is large, and is taken into account in the equation of motion (2.66) by introduction of the function $\psi(D)$:

$$\psi(D) = \frac{F_F \cdot c_F}{F_M \cdot c_M},$$

where $D = \frac{\rho_B \cdot u^2 a}{\sigma}$ — criterion of equilibrium deformation of the drop;

u — blowing velocity of the drop;

σ — coefficient of surface tension of the liquid;

F_M, c_M — center section and drag coefficient of a spherical drop;

F_D, c_D — center section and drag coefficient of a deformed drop.

The experimental dependence of function ψ on D is determined by experimental data and is shown in Fig. 2.28.

According to experimental data, in the region $Re = 700$ to 1700 , function ψ does not depend on Re .* Experimental dependence ψ on D in the region of D (0 to 10) can be approximated by the expression

$$\psi(D) = e^{0.03D^{1.5}}. \quad (2.70)$$

Let us describe the process of deformation of the drop. In the first moment, forces of the flow cause fast deformation of the drop. This deformation from its beginning to the moment of maximum flattening ($\psi = \psi_{\max}$) is unbalanced (interval

AC in Fig. 2.29) — external pressure greatly exceeds the pressure of surface tension.

From the moment corresponding to $\psi = \psi_{\max}$, when there exists approximate equilibrium of forces of surface tension and the flow, deformation decreases statically or quasi-statically (interval CO); on this interval the measure of deformation ψ is determined by current values of criterion D .

With entrainment of the drop by the flow, its relative velocity and criterion

D decreases, and function ψ decreases, tending to 1 for the limiting case of a spherical drop.

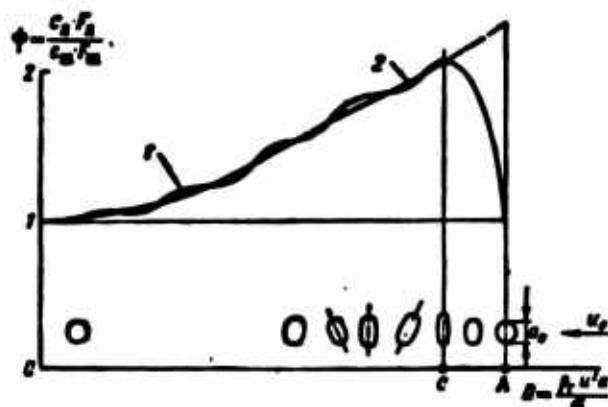


Fig. 2.29. Deformation of a drop entrained by a flow: 1 — actual change of ψ , 2 — accepted dependence $\psi(D) = e^{0.03D^{1.5}}$.

*It is possible to expect that in other ranges of Reynolds numbers, the influence of Re on ψ will not be great.

The value of ψ_{\max} (see Fig. 2.29) depends on magnitude of D at the time of the maximum stage of deformation. If in the beginning of motion the value of D_0 is so large that by the moment of its maximum deformation $D > D_{kp}$, ≈ 10 , then the drop will be split up by the flow.

Calculations show that, for instance, a drop with $a = 200 \mu$ will not be split-up in a flow by PD which is usual for chambers, even at

$$D_0 = \frac{\rho \cdot a^2 \cdot g}{\sigma} \approx 40.$$

The time of critical deformation can be estimated by formula (2.2). Time of stay of the drop in the deformed state ($\psi \neq 1$) is estimated by the formula (2.71). Below there will be derived a formula for determination of time of motion of the drop (2.75). If we assume that in it $k = 0$; $\varphi = 1$, then the formula will take the form

$$\tau_1 = \frac{A}{V u_0} \left[\sqrt{\frac{u_0}{a}} - 1 \right]. \quad (2.71)$$

where

$$\frac{u}{u_0} = \sqrt{\frac{2}{D_0}} \quad (\text{at } D = 2, \psi = 1, \text{ see Fig. 2.28}).$$

From approximate calculations on determination of $\tau_{kp,д}$ [see formula (2.2)] and $\tau_д$, it follows that time of flattening of the drop $\tau_{kp,д}$ composes a small fraction of the total time of stay of the drop in the deformed state (about 2 to 3%). Therefore, during solution of the equation of motion we will disregard change of $\psi(D)$ during the time of flattening of the drop. We will consider that at $\tau = 0$ the drop already is in the deformed state, and with its entrainment by the flow becomes spherical (curve 2 on Fig. 2.29).

If the initial value of $D_0 > D_{kp}$ ($D_{kp} \approx 10$), then we consider that at the time of maximum deformation the magnitude of $\psi(D)$ will reach $\psi(D_{kp}) = 2.56$ (see Fig. 2.28), and during the time of change of D from D_0 to $D_{kp} = 10$, the value of ψ is constant and equal to the average between initial $\psi(D_0)$ and maximum $\psi(D = 10)$:

$$\psi_{\varphi} = \frac{\psi(D_0) + \psi(10)}{2} = \frac{1 + 2.56}{2} = 1.78.$$

As a result of these assumptions during the solution of equation (2.31), the influence of deformation of the drop at the time of its flattening is exaggerated, but errors in the solution will be small, since the initial period of flattening of the drop composes a small fraction of the time of stay of the drop in its deformed state.

Let us proceed to the solution of equation (2.30). Decrease of diameter of the vaporizing drop will be considered by formula (2.163)

$$\left(\frac{u}{u_0}\right)^3 = \left(\frac{u}{u_0}\right)^k.$$

Putting in equation (2.66) values of $d\bar{v}$ from (2.68) and of $a(u)$ from (2.163) and separating variables, we will obtain

$$\frac{1}{\phi\left(\frac{u}{u_0}\right)} \cdot \frac{d\left(\frac{u}{u_0}\right)}{\left(\frac{u}{u_0}\right)^{\frac{1-k}{2}}} = -\frac{2\sqrt{u_0}}{A} dt; \quad (2.72)$$

$$\frac{1}{\phi\left(\frac{u}{u_0}\right)} \cdot \frac{d\left(\frac{u}{u_0}\right)}{\left(\frac{u}{u_0}\right)^{\frac{1-k}{2}}} = -\frac{2}{A\sqrt{u_0}} dL; \quad (2.73)$$

$dL = u dt,$

where L is the coordinate of the drop in a system moving together with the flow with velocity w [see formula (2.67)]:

$$A = \frac{0.197 u_0^{3/2}}{\sqrt{D_0 \gamma_r}}.$$

Function $\phi\left(\frac{u}{u_0}\right)$ in the interval of change of $\frac{u}{u_0} \left[1 + \left(\frac{u}{u_0}\right)_{D=10}\right]$ for the case $D_0 > 10$ will be equal to $\phi\left(\frac{u}{u_0}\right) = \phi_{cr} = 1.78$, and in the interval of $\frac{u}{u_0} \left[\left(\frac{u}{u_0}\right)_{D=10} \text{ to } 0\right]$ at $D_0 \leq 10$

$$\phi\left(\frac{u}{u_0}\right) = e^{0.03 D^{1.5}}.$$

In order to integrate equations (2.72) and (2.73), we will expand function $\frac{1}{\psi(D)}$ in a series:

$$\frac{1}{\psi(D)} = e^{-0.03 D^{1.5}} \approx 1 - 0.03 D^{1.5} + \frac{(0.03)^2}{2} D^3 - \frac{(0.03)^3}{6} D^{4.5} \quad (2.74)$$

(error 6%), where D , if we take into account decrease of the diameter of the vaporizing drop [see (2.163)], is equal to

$$D = D_0 \left(\frac{u}{u_0}\right)^{\frac{3+k}{3}}; \quad D_v = \frac{u_0 x_0^2 p_0}{u_r (k_{cr})}.$$

After integrating equations (2.72) and (2.73), we will obtain

$$\tau = \frac{1}{1-k} \frac{A}{\sqrt{u_0}} \left[\left(\frac{u}{u_0}\right)^{\frac{1-k}{2}} - \eta_1\left(D_0, k, \frac{u}{u_0}\right) \right]; \quad (2.75)$$

$$L = \frac{1}{1+k} A \sqrt{u_0} \left[\eta_1\left(D_0, k, \frac{u}{u_0}\right) - \left(\frac{u}{u_0}\right)^{\frac{1+k}{2}} \right]. \quad (2.76)$$

where $D_0 \leq 10$

$$\begin{aligned} \varphi_1\left(D_0, k, \frac{u}{u_0}\right) &= 1 + \frac{1-k}{2} \left\{ \frac{0.03 D_0^{1.5}}{2.5+k} \left[1 - \left(\frac{u}{u_0}\right)^{2.5+k} - \right. \right. \\ &\quad \left. \left. - \frac{(0.03)^2 D_0^3}{2(5.5+1.5k)} \left[1 - \left(\frac{u}{u_0}\right)^{5.5+1.5k} \right] + \frac{(0.03)^2 D_0^{4.5}}{6(8.5+2k)} \times \right. \right. \\ &\quad \left. \left. \times \left[1 - \left(\frac{u}{u_0}\right)^{8.5+2k} \right] \right\} \right\}, \\ \varphi_2\left(D_0, k, \frac{u}{u_0}\right) &= 1 - \frac{1+k}{2} \left\{ \frac{0.03 D_0^{1.5}}{3.5+k} \left[1 - \left(\frac{u}{u_0}\right)^{3.5+k} \right] - \right. \\ &\quad \left. - \frac{(0.03)^2 D_0^3}{2(6.5+1.5k)} \left[1 - \left(\frac{u}{u_0}\right)^{6.5+1.5k} \right] + \frac{(0.03)^2 D_0^{4.5}}{6(9.5+2k)} \left[1 - \left(\frac{u}{u_0}\right)^{9.5+2k} \right] \right\}. \end{aligned}$$

at $D_0 > 10$

$$\left. \begin{aligned} \varphi_1\left(D_0, k, \frac{u}{u_0}\right) &= \frac{1}{\psi_{cp}} + \frac{\psi_{cp}-1}{\psi_{cp}} \left(\frac{D_0}{10}\right)^{\frac{1-k}{2\left(2+\frac{k}{3}\right)}} + \\ &\quad + \varphi_1\left(10, k, \frac{u}{u_0}\right) - 1, \\ \varphi_2\left(D_0, k, \frac{u}{u_0}\right) &= \frac{1}{\psi_{cp}} + \frac{\psi_{cp}-1}{\psi_{cp}} \left(\frac{10}{D_0}\right)^{\frac{1+k}{2\left(2+\frac{k}{3}\right)}} + \\ &\quad + 1 - \varphi_2\left(10, k, \frac{u}{u_0}\right). \end{aligned} \right\} \quad (2.77)$$

Inasmuch as functions φ_1 , φ_2 (2.77) represent complicated polynomials in u/u_0 , formulas (2.75) and (2.76) are difficult to use during calculations and further analytic computations. Let us simplify these relationships, representing functions φ_1 and φ_2 in dependence only on the initial value D_0 . At $D = 2$, values of ψ differ little from 1 (see Fig. 2.28), and further consideration of the influence of deformation (at $D < 2$) on the trajectory of motion of the drops is not needed. From analysis of formulas (2.77), one may also see that with decrease of relative velocity u , functions φ_1 and φ_2 rapidly approach constant values.

Inasmuch as blowing velocity of the drop sharply decreases over the length (accordingly criterion D decreases still faster), the section of change of D (D to 2) is very small ($x \leq 100$ to 200 mm).

Therefore, during use of solutions (2.75) and (2.76) on the section $x \geq 100$ to 200 mm, functions φ_1 and φ_2 can be simplified by putting in formulas (2.77) the

value $\frac{u}{u_0} = \left(\frac{2}{D_0}\right)^{2+\frac{k}{3}}$. In this case, functions φ_1 , φ_2 will depend only on two variables

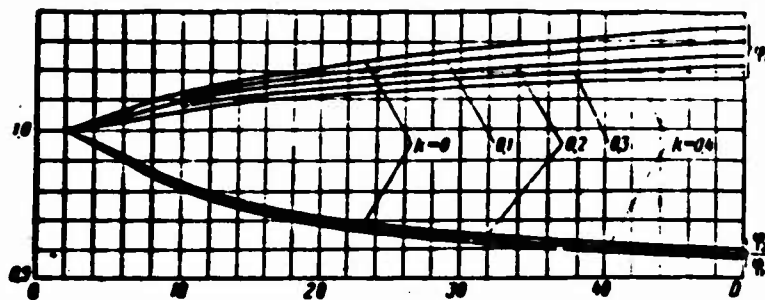


Fig. 2.30. Graph of functions $\varphi_1(D)$ and $\frac{\varphi_2(D)}{\varphi_1(D)}$.

D_0, k . Graphs of the dependence of $\varphi_1, \frac{\varphi_2}{\varphi_1}$ on D_0, k are shown in Fig. 2.30.

In solutions (2.75)-(2.76) and during further computations, instead of the complicated expressions of φ_1, φ_2 (2.77) we will use numerical values of the constants $\varphi_1, \varphi_2/\varphi_1$.

Let us represent equations of the trajectory of the droplet in absolute coordinates. Projections of absolute velocity of the droplet on axes x, y are equal to

$$\left. \begin{aligned} v_x &= u \cos \gamma + w \text{ or } \frac{dx}{dt} = \frac{dL}{dt} \cos \gamma + w, \\ v_y &= u \sin \gamma \text{ or } \frac{dy}{dt} = \frac{dL}{dt} \sin \gamma, \end{aligned} \right\} \quad (2.78)$$

where $\gamma = \text{const.}$

After integration of (2.78) we will have

$$\left. \begin{aligned} x &= w\tau + L \cos \gamma, \\ y &= L \sin \gamma. \end{aligned} \right\} \quad (2.79)$$

In formulas (2.75), (2.76) and (2.79), values of τ, x, y are represented as functions of u . In such a form these formulas are inconvenient for calculations. Let us represent τ, y in dependence upon u, x . For shortening of further computations, we will introduce new variables:

$$\left. \begin{aligned} \bar{\tau} &= \frac{\tau}{u}, \quad \bar{s} = \varphi_1(D_0, k) \frac{1}{1-k} \cdot \frac{A}{\sqrt{u_0}} \cdot \frac{w}{x}, \\ \bar{y} &= \frac{y}{x \tan \gamma}, \quad \bar{u}_x = \frac{\varphi_1(D_0, k)}{\varphi_2(D_0, k)} \frac{1-k}{1+k} \cdot \frac{u_0 \cos \gamma}{u}. \end{aligned} \right\} \quad (2.80)$$

After change of variables, equations (2.75), (2.79) will take the form

$$\bar{\tau} = \bar{s} \left[\frac{1}{\bar{u}_x} \left(\frac{u}{u_0} \right)^{\frac{1-k}{1+k}} - 1 \right]. \quad (2.81)$$

$$1 = \bar{\tau} + \bar{y} \cdot \bar{u}_x. \quad (2.82)$$

$$\bar{y} = \bar{u}_{0x} \left[1 - \frac{1}{\tau_1} \left(\frac{x}{a_0} \right)^{\frac{1+k}{2}} \right]. \quad (2.83)$$

From equations (2.80) and (2.82) it follows that

$$y_p(a, x) = x \lg \tau (1 - \bar{\tau}). \quad (2.84)$$

Replacing u in formula (2.83) by $\bar{\tau}$ from (2.81) and substituting $\bar{y}(\bar{\tau})$ in formula (2.82), we will determine $\bar{\tau}(a, x)$:

$$\bar{\tau}(a, x) = \sqrt{\left[\frac{\bar{a}(1 + \bar{u}_{0x}) - 1}{2} \right]^2 + \bar{a}[1 - \bar{a}\bar{u}_{0x}\Delta] - \left[\frac{\bar{a}(1 + \bar{u}_{0x}) - 1}{2} \right]}. \quad (2.85)$$

where

$$\Delta = 1 - \frac{1}{\frac{v_1}{v_1} \tau_1^{\frac{2}{1-k}} \left(\frac{\bar{\tau}}{\bar{a}} + 1 \right)^{\frac{2k}{1-k}}}.$$

It will not be possible to express function $\bar{\tau}$ in explicit form ($\bar{\tau}$ is contained in Δ).

Values of $\bar{a}\bar{u}_{0x}\Delta$ are order of magnitude less than 1; therefore, τ can be determined by successive approximation; setting $\Delta = 0$, we determine $\bar{\tau}_1(\bar{a}; \bar{u}_{0x})$ by the

nomograph (Fig. 2.31), calculate $\Delta(\bar{\tau}_1)$ and by formula (2.85) calculate $\bar{\tau}_2[\bar{a}; \bar{u}_{0x}; \Delta(\bar{\tau}_1)]$. Maximum divergence between $\bar{\tau}_2$ and $\bar{\tau}_1$ for large drops (100 to 200 μ) will be 5-10% (see § 11 of the present chapter). According to the definition of $\bar{\tau}$ (2.80), time of stay of the drop a_0 on the section 0-x is equal to

$$\tau(a_0, x) = \bar{\tau}(a_0, \bar{u}_{0x}, \Delta) \frac{x}{w}, \quad (2.86)$$

where τ will be determined from (2.85) or (2.88).

Depending upon direction and magnitude of initial velocity of the drops, $\bar{\tau}$ changes in the following way:

- at $\bar{u}_{0x} < 0$ or ($v_0 \cos \alpha < w$); $\bar{\tau} > 1$ — the drop is entrained by the flow;
- at $\bar{u}_{0x} < 0$ or ($v_0 \cos \alpha > w$); $\bar{\tau} < 1$ — the drop is decelerated in the flow;

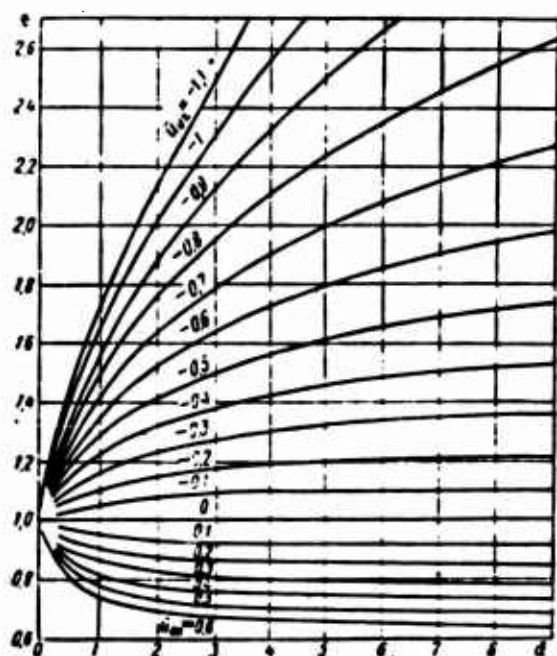


Fig. 2.31. Graph of the function $\bar{\tau}(\bar{a}; \bar{u}_{0x})$.

at $\bar{u}_{Ox} = 0$ or ($v \cos \alpha = w$); $\bar{\tau} = 1$ — the drop moves along axis \bar{Ox} with the flow velocity.

Thus, $y_p(a; x)$ and $\tau(a; x)$ depend on function τ , which in turn depends on variables \bar{a} , \bar{u}_{Ox} [see formulas (2.80) and (2.85)]. During motion of an undeformed drop in a flow, these variables will have the form

$$\begin{aligned} \tau(D_0; k) &= \tau_1(D_0; k) = 1; \\ \Delta &= 1 - \frac{1}{\left(\frac{\bar{\tau}}{\bar{a}} + 1\right)^{\frac{2k}{1-k}}}; \\ \bar{a} &= \frac{1}{1-k} \cdot \frac{A}{\sqrt{u_0}} \cdot \frac{w}{x}, \quad \bar{u}_{Ox} = \frac{1-k}{1+k} \cdot \frac{u_0 \cos \gamma}{w}. \end{aligned}$$

During motion of a nonvaporizing drop ($k = 0$)

$$\bar{a} = \tau_1(D_0; k) \frac{A}{\sqrt{u_0}} \frac{w}{x}; \quad \bar{u}_{Ox} = \frac{\tau_1}{\tau_1} \frac{u_0 \cos \gamma}{w}; \quad \Delta = 1 - \frac{1}{\tau_1^2 - \frac{\tau_1}{\tau_1}}.$$

If the drop moves in a flow without vaporization or deformation, then

$$k=0, \Delta=0, \bar{a} = \frac{A}{\sqrt{u_0}} \frac{w}{x}, \quad \bar{u}_{Ox} = \frac{u_0 \cos \gamma}{w}. \quad (2.87)$$

In this case function $\bar{\tau}$ will depend on two parameters \bar{a} , \bar{u}_{Ox} :

$$\bar{\tau}(\bar{a}, \bar{u}_{Ox}) = \sqrt{\left[\frac{\bar{a}(1+\bar{u}_{Ox})-1}{2}\right]^2 + \bar{a}} - \left[\frac{\bar{a}(1+\bar{u}_{Ox})-1}{2}\right]. \quad (2.88)$$

For convenience of determination of $y_p(a; x)$ and $\tau(a; x)$, on the graph in Fig. 2.31 there is given a nomograph of function $\bar{\tau}(\bar{a}, \bar{u}_{Ox})$. Calculations show that in the case of motion of a deforming vaporizing drop, values of $\bar{\tau}$ can be with sufficient accuracy determined by such a nomograph. Thus, for $k \leq 0.05$ ($t_b < 100^\circ\text{C}$) $D \leq 5$ parameters \bar{a} , \bar{u}_{Ox} can be determined by formulas (2.87) (error in values of $\bar{\tau}$ will not exceed ~5%). When values of k and D_0 are respectively within the limits (0.05-0.1) and (5-10), quantities \bar{a} and \bar{u}_{Ox} should be determined by formula (2.80). Error with use of the nomograph will be not more than 10%. At $k > 0.1$ and $D > 10$, values of $\bar{\tau}$, especially during determination of $y_p(a; x)$, must be determined by the more exact formula (2.85). The case $k < 0.1$; $D_0 < 10$ corresponds to a wide range of regime of motion of the drops. With increase of intensity of vaporization and deformation, the drops are more rapidly entrained by the flow. Large drops of the fuel jet are more strongly deformed and remain longer in the deformed state; therefore, the

influence of deformation on the time of stay in the flow and on coordinates $y_F(a; x)$ of large drops will be larger than for small drops.

Motion of a Droplet in a Flow with Variable Velocity

The problem of motion of a drop in a flow of variable velocity has practical significance during the calculation of trajectories and vaporizability of fuel particles in a combustion chamber. For instance, in a turbojet combustion chamber (TPД), the injector is usually installed directly after the swirler, and drops fall

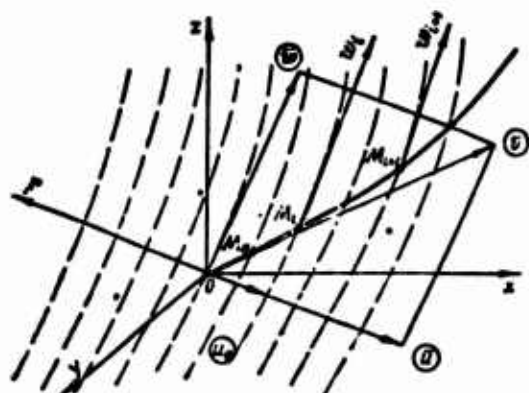


Fig. 2.32. For derivation of the equation of motion of a drop in a flow with variable parameters. — trajectory of drop; — — — flow lines.

within a region of variable velocity. In the chambers of ramjet engines (ПВРД), two-phase flow which contains drops. Thus it is important to establish whether drops flow around the body, following flow lines of the gas, or settle on its surface, moving by inertia (see, for instance, [5]). Furthermore, in considering a variable flow velocity, it is necessary to determine how drops are vaporized in the combustion zone, where speed of gases increases along the length of the combustion chamber.

We will write equations of motion of a drop in field of variable velocity, for which we will select coordinate axes xyz , placing their origin O at the point of beginning of motion (Fig. 2.32). For simplicity we will consider the case of a non-vaporizing drop at maximum deformation $n = \text{const} \approx 29$. Maximum deformation will correspond to the case of the most intense entrainment of the particle by the gas.

Let us assume that

$\bar{v}(v_x; v_y; v_z)$ — absolute velocity of drop;

$\bar{w}(w_x; w_y; w_z)$ — flow velocity (velocity of following);

$\bar{u}(u_x; u_y; u_z)$ — relative velocity of drop at a given point of the flow.

According to equation (2.1) we will write

$$\rho_m \frac{\pi a^3}{6} \frac{d\bar{v}}{dt} = - \frac{n}{\sqrt{\frac{a}{v_a}}} \frac{\rho_m a^3}{2} \frac{\pi a^3}{4} \frac{\bar{u}}{a} \quad (2.89)$$

or

$$\frac{d\bar{v}}{dt} = - \frac{4}{3} n \frac{\rho_m}{\rho_m} \frac{v_a^{\frac{1}{3}}}{a^{\frac{1}{3}}} \sqrt{\bar{u} \cdot \bar{u}} = - \Lambda \sqrt{\bar{u} \cdot \bar{u}}, \quad (2.90)$$

where

$$A = + \frac{3}{4} \pi \frac{\rho_0}{\rho_m} \frac{v_0^{\frac{1}{3}}}{a^{\frac{1}{3}}}.$$

We will write equation (2.90) in projections on the coordinate axes, remembering that $\bar{u} = \bar{v} - \bar{w}$:

$$\left. \begin{aligned} \frac{dx}{dt} &= -A w_x u_x = -A \sqrt{(v_x - w_x)^2 + (v_y - w_y)^2 + (v_z - w_z)^2} (v_x - w_x), \\ \frac{dy}{dt} &= -A w_y u_y = -A \sqrt{(v_x - w_x)^2 + (v_y - w_y)^2 + (v_z - w_z)^2} (v_y - w_y), \\ \frac{dz}{dt} &= -A w_z u_z = -A \sqrt{(v_x - w_x)^2 + (v_y - w_y)^2 + (v_z - w_z)^2} (v_z - w_z), \end{aligned} \right\} \quad (2.91)$$

where w_x ; w_y ; w_z are components of flow velocity.

Initial conditions are $\tau = 0$; $x = x_0$; $y = y_0$; $z = z_0$; $v_x = v_{x0}$; $v_y = v_{y0}$; $v_z = v_{z0}$.

System (2.91) is made up of nonlinear second order differential equations

$\left(v_x = \frac{dx}{dt}; v_y = \frac{dy}{dt}; v_z = \frac{dz}{dt} \right)$ in the functions $x = x(\tau)$; $y = y(\tau)$; $z = z(\tau)$ and cannot

be reduced to quadratures, as this can be done during motion of a drop in a flow with constant velocity. Very frequently it is necessary to deal with an axially symmetric flow. Therefore, we will consider integration of equations for the case of plane motion; we will select a plane passing through the flow axis and the vector of initial velocity of the drop ($v_z = w_z = u_z = 0$). For convenience we will introduce the following designations:

$$u_x = p, \quad u_y = q, \quad v_x x + v_y y = r$$

then system (2.91) will be written in the form

$$\left. \begin{aligned} \frac{dx}{dt} &= -A \sqrt{(x-p)^2 + (y-q)^2} (x-p), \\ \frac{dy}{dt} &= -A \sqrt{(x-p)^2 + (y-q)^2} (y-q), \end{aligned} \right\} \quad (2.92)$$

where $p = p(x; y)$; $q = q(x; y)$ are given functions of the velocity field.

Let us give the most simple method of approximate solution of system (2.92); the path of motion of the drop is divided into small intervals, corresponding to $\Delta\tau$; the flow velocity field at point of every interval is considered to uniform — for instance such that components of the field p and q are equal everywhere on the interval to their values at the initial point of the interval of the partition. Then on every interval equations (2.92) can be twice integrated by one of the methods, presented in the preceding paragraphs. Shifting from interval to interval, we will obtain an approximate solution in the entire region; it will be more accurate, the smaller the

interval $\Delta\tau$. After appropriate transformations, we will find the following relationships in the form of recurrence formulas:

$$u_{i+1} = \pm \frac{4}{(m_i \Delta\tau_i + A_i)^2} + p_i(x_i; y_i), \quad (2.93)$$

$$v_{i+1} = \pm \frac{4}{(m_i \Delta\tau_i + B_i)^2} + q_i(x_i; y_i); \quad (2.94)$$

$$x_{i+1} = x_i + p_i \Delta\tau_i \pm \left\{ -\frac{4}{m_i^2 \Delta\tau_i + m_i A_i} + \frac{4}{A_i m_i} \right\}, \quad (2.95)$$

$$y_{i+1} = y_i + q_i \Delta\tau_i \pm \left\{ -\frac{4}{m_i^2 \Delta\tau_i + m_i B_i} + \frac{4}{B_i m_i} \right\}. \quad (2.96)$$

where

$$m_i = -A \sqrt{u_i} \sqrt{1 + \left(\frac{q_i - v_i}{p_i - u_i} \right)^2};$$

$$A_i = -\frac{2}{\sqrt{|p_i - u_i|}}; \quad B_i = -\frac{2}{\sqrt{|q_i - v_i|}}.$$

Signs (\pm) in formulas (2.93) and (2.95) are taken respectively at $u_i > p_i$ and $u_i < p_i$; signs (\pm) in formulas (2.94) and (2.96) - at $v_i > q_i$, $v_i < q_i$. The given equations permit us to determine parameters of motion corresponding to the initial point $M_{i+1, i+1}$ -th of the interval according to data on parameters of motion of the initial point M_0 . Data for point M_1 are determined from initial conditions at point M_0 . As an example we will present calculations of motion of a drop in the field of an ideal vortex and in the flow around a plate.

Motion of a drop in the field of a vortex. Let us consider a drop which starts to move from the periphery of an air core, being located at the initial moment at a distance $r_0 = 10$ mm from its center; the velocity field of the vortex is determined by expressions known in hydrodynamics:

$$p = \frac{\Gamma y}{x^2 + y^2}; \quad (2.97)$$

$$q = \frac{\Gamma x}{x^2 + y^2}; \quad (2.98)$$

$$r = \sqrt{x^2 + y^2}, \quad (2.99)$$

where $\Gamma = 2\pi w r$.

The magnitude of circulation Γ will be selected from conditions at $r = 10$ mm, $w = 40$ m/sec, which can approximately correspond to the order of magnitude of velocity in the zone counter currents behind the flame-holder; then $\Gamma = 0.4$ m²/sec. Initial velocity of the drop $v = 30$ m/sec and is directed at an angle $\beta_0 = 15^\circ$ to axis Ox . Dimensions of the drops will be selected equal to $a = 10; 20; 40; 60$ μ ; this corresponds to the region of small drops in injectors spectra. The interval of the partition will be taken to be $\Delta\tau = 2 \cdot 10^{-5}$ sec.

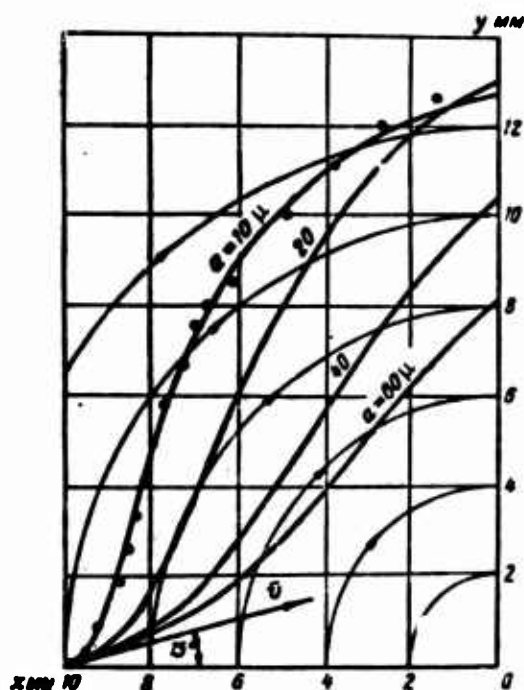


Fig. 2.33. Motion of a drop in a vortex field. $\Gamma = 2\pi w r = 25 \text{ m}^2/\text{sec}$, $w = 40 \text{ m/sec}$ at $r = 10 \text{ mm}$, $v = 30 \text{ m/sec}$.

by the well-known, but more complicated method of Adams [18] for a drop $a = 10 \text{ } \mu$. It is possible to ascertain that results of integration by the simplified method and by the method of Adams turn out to be close.

In Fig. 2.33 there are given results of calculation; from the curves it is seen that a drop possessing sufficient inertia only distorts its own trajectory, having time nevertheless to emerge from the sphere of the vortex (which is arbitrarily bounded by the circle with $r = 10 \text{ mm}$). The smaller the drop, the nearer the slope of its trajectory to the slope of flow lines of the vortex; however, not one of them is involved in vortex motion. In reality, influence of the vortex will be still weaker, since the real value of $n < 30$. This result will agree with experimental data about the almost complete absence of drops behind the flame-holder.

In Fig. 2.33 there are also plotted points which are the result of integration of equations

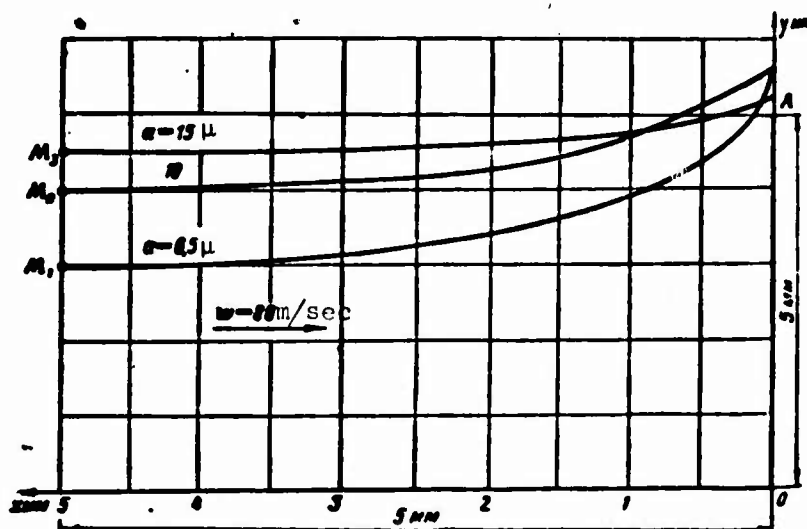


Fig. 2.34. Motion of a drop in a flow around a plate.

Motion of a drop in a flow around a plate. For simplicity, during solution of the problem there were used formulas of flow around a plate set transverse to the flow, which are given in the book of Milovich [19].

In Fig. 2.34 there are plotted trajectories of particles which move together with the flow through points M_1 ; M_2 ; M_3 . The positions of these points are selected so that drops passing through them with the dimension indicated on the drawing will approximately pass near the outer edge of the plate. Larger and larger drops moving through these points (for instance, a drop with $a \approx 10 \mu$ moving through point M_1) must settle on the surface of the plate.

The main mass of particles of liquid, can be seen from Fig. 2.34 (drops with $a \leq 6.5 \mu$ usually correspond in the spectra to 0.2 to 3% of the liquid) during flow around a plate will settle on its surface.

Drops poorly follow flow lines during flow around obstacles, or, in general, during sharp distortion of the flow. This is obtained even for the exaggerated values of drag coefficients of the drops used in calculation, and is explained by the considerable inertia of a drop, the specific gravity of which by almost 800 times exceeds the specific gravity of the flow.

§ 9. MOTION OF DROPS IN A FUEL JET

During calculation of the distribution of fuel, it is necessary to know the trajectories of the drops. Conditions of motion drops in a fuel jet will differ from conditions of motion of a single drop. Experiments in measurement of the distribution drops of the jet in a flow showed that:

1) separation of drops by the flow ($a_0 = 20-200 \mu$) occurs quite weakly; curves of distribution of drops of the given diameter cover almost half of the width of the fuel jet (Figs. 2.35; 2.36);

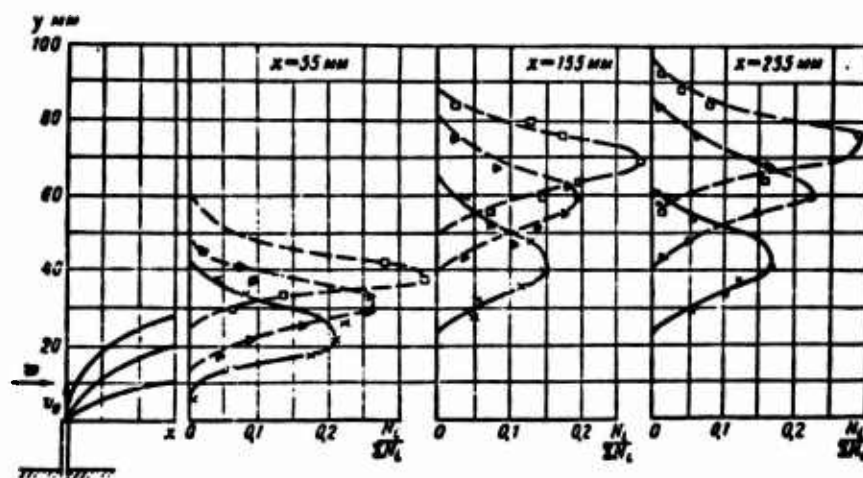


Fig. 2.35. Distribution of drops from a direct-spray injector. Kerosene. $p_B = 1 \text{ atm (abs.)}$, $t_B = 50^\circ\text{C}$, $w = 56 \text{ m/sec}$, $\Delta p_T = 5 \text{ atm (gage)}$, $d_c = 0.4 \text{ mm}$; $\times - a = 41.2 \mu$, $\Delta - a = 82.4 \mu$, $\square - a = 144 \mu$.

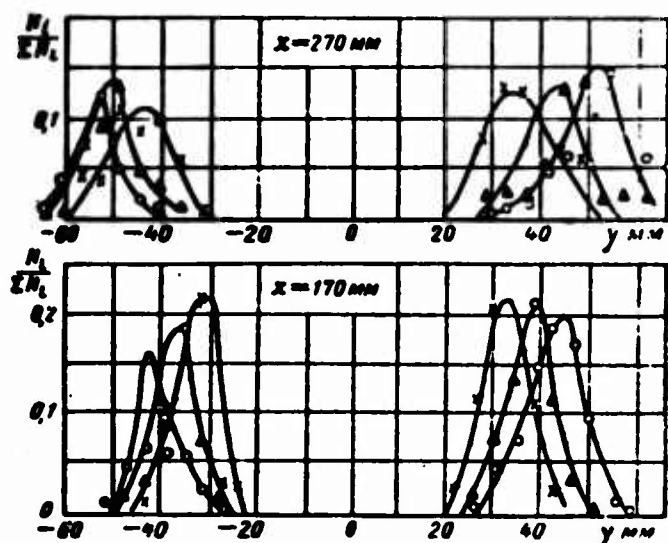


Fig. 2.36. Distribution of drops from swirl injector directed against the flow. Kerosene.

$p_0 = 1 \text{ atm (abs.)}$, $t_0 = 50^\circ\text{C}$, $w = 58 \text{ m/sec}$,
 $\Delta p_T = 5 \text{ atm (gage)}$, $d_0 = 0.8 \text{ mm}$; $x - a =$
 $= 41.2 \mu$, $\Delta - a = 61.8 \mu$, $O - a = 144 \mu$.

2) curves of distribution of drops have clearly pronounced maxima; coordinates of maxima $y_{\text{exc}}(a_1; x)$ represents points of the trajectories of ordered motion of the drops;

3) dispersions of drops of different diameters relative to their trajectories of ordered motion are identical in order of magnitude: small drops ($a_0 = 20 \text{ to } 80 \mu$) are dispersed somewhat more than large drops ($a_0 \approx 100 \text{ to } 200 \mu$).*

Comparison of calculated data on trajectories of ordered motion of drops with experimental data showed the following:

When the swirl injector is directed against the flow or when a direct-spray injector is directed at an angle to the flow experimental trajectories of drops lie above calculated trajectories (Fig. 2.37a). Then the differences $\Delta y = y_{\text{exc}}(a_1; x) - y_p(a_1; x)$ do not depend on diameter of the drops or distance from the nozzle of the injector to section x .

When the swirl injector is directed along the flow, experimental trajectories of ejected drops lie below calculated trajectories (Fig. 2.37b), where the differences $y_p(a_1; x) - y_{\text{exc}}(a_1; x)$ increase with increase of diameter a and distance x .

When the injector is directed along the flow, initial blowing velocities u_0 and

*Spectra of atomization and distribution of drops over the cross section of a fuel jet were determined by the method of catching of drops on a layer of carbon black.

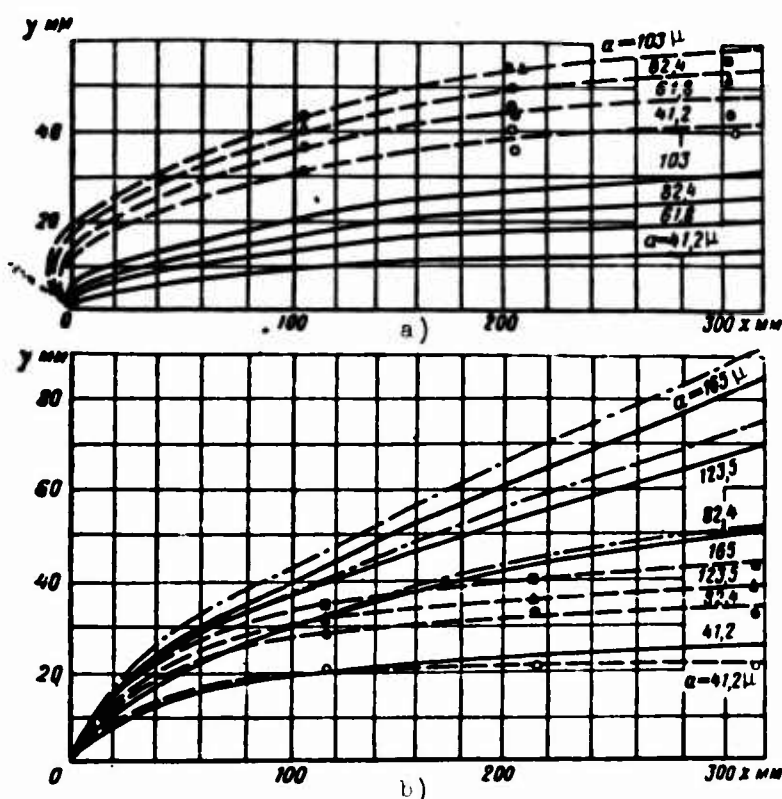


Fig. 2.37. Comparison of calculated trajectories of drops with experimental. a) centrifugal injector swirl injector is directed against the flow. $p_B = 1$ atm (abs.), $t_B = 50^\circ\text{C}$, $w = 58$ m/sec, $\Delta p = 5$ atm (gage), $d_C = 0.8$ mm, $2\alpha = 60^\circ$, $G_m = 5.3$ g/sec; b) direct-spray injector is directed perpendicular to the flow. Kerosene. $p_B = 1$ atm (abs.), $t_B = 50^\circ\text{C}$, $w = 66.4$ m/sec, $\Delta p_T = 8$ atm (gage), $d_C = 0.8$ mm, $2\alpha = 60^\circ$, $G_T = 6.5$ g/sec. — calculated trajectories; — experimental, — calculated trajectories without taking into account deformation of the drop.

accordingly criteria D_0 will be less than 10. At such small values of D_0 , trajectories of drops, if we take into account deformation, differ little from trajectories of undeformed drops (Fig. 2.37b).

Independence of values of $y_{\text{calc}}(a_i; x) - y_p(a_i; x)$ from the diameter of the drop (in the case when the swirl injector is directed against the flow and direct-spray injector is directed perpendicular to the flow) indicates that the influence of deformation on trajectories of drops has been satisfactorily taken into account. Disparity between calculated and experimental trajectories of motion occurs due to interaction of the fuel jet as a whole with the gas flow. Actually, in the region of the root of the fuel jet at a small distance from the injector nozzle, density of distribution of drops is so high that the uniform flow is strongly distorted, penetrating inside the jet. Depending upon the shape of the fuel jet, there will appear different conditions of the flow around it.

Thus, flow around the fuel jet of an injector directed against the flow is similar to flow around a disk, and flow in the region of the jet occurs just as flow around a solid obstacle. Data on measurement of the velocity field before the fuel

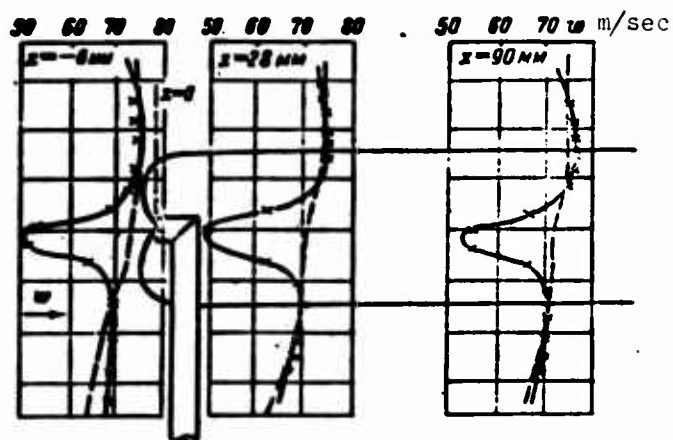


Fig. 2.38. Distribution of air velocity field in the fuel jet of a swirl injector directed against the flow. $p_B = 1 \text{ atm (abs.)}$, $w = 75 \text{ m/sec}$, $\Delta p_T = 20 \text{ atm (gage)}$, $d_c = 0.8 \text{ mm}$.

jet and in its zone (Fig. 3.28) confirm these conclusions.* The higher the feed pressure, the larger the dimensions of the obstacle (fuel jet) and the larger the velocity defect in the wake. The losses occur basically during flow around an obstacle (the jet), and not due to entrainment of the drops. Approximate calculations show that losses of momentum of flow due to entrainment of drops compose 20 to 30% of

total losses calculated according to the velocity defect.

When the swirl injector is directed along the flow, the fuel jet is a well streamlined body, and in this case, as measurements show, perturbations in the flow due to the jet are insignificant. Changes of direction of velocities before the fuel jet cannot be detected by deflections of a silk thread placed in the flow. Losses in the flow around a fuel jet are small, since initial velocities of drops usually are close in magnitude and direction to the flow velocity.

In spite of the fact that perturbations in the flow due to the fuel jet of the injector directed along the flow are small, disparities between calculated and experimental trajectories of motion of drops are obtained to be large (see Fig. 2.37b), because the zone of the fuel jet, due to the high concentration of drops, has high flow friction, and, furthermore, flow of air inside this zone is hampered. The atomization jet is compressed by the flow; this leads to decrease of the atomization angle and displacement of trajectories of particles toward the flow axis.

In other regimes other factors start to have an influence — air located in the zone of the droplets is entrained by them; due to this, inside the jet there occurs rarefaction. The current of air approaching the zone of rarefaction carries drops to the center of the jet. Such influence of the fuel jet on trajectories of drops is analogous to the effect of narrowing of jet with increase of feed pressure of fuel

*Total pressure in a flow containing drops was measured by a special tube, which was made in such a way that in the tube leading to the manometer there did not appear liquid plugs from drops entering the heads. Directions of velocities were determined by deflections of silk thread.

atomized in motionless air. In a flow, this effect of narrowing is more weakly pronounced due to decrease of relative blowing velocity.

It is possible to assume that at high flow velocity and low fuel feed pressure, the first factor will predominate, but at low flow velocity and high feed pressure — the second factor (rarefaction inside the jet) will predominate.

Thus, as a result of interaction of fuel jet with flow, trajectories of ordered motion drops of the jet differ from trajectories calculated for conditions of motion of a single drop. From comparison of calculated data on $y(a_1; x)$ with experimental data there was estimated the influence of flow on the fuel jet and on change of trajectories of the drops.

Formulas for determination of trajectories of drops moving in the presence of a fuel jet have the form

$$y(a; x) = y_p(a; x) + \Delta y,$$

where Δy — experimental correction to computed value of coordinate of drop $y_p(a; x)$.

For a swirl injector directed against the flow:

$$y(a; x) = y_p + 0,049(1 - 1,95k) \mu \quad (2.100)$$

at $k[0.25 - 0.45]$.

For a direct-spray injector

$$y(a; x) = y_p + 0,015[1 + 0,024k] \mu \quad (2.101)$$

at $k[4 - 23]$,

where

$$k = \frac{\tau_1 a_1^2 w}{g r_0} \sin \gamma (\lg \gamma).$$

For a swirl injector directed along the flow:

$$y(a, x) = y_p(a; x) \left[1 - \frac{0,4}{\tau(a_1; x) - 1} \left(\frac{a_0 \cos \gamma}{w} \right) \right] \mu \quad (2.102)$$

at $x[0,1 - 0,5 \mu]; \cos \gamma < 0$.

When the swirl injector is directed along the flow, there are possible three cases of motion of drops from the injector nozzle:

at $\bar{u}_{ax} < 0 \left(\cos \gamma - \frac{a_1 - w}{a_0} < 0 \right);$

at $\bar{u}_{ax} = 0 \quad (\cos \gamma = 0);$

at $\bar{u}_{ax} > 0 \quad (\cos \gamma > 0).$

In the first case the projection of initial velocity of drops on axis Ox is less than the flow velocity; drops are entrained, and the greater the difference between v_{Ox} and w , the stronger will be the influence of flow on the fuel jet on the whole [see formula (2.102)].

In the second case ($\cos \gamma = 0$; $v_{Ox} = w$), influence of flow on the fuel jet will be minimum, and the coordinate of a droplet of the jet should coincide with the coordinate during motion of a single drop $y_p(a_m)$, ($y = y_p$; $\Delta y = 0$).

In the third case ($v_{Ox} > w$; low flow velocities and high feed pressure of fuel) it will be narrowed from rarefaction inside the jet, and coordinate $y(a; x)$ will again become less than $y_p(a; x)$.

For approximate calculations at $\cos \gamma \approx 0$, it is possible to consider that $y = y_p$. Maximum error during determination of $\Delta y(a_1; x)$ can attain 30 to 50%; inasmuch as $y > \Delta y$ (on the average by 2-3 times), error during determination of $y(a_1; x)$ will be about 10 to 15%.

§ 10. DISPERSION OF DROPS RELATIVE TO TRAJECTORIES OF ORDERED MOTION

As was shown above, drops of fuel jet are incompletely separated by flow, and with removal from injector nozzle are noticeably dispersed from their trajectories of ordered motion (see Figs. 2.35 and 2.36).

Dispersion of drops over cross section of flow occurs basically:

- 1) due to turbulence of flow and turbulence induced by fuel jet;
- 2) due to random deviations in initial conditions of motion of drops, namely:
 - disintegration of sheet and splitting up of drops occurs not in the nozzle section, but in a certain volume near it;
 - during disintegration of sheet and splitting up of drops, values and directions of velocities of liquid particles $[v_0(a)]$ will differ from velocity of liquid in the sheet (v_0) - this occurs due to oscillations in the disintegrating sheet and breakaway of drops from its surface;
- 3) due to incomplete separation. As already was said, the region of disintegration of the sheet is weakly ventilated by the flow; therefore separation of drops of the jet will occur very sluggishly; random distribution of particles in the root of the jet will be as if "frozen" on a certain section of motion.

Influence of these factors on dispersion of drops has a random statistical character; therefore, it is possible to expect that experimental distribution of drops will obey the law of normal distribution.

Distribution of drops with diameter a_1 relative to a direct-spray injector can

be represented as diffusion of drops from a point source located on the trajectory of ordered motion of the drop:

$$\bar{N}(a_i; y) = \bar{N}_{\max} y(a_i; x) e^{-\left[\frac{y - y(a_i; x)}{l(a_i; x)}\right]^2}, \quad (2.103)$$

where $y(a_i; x)$ — coordinate of trajectory of ordered motion of drop; $l(a_i; x)$ — mean-square displacement of drops from trajectory $y(a_i; x)$; $\bar{N}(a_i; y) = \frac{N(a_i; y)}{\sum N(a_i)}$; $\sum N(a_i)$ — sum of drops of diameter a_i over cross section of flow; $\bar{N}_{\max}[y(a_i; x)]$ — maximum relative concentration of drops.

Let us check to what degree experimental distribution curves obey the Gauss law (2.103). For this we will represent experimental data on the distribution of drops in the coordinates

$$-\ln \frac{\bar{N}(a_i; y)}{\bar{N}_{\max}(a_i)}, [y - y(a_i; x)]^2. \quad (\text{Fig. 2.39})$$

Experimental points may be plotted in straight lines, and confirm the linear dependence (2.104). Consequently, values of $1/l^2 = \text{const}$ and distribution of drops satisfies the Gauss law:

$$-\ln \frac{\bar{N}(a_i; y)}{\bar{N}_{\max}(a_i)} = \frac{1}{[l(a_i; x)]^2} [y - y(a_i; x)]^2. \quad (2.104)$$

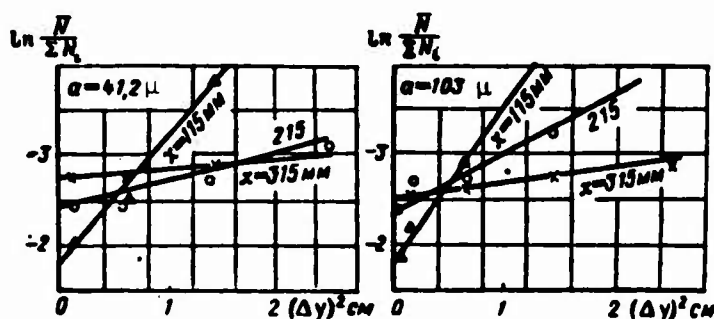


Fig. 2.39. Determination of mean-square displacement of drops $l(a_i; x)$ (swirl injector directed along the flow, $w = 66.4$ m/sec, $\Delta p_T = 8$ atm (gage); $d_c = 0.8$ mm).

For determination of magnitude of $l(a_i; x)$ and its dependence on regime parameters, all data on distribution of drops from direct-spray and centrifugal* injectors

*Distribution of drops from swirl injectors could have been represented as diffusion of drops from an annular source. Inasmuch as experimental curves of distribution are determined approximately, we will represent distribution of drops from swirler by a Gaussian curve.

were processed in the coordinates $-\ln \frac{N(a_i; y)}{N_{max}(a_i)}, [y - y(a_i; x)]^2$. Then according to data

on slopes averaging experimental points of the lines and formula (2.104), there were

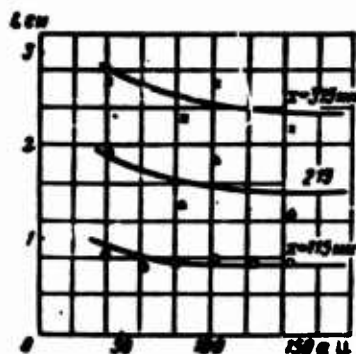


Fig. 2.40. Dependence of displacement $l(a_1; x)$ on diameter of drops (swirl injector, $w = 66.4$ m/sec; $\Delta p_T = 8$ atm (gage); $d_C = 0.8$ mm).

determined values of $l(a_1; x)$. Values of l depending upon surrounding conditions changed in the following way: they increase with increase of x , and weakly decrease with increase of drop dimension (big drops are more weakly entrained by turbulent pulsations).

Dependence of l on diameter of drop and x is shown in Fig. 2.40. During determination of dependence of l on diameter of drops and regime parameters, we considered that mean-square displacement l is the sum of two displacements: displacement of drop under influence of turbulent pulsations $l_{T.K}$ and displacement l_0 appearing due to dispersion of trajectories of drops

as a result of random deviations of initial data and incomplete separation of drops in the root of the jet:

$$l = l_0 + l_{T.K}. \quad (2.105)$$

Displacement l_0 is taken to be proportional to displacement drops of jet perpendicularly to flow, and will be represented in the following form:

$$l_0 \approx B_y,$$

where

$$y \sim u_0 \sin \gamma \cdot \tau; \quad \tau = \frac{x}{w};$$

$$l_0 = Bx \frac{u_0}{w} \sin \gamma. \quad (2.106)$$

Displacement of drops due to turbulent transfer ($l_{T.K}$) will be determined from approximate solution of equation of motion of a drop, carried by turbulent pulsations:

$$\frac{G}{g} \frac{dw}{dt} = -c_x F \frac{\rho_a (u')^2}{2}, \quad (2.107)$$

where

$$\frac{dw}{dt} \approx \frac{w'}{T}; \quad T = \frac{l'}{w}; \quad l' = 0.018 D_{T.};$$

$$w' = c_T \cdot w; \quad u' = w' - u';$$

$$c_x = \frac{40}{Re'} \text{ (see Fig. 2.27)}; \quad Re' = \frac{w w'}{\nu} [4 \div 30];$$

$$G = \gamma \cdot \frac{\pi}{6} a^3; \quad F = \frac{\pi}{4} a^2.$$

Solving (2.107) with such determinations of $dv/d\tau$, c_x , we will obtain

$$v' = \frac{v'}{1 + \frac{a^2 \gamma_r v'}{30 g \mu_s l'}}.$$

Displacement of drop $l'_{T.K}$ in the period T will be determined as

$$l'_{T.K} = v' T.$$

Number of displacements of the drop during time τ is equal to

$$n = \frac{\tau}{T} = \frac{x}{v'}; \quad \tau = \frac{x}{v'}.$$

Displacement of drop under influence of turbulent oscillations of flow in the section x will be

$$l'_{T.K} = n \cdot l'_{T.K} = \frac{x v_T}{1 + \frac{a^2 \gamma_r v_T}{30 g \mu_s l'}}. \quad (2.108)$$

Putting values of l_0 (2.106) and $l'_{T.K}$ (2.108) in (2.105), we will determine l :

$$l = Bx \frac{v_T}{v} \sin \gamma + \frac{x v_T}{1 + \frac{a^2 \gamma_r v_T}{30 g \mu_s l'}}. \quad (2.109)$$

where $B \approx 0.17$.

Constant B is determined after a large number of comparisons of l_{excn} with l_{pacu} . Thus, as a result of more exact solution of equation of motion (2.66) there are found new formulas for calculation of coordinates of drops and time of their stay in the flow, taking into account deformation and vaporization. On the basis of experimental material on distribution of drops in the flow, there is obtained an expression for determination of dispersion of drops from trajectories of ordered motion.

In work [5], distribution of fuel over cross section of flow is considered as a process of turbulent diffusion of drops. Thus, distribution of fuel from a direct-spray injector directed along the flow is represented by the equation of turbulent diffusion of drops from a point source:

$$\frac{\partial f}{\partial x} = \frac{D_x}{v} \left(\frac{1}{y} \frac{\partial f}{\partial y} + \frac{\partial^2 f}{\partial y^2} \right).$$

Solution of the equation has the form

$$f(x, y) = \frac{a_r \cdot \pi R_{tp}^2}{a_s \cdot 4 \pi D_{ex}} e^{-\frac{y^2}{4 D_{ex} \frac{x}{v}}}. \quad (1.09')$$

where $f(x; y) = \frac{c_{\pi}(xy)}{\gamma_B \cdot w}$ — local ratio of fuel to air flow rates;

R_{tp} — radius of pipe;

G_B, G_T - flow rates of air and fuel;

D_R - coefficient of turbulent diffusion of drops.

$$D_R = \frac{\omega r}{1 + \left(\frac{\omega}{2k}\right)^2}; \quad k = \frac{G_B \cdot G}{r \cdot \omega^2};$$

ω - frequency of turbulent oscillations of flow.

Distribution of fuel from swirl injector or direct-spray injector directed against the flow is considered as a process of turbulent diffusion of drops from an annular source of radius R_0 :

$$I(x, y) = \frac{G_T}{G_B} \frac{R_0^2}{R_0^2} \left[I_0 \left(2k \cdot \frac{y}{R_0} \right) \right] e^{-\left(1 + \frac{x^2}{R_0^2}\right)},$$

where

$$k = \frac{R_0^2}{4D_R \cdot \frac{x}{\omega}};$$

I_0 - Bessel function of zero order.

Values of R_0 are determined by experimental dependence of $\frac{R_0}{r}$ on $\frac{\rho_B w^2}{\rho_r v_0^2}$, where r is radius of injected stream of fuel.

Let us determine to what effective values of the coefficient of diffusion of drops the mean-square displacements $l(a_1; x)$ will correspond. From comparison of expression (2.103) and (2.109'), it follows that $D_{\text{eff}} = \frac{w[l(a_1; x)]^2}{4x}$.

According to data on $l(a_1; x)$ (Fig. 2.40), we have

x in cm	11,5	21,5	31,5
l in cm	0,8	1,6	2,5
D_{eff} cm ² /sec	90	195	320

Coefficient of turbulent exchange under these circumstances is equal to

$$D_T = w' l' = 86 \text{ cm}^2/\text{sec},$$

where

$$w' = \varepsilon \cdot w = 0.05 \cdot 64 = 3.2 \text{ m/sec};$$

$$l = 0.018 \cdot D = 0.0027 \text{ m}.$$

It appears that coefficient of diffusion of drops D_{eff} is larger than the coefficient of turbulent exchange in the flow D_T , which, of course, is incorrect. Fictitious values of D_{eff} exceed values of D_T due to the large value of l_0 [see expression

(2.105)], i.e., due to the fact that particles are dispersed in the flow mainly not from turbulent diffusion of drops, but due to variation of initial conditions of motion of drops along their trajectories. If we determine D_{eff} by values of l_T (2.108), then D_T will be, as we see, larger than D_{eff} .

By means of selection of correction factors to the diffusion coefficient, the authors of work [5] succeed in obtaining agreement between calculated data on distribution of fuel with experimental data, but, as follows from the given materials about motion and dispersion of drops, such a description of the process does not encompass the main physical phenomena, and therefore is limited.

§ 11. DISTRIBUTION OF LIQUID PHASE OF FUEL

On the basis of what has been presented about motion of drops of a fuel jet and dispersion of them, it is possible to present the following model of the phenomenon

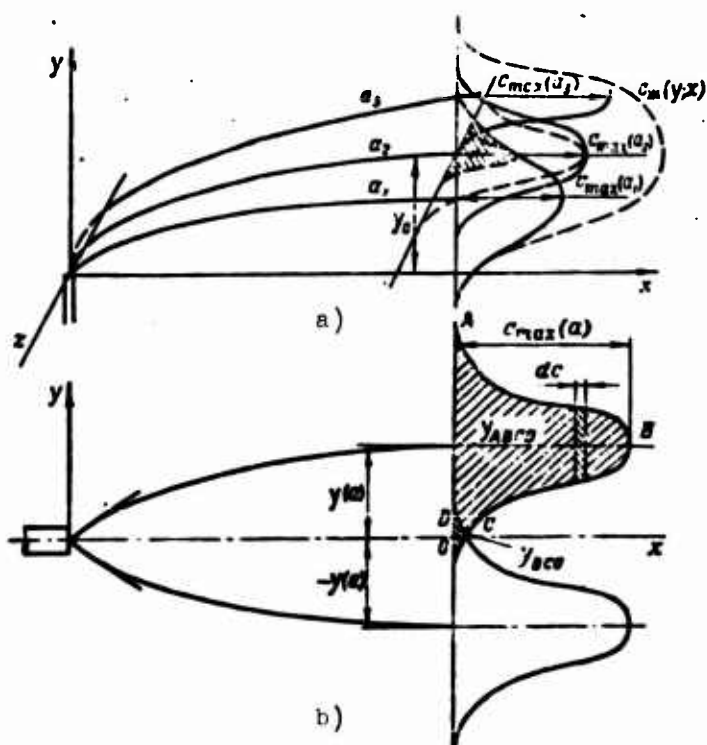


Fig. 2.41. For calculation of distribution of liquid phase of fuel. a) for direct-spray injector; b) for swirl injector.

and a scheme of calculation of distribution of liquid phase of fuel in the jet.

During atomization of an injector of fuel with flow rate G_T , there will be formed a spectrum of drops $V(a_1)$. For carrying out of calculation, we will break the spectrum of drops into groups with average diameter a_1 in the interval of every group. As a result of motion of particles and dispersion of them relative to average trajectories, we will have in section x a series of distribution of curves of drops a_1 for a direct-spray injector (Fig. 2.41a) and for a swirl injector (2.41b).

Absolute density of distribution of the drops a_1 will depend on the percentage of the drops in the spectrum and is proportional to $\Delta V(a_1)G_T$.

Specific fuel flow rate from group of drops a_1 at point $(y; x)$ is proportional to density of distribution of the drops [see expression (2.103)] and is equal to

$$\frac{c(a; y)}{c_{\max}(a; x)} = e^{-\left[\frac{y-y(a; x)}{l(a; x)}\right]^2}. \quad (2.110)$$

Composing the weight balance by formulas (2.111) and (2.113), we will determine c_{\max} . For a direct-spray injectr

$$\Delta V(a) G_r = 2\pi \int_0^{\bar{y}} c(a; y) |y - y(a; x)| dy. \quad (2.111)$$

Integrating (2.111), we will obtain

$$c_{\max}(a; x) = \frac{\Delta V(a) G_r}{\pi [l(a; x)]^2}. \quad (2.112)$$

For a swirl injectr

$$\begin{aligned} \Delta V(a) G_r = F_{ABCD} + F_{DC0} = \pi \int_0^{\bar{y}} \left\{ \left[y(a; x) + l(a; x) \sqrt{\ln \frac{c_{\max}}{c}} \right]^2 - \right. \\ \left. - \left[y(a; x) - l(a; x) \sqrt{\ln \frac{c_{\max}}{c}} \right]^2 \right\} dc + 4\pi c_{\max} \int_0^{\bar{y}} e^{-\left[\frac{y-y(a; x)}{l(a; x)}\right]^2} \times \\ \times y dy. \end{aligned} \quad (2.113)$$

According to (2.110),

$$y = y(a; x) \pm l(a; x) \sqrt{\ln \frac{c_{\max}}{c}};$$

during integration of the first term we use the substitution:

$$\ln \frac{c_{\max}}{c} = e^t.$$

After integration of (2.113), we will obtain

$$c_{\max}(a; x) = \frac{\Delta V(a) G_r}{2\pi^{3/2} l(a; x) y(a; x) Y \left[\frac{y(a; x)}{l(a; x)} \right]}, \quad (2.114)$$

where

$$Y \left[\frac{y(a; x)}{l(a; x)} \right] = \frac{l(a; x)}{y(a; x)} e^{-\left[\frac{y(a; x)}{l(a; x)}\right]^2} + \Phi \left[\sqrt{2} \frac{y(a; x)}{l(a; x)} \right]$$

(Φ - Laplace function).

For $\frac{y(a_1; x)}{l(a_1; x)} \geq 1$, function $Y \approx 1$.

Cases when $\frac{y(a_1; x)}{l(a_1; x)} < 1$ occur very rarely (at high flow rate and low feed pressure of fuel).

During calculation of distribution of fuel in the jet, we consider that during motion and dispersion of drops, between them there is no interaction. Then specific

flow rate of liquid phase at every point of the jet can be represented as the sum of specific flow rates of fuel made up of those drops of the spectrum which land at the given point:

$$c_{\Sigma}(y, x) = \sum_{a_{\min}}^{a_{\max}} c_{\max}(a_i, x) e^{-\left[\frac{y - y(a_i, x)}{4(a_i, x)}\right]^2}, \quad (2.115)$$

where for a direct-spray injector we will determine c_{\max} by formula (2.112); $y(a_i, x)$ - by (2.101); for a swirl injector we will determine c_{\max} by formula (2.114); $y(a_i, x)$ - for the injector directed along the flow by formula (2.102); against the flow - by (2.100); $l(a_i, x)$ - by formula (2.109).

During vaporization of drops, distribution of liquid phase at a given point of the fuel jet can be determined by the formula

$$c_{\Sigma, \text{vap}}(x, y) = \sum_{a_{\min}}^{a_{\max}} c_{\max}(a_i, x) \left(\frac{a}{a_0}\right)^3 e^{-\left[\frac{y - y(a_i, x)}{4(a_i, x)}\right]^2}. \quad (2.116)$$

Determination of $\left(\frac{a}{a_0}\right)^3$ is given in § 16 of the present chapter.

In the particular case, distribution of fuel in section z (Fig. 2.41a) during its atomization by a direct-spray injector is equal to

$$c(z, y_0, x) = \sum_{a_{\min}}^{a_{\max}} c_{\max}(a_i, x) e^{-\left[\frac{\sqrt{x^2 - y_0^2} - y(a_i, x)}{4(a_i, x)}\right]^2}.$$

Comparison of Calculated Data on Distribution of Liquid Phase of Fuel with Experimental Data

Data on distribution of fuel in the case of intense vaporization for swirl injectors directed along or against the flow, are shown in Figs. 2.42; 2.59; 2.60.

Distribution of liquid phase of fuel was determined by the volume of liquid ΔV entering intake pipes of the rake probe:

$$c_{\Sigma} = \frac{\gamma \cdot \Delta V}{\frac{\pi}{4} d_{\text{tp}}^2 \cdot h} = \frac{\gamma \cdot h}{\pi} \left(\frac{d}{d_{\text{tp}}}\right)^2 \text{ g/cm}^2 \text{ sec.}$$

where h - height of column of liquid in measuring holes (or tubes) into which liquid flows from the probe;

d - diameter of measuring holes;

d_{tp} - diameter of inlets of intake tubes of rake probe.

Comparison of calculated and experimental results on the distribution of liquid phase at different preheating temperatures of fuel is shown in Fig. 2.60. This

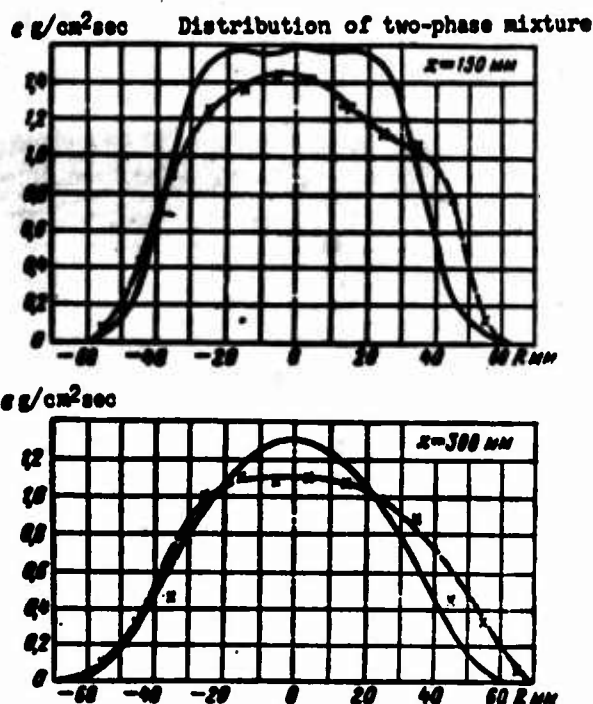
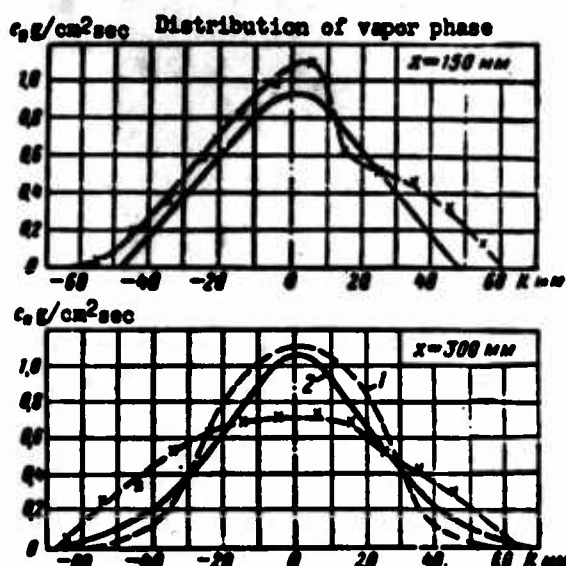
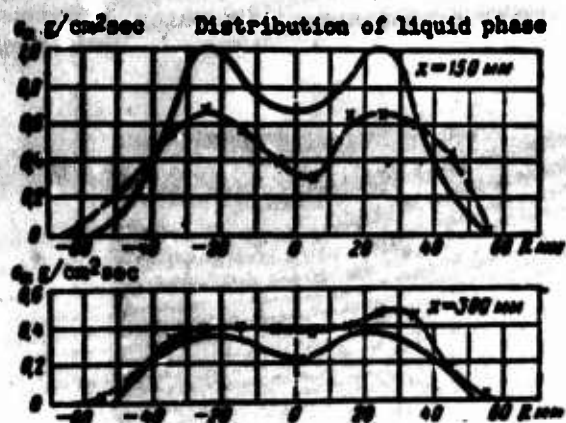


Fig. 2.42. Comparison of calculated data on distribution of fuel with experimental data (swirl injector directed against the flow; fuel is gasoline). $p_B = 1$ atm (abs.), $t_B = 45^\circ\text{C}$, $w = 55$ m/sec, $\Delta p_T = 15$ atm (gage), $t_{O_T} = 20^\circ\text{C}$, $G_T = 7.5$ g/sec, $d_c = 0.75$ mm, $2\alpha = 60^\circ$. —x— equipment, — calculation. 1 — distribution of vapor due to removal of vapor by the flow; 2 — distribution of vapor taking into account turbulent diffusion.

example is interesting due to the fact that at experimental values of p_T , α_{pacn} , w projection of outflow velocity of fuel v_{Ox} was close to flow velocity w .

As was noted above (see § 3 of the present chapter), for such conditions it is possible to disregard influence of flow on the fuel jet, and during determination of $c_{\text{max}}(x; y)$ to consider that $y(a_1; x) = y_p(a_1; x)$. Satisfactory coincidence of experimental and calculated data on the distribution of $c_{\text{max}}(x; y)$ (see Fig. 2.60) showed that narrowing of the jet with increase of preheating temperature occurs only due to displacement of trajectories of drops toward center of the jet as a result of this vaporization and deformation.

From the given material it is clear that calculated data on distribution of liquid phase of fuel will on the whole satisfactorily agree with experimental data.

Consequently, methods of calculation by determination of the atomization spectrum, trajectories of drops, their vaporization and dispersion are basically correct.

As will be shown below, consideration of dispersion of drops during consideration of distribution of liquid phase is necessary for calculation of distribution of degree of vaporization over the cross section of the fuel jet. Data on distribution of only liquid phase can be rapidly calculated by the formula proposed by Yerastov:

$$c_x(x, y) = \frac{G_T \Delta V(a_i)}{2x \cdot y(a_i; x) \cdot \Delta y},$$

where

$$\Delta y = \frac{y(a_{i+1}; x) - y(a_{i-1}; x)}{2}.$$

This formula is valid under the assumption that drops of the fuel jet are separated by the flow and in the ring Δy there will travel only particles of dimension a_i , the amount of which is $G_T \Delta V(a_i)$. Values of $y(a_i; x)$ should be determined by formula (2.84), and parameters \bar{a} , \bar{u}_{Ox} — without taking into account deformation of drops $\varphi_1 = \varphi_2 / \varphi_1 = 1$.

Influence of interaction of fuel jet with flow on change of trajectories of drops is considered by introduction of empirical corrections n to parameter \bar{a} :

$$\bar{a} = \bar{a} \frac{1}{1-k} \cdot \frac{A}{\sqrt{u_0}} \frac{w}{x},$$

where when injector is directed along the flow $n = 29$ to 31 ; when injector is directed against the flow $n = 18$ to 20 .

For illustration of the above formulas, we will consider the following example.

Example of Calculation of Distribution of Liquid Phase of Fuel

I. Initial Data for Calculation

1. Temperature of flow $t_B = 200^\circ\text{C}$.
2. Flow velocity $w = 86$ m/sec.
3. Pressure in flow $p_B = 1$ atm (tech.).
4. Intensity of turbulence $\epsilon_T = 5\%$.
5. Scale of turbulence $l' = 0.0818 \cdot D_{Tp} = 2.7$ mm, $D_{Tp} = 150$ mm.
6. Swirl injector directed against flow (fuel is kerosene).
7. Angle of atomization cone $2\alpha = 82^\circ$.
8. Feed pressure of fuel $\Delta p_T = 2$ atm (gage).
9. Fuel flow rate $G_T = 8.73$ g/sec.

10. Relative initial velocity of drops $u_0 = 103$ m/sec.
11. Angle of inclination of relative velocity vector to axis $\gamma = 108^\circ 30'$.
12. Atomization spectrum of drops $V(a)$ (see § 4 of the present chapter).
13. Initial temperature of fuel $t_0 = 45^\circ\text{C}$.
14. Length of section of motion of drops $x = 365$ mm.

Data of calculation are reduced to the following table.

Number	$a \mu$	30	40	60	80	100	120		
1	D_0	6,3	12,6	18,9	25,2	31,5	38		
2	$\varphi_1(D_0)$	1,06	1,14	1,18	1,22	1,25	1,27		
3	φ_2/φ_1	0,91	0,785	0,710	0,67	0,64	0,62		
4	σ	0,0085	0,072	0,518	0,82	1,17	1,57		
5	$\frac{\sigma}{\rho_B}$	-0,66	-0,73	-0,675	-0,635	-0,61	-0,59		
6	$\frac{\sigma}{\rho_B u_0}$	1,08	1,15	1,25	1,325	1,39	1,435		
7	$\frac{\sigma}{\rho_B u_0^2}$	1,071	1,174	1,27	1,39	1,46	1,50		
8	$y_p(a_i; x)$ см	0,357	0,875	1,36	1,95	2,31	2,52		
9	$y(a_i; x)$ см	3,4	3,91	4,4	4,99	5,35	5,56		
10	$l(a_i; x)$ см	2,15	1,58	1,34	1,24	1,19	1,16		
11	$\Delta V(a_i)$	0,15	0,235	0,23	0,17	0,086	0,07		
12	$c_{\max}(a_i; x)$	0,0172	0,0298	0,0306	0,0215	0,0105	0,0085		
13	$(a/a_0)^3$	0	0,425	0,63	0,735	0,80	0,84		
14	$c_{\max \text{ ncn}}(a_i; x)$	0	0,0125	0,0193	0,0158	0,0084	0,0071		
15	$c_{\max \text{ ncn}}(a_i; x) \times$ $\times \sigma \left[\frac{\bar{y} - y(a_i; x)}{l(a_i; x)} \right]$	y см							
		1		0,000126					
		2		0,00042					
		3		0,0091	0,000775				
		4		0,01245	0,00657	0,00126			
		5		0,00787	0,0176	0,0063	0,00017		
		6		0,00222	0,0158	0,0158	0,0077		
	7		0,00032	0,0046	0,00812	0,00528			
				0,000185	0,00117	0,00125	0,00153		
Number	y см	0	1	2	3	4	5	6	7
16	$c_{\text{н. нcn}}(x; y)$	0,000252	0,00042	0,0097	0,0206	0,0378	0,0472	0,0255	0,0041
17	$c_{\text{н}}(x; y)$	0,00354	0,00594	0,0139	0,0588	0,0782	0,078	0,0383	0,0158
18	$Z \%$	99,3	99,3	71	55	51,7	39,5	33,5	24

II. Notes and Auxiliary Calculations (According to Reference Numbers of the Table)

$$1. D_0 = \frac{\rho_B u_0^2}{\sigma} = 31.5 \frac{\sigma}{100} \mu,$$

where

$$\sigma = 0.0258 \text{ kg/m}; \quad \rho_B = 0.0074 \text{ kg} \cdot \text{sec}^2/\text{m}^4; \quad u_0 = 103 \text{ m/sec}.$$

2. According to Fig. 2.49, at $t_B = 200^\circ\text{C}$ and $p_B = 1 \text{ atm (abs.)}$, $t_p = 112^\circ\text{C}$.

By formula (2.169) we will determine t_p' : $t_p' = 103.5^\circ\text{C}$.

3. By Fig. 2.52 we will determine $k(t_p') = 0.114$.

Values of $\varphi_1(k, D_0)$ and φ_2/φ_1 will be determined by Fig. 2.50 at $k = 0.114$.

$$4. \quad \bar{a} = \frac{0.19 \gamma_1 (a_1)^{2/3}}{\sqrt{g \gamma_1 (a_1)^{2/3} \gamma_2 (a_2)^{2/3}}} \cdot \frac{v}{x} \cdot \frac{\gamma_1}{1-k} = 0.94 \gamma_1 \left(\frac{a_1 \mu_1}{100} \right)^{2/3}.$$

$$5. \quad \bar{a}_{0x} = \frac{a_1 \cos \gamma}{u} \cdot \frac{1-k}{1+k} \cdot \frac{\gamma_1}{\gamma_2} = -0.95 \frac{\gamma_1}{\gamma_2}; \quad \cos \gamma = -0.985.$$

6. We will determine $\bar{\tau}_0$ for given \bar{a} , \bar{u}_{0x} by Fig. 2.31.

7. We will determine $\bar{\tau}_0$ at given $\bar{\tau}_0$, \bar{a} , \bar{u}_{0x} by formula (2.85).

$$8. \quad y_p(a_i; x) = x \lg \gamma (1-\bar{\tau}) = 3.3(1-\bar{\tau}) \text{ cm}; \quad \lg \gamma = -0.1485;$$

$$9. \quad y(a_i; x) = y_p + \Delta y = y_p + 3.06 \text{ cm}.$$

$$10. \quad l(a_i; x) = x \left[0.17 \frac{a_1 \sin \gamma}{u} + \frac{c_r}{1 + \frac{c_r^2 \gamma_1 u'}{30 g \cdot \rho \cdot d^2}} \right] = 1.00 + \frac{0.064}{1 + 16.4 \left(\frac{a_1 \mu_1}{100} \right)^2} \text{ cm}.$$

11. Data on the atomization spectrum will be determined from the example given in § 4, Chapter II.

$$12. \quad c_{\max}(a_i; x) = \frac{\Delta V(a_i) G_r}{2 \pi^{1/2} \gamma \cdot l(a_i; x) \cdot y(a_i; x)} = 0.785 \frac{\Delta V(a_i)}{l(a_i; x) y(a_i; x)} \gamma = 1$$

13. See data on vaporization of drops in § 16, Chapter II.

Comparison of calculated data of this example on the distribution of liquid phase of fuel and degree of vaporization with experimental data is shown in Fig. 2.59b. Agreement of calculated and experimental data on $c_{\text{ж.исп}}$ is satisfactory; disagreement between them with respect to degree of vaporization is due to the insufficient accuracy of calculations of dispersion of drops in the center of the jet.

§ 12. DISTRIBUTION OF VAPOR PHASE AND TWO-PHASE MIXTURE DURING ATOMIZATION OF FUEL IN A SWIRL INJECTOR

Distribution of vapor fuel in a flow during vaporization of drops of the jet occurs in the following way: fuel vapors are blown off from drops, and by the action

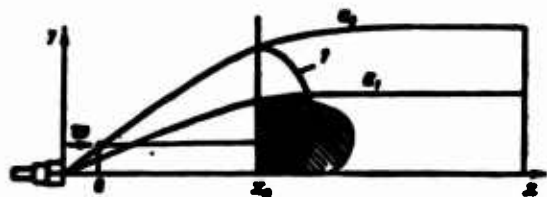


Fig. 2.43. For calculation of distribution of vapor phase formed as a result of removal of vaporized fuel from drops by the flow. 1 - distribution of vapor from drop a_2 .

of turbulent diffusion are spread over the cross section of the flow. During entrainment of drops (section 0- x_0 in Fig. 2.43) the blown off vapors pass along flow lines, and trajectories of motion of particles of vapor do not coincide with trajectories of motion of the drops. When drops are entrained by the flow (section x_0 - x), we may assume that trajectories of motion of

vapors blown from the drops coincide with trajectories of motion of the drops.

We will determine the distribution of vapor without taking into account turbulent diffusion. The section of entrainment of drops where their trajectories of motion are strongly distorted is small. Therefore, for simplification of calculation of removal of vapors on this section we will make the following assumptions:

- 1) rate of vaporization of drops along path $y[0 \text{ to } y(a_1; x)]$ is constant;
- 2) we will not consider dispersion of drops;
- 3) we do not consider the fact that during passage of the flow through the fuel jet, flow lines will be distorted (we consider that fuel vapors will move along the straight lines of initial motion of the flow).

Under these conditions, distribution of vapor in section x_0 can be determined by the formula

$$q(y; x_0) = \frac{G_r}{2xy\Delta y} \Sigma \Delta V(a_i) \Delta Z(a_i; x_0). \quad (2.117)$$

where Δy — interval of partition over the depth of the jet (usually $\Delta y = 0.5$ to 1 cm);

$\Delta Z(a_1; x_0)$ — degree of vaporization during passage of drop through interval Δy ;

$$\Delta Z(a_i; x_0) = \frac{Z(a_i; x_0)}{\frac{y(a_i; x_0)}{\Delta y}};$$

at $y_1 > y(a_1; x)$ we have $\Delta Z = 0$, $y(a_1, x_0)$ — coordinate of drop a_1 in section x_0 .

Determination of $Z(a_1; x_0)$ is given in § 15, Chapter II.

On section x_0-x , where drops are mainly entrained by the flow, distribution of vapor formed during vaporization of drops on the interval $\Delta x = x_{k+1} - x_k$ will be determined by the relationship

$$\Delta q(y; x_{k+1}) = \Sigma_{a_{k+1}}(a_i; x_{k+1}) \left\{ \left[\frac{a(x_0)}{a_0} \right]^2 - \left[\frac{a(x_{k+1})}{a_0} \right]^2 \right\} \frac{1 - \frac{y(a_i; x_{k+1})}{y(a_i; x_0)}}{\left[\frac{a(x_{k+1})}{a_0} \right]^2}. \quad (2.118)$$

Summing specific vapor flow rates calculated on the section of entrainment of drops (0 to x) and on the section where drops are entrained (x_0 to x_1), we will determine distribution of vapor fuel formed as a result of removal of vapors by the flow:

$$q(x, y) = q(x; y) + \sum_b \Delta q(x_b; y). \quad (2.119)$$

Let us consider how the profile of concentrations of vapor obtained on the assumption of removal of vapor is spread out due to turbulent mixing. Equation of diffusion in cylindrical system of coordinates with axis Ox located along the axis of the injector for nonswirling flow can be written as:

$$\frac{\partial \bar{c}}{\partial x} = \frac{D_T}{\sigma} \left(\frac{1}{y} \frac{\partial \bar{c}}{\partial y} + \frac{\partial^2 \bar{c}}{\partial y^2} \right) + \frac{\partial q}{\partial x}, \quad (2.120)$$

where $\frac{\partial}{\partial x} q$ — density of sources of vapor fuel;

D_T — coefficient of turbulent diffusion;

\bar{c} — concentration of vapor in g/cm³.

Concentration of vapor is connected with specific flow rate by the expression

$$\bar{c} = c_n \cdot w.$$

According to data of Gol'denberg [20], coefficient of turbulent mixing has the following values:

$$D_T = 1.1 \cdot 10^{-3} \cdot w_{cp} \cdot d_{cp} \quad (Re > 4 \cdot 10^4);$$

$$D_T = \frac{9 \cdot 10^{-3}}{Re^{0.16}} w_{cp} \cdot d_{cp}; \quad (Re [3,000 \div 3 \cdot 10^4]).$$

$$Re = \frac{w_{cp} \cdot d_{cp}}{\nu_s}.$$

where w_{cp} — average volume rate of flow.

In the diffusion equation (2.120), sources of vapor (evaporating drops) are distributed over the entire volume of the fuel jet; representation of function q by an analytic expression with which it would be possible to solve this equation is impossible.

Representing derivatives $\frac{\partial \bar{c}}{\partial y}$, $\frac{\partial^2 \bar{c}}{\partial y^2}$, $\frac{\partial \bar{c}}{\partial x}$ in terms of their finite increments, we will write equation (2.120) in the following form:

$$\bar{c}_{k,k+1} - \bar{c}_{k,k} + \frac{\Delta q_{k+1,k}}{\sigma(x_{k+1,k})} + \frac{\Delta x D_T}{(\Delta y)^2} \left(\bar{c}_{k+1,k} + \bar{c}_{k-1,k} - 2\bar{c}_{k,k} + \frac{\bar{c}_{k,k} - \bar{c}_{k-1,k}}{\frac{y}{\Delta y}} \right). \quad (2.121)$$

Boundary conditions:

in center of the jet $\bar{c}_{1,k} = \bar{c}_{-1,k}$ (we assume a symmetric distribution of vapor relative to an axis Ox);

on the wall $D_T = 0$.

Initial conditions:

as the initial distribution of vapor $\bar{c}_{1,1}$ we take the distribution of vapor calculated

on the interval $[0+x_0]$ $\left(\bar{c}_{1,1} = q \frac{(y_0 x_0)}{u(y_0 x_0)}\right)$.

Distribution of specific flow rates of two-phase mixture of fuel can be expressed by the formula

$$c(x, y) = c_m(x, y) + c_a(x, y). \quad (2.122)$$

where $c_m(x, y)$ — will be determined by formula (2.116);

$$c_a(x, y) = \bar{c}(x, y) \cdot w(x, y).$$

Comparison of calculated data with experimental data on the distribution of vapor in a two-phase mixture is shown in Fig. 2.42. Calculation of distribution of vapor

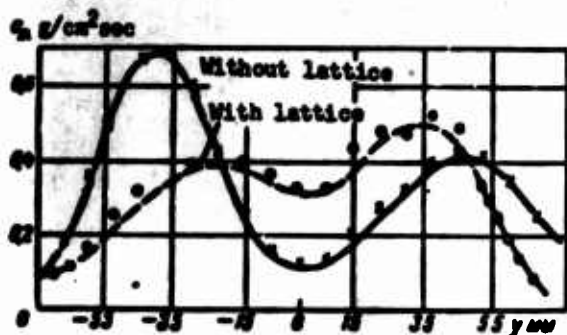


Fig. 2.44. Influence of turbulence induced by a lattice on the distribution of liquid phase of fuel (swirl injector directed against the flow; fuel — kerosene). $p_0 = 1$ atm (abs.), $t_0 = 240^\circ\text{C}$, $w = 76$ m/sec, $\Delta p_T = 1.3$ atm (gage), $t_{OT} = 57^\circ\text{C}$, $d_0 = 1.2$ mm.

is very labor-consuming. Therefore, it is of interest, on the basis of working formulas for determination of liquid and vapor phases of fuel and experimental data, to conduct qualitative analysis of the influence of parameters of the flow and conditions of atomization of fuel on its distribution in the flow.

Influence of surrounding conditions (turbulence and pressure in flow, preheating of fuel, feed pressure, characteristics of injector d_0 , 2α , μ_0 and its position in

the flow) on distribution of vapor phase and two-phase mixture will mainly show up in the change of the distribution of the liquid phase of the fuel.

Influence of turbulence. With increase of intensity of turbulence ϵ_T by means of installation of turbulizing lattices, distribution of liquid phase of fuel is changed in the following way:

During atomization of fuel by a direct-spray injector, the inner boundary of the jet (where small drops move) becomes indistinct and the outer boundary remains constant; during atomization of fuel by a swirl injector, distribution of fuel in center of jet becomes more uniform (Fig. 2.44). Such changes in distribution of liquid phase with increase of ϵ_T are due to increase of dispersion of small drops of the jet.

On the whole, the influence of turbulence of flow on distribution of liquid phase is small, but diffusion rate of vapor will noticeably increase with increase of intensity of turbulence. since $D_T = l'w'$, and $w' = \epsilon_T w$.

Influence of pressure in a flow. Change of pressure strongly affects distribution of liquid phase of fuel. Change of pressure affects distribution of vapor phase of fuel by change of distribution of liquid phase (sources of vapor) and coefficient of turbulent diffusion $D_T \sim \epsilon_T$, and $\epsilon_T \sim (p/p_0)^{0.25}$.

With decrease of pressure drops will be more slowly entrained by the flow, the fuel jet will "open up," and the distribution of vapor will be more uniform over the

flow section. With increase of pressure, flow will "close" the fuel jet - accordingly evaporated fuel will be concentrated in a narrow zone.

As it was shown in §§ 4 and 15, Chapter II, change of pressure within the range of 0.5-2 atm (tech.) weakly affects atomization of fuel and speed of evaporation of drops.

Influence of preheating of fuel.

Spreading out of liquid and fuel without preheating ($t_{OT} \approx 20$ to 40°C) occurs in the following way:

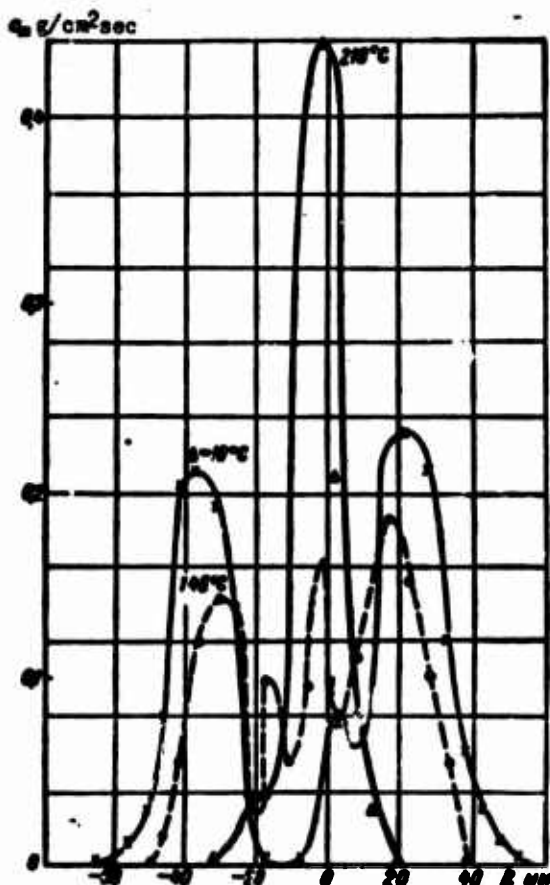


Fig. 2.45. Influence of preheating of fuel on its distribution over the flow section (swirl injector directed along the flow, fuel - kerosene).

$p_B = 1$ atm (abs.), $t_B = 50^\circ\text{C}$, $w = 53$ m/sec, $\Delta p = 20$ atm (gage), $x = 100$ mm).

G in g/sec	0.8	0.1	7.8
t_B in $^\circ\text{C}$	10	140	210
$q_{0.5}$	0.77	0.72	0.11

G - fuel flow rate according to data of distribution of specific flows of liquid phase in a flow.

Close to the injector (see Fig. 2.42; $x \approx 150$ mm), the profile of liquid phase has two sharply outlined maxima. Moreover, as a result of intense evaporation of small drops, in the center of the jet there will be formed much vapor, and the profile

of evaporated fuel will have a maximum in its center. With further increase of distance from the injector, due to turbulent mixing, profiles of liquid and vapor fuel ($x = 300$ mm) are equalized.

If fuel is preheated (gasoline to 20 to 80°C, kerosene to 40 to 160°C), then due to the more intense evaporation, the picture of distribution of liquid and vapor fuel will be sharply changed (Fig. 2.45). Atomized fuel almost immediately at the root of the jet will cross over to the vapor state. The higher the temperature of preheating, the more evaporated fuel there will be in the root of the jet, and the less will be the area over which liquid and vapor fuel will be distributed.

If fuel is above its boiling point (for gasoline $t_{\text{кип}} \approx 90^\circ\text{C}$, for kerosene $t_{\text{кип}} \approx 160^\circ\text{C}$), then operation of injector is disturbed, fuel jet is "closed," swirl injector starts to work as a direct-spray injector (Fig. 2.45, $t_{\text{OT}} = 210^\circ\text{C}$). Calculation of distribution of vapor fuel in this case can be reduced to the problem of turbulent propagation of gas proceeding from a point source.

Limits of preheating of fuel. If fuel is heated above its boiling point at a given pressure in its environment (p_g), then during outflow through the swirl chamber and injector nozzle, it starts to be rapidly evaporated; then the atomization cone will become a narrow stream and fuel flow rate will decrease. Distribution of fuel in a flow with such operating conditions of the injector will become very non-uniform.

With further heating of fuel above the boiling point of its light fractions at a given pressure in the fuel manifold, there will start vaporization, and flow rate

of liquid will almost be ceased.

When fuel is atomized by a swirl injector, it should not be heated above its boiling point at a given pressure in its environment p_g , so that pressure of saturated vapor does not exceed the pressure in the environment, and the fuel does not boil during outflow from the injector.

During atomization of fuel by direct-spray injectors, to avoid vaporization in feed lines and cessation of flow rate of

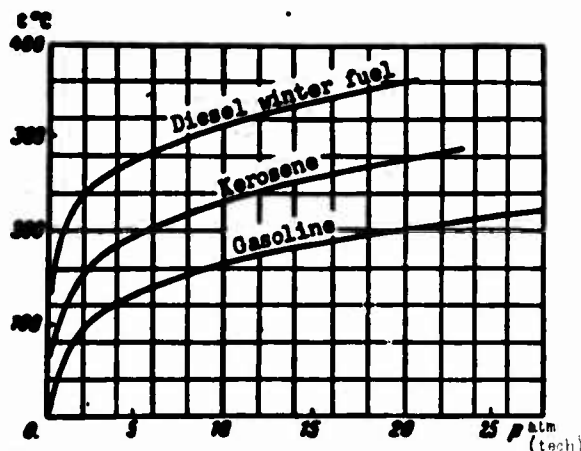


Fig. 2.46. Dependence of permissible preheating temperatures of fuel on feed pressure.

liquid through injectors, one should not heat it above the boiling point of its light fractions at the given feed pressure.

Values of limiting preheating temperatures at given pressure of fuel in feed lines are shown in Fig. 2.46.

§ 13. DISTRIBUTION OF SPECIFIC FUEL RATES DURING ATOMIZATION OF FUEL BY THE MANIFOLDS

During design of a fuel manifold (selection of type of injectors and their distribution), it is necessary to know how flows of drops interact when fuel jets

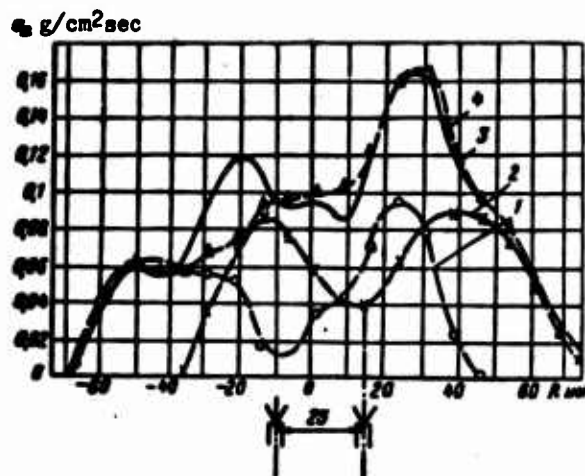


Fig. 2.47. Determination of specific flow rates of liquid phase of fuel during joint operation of two injectors (swirl injectors directed along the flow; fuel - gasoline). $p_B = 1$ atm (abs.), $t_B = 30^\circ\text{C}$, $w = 61$ m/sec, $\Delta p = 10$ atm (gage), $d_c = 0.8$ mm, $2\alpha = 60^\circ$, $x = 125$ mm. 1 - left injector is operating, the right one is suppressed; 2 - right injector operates, the left is suppressed; 3 - injectors operate together; 4 - distribution of fuel from addition of specific flow rates of liquid phase of left and right injectors.

jets is quite small, and changes in distribution of fuel due to collision of drops are insignificant. Thus, it has been experimentally verified that the general profile of specific flow rates at the given distances between injectors can be determined by addition of specific flow rates of liquid phase of fuel from each injector.

In Fig. 2.48 there are compared experimental and calculated data on the distribution of liquid phase of fuel from a manifold with diameter of 300 mm in a pipe with $D = 400$ mm. For equal distribution of fuel over the flow section, injectors of the manifold were located in a hexagonal system.

In examining experimental data, it is possible to note that in spite of the

intersect. For clarification of this question there were conducted experiments to determine specific flow rates of fuel in the region of intersection of jets of two injectors. At first there was measured distribution of fuel from two simultaneously working injectors (curve 3 on Fig. 2.47), and then (in the same regime) from each injector separately.

As can be seen, the profile of distribution of fuel obtained by means of addition of specific flow rates in the region of intersection of jets satisfactorily coincides with the profile of distribution of fuel obtained during simultaneous operation of the injectors. Consequently, fuel streams at the indicated distances between injectors freely pass through each other. Density of distribution of drops at the place of intersection of

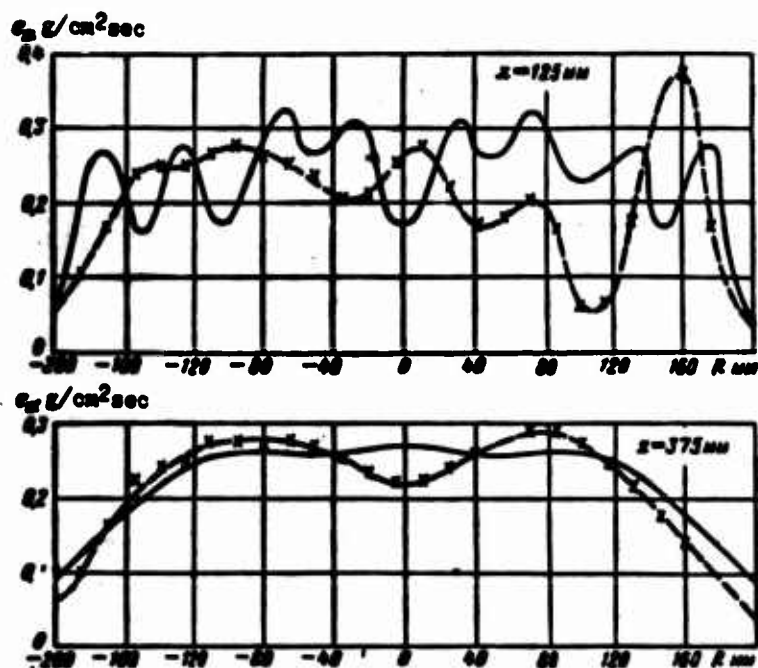


Fig. 2.48. Comparison of calculated data on the distribution of liquid phase of fuel from a manifold with 18 injectors with experimental data (swirl injectors directed along the flow; fuel is kerosene). $p_B = 1.06$ atm (abs.), $t_B = 50^\circ\text{C}$, $w = 73$ m/sec, $\Delta p_T = 29$ atm (gage). —x—x experiment, — calculation.

large number of injectors in the manifold, fuel near the manifold ($x = 125$ mm) is distributed nonuniformly. With increase of distance from the manifold, the profile of specific flow rates of fuel is equalized ($x = 375$ mm).

Calculated data on distribution of liquid phase agrees well with experimental data in the section $x = 375$ mm, and unsatisfactorily in the section $x = 125$ mm (see Fig. 2.48). In the second case fuel is distributed from every injector nonuniformly about its axis, but the number of injectors in the manifold is insufficient for statistical averaging of nonuniformities created by the injectors.

At a large distance from the manifold ($x = 375$ mm), nonuniformities in fuel jets of injectors will decrease. Conditions of experiment in this case will be nearer to the assumptions of the calculation scheme, and experimental data will agree better with calculated data.

§ 14. HEAT-MASS TRANSFER OF A DROP

Drops of fuel atomized in a ramjet engine combustion chamber are evaporated under the following conditions. Drops of liquid formed after disintegration of the sheet are entrained by the flow and heated (cooled) from the temperature of the

atomized fuel (t_0) to the temperature of equilibrium vaporization (t_p - temperature at which all of the heat flow proceeding to the drop is expended on its vaporization).

If fuel is overheated ($t_0 > t_p$), then at the time of cooling of drops from initial temperature to equilibrium temperature, rate of evaporation of them is determined basically by enthalpy of the drops and weakly depends on conditions of heat addition from without. But, conversely, evaporation of cold fuel ($t_0 < t_p$) very strongly depends on rate of heat addition from without.

At the time of entrainment of drops, they are blown by the flow - heat addition and evaporation thus occurs more intensely than evaporation of entrained drops. On the section from manifold to flame front, not all drops are unevaporated; part of fuel will enter zone of burning in unevaporated form. Due to thermal expansion of the burning mixture, flow in the zone of burning is accelerated; drops of fuel, as heavier particles, will be more slowly entrained by the flow (relative to the drops there again occurs blowing).

Thus, drops in the combustion chamber are evaporated under complicated conditions: at variable temperature and blowing velocity, during change of physical properties of fuel due to its fractionation during evaporation. Let us consider the influence of all these factors on evaporation.

Evaporation of a Drop Which is Motionless Relative to the Air

During evaporation of a drop in a medium with high temperature (for kerosene, gasoline, water, at $t_g > 100$ to 200°C), flowoff of vapor from the drop retards heat addition to it, and in this case processes of diffusion and heat exchange are mutually related.

Let us write the equations of heat- and mass transfer of a drop with its surrounding medium.

Heat flow through a sphere of radius r around the drop is equal to

$$Q = 4\pi r \lambda_{\text{gas}} \frac{dt}{dr} + Q_{\text{rad}} - 4\pi r^2 c_{\text{fuel}} \cdot \gamma_{\text{fuel}} \cdot v. \quad (2.123)$$

The first term of the right side of equation (2.123) represents flow of heat to the drop due to thermal conduction of the gas; 2nd term - flow of heat to the drop due to radiation; 3rd term - flow of heat in the mixture of gases due to flowoff of vaporized fuel from the drop.

On the surface of the drop flow will be

$$Q = \frac{dQ}{dt} \cdot t + Q_{\text{ev}} - 4\pi r^2 c_{\text{fuel}} \cdot \gamma_{\text{fuel}} \cdot v. \quad (2.124)$$

where v — flowoff rate of gas mixture;

$$v = \frac{\frac{dG}{dt}}{4\pi r^2 \cdot \gamma_{cm}}, \quad (2.125)$$

$\frac{dG}{dt}$ — rate of vaporization of drop; l — heat of vaporization of fuel; Q_{np} — flow of heat to drop to heat it from initial temperature to the temperature of equilibrium vaporization (see below); λ_{cm} — coefficient of thermal conductivity of mixture of fuel vapor and air; c_{pcm} — specific heat of mixture of fuel vapor and air;

$$c_{pcm} = c_{ps} \cdot c + c_{pa} (1 - c),$$

c — dimensionless concentration of fuel vapor;

$$c = \frac{\gamma_a \cdot \frac{p_a}{p}}{\gamma_{cm}}; \quad \gamma_{cm} = \gamma_a \frac{p_a}{p} + \gamma_b \frac{p - p_a}{p}, \quad (2.126)$$

p — pressure of surrounding medium of drop; p_a — partial pressure of fuel vapor, which is equal on the surface of the drop to the pressure of saturated vapor.

Considering (2.125), we will determine flow of heat due to flowoff:

$$4\pi r^2 \cdot c_{pcm} \cdot v = c_{pcm} \cdot \frac{dG}{dt}. \quad (2.127)$$

Equating heat flow through spheres r and r_k and considering (2.127), we will represent equation of heat exchange of drop in the following form:

$$4\pi r^2 \lambda_{cm} \frac{dt}{dr} + Q_L = Q_{np} + \frac{dG}{dt} [l + c_{pcm}(t - t_a)]. \quad (2.128)$$

Equation of mass transfer of drop taking into account flowoff of vapor has the form

$$\frac{dG}{dt} = 4\pi r^2 D_a \cdot \gamma_{cm} \frac{dc}{dr} + 4\pi r^2 \gamma_{cm} \cdot c \cdot v. \quad (2.129)$$

1st term of right side represents flow of fuel vapor due to diffusion;

2nd term — transfer of vapor due to flowoff; considering (2.125), we will simplify it:

$$4\pi r^2 \gamma_{cm} c \cdot v = c \frac{dG}{dt}.$$

Then the equation of mass transfer will be written in the following form:

$$4\pi r^2 D_a \cdot \gamma_{cm} \frac{dc}{dr} = \frac{dG}{dt} (1 - c). \quad (2.130)$$

During solution of equations (2.128) and (2.130), dependence of complexes λ_{cm}/c , γ_{cm} , $\gamma_{cm} \cdot D_a$ on temperature is not considered, and their values are determined

at average temperature $t_{cp} = \frac{t_s + t_k}{2}$.

Eliminating r from equations (2.128) and (2.129), we will obtain

$$\int_{t_s}^{t_k} \frac{dt}{t - t_s + \frac{l}{c_{pcu}} + \frac{Q_{np} - Q_1}{c_{pcu} \frac{dG}{dt}}} = \pi \int_{c_0}^{c_s} \frac{dc}{c-1}, \quad (2.131)$$

where

$$\pi = \frac{\gamma_{cu} \cdot D_n}{\frac{\lambda_{cu}}{c_{pcu}}} = \frac{D_n}{a_{cu}}. \quad (2.132)$$

Let us determine the dependence of temperature of the drop on air temperature, for this integrating expression (2.131):

$$t_k - t_s - \left[\frac{l}{c_{pcu}} + \frac{Q_{np} - Q_1}{\frac{dG}{dt} c_{pcu}} \right] \left[\left(\frac{1 - c_s}{1 - c_0} \right)^{\pi} - 1 \right]. \quad (2.133)$$

Equation (2.131) is integrated on the assumption that Q_{np} and dG/dt are constant. In reality these magnitudes depend on temperature; therefore, formula (2.133) is approximate and presents interest only for appraisal of the influence of Q_{np} , Q_1 , dG/dt on temperature of the evaporating drop.

When rate of heat addition to the drop is equal to rate of heat removal by evaporating fuel ($Q_{np} = 0$), there will occur thermal equilibrium between evaporating drop and its environment, and temperature of the drop will remain constant until full evaporation.* According to (2.133), temperature of equilibrium evaporation (vaporization) of drop at $Q_{np} = 0$ will be equal to

$$t_p = t_s - \frac{l(t_p)}{c_{pcu}(t_p)} \left[\left(\frac{1 - c_s}{1 - c_0} \right)^{\pi} - 1 \right]. \quad (2.134)$$

For gasoline and kerosene, dependence of temperature of equilibrium evaporation on temperature of air is shown in Fig. 2.49.

We will determine rate of evaporation of drop dG/dt . Integrating equation (2.123) at $r = r_0$; $t = t_k$, $r = \infty$; $t = t_p$, we will obtain

$$\frac{dG}{dt} = -\frac{4\pi r_0 \lambda_{cu}}{c_{pcu}} \ln \left[1 + \frac{(t_s - t_k) c_{pcu}}{l + \frac{Q_{np} - Q_1}{dG/dt}} \right]. \quad (2.135)$$

*These reasonings are completely accurate for evaporation of pure liquids; during evaporation of complicated fuel temperature of drop will increase with fractionation (see § 16, Chapter II).

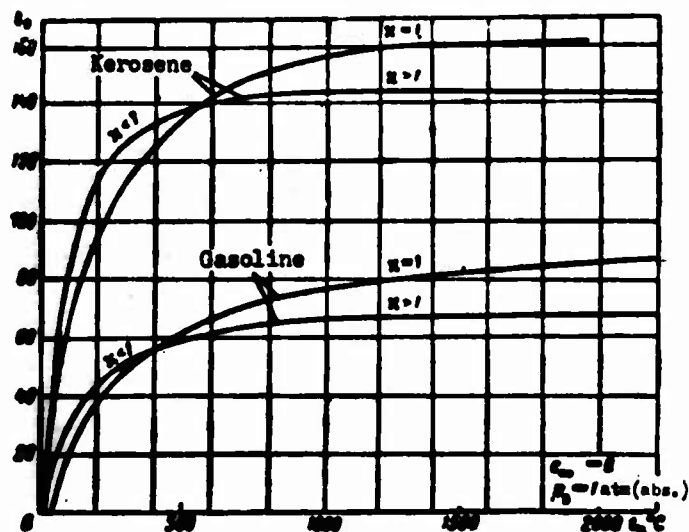


Fig. 2.49. Dependence of temperature of equilibrium vaporization on temperature of air.

During equilibrium evaporation of drop for $Q_{\pi} = 0$, expression (2.135) will take the form

$$\frac{d\theta}{dt} = -\frac{4\pi r_{\text{eq}}(t_p)}{c_{p\text{eq}}(t_p)} \ln \left[1 + \frac{(t_a - t_p) c_{p\text{eq}}(t_p)}{l(t_p)} \right]. \quad (2.136)$$

Considering (2.134), we will represent (2.136) in the form

$$\frac{d\theta}{dt} = -4\pi r_{\text{eq}}(t_p) D_v(t_p) \ln \frac{1 - c_a}{1 - c_0}. \quad (2.137)$$

Considering that

$$\frac{d\theta}{dt} = \gamma_r \frac{\pi}{6} \frac{ds^2}{dt}, \quad (2.138)$$

we will represent equation (2.137) in the form

$$ds^2 = -6dt,$$

where

$$\theta = \frac{8 \cdot \gamma_r D_v}{\gamma_r} \ln \frac{1 - c_a}{1 - c_0} = \frac{8 l_{\text{eq}}}{\gamma_r c_{p\text{eq}}} \ln \left[1 + \frac{(t_a - t_p) c_{p\text{eq}}}{l} \right], \quad (2.139)$$

and integrate it:

$$c_a^2 - c_0^2 = 6t. \quad (2.140)$$

Formula (2.140) is convenient for experimental verification of dependence of θ on parameters of medium surrounding the drop (t ; p) and physical properties of the liquid. The drop is usually suspended on a quartz fiber, and by decrease of a with respect to r during evaporation or burning, there are determined experimental

values of θ .

We will determine criteria Nu and Nu' . By definition

$$\left. \begin{aligned} Nu &= \frac{\alpha}{\lambda}, \\ Nu' &= \frac{\beta}{D_a}, \end{aligned} \right\} \quad (2.141)$$

where

$$\left. \begin{aligned} \alpha &= \frac{l \cdot \frac{dG}{dt}}{\pi a^2 (t_a - t_n)}, \\ \beta &= \frac{\frac{dG}{dt}}{\pi a^2 c_m (c_0 - c_\infty)}. \end{aligned} \right\} \quad (2.142)$$

Substituting dG/dt from (2.147) and $t_B - t_p$ from (2.134) into the expression for α, β (2.141), we find Nu and Nu' :

$$\left. \begin{aligned} Nu_{CT} &= \frac{2\pi}{\left(\frac{1-c_\infty}{1-c_0}\right)^2 - 1} \ln \frac{1-c_\infty}{1-c_0}, \\ Nu'_{CT} &= \frac{\left(\frac{1-c_\infty}{1-c_0}\right)^2 - 1}{2(c_0 - c_\infty)} Nu_{CT} \end{aligned} \right\} \quad (2.143)$$

Let us consider how consideration of the inequality of thermal and diffusion fluxes [$\kappa \neq 1$; see (2.133)] influences criteria of transfer Nu and Nu' and dependence $t_p(t_B)$.

At $\kappa = 1$, functions $t_p(t_B)$, Nu_{CT} , Nu'_{CT} will have the form

$$\left. \begin{aligned} Nu_{CT} &= \frac{1-c_0}{c_0 - c_\infty} \ln \frac{1-c_\infty}{1-c_0}, \\ Nu'_{CT} &= \frac{1}{1-c_0} Nu_{CT} \end{aligned} \right\} \quad (2.144)$$

$$t_p = t_0 - \frac{l(t_p)c_0 - c_\infty}{c_{p,m}(t_p)1 - c_0}. \quad (2.145)$$

Numerical difference between values of $Nu_{CT}(\kappa \neq 1)$ and $Nu_{CT}(\kappa = 1)$ is considerable (Fig. 2.50).

Dependence of temperature of equilibrium vaporization on temperature of air at $\kappa \neq 1$ (2.134) also differs from dependence $t_p(t_B)$ at $\kappa = 1$ (2.145) (Fig. 2.49), and this difference in values of t_p noticeably affects rate of vaporization of drops.

In region of low temperatures $\kappa < 1$; this means that $D_\pi < a_{T,CM}$ [see formula (2.131)]. Consequently, rate of vaporization will be limited not by the magnitude of heat addition, but by the rate of diffusion transfer. Thermal equilibrium of the

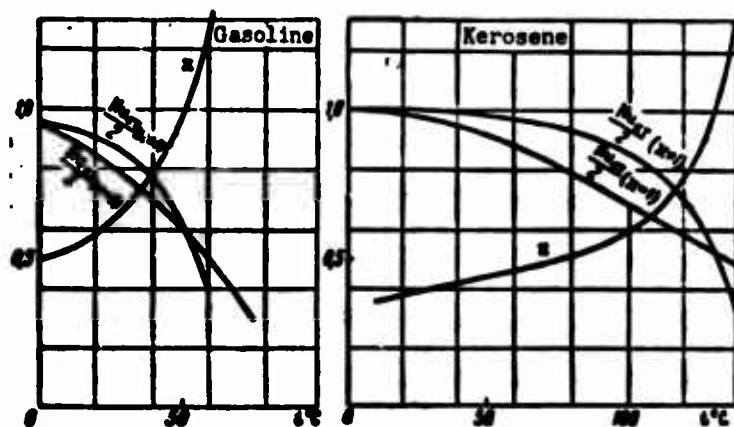


Fig. 2.50. Dependence of Nusselt number Nu on temperature of drop.

drop in this case will be established at higher temperature (t_p) than for $\kappa = 1$.

With increase of temperature, values of κ will be larger than unity; i.e., diffusion transfer will become greater than heat transfer. In this case, rate of vaporization of drop will be limited by rate of heat addition, which at high temperatures is strongly hindered due to losses of heat in the heating of vaporized fuel.

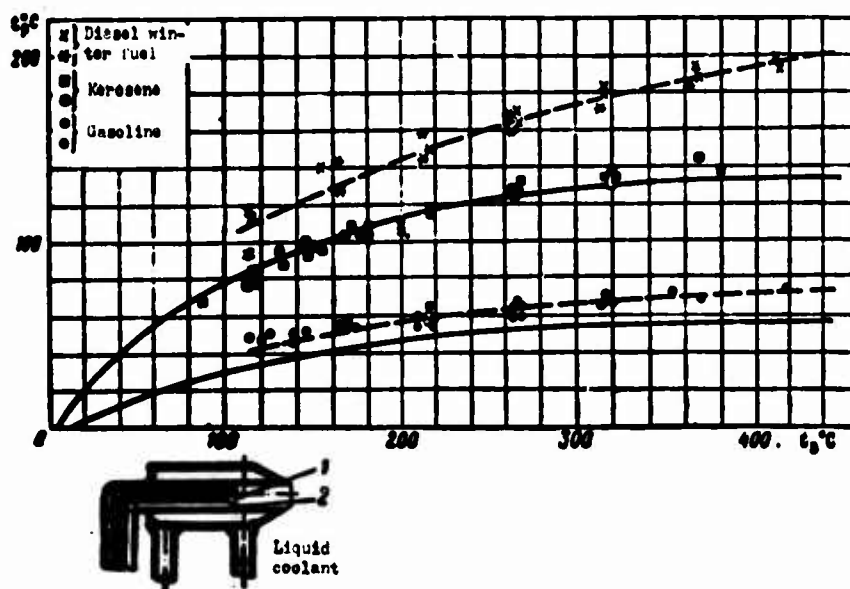


Fig. 2.51. Comparison of calculated data with experimental data on the dependence of equilibrium temperature of droplet on temperature of air. — calculated curves, - - - curves averaging experimental points.

At high temperatures, losses of heat flow in heating of vapor considerably exceed the value of heat flow necessary for vaporization of drops, and increase proportionally to increase of temperature. Therefore, heat flow proceeding to

vaporization of the drop increases very weakly with temperature rise; thus, temperature of equilibrium vaporization tends to a maximum value (close to boiling point at given pressure in the environment) and rate of vaporization increases only from increase of diffusion coefficient with temperature rise.

Comparison of calculated data on $t_p(t_B)$ with experimental data (Fig. 2.51) showed that at $t_B = 80$ to 420°C (where $n < 1$), values of $t_p(t_B)_{n \neq 1}$ correspond better to experimental data than $t_p(t_B)_{n=1}$.

Measurement of temperature of atomized fuel was conducted by means of thermocouples, which were built into the cooled collector tube (see Fig. 2.51). Temperature of liquid entering collector tube from the flow was measured by thermocouple 1 at that moment when differential thermocouple 2 showed absence of difference of temperatures between temperature of wall and temperature of liquid flowing through internal cavity of tube.

Thus, from the given comparisons it is clear that the theoretical expression for $t_p(t_B)$ determined without assumption of equality of thermal and diffusion fluxes ($D_n = a_{T.CM}$) is more exact.

Vaporization of a Drop in a Flow

Determination of dependence of Nu (Re) is conducted in the following way: Assuming that profile of temperatures in boundary layer on a drop located in a flow will be the same as during evaporation in motionless air, we will determine thickness of layer around the drop in which heat exchange is carried out. Knowing thickness of boundary layer, we will compose heat balance of evaporating drop and will find dependence of Nu on Re.

In case of evaporation of a drop in motionless air, profile of temperatures is determined by formula (2.146), which we will obtain by integrating equation (2.128) at $q_n = 0$, $q_{np} = 0$:

$$t(r) - t_p(r_s) = \frac{1}{\epsilon_{\text{pr}}} \left[e^{\left(1 - \frac{n}{r}\right) - \frac{\epsilon_{\text{pr}} \cdot \frac{d^2}{4\pi \alpha r^2}} - 1} \right] \quad (2.146)$$

at $r = R$, $t(r) = t_B$. By definition,

$$\text{Nu} = \frac{q \cdot 2R}{4\pi R^2 (t_B - t) \lambda_{\text{air}}} \quad (2.147)$$

Placing in expression (2.147) the value of $t_B - t_p$ from (2.146), we will obtain

in dependence of Nu on r/R (at $t = t_p$, $q = l \frac{dG}{dt}$):

$$Nu = \frac{q}{\left(1 - \frac{r}{R}\right)^{\frac{q}{2}} - 1}, \quad (2.148)$$

where

$$q = \frac{2r_0 \frac{dG}{dt}}{4\pi r_0^2 \gamma_{\text{sat}} D_n}. \quad (2.149)$$

Solving equation (2.148) for r/R , we will find

$$\frac{R}{r} = \frac{1}{1 - \frac{Nu}{q} \cdot \frac{2}{Nu} \ln \left(1 + \frac{q}{Nu}\right)}. \quad (2.150)$$

Function $\frac{Nu}{q} \cdot \frac{2}{Nu} \ln \left(1 + \frac{q}{Nu}\right)$ is equal to $\frac{Nu_{cr}}{Nu}$.

Actually, from comparison of (2.148) and (2.134) with (2.146), it follows that

$$\begin{aligned} \frac{q}{Nu} &= e^{-\left(1 - \frac{r_0}{r}\right)^{\frac{q}{2}}} - 1 = \left(\frac{1 - c_0}{1 - c_0}\right)^2 - 1; \\ 1 + \frac{q}{Nu} &= \left(\frac{1 - c_0}{1 - c_0}\right)^2; \\ \ln \left(1 + \frac{q}{Nu}\right) &= 2 \ln \frac{1 - c_0}{1 - c_0}; \\ \frac{Nu_{cr}}{Nu} &= \frac{2Nu}{Nu} \ln \left(1 + \frac{q}{Nu}\right) = \frac{2x}{Nu \left(\frac{1 - c_0}{1 - c_0}\right)^2 - 1} \ln \frac{1 - c_0}{1 - c_0}. \end{aligned} \quad (2.151)$$

Considering (2.151), we will represent (2.150) in the following form:

$$\frac{R}{r_0} = \frac{1}{1 - \frac{Nu_{cr}}{Nu}}. \quad (2.152)$$

Heat balance in boundary layer of drop has the form

$$k^2 \gamma_{\text{sat}} \bar{u} (t_0 - t_n) \pi (R^2 - r_0^2) = c_{p,n} \frac{dG}{dt} (t_0 - t_n) + q \quad (2.153)$$

$$\left[\text{heat flow from surrounding gas} \right] = \left[\text{heat content of} \right] + \left[\text{heat flow going into heating} \right]$$

[into boundary layer of drop] [flowoff of gas] [and vaporization of the drop]

(k — proportionality constant determined from experiment).

Multiplying (2.153) by the complex

$$\frac{2r_0}{4\pi r_0^2 \gamma_{\text{sat}} (t_0 - t_n) c_{p,n} \gamma_{\text{sat}}},$$

taking into account (2.147) and (2.149), we will obtain

$$k^2 \frac{Re}{4} \left[\left(\frac{R}{r_0} \right)^2 - 1 \right] = \frac{2r_0 \cdot \frac{dQ}{dt}}{4\pi r_0^2 \gamma_{cu} \cdot D_n} \cdot \frac{c_{pcu} \gamma_{cu} \cdot D_n}{\lambda_{cu}} \cdot \frac{\lambda_{cu}}{\lambda_a} \cdot \frac{\lambda_a}{v_a c_{pa} \gamma_a} +$$

$$+ \frac{q \cdot 2r_0}{4\pi r_0^2 (t_a - t_n) \lambda_{cu}} \cdot \frac{\lambda_{cu}}{\lambda_a} \cdot \frac{\lambda_a}{v_a c_{pa} \gamma_a} = \frac{1}{Pr_a} \cdot \frac{\lambda_{cu}}{\lambda_a} Nu \left(1 + \frac{v_f}{Nu} \right).$$

Putting in this formula the value of R/r_0 from (2.152) and $(1 + \frac{v_f}{Nu})$ from (2.151), we will obtain

$$k^2 \frac{\lambda_a}{\lambda_{cu}} \frac{Pr_a Re}{4} = \frac{\left(\frac{1-c_a}{1-c_0} \right)^2 \cdot Nu}{\left[\left(1 - \frac{Nu_{cr}}{Nu} \right)^2 - 1 \right]}.$$

After transformations, dependence of Nu on Re will have the form

$$Nu = Nu_{cr} + k \sqrt{1 - \frac{Nu_{cr}}{2Nu}} \cdot \sqrt{\frac{\frac{Nu_{cr}}{2}}{\left(\frac{1-c_a}{1-c_0} \right)^2}} \sqrt{\frac{\lambda_a}{\lambda_{cu}}} \times \sqrt{Pr_a} \sqrt{Re}. \quad (2.154)$$

Complex $\sqrt{1 - \frac{Nu_{cr}}{2Nu}}$ is a weakly variable function of Nu , whose value is close to 1. Maximum deviation from 1 will be equal to 0.13 at $Nu_{cr} = 2$ and $Nu = 3$. Under real conditions, $Nu_{cr} < 2$; and Nu changes within the limits 3-10, so that deviation of $\sqrt{1 - \frac{Nu_{cr}}{2Nu}}$ from 1 during change of Nu will be less than 0.13. Therefore, dependence of $\sqrt{1 - \frac{Nu_{cr}}{2Nu}}$ on Nu can be disregarded.

Analysis of equations of heat and mass transfer from the surface of a plate shows that in the boundary layer when there is flowoff of vapor, dimensionless profiles of temperatures and velocities are similar, and ratio of energy thickness to hydrodynamic layer almost does not depend on intensity of vapor flowoff; i.e., hydrodynamics of flow around the body weakly depends on intensity of flowoff. Consequently, for determination of constant k [see formula (2.154)] it is possible to use experimental data on dependence Nu (Re) for weak intensity of flowoff (vaporization) of drops.

Experimental data [21, 22] (for the region Re [10 to 500]) are well expressed by the dependence

$$Nu = 2 + 0.6 \cdot \sqrt{Pr_a} \sqrt{Re}.$$

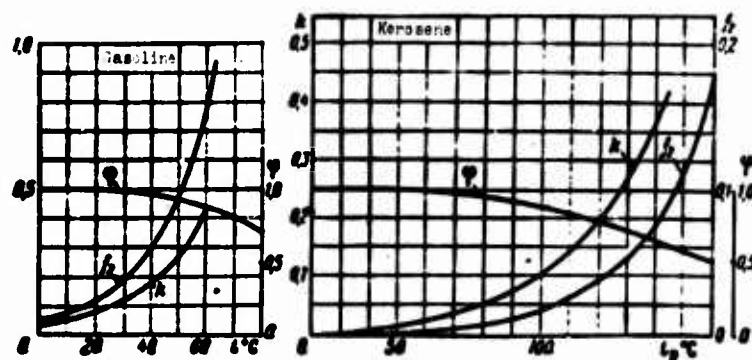


Fig. 2.52. Dependence of function f_2 , k and φ on temperature of fuel ($p_B = \text{atm (abs.)}$).

We will take k equal to 0.6. Then

$$Nu = Nu_{cr} + 0.51 \sqrt{\frac{\lambda_2}{\lambda_{cr}}} \cdot f(c_0; c_\infty) \sqrt{Re}$$

or

$$Nu = Nu_{cr} \left(1 + 0.255 \sqrt{\frac{\lambda_2}{\lambda_{cr}}} \cdot \varphi(c_0; c_\infty) \sqrt{Re} \right). \quad (2.145)$$

where

$$0.51 = 0.6 \sqrt{Pr_s}; \quad Pr_s = 0.72;$$

$$\varphi(c_0; c_\infty) = \frac{f(c_0; c_\infty)}{\frac{Nu_{cr}}{2}}; \quad f(c_0; c_\infty) = \sqrt{\frac{\frac{Nu_{cr}}{2}}{\left(\frac{1-c_\infty}{1-c_0}\right)^2}}.$$

Dependence of function $\varphi(c_0; c_\infty)$; $Nu_{cr}/2$ on temperature of fuel for kerosene and gasoline is shown in Fig. 2.52. In the interval of temperatures (0 to 80°C) for gasoline and (0 to 140°C) for kerosene, the values of $\sqrt{\frac{\lambda_2}{\lambda_{cr}}} \approx 1$ (with accuracy of up to 3%). With increase of temperature of drop, vapor flowoff from it increases, which will lead to decrease of inflow of heat to the drop. Decrease of heat addition to the drop is taken into account by change of function $f(c_0; c_\infty)$.

§ 15. INFLUENCE OF PRESSURE OF MEDIUM, NONUNIFORMITY OF HEATING AND FRACTIONATION OF FUEL ON RATE OF VAPORIZATION OF DROPS

Influence of pressure. From analysis of equation (2.139), it follows that influence of pressure on rate of vaporization can be traced by change of the equilibrium temperature. Placing in (2.145) values of c_0 from (2.136), we will represent

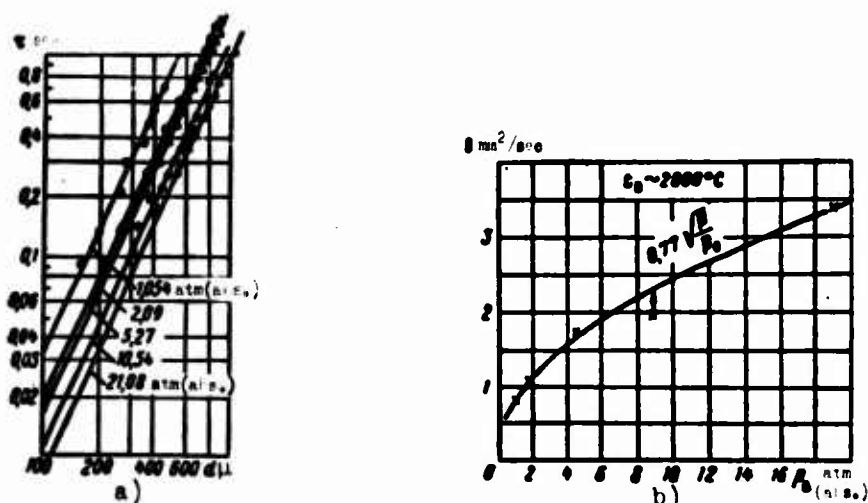


Fig. 2.52. Influence of pressure on vaporization of a drop (τ - lifetime of drop in sec).

dependence of t_p on p in explicit form:

$$t_p = t_0 - \frac{l}{c_{pca}} \frac{M_0}{M_1} \frac{1}{\frac{p}{p_0} - 1}; \quad p_0 = c_0 = 0, \quad z = 1.$$

With increase of pressure, t_p grows; accordingly rate of vaporization (2.136) will weakly decrease. Calculations show that with increase of p in the interval 0.5 to 3 atm (abs.), rate of vaporization decreases by 3%. One may assume that in the interval of p (0.5 to 3) atm (abs.) rate of vaporization of the drop located in a flow does not depend on pressure.

Using formulas (2.155), (2.143), (2.141), (2.142), we will represent the expression for rate of vaporization of the drop located in a flow in the following form [see formula (2.159)]:

$$\frac{dG}{dt} = -2\pi\alpha_{1ca}D_0 \ln \frac{1-c_{1a}}{1-c_{1a}^0} [1 + 0.255\varphi(c_0, c_a) \sqrt{Re}].$$

Change of pressure will affect rate of vaporization of the drop as a result of change of density in the value of Reynolds number Re of the flow, i.e., rate of vaporization of proportional to \sqrt{p} . This is confirmed by experimental data of work [23] (Fig. 2.53a), in which there are described experiments on vaporization of a drop of water suspended on a quartz fiber. If by the slope of line a^2 with respect to τ we determine ϵ , then these data on ϵ are averaged well by curve $0.77 \sqrt{p/p_0}$; ($p_0 = 1$ atm (abs.)) (Fig. 2.53b).

Influence of nonuniformity of heating of drops. Rate of vaporization depends on surface temperature of the drop, on heat losses on its heating. Time of temperature rise during heating of a drop (from t_0 to t_p) depends on rate of propagation of

heat through its volume, which is determined by the values of criteria Bi, F_0 :

$$Bi = \frac{\frac{a}{2}}{\lambda_m} = \frac{\lambda_r}{\lambda_m} \frac{Nu}{2}; \quad F_0 = \frac{a_T \tau}{\left(\frac{a}{2}\right)^2},$$

where λ_r , λ_m — coefficient of thermal conductivity of the gas or liquid surrounding the drop;

a_T — coefficient of thermal diffusivity of the liquid.

For drops vaporizing in an air flow at values of Nu (2 to 15), τ (0 to 0.01) sec, a (0 to 200 μ), $a_{T, \text{ker}} = 0.007 \cdot 10^{-6} \text{ m}^2/\text{sec}$, the criteria Bi and F_0 change within the limits Bi = 0.2 to 1; $F_0 = 0$ to 0.1.

From consideration of nomographs of solution of the problem about nonstationary heating of a sphere [24], it is clear that at such values of Bi and F_0 , heat flow proceeding to the drop weakly spreads throughout its volume and is expended basically on heating the outer layer of the drop.

It is possible to expect that the temperature field inside the drop will be equalized from the forced convection appearing as a result of entrainment of the outer layer of the drop by the air flow, and by free convection appearing in the liquid volume due to the temperature gradient.

Entrainment of the outer layer is observed during laminar flow around large drops [25]. Now it is difficult to estimate to what degree the outer layer of the drop will be entrained during turbulent flow around it.

The influence of free convection on increase of heat transfer inside the drop can be estimated by the magnitude of the correction ϵ_{KONB} to the coefficient of thermal conductivity [24]:

$$\epsilon_{\text{KONB}} = \frac{\lambda_{\text{eff}}}{\lambda_m} = 0.185 \left[\frac{\beta g (t_n - t_{\text{II}}) \text{Pr}_m}{\nu_m^2 \delta} \right]^{0.25}, \quad (2.156)$$

where t_n , t_{II} — temperature of surface, center of drop;

β — coefficient of volume expansion of the liquid;

Pr_m — Prandtl number of liquid;

δ — thickness of layer in which there occurs the temperature drop $t_n - t_{\text{II}}$.

Calculations show that for kerosene at $a = 2000 \mu$, $\delta = 500 \mu$ and $\Delta t = t_n - t_{\text{II}} = 50^\circ\text{C}$, $\epsilon_{\text{KONB}} > 1$. This means that convection mixing inside the drop takes place, and it should be taken into account. At $a = 200 \mu$, $\delta = 50 \mu$, and $\Delta t = t_n - t_{\text{II}} = 50^\circ\text{C}$, $\epsilon_{\text{KONB}} < 1$; this means that convection mixing inside the drop does not appear, $\lambda_{\text{eff}} = \lambda_m$. Thus, at values of a , Δt , and Pr_m which are typical for drops of fuel atomized

In the combustion chamber of an engine, convection mixing of liquid inside droplets is not observed.

Analysis of heating conditions shows that the drop is heated nonuniformly. Thus it is impossible to consider that when the drop enters the flow, its outer layer is instantly heated from initial temperature to equilibrium. This is confirmed by experimental data.

Experiments on measurement of temperature of a burning drop with diameter of $a = 1$ to 2 mm suspended on a thermocouple (see § 4, Chapter VII) show that heating times for gasoline and kerosene are 10% and 25% of their time of vaporization respectively. The drop of kerosene is heated to 160°C , and the drop of gasoline is heated to 80°C .

Influence of fractionation. The process of fractionation of complex fuel during vaporization of a drop was studied by Yerastov [26]. Experiments were conducted in the following way: Into a heated flow, kerosene was atomized. Incompletely vaporized

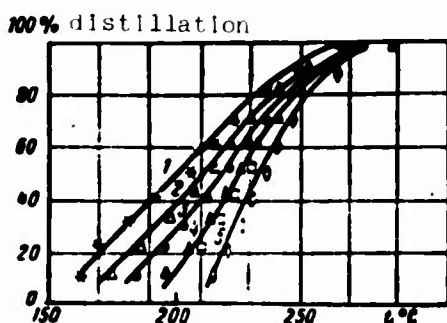


Fig. 2.54. Distillation curves of fuel for different degrees of its vaporization in a flow. $p_B = 1$ atm (abs.), $t_B = 207^{\circ}\text{C}$, $v = 4$ m/sec, $\Delta t_T = 30$ atm (gage), $t_{OT} = 25^{\circ}\text{C}$.

Degree of vaporization drops in a flow. 1 - $z = 0\%$ (initial sample), 2 - $z = 15\%$, $x = 80$ mm, 3 - $z = 26\%$, $x = 80$ mm, 4 - $z = 40\%$, $x = 180$ mm - \square , $x = 30$ mm - Δ ; 5 - $z = 63\%$, $x = 240$ mm.

drops were removed from the flow by an intake tube. By the removed samples of fuel there was determined the degree of vaporization, and then there was conducted Engler distillation of the fuel.

On Fig. 2.54 it is shown how the proportion of heavier components of the fuel increases due to the predominant vaporization of the light fractions. This leads to decrease of saturated vapor pressure and increase of equilibrium vaporization temperature. As calculations show, in spite of increase of equilibrium vaporization temperature with fractionation of the fuel, saturated vapor pressure on the surface of the drop decreases. Consequently, rate vaporization will decrease during fractionation of fuel. During 60% vaporization of drops, saturated vapor pressure decreased by 20% (rate of

vaporization will decrease by approximately the same amount). However, there are data showing that diffusion burning drops of fuels consisting of mixtures of hydrocarbons proceeds without noticeable influence of fractionation on the rate of vaporization. Obviously, in case there is intense heat addition, rate of vaporization of the drops exceeds the rate of fractionation.

Fractionation of fuel can be influenced by a nonuniformity of heating. Nonuniformity of heating of a drop promotes uniform vaporization of all fractions of the fuel from the heated outer layer. Inasmuch as the inner part of the drop will not be heated, then diffusion of light fractions into the outer layer will occur weakly.

Thus, it may be concluded that for low rate of evaporation and low viscosity of fuel, evaporation will occur with fractionation and deceleration of evaporation of the drops. For high rate of evaporation, the influence of fractionation of fuel on deceleration of evaporation of drops will be insignificant. Under conditions typical for the combustor of a ramjet engine, the influence of fractionation of fuel on deceleration of evaporation can be disregarded.

§ 16. EVAPORATION OF DROPS IN A FUEL JET (SPRAY)

Fuel atomized in a flow is evaporated under complicated conditions. Drops formed during disintegration of the liquid sheet and splitting up are entrained by the flow. Thus, temperature of the drops is changed little from initial to equilibrium. Change of blowing velocity and temperature of the drops very strongly affects the rate of evaporation.

In order to take into account the influence of blowing and change of temperature of a drop on its evaporation, it is necessary to solve simultaneously the equations of evaporation and heating:

$$\frac{dQ}{dt} = -\beta S \gamma_{\text{ev}} (c_0 - c_{\infty}); \quad (2.157)$$

$$G c_p \frac{dt}{dt} = \alpha S (t_0 - t) - l \frac{dQ}{dt}. \quad (2.158)$$

We solve these equations under the following assumptions:

- 1) We consider that temperature and air velocity are constant over cross section and along the flow;
- 2) We do not consider that during change of temperature of the drop from t_0 to t_p the drop is nonuniformly heated over its volume (by temperature of the drop we imply the average volume, or the surface temperature).

Let us transform equation (2.157). By means of successive substitution of β through Nu' (2.141), Nu' through Nu (2.143), and Nu through (2.155), we will determine β , place it in equation (2.157), and, transforming it, will obtain

$$\frac{dQ}{dt} = -\frac{8 D_{\text{air}} \gamma_{\text{ev}}}{\gamma_r} \frac{\gamma_{\text{ev}}}{\gamma_{\text{a}}} \ln \frac{1 - c_{\infty}}{1 - c_0} \left[1 + 0.255 \sqrt{Re} \right]. \quad (2.159)$$

Let us take $\sqrt{\frac{\lambda_p}{\lambda_{\infty}}} = 1$

We will express Reynolds number Re in terms of τ ; then we will consider the influence of deformation and evaporation of the drop on change of blowing velocity and diameter.

Let us determine the decrease of diameter of an evaporating drop at the moment of its entrainment by the flow. For this, the dependence of Nu on Re (2.155) will be represented as

$$Nu = Nu_{cr} + 0.54f \sqrt{\frac{\lambda_p}{\lambda_{\infty}}} \sqrt{Re} \approx 0.75f \sqrt{Re}. \quad (2.160)$$

The equation of evaporation (2.157), after determination of β taking into account (2.160), will have the form

$$\frac{dG}{d\tau} = -0.75 \cdot \pi \cdot a D_p \gamma_{mf} \cdot \left[\frac{\left(\frac{1-\epsilon_{\infty}}{1-\epsilon_0} \right)^{\frac{1}{2}} - 1}{\frac{1}{2}} \right] \sqrt{Re}. \quad (2.161)$$

Simultaneously solving equations of motion (2.72) and evaporation (2.161), we will obtain

$$\frac{d(\sigma^2)}{d\tau} = \frac{k}{\psi(D)} \frac{d\tau}{\tau}, \quad (2.162)$$

where

$$k = 0.43 \frac{D_p \gamma_{mf}}{g \cdot r_0} f_1(\eta);$$

$$f_1 = \frac{\left(\frac{1-\epsilon_{\infty}}{1-\epsilon_0} \right)^{\frac{1}{2}} - 1}{\frac{1}{2}} \sqrt{\frac{Nu_{cr}}{\left(\frac{1-\epsilon_{\infty}}{1-\epsilon_0} \right)^{\frac{1}{2}}}}.$$

Function $\psi(D)$ takes into account the influence of deformation of the drop on change of blowing velocity, and accordingly of rate of evaporation of the drop. Theoretical analysis and calculations have shown that the influence of deformation of drops on decrease of degree of evaporation can be disregarded. Error does not exceed 5 to 8%. Therefore, during integration we will set $\psi(D) = 1$.

During integration of equation (2.162), we assume that evaporation of drops occurs at equilibrium temperature ($t = t_p$; $k(t_p) = \text{const}$).

After integration of (2.162) we will obtain

$$\left(\frac{\sigma}{\sigma_0} \right)^2 = \left(\frac{\tau}{\tau_0} \right)^k. \quad (2.163)$$

Taking into account (2.163),

$$Re = Re_0 \left(\frac{a}{a_0} \right)^{1 + \frac{k}{3}},$$

where

$$Re_0 = \frac{\rho_0 u_0}{\eta_0(u_0)}.$$

With the help of (2.8'), the value of u/u_0 will be expressed in terms of $\bar{\tau}/\bar{a}$:

$$\frac{a}{a_0} = \frac{1}{\left[\eta \left(\frac{\bar{\tau}}{\bar{a}} + 1 \right) \right]^{\frac{3k}{1-k}}}. \quad (2.165)$$

The value of Reynolds number Re from equation (2.159), with the help of expressions (2.164) and (2.165), will be represented as a function of $\bar{\tau}/\bar{a}$:

$$VRe = \frac{VRe_0}{\eta \left(\frac{\bar{\tau}}{\bar{a}} + 1 \right)^{1 + \frac{k}{3}}}. \quad (2.166)$$

Placing (2.166) in equation (2.159), we will obtain

$$d(a^3) = -\frac{8D_n \gamma_n}{\gamma_T} \cdot f_2(t) \left\{ 1 + \frac{0.255 \gamma (c_0; c_\infty) VRe_0}{\left[\eta \left(\frac{\bar{\tau}}{\bar{a}} + 1 \right) \right]^{1 + \frac{k}{3}}} \right\} d\tau, \quad (2.167)$$

where

$$f_2(t) = \frac{\gamma_{cn}}{\gamma_n} \ln \frac{1 - c_\infty}{1 - c_0}; \quad \gamma_n = \frac{p}{R_i T}.$$

During change of temperature of the drop from t_0 to t_p , physical constants of fuel and gas in the expressions, $D_n \cdot \gamma_n / \gamma_T$, Re_0 , \bar{a} , φ_1 , and function $\varphi(c_0; c_\infty)$ change very little. Therefore, during integration of equation (2.167) we will consider

them to be constants, and determine $\varphi(c_0; c_\infty)$ at $t = t_p$, and $\frac{D_n \gamma_n}{\gamma_T}$, Re_0 , \bar{a} , $\varphi =$ at

$$t_{cp} = \frac{t_0 + t_p}{2}.$$

Function $f_2(t)$ very strongly depends on temperature of the drop. During integration of equation (2.167) in the case of nonequilibrium evaporation, it is necessary to take into account the dependence of function $f_2(t)$ on temperature.

The equation of evaporation of a drop (2.167) will be solved for two cases:

- 1) Evaporation occurs at equilibrium temperature;
- 2) Initial temperature of the drop differs from equilibrium temperature. In the second case, evaporation of the drop for a certain period of time of the entire "lifetime" of the drop will occur at varying temperature and, accordingly, with

varying rate of evaporation. As is shown in § 15, drops of fuel are heated (or cooled) nonuniformly with respect to depth.

Solution of the problem of evaporation of a drop at variable temperature, taking into account nonuniformity of heating, will be very complicated, and unacceptable for practical calculations. Therefore, the problem of heating (cooling) of an evaporating drop will be considered under two extreme assumptions:

- 1) at the moment of change of temperature of the drop from t_0 to t_p , it is uniformly heated over its entire volume; i.e., we assume that $\lambda_{\infty} = \infty$;
- 2) during change of temperature from t_0 to t_p , only the evaporating part of the outer layer of the drop is instantaneously heated; i.e., we consider that $\lambda_{\infty} = 0$.

In the case $t_0 = t_p$, function $f_2(t_p)$ will be constant in time, and equation (2.167) is easily integrated:

$$1 - \left(\frac{a}{a_0}\right)^3 = \frac{8D_0 \tau_0}{\tau_r(t_p) a_0^3} f_2(t_p) \left[1 + \frac{0.255 \tau(t_p) \sqrt{Re_0}}{\tau_0^{1+m}} \cdot \Phi\left(\frac{\tau}{a}; m\right) \right] \times \tau(a; x). \quad (2.168)$$

where

$$m = \frac{4}{3} \frac{h(t_p)}{1 - h(t_p)}; \quad \Phi\left(\frac{\tau}{a}; m\right) = \frac{1}{m} \frac{a}{\tau} \left[1 - \left(\frac{\tau}{a} + 1\right)^{-m} \right].$$

For facilitation of calculations, in Fig. 2.55 there is given a graph of function $\Phi(\tau/a; m)$. Values of functions $\varphi(t)$, $f_2(t)$, $k(t)$ are given in Fig. 2.52.

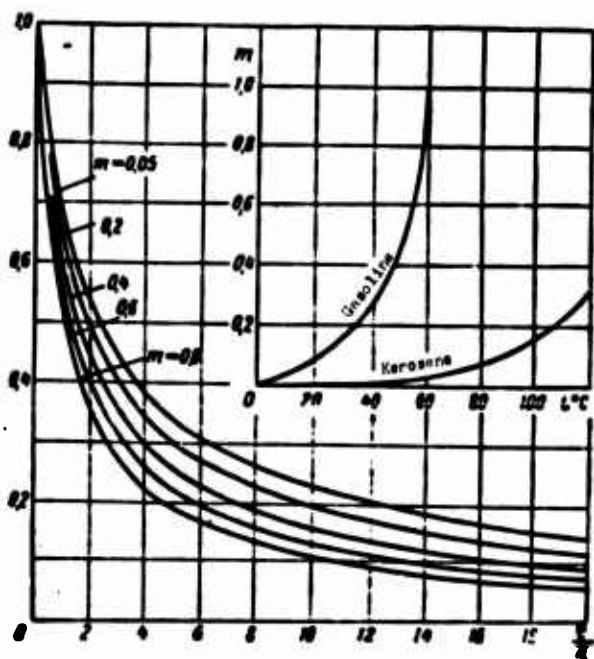


Fig. 2.55. Graph of function $\Phi\left(\frac{\tau}{a}; m\right)$.

If Re_0 of airflow around the drops is small, it is possible to disregard the second term in the right side of equation (2.168) and to consider evaporation of the drop under static conditions [see formula (2.142)].

We will consider the problem of non-equilibrium evaporation under the assumption that only the outer layer of the evaporated part of the drop is heated.

Heat flow expended in heating the outer layer is equal to

$$Q_p = c_f (t_p - t) \frac{dQ}{dt},$$

where c_f is specific heat of the liquid fuel.

According to (2.136), with such a definition of $Q_{\text{нл}}$ and $Q_{\text{л}} = 0$, temperature of the evaporating outer layer of the drop is determined by the following expression:

$$t_p' = t_0 - \frac{l + c_r(t_p' - t_0)}{c_{\text{pcu}}} \left[\left(\frac{1 - c_{\infty}}{1 - c_0} \right)^3 - 1 \right]. \quad (2.169)$$

Inasmuch as $t_p' = \text{const}$, function $f_2(t_p')$ will also be constant. Solution of equation (2.167) in this case will be the same as for the case of equilibrium evaporation (2.168), except that values of function f_2 , φ and m will be determined at $t_p' = t_p'$.

On the assumption of instantaneous heating of the drop over its entire volume, the problem of nonequilibrium evaporation is solved in the following way:

Transforming equation (2.158) to the form

$$\frac{dG}{G} = \frac{c_r dt}{aS(t_0 - t) - l}, \text{ where } \frac{dG}{G} = \frac{da^3}{a^3} + \frac{d[\gamma_r(t)]}{\gamma_r(t)}$$

and integrating it within the limits $a = a_0$; $a = a_p$; $t = t_0$ and $t = t_p$, we will obtain

$$\ln \left(\frac{a_p}{a_0} \right)^3 = - \int_{t_0}^{t_p} \left[\frac{\frac{c_r}{l}}{\frac{t_0 - t}{h(t)} - 1} - \frac{k}{\gamma_r(t)} \right] dt, \quad (2.170)$$

where k is the coefficient of thermal expansion of the liquid: $\gamma_T = \gamma_0 - kT$:

$$\frac{t_0 - t}{h(t)} = \frac{aS(t_0 - t)}{\frac{dG}{dt} \cdot l}.$$

Taking into account (2.142) and (2.145),

$$h(t) = \frac{l}{c_{\text{pcu}}} \left[\frac{1 - c_{\infty}}{1 - c_0} - 1 \right].$$

The analytic dependence of $f_3(t)$ on t is very complicated; therefore, the integral in equation (2.170) is solved by numerical methods:

$$\left(\frac{a_p}{a_0} \right)^3 = e^{- \sum_{t=t_0}^{t_p} \frac{\frac{c_r}{l} \Delta t}{\frac{t_0 - t}{h(t)} - 1} - \ln \frac{\gamma_r(t_p)}{\gamma_r(t_0)}}. \quad (2.171)$$

Knowing the dependence of $(a_p/a_0)^3$ and $f_p(t)$ on t , we will construct a graph of the dependence of $f_2(t)$ on $(a/a_0)^3$. Then f_2 will become a function only of value ratio $(a/a_0)^3$, and it will be possible to transfer it to the left side of equation (2.167) and numerically integrate it. Then equation (2.167) will take the form

$$\int_1^{\frac{a_p}{a_0}} \left[\frac{h(t_p)}{h(t)} - 1 \right] d \left[\left(\frac{a}{a_0} \right)^2 \right] + \int_1^{\frac{a_p}{a_0}} d \left[\left(\frac{a}{a_0} \right)^2 \right] = - \frac{8 D_{nTn}}{a_0^2 \gamma_r(t_p)} \times$$

$$\times h(t_p) \int_1^{\frac{a_p}{a_0}} \left\{ 1 + \frac{0.255 \gamma \sqrt{R c_0}}{\left[\gamma_1 \left(\frac{\tau}{a} + 1 \right)^{1 + \frac{1}{3}} \right]} \right\} d \tau, \quad (2.172)$$

where a_p/a_0 is relative diameter of the drop upon achievement of $t = t_p$.

Inasmuch as function $\left[\frac{h(t_p)}{h(t)} - 1 \right]$ is determined only graphically, the first integral in the left side of equation (2.172) must be solved by a numerical method:

$$\int_1^{\frac{a_p}{a_0}} \left[\frac{h(t_p)}{h(t)} - 1 \right] d \left[\left(\frac{a}{a_0} \right)^2 \right] \approx \sum_{\left(\frac{a}{a_0} \right)_i=1}^{\frac{a_p}{a_0}} \left[\frac{h(t_p)}{h(t)} - 1 \right]_{\left(\frac{a}{a_0} \right)_i} \Delta \left(\frac{a}{a_0} \right)_i^2 = \Sigma. \quad (2.173)$$

After integration of equation (2.172), we will obtain

$$1 - \left(\frac{a}{a_0} \right)^2 \pm \Sigma = \frac{8 D_{nTn} f_1(t_p)}{a_0^2 \gamma_r} \left[1 + \frac{0.255 \gamma \sqrt{R c_0}}{[\gamma_1(D_0)]^{1+m}} \cdot \Phi \left(\frac{\tau}{a}; m \right) \right] \tau(a; x). \quad (2.174)$$

Influence of the period of nonequilibrium evaporation on the total percentage of evaporation of drops in the last formula is taken into account by the function Φ . (+ is heating of the drop, - is cooling).

Let us determine the degree of evaporation over the cross section of the fuel spray.

Degree of evaporation of a drop strongly depends on its initial diameter. As a result of dispersion of particles, at any given point of the fuel spray there will be drops of different diameters, and the degree of evaporation at a given point of the spray (jet) will be determined by the concentration and evaporation of the drops of those diameters which occur at the given point, i.e.,

$$Z(x, y) = 1 - \frac{c_{\Sigma, \text{всп}}(x, y)}{c_{\Sigma}(x, y)} \quad (2.175)$$

(definition of $c_{\Sigma, \text{всп}}$ and c_{Σ} is given in § 11, Chapter II).

Degree of evaporation of the entire fuel jet at distance x from the injector nozzle is equal to

$$Z_0(x) = 1 - \sum_{a_i=a_{\text{min}}}^{a_{\text{max}}} \Delta V(a_i) \left(\frac{a}{a_0} \right)_i^3. \quad (2.176)$$

During derivation of the working formulas, there were made several assumptions, as a result of which errors in the calculations are possible. Let us estimate magnitudes of these errors in examples.

1. During derivation of formula (2.174), there was not considered change of specific gravity of the fuel at the time of nonequilibrium evaporation during change of temperature of the drop from t_0 to t_p [we consider that $\gamma(t) = \gamma(t_p)$].

During change of temperature of kerosene from $t_0 = 20^\circ\text{C}$ to $t_p = 160^\circ\text{C}$, absolute error in determination of the degree of evaporation will be equal to

$$\Delta Z \approx \frac{3}{2} \theta \left[\frac{\frac{\gamma(t_0) + \gamma(t_p)}{2}}{\gamma(t_p)} - 1 \right] \approx \frac{3}{2} 0.075 \theta.$$

During the period of nonequilibrium evaporation, not more than 30% of the drop will evaporate (consequently, $\theta \approx 0.2$). Then the highest possible error for complete evaporation of the drop will be

$$\frac{\Delta Z}{Z} = \frac{\frac{3}{2} \cdot 0.075 \cdot 0.2 \cdot 100}{100} \approx 2.25\%.$$

2. During determination of τ by equations (2.85) and (2.88), values of $k(t)$ are taken at t_p without considering the fact that at the time of nonequilibrium evaporation $k(t)$ will be variable. Error due to change of k under the conditions $t_0 = 45^\circ\text{C}$, $k(t_0) = 0.005$, $\bar{a}(t_0) = 1.07$, $\bar{u}_{ox}(t_0) = -1.18$, $t_p = 103^\circ\text{C}$, $k(t_p) = 0.014$,

$$a(t_p) = 1.17, \bar{u}_{ox}(t_p) = -0.61 \quad (a = 100 \mu; x = 0.355 \text{ m};$$

$$w = 86 \text{ m/sec (see § 11, Chapter II)}).$$

will be

$$\Delta \bar{\tau} = \frac{\bar{\tau}_0[k(t_0)] + \bar{\tau}_0[k(t_p)]}{2} - \bar{\tau}[k(t_p)] = \frac{1.52 + 1.39}{2} - 1.52 = 0.65.$$

Error in the value of τ will be equal to

$$\begin{aligned} \Delta \tau &= \frac{x}{w} \Delta \bar{\tau} = \frac{0.355}{86} \cdot 0.65 = 0.27 \text{ m sec} \frac{\Delta \tau}{\tau(a = 100 \mu)} = \\ &= \frac{0.27 \cdot 100}{6.13} \approx 4.5\%. \end{aligned}$$

During use of formula (2.163), we do not consider that the dependence $Nu(k)$ (2.160) used in its derivation is inaccurate for small values of Re .

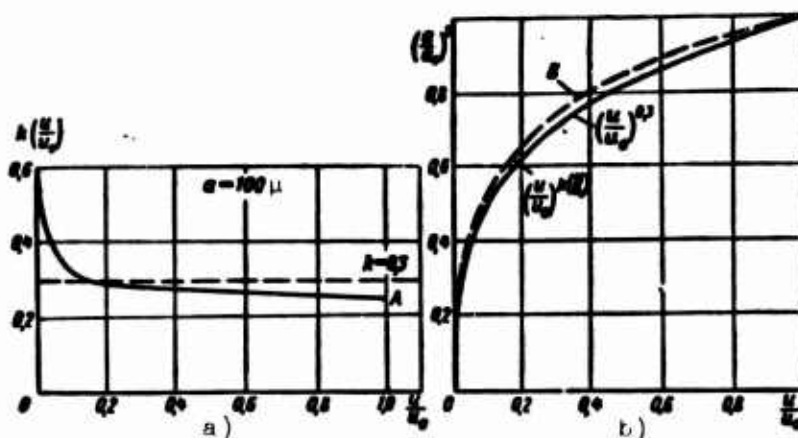


Fig. 2.56. For estimation of errors during analysis of evaporation of drops due to inaccurate determination of the dependence Nu (Re).

In Fig. 2.56a (for the specific example $k = 0.3$), curve A shows change of k calculated by the more exact dependence $Nu_3(Re)$ [see equation (2.155)]. The dependence of $(a/a_0)^3$ on (u/u_0) , which is determined for varying values of $k(u/u_0)$ (Fig. 2.56b, curve B), differs little from that calculated by formula (2.163).

The biggest divergence will be in the region $\frac{u}{u_0} < 0.03$, but at such small relative velocities, when the drops are almost entrained, there is no need to consider the influence of decrease of diameter of the drop for its time of stay and trajectory in the flow. Thus, on the basis of these estimates it is possible to state that errors which are possible during calculation of values of $Z(a_1; x)$, $\tau(a_1; x)$ and $y(a_1; x)$ will not exceed 10%.

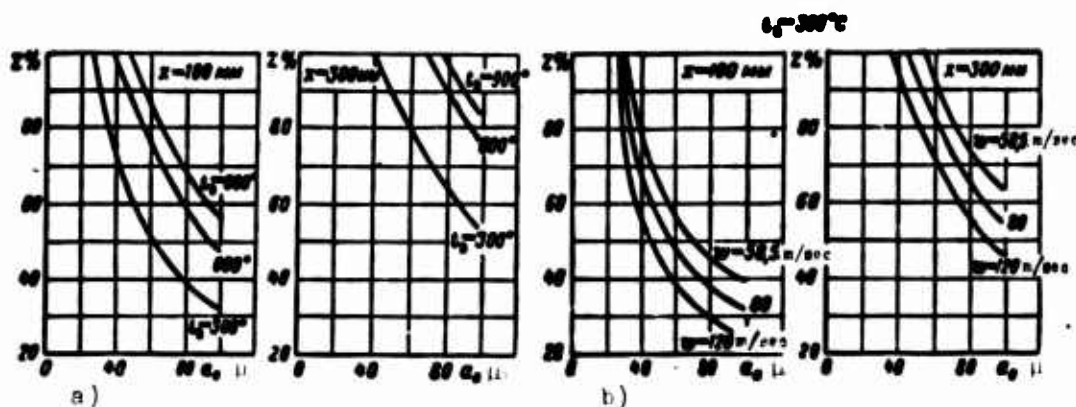


Fig. 2.57. Influence of temperature of air (a), flow velocity (b) on degree of evaporation of drops at equilibrium temperature.

For estimate of the influence of parameters of the flow and conditions of atomization of fuel on the degree of evaporation of drops in Figs. 2.57 and 2.58 there are given calculated data on the evaporation of drops. Calculations were

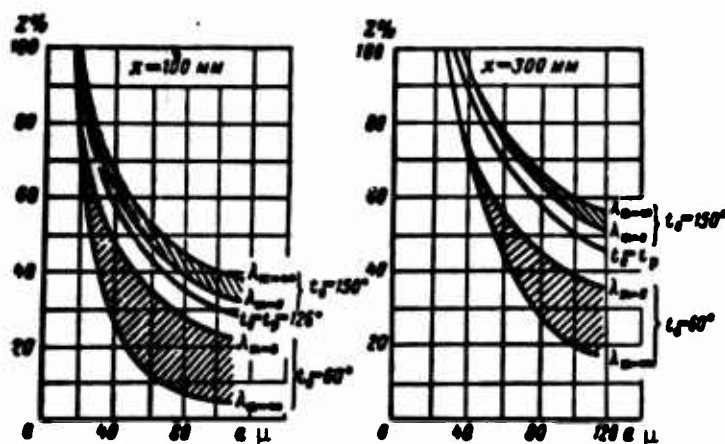


Fig. 2.58. Comparison of calculated data on nonequilibrium evaporation on the assumption of surface ($\lambda_{\kappa} = 0$) and volume ($\lambda_{\kappa} = \infty$) heating of the drops.

conducted for the following conditions: a swirl injector directed upstream (against the flow); $2\alpha = 60^\circ$; fuel — kerosene: $p_B = 1 \text{ atm (abs.)}$; $w = 80 \text{ m/sec}$; $p_T = 6 \text{ atm (gage)}$; $x = 100; 300 \text{ mm}$; $a [20 \text{ to } 100] \mu$.

There was determined the influence of temperature of the flow (Fig. 2.57a), velocity (Fig. 2.57b) and initial temperature of fuel (Fig. 2.58). Calculations show that evaporation of drops is influenced basically by initial diameter, air temperature and initial temperature of the fuel.

Influence of flow velocity on degree of evaporation of the drops mainly shows up in change of their time of stay in the chamber: the higher the velocity, the shorter the time of evaporation of the drops ($\tau \sim x/w$).

In Fig. 2.58 there are compared data on nonequilibrium evaporation of drops which were calculated on the assumption of volume ($\lambda_{\kappa} = \infty$) and surface ($\lambda_{\kappa} = 0$) heating of the drops.

According to data of the calculation, it is possible to be sure only of the fact that real values of evaporation of drops will fall within the regions: $Z_{\lambda_{\kappa}=0}$ to $Z_{\lambda_{\kappa}=\infty}$.

From analysis of data on heating of drops and fractionation of fuel (see [10], Chapter II), it is possible to assume that in the region of low temperatures of the environment, when processes of heating and evaporation of drops occur slowly, calculation on the assumption of volume heating will be more correct, and at high temperatures and large heat flow, results of calculation on the assumption of surface heating will be nearer to actual data.

Example of Analysis of Evaporation of Drops of a Fuel Jet

The list of initial data is the same as the one used in calculation of the distribution of liquid phase (see § 10, Chapter II). Calculated data are given in Table 2.1.

Table 2.1

Ref. No.	$a \mu$	20	40	60	80	100	120
1	$\frac{\tau}{a}$	12	4,26	2,41	1,65	1,22	0,94
2	Re_0	56	112	168	224	280	326
3	$\Phi\left(\frac{\tau}{a}; m\right)$	0,173	0,34	0,46	0,545	0,61	0,665
4	$\frac{0,255 \varphi \sqrt{Re_0}}{\varphi_1^{1+m}} \Phi$	0,162	0,286	0,37	0,42	0,46	0,485
5	$\tau \text{ m} \cdot \text{sec}$	4,99	4,92	5,33	5,81	5,13	6,30
6	$1 - \left(\frac{a}{a_0}\right)^2$	1,210	0,437	0,253	0,187	0,142	0,112
7	$\left(\frac{a}{a_0}\right)^3$	0	0,425	0,630	0,735	0,800	0,820

Notes and supplementary calculations are given according to reference numbers of the table.

1. Values of τ/\bar{a} are determined according to data given in § 10, Chapter II.

$$2. \quad Re_0 = \frac{u_0 a_0}{\nu(t_p)} = 280 \left(\frac{a[\mu]}{100} \right).$$

3. At $t_p = 200^\circ\text{C}$; $t_p' = 103.5^\circ\text{C}$;

$$k(t_p') = 0,114; \quad m = \frac{4}{3} \frac{k}{1-k} = 0,172;$$

$$I_2(t_p') = 0,194, \quad \varphi(t_p') = 0,87.$$

For given τ/\bar{a} and \bar{m} , we will determine the value of function $\Phi(\tau/\bar{a}; m)$ (see Fig. 2.55).

$$4. \quad \frac{8D_0 \gamma_0}{a_0^2 \gamma_0(t_p')} I_2(t_p') \left[1 + \frac{0,255 \varphi(t_p') \sqrt{Re_0}}{\varphi_1^{1+m}} \Phi\left(\frac{\tau}{a}; m\right) \right] =$$

$$= \frac{1,67}{\left(\frac{a[\mu]}{100}\right)^2} \left[1 + \frac{3,72 \sqrt{\frac{a[\mu]}{100}}}{\varphi_1^{1+m}} \Phi\left(\frac{\tau}{a}; m\right) \right].$$

$$\tau = \frac{x}{u} \bar{a} = 4,18 \bar{a}.$$

A comparison of calculated data with experimental data is given in § 17. Calculated data on this example are used in determination of the degree of evaporation of the entire spray (see Table 2.2).

Table 2.2. Comparison of Calculated and Experimental Data on the Evaporation of a Fuel Jet ($p_B = 1$ atm (abs.), $t_p = 112^\circ\text{C}$; Fuel - Kerosene).

Ref. No.	x m	t_c $^\circ\text{C}$	t_p $^\circ\text{C}$	θ n. sec	Δp_T atm (gase)	Position of injector	a_u μ	Z_p ($x=0$) %	$Z_{p,c}$ %	Z_p ($x=\infty$) %
1	0,41	200	90	94	8	Along the flow $d_c=0,8$ $\alpha=30^\circ$	90	46,2	44,8	
2	0,355	200	45	86	2	Against the flow $d_c=1,2$ $\alpha=40^\circ$	57,5	51,6	54,8	
3	0,08	200	20	60	30	Along the flow $d_c=0,75$ $\alpha=30^\circ$	68	18	11	2
4	0,08	200	125	60	30	Along the flow $d_c=0,75$ $\alpha=30^\circ$	65	24	25,7	24
5	0,08	200	175	60	30	Along the flow $d_c=0,75$ $\alpha=30^\circ$	61	35	43,5	63

§ 17. COMPARISON OF CALCULATED AND EXPERIMENTAL DATA ON EVAPORATION OF A FUEL JET

As was noted above, calculated data on evaporation of a fuel jet and distribution of the liquid vapor phases depend on the accuracy of calculation of "elementary" processes: 1) atomization spectrum; 2) trajectories of drops; 3) dispersion; 4) evaporation; and 5) removal of vapor from drops by the flow, and its turbulent mixing over the flow section.

Comparison of data on degree of evaporation of the jet and distribution of the liquid phase of the fuel is shown in Figs. 2.59 and 2.60. Divergence between calculated and experimental values of $Z(x; y)$ are due to inaccuracies in the calculation of dispersion of droplets. As can be seen from comparison of data on evaporation of the jet (Table 2.2), results of calculations on evaporation of drops of the jet on the whole Z_p (2.176) agree better with experimental data than the data on distribution of degree of evaporation over the cross section of the jet.

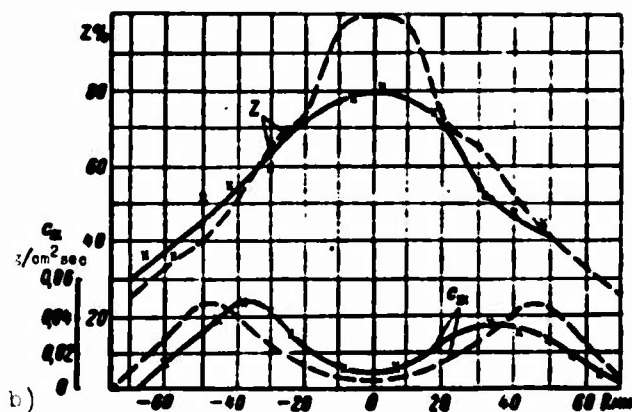
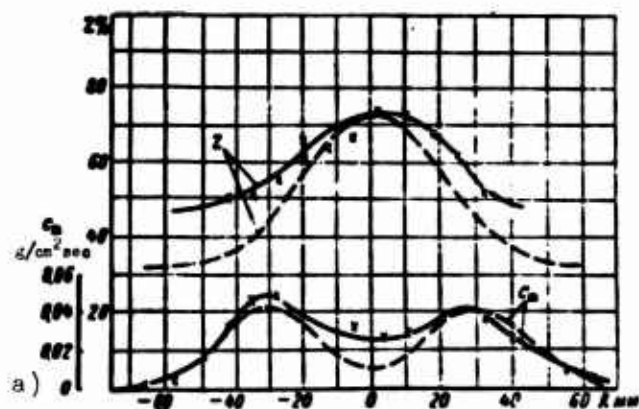


Fig. 2.59. Comparison of calculated data on evaporation and distribution of fuel with experimental data. a) swirl injector directed along the flow; fuel - kerosene; $d_c = 0.8$ mm; $p_B = 1$ atm (abs.); $t_B = 200^\circ\text{C}$, $w = 94$ m/sec; $\Delta p_T = 8$ atm (gage); $t_{O_T} = 90^\circ\text{C}$, $x = 410$ mm. b) swirl injector directed against the flow; fuel - kerosene; $d_c = 1.2$ mm; $p_B = 1$ atm (abs.); $t_B = 200^\circ\text{C}$; $w = 86$ m/sec; $\Delta p_T = 2$ atm (gage); $t_{O_T} = 46^\circ\text{C}$, $x = 355$ mm.

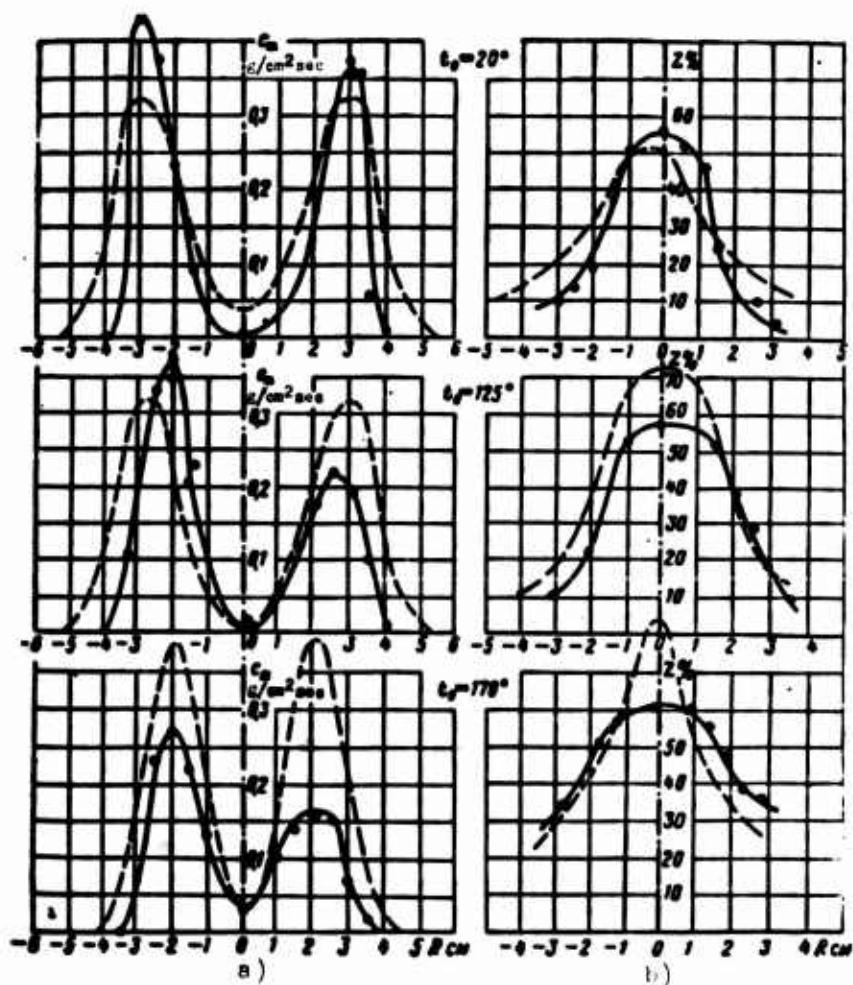


Fig. 2.60. Comparison of calculated data on evaporation and distribution of fuel with experimental data at different preheating temperatures of fuel (swirl injector directed along the flow; fuel - kerosene). $p_B =$

$= 1.1 \text{ atm (abs.)}$; $t_B = 200^\circ\text{C}$; $w = 60 \text{ m/sec}$; $\Delta p_T =$

$= 30 \text{ atm (gage)}$; $x = 80 \text{ mm}$. --- calculation.

— experiment. a) distribution of liquid phase of fuel; b) distribution of degree of evaporation over the cross section of the fuel jet (data of Yerastov).

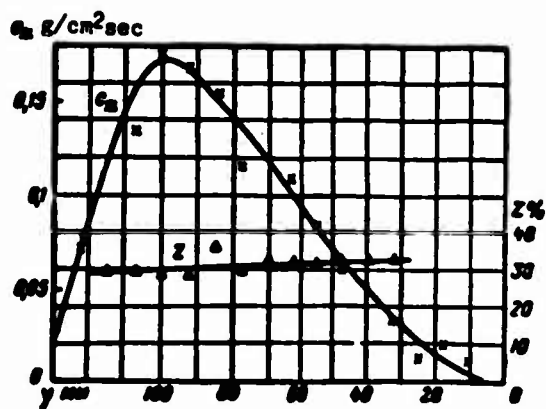


Fig. 2.61. Distribution of degree of evaporation over the cross section of the jet during atomization of heated fuel into a cold flow (direct-spray injector directed perpendicularly to the flow). $d_c = 0.7 \text{ mm}$;

$p_B = 1 \text{ atm (abs.)}$; $t_B = 40^\circ\text{C}$; $w = 36 \text{ m/sec}$;

$\Delta p = 2 \text{ atm (gage)}$; $t_c = 35^\circ\text{C}$.

In Fig. 2.60 there are compared data on degree of evaporation of the jet and distribution of liquid phase for different preheating temperatures of the fuel. Calculated curves on degree of evaporation taking into account dispersion of droplets agree relatively well with experimental data.

Comparison of experimental and calculated data on evaporation of the jet on the whole (see Table 2.2, 3, 4, 5) has shown that experimental data on evaporation of the jet are intermediate between those calculated at $Z_{\lambda=0}$ and $Z_{\lambda=\infty}$. Consequently, both schemes of calculation of nonequilibrium evaporation of drops give limiting results and are useful only for approximate calculations. At low ambient temperatures, a more correct explanation of experimental data is obtained if we assume volume heating of the drops.

In Fig. 2.61 there are shown experimental data on Z during nonequilibrium evaporation of drops of heated fuel in a cold flow. The degree of evaporation is almost constant over the entire cross section of the jet; consequently, evaporation of all drops of the spectrum should be identical.

Identical evaporation of drops of the spectrum is not considered in the scheme of calculation assuming surface heating, but it is possible to explain it completely if we assume volume heating of drops. Actually, during evaporation of heated fuel in a cold flow, heat addition to drops $\alpha S(t_g - t)$ will be small, and rate of evaporation of drops will be high.

In formula (2.171) function $\frac{S(t_g - t)}{l \cdot \frac{du}{dt}} = \frac{t_g - t}{l_0(t)}$ will be close to zero.

Then formula (2.171) can be represented as

$$\left(\frac{a}{a_0}\right)^3 = e^{-\frac{\alpha}{l}(t_g - t)} \sim 1 - \frac{\alpha}{l}(t_g - t_p)$$

or

$$Z = 1 - \left(\frac{a}{a_0}\right)^3 \approx \frac{\alpha}{l}(t_g - t_p). \quad (2.177)$$

Thus, nonequilibrium evaporation of drops in this case occurs basically due to internal heat content of the drops. This is confirmed by comparison of experimental data with calculated data. According to data shown in Fig. 2.61, $Z_{\text{экспер}} \approx 50\%$. During calculation by formula (2.177), $Z_{\text{расч}} = 27\%$.

For practical calculations on the determination of nonequilibrium evaporation of drops at high ambient temperature, it is more convenient to use the scheme of

calculation, proposed by Yerastov (with the assumption of surface heating of drops). Thus we should remember that at $t_0 < t_p$, computed values of $Z(a_i; x)$ will be somewhat higher than experimental values and, conversely, at $t_0 > t_p$, $Z_{\text{расч}} < Z_{\text{эксп}}$.

In those cases when it is necessary to estimate degree of evaporation of the jet rapidly, it is possible to calculate it by the method derived by Probert [27], which deal with evaporation of drops of the spectrum with mean evaporative diameter. In the case of constant rate of evaporation of a drop, and with determination of the spectrum by formula (2.23), mean evaporative diameter a_{cp} will be equal to

$$a_{cp} = \bar{a} \sqrt{\frac{\Gamma(1 + \frac{2}{n})}{2}}.$$

where

$$\bar{a} = \frac{a_n}{(\ln 2)^{\frac{1}{n}}}.$$

or

n	2	2,5	3	3,5	4
$\frac{a_{cp}}{a_n}$	1,2	1,12	1,07	1,05	1,03

Mean evaporative diameter is close to the median diameter.

On the section in which drops are entrained by the flow, during nonequilibrium evaporation the rate of evaporation of droplets is variable; accordingly, mean evaporative diameter will change. In this case it is possible to estimate evaporation of the jet by evaporation of a drop of median diameter only approximately.

§ 18. EVAPORATION OF DROPS IN THE COMBUSTION ZONE

Not all drops in the mixture will be evaporated in the section before the flame front. Part of the larger drops of the spectrum will continue to be evaporated in the combustion zone at increasing temperature and flow rate. The percentage of unevaporated fuel and rate of evaporation of drops in the combustion zone will affect development of combustion and the magnitude of physical incompleteness of burning.

With variable temperature and flow velocity, equations of motion (2.66) and evaporation (2.167) cannot be solved in quadratures. It is necessary to solve them by the method of numerical integration. The given profile of temperatures and velocities in the flow is partitioned into intervals; we will consider that during motion and evaporation of drops on each interval Δx there are satisfied the following conditions:

1. Temperature and velocity of the flow are constant and equal to the average magnitudes t_{icp} , w_{icp} .

2. We consider that a drop in the combustion zone is carried along the flow lines; if the flow lines are parallel to axis Ox, then velocity of the drop will be equal to V_x .

3. We will not take into account deformation of the drops.

4. During change of temperature of the flow (from interval to interval), temperature of the drop will change. Nonequilibrium of evaporation of the drop will be considered by the scheme of calculation which assumes surface heating of drops; temperature of a drop $t_p(t_{icp})$ will be determined by the formula (2.169).

5. During solution of the equation of motion and the equation of evaporation on the i-th interval, we consider that the value of the diameter of the drop is constant and equal to a_{i-1} .

Integrating the equation of evaporation (2.167) under these assumptions, we will obtain

$$1 - \left(\frac{a}{a_0}\right)^3 = \sum \frac{\theta_i \Delta \tau_i}{a_0^3} \quad (2.178)$$

where

$$\theta_i = \frac{8D_n(t_{icp}) \gamma_n(t_{icp})}{\gamma_r(t_{icp})} f_2(t'_p) \left[1 + 0.255 \gamma(t'_p) \sqrt{\frac{a_{i-1} u_{icp}}{v_n(t_{icp})}} \right]; \quad (2.179)$$

$$\Delta \tau_i = \frac{\Delta x}{u_{icp}}; \quad v_{icp} = \frac{v_{i-1} + v_i}{2}; \quad v_i = w_i - u_i; \quad u_{icp} = \frac{u_{i-1} + u_i}{2}.$$

The value of u_1 will be determined from solution of the equation of motion (2.66) on interval Δx for a constant value of w_{icp} :

$$\sqrt{u_i} = \sqrt{y_i^2 + w_{icp} + y_i} \quad (2.180)$$

where

$$y_i = \frac{1}{2} \left[\sqrt{u_{i-1}} - \frac{w_{icp}}{\sqrt{u_{i-1}}} - \frac{\Delta x}{A_{i-1}} \right];$$

$$A_{i-1} = \frac{0.19 \cdot \gamma_r(t_{icp}) a_0^{3/2} \left(\frac{a}{a_0}\right)_{i-1}^{3/2}}{\sqrt{g \cdot P_n(t_{icp}) \gamma_n(t_{icp})}};$$

$\left(\frac{a}{a_0}\right)_{i-1}$ is taken from the calculation of evaporation by formula (2.178) on the interval $i - 1$.

Calculations on evaporation of drops in the combustion zone were carried out for specific conditions existing in special experiments for clarification of the influence of atomization spectrum on combustion of the mixture (see § 7, Chapter VIII).

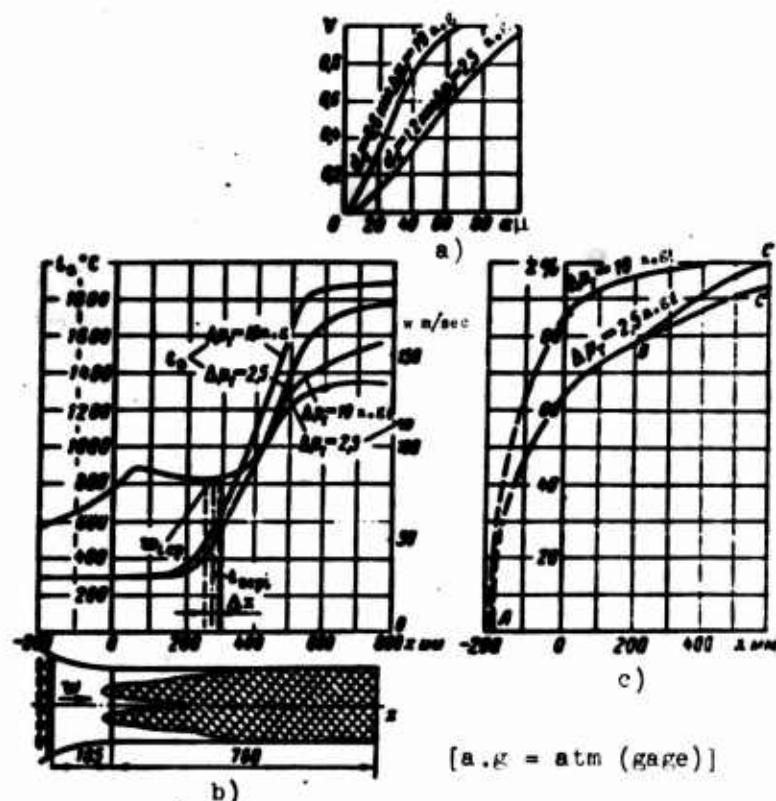


Fig. 2.62. Evaporation of fuel in the combustion zone (fuel is kerosene; the manifold consists of 12 swirl injectors and is directed upstream). $\alpha_{\text{смеси}} = 1.16$.

$p_0 = 1 \text{ atm (abs.)}$, $w_0 = 55 \text{ m/sec}$, $t_{00} = 300^\circ\text{C}$. a) atomization spectra of fuel; b) experimental data on change of temperature and flow velocity along the axis Ox; c) calculated data on evaporation of a fuel spray in the combustion zone (for $\Delta p_T = 2.5 \text{ atm (gage)}$) — section BC; curve BC corresponds to evaporation of drops under the assumption that velocity and temperature of gas in the combustion zone ($x = 200$ to 1200 mm) increases linearly in the intervals of $t_g [300-2000^\circ\text{C}]$ and $w [90-400 \text{ m/sec}]$.

Experiments were conducted under the following conditions: in a rectangular channel there was directed upstream (against the flow) a manifold of swirl injectors (see Fig. 2.62a and Fig. 8.23). Fuel from the manifold at constant air-fuel ratio $\alpha = 1.16$, but with different fineness of atomization, proceeded to the flameholders and burned in a half-open stream. The atomization spectrum was changed by means of selection of injectors and feed pressure of fuel. The rate of combustion of the mixture was determined by the change of concentration of CO_2 measured on the flow axis, temperature and velocity.

For analysis of experimental data, there was considered two cases ($\Delta p_T = 2.5 \text{ atm (gage)}$, $d_c = 1.2 \text{ mm}$ and $\Delta p_T = 19 \text{ atm (gage)}$, $d_c = 0.5 \text{ mm}$). These regimes

had their own individual spectra (Fig. 2.62a) (which were calculated by the formulas of § 4, Chapter II) and temperature and velocity profiles (Fig. 2.62b). Results of calculations for evaporation of the jet in the section before the front and in the combustion zone are shown in Fig. 2.62c.

Degree of evaporation of fuel in the sprays at $\Delta p_T = 2.5$ atm (gage) and $\Delta p_T = 19$ atm (gage) in the section before the front AB ($x = 385$ mm, see Fig. 2.62c) was 95% for $\Delta p_T = 19$ atm (gage) and 78% for $\Delta p_T = 2.5$ atm (gage). In both cases equal quantities of evaporated fuel entered the combustion zone; therefore, combustion of mixtures at $\Delta p_T = 2.5$ atm (gage) and $\Delta p_T = 19$ atm (gage) proceeded almost identically (temperature and velocity profiles at $\Delta p_T = 2.5$ and 19 atm (gage) differ slightly from each other) (see Fig. 2.62b).

In spite of the temperature rise in the combustion zone, evaporation of the remainder (section BC on Fig. 2.62c) proceeds quite slowly. Degree of evaporation of the remainder increases only slightly because due to acceleration of flow and increase of velocity of the entrained drops, time of their stay in the flow in each interval Δx decreases more rapidly than the rate of evaporation increases due to increase of temperature of the gas.

Curve BC' shows evaporation of the remainder under the following conditions: on the interval $x = 400-1200$ mm, temperature and velocity in the combustion zone increase linearly within the limits $t = 300-2000^\circ\text{C}$ and $w = 91-400$ m/sec. In this case, due to decrease of time of stay of drops in the flow, the remainder is evaporated still more slowly (line BC').

It is necessary to note that calculations on evaporation of drops in the combustion zone are not very rough, and are conducted with exaggerated degree of evaporation. Thus, according to calculations, the coefficient of evaporation of drops $\theta = \frac{8D_0\gamma_r}{\gamma_r}$ at $t_B = 2000^\circ\text{C}$ is equal to 0.0127 cm²/sec, and according to experimental data on the burning of a drop surrounded by a diffusion flame front, in which the gas temperature is also approximately equal to 2000°C , the coefficient $\theta = 0.0096$ cm²/sec (§ 4, see Chapter VII).

During calculations it was noticed that the second term of formula (2.179), which takes into account the influence of accelerated flow around the drop, is small and changes little. Thus, according to calculated data, due to the high gas velocity it is very difficult to evaporate drops in the combustion zone. Therefore, to avoid physical incompleteness of burning, it is desirable to select according to

parameters of the flow and fuel conditions under which evaporation of drops is mainly completed before they reach the combustion zone.

LITERATURE

1. Rayleigh. Theory of sound, Vol. II. State Technical and Theoretical Press, 1955.
2. K. Weber. Disintegration of a stream, Internal-combustion engines, Vol. I. ONTI NKGB [Department of Scientific and Technical Information of the Peoples Commissariat of State Security] USSR, 1936.
3. M. S. Volynskiy. Splitting up of drops of liquid in a main flow. Reports of the Academy of Sciences of the USSR, Vol. 62, No. 3, 1948.
4. M. S. Volynskiy. Study of splitting up of drops in a gas flow. Reports of the Academy of Sciences of the USSR, Vol. XVIII, No. 2, 1949.
5. B. Lewis, R. N. Pease and H. S. Taylor. High-speed aerodynamics and jet engineering. Gosfizmatgiz, 1961.
6. Yu. D. Dityakin, V. I. Yagodkin and V. A. Borodin. Splitting up of a spherical drop in a gas flow. Journal of applied mechanics and technical physics, 1962, No. 1.
7. L. I. Sedov. Methods of dimensional theory and similarity in mechanics. OGIZ [Union of State Publishing Houses] 1944.
8. G. N. Abramovich. Applied gas dynamics. State Technical and Theoretical Press, 1953.
9. M. Doumas and R. Laster. Liquid Film Properties for Centrifugal Spray Nozzles. Chem. Engng. Props., 1953, 49, No. 10, pp. 518-526.
10. E. Giffen and A. Muraszew. The Atomization of Liquid Fuels. London, 1953.
11. R. A. Miquell and H. D. Evans. Droplet Size Distribution in Sprays. Industrial and Engineering Chemistry, 1951, Vol. 43, No. 6.
12. M. S. Volynskiy. Investigation of atomization of liquid in a supersonic flow. Third all-union conference on the theory of combustion. Vol. II. Academy of Sciences of the USSR, Moscow, 1960.
13. R. Dunlap, R. L. Erehm and I. A. Nicholls. A Preliminary Study of the Application of Steady-State, Detonative Combustion to a Reaction Engine. Jet Propulsion, 1958, Vol. 28, No. 7.
14. T. Pearcey and G. W. Hall. The Accelerated Motion of Droplets and Bubbles. Austral. J. Phys., 1956, 9, No. 1.
15. N. A. Fuks. "Mechanics of aerosols." Publishing House of the Academy of Sciences of the USSR, 1955.
16. V. A. Olevskiy. Collection of scientific research works of the Scientific research and design institute for mechanical processing of useful minerals, 1963, No. 8, pp. 7-43.
17. D. N. Vyrubov. Heat transfer and evaporation of droplets. ZhTF [Journal of Theoretical Physics] 1939, No. 9.
18. A. N. Krylov. Lectures on approximate calculations. State Technical Press, 1950.
19. A. Ya. Milovich. Theory of dynamic interaction of bodies and liquids. State publishing house of literature on construction and architecture, 1965.

20. S. A. Gol'denberg. Certain empirical laws in the area of turbulent diffusion. Publishing House of the Academy of Sciences, OTN, 1950, No. 4-5.
21. N. Frossling. Über die Verdunstung fallender Tropfen. Ger. Beil. zur Meteorophysik, 1938, Bd. 52, H 1/2.
22. W. R. Marschall and Ranz. Evaporation from Drops. Chemical Engineering Progress, 1952, Vol. 48, No. 3, 4.
23. A. R. Hall and Y. Diederichsen. An Experimental Study of the Burning of Single Drops of Fuel in Air at Pressures Up to Twenty Atmospheres. IV Symposium of Combustion, 1953.
24. M. A. Mikheyev. Fundamentals of heat transfer. GEL [State Power Engineering Publishing House] 1949.
25. V. G. Levich. Physicochemical hydrodynamics. Academy of Sciences of the USSR, 1952.
26. K. N. Yerastov. Third All-Union conference on the theory of combustion. Vol. II. Academy of Sciences of the USSR, Moscow, 1960.
27. R. I. Probert. Phil. Mag., 1946, 37, 94.
28. W. R. Lane. Shatter of Drops in Streams of Air. Industrial and Engineering Chemistry, 1951, Vol. 43, No. 6, p. 1312.

CHAPTER III

FORCED IGNITION AND BURNING OF UNIFORM FUEL-AIR MIXTURES IN A LAMINAR FLOW

At present there exist a large number of works, [1] to [10] on the theory of normal burning. Therefore we will note only the main results of the thermal theory of Zel'dovich which are necessary for explanation of the influence of different factors on burning velocity, using for this dimensional considerations. Normal burning is characterized by only two dimensional parameters: the molecular diffusion coefficient a (thermal diffusivity), which determines the rate of supply of active centers (heat) into the fresh mixture from the reaction zone (combustion products), and the rate of heat emission Φ_{\max} , which determines the characteristic time scale of combustion:

$$\tau \sim \rho_1 c_p T_1 / \Phi_{\max}.$$

Using these parameters, we can write a series of dimensional relationships, which are useful for qualitative analysis of experimental data:

$$u_n \sim \sqrt{a/\tau}; \quad \delta_n \sim a/u_n; \quad \tau \sim \frac{\rho_1 c_p T_1}{\Phi_{\max}} \sim p e^{-\frac{E}{RT_1}}, \quad (1.1)$$

where δ_n — characteristic scale of width of the laminar flame front;

p — pressure in the fuel mixture.

§ 1. INFLUENCE OF DIFFERENT FACTORS ON BURNING VELOCITY

At present there exists quite extensive experimental material on the influence of different factors on burning velocity: mixture ratio, initial temperature, pressure, molecule structure of the fuel and impurities. Let us note briefly the role of these factors.

Influence of mixture ratio. Normal velocity of the flame attains maximum value at some concentration of fuel and monotonically decreases with change of the mixture ratio in the direction of either impoverishment or enrichment of the fuel mixture.

Typical graphs of these dependencies for a series of hydrocarbon fuels applied in technology (gasoline, kerosene) and for simple gas fuels (methane, propane, and so forth) are shown in Fig. 3.1. An interesting peculiarity of these curves is that the maximum burning velocity for air mixtures never corresponds to a stoichiometric mixture ratio, but always is somewhat displaced in the direction of surplus fuel content. For hydrocarbon fuels this displacement is small. For instance, the maximum value of burning velocity for gasoline is attained at $\alpha = 0.93$ to 0.95 (Fig. 3.2).

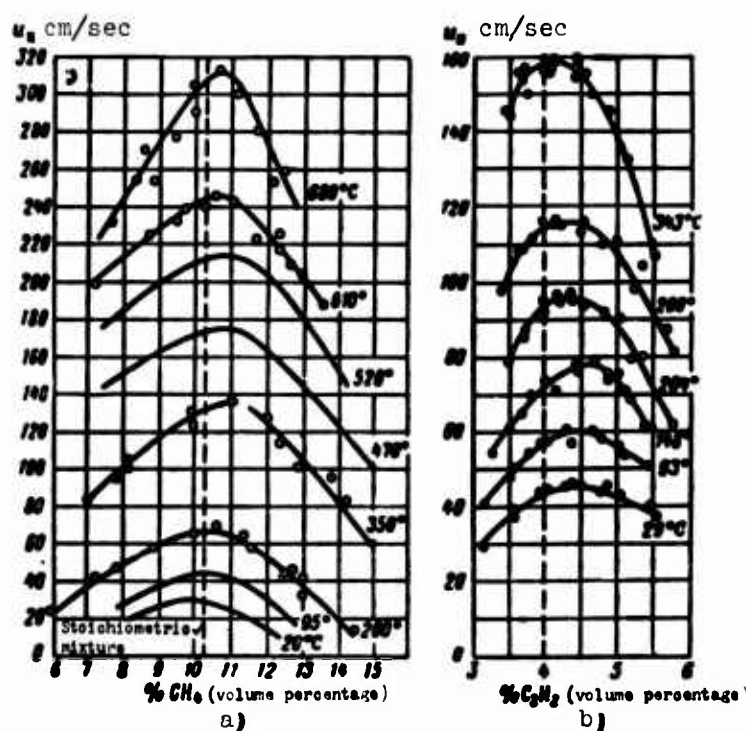


Fig. 3.1. Influence of mixture ratio and initial temperature on burning velocity of methane and propane. a) methane, b) propane (diameter of burner $5/8$ mm, $Re = 1500-2000$).

From the graphs one may also see that the velocity-versus-composition curve is asymmetric relative to its maximum value. A number of authors indicate that curves can be made more symmetric if we construct a function of mass rate $p\Delta u_H$ [$g/cm^2 \text{ sec}$] versus volume percent fuel content of the mixture [11]. Shift of the maximum velocity toward richer mixtures and asymmetry of the velocity-versus-composition

curve are not explained by simple dimensional formulas of the type of (3.1). Causes for them should be sought by more exact solution of the problem, possibly by taking into account inequality of diffusion rates of oxygen and fuel.

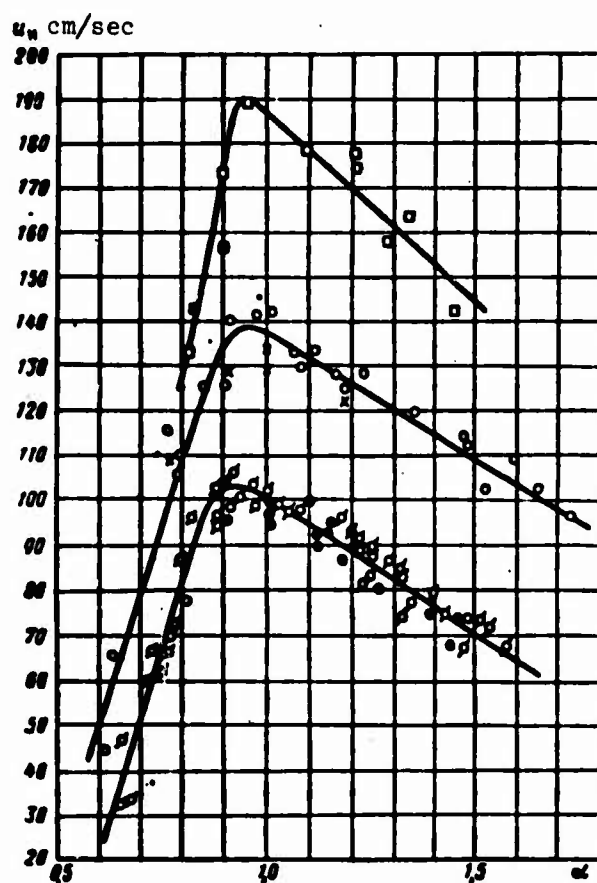
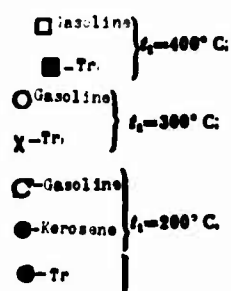


Fig. 3.2. Comparative $u_H = f(\alpha)$ characteristic for curves mixtures of gasoline, kerosene and Tr* with air for different initial temperatures.



*Tr is a direct transliteration of the Cyrillic Tp. It may refer to a type of jet fuel, Tp being an abbreviation for tybpoektubhoe, i.e., turbojet. [Tr. Ed. note].

Influence of initial mixture temperature. With increase of initial temperature of the fresh mixture, burning velocity also increases in accordance with results of thermal diffusion theories. The experimental dependence is well described by the relationship

$$u_H \sim T_1^{1.5-2.0}, \quad (3.2)$$

where T_1 - absolute temperature of the fresh mixture.

On Fig. 3.3 there are given the experimental data of a number of authors concerning the dependence of maximum velocity of flame propagation on temperature of the fresh mixture for a series of the most widely used hydrocarbon fuels and for hydrogen. Let us note that although this

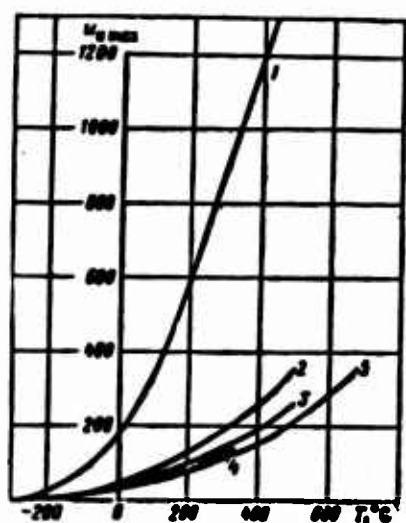


Fig. 3.3. Influence of initial temperature on maximum burning velocity. 1) hydrogen H_2 (data of Passauer); 2) ethylene C_2H_4 (data of Passauer and Daguerre); 3) gasoline (data of N. N. Inozemtsev); 4) propane (data of Daguerre); 5) methane CH_4 (data of Passauer and Daguerre).

dependence is strong, it is much weaker than the exponential dependence of flame speed on burning temperature T_2 [see formula (3.1)]. Experiment shows, in accordance with the theory, that between the quantities u_H and T_2 there is observed the following relationship for fuel-air mixture: burning velocity turns out to be higher, the higher the temperature of the combustion products, independently of whether or not mixture ratio or type of fuel changes [11].

Influence of pressure. The exact dependence of u_H on pressure has not been established at present. This is explained by the small degree of this dependence and the considerable errors of measuring methods. Many of the errors also depend on pressure. Therefore, it is expedient to give a table of experimental data obtained by various methods for different mixtures and ranges of pressures.

Data of foreign authors are taken from the monograph of NACA [17]. Knowledge of the dependence of u_H on pressure permits us to judge the total order of the chemical reaction for the given mixture (in the flame).

Table 3.1. Dependence of Burning Velocity on Pressure

Mixture	Air-fuel ratio α	Range of pressure p atm	Dependence of u_H on pressure	Total order of reaction	Method of measurement and author
Methane - air	1.00	0.7-1.0	-	2.0	Constant-volume bomb. Lewis (1953)
	1.00	0.33-1.0	-	2.0	Method of burner according to cone. Lewis (1953)
	1.00 or α_{\max}	0.25-1.0	$p^{-0.24}$	1.52	Burner. Wohl and Kapp (1949)
	0.685	1.0-6.3	$p^{-0.45}$	1.1	The same
	0.625-0.605	0.25-6.3	$p^{-0.5}$	1.0	The same
		0.26-0.66	$p^{-0.49}$	1.02	Method of flat flame. Edgerton and Seen (1953). Burner
Propane - air		1-4			Ubbelode and Kelliker (1916)
	1.00	0.7-1.0	-	2.0	Constant-volume bomb. Lewis (1953)
	1.00	0.33-1.0	-	2.0	Burner. Lewis (1953)
	1.00		$\log p$	-	Burner. Kallen (1953)
	0.642	0.26-0.66	$p^{-0.30}$	1.4	Method of flat flame. Edgerton and Seen (1953)
	α_{\max}	1-5	-	2.0	Ribaud and Gaudri (1936)
Butane - air	0.84	0.25-1.00	$p^{-0.30}$	1.4	Burner. Inozemtsev (1956)
	α_{\max}	0.2-1.0	$p^{0.17}$	2.34	Burner method. Wohl and Kapp (1949)
n-heptane - air	1.00	0.25-0.99	$p^{-0.36}$	1.28	Garner, Ashford and Long (1951) Burner. Ubbelode and Kelliker (1916)

Table 2. Continued

Mixture	Air-fuel ratio α	Range of pressure p atm.	Dependence of t_H on pressure	Total order of reaction	Method of measurement and author
Isocetane - air	1.00	0.53-0.22	$p^{-0.39}$	1.22	Garner, Ashford and Long (1951)
Ethane - air	1.00	0.33-1.0	$\log p$	-	Burner. Kallen (1953)
	1.00	0.05-1.5	-	2.0	Constant-volume bomb. Lewis (1953)
	0.325-0.807	0.30-0.80	-	2.0	Soap-bubble method. Pickering and Linnet (1951)
	0.714	0.35-1.0	$p^{-0.39}$	1.22	Burner. Linnet, Vitli (1949)
	0.683	0.26-0.66	$p^{-0.31}$	1.38	Flat flame. Edgerton and Seen (1953)
Acetylene - air		0.4-1.00			Burner. Ubbellyude and Kelliker (1916)
	α_{\max}	0.01-1.0		2.0	Burner. Wolfhard (1943)
	3.03	0.26-0.66	$p^{-0.47}$	1.06	Flat flame. Edgerton and Seen (1953)
Acetylene - O_2		1-2.00			Burner. Ubbellyude and Kelliker (1916)
	α_{\max}	0.01-1.0	-	2.0	Burner. Wolfhard (1943)
Gasoline - air	1.00	0.40-0.92	$p^{-0.31}$	1.38	Garner, Ashford and Long (1951)
	1.00 or α_{\max}	0.25-1.00	$p^{-0.15}$	1.7	Burner. Inozemtsev (1956)
		0.4-1.00			Burner. Ubbellyude and Kelliker (1916)

From relationship (3.1) it is clear that u_H is connected with parameters depending on pressure in the following manner:

$$u_H \sim \sqrt{\frac{a \cdot \Phi_{\max}}{h}}, \quad (3.3)$$

where according to the kinetic theory of gases

$$a \sim 1/\rho, \quad \Phi_{\max} \sim p \quad \text{and} \quad \rho_1 \sim p,$$

so that

$$u_H \sim p^{1/2-1} = p^{-1/2}.$$

Values of ν given in Table 3.1 show that for hydrocarbon-air mixtures, total order of reaction lies somewhere between units and two, so that with decrease of pressure, normal velocity increases on the average. For tentative calculations it is possible, apparently, to take average value of m equal to 0.25. Growth is observed only up to certain finite values of pressure ($P \geq 0.3$ atm), after which velocity starts to drop due increase of role thermal losses to walls, and so forth (see § 2, Chapter III). For fuel-oxygen mixtures, behavior of u_H noticeably differs with change of pressure. Majority of authors indicate independence of u_H from pressure; i.e., for oxygen mixtures $m \approx 0$ and $\nu \approx 2$.

The influence of impurities on flame speed is two-fold. If we add to the fuel mixture as impurities inert gases such as CO_2 ; N_2 ; He; Ar, then this will not cause chemical changes of the given mixture, but will change only its physical properties: relative concentration of fuel (oxidizer), heat capacity, thermal diffusivity, and "mass transfer" of the mixture, etc. Therefore, deceleration of normal burning by dilution of the fuel mixture should be for any inert diluent (including for dilution of oxidizer or fuel) practically identical, if when there is high dilution, change of other physical parameters (besides relative mixture ratio) turns out not to be large. Experiment confirms these simple physical considerations.

In Fig. 3.4 [11] there are given graphs of the dependence of maximum flame speed for CO , CH_4 and H_2 on the percentage substitution of nitrogen and carbon dioxide for oxygen. More detailed observations taking into account other factors (thermal conduction, heat capacity of the diluent, and so forth) show that according to degree of "legmatizing" action, it is possible to arrange inert gases in the following order: CO_2 ; N_2 ; He; Ar (the quantity $(\lambda/c_p) \cdot 10^5$ is equal respectively to 15, 25, 27, 55 cm [11]).

Active impurities affect the magnitude of u_H absolutely differently. When a small amount of them are added, they change chemical reaction rate considerably (usually increase it). Additions of active impurities make it possible for a chemical reaction to go in different ways, with lower activation energies and accordingly with high rates. A classical example is the process of ignition and burning of carbon monoxide with oxygen. It is known that a thoroughly dried mixture carbon monoxide with oxygen does not ignite at all (flame speed is equal to zero), but it is sufficient to add a small quantity of water vapor to cause the flame speed to attain a noticeable magnitude; then increases with further increase of concentration of water vapor. In this case, water vapor gives active OH radicals, which are the necessary additional link in the chain of reactions proceeding with high rate.

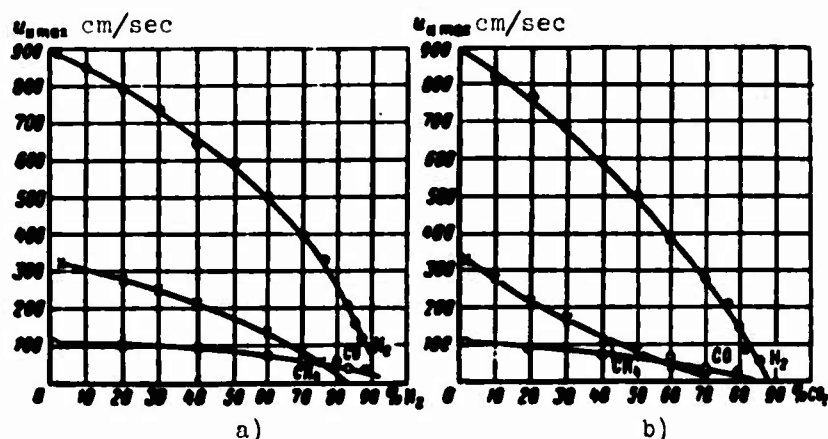


Fig. 3.4. Change of maximum flame speed depending upon percentage substitution of nitrogen (a) and carbon dioxide (b) for oxygen.

With further increase of concentration of the active impurity, it starts to play the role of an inert diluent, so that at some concentration of it magnitude of u_H attains maximum value, after which it decreases. For instance, for a wet mixture of CO with air at atmospheric pressure, the optimum value of u_H is attained at approximately 9% concentration of water vapor. Mixtures of different fuels can serve as active impurities with respect to one to another. Thus, for instance, a mixture of carbon monoxide with methane and air gives flame speed higher than the flame speed in mixtures of air with each of these gases separately (flame speed in these mixtures are approximately identical: $u_H = 38$ cm/sec for CH_4 and 43 cm/sec for CO). Combination of CO and CH_4 vapor exactly creates the possibility for appearance in the burning zone of the concentration of active OH radicals necessary for high reaction rate of CO with air.

The optimum value of flame speed in such a complex mixture, which is equal to 65 cm/sec, is obtained at concentrations of CO and CH₄ which are 94% and 5% of the total quantity of fuel respectively [11]; this indicates a unilateral influence: methane is the active impurity with respect to carbon monoxide. In principle there is possible a mutual activating influence of two or more fuels in a complex mixture. At present, the influence of impurities on burning rate of fuel-air mixtures is the object of extensive independent experimental investigations, which are undoubtedly of practical interest. It is sufficient to compare the burning rates of the applied hydrocarbon fuels with the burning rate of hydrogen (see Fig. 3.3) in order to be convinced that burning rates of these fuels are not the limit.

Influence of molecular structure of the fuel. Accumulated experimental material on u_H for different hydrocarbons permits us to express certain considerations about the influence of molecular structure of hydrocarbon fuels on the magnitude of u_H .

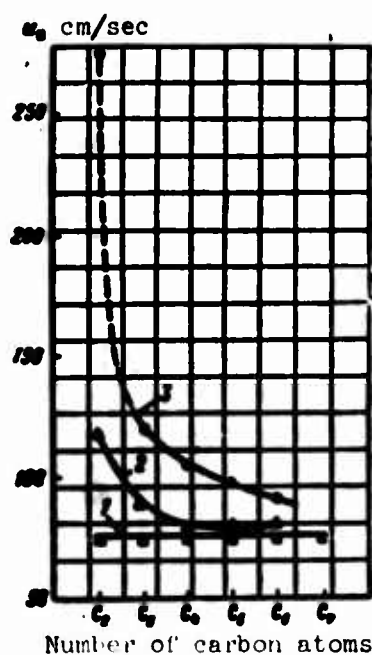


Fig. 3.5. Maximum flame speed for normal hydrocarbons depending upon number of carbon atoms in the molecule. 1) H -- alkanes C-C-R; 2) H -- alkenes C=C-R; 3) H -- alkynes C≡C-R.

In Fig. 3.5 there are given data of Gershteyn, Melvin and others [11] [17] on the influence of number of carbon atoms on maximum flame speed for different classes of hydrocarbon fuels. There is given the dependence of u_H on number of carbon atoms within one class and the dependence of u_H for identical number of carbon atoms for hydrocarbons of three different classes:

1. Alkane class - saturated hydrocarbons: ethane (C₂H₆), propane (C₃H₈), butane (C₄H₁₀), pentane (C₅H₁₂), hexane (C₆H₁₄).
2. Alkene class - unsaturated hydrocarbons having a double bond: ethylene (C₂H₄), propylene (C₃H₆), butene-1 - (C₄H₈), pentene-2 (C₅H₁₀), hexene-1 (C₆H₁₂).
3. Alkyne class - unsaturated hydrocarbons having one triple bond: propyne (C₃H₄), butyne-1 (C₄H₆), pentyne-1 (C₅H₈), hexyne-1 (C₆H₁₀).

In Fig. 3.5 it is seen that flame speed decreases with increase of saturation of molecular bonds. For saturated hydrocarbons (molecules with multidimensional bond, alkane class) this speed is least; its magnitude does not change with increase of

the number of carbon atoms. Increase of flame speed as compared to that of saturated hydrocarbons turns out to be more noticeable, the greater the degree of non-saturation. For instance, the difference for transition from hydrocarbons with double bond to hydrocarbons with single bond (saturated hydrocarbons) to hydrocarbons with double bond. As molecules become heavier, flame speed for unsaturated hydrocarbons tends to the flame speed for saturated hydrocarbons. All these peculiarities are fully explainable: the fewer the free bonds of a molecule, the more difficult it is for it to enter into a compound with oxidizer molecules, the heavier it is, the less is its inclination to break old bonds during thermal collisions and to form new ones; all this, in the final result; leads to deceleration of burning.

§ 2. FORCED IGNITION

Above it was noted that in combustion chambers, the mixture does not ignite by itself. In order to ignite it, it is necessary to somehow accelerate the chemical reaction in a small volume of the given mixture. This can be done by introduction of a catalyst into the mixture, a source of active centers and a source of heat. A heated wire, pilot flame, hot gas, shock wave, electric spark (capacitive or inductive) etc., can serve as the heat source. During attempts to ignite the mixture, it is seen that there exist ignition boundaries (with respect to composition, temperature and pressure of the mixture), beyond which the mixture is not ignited by the given heat source, and also ignition limits, beyond which the mixture is not ignited by any source under any ignition conditions. It is fully understandable that it is necessary to establish the boundaries and limits of ignition for fire safety and for determination of the reliability of operation of the combustion chambers under different conditions.

To this question there have been dedicated a large number of theoretical and experimental works. The existence of the concentration boundaries of ignition was shown for the first time in the work of Mallard and LeChatelier (1883). They established that in a given vessel, for a given heat source, there exist fully defined limiting values of fuel concentration, beyond which a mixture will not be ignited. The boundary corresponding to the smallest percentage of fuel is called the lower boundary, and the boundary corresponding to the largest percentage is called the upper boundary. If we construct for the given vessel values of boundary concentrations of different fuels as functions of the heat source power necessary for ignition, then we will obtain curves of the same type, which are shown in Fig. 3.6.

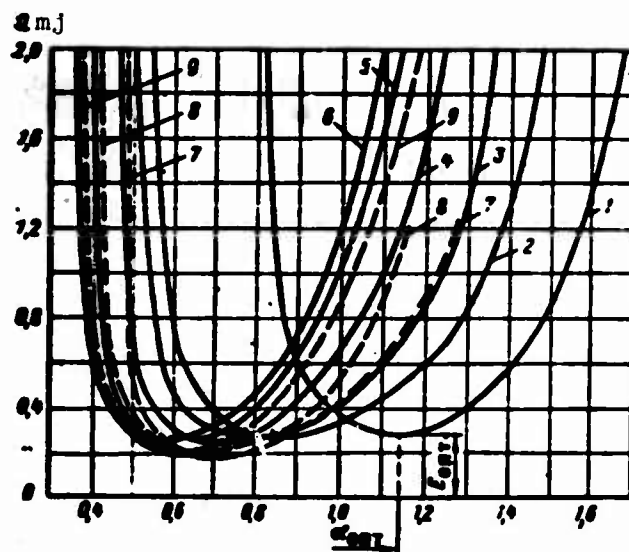


Fig. 3.6. Ignition energy depending upon composition of fuel-air mixture. ($p = 760$ mm Hg; $t \approx 20^\circ\text{C}$). 1) methane; 2) ethane; 3) propane; 4) butane; 5) hexane; 6) heptane; 7) cyclopropane; 8) diethyl ether; 9) benzene.

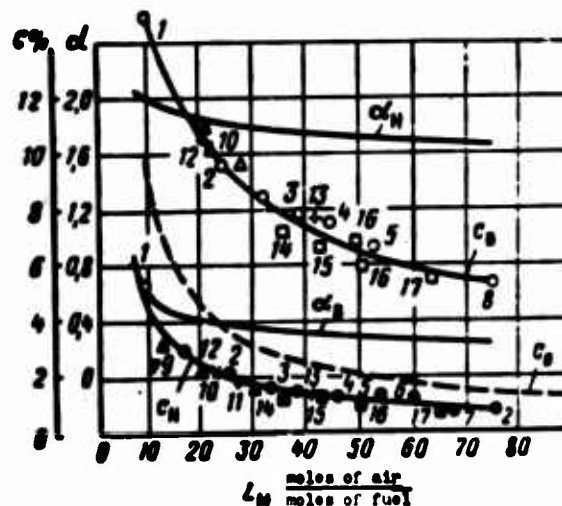


Fig. 3.7. Concentration limits of flame propagation in hydrocarbon-air mixtures in dependence on stoichiometric coefficient.

($t \approx 20^\circ\text{C}$; $p = 760$ mm Hg) $\circ \bullet - \text{C}_n\text{H}_{2n+2}$;

$\Delta \Delta - \text{C}_n\text{H}_{2n}$; $\Delta \nabla - \text{C}_n\text{H}_{2n-2}$;
 $\square \square - \text{C}_n\text{H}_{2n-4} + \chi - \text{C}_n\text{H}_{2n-6}$ (cycloolefins)

1) methane; 2) propane; 3) n-pentane; 4) n-hexane; 5) n-heptane; 6) n-octane; 7) n-nonane; 8) n-decane; 9) n-ethylene; 10) propylene; 11) butyne-1; 12) cyclopropane; 13) cyclohexane; 14) benzene; 15) toluene; 16) o-xylene; 17) n-butylbenzene.

From Fig. 3.6 it is clear that for every mixture there is a minimum source power: a source of less power will not ignite the mixture regardless of its composition. In Fig. 3.7 it is shown that both branches of boundary concentrations of fuel (they are frequently called, referring to the fuel, "poor" and "rich" branches) asymptotically tend to the limiting values, beyond which the mixture will not ignite, regardless of the source power. If ignition is carried out in a sufficiently large volume, far from the walls of the vessel, then these limiting values of concentration are called by the concentration limits of ignition.

§ 3. CONCENTRATION LIMITS OF IGNITION OF A COMBUSTIBLE MIXTURE

Concentration limits of ignition to a considerable degree are physicochemical constants of fuel mixtures, inasmuch as by definition they do not depend on heat source power or dimensions of the vessel, but only on properties of the mixture itself: kind of fuel, temperature, pressure, and so forth. Attainment of full independence of ignition limits from conditions of experiment turns out to be not always possible in practice. For instance, at pressures lower than 0.3 atm, the source strongly increases, so that concentration limits of ignition obtained at such low pressures as a function of pressure should be considered only as ignition boundaries of the fuel mixture obtained on the given experimental installation with the given ignition source (Fig. 3.8). Therefore, concentration limits of ignition are usually given at pressure considerably higher than 0.3 atm. Under such conditions, values of concentration limits obtained by different authors on different experimental installations turn out to be practically identical. In Table 3.2 there are given data on concentration limits of ignition of a series of fuels at $t = 20^{\circ}\text{C}$ and pressure of 1 atm.

Analogous, but more extensive tables are given in the books: Iost [12], Lewis and Elbe [13], Khitrin [11] and in the NACA monograph [17].

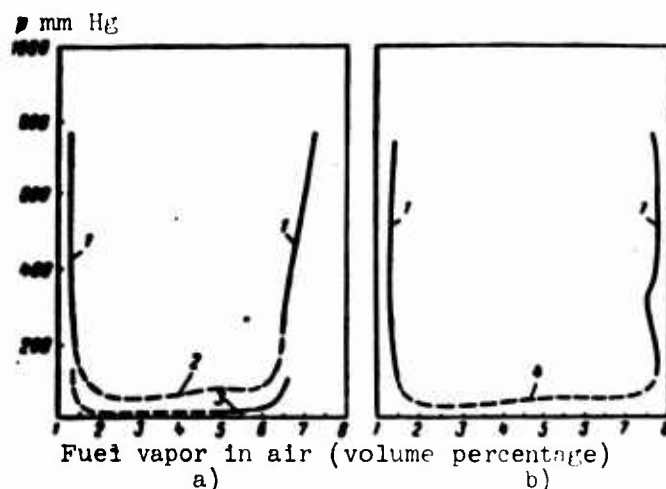


Fig. 3.8. Limits (boundaries) of flame propagation for petroleum fuels at lowered pressures in a closed pipe with diameter of 50.8 mm. a - aviation gasoline of type 100/130 (temperature 25°C). 1) limits of flame propagation; 2) ignition boundaries using a heating spiral of Ford brand; 3) ignition boundaries using a generator of the Bureau of Mines; 6) rocket fuel of type JP-3 (temperature 26°C); 1) limits of propagation of flame; 4) ignition boundaries using a transformer (15 kilowatts, 30 atm (abs.)).

Table 3.2. Stoichiometric Coefficients, Concentration Limits of Ignition and Normal Flame Propagation Velocity

Fuel	Chemical formula	Stoichiometric coefficient		Concentration of fuel in volume %			Air-fuel ratio at ignition limits		Maximum normal flame propagation velocity v_{H_0} in cm/sec	Fuel concentration in volume % at v_{H_0}
		L_0 kg air kg fuel	L_m moles of air moles of fuel	stoichiometric composition C_0	lower concentration limit C_L	upper concentration limit C_B	lower	upper		
Hydrogen	H_2	34.5	2.39	29.50	4.0	75	10.1	0.14	315	42.2
Acetylene	C_2H_2	13.25	11.96	7.75	2.5	81	3.57	0.018	170	5.9
Ethylene	C_2H_4	14.8	14.36	6.56	2.7	34	2.51	0.135	68.3	7.40
Methane	CH_4	17.23	9.56	9.5	5	15	1.98	0.59	55.8	9.9
Benzene	C_6H_6	13.3	35.85	2.73	1.4	7.1	1.96	0.36	40.7	5.34
Propylene	C_3H_6	14.8	21.5	4.47	2.0	11	2.28	0.37	45.8	6.04

From Table 3.2 it is clear that the range of concentrations in which propagation of flame is possible, turns out to be wider, the higher the maximum burning velocity, or, accordingly, the higher the maximum flame temperature. Existing data on limits show that "lean" limits turn out to be approximately identical for all types, but "rich" limits have a tendency to increase with decrease of molecular weight, so that the limiting range of ignition is expanded.

Isoparaffins have a somewhat narrower concentration range of ignition than linear hydrocarbons. Cycloparaffins have approximately the same range of ignition as normal paraffins with the same number of carbon atoms [17]. Experiment also shows that for the majority of fuels, the temperatures of combustion products at the ignition limits turn out to be approximately identical, equal to $\sim 1600^\circ\text{K}$. Thus, burning velocities also turn out to be approximately identical for the lower and upper limits. According to experiments of Edgerton [11], for a plane flame the minimum critical mass rate for different hydrocarbon fuels practically does not depend on pressure ($p \geq 0.3 \text{ atm}$), mixture ratio, impurities, etc., and is equal to

$$m_{cr} = \rho_1 u_n = (3+4) \cdot 10^{-3} \text{ g/cm}^2 \text{ sec.}$$

According to measurements conducted under nonoptimal conditions (for determination of the influence of walls of the vessel, etc.), limiting rates turn out to be somewhat higher, but of the same order, $\sim 10 \cdot 10^{-3} \text{ g/cm}^2 \text{ sec}$ [11]. The given peculiarities of concentration limits of ignition are sufficiently well generalized by the universal curves shown in Fig. 3.7.

On the graph, along the axis of abscissas, there is plotted the magnitude of the stoichiometric coefficient expressed in moles (stoichiometric coefficient expressed in moles L_M is connected with the weight stoichiometric coefficient L_0 by the relationship $L_M = \frac{\mu_T}{\mu_B} L_0$, where μ_T and μ_B are molecular weights of propellant and air respectively); along the axis of ordinates there are plotted: limiting concentrations of fuel (in volume %) at the lower (c_H) and upper (c_B) ignition limits, fuel concentrations for stoichiometric mixture ratio (c_0), and also values of air-fuel ratio at the lower and upper limits (α_H and α_B). From Fig. 3.7 it is clear that values of α_H and α_B for different fuels decrease with increase of L_M . Thus the difference ($\alpha_H - \alpha_B$) remains approximately constant and equal to 1.4. The dependence of ignition limits on pressure, percent of inert impurities and other physicochemical properties of the mixture is more conveniently considered together

with corresponding dependences of the ignition boundaries, inasmuch as these dependencies are qualitatively identical, so that it is not always possible to say whether or not the obtained extreme boundaries are really limiting and do not depend on power or form of the ignition source or other specific conditions of the experiment.

What is the physical nature of the existence of concentration limits of flame propagation? The above mentioned solution of Zel'dovich for the quantity u_H does not give such limits (according to this solution, at continuous "leanness" or "richness" of the mixture, burning velocity continuously decreases to zero). As Zel'dovich indicated for the first time [1], the limit to the existence of flame speed is determined by radiation losses occurring in the plane flame front and heat removal in the direction of the cooler combustion products behind the front. The relative role of rate of heat losses increases with decrease of rate of heat release in the front. At certain finite values of rate of heat emission and rate of thermal losses, the surplus rate of heat emission turns out to be insufficient to provide heating of the following cold layers of fresh mixture. Therefore, the flame front turns out to be incapable of propagating through the given mixture, no matter in what pipe it is located or what the ignition source is. Another possible cause of ignition limits may be specific characteristics of the chemical reactions: transition of the statistical system of the mixture beyond known concentration limits into a new, more stable state.

In distinction from ignition limits, concentration boundaries of ignition further depend on a series of other, not always present sources of heat losses, which are determined by specific experimental conditions (geometry of the pipe, and power, geometry and form of ignition source, etc.). Therefore, establishment of boundaries of forced ignition essentially reduces to clarification of the influence of each of these factors on ignition boundaries. Let us consider the main factors.

§ 4. INFLUENCE OF DIFFERENT FACTORS ON CONCENTRATION BOUNDARIES OF IGNITION

Influence of pipe diameter. Due to heat removal through walls of the pipe (or active centers on the wall), concentration boundaries of u_H will decrease. According to Zel'dovich [1], this influence will be decisive when the pipe diameter is comparable with the width of the laminar flame front δ_L . On the basis of this consideration, we will determine a series of dependences of the limiting diameter of

the pipe, in which a flame still exists, on physicochemical properties of the mixture: magnitude of u_H , pressure, temperature, and etc:

$$d_{tp} \sim \sigma_1 \sim a/u_H \sim \lambda/c_p \rho_1 u_H \sim 1/p \cdot u_H. \quad (3.4)$$

Experimentally a dependence of the form $u_H \rho_1 c_p d_{tp} / \lambda = \text{const}$ was verified experimentally by Lewis and Elbe.

For hydrocarbon-air mixtures with stoichiometric composition at normal pressure and a temperature of 100°C , values of limiting diameters oscillate within the interval 1.67-1.85 mm [17]. With increase of pipe diameter, the influence of the walls asymptotically decreases. On Fig. 2.9 [17] there are given concentration boundaries of ignition as a function of the pressure of a propane-air mixture (lean branch) for different pipe diameters (with a source of maximum power). Only for pipe diameters $d_{tp} > 66$ mm is this influence weak in practice. Therefore, the majority of investigations of boundaries and limits of ignition are conducted in pipes with open ends (to avoid the influence of variable pressure) with diameter of ≈ 66 mm, set vertically (to avoid nonuniformities due to the influence of convection, gravitation and other effects). There are investigated the concentration limits of flame propagation during its motion from bottom to top and from top to bottom (see Table 3.2). These limits during motion of the flame from bottom to top turn out to be usually somewhat wider than during its motion from top to bottom or in the case of its horizontal propagation.

The minimum distance between the end of the pipe and the edges of the flame cone of a Bunsen burner, (i.e., the distance at which heat loss to the walls of the burner is decisive) has the same properties as the limiting diameter but absolute values of these distances turn out to be (according to [17]) more than twice as small as values of the limiting diameters.

Influence of form, material and geometry of the ignition source. An ignition source of any form (catalyst, heat source, source of active centers) creates in some volume of mixture a certain excess quantity of heat or active centers. This quantity of heat (centers) should be sufficient to cause [by diffusion of heat (centers)] burning in adjacent layers of the mixture and to thereby begin the propagation of flame from the given volume throughout the entire mixture. The excess quantity of heat (centers) in the considered volume is created, on the one hand, by the external source, and on the other — by chemical reaction in this volume. The relative roles

of heat added from without and heat released by the chemical reaction essentially depend on the temperature at which the heat is added.

If heat is brought in at a temperature lower than the temperature of products of total combustion of the given mixture, then ignition conditions essentially depend on the heat released during the chemical reaction, since namely this heat should lead,

in the final result, to formation of a flame front around the igniting volume. Therefore, ignition under such conditions should depend essentially on such factors as temperature of the ignition source, its time of stay in the igniting volume, its catalytic action on the chemical reaction, material of the ignition source, direction of heat flow (geometry of the source), and so forth.

If, however, heat is brought in at very high temperature, to a very small volume, then the fraction of heat released in this volume by the chemical reaction may be small by itself, and factors determining the length of time for its release become immaterial, since this time is quite short, and therefore is not a limiting factor. Thus, the role of the specific characteristics of the ignition source continuously decreases with decrease of its dimensions and increase of the temperature at which the heat is brought in.

Determination of ignition conditions at temperatures less than the temperature of products of total combustion of the mixture turns out to be a more complicated problem than determination of ignition conditions at higher temperatures. Of the existing theoretical solutions of problems of this type, apparently not one can be considered to be correct, since none of these solutions consider the factor of time which is essential for these problems, (the non-stationary character of the problem). In combustion chambers, ignition of the first type is not met in practice: the limiting case is burning behind a flame holder, where temperature of the igniting volumes is exactly equal to T_2 .

The most widely used ignition source is an electric discharge (spark). An electric spark creates a surplus of heat, as well as a surplus of active centers — charged molecules, atoms and radicals — which accelerate the oxidation reaction.

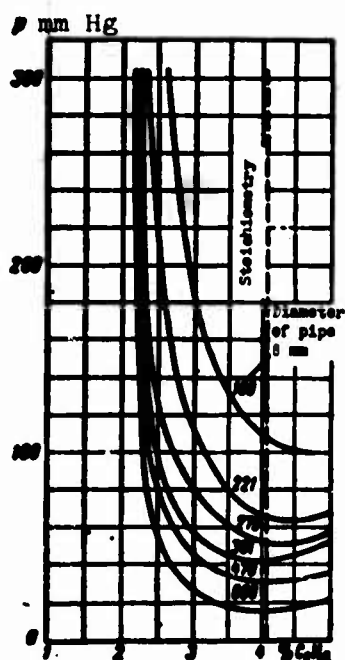


Fig. 3.9. Influence of pipe diameter on ignition boundaries as a function of pressure (lean branch). Propane in air.

There appears the question: what mechanism of ignition (thermal or ionic) will play the decisive role? Analysis of existing experimental data permits us to expect that also in this case, thermal acceleration of chemical reactions is predominant, especially at sufficiently high pressures (higher than 50 to 100 mm of Hg). This is indicated in particular by the fact that when thermal power of the electric spark is sufficiently high, concentration boundaries of ignition turn out to be sufficiently stable, and close to the ignition boundaries for purely thermal sources. Only at very low pressures and high discharge velocity is it possible to expect that the chemical reaction will be accelerated mainly due to activation caused by ionized molecules moving with high speeds under the action of the electrical field. Any other possible ignition source (pilot flame, hot gas, incandescent body, etc.) is chiefly a thermal source. Therefore, for all methods of ignition interesting in practice, it is possible to assert that not the form of the ignition source will be decisive, but its thermal power.

§ 5. CONDITIONS OF FORCED IGNITION (INFLUENCE OF THERMAL POWER OF IGNITION SOURCE)

It is necessary to distinguish the power necessary for ignition of a mixture by a given ignition source in a given pipe from the minimum power sufficient for ignition of the given mixture. Required power includes all possible losses of heat, which are determined by conditions of the experiment, and also the minimum power. Minimum power is a physicochemical parameter of the given mixture, whereas required power can depend to a great extent on diameter of the pipe, geometry and material of the ignition source and so forth. Creation of the best conditions for ignition reduces, obviously, to decrease of the required power to a minimum. Let us estimate the magnitude of minimum power sufficient for ignition.

Let us consider at first the case when in the mixture there instantly appears a rectangular temperature profile of the total combustion products of the given mixture, and accordingly a rectangular profile of zero fuel concentrations. Shape of the initial igniting volume can be a sphere, cylinder or a plane of finite thickness. It is necessary to determine the dimensions of this volume which are sufficient for formation of a laminar flame front around it. Inasmuch as combustion products are motionless, the formed flame front will move relative to the axis of the volume with velocity $u_1 T_2 / T_1$. If the initial dimension of the volume R (radius of a sphere or cylinder or half-width of a plane) is sufficiently large, then the total thermal

width of the front will continuously increase from zero to its limiting value $\sim \sigma_{\Pi}$. Otherwise, velocity $u_1(t)$, after attaining a certain limit less than u_H , will start to decrease continuously (due to decrease of the total integral of heat emission), and speed of increase of the width of the front, after attaining a minimum different from zero, will again start to increase and to approach as a limit the diffusion speed of "erosion" of boundaries of the initial igniting volume.

The dimension of the volume which is necessary and sufficient for ignition, can be determined by the condition

$$R + \frac{T_2}{T_1} \int_0^{\tau^*} u_1(t) dt \sim \sigma_{\Pi} \quad (3.5)$$

(τ^* - characteristic time of formation of the front; this is a quantity of the same order of magnitude as the characteristic burning time τ , but, apparently, smaller) or

$$R \sim \sigma_{\Pi} - \frac{T_2}{T_1} u_{\Pi} \tau \sim \sigma_{\Pi} \left(1 - k \frac{T_2}{T_1}\right) \quad (k - \text{an empirical constant}). \quad (3.5a)$$

If we disregard the second term in the right side of expression (3.5a), we will obtain

$$R \sim \sigma_{\Pi} \quad (3.5b)$$

This condition, which determines the dimension of the minimum igniting volume, is sufficient, but not necessary, since, according to (3.5a), at large T_2/T_1 smaller dimensions of the volumes igniting the mixture are possible. The dimension determined by condition (3.5b) is, as it were, the dimension, which guarantees ignition. The quantity of heat contained in such a volume is composed of the heat brought in from without and the heat released by the chemical reaction. The fraction of heat supplied from without is determined by a series of factors, including the dependence of heat capacity on temperatures and length of time of heat addition. If heat brought in from without instantaneously brings the temperature of the mixture to T_2 , at which the heat capacity of the gas is high, then subsequently the temperature of the volume practically does not change due to the chemical reaction, so that for simplicity of calculation it is possible to take the upper limit of the minimum energy guaranteeing ignition to be equal to the energy of complete combustion of the fresh mixture in a volume with dimension of $\sim \sigma_{\Pi} \cdot \rho_2 / \rho_1$. Thus, in the case of a sphere, cylinder or plane, the minimum powers guaranteeing ignition, with accuracy up to that of the empirical coefficient, are determined (taking into account further thermal expansion) respectively as

$$\left. \begin{aligned} Q &\sim c_p \rho_2 (T_2 - T_1) \sigma_n^2 \\ Q &\sim c_p \rho_2 (T_2 - T_1) \sigma_n^2 \\ Q &\sim c_p \rho_2 (T_2 - T_1) \sigma_n \end{aligned} \right\} \quad (3.6)$$

Let us consider now the case when the igniting volume has an arbitrary temperature profile, with maximum temperature higher than the temperature of total combustion products of the given mixture. After cessation of supply of heat into the igniting volume, it will start to expand with time due to diffusion and combustion of the available fresh mixture, but the maximum value of temperature will begin to decrease due to diffusion the total reserve of introduced heat remains constant. As such an example, we may mention the electric spark. An electric discharge creates (practically, instantaneously relative to the burning times) in an infinitesimal volume a field of temperatures of the order of 10,000-20,000°C. In this case the length of time of formation of the igniting volume will be the largest; therefore, the fraction of additional heat emission due to combustion of the mixture in the formed volume will be the largest. However, it is possible to consider that in this case its role will be immaterial, since combustion of the mixture in the high-temperature region of the initial volume will change these temperatures insignificantly. Therefore, for practical calculations it is possible to disregard change of the temperature profile of the igniting volume due to chemical reaction, and to consider this change to be purely diffusional.

Conditions for selection of the quantity of thermal energy sufficient for ignition may be in this case, or any other intermediate case, formulas as follows: time for drop of maximum temperature to the value T_2 should be larger than, or in the limiting case equal to the time of expansion of the igniting volume to the characteristic dimension R , which is approximately equal to σ_n . Then the dimensions of the arbitrary initial temperature profile will, in time, approach those of the square profile considered above, for which ignition was guaranteed. In the case of diffusion the time necessary for drop of temperature to the value T_2 will be determined for a sphere, cylinder and plane respectively by the relationships

$$\begin{aligned} c_p \rho_2 (T_2 - T_1) &= Q \sqrt{2\pi} \sigma_n^2; \quad c_p \rho_2 (T_2 - T_1) = Q \sqrt{2\pi} \sigma_n^2; \\ c_p \rho_2 (T_2 - T_1) &= Q \sqrt{2\pi} \sigma_n \end{aligned}$$

where Q is the initial quantity of heat introduced into the mixture.

For an initial volume close to a cylinder or to a plane, this quantity of heat pertains to a unit of length of the cylinder or to a unit of area of the plane;

σ — characteristic scale of diffusion of the igniting volume: $\sigma^2 = 2at$,

where $a = \lambda / c_p \rho_1$ — coefficient of thermal diffusivity.

The characteristic dimension of the igniting volume attains a value of $\sim \sigma$ in the time $t = \sigma^2 / 2a$. The above formulated boundary conditions, which guarantee ignition, will be written in the form

$$Q \sim c_p \rho_2 (T_2 - T_1) \sigma_1^2; \quad Q \sim c_p \rho_2 (T_2 - T_1) \sigma_2^2; \quad Q \sim c_p \rho_2 (T_2 - T_1) \sigma_3 \quad (3.7a)$$

or

$$\left. \begin{aligned} Q &\sim c_p \rho_2 (T_2 - T_1) a^3 / u_1^3; \quad Q \sim c_p \rho_2 (T_2 - T_1) a^2 / u_2^2; \\ Q &\sim c_p \rho_2 (T_2 - T_1) a / u_3 \end{aligned} \right\} \quad (3.7b)$$

These conditions, as can be seen, coincide with conditions (3.6). Condition (3.7) for a spark (sphere) was for the first time formulated by Zel'dovich [3] in the form of a working hypothesis. This condition, just as condition (3.6), is sufficient, but not necessary: it guarantees ignition, but this does not mean that ignition cannot occur with lower power of the spark. If these conditions are considered as necessary (as the ignition criterion), then this is true only with accuracy up to that of the previously made assumptions. In combustion chambers, ignition is carried out in moving mixtures. The ignition source can be either single-action (spark) or continuous-action (an incandescent body maintained at constant temperature, flame holder, etc.). In the first case, minimum source power is determined by the relation (3.7a) or (3.7b), depending upon the shape of the initial igniting volume.

In the case of ignition by an incandescent body, the body gives its heat to the flow only in the thin laminar boundary layer adjacent to the surface of the body. Being heated approximately to the temperature of the body T_s , this layer will run off behind the body in the form of a sheet, whose width is equal to the maximum

thickness of the heated boundary layer grown on the body $\delta_n \sim \sqrt{\frac{d \cdot a}{v}}$ (v — velocity

of the flow; d — dimension of the body, which determines the length of the section in which the boundary layer is built up; a — coefficient of thermal diffusivity).

If flow is laminar and continuous, then this sheet will be in the form of a plane

after a linear heat source or in the form of a cylinder after a point source. During turbulent, detached flow around the body, the laminar heated shell will break up immediately behind the body into separate "hot" vortices. The total rate of heat transfer of the body increases due to increase of the total surface of the turbulent sheet, although the characteristic dimension of the vortex and the temperatures in it remain the same. Thus, ignition conditions in the flow of the mixture reduce to the conditions considered above. If, for instance, by the moment of separation of the layer from the body the characteristic temperature in it is close to T_2 , then the ignition condition will be simple:

$$\left. \begin{aligned} \delta &\sim \sqrt{\frac{d \cdot a}{v}} \sim a, = \sqrt{a \cdot \tau} \\ \frac{d}{v} \cdot \tau &\sim e^{-\frac{E}{RT_2}} \end{aligned} \right\} \quad (3.8a)$$

This condition, which is frequently given in the literature, is derived on the basis of the most diverse ideas, which are sometimes not quite correct. However, to a certain extent it is justified if T_s and T_2 are of the same order, and if it is not applied to the case when T_s is much less than or much greater than T_2 . In this case, also very approximate, but more correct will be the condition

$$(T_s - T_1) \sqrt{\frac{da}{v}} \sim (T_2 - T_1) a. \quad (3.8b)$$

The thermal power of such an ignition source is determined, obviously, by the quantity of heat necessary for maintaining in it a temperature equal to T_s , when flow velocity and source dimensions are determined by relationships (3.8a and b). The condition for ignition by an incandescent body should not be confused with the condition for stabilization of the flame by the same body, although in practice these conditions may not be distinguishable. The nature of stabilization is apparently basically the same as the nature of forced ignition by an incandescent body. Turbulent exchange from the stagnant zone after the stabilizer, which is filled, as experiment shows, with products of total combustion of the mixture, ejects into the flow individual moles of burnt mixture. Rate of exchange (turbulent rate of ejection), as experiment shows, is proportional to flow velocity, so that conditions for ignition of the mixture of the incident flow again lead to consideration of

relationships between the necessary and sufficient dimension of a mole and the width of the flame front in the turbulent flow. With the help of a series of hypotheses, stabilization conditions usually lead to relationships of the form (3.8).

If for instance, we assume that turbulent exchange between the zone and the flow around it is carried out by turbulent vortices formed during flow around the stabilizer, then stabilization conditions will be written in a form analogous to the relationship (3.8).

The above mentioned conditions of ignition and stabilization qualitatively correspond to conditions obtained experimentally if the required power is practically equal to the minimum power which guarantees ignition, i.e., if loss of the heat supplied by the ignition source is insignificant. Radiation heat losses can apparently always be disregarded, since they are relatively small and, furthermore, are approximately identical, which is taken into account by the empirical constant. Heat loss to the surface of the incandescent body and stabilizer also is practically absent. An exception is the spark at electrodes located very close to each other. In this case, while the igniting volume passes with local flow velocity past the cold electrodes, the electrodes have time to "withdraw" from it a sufficiently large quantity of heat, so that the heat, remaining in the igniting volume turns out to be insufficient for formation of a flame front around it. In order to ignite the mixture under conditions, there is required a power which is much higher than the minimum power. Required power in this case greatly increases with further decrease of distance between the electrodes and with increase of "cooling" area of the electrodes, and naturally depends on the shape, as well as on the material of the electrodes. In Fig. 3.10 there is shown an example of such a dependence (data are taken from work [13]; analogous curves are given in work [17]).

As can be seen from the graphs shown in Fig. 3.10 and 3.11, for the given mixture there exists a minimum discharge gap δ_{\min} , starting at which heat withdrawal does not play an important role. The magnitude of this gap, in physical meaning, as well as in absolute value, coincides with the magnitude of the limiting diameter of a pipe at which a flame is extinguished. For instance, a flame cannot propagate from electrodes with flat side-pieces with a gap between them smaller than the magnitude of the limiting diameter (δ_{\min}), no matter what the quantity of heat released by the spark is, since all, or almost all, of this heat will be withdrawn from the interelectrode volume through the electrodes. For determination of the

magnitude of δ_{\min} under different conditions, it is obviously possible to use relation (3.8a) which are given for the limiting diameter. For a gap larger than δ_{\min} , required power is practically equal to minimum power, which, as one may see from Fig. 3.10, does not depend on specific characteristics of the ignition source (distance between electrodes, shape and material of electrodes, and so forth).

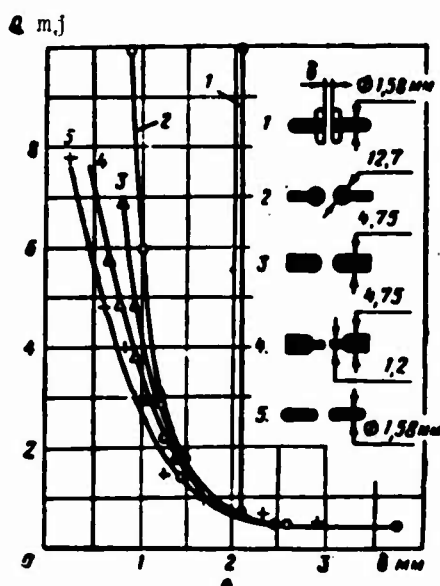


Fig. 3.10. The influence of discharge gap, shape and material of electrodes on minimum ignition energy of the electric discharge ($p = 1$ atm (abs.), $t = 20^\circ\text{C}$). 1, 2 and 5) mixture (8.5% natural gas + air); 3 and 4) mixture (8.5% methane + air).

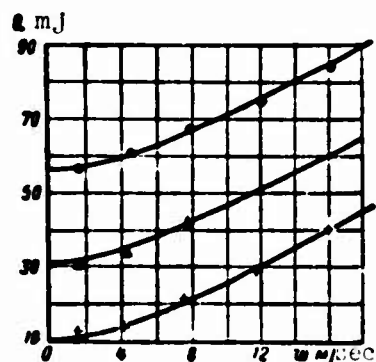


Fig. 3.11. Ignition energy depending upon velocity of propane-air mixture.

$\alpha = 0.77$.

$\tau_{\text{pasp}} = 600 \mu\text{sec}$, $t = 26.6^\circ\text{C}$;
discharge gap $\delta = 6.35$ mm.

Designations	●	▲	+
p in mm Hg	50.8	76.2	101.6

§ 6. DEPENDENCE OF MINIMUM IGNITION SOURCE POWER ON PHYSICOCHEMICAL PARAMETERS OF THE MIXTURE

The dependence of minimum ignition power of a spark on mixture ratio for a series of hydrocarbon fuels is shown in Fig. 3.12. This power mainly changes due to change of the magnitude of u_H [according to (3.7b), $Q \sim 1/u_H^3$] and attains its least value Q_{ONT} at a mixture ratio close to stoichiometric, but displaced in the direction of richer mixtures. This displacement is increased with increase of molecular weight of the hydrocarbons and is explained (just as displacement of the maximum of u_H) by a certain difference in diffusion coefficients of oxygen and fuel. The given dependence is typical for the majority of fuel mixtures. Q_{ONT} decreases upon transition from alkane hydrocarbons to alkene, and further to alkyne hydrocarbons (in accordance with the magnitude of u_H for these hydrocarbons; see § 1, Chapter III). Aromatic

hydrocarbons and linear hydrocarbons containing identical numbers of carbon atoms ignite at approximately identical values of Q_{OPT} . For the majority of carbon-air mixtures of optimum composition ($\alpha = \alpha_{\text{OPT}}$), ignition energy at atmospheric pressure and room temperature changes within the limits 0.18 to 0.30 mJ. Values of Q_{OPT} for a series of fuels are given in Table 3.3.

Table 3.3. Minimum Energies of an Electric Discharge Necessary for Ignition of Different Fuel-Air Mixtures ($t \approx 25^\circ\text{C}$, $p = 1 \text{ atm}$ (abs.)

Fuel	Optimum mixture ratio		Stoichiometric mixture ratio	
	$c_{\text{OPT}} \%$	$Q_{\text{OPT}} \text{ mJ}$	$c_{\text{stex}} \%$	$Q \text{ mJ}$
Methane.....	8.8	0.28	9.50	0.48
Ethane.....	6.5	0.25	5.68	0.28
Propane.....	5.5	0.26	4.04	0.39
Butane.....	4.53	0.26	3.14	0.38
Pentane.....	—	—	2.56	0.49
Hexane.....	3.64	0.24	2.17	—
Heptane.....	3.36	0.25	1.87	0.70
Ethylene.....	—	—	6.56	0.096
Cyclopropane.....	6.34	0.18	4.45	0.35
Cyclohexane.....	3.94	0.24	2.28	1.00
Benzene.....	4.67	0.21	2.73	0.55
Diethyl ether.....	5.30	0.19	3.40	0.52
Hydrogen.....	—	—	29.5	0.019

The influence of inert and active impurities on ignition energy is the same as their influence on burning velocity u_H — monotonic increase of percentage of inert impurities monotonically decreases burning velocity, and consequently increases ignition energy according to (3.7b). Any positive influence of active impurities on u_H decreases the magnitude of ignition energy. The influence of additions of oxygen on the magnitude of ignition energy also shows up mainly through the value of u_H . Between minimum ignition energy and relative concentration of oxygen ψ , where $\psi = O_2/O_2 + N_2$, there exists the relation $Q \sim 1/\psi^3$, which has been experimentally verified for methane, ethane and propane for change of ψ from 1.0 to 0.21 and at

pressures of the medium from 1.0 to 0.2 atm. From relation (3.7b) it follows that minimum ignition energy is inversely proportional to the square of pressure and the cube of initial temperature (since according to (3.7b) $Q \sim pa^3/u_H^3$, where $a \sim 1/p$; $u_H \sim T_1^2$; $a \sim T_1$), which agrees well with experiment. With increase of flow velocity, the magnitude of the coefficient of micro-turbulent diffusion increases. For a well-developed turbulent microstructure (Reynolds number Re of the flow $\geq 10^5$), the micro-diffusion coefficient $D_{M,T}$ is proportional to flow velocity. In relationship (3.7b), for ignition of a mixture in a turbulent flow, in place of the quantity $a = D_{M,T}$ we should substitute $D_M + D_{M,T}$, then the relationship will be written as

$$Q \sim p_2(T_2 - T_1)(V \sqrt{D_M(D_M + D_{M,T})} u_H)^3. \quad (3.9)$$

The dependence of ignition energy on flow velocity will take in this case the form

$$Q \sim Q_0 + Av^{1.5}. \quad (3.10)$$

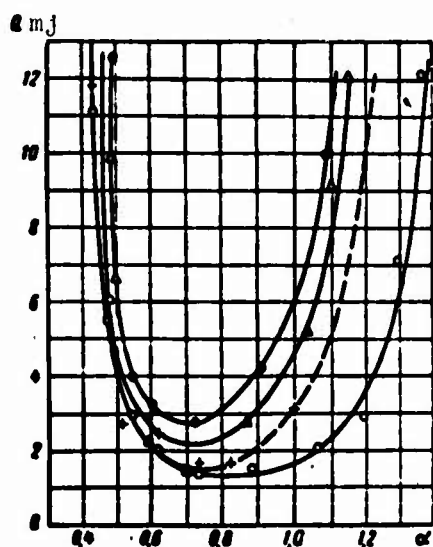


Fig. 3.12. Ignition energy vs composition and rate of motion of gasoline-air mixture. $p = 760$ mm Hg; $t = 100^\circ\text{C}$; $\delta = 0.4$ mm; pointed electrodes.
 0 - $w = 0$ m/sec;
 + - $w = 25$ m/sec;
 Δ - $w = 40$ m/sec;
 \bullet - $w = 50$ m/sec.

Experimental data on ignition of benzene-air and propane-air mixtures confirm this relationship (see Fig. 3.11). With increase of flow velocity, the region of ignition is narrowed and displaced in the direction of "richer" mixtures (Fig. 3.12). The cause of the shift is apparently common to all curves of such type: the inequality of the diffusion coefficients of fuel D_T and oxidizer D_K . This shift is always greater, the smaller the ratio (D_T/D_K) . Ignition boundaries $(c_B - c_H)$ of different hydrocarbon fuels at different pressures (0.2 to 1 atm and different fractions of oxygen ($\psi = 1.0$ to 0.35)) as a function of minimum ignition source power can be represented in the form of a universal curve, if we construct them in corresponding dimensionless coordinates. In Fig. 3.13, which is taken from work [13], there is given such a curve for methane, ethane

and propane. Along the axis of ordinates there is plotted the ratio of ignition boundaries $(c_B - c_H)$ depending on ignition source power to the ignition limits $(c_B - c_H)_n$, which do not depend on source power; along the axis of abscissas there are plotted logarithms of the ratio of minimum power of ignition to optimum power. The given graph permits us to determine ignition boundaries if concentration limits of propagation of the flame, Q_{opt} and c_{opt} are known.

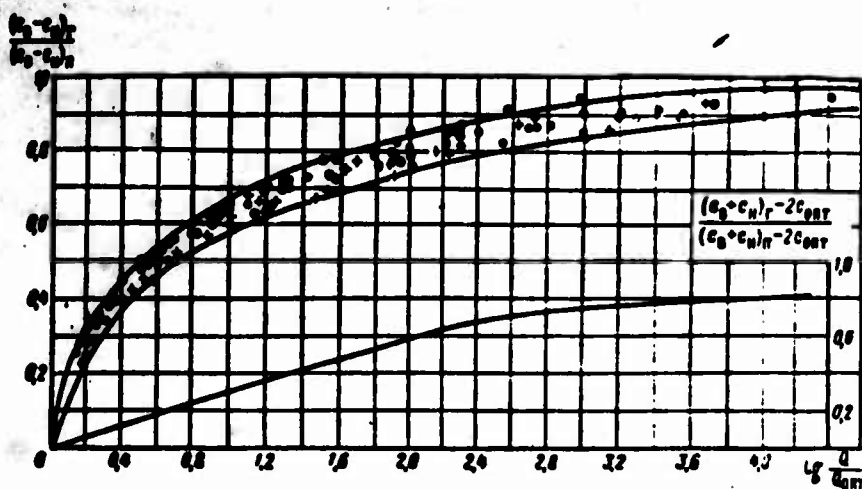


Fig. 3.13. The influence of ignition energy on change of the region of ignition of mixtures of hydrocarbons + oxygen + nitrogen (according to data of [3, 13]). The value of $(c_B - c_H)_n$ at $0.2 \leq p \leq 10$ atm (abs.).

ψ	1.0	0.67	0.5	0.35
Methane ●	53.8	42.2	33.3	23.1
Ethane ○	50.0	39.3	31.0	21.5
Propane +	42.5	32.6	25.3	16.3

§ 7. INFLUENCE OF PHYSICOCHEMICAL PROPERTIES OF A MIXTURE ON CONCENTRATION BOUNDARIES OF IGNITION

The study of the dependence of ignition boundaries on pressure, temperature, percentage of inert impurities and so forth is usually conducted at constant ignition source power. Thus it is attempted to take an ignition source of sufficiently high power and to conduct measurements in pipes of sufficiently large diameter, so that the obtained ignition boundaries can to a certain degree be considered also as ignition limits. Only at very low pressures, when the influence of the particular experimental conditions is great (influence of source and dimensions of pipe), do we stipulate with what source and in what pipe ignition was conducted, thereby stressing

the particular character of the experiment.

Typical boundary curves of ignition depending on pressure for simple hydrocarbons (normal paraffins) are shown in Fig. 3.14.* Boundaries (limits) of ignition slightly change in the range of pressures from 4 to 0.3 atm and have the same limiting values

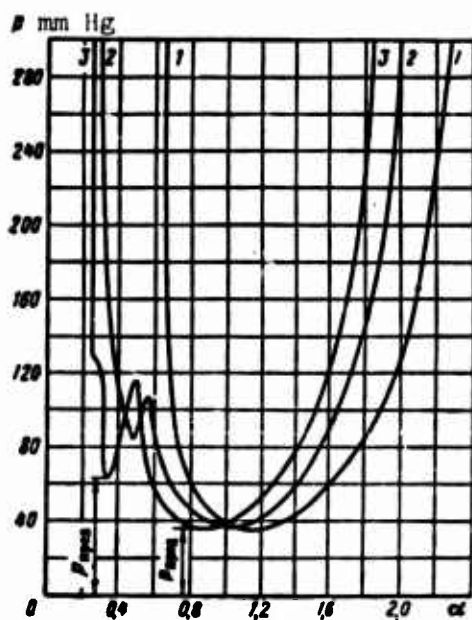


Fig. 3.14. Concentration limits of flame propagation in fuel-air mixtures depending upon pressure. $t = 20^\circ\text{C}$; $Q = 600$ joules, heating coil, 1) methane, 2) butane, 3) hexane.

of concentration as at atmospheric pressure.

With decrease of pressure they rapidly approach each other, and at a certain limiting pressure merge into one point. This is explained, apparently, by increase of the cooling influence of the walls (see Fig. 3.9). As can be seen from Fig. 3.9, at pressures lower than 33 mm Hg, the flame can not propagate in a pipe with diameter of 50 mm for all mixtures and ignition sources. For all hydrocarbon fuels, with the exception of methane, there are noted two limiting values of pressure $P_{\text{пред}}$ ("rich" and "lean" limits). The "lean" limit corresponds to the limits of propagation of normal flames, and the "rich" limit is a result of the appearance of "cold" flames with a different

mechanism of propagation. Limiting pressure can be lowered to 2 to 10 mm Hg by replacing air with oxygen or considerably increasing initial temperature of the mixture [20], [21].

There also investigated boundaries (limits) of ignition of complex hydrocarbon fuels (petroleum fuels). Ignition was carried out in the same pipe with diameter of 50 mm, but by an electric spark. Thus there were not observed cold flames, and consequently there appeared one limiting pressure (see Fig. 3.8). In Fig. 3.8 there are given data at $t = 25^\circ\text{C}$ for aircraft gasoline of type 100/130 and for the American rocket fuel JP-3. The fuel mixture was obtained by mixing only the first 20% of the

*In Fig. 3.14 there are represented certain data from extensive investigations of "lean" and "rich" ignition limits of different fuels, which were conducted at NACA (Lewis Laboratory). Measurements were conducted in a pipe with diameter of 50 mm; ignition was carried out by a heated wire (600 joules) at a temperature of 20°C .

distillation products of the petroleum fuel with air, i.e., the percentage of heavy fractions in the mixture was small. In view of the uncertainty of average molecular weight of the fuel vapor, concentration boundaries (limits) are given in volume percent fuel in air. Since the given data depend on experimental conditions, they are particular boundary conditions of ignition, and are interesting by the fact that they indicate the possibility of existence of flame at pressures less than 25 mm Hg. At higher pressures, vertical branches of the curves lie approximately in the region within the concentration limits of ignition existing at atmospheric pressure for normal paraffins (in the region of butane and heptane). The character of change of concentration boundaries of ignition as a function of pressure shown in Fig. 3.8, is qualitatively described by the theoretical condition of ignition (3.7).

Increase of initial temperature of the mixture expands the boundaries (limits) of ignition, but only slightly. The "lean" boundaries (limits) practically do not change with increase of temperature, or very slightly shift in the direction toward lower concentrations of fuel; "rich" boundaries (limits) more noticeably increase, in linear dependence on the initial temperature of the mixture. A typical graph of the dependence of concentration boundaries of ignition on initial temperature of the mixture for hydrogen, carbon monoxide and methane is presented in Fig. 3.15.

Experiment shows that from the known concentration boundaries (limits) of ignition at one initial temperature of the mixture, it is possible to calculate boundaries at any other initial temperature within quite a wide range of temperatures (to 400°C), proceeding from the condition of constancy of enthalpy ($c_p T_1 + q \cdot c = c_p T_2$), since at the ignition boundaries $T_2 \approx \text{const}$ and $T_1 = \text{var}$.

With increase of the percentage of inert impurities in the mixture, boundaries (limits) of ignition approach each other, and finally, at some quantity of impurities, merge into one value. In Fig. 3.16 there are given data on the influence of additions of argon, helium, nitrogen and carbon dioxide on ignition boundaries of methane. The influence of all impurities besides CO_2 is identical — a weak influence on the lower boundary and a strong displacement of the upper boundary. Addition of CO_2 also noticeably displaces the lower boundary. This displacement is due to the fact that carbon dioxide is not a completely inert impurity. The small influence of inert impurities on the lower boundary can be explained by the fact that at the lower boundary the mixture contains an excess of oxygen, and replacement of part of this oxygen by an inert addition cannot essentially change the minimum percentage of fuel

at the lower boundary. The same can be said of the upper boundary if it is characterized by percentage of oxygen: the minimum percentage of oxygen at the upper boundary practically does not depend on the percentage of inert impurity contained in the mixture. Complete flegmatization of the mixture occurs when there are considerable quantities of impurity. With regard to degree of flegmatization, inert additions affect both the ignition boundaries and the quantity u_{HMAX} (see § 1, Chapter III). This influence is basically determined by purely physical action, and

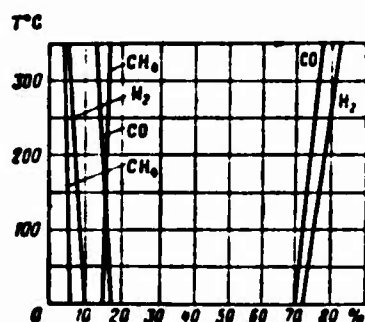


Fig. 3.15. Dependence of concentration boundaries of different gases on temperature.

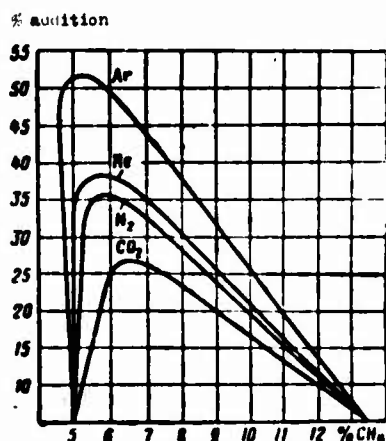


Fig. 3.16. Displacement of concentration boundaries of a methane-air mixture with different inert additions (according to Parker, Burgess and Wheeler).

is characterized by the ratio λ/c_p (of the c_p addition, the weaker is its flegmatizing action). In distinction from inert additions, an active flegmatizing addition acts not only as a simple diluent, but also actively participates in the chemical process, by chemically combining with oxidizer and so forth.

Curves determining the action of active additions are qualitatively the same, but complete flegmatization of the mixture may occur at only a 1-6% content of active additions in the mixture. As active flegmatizing additions there are used such organic compounds as ethyl bromide and ethyl iodide, methyl iodide, ethylene bromide, bromoform, methylene bromide, carbon tetrachloride, chloroform, and others [11].

The influence of mean flow velocity on boundaries (limits) of ignition appears both through turbulence and characteristic time of stay of the igniting volume within the sphere of influence of the ignition source. For an electric spark with discharge gap, larger than b_{min} , the influence of flow velocity appears

only through turbulence. From condition (3.9) it is clear that at constant spark power, with increase of mean flow velocity ignition boundaries are narrowed (at $D_{M.T} \approx v$ the value of u_H necessary for ignition increases). At some sufficiently high mean velocity $v_{пред}$, concentration boundaries merge into one point at the value u_{HMAX} of the given mixture.

In expression (3.9) there is contained the minimum source power. The majority of data known to us are based on required power, which takes into account heat transfer to the electrodes (when the gap between electrodes is smaller than δ_{\min}). For instance, according to work [23] (Fig. 3.10), for a gap of 0.4 mm between electrodes, heat supplied by the spark is for the most part transferred to the electrodes. Therefore, heat transfer characteristics, not condition (3.9), are the decisive factor. According to relationship (3.9), at a given minimum spark power, the maximum flow velocity of the mixture being ignited increases with decrease of pressure, but according to work [23], velocity, on the contrary, decreases due to the strong influence of heat transfer with decrease of pressure; i.e., it is necessary to investigate physicochemical conditions of ignition of the form (3.9) at $\delta \geq \delta_{\min} \approx \approx T_{\text{пред}}$.

The presence of side factors determined by the specific characteristics of the experiment leads to disagreement between existing experimental data. At present there are not yet clear and consistent data on the influence of turbulence and flow velocity (through the factor of time) on boundaries and limits of ignition. Nonetheless, the majority of experimental data and condition (3.9) permit us to assert that ignition boundaries (limits) of a homogeneous mixture are narrowed with increase of mean flow velocity. As an exception we have two-phase mixtures, for which with increase of mean velocity (increase of turbulence) ignition boundaries (limits) may be expanded due to the improvement of local mixture ratio by turbulent diffusion.

§ 8. IGNITION LIMITS OF TWO-PHASE (HETEROGENEOUS) MIXTURES

Till now we have considered boundaries and limits of ignition of homogeneous, gas-fuel mixtures, when the fuel component is in the vapor phase. In combustion chambers, atomization of liquid fuel occurs in direct proximity to the burning zone, so that fuel droplets will not have time to be completely vaporized or uniformly mixed with air directly before the burning zone. Therefore, it is required to establish the ignition limits of such two-phase (heterogeneous) mixtures. At present there are still relatively few works dedicated to this problem. This is explained by the methodological difficulties connected with such investigations, and also by the necessity of obtaining stable mists (sprays) of fuel in air, and of measurement of the average dimension of the drops if it is impossible to obtain a sufficiently uniformly dispersed mist. Finally, the mist is sufficiently stable if physical

parameters of the medium are constant, whereas distributions of liquid and vapor phases of fuel in a real combustion chamber are essentially not stable. A typical example of such an unstable distribution is the atomization spray after a swirl injector. Therefore, in all such investigations it is necessary to stipulate the diameter of the pipe and the length of the pipe from the place of atomization to the flame front.

The first observations of the ignition limits of a mist showed that mists have approximately the same limits as mixtures of completely vaporized fuel. In work [17] drops of kerosene (dimensions of the drops were from 9 to 80 μ) were injected into butane-air and acetylene-air mixtures in a Bunsen burner. According to data of this work, drops with dimension of up to 30 μ under the conditions of the experiment are completely evaporated before they reach the inner cone of the burner, and drops of fuel with dimension of 10 μ are obtained by condensation of the vapor-air mixture (the mixture is composed of the American rocket fuel JP-1 + air) at a temperature of 0°C. By recalculation of ignition limits of the liquid-vapor-air mixture (mist) and the vapor-air mixture for identical temperature, the authors of [17] arrive at the conclusion that the "lean" limit for a mist is very close to the corresponding limit for a vapor-air mixture (ratio of fuel to air is 0.04). The "rich" limit for the mist, however, is observed at lower concentrations than would have been expected proceeding from the data for homogeneous mixtures (ratio of fuel to air is 0.13 instead of 0.3 for the homogeneous mixture). The "lean" limits for all mists are approximately identical, equal to the limit usually observed for hydrocarbon vapors (weight ratio of fuel to air oscillated within the range from 0.035 to 0.043), and the "rich" limit is different and, on the average, lower than for hydrocarbon vapors. In this same work there is noted a stronger plegmatizing action of inert additions on ignition limits of the mist (for a mist lubricating oil No. 5, the limit was observed at 30% N_2 or at 22% CO_2 , whereas for heptane, complete plegmatization was observed only at 42% N_2 and 29% CO_2).

More exact quantitative results on ignition limits of mists are given in the work of Gayone [17]. A uniform mist was obtained by condensing fuel vapor on condensation center supplied by the vaporization of fuel salt from a heated coil. In such a way, it is possible to obtain sufficiently uniformly dispersed mists with different average dimensions of drops. Tetralin was used as fuel. Average dimension of drops can be varied from 7 to 11 μ . The mixture flowed in a vertical pipe, from

top to bottom, with velocity not exceeding 3 cm/sec, and was ignited from below, so that the flame propagated from bottom to top. During the time of motion through the pipe, the dispersed composition of the mist did not change essentially (drops did not have time to be enlarged due to collisions with each other during the time of their motion to the flame front). Results of measurements showed that the nature of the flame completely changes over the range of dimensions of drops from 7 to 50 μ .

In Fig. 3.17 and 3.18 there are plotted the "lean" limits of ignition for a tetralin mist as a function of diameter of the droplets of mist. For the smallest dimensions of drops, the weight ratio of fuel to air (0.039) was approximately equal to the ratio for the vapor mixture. With increase of diameter of droplets, the magnitude of this ratio continuously decreases. Thus, for drops having the smallest dimensions, the flame is similar to the flame existing in gas mixtures at the "lean" limit, but with increase of dimensions of the drops, the flame becomes more and more concentrated at discrete centers of burning around individual droplets.

Unfortunately, in the work of Furgoyne, dimensions of the vapor phase of the fuel are not given, but there is given only the quantity of liquid phase, and also some data on the ignition limit during motion of the flame top to bottom. The limit for this case could be measured only for the drops of smallest dimensions. For drops of 7 μ , the limit during motion of the flame upwards occurred at a ratio of fuel to oxidizer equal to 0.039, and during motion downwards - at 0.044; i.e., the difference between the values was in order of magnitude the same as for the "lean" limit of gas mixtures. The quantity of fuel was measured only for the liquid phase. In the work of Furgoyne there was also investigated the influence of additions of nitrogen on the "lean" limit for drops with diameter of 10, 19 and 45 μ (Fig. 3.19). It turned out that the larger the drops, the greater the percentage of nitrogen which is required for cessation of flame propagation. For the smallest dimension of the drops, the "lean" limit as a function of the minimum percentage of oxygen ($\sim 12\%$) coincides with the limit for hydrocarbon gas flames (see Table 1.4).

The conclusion concerning displacement of the "lean" limit in the direction of lower fuel concentrations with increase of dimensions of drops and the analogous physical interpretation of this phenomenon are given in works of Rud'ko [22] and Tikhomirov, who conducted similar investigations with atomization spray. Tikhomirov [25], for instance, investigated the rate and limits of combustion of a flame jet after a burner placed at fixed point of the atomization spray, under a swirl injection.

In the work of Golovina [26], dedicated to the same problem, there is considered the influence of ratios of liquid and vapor phases of the fuel on concentration boundaries of ignition. Ignition of two-phase and homogeneous gasoline-air mixtures and two-phase kerosene-gasoline-air mixtures (kerosene was in the liquid phase) was carried out by a spark in a pressure chamber (at $p = 760$ to 20 mm Hg). On the basis of the obtained data there was made the conclusion that for ignition of a two-phase mixture

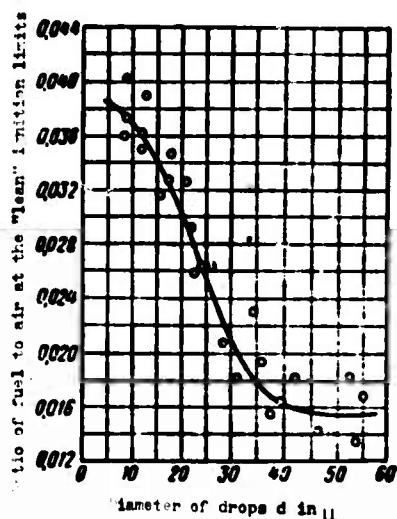


Fig. 3.17. Influence of diameter of drops on "lean" ignition limits in homogeneous tetralin mists.

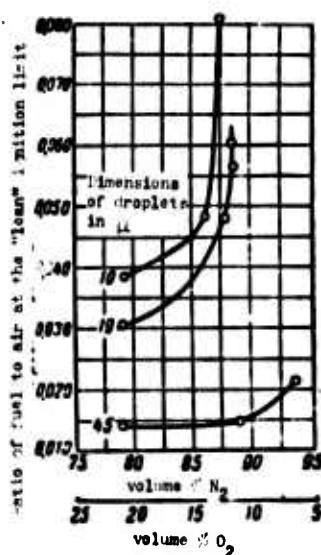


Fig. 3.18. Influence of dilution of a mixture with nitrogen on the "lean" ignition limits of tetralin mists.

(initial ratio of vapor to total amount of fuel was changed from 0.2 to 0.7), it is necessary to have a mean value of the air-fuel vapor ratio, equal for the "lean" ignition boundary to $\alpha_{\text{nap}} \approx 3$, and for the "rich" boundary — to $\alpha_{\text{nap}} \approx 0.32$. Coarseness of atomization of drops in the work was so great (100μ) that ignition boundaries with respect to total quantity of fuel were noticeably shifted in the direction of "richer" mixtures. At atmospheric pressure, for the two-phase gasoline-air mixture, values of total α at the "lean" and "rich" boundaries were equal respectively to 1.6 and 0.3, whereas for the homogeneous mixture these values were equal respectively to 1.9 and 0.4.

Quantitative results of the work, in spite of their preliminary and specific character, are interesting due to the fact that they indicate the important role of the fuel vapor phase under ignition conditions. In the region of ignition there should always be determined the average level of concentration of fuel vapor, and the wider the spectrum of oscillations of concentration of vapor about the mean value, the greater is the possibility that there will occur ignition at a lower average level.

Thus, in heterogeneous mixtures the flame can propagate within approximately the same

limits (and within even wider limits) as in homogeneous mixtures of these fuels. Such behavior of the limits for mists and atomization sprays can apparently be explained by the fact that an atomization spray or mist gives the most varied local distributions of ratios of fuel vapor phases to oxidizer, including the most favorable distribution, which lie within the ignition region and can serve as a constant ignition source for close-lying distributions of another, unignited composition. Thus, ignition can be realized even if the total average quantity of fuel turns out to be less than or greater than in the homogeneous mixture respectively at the "lean" and "rich" ignition boundaries.

Table 3.4. Comparison of Ignition Limits of Atomization Sprays of a Number of Liquid Fuels (in Terms of Minimum Oxygen Concentration) and Vapors of a Number of Hydrocarbons in Nitrogen-Oxygen Mixtures

Fuel liquid	Ignition limit of atomization spray, % O_2 in O_2-N_2	Fuel (vapor)	Minimum concentration of O_2 necessary for ignition of fuel vapor, % O_2 in O_2-N_2 mixture
Gasoline	12	Gasoline	11.2
P-hexadecane	12	Methane	12.1
Aircraft hydraulic fluid AN-VV-0-366B	12	Propane	11.4
Marine lubricating oil NS2135	—	Pentane	12.1
		Hexane	11.9

LITERATURE

1. Ya. B. Zel'dovich and D. A. Frank-Kamenetskiy. Theory of thermal propagation of flame, Journal of Physical Chemistry ZhFKh, 1938, Vol. 12, Issue 7, p. 100; Theory of limits of propagation of a normal flame. Journal of Experimental and Theoretical Physics ZhETF, 1941, No. 11.
2. N. P. Drozdov and Ya. B. Zel'dovich. Diffusion phenomena at flame distribution limits. Journal of Physical Chemistry, 1943, Vol. 17, Issue 3, p. 144.
3. Ya. B. Zel'dovich and N. N. Simonov. On the theory of spark ignition of gas explosive mixtures. Journal of Physical Chemistry, 1949, Vol. 23, No. 11; Journal of Physical Chemistry, 1949, XXIII, Issue 11, p. 1361.
4. Ya. B. Zel'dovich. On the theory of burning of unmixed gases. Journal of Technical Physics ZhTF, 1949, Vol. 19, No. 10.
5. Ya. B. Zel'dovich and K. Ye. Zarembo. Investigation of the structure of a Bunsen flame. Journal of Physical Chemistry, 1948, Vol. XXII, Issue 4, p. 427-441.

6. Ya. B. Zel'dovich and N. N. Semenov. Kinetics of chemical reactions in a flame, *ZhETF*, 1940, Vol. 10, No. 9-10, pp. 1110 and 1427.
7. Ya. B. Zel'dovich. Theory of combustion and detonation of gases. Academy of Sciences of USSR, Moscow-Leningrad, 1944.
8. N. N. Semenov. Basic questions of the contemporary theory of homogeneous burning of homogeneous gas mixtures. News of the Academy of Sciences of the USSR, Department of Technical Services (DTN), 1953, No. 5, Progress of Physical Sciences (VFN) of the Academy of Sciences of the USSR, 1940, 24, 433.
9. D. A. Frank-Kamenetskiy and Ye. M. Minskiy. Microdiffusion turbulent burning. Reports of the Academy of Sciences of the USSR, 1945, Vol. 50, pp. 353-354.
10. D. A. Frank-Kamenetskiy. Diffusion and heat transfer in chemical kinetics. Publishing House of the Academy of Sciences of the USSR, 1947.
11. L. N. Khitrin. Physics of combustion and explosion. Moscow State University Press, 1957.
12. V. Iost. Explosions and burning in gases, IL, 1952.
13. E. Lewis and G. El'be. Burning, flame and explosions in gases, IL, 1948.
14. A. G. Gaydon and H. G. Wolfhard. Flames, their Structure, Radiation and Temperature Ind., Chapman and Hall, 1953.
15. N. N. Inozemtsev. Investigation of the normal velocity of propagation of flame in hydrocarbon fuels, News of higher educational institutions, University of Higher Education (MVD) of the USSR, No. 4, Series "Aircraft Technology," 1958.
16. N. N. Inozemtsev. The influence of initial temperature and pressure on the normal velocity of propagation of flames of different hydrocarbon-air mixtures. Journal of Engineering Physics, 1959, Vol. II, No. 10.
17. Report 1300, Basic Considerations in the Combustion of Hydrocarbon Fuels with Air. By Propulsion Chemistry Division Lewis Flight Propulsion Laboratory Cleveland, Ohio, Edited by Henry C. Barnett and Robert E. Hibbard
18. V. G. Voronkov and A. S. Sokolik. Normal burning of oxygen and air mixtures of carbon monoxide. Journal of Physical Chemistry, 1953, Vol. 6, Issue 10.
19. A. S. Sokolik. Fundamentals of the theory of the process of normal combustion in engines utilizing spark ignition, Collection of articles "Combustion in Transport Piston Engines," Academy of Sciences of the USSR, 1961.
20. Ye. M. Abezgauz. Ignition limits of fuel-gas mixtures, Dissertation, Moscow State University Press, 1947.
21. A. V. Bondarenko. Investigation of limiting phenomena of forced ignition of gas mixtures containing an inert diluent, Dissertation, Moscow State University Press, 1962.
22. Burning of two-phase mixtures, Collection of the Power Institute in G. M. Frzhichanskiy (ENIN), Academy of Sciences of the USSR, 1958.
23. N. F. Dubovkin. Reference book on hydrocarbon fuels and their combustion products. State Power Engineering Publishing House, 1962.
24. N. N. Zenger. Investigation of ignition in a spark discharge, Combustion in transport piston engines, Academy of Sciences of the USSR, 1961.
25. V. S. Tikhomirov. Collection "Combustion in Turbulent Flow," Publishing House of the Academy of Sciences of the USSR, 1959.

26. Ye. S. Golovina. Collection "Combustion in Turbulent Flow," Publishing House of the Academy of Sciences of the USSR, 1959.

27. Charles Tranford and Robert N. Pease. Theory of Burning Velocity. II The Square Root Law for Burning Velocity, Journ. Chem. Phys., Vol. 15, No. 12, Dec. 1947, pp. 861-865.

CHAPTER IV

TURBULENCE IN AIR FLOWS

The various elements of the working process in combustion chambers of air-breathing jet engines — carburetion of the fuel mixture, stabilization and propagation of the flame, heat exchange between combustion products and chamber walls and nozzle — to a considerable degree are determined by properties of turbulence in the flow. Below, there are briefly expounded present-day physical concepts and experimental data on turbulence which have a direct relation to elements of the working process in combustion chambers of air-breathing jet engines.

§ 1. DESCRIPTION AND DEFINITION OF TURBULENT MOTION FOLLOWING EULER'S TREATMENT

By measuring the flow parameters in a combustion chamber with the help of quick-response instruments (hot-wire anemometer, resistance thermometer and so forth), we can show that the instantaneous value of a parameter, even in a stationary flow, does not remain constant in time, but fluctuates about its mean value, i.e.,

$$v = \bar{v} + v', \quad T = \bar{T} + T', \text{ etc.} \quad (4.1)$$

where \bar{v} , \bar{T} , v' , T' are respectively the mean and fluctuating values of velocity and temperature at the considered point of the flow.

Fluctuation can be either acoustic or turbulent in nature.

Acoustic pulsations constitute a system of random waves — longitudinal, adiabatic compressions of the medium. This is what is perceived as audible noise; it always exists in a flow moving through a pipe, in a flow passing out into a filled space, and so forth. In acoustic pulsations, velocity of the medium coincides with direction of propagation of the wave, but its magnitude is insignificantly small

in comparison with the velocity of wave, propagation, which is equal, as it is known, to the speed of sound. An acoustic wave does not transfer an elementary volume of the medium through space, but causes it to oscillate about its mean position with an amplitude not usually exceeding fractions of a millimeter, whereas the energy of this



Fig. 4.1. Schematic diagram of the field of turbulent velocities (a) and the distribution of transverse turbulent velocities along the x-axis (b).

Acoustic pulsations owe their existence to compressibility and elasticity of the medium.

Turbulent fluctuations are a random, disordered set of vortical motions of a medium (eddies) of different scales (Fig. 4.1). An idea of turbulent motion can be obtained, for instance, by observing the wake after an object moving in water. The velocity of the volumes of the turbulent medium is determined by the velocity of rotation of the eddies v' . These volumes, along with whatever substance they contain or properties they have (impurities, temperature, turbulent energy, etc.) can move through the turbulent medium practically without limit with a velocity determined by the coefficient of turbulent diffusion. For turbulent fluctuations, a continuous distribution of the energy of the fluctuations with frequency is characteristic. Turbulent pulsations are not connected with compressibility of the liquid, and owe their existence basically to one property of the liquid — its fluidity.

The entire contemporary theory of turbulence is based primarily on the condition of incompressibility of a liquid. In reality, compressibility of a liquid puts its own imprint on the physical picture of a turbulent field: in an end, of a "compressible" liquid, there is a certain time-varying distribution of static

wave propagates through the pipe with the speed of sound practically without limit. For acoustic pulsations, a discrete distribution of energy of the pulsations with respect to frequency is characteristic. For flow in a pipe there is, as it is known, a fundamental frequency (fundamental tone), which is determined by the length of the pipe, and an infinite series of higher frequencies ("harmonics"), which are multiples of the fundamen-

pressures, and therefore densities, so that any eddy is at the same time a source of acoustic oscillations. Any disintegration of an eddy or formation of a new eddy is accompanied either by the disappearance or formation of new acoustic oscillations, which propagate over the entire turbulent field. Therefore, on a field of turbulent velocities there is always superimposed a background of acoustic noises. For this reason we can "hear" a stream of air flowing out into a filled space, the whistle of wind in the rigging of a ship, etc.

Thus, acoustic and turbulent pulsations exist in a flow simultaneously, and are not divisible. However, inasmuch as their roles in the process of turbulent exchange are different,* it is necessary, for quantitative description of turbulence, sometimes to separate them artificially. All hot-wire anemometric methods of measurement of pulsations obviously do not distinguish between classes of pulsations (the filament of a hot-wire anemometer simply registers the total magnitude of the pulsations). All diffusion methods based on features of turbulent transfer mainly measure only characteristics of turbulent pulsations.

Comparison of measurements of the magnitude of velocity pulsations by these two different methods indicates that in industrial pipes, in most cases, the magnitude of acoustic pulsations of velocity can apparently be disregarded. In the foreign literature recently, along with the measured total magnitude of velocity pulsations, there is also given the value of the level of acoustic noise. Acoustic pulsations can give a large error in measurement by a hot-wire anemometer of turbulent scales by correlation of longitudinal velocity pulsations, since the correlation of acoustic velocities is practically not limited with respect to length. It is possible, for example to observe the correlation between acoustic velocity pulsations on filaments of hot-wire anemometers located at the ends of a long pipe. Therefore, experimental data on turbulence obtained with the help of a hot-wire anemometer without consideration of the influence of noises must be used with caution. Subsequently we will, without stipulating more than this, consider only the field of turbulent pulsations (for acoustic pulsations, see Chapter VI).

Inasmuch as the mean value of pulsations is by definition equal to zero, then for determination of the magnitude of pulsations we use the mean-square \overline{v}^2 or

*Acoustic pulsations affect the process of microturbulent mixing, but practically do not affect the process of macro-exchange. According to results of a series of foreign and Soviet works, their influence on the rate of turbulent combustion is positive.

root-mean-square value of the considered pulsations $\sqrt{\overline{v'^2}}$. In practice, instead of root-mean-square value of the modulus of velocity, there are used values of its projections on the coordinate axes x, y, z - respectively $\sqrt{\overline{u'^2}}, \sqrt{\overline{v'^2}}, \sqrt{\overline{w'^2}}$ or the more convenient relative magnitudes $\sqrt{\overline{u'^2}/\overline{u^2}}, \sqrt{\overline{v'^2}/\overline{v^2}}, \sqrt{\overline{w'^2}/\overline{w^2}}$, which are called intensities of turbulence (in the given direction). The last parameter is frequently called the Kármán number.

Turbulence is called uniform in a certain space direction (uniform in time), if values of its average parameters are identical at any point along the given space direction (identical with respect to time).

An example of uniform turbulence is turbulence along the axis of a one-dimensional steady turbulent flow in a pipe (but not perpendicularly to the axis of the pipe!).

Turbulence is called isotropic if its averaged parameters are identical in any direction. In isotropic turbulence, orientation of the turbulent vortice turns out to be on the average identical in all directions (in particular $\sqrt{\overline{u'^2}} = \sqrt{\overline{v'^2}} = \sqrt{\overline{w'^2}}$). Subsequently we will describe only this simple case of turbulence, while stipulating what changes are introduced into the relationships considered below by nonuniformity and anisotropy.

The description of turbulence can be conducted as in Euler's treatment, considering statistical properties of the distribution of turbulent velocities throughout space at a given moment of time, as well as in Lagrange's treatment, considering statistical properties of turbulent velocities of particles of the liquid at different moments of time.

All data necessary for a complete statistical description of turbulence in Euler's treatment can be obtained by placing the filament of an ideal hot-wire anemometer at the point of the turbulent flow which is of interest to us. This instrument will give an oscillogram of longitudinal u' or transverse v' (in dependence on the design of the instrument) components of turbulent velocity. Since usually the average flow velocity is much higher than the turbulent velocity ($\overline{u} \gg \overline{u'}$), then the oscillogram of the longitudinal component of turbulent velocity turns out to be practically identical to the oscillogram of this same velocity recorded instantaneously along coordinate x along the flow axis. Here a change in turbulent velocity, e.g., from zero to u' with frequency k , on the "time" oscillogram indicates

the passage, across the filament, of a single vortex with the scale of the longitudinal velocity component u' and a scale of length $l_1 = \bar{v}/k_1$.

According to the given oscillogram, it is possible to construct the probability density function of the quantity $dv'^2/2dk = E(k)$ over frequencies k (or over scales l). Quantity $E(k)$ is called the spectral energy density and characterizes the magnitude of turbulent energy of a unit of mass per unit interval of frequencies in the region of frequency k . Typical graphs of this function are shown in Fig. 4.2.

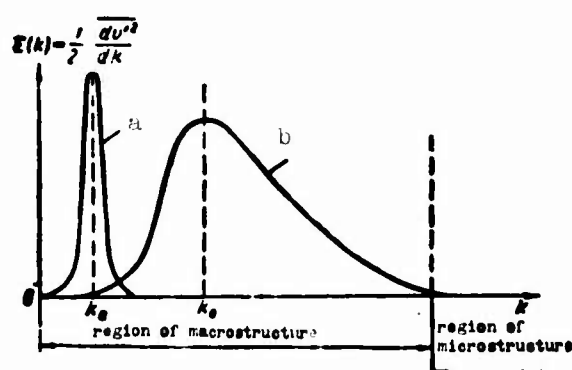


Fig. 4.2. Spectral energy density at small (a) ($Re \sim Re_{kp}$) and large (b) Reynolds numbers ($Re \gg Re_{kp}$).

From these graphs it is clear that for a given distribution there exist certain frequencies (scales) to which the largest fraction of the turbulent energy belongs (frequencies in the region of the value k_0). Let us note that on the same graph, the distribution of noise energy in the flow would be in the form of an infinite series of discrete values of k (multiples of the fundamental frequency). Knowledge of \bar{v}/k_0 (the scale to which the maximum of turbulent energy drops) can be taken as the characteristic of the average scale of turbulent vortices.

Usually there is used another scale which is more convenient in the sense of theoretical analysis and measurement, the so-called integral Euler scale of turbulence l_E . It is defined in the following way: With the help of two hot-wire anemometers located at a distance r from each other, there is measured the correlation coefficient:

of longitudinal velocities

$$R_u(r) = \frac{\overline{u'(x) \cdot u'(x+r)}}{\overline{u'^2}} \quad (4.2)$$

and transverse velocities

$$R_v(r) = \frac{\overline{v'(x) \cdot v'(x+r)}}{\overline{v'^2}}$$

*Here $\bar{v}^2 = \bar{u}^2 + \bar{v}^2 + \bar{w}^2$ is the square of the modulus of turbulent velocity; k is the modulus of the wave vector with components k_1, k_2, k_3 .

as a function of r . The correlation coefficient serves as a measure of the statistical relationship between turbulent velocities at two points separated by a distance r . It changes from unity, when $r = 0$ (complete correlation), to zero, when with increase of r ($r \rightarrow \infty$) this correlation disappears. It is obvious that the larger dimensions of the eddies are on the average, the higher is the probability of encountering turbulent velocities of the same sign at the two points, i.e., the less steeply function $R(r)$ decreases from unity to zero. Therefore, as the measure of the average scale of eddies, it is possible to introduce the scale defined as

$$l_{Eu} = \int_0^\infty R_r dr \text{ and } l_{Ev} = \int_0^\infty Rv(r) dr. \quad (4.3)$$

From the condition of continuity of the medium, for uniform and isotropic turbulence the theory gives

$$l_{Eu} = 2l_{Ev}. \quad (4.4)$$

For isotropic turbulence the theory also gives the relation between the longitudinal scale and the spectral energy function [1]:

$$l_{Eu} = \frac{3\pi}{4} \int_0^\infty k^{-1} \cdot E(k) dk' \int_0^\infty E(k) dk \quad (4.5)$$

(usually there is used only the scale l_{Eu} is then omitted).

The Euler scale of turbulence can also be obtained from the "time" oscillogram with the help of the following relationships:

$$R_r(\tau) = \frac{\overline{u'(t)u'(t+\tau)}}{\overline{u'^2}}; \quad l_{Eu} = v \int_0^\infty R_r(\tau) d\tau. \quad (4.6)$$

The value of l_E measured by the two methods turn out to be identical [25], which once again confirms the identity of the distributions of turbulent velocities in time and space.

For measurement of parameters $\overline{u'^2}$; l_E ; $E(k)$ at high flow velocities, it is necessary to have an instrument with high frequency resolving power in all of its units (higher than 10,000 cps); otherwise the instrument will measure not the curve $E(k)$, but its own frequency-response curve.

The whole spectrum of turbulent pulsations can arbitrarily be divided into two regions: a macrostructure region and a microstructure region. In the literature these concepts have still not been established finally. Depending upon the purpose of their investigation, some authors define the macrostructure region as only the

region of the largest, slowest, anisotropic eddies, the dimensions and orientation of which are determined by the characteristic scale and geometry of the flow (diameter and shape of an obstacle in the flow, of the pipe, and so forth), i.e., the region of frequencies $k \ll k_0$. Others define it as only the spectrum of frequencies in the region of k_0 , in which the main part of the energy of the turbulent pulsations falls (without the biggest, anisotropic eddies). A third group understand by the term "macrostructure" all frequencies less than or equal to, in order of magnitude, the frequency k_0 . For problems of turbulent combustion the last definition is sufficient. Values of turbulent parameters \bar{v}^2 ; l_E are determined basically by eddies of the macrostructure. The theory of turbulence does not give relationships for calculation of these magnitudes, and they are still determined experimentally.

By the term "microstructure", we understand the region of frequencies much higher than k_0 (see Fig. 4.2). The theory of the microstructure of turbulence is most fully developed for very high Reynolds numbers Re ; this is the so-called theory of local turbulence of A. N. Kolmogorov [9], [14]. This theory is based on the following physical concepts. At sufficiently large Reynolds numbers $Re(\bar{v} \cdot d/\nu > 1)$, forces of inertia of the flow start to exceed forces of viscosity; the main flow becomes unstable and vortices (eddies) with dimensions l comparable with dimensions of pipe d , the turbulence producing obstacle, etc., develop. Distribution of energy of the eddies is grouped near the frequency $k_d \sim d/\bar{v}$ (see Fig. 4.2a). With further increase of average flow velocity, the appearing eddies also become unstable ($\bar{v}l/\nu > 1$) and are broken up into eddies of still smaller scale, which in turn are again broken up, etc. This process continues up to scales of eddies for which viscosity plays the dominant role ($\bar{v}l/\nu \leq 1$). As a result, at very large Reynolds numbers Re of the flow, in the flow there is obtained a cascade of eddies with continuous distribution of energy with respect to scales (Fig. 4.2).*

In such a cascade process of energy transfer, every eddy obtains on the average energy from the bigger eddies, and the biggest eddies obtain energy directly from the averaged motion of the flow. The smaller the eddy, the more weakly it is connected with the averaged flow (with its direction and geometry). Therefore it is possible to expect that with decrease of dimensions of eddies, their statistical properties will approach conditions of uniformity and isotropy. The farther the

*The idea of cascade energy transfer was expressed for the first time by Richardson.

considered turbulence is located from walls of the pipe (from the surface of the obstacle), the larger will be the scales in which it will be possible to expect observance of these conditions.

Energy of large eddies is practically not dissipated by viscosity, since the influence of viscosity on these eddies is insignificantly ($v'l/\nu \gg 1$). If turbulence on the average attenuates with time (i.e., is non-stationary), then this dissipation is due to the fact that large eddies transmit part of their energy to smaller eddies with exactly the same rate with which energy is dissipated by the small eddies due to viscosity. It follows from this that local turbulences not only is uniform, but also stationary — rate of energy supply from large eddies is equal to energy dissipation by viscosity — and that, although the dissipation of turbulent energy is determined by viscosity, the rate of this dissipation is established (determined) by properties of the turbulent macrostructure.

From parameters determining turbulent macrostructure it is possible to compose a unique expression for the dimension of rate of dissipation ϵ (erg/g·sec) — the average quantity of energy, dissipated per unit time, per unit mass of liquid:

$$\epsilon \sim (V_{\overline{u}}^3)/l_g. \quad (4.7)$$

For turbulence caused by grids in the flow, by definition this quantity is also equal to $\epsilon = \frac{3}{2} d\overline{u}^2/dt$, so that there should be satisfied the approximate equality

$$\frac{d\overline{u}^2}{dt} \approx \frac{(V_{\overline{u}}^3)}{l_g} \text{ or } \frac{d\overline{u}^2}{dt} = -A \frac{\overline{u}^3}{l_g}, \quad (4.8)$$

where

$$A = \frac{V_{\overline{u}}^3}{\overline{u}^3}.$$

For turbulence after the grids in wind tunnels, this equality is indeed satisfied with good accuracy [1].

Inasmuch as the actual existence of local turbulence is determined only by the rate of energy supply to it from the macrostructure and by the action of viscosity, then the only dimensional parameters determining local turbulence are ϵ and ν .

Instead of these, it is more convenient to use two other parameters of the dimension of velocity v and length η derived from them:

$$v = (\nu\epsilon)^{1/2} \text{ and } \eta = (\nu^3/\epsilon)^{1/2}. \quad (4.9)$$

Parameter η does not have an established name. It is sometimes called the internal scale of turbulence (in distinction from l_E , "the external" scale of turbulence), the scale of the smallest eddies, the Kolmogorov scale, etc. The parameter v in general has no name. In physical meaning, these parameters are characteristic scales of velocity and dimension of eddies for which forces of inertia and forces of viscosity are in equilibrium ($v \times \eta/\nu = 1$). This means that there exist eddies smaller than η , but they are extinguished by viscosity more rapidly than they can transmit energy to still smaller eddies. The condition $v \cdot \eta/\nu = 1$ also signifies that the coefficient of turbulent diffusion of these eddies is of the same order as the coefficient of molecular diffusion.

Scale η divides the spectrum of scales of local turbulences into two regions — regions of scales of larger and smaller η . For the region of scales $\eta \ll l \ll l_E$, viscosity does not play a significant role, so that one parameter ε remains decisive. Therefore, it is possible to write the following expression of the dimension of velocity (Kolmogorov-Obukhov law [9], [14]):

$$v_l \sim (\varepsilon l)^{1/3} \quad \text{or} \quad \frac{v_l}{\sqrt{\varepsilon l}} \approx \left(\frac{l}{l_E}\right)^{1/3}. \quad (4.10)$$

For the region of scales $l \ll \eta$, it is possible to write from the same dimensional considerations [10]

$$v_l \approx v \left(\frac{l}{\eta}\right). \quad (4.11)$$

The parameter v_l , in physical meaning, determines the order of total velocity of all eddies located in the interval from zero to l , or the order of change of the velocity of turbulent motion over a distance of the order of l .

Turbulent macrostructure is described mainly by correlation functions of form $\overline{u^i(x)u^i(x+r)}$, but microstructure is basically described by structural functions of the form $\overline{|u^i(x) - u^i(x+l)|^2}$. In structural functions there are contained differences between turbulent velocities at two points located a distance l from each other. All eddies larger than l have at these points identical values of velocity and therefore do not give any contribution to the structural function, i.e.,

$$\overline{|u(x) - u(x+l)|^2} \sim v_l^2.$$

For this reason values of derivatives of the turbulent parameters (quantities of the type $\overline{(\partial u/\partial x)^2}$; $\overline{(\partial u/\partial t)^2}$, and so forth) are also determined basically by properties of the turbulent microstructure.

The theory of A. N. Kolmogorov has received at present wide recognition and acceptance, and also certain experimental confirmation. Mathematical bases of this theory are presented in the works [9], [10], [14].

§ 2. DESCRIPTION OF TURBULENCE ACCORDING TO THE LAGRANGE TREATMENT

The basis of the theory of turbulence in the treatment of Lagrange is composed of the experimental Gauss law of probability distribution of displacements of volumes of the turbulent medium and Taylor's equation. Let us dwell on this in greater detail. Let us imagine a cold flow with temperature T_1 flowing with velocity v around an infinitely long and infinitely thin filament heated to the temperature T_2 (Fig. 4.3). We will direct axis x along the flow and axis z — along the filament. Instead of temperature, it is also possible to consider an impurity released in the flow, intermediate chemical reaction products on the boundary of molecular mixing of two reacting gases, and so forth.

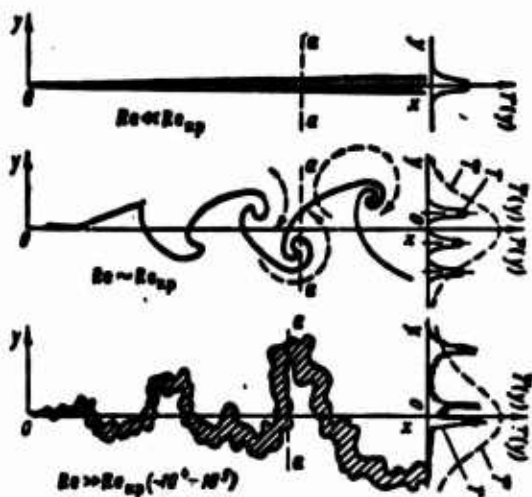


Fig. 4.3. Diffusion wake behind a linear source. Thermal diffusion (diffusion of matter) behind a linear source in a flow at different Reynolds numbers Re (along the diameter of the pipe).

where a_0 — initial width of the sheet (diameter of the filament);

$\overline{Y_M^2} = \frac{2D}{v} x$ — variance of "widening" of the layer in the laminar flow;

In the absence of turbulence ($Re < Re_{kp}$), behind the filament there will extend a heated layer, which widens with increase of x under the action of molecular diffusion. The temperature profile over the thickness of the heated layer at distance x from the filament for

$$\sqrt{\overline{Y_M^2}} \gg a_0$$

will be determined, as is known, by Gaussian law:

$$\frac{T - T_1}{T_2 - T_1} = \frac{a_0}{\sqrt{2\pi \overline{Y_M^2}}} e^{-\frac{x^2}{2\overline{Y_M^2}}}, \quad (4.12)$$

$\sqrt{\bar{Y}^2}$ - characteristic width of the "widened layer";

D_M - molecular diffusion coefficient (coefficient of thermal diffusivity).

Relationship (4.12) is a particular solution of the molecular diffusion equation

$$\frac{\partial T}{\partial x} = \frac{D_M}{v} \frac{\partial^2 T}{\partial y^2}.$$

We will superimpose a field of turbulent velocities on the incident flow.

Experiment shows that also in this case the profile of average temperatures satisfies the Gauss law with great accuracy:

$$\frac{T - T_1}{T_2 - T_1} = \frac{q}{\sqrt{2\pi Y^2}} e^{-\frac{y^2}{2Y^2}} = a_0 p(y),$$

which is a particular solution of the differential equation

$$\frac{\partial T}{\partial x} = \frac{1}{2} \frac{dY^2}{dx} \frac{\partial^2 T}{\partial y^2},$$

where T - the value of temperature at point x, y of the heated turbulent wake after the filament averaged over time (or over z); in the heated molecular wake, average and instantaneous values of T coincide; here, however, these are different concepts;

\bar{Y}^2 - variance of diffusion in the turbulent flow, which includes molecular diffusion \bar{Y}_M^2 , purely turbulent transfer \bar{Y}_T^2 and the mutual influence of molecular diffusion and turbulence $\bar{Y}_{M,T}^2$.

Let us find the variance of turbulent transfer \bar{Y}_T^2 , which determines the mean square of the displacement of a unit of volume of liquid in the turbulent field during the time t . During that time every particle of the unit volume, after leaving the filament, will pass along the flow over a distance $x = \bar{v}t$ (more exactly $x = (\bar{v} + \bar{v}')t$, but, with error not exceeding \bar{v}'^2/\bar{v}^2 , it is possible to write the average distance for the assembly of particles), and in direction y - a distance equal to

$$Y_T = \int_0^t v'(t') dt'. \quad \text{Multiplying both sides of the last equality by the quantity}$$

$dY_T/dt = v'(t)$ and bringing the constant $v'(t)$ under the integral sign, we will obtain after averaging over the assembly of particles leaving the filament the well-known Taylor equation

or

$$\left. \begin{aligned} \frac{1}{2} \frac{d\overline{v^2}}{dt} &= \int \overline{v'(t)v'(t')} dt' - \overline{v^2} \int R(\tau) d\tau \\ \frac{1}{2} \frac{d\overline{v^2}}{dx} &= \frac{\overline{v^2}}{v} \int R(x) dx, \end{aligned} \right\} \quad (4.13)$$

where

$$t = t' + \tau, \quad R(\tau) = \frac{\overline{v(t)v(t+\tau)}}{\overline{v^2}}.$$

The correlation coefficient $R(x)$ (or $R\tau$) coincides in form with Euler's correlation coefficient, which was given above, but there we took velocities at different points of space (different particles) at the same moment of time and averaged over space (over time), and here we take the same particles, but at different moments of time, and averaging is conducted over an assembly particles.

Taylor's equation has two limiting solutions:

$$P_T^2(x) = \frac{\overline{v^2}}{2} x^2 \text{ for } x < l_L v / \sqrt{\overline{v^2}} = \frac{D_T v}{\overline{v^2}}; \quad (4.14)$$

$$P_T^2(x) = \frac{2\overline{v^2}}{v} \int_0^x R(\tau) d\tau \cdot x - 2 \frac{D_T}{v} x \text{ for } x \gg l_L v / \sqrt{\overline{v^2}}, \quad (4.15)$$

where

$$\int_0^\infty R(\tau) d\tau = T_L - \text{the Lagrange time scale};$$

$$\sqrt{\overline{v^2}} T_L = l_L - \text{the Lagrange integral turbulence scale (mixing length);}$$

$$\sqrt{\overline{v^2}} l_L = D_T - \text{turbulent diffusion coefficient (turbulent transfer coefficient)}.$$

From comparison of equation (4.14) for small diffusion times with the well-known experimental Gauss law of the distribution of turbulent velocities, it ensues that

$$p(v) = \frac{1}{\sqrt{2\pi\overline{v^2}}} e^{-\frac{v^2}{2\overline{v^2}}}. \quad (4.16)$$

where $p(v')dv'$ is the probability of appearance of a value of turbulent velocity in the interval from v' to $v' + dv'$.

It is clear that the probability distribution of turbulent displacements of volumes of liquid $p(y_T)$ also satisfy the Gauss law. For large diffusion times, the Gauss law $p(y_T)$ has not yet been proven; it is taken as a postulate.

The quantity \bar{Y}^2 , and thus means also the profile of average temperatures in the turbulent flow, depends not only on turbulent transfer \bar{Y}_T^2 and molecular diffusion, but also on the mutual influence of these factors (turbulence and molecular diffusion). This influence is apparently always positive: turbulent transfer on the average increases molecular diffusion (i.e., $\bar{Y}^2 > \bar{Y}_T^2 + \bar{Y}_M^2$). The value $\bar{Y}_{M.T}^2 = \bar{Y}^2 - \bar{Y}_T^2 - \bar{Y}_M^2$ will be called the variance of accelerated molecular diffusion.

Accelerated molecular diffusion starts from the smallest scales. Starting from time η/v , each turbulent vortex incident on the heated layer of the flow, instead of displacing it in a translatory manner, rotates the element of this layer about its axis and deforms it so that its average instantaneous width in the direction of axis y becomes noticeably larger than the value $\sqrt{\bar{Y}_T^2}$ (see Fig. 4.3); this is seen on the average as increase of molecular diffusion in the direction of axis y . With increase of instantaneous width of the heated layer, larger and larger eddies can enter it, thereby increasing the diffusion rate inside the layer. The rate of accelerated molecular diffusion $\frac{1}{2} \frac{d\bar{Y}_{M.T}^2}{dt}$ tends to a constant value, inasmuch as $\frac{1}{2} \frac{d\bar{Y}^2}{dt} \rightarrow D = \text{const}$ for $t > l/v^2$ (according to experiment) and $\frac{1}{2} \frac{d\bar{Y}_T^2}{dt} \rightarrow D_T$ [according to the Taylor equation (4.15)].

For diffusion times smaller than η/v , molecular broadening of the heated layer in the direction of axis y remains practically the same as without turbulence: the influence of turbulence reduces only to the fact that the center of a unit volume, where the heated layer is located, oscillates in time about the axis x according to the Gauss law, with variance \bar{Y}_T^2 . Therefore, for these times, the total variance of diffusion will be approximately equal to

$$\bar{Y}^2 \approx \bar{Y}_T^2 + \bar{Y}_M^2 \text{ for } t < \eta/v = \frac{D_T}{\nu}. \quad (4.17)$$

For times larger than $t > \eta/v$, an exact analytic expression for \bar{Y}^2 does not exist. There are known only a few works [11], [49] in which there is made an attempt to estimate theoretically and experimentally the effect of accelerated molecular diffusion for times of the order of η/v .

In combustion chambers, the level of turbulence is very high, so that values of D_T are several orders of magnitude higher than values of D_M . Therefore, it is possible to disregard not only molecular diffusion \bar{Y}_M^2 , but also accelerated molecular diffusion $\bar{Y}_{M.T}^2$ as compared to turbulent transfer \bar{Y}_T^2 , i.e., to consider that

$$\bar{Y}^2 \approx \bar{Y}_T^2 \text{ (for } t > D_T/\nu^2) \text{ at } D_T \gg D_M. \quad (4.18)$$

Using (4.17) and the Taylor equation, we can determine the parameters of turbulence in Lagrange's treatment according to measurements of fields of average temperatures (concentrations) behind a linear or a point source (the so-called diffusion method of determination of parameters of turbulence, in distinction from the hot-wire anemometric method).

The diffusion method can be used with accuracy sufficient for practice in the case of nonuniform and anisotropic turbulence. Then, in relationship (4.14) it is necessary to substitute the intensity of transverse turbulent pulsations at the point of location of the source, and in relationship (4.15) — the turbulent diffusion coefficient (transfer) $D_T D$ as a function of x .

Turbulent velocity, mixing length l_L , correlation coefficient, etc., measured by the diffusion method are determined just as the corresponding Euler parameters, with accuracy up to molecular and microturbulent mixing, by properties of the turbulent macrostructure. With the same assumption ($\bar{Y}^2 \approx \bar{Y}_T^2$), it is possible to determine the field of average temperatures in the zone of turbulent mixing of nonisothermal flows, in a turbulent flame, etc., fields of average turbulent velocities in the mixing zone of flows with unequal turbulence, etc. In this case the entire problem is reduced to determination of the probability of appearance of volumes with the given temperatures T_1 and T_2 or velocities $(\sqrt{v_1^2}; \sqrt{v_2^2})$ at the considered point.

The influence of turbulence on molecular diffusion can be disregarded in the examining of processes determined directly by molecular mixing (burning of drops, diffusion and homogeneous reaction in burning layers of diffusion and homogeneous flames, and so forth). This influence can arbitrarily be divided into the influence of large eddies, whose scales are larger than the instantaneous width of the sheet (molecular mixing layer), and the influence of small eddies, with scales equal to or smaller than the instantaneous width of the sheet. Large eddies increase molecular diffusion in the direction of axis y basically due to increase of the number of intersections of the sheet with axis y . Instantaneous width of the sheet in the direction of axis y is obtained to be equal at certain moments not to $\sqrt{Y_2}$ but to

$3\sqrt{Y_2}; 5\sqrt{Y_2}$ etc. (see Fig. 4.3). Smaller eddies increase molecular diffusion due to acceleration of the exchange inside the sheet itself, and due to rotation of an element of the sheet at an angle to the axis y .

The roles of large and small eddies in accelerated molecular diffusion for various Reynolds numbers Re turn out to be different. For numbers Re close to critical, small eddies practically do not exist; large eddies turn out to be sufficiently stable. The large eddies "roll up" the sheet on themselves, thereby increasing the average number of its intersections with axis y , until they are extinguished by viscosity (see Fig. 4.3). With increase of Reynolds number, the rate of disintegration of large eddies into smaller one increases, which leads to decrease of the degree of curvature of the surface of the sheet by big eddies and to increase of the role of small eddies.

For sufficiently large Reynolds numbers Re , the average lifetime of an eddy of the macrostructure turns out to be equal to $\sim l_e \sqrt{\nu}$. This means that, turning on the length of its radius, a large eddy is broken up into a series of small eddies before it can distort the surface of the sheet. The average number of intersections of the sheet with axis y thus turns out to be of the order of unity.

The influence of turbulence on molecular diffusion depends not only on Reynolds number Re , but also on the relationship between coefficient of molecular diffusion and kinematic viscosity. The larger the coefficient of molecular diffusion (the wider the sheet) and the smaller the coefficient of viscosity (the smaller the dimension of the smallest eddies), the greater will be the microturbulent diffusion of the sheet.

Accelerated molecular diffusion begins earlier, the greater the initial width of the sheet a_0 , and increases in time, reaching, as experiment shows, a limiting value. From the point of view of calculation of accelerated molecular diffusion, it makes no difference what causes \bar{Y}_{MT}^2 to increase — whether it is increase of the average number of intersections of the sheet with axis y , increase of the average slope of the sheet to axis y , or average increase of thickness of the sheet by microturbulent diffusion. Let us note that for large Reynolds numbers Re , when there does not exist a clearly defined boundary of the sheet (see Fig. 4.3), these effects can not always be separated, even in principle; i.e., the concept of a boundary between large-scale and small-scale acceleration of molecular diffusion for large Reynolds numbers Re is arbitrary, and at the existing level of knowledge, distinguishing between these processes is not necessary. It is sufficient to operate with the generalized concept of the coefficient of accelerated molecular diffusion:

$$D_{a.}(t) = \frac{1}{2} \frac{d\bar{Y}_{a.}^2}{dt}.$$

On the basis of the expressed physical and dimensional considerations, for the coefficient of accelerated molecular diffusion it is possible to write the criterial equation

$$\frac{D_{M,T}}{D_r} = f\left(Re_r; \frac{D_M}{\nu}; \frac{q}{l_L}; \frac{\sqrt{\overline{v^2}}}{l_L} t\right). \quad (4.19)$$

For sufficiently large diffusion times, dependence on initial conditions and time can be disregarded, so that

$$\frac{D_{M,T}}{D_r} \sim (Re_r)^n \left(\frac{D_M}{\nu}\right)^s, \quad (4.20)$$

where

$$Re_r = \sqrt{\overline{v^2}} l_L / \nu.$$

The quantity value $D_{M,T}$ can apparently be considered to be completely equivalent to the coefficient of molecular diffusion in the first approximation. There exist a number of methods of experimental estimate of $D_{M,T}$: the Townsend method [11], by measurements of total variance $\overline{Y^2}$ and variance of turbulent transfer $\overline{Y_T^2}$ by the method of determination of rate of molecular mixing according to the rate of discoloration of a stream of phenolphthalein containing acid in an alkali, etc. For gases it is possible to indicate an analogous method, the basis of which consists of the following: A "cold" gas (T_1) containing uniformly distributed vapor of NaCl is mixed with a "hot" gas of sufficiently high temperature T_2 . The distribution of average intensity of resonant radiation over the depth of the mixing zone is determined by a relationship analogous to the distribution of average rate of heat emission:

$$J(x) \sim (T_2 - T) \exp(-h\nu/RT), \quad (4.21)$$

where h — Planck's constant;

ν — frequency of the radiation.

The distribution of relative intensity over y determines the scale $Y_T(t)$, and the integral of intensity (for known physical constants) determines the scale $Y_M + Y_{M,T}$, which determines $D_M + D_{M,T}$.

All physical peculiarities of turbulent diffusion analyzed in on the simple example of a two-dimensional problem (diffusion behind a filament) can be generalized to all other cases with the help of the differential equation of turbulent diffusion.

The equation of turbulent diffusion can also be obtained in the Euler treatment of the process. In Euler coordinates, in the conservation equation (temperature, mass, impurity, and so forth) there are contained unknown correlation moments of the form $\overline{T'v'}$; $(\overline{c'v'})$, which determine the average rate of turbulent transfer. The meaning of these moments is clarified from direct comparison of the conservation equation with the equation of turbulent diffusion. It turns out that the part of the temperature fluctuations correlating with turbulent velocity is equal to

$$T'_x = \frac{\partial T}{\partial y} Y, \quad (4.22)$$

where Y is random displacement of temperature during the time t .

This relationship coincides in form with the known relation of Prandtl, which is assumed at the basis of the so-called semi-empirical theory of turbulence; but in the given case, this is a strict analytical relation. The root-mean-square value of displacement is not the mixing length of Prandtl. At various moments of time it may be less than or greater than the scale of turbulence. This is not an empirical coefficient, since its principle part is described by the Taylor equation.

Let us note that the magnitude of temperature fluctuations which correlated with velocity is less than the total magnitude of temperature fluctuations. If, for instance, there are mixed only two media with temperatures T_1 and T_2 , then the average temperature and magnitude of $\overline{T'^2}$ in the mixing zone is determined with accuracy up to accelerated molecular diffusion by relationship (4.6). The mean square of the correlating part of the pulsations for a one-dimensional zone is equal to

$$T'^2_x = \left(\frac{\partial T}{\partial y} \right)^2 \overline{Y^2} = \frac{(T_1 - T_2)^2}{2\pi} e^{-\frac{r^2}{2l^2}}. \quad (4.23)$$

In particular, in the center of the one-dimensional zone of turbulent mixing of the two media

$$\overline{T'^2_x} / \overline{T'^2} = 2/\pi.$$

The equation of turbulent diffusion extends with sufficient logical grounds to the three-dimensional case and to the case of nonuniform and anisotropic turbulence at constant or slightly changing average flow rate [4], [7]. With practical accuracy it is also possible to extend it to the case of flows with large gradients of average velocities. Experiment shows that with practical accuracy it is also possible to consider that

$$\overline{u'v'} = -\nu_T \frac{\partial \bar{u}}{\partial y}, \quad (4.24)$$

where $\nu_T = \overline{l'^2 v'}$, by analogy with the coefficient of kinematic viscosity, is called the coefficient of turbulent viscosity.

This relationship, which was obtained for the first time by Boussinesq and later by Prandtl on the basis of the physical model of turbulent transfer developed by him, justifies itself in engineering calculations for problems involving a turbulent boundary layer, a submerged stream, and so forth, although it does not have the physical basis which Prandtl attributed to it. Formulas (4.24) can also be generalized to the case of three-dimensional nonuniformity of turbulent flow.

§ 3. EXPERIMENTAL DATA ON TURBULENCE

Turbulence in flows with large Reynolds numbers Re possesses one general remarkable property, which greatly facilitates its study. This property is self-similarity with respect to velocity. The earliest measurements of Schubauer, Dryden, Reichardt, Minskiy and others (1935) showed that intensity of turbulence $\sqrt{\overline{u'^2}}/v$ for Re numbers of the flow larger than 10^5 practically does not depend on the absolute value of average flow velocity. The later and considerably improved measurements of Townsend, Corrsin, Uberoi, Kovazhnyy, Laurence, Balnes and Peterson and others in subsonic flows, and also numerous working measurements confirmed this result. Hot-wire anemometric and diffusion measurements also showed the independence from flow velocity (more accurately, the independence from Reynolds number Re) of such parameters l_E ; l_L ; D_T/v ; $R_E(x/l_E)$; $R_L(\tau/T)$; $E(k \cdot l_E)$ and others. Therefore, subsequently, considering properties of turbulence at Reynolds numbers Re larger than 10^5 , it will not always be stipulated at what flow velocity they are obtained.

Pipe turbulence of a steady flow. Steady flow in a pipe can be obtained by the most diverse methods; therefore, the length of the section of establishment of steady flow can also vary greatly. By means of creation of a soft inlet of flow into the pipe and several other measures, it is possible to extend this section to values noticeably larger than 50 caliber (with respect to diameter of pipe). Without taking special precautionary measures, Nikuradze observed full establishment of a turbulent profile of average velocities over a length equal to $40d(Re = 10^6)$. This length can be shortened by installation of a turbulizing grid at entrance into the pipe; it will be shortened more, the larger the coefficient of turbulent diffusion given by the grid. In combustion chambers turbulence tends to a limiting value usually not from

below, but from above, the level of turbulence in the diffuser or from the level of turbulence after the straightening grid after the diffuser. In these cases, length of section of establishment of steady flow is determined according to the data below on rate of attenuation of turbulence to be 20-30 caliber with respect to characteristic scale of holes of the grid, scale of vortices after the diffuser, after the elbow or a connecting channel, and so forth. In a steady flow, parameters of turbulence do not change along the flow.

The character of change of parameters of turbulence over the cross section of the flow is represented in Fig. 4.4 and 4.5 [16], [22]. From the figures it is clear that on the flow axis the intensity of the longitudinal component of turbulence does not depend on Reynolds number Re . With approach to the wall, the intensity increases; this increase is greater, the smaller Reynolds number Re is. At Reynolds numbers Re larger than 10^5 , the form of the curve does not change (turbulence is self-similar). The vertical component of turbulent velocity changes still less, and on the pipe axis coincides with the horizontal component, which indicates isotropy of turbulence on the flow axis.

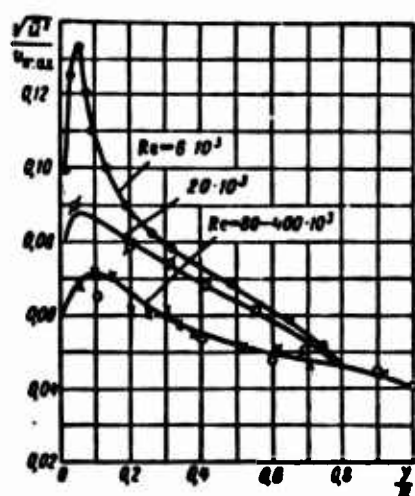


Fig. 4.4. Distribution of intensity of turbulence over the flow section.

- | | |
|---|---|
| ○ - in circulatory flow
$Re = 2 \cdot 10^4$; | } according
to
experi-
ments of
Minskiy |
| X - in a flat pipe
$Re = 2.4 \cdot 10^4$;
$V = 10$ m/sec; | |
| ⊘ - in a round pipe; | |
| ● - in a flat pipe $Re = 6 \cdot 10^3$,
$V = 1$ m/sec (according to
experiments of Reichardt). | |

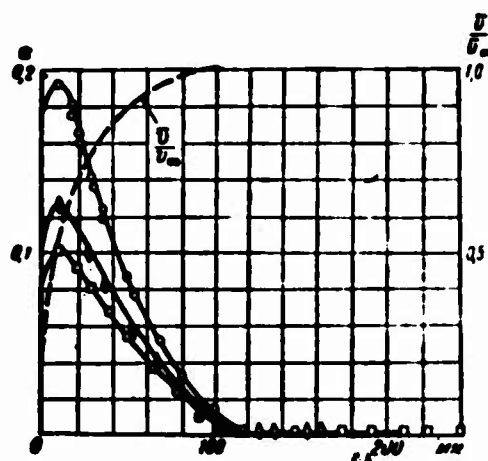


Fig. 4.5. Intensity of turbulence in a boundary layer at $x = 2600$ mm (data of Corrsin).

- | |
|------------------------|
| ○ - $\frac{v'}{v_m}$; |
| □ - $\frac{v'}{v_m}$; |
| ◇ - $\frac{v'}{v_m}$. |

Experimental material accumulated up to the present time shows that intensity on the pipe axis weakly depends on degree of roughness of the pipe, changing from 4% for the mirror surface of hydraulic chutes to 5% for usual technical pipes. These values include all hot-wire anemometric and diffusion measurements with their systematic errors. On the flow axis in products of complete combustion ($T_2 \approx 2000^\circ\text{K}$), the value of intensity of turbulence is also equal to 5% [25]. This magnitude can be taken as the characteristic of intensity of turbulence in the central part of the flow.

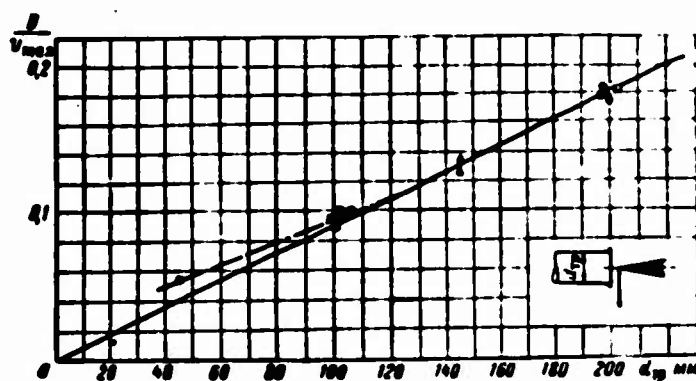


Fig. 4.6. Dependence of coefficient of turbulent diffusion at the flow axis on velocity and pipe diameter.

$$\frac{D}{v_{\max}} = 0.0009 d_{tp} \text{ for } Re > 10^5$$

$$\frac{D}{d_{tp} v_{\max}} = 0.009 \left(\frac{v_{cp}}{v_{\max}} \right) Re^{-0.16} \text{ for } Re < 10^5$$

(formula of Gol'denberg)

Method of measurement	$\frac{D}{v_{\max}}$ mm	d_{tp} mm	v_{cp} m/sec	Conventional designations
○	0.18	200	20 ± 60	diffusion of CO ₂
●	0.18	200	35 ± 60	optical-diffusion method
▲	0.13-0.14	145	60	
■	0.1	100	30 ± 40	
□	0.065	45	40	

In Fig. 4.6 there is represented the dependence of the coefficient of turbulent diffusion D at the flow axis on flow velocity and pipe diameter [26]. It is clear that the coefficient of turbulent diffusion satisfies the condition of geometric similarity and velocity similarity, where

$$\frac{D}{v_{\max}} d_{tp} \approx 0,0009 \text{ for } Re > 10^5, \quad (4.25)$$

$$\frac{l_L}{d_{tp}} = 0,018 \text{ at } \epsilon = 0,05 \text{ for } Re > 10^5.$$

It is necessary to distinguish the coefficient of turbulent diffusion and the scale of turbulence l_L of Lagrange from the coefficient of turbulent diffusion D_p and the mixing length l_p of Prandtl, which were calculated by Nikuradze according to experimental values of turbulent friction and the gradient of average velocities in the pipe cross section, with the help of the hypotheses of Prandtl. Prandtl's hypotheses are not applicable to turbulence in the central part of the flow.

Therefore, distributions of diffusion coefficient D_p and scale l_p over the pipe cross section obtained by Nikuradze are devoid of physical meaning, and contradict direct experiments. For instance, according to the calculations of Nikuradze with the help of Prandtl's hypothesis, the coefficient of turbulent diffusion attains its maximum value in the region of maximum gradient of average velocity, and tends to zero with approach to the flow axis, whereas in reality it practically does not change over the flow cross section. Turbulent velocity and scale practically do not change in the central part of the flow, but at walls of the pipe velocity increases, and the scale decreases, so that the diffusion coefficient $\sim l \cdot \sqrt{v^2}$ remains practically constant over the cross section of the pipe. The value $l_p = 0,07 d_{tp}$ on the flow axis obtained by Nikuradze by means of extrapolation, as can be seen from comparison with (4.25), is three times as large as the value of the scale of turbulence of Lagrange.

On the other hand, it is interesting to note the following curious fact: The value of D_p obtained by Nikuradze averaged by Gol'denberg [27] over the cross section of a pipe coincides well with the above mentioned data of direct measurements. Averaging calculations of Nikuradze over the cross section of a pipe, Gol'denberg obtained the relationship

$$\left. \begin{aligned} \frac{D_p}{v_{cp} d_{tp}} &= 0,009 Re^{-0,16} \text{ for } Re < 10^5 \\ \frac{D_p}{v_{cp} d_{tp}} &\approx 0,0011 \text{ for } Re > 10^5 \end{aligned} \right\} \quad (4.26)$$

and

where v_{0r} is the average velocity over the pipe cross section.

Such coincidence indirectly indicates the fact that, although calculations of Nikuradze are not correct in the details, on the average they give results close to correct, so that with certain grounds it is possible to use the first formula of Gol'denberg in the region of small Re, holds numbers Re, where systematic direct measurements of the coefficient of turbulent diffusion are not available.

It is also interesting to compare the scale of turbulence l_L with the longitudinal scale l_E ; all the more so, because in the majority of investigations of turbulence there appears the Euler scale. Comparisons of exact measurements behind grids, conducted by Taylor [28] and later by Townsend [13], showed that between these scales there exists the approximate relationship

$$l_L \approx 0.5l_E, \quad (4.27)$$

i.e., the path of transfer of particles of liquid by a turbulent vortex (l_L) is on the average twice as small as the dimension of the vortex l_E .

In the foreign literature, for pipe turbulence there is frequently used for estimation the relationship

$$l_L d_p = 0.05 \quad (4.28)$$

which with accuracy up to the spread of values of ϵ from 0.04 to 0.05 will also agree with the above equations (4.25) and (4.27).

Turbulence behind grids. The level of turbulence can be greatly increased by installing a turbulizing grid in the flow. The turbulizing grid is usually composed of a row of parallel rods with diameter b and with distance between axes M (parallel grid); it is also possible to install two rows of such rods one after the other, such that the rods are mutually perpendicular (orthogonal grid). As a grid there can also serve a perforated sheet of iron with holes of diameter $\approx M$ and with distances between holes of $\approx b$. The ratio M/b is usually larger than 3 to 5 (for small hydraulic losses).

Scales of turbulent motion and lengths on which turbulence is formed are determined to a greater degree by dimensions of holes of the grid M , and the absolute level of intensity of turbulence is determined to a greater degree by width of the crosspieces b . This is a rough qualitative estimate, since experiment shows that with change of either the value of M , or the value of b the intensity and scale of turbulence changes. In general, the behavior of the intensity and scale of turbulence depends not only on M and b , but also on parameters of turbulence of the flow incident

on the grid and on the scale of the flow (diameter of the pipe). During investigation of the nature of attenuation of turbulence, the last two factors only complicate the problem. Therefore, we try to eliminate them. For this, we extinguish turbulence of the incident flow and conduct measurements on the flow axis in pipes of relatively large diameters (wind tunnels), at absolute distances from the grid where the influence of pipe walls does not show up.

On turbulence in wind tunnels there has been accumulated up to now much experimental material, which has been reinforced by the theoretical considerations of a number of authors [1], [30], [31]. It turns out that in a wind tunnel, the region of variation of turbulence behind the grid can be conditionally divided into three sections: into the initial section of formation of the turbulent field behind the grid and on the initial and final sections of attenuation of the turbulence. The initial section extends from the grid to cross sections $\sim (5 \text{ to } 15)M$, where gradients of average velocities after the grid become practically equal to zero, the arrival of energy from average motion is practically ceased, and the field of average and turbulent velocities becomes constant over the cross section of the pipe. In this section, turbulence receives energy from the average flow in layers of maximum gradients of the average velocities, which then is distributed by turbulent transfer over the entire flow cross section. Turbulence in the initial section is not only nonuniform, but also anisotropic: eddies predominate, the scales and orientation of which are determined by the geometry of the grid. For a parallel grid (axis y direction along the rods) fluctuations of velocity in the direction of axes x and z predominate; for an orthogonal grid, fluctuations of velocity in the direction of axis x predominate, since in this direction there are added the velocities from eddies generated by the horizontal and vertical rows of rods.

Toward the end of the initial period, forces of inertia distribute turbulent energy continuously over the spectrum of scales, and forces of pressure — uniformly over all directions, so that turbulence becomes, as measurements show, isotropic. Values of $\overline{u'^2}$; $\overline{v'^2}$; $\overline{w'^2}$ and values of corresponding correlation functions with respect to different directions become identical for parallel, orthogonal and other lattices [1]. Toward the end of the initial section, supply of energy from average motion is ceased, and turbulence, "left to itself", starts to attenuate under the action of viscosity forces. Viscosity forces extinguish turbulent vortices (convert their energy into heat). Small eddies are the most rapidly extinguished, so that the average

scale of turbulent vortices increases on the average with increase of distance from the grid (larger and larger eddies remain). This process in the initial section of attenuation is well described by the theoretical relationship (4.8). If we represent the law of attenuation of turbulence in the form

$$\overline{v^2}/v = \overline{u^2}/v^2 \approx B(x - x_0)^{-n} \quad (4.29)$$

(B is an empirical constant; x_0 is an arbitrary reference point; in order of magnitude the value of x_0 coincides with the cross section where the initial formation section of ends), then in virtue of equation (4.19) change of the scale of turbulence will be

$$l_x = \frac{\Lambda \sqrt{B}}{n} (x - x_0)^{1-n}, \quad (4.30)$$

and change of the coefficient of turbulent diffusion

$$D_x/v = B(x - x_0)^{1-n}. \quad (4.31)$$

Hence, in particular, it follows that the diffusion coefficient remains constant with increase of distance from the grid for $n = 1$, increases for $n < 1$ and decreases for $n > 1$.

Experiment shows that in the range of distances from 15 to 200 M there is observed the value $n = 1$. In the coordinates $1/\epsilon^2$, x experimental points fall on a straight line. With further increase of distance from the grid, the value of n changes from $10/7$ (the Kolmogorov-Frenkil law) to $5/2$ (law of Millionshchikov-Loytsyanskiy) in the final period of attenuation. In the final period of attenuation in the turbulent spectrum, as a result of faster attenuation of small eddies large eddies which depend on the specific character of the lattice, start to predominate; i.e., there is observed a return of the turbulence to anisotropy (for instance, for an orthogonal grid, for values of x/M larger than 200). The value of $\overline{u'^2}$ becomes approximately one and a half times as large as the value of $\overline{v'^2}$ [1].

In Fig. 4.7 there are presented typical curves of change of ϵ obtained by Townsend and Stewart with an orthogonal grid with $M = 26.4$ mm and $b = 4.77$ mm, with a grid of parallel rods of rectangular cross section 49.6×9.6 mm with $M = 26.4$ mm and $b = 9.6$ mm. As can be seen, the grids were selected so that at identical values of M they have values of b increasing in the proportion 1:1, 1:2. If we take as the beginning of the initial attenuation section a value of x_0 identical for all three grids and equal to $\sim 13M$ (Fig. 4.7a), then all three graphs of the intensity of turbulence are plotted in coordinates x/b on one dimensionless graph (Fig. 4.7b).

This result indicates that the length of the section of formation does not depend on the dimension of the crosspiece, whereas the magnitude of intensity depends only on its dimension (for the given grids).

In Fig. 4.8 there are given typical curves of change of D/v ; l_E ; l_L over the length of the flow. Data for l_E are constructed according to measurements of Townsend [11], which, as can be seen, agree well with the theoretical formula (4.30) in the initial region of attenuation at $A \approx 0.9$; data for l_L are constructed according to values of D_T measured by Townsend for an orthogonal grid [2]. In Fig. 4.8 these parameters are reconstructed in dimensionless coordinates $(x - x_0)/b$.

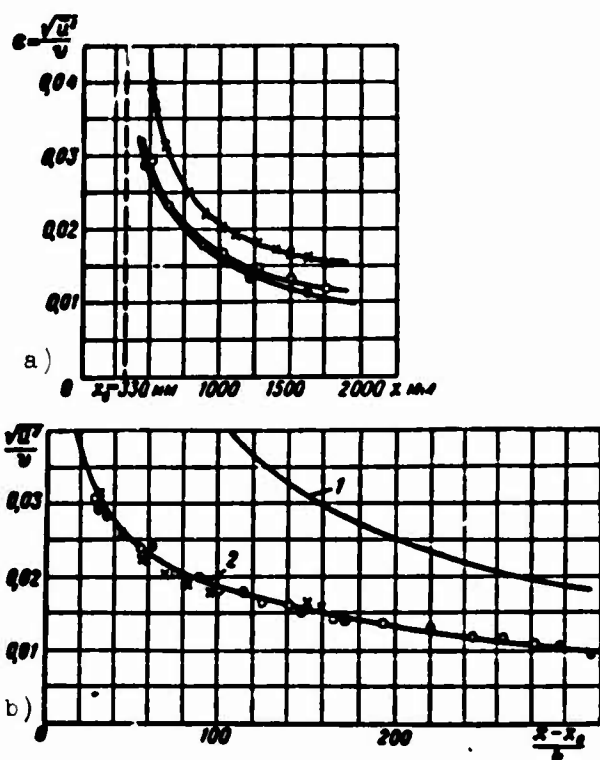


Fig. 4.7. Attenuation of intensity of turbulence behind a grid in a wind tunnel (data of Townsend, Batchelor, Stewart and Baines and Peterson).

a) grids (according to Townsend, Batchelor and Stewart).

× — $M = 25.4$, $b = 95$ mm (parallel rods);

○ — $M = 25.4$, $b = 5.35$ mm (parallel bars);

● — $M = 25.4$, $b = 4.77$ mm (orthogonal grid of rods).

b) grids (data of Baines and Peterson, Townsend, Batchelor and Stewart).

$$1 - \frac{\sqrt{u^2}}{v} = 1.12 \left(\frac{x - x_0}{b} \right)^{-\frac{1}{3}} \quad (\text{data of Baines and}$$

Peterson, $b = 25.4$ mm, $M = 3.8; 51; 68; 102; 203$ mm);

$$2 - \frac{\sqrt{u^2}}{v} = 0.02 \left(\frac{x - x_0}{b} \right)^{-\frac{1}{3}} \quad (\text{data of Townsend, Batchelor and Stewart}).$$

Among investigations of turbulence there is no single opinion about the best method of construction of dimensionless empirical formulas by which it would be possible to determine parameters of turbulence for any grid simply, inasmuch as such universal formulas apparently do not exist. Therefore, the dimensionless graphs shown in Fig. 4.8 should not be considered as unique and universal. A number of authors, such as, for example Batchelor, Townsend and Stewart, consider the decisive parameter to be the dimension of the hole M , and construct all curves in coordinates x/M , even if the value of M remains constant, and only the dimension of the crosspiece b is changed. Data from the book of Batchelor [12] shown in Fig. 4.8 are constructed together with data from a number of other grids with constant b and variable M in the coordinates x/M , but for each (above mentioned) lattice there was taken an effective scale, respectively equal to 1; 1.1 and 2. Other authors (Baines and Peterson and others) take as the controlling scale the dimension of the crosspiece. In the work of Baines and Peterson [24] there were measured parameters of turbulence mainly after grids with constant width of the rods $b = 25.4$ mm and with dimensions of holes equal to 38, 51, 68, 102, and 203 mm (cross section of the working part of the pipe was 1.8×1.2 m; $v = 0.3$ to 7.5 m/sec), and the authors prefer to construct empirical formulas in coordinates x/b and, following the theoretical formula of Kolmogorov and Frenkil, also give, in particular, the empirical relationships:

$$\begin{aligned} \sqrt{u'^2}/v &= 1.12 (x/b)^{-1.7}, \\ l_{20}/b &= 2l_{20}/b = 0.156 (x/b)^{0.53+0.56} \end{aligned} \quad (4.32)$$

Graphs of these curves are given for comparison in Fig. 4.8. One may see that curves of intensity obtained by different authors turn out to be absolutely different. This difference lies outside limits of accuracy of the measurements and is apparently explained by the difference in type of lattice — mainly by the difference between absolute values of scales. In the first case the value of b was varied, and the range of values of b and M was the same; in second case, the value of M was varied, and the ranges of values of b and M were absolutely different. Curves of scales do not coincide either, although the difference between the curves lies within the limit of accuracy of their measurements.

How is turbulence after the grids installed in technical pipes with high level of turbulence changed? If the grid stands immediately after a nozzle with high compression ratio (ratio of average velocities v_2/v_1 equal to 3-4), then the behavior

of turbulence after it will be analogous to that considered above, at least up to distances (of the order of 20-30 M), at which the intensity of turbulence after the grid is higher than the intensity in the pipe (Fig. 4.9). If the diffusion coefficient after the grid then is much less than the diffusion coefficient of pipe turbulence, then the considered grid cannot accelerate the process of restoration of the level of pipe turbulence very much (after the nozzle), so that the intensity of turbulence will reach some minimum value (noticeably less than 5%) at distances larger than 20-30 M, after which it will again begin to increase to the level of pipe turbulence.

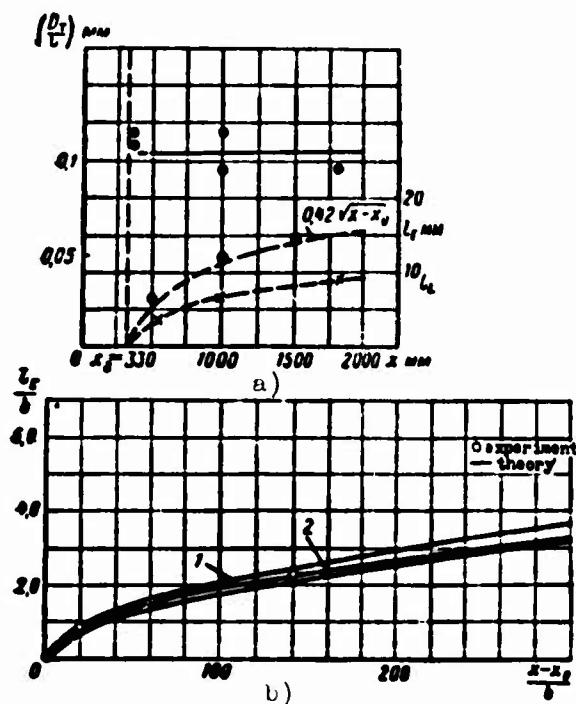


Fig. 4.8. Change of diffusion coefficient and scales after grids in a wind tunnel.

a) grid (data of Townsend and Batchelor)
 $M = 25.4 \text{ mm};$

$$b = 4.77,$$

$$\bullet - \frac{l_E}{l_T};$$

$$\bullet - l_{E^v} = 13 \text{ m/sec};$$

$$X - l_{L^v} = 13 \text{ m/sec};$$

b) grid (data of Baines and Peterson),

$$\frac{l_E}{b} = 0.156 \frac{x - x_0}{b}^{0.5} \text{ (curve 1);}$$

and grid (data of Batchelor and Townsend)

$$\frac{l_E}{b} = 0.19 \sqrt{\frac{x - x_0}{b}} \text{ (curve 2).}$$

For a diffusion coefficient of the grid equal to or greater than the diffusion coefficient of the pipe turbulence, the length of the section of formation of pipe turbulence will be much shorter than without the grid, so that in the limit, turbulence after the grid at distances of 20-30 M attains the level of pipe turbulence, after which it remains constant. In the case of combustion chambers, the grid is usually placed where the turbulence before it is either practically equal to pipe turbulence (after the connecting channel), or higher (after the diffuser, bend, etc.). Under these conditions, the grid also can be used to generate turbulence under the condition that it give diffusion coefficient a larger than in the incident flow. Experiment shows that for this the grid should have a relatively large coefficient ($b/M \approx 1$) and relatively large absolute values of scales M and b .

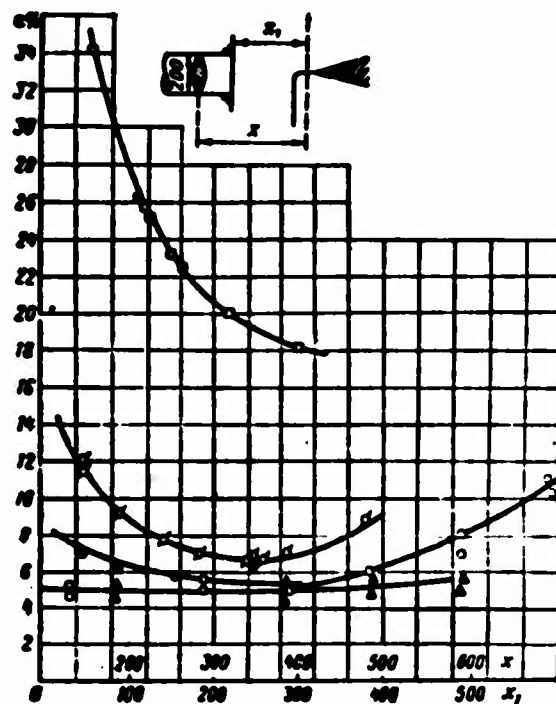


Fig. 4.9. Change of intensity of turbulence after grids in an open flow.

○ — without grid $d_{Tp} = 200$ mm;

▲ — grid $M = b = 6$ mm;

● — grid $M = b = 12$ mm;

✕ — grid $M = b = 18$ mm;

□ — grid of swirl vanes.

In Figs. 4.8-4.12, for example, there are given data on ε , D/v and l_L for a series of such grids. Three grids are perforated sheets of iron with diameters of holes respectively equal to $M = 6, 12$, and 18 mm. Holes were drilled so that between them there were located blanketed areas of approximately the same characteristic dimensions $b = 6, 12$, and 18 mm. Such grids can be considered as analogs of a fuel manifold with injectors in blanketed areas, as an analog of a group of stabilizers uniformly located over the cross section of the pipe, and so forth. The fourth grid is a group of seven swirl vanes, filling the entire cross section of the pipe (see Fig. 4.10). The blade length of the swirl vane is equal to $d_{TP}/6$. Grids were located in a 200 mm pipe with well-developed pipe turbulence. Measurements were conducted at the end of the pipe.

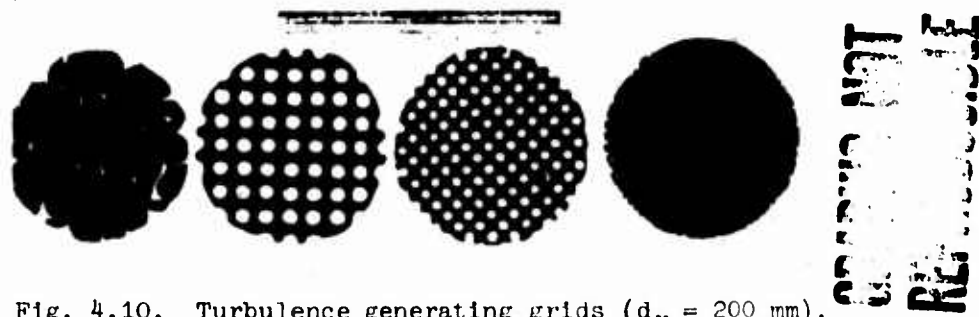


Fig. 4.10. Turbulence generating grids ($d_K = 200$ mm).

In Fig. 4.9 for comparison there is also given the distribution of intensity of turbulence on the axis of a pipe without a grid. It is clear that the core of constant turbulent velocity is considerably shorter than the core of average velocities (see also Fig. 4.13). Turbulence generating grids very slightly shorten the length of the core: growth of turbulent velocity is observed at practically the same relative distance ($2-1.5d_{TP}$), but at correspondingly higher absolute values of turbulent velocity.

The first turbulence generating grid ($b \approx M \approx 6$ mm) does not create additional turbulence; it even plays the role of a turbulence-attenuating grid; the diffusion coefficient after this grid is somewhat lower than the turbulent diffusion coefficient of a flow without the grid; this shows up in the slower rate of increase of turbulent velocity (in the case of the grid) outside of the core (see Fig. 4.9). The second grid gives higher intensity, but at absolute distances larger than 200 mm it practically has no influence; more exactly, its influence due to excess hydraulic losses will be only negative. The third and fourth grids considerably increase the intensity of turbulence above the 1% level of pipe turbulence, but again at distances

smaller than 20 calibers with respect to the characteristic dimension of the grid.

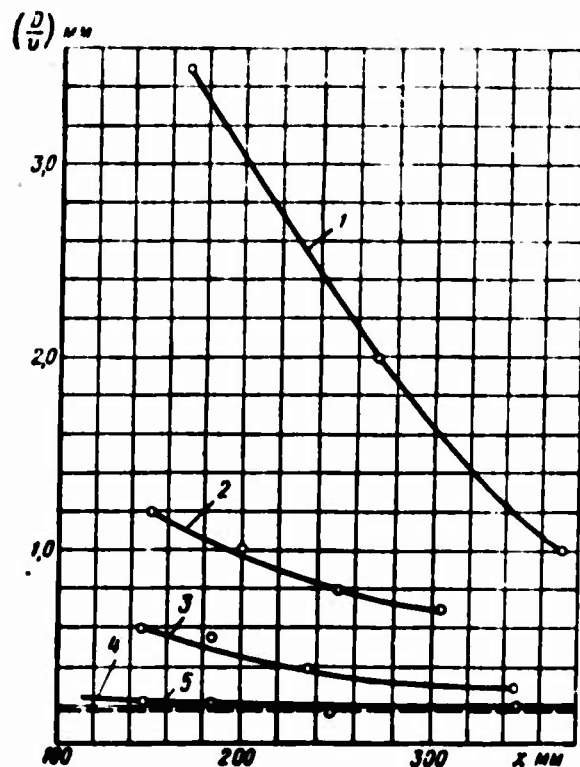


Fig. 4.11. Change of coefficient of diffusion after strongly turbulizing grids in technical pipes.

- 1 - grid of swirl vanes, $d_{TP} = 145$ mm;
- 2 - grid of swirl vanes, $d_{TP} = 100$ mm;
- 3 - grid $M = b = 18$ mm, $d_{TP} = 200$ mm;
- 4 - grid $M = b = 12$ mm, $d_{TP} = 200$ mm;
- 5 - without grid, $d_{TP} = 200$ mm.

Let us note a number of other peculiarities of turbulence which are characteristic for grids set in a flow with high initial level of turbulence. The absolute value of intensity of turbulence after the grid will be obtained to be higher, the larger the diameter of the pipe. The same grid in a pipe with very large diameter acts as an attenuating grid with respect to the large-scale turbulence of the incident flow and as a turbulence generator in a pipe with small diameter. The three first grids ($b \approx M$; 6, 12, and 18 mm), which were set in a pipe with diameter of 100 mm, give at the same absolute distances a noticeably larger value of intensity of turbulence than in a pipe with diameter of 200 mm. If the grid is placed after the diffuser, then it breaks up large eddies, appearing in the diffuser into smaller eddies (of the order of M). Then, immediately after the grid, the intensity of turbulence can be

higher than without the grid, but it will be concentrated in smaller scales and therefore will attenuate at closer absolute distances (20 M).

Large-scale, intense eddies after the diffuser play a negative role in the process of burning, decreasing stability and uniformity of burning, rather than a positive role, increasing rate of combustion; therefore, installation of a grid with

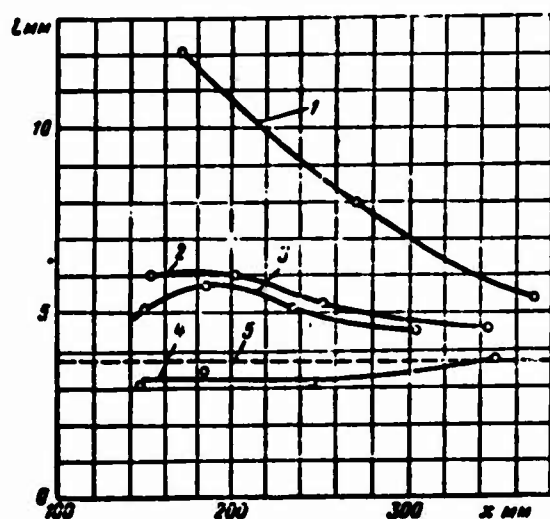


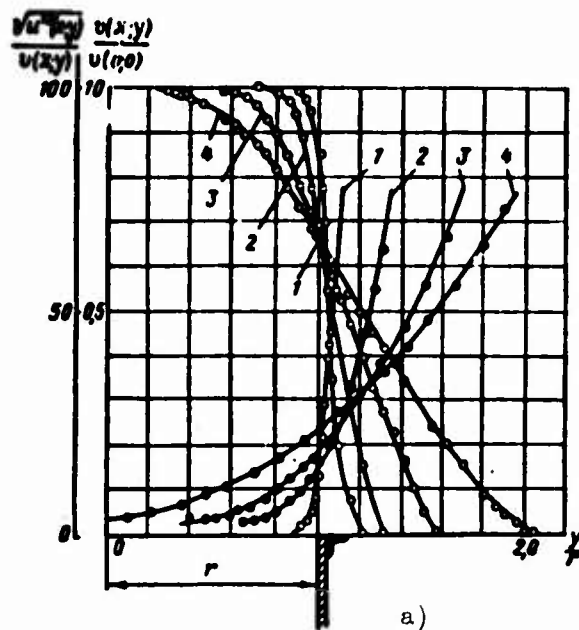
Fig. 4.12. Change of scale l after strongly turbulizing grids in technical pipes.

- 1 - grid of swirl vanes, $d_{TP} = 145$ mm;
- 2 - grid of swirl vanes, $d_{TP} = 100$ mm;
- 3 - grid $M = b = 18$ mm, $d_{TP} = 200$ mm;
- 4 - grid $M = b = 12$ mm, $d_{TP} = 200$ mm;
- 5 - without grid, $d_{TP} = 200$ mm.

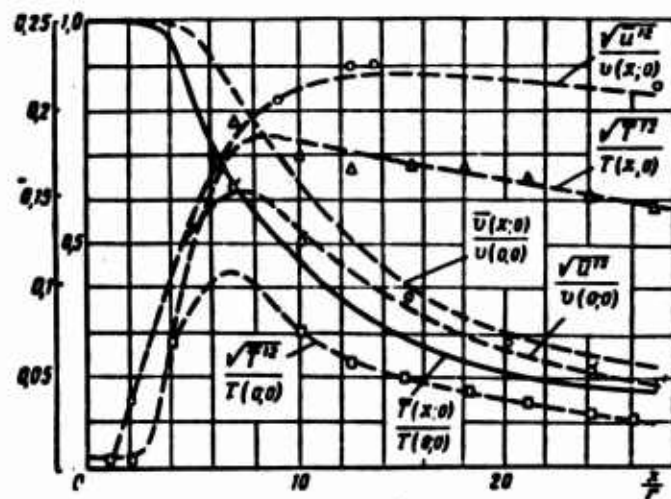
in the pipe, after which it remains constant, or until it attains its least value at the boundary of the core of constant turbulence in an open flow after which it starts to increase (in a submerged stream). In Fig. 4.14 there are given typical curves of change of intensity of turbulence after the third and fourth grids in a pipe with diameter of 200 mm and after the third grid in a pipe with diameter of 100 mm. In coordinates $1/\varepsilon^2$ and x , all experimental points obtained within the bounds of the core of turbulent velocities fall on straight lines. The value of x_0 turns out to be identical for all grids, of the most diverse types (including others not shown in Fig. 4.14), and to be equal to $x_0 = 80$ mm (2-4 M) at $v = 20$ to 60 m/sec, $d_{TP} = 100$ to 200 mm.

sufficiently small flow friction is usually expedient. In this case the grid plays the role of a flow straightener. Let us note that turbulence after the grid depends on turbulence of the incident flow more weakly, the greater the height of channels of holes of the grid. The grid completely destroys all eddies of turbulence of the incident flow if the time of passage of flow through the grid is equal to or larger than the time scale of this turbulence $(l_0/\sqrt{u'^2})$.

The rate of attenuation of intensity of turbulence obeys a linear law of attenuation (the value of n in formula (4.29) is equal to unity) practically until the moment when it reaches the average level of intensity of turbulence



a)



b)

Fig. 4.13. Turbulent characteristics of flow over the cross section and axis of a stream. a) distribution of turbulence and average velocity over the cross section of a stream (data of Laurence).

$Re = 1.92 \cdot 10^5 - 7.25 \cdot 10^5$; $M = 0.2$ to 0.7 , $d_{TF} = 89$ mm;

● — $\frac{\sqrt{u'^2}}{u(x,0)}$; ○ — $\frac{u(x,0)}{u(0,0)}$. 1 — $\frac{x}{r} = 1.14$, 2 — $\frac{x}{r} = 2.27$, 3 — $\frac{x}{r} = 4.38$, 4 — $\frac{x}{r} = 7.8$.

b) distribution of pulsations along the axis of the stream (hot stream $d_{TF} = 25.4$ mm; $T = 170^\circ C$ (data of Corrsin)).

From comparison of the given data with data of Batchelor and Townsend and with data of Baines and Peterson, it is clear that the ranges of variation of absolute distances from the grids are absolutely different in all cases: measurements of parameters of turbulence in wind tunnels are usually conducted at absolute distances at which the level of turbulence is already known to be constant in technical pipes. Therefore dimensionless graphs and empirical formulas obtained under different conditions usually do not coincide. For estimation of the value of intensity of turbulence in every specific case, one should take data obtained under conditions which are as close as possible to the considered case.

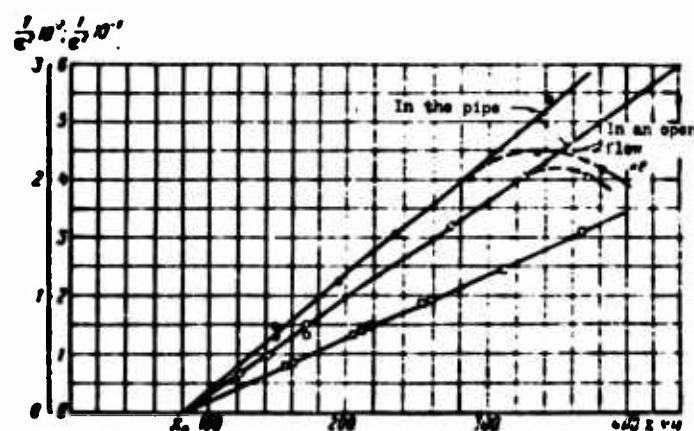


Fig. 4.14. Law of attenuation of turbulence after strongly turbulizing grids in technical pipes.

$$\frac{l}{x} \frac{u'}{u} = \frac{\text{const}}{x - x_0}$$

Lattices

● — $M = b = 18 \text{ mm}$; $d_{TP} = 200 \text{ mm}$,

○ — $M = b = 18 \text{ mm}$; $d_{TP} = 100 \text{ mm}$,

□ — grid of swirl vanes.

The characteristic growth of the scale of turbulence after grids in technical pipes is observed only at relatively short distances from the grid ($\leq 10 M$); at larger distances, the scale of turbulence decreases, and at distances larger than 20-30 M practically attains the magnitude of the scale of pipe turbulence, after which it remains constant (see Fig. 4.12). If the initial scale of turbulence is much larger than the scale of pipe turbulence, as for instance after a grid composed of seven swirl vanes for pipes of diameter 100, 140-200 mm, then the section of growth of scale almost does not exist: the scale immediately monotonically tends to the scale of pipe turbulence. Such behavior of the scale can apparently be explained by the

fact that eddies with dimensions much larger than the scale of pipe turbulence cannot exist for a long time in the given pipe; as a result of this the integral scale of turbulence approaches its limit — the scale of pipe turbulence (from below — due to faster damping of small eddies, and from above — due to faster damping of small eddies much larger than this limit).

The diameter of the pipe also affects absolute values of scales of turbulence, if the latter are much larger than the scale of pipe turbulence. For instance, for a grid of swirl vanes set in pipes with diameter of 200, 145 and 100 mm, the scale decreases not proportionally to \sqrt{b} , according to the formula (4.32), but proportionally to $b^2 \sim b \cdot d_{TP}$ ($b \sim d_{TP}$ is the dimension of the blade). By measurements of the intensity of turbulence and diffusion coefficient, it is also possible to calculate other parameters of turbulence, such as the Lagrange scale of turbulence, the rate of dissipation of turbulence, the Kolmogorov scale, and so forth. An example of such calculation for a grid ($M \approx b = 18$ mm) in a pipe with diameter of 100 mm is given in Table 4.1. The value of D/v is arbitrarily taken to be constant for all distances from the grid, although it in reality decreases with increase of x within the bounds of the core of turbulence in an open flow, and increases outside of the core.

Table 4.1. Parameters of Turbulence after a Grid

$$\epsilon^{-2} \approx 1.7; \left(\frac{x}{M} - 4\right); M \approx b \approx 18 \text{ mm}, \nu = 0.15 \text{ cm}^2/\text{sec}; d_{TP} = 100 \text{ mm}$$

x mm	$\epsilon \%$	$\frac{D}{v}$ mm	l_L mm	E cm ² /sec ³	η mm	v m/sec	$Re = \frac{V \sqrt{l_L}}{\nu} = \frac{D}{\nu}$
122	17 to 18	0.6	3.5	$8 \cdot 10^7$	0.03	20	810
172	11.5	0.6	5.3	$11 \cdot 10^6$	0.04	20	810
344	6.5	0.6	9.4	$2 \cdot 10^6$	0.10	20	810
122	17 to 18	0.6	3.5	$22 \cdot 10^8$	0.01	60	2430
172	11.5	0.6	5.3	$4.5 \cdot 10^8$	0.02	60	2430
344	6.5	0.6	9.4	$5.4 \cdot 10^7$	0.03	60	2430

Turbulence after a bluff body (stabilizer), in a boundary layer and in a submerged stream. Properties of this turbulence for a long time were not investigated in detail (there were measured only fields of average parameters of the flow:

velocities, temperatures and so forth). In recent years, thanks to progress in the region of hot-wire anemometry, there has appeared a series of works (of Townsend [12], Corrsin [21], Laurence [23] and others) which has provided a beginning for such investigations. According to results of these works in all three cases, which are different at first glance, the structure of turbulence turns out to be identical. In the wake after a stabilizer, in a boundary layer and in a stream there will be formed a region of increased turbulence separated from the nonturbulent (potential) part of the flow by quite a sharp boundary — a laminar superlayer (Fig. 4.15). The surface of this boundary is distorted by the action of large, slow, anisotropic eddies (with orientation determined by the geometry of the problem) and moves toward the nonturbulent part of the flow, so that average width of the turbulent region increases downstream along the flow.

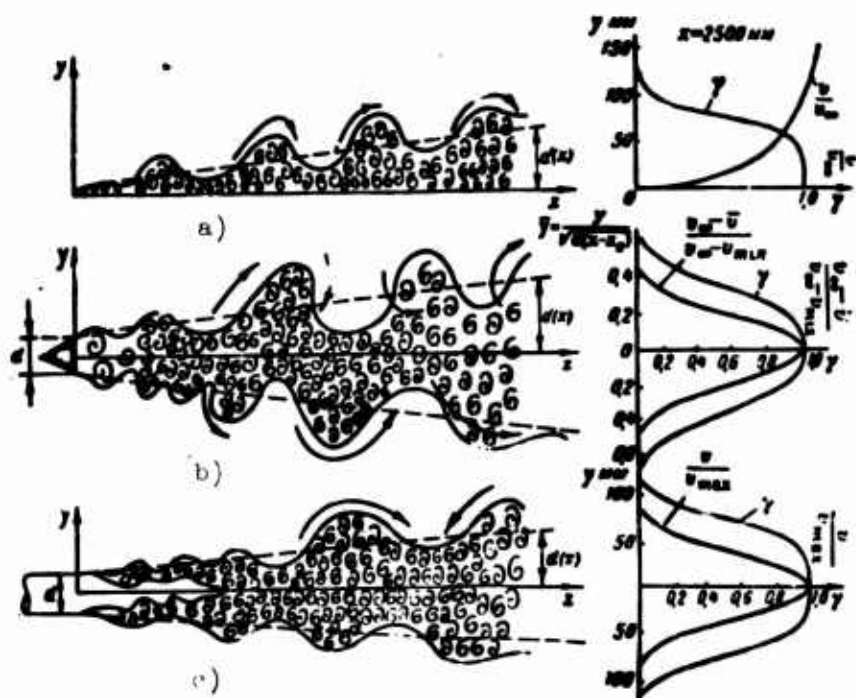


Fig. 4.15. Three forms of turbulence. a) turbulent boundary layer on a plate (data of Corrsin); b) plane turbulent wake (data of Townsend); c) turbulent stream (data of Corrsin).

The region of increased turbulence can be represented with practical accuracy as a region of isotropic turbulence, which is homogeneous over the cross section of the wake (layer) and which satisfies the condition of Kolmogorov's theory. Variation of parameters of turbulence become considerable only in direct proximity to the inner boundary (wall) or to the outer boundary (laminar superlayer) of this region, since exactly at the wall and outside of the surface of the superlayer, turbulent

pulsations are equal to zero. The average (in time) value of a given parameter of turbulence measured at a fixed point of the wake (layer, stream) is composed of values of the parameter from the region of increased turbulence at this point and values of the nonturbulent region; i.e., it is possible to write

$$\left. \begin{aligned} \bar{u}^2 &= \bar{u}_1^2 \gamma + (1 - \gamma) \bar{u}_2^2, \\ \bar{v}^2 &= \bar{v}_1^2 \gamma + (1 - \gamma) \bar{v}_2^2, \\ \overline{uv} &= \gamma (\overline{uv})_1 = -\gamma \cdot a \sqrt{\bar{u}_1^2} \cdot \sqrt{\bar{v}_1^2} \approx -a \gamma \bar{u}^2 (a \approx 0.4) \\ \text{etc.,} \end{aligned} \right\} \quad (4.33)$$

where $\gamma(x, y) = \frac{\bar{u}^2 - \bar{u}_2^2}{\bar{u}_1^2 - \bar{u}_2^2} = \frac{\bar{v}^2 - \bar{v}_2^2}{\bar{v}_1^2 - \bar{v}_2^2}$, etc., is the probability of appearance of a turbulent region.

Subscript "1" denotes parameters measured only in the turbulent region; subscript "2" denotes parameters measured in the nonturbulent region (in the incident flow), if they are large.

In the above cited works, function $\gamma(x, y)$ is called "discontinuity factor" or "intermittence". The probability of appearance of a turbulent region at the considered point is well described by Gauss's law. Analytic expressions $\gamma(x, y)$ in all three cases will be analogous to the below considered expressions of physical completeness of combustion $P_2(x, y)$ in a turbulent flame, but values of the average boundary of the turbulent region $a(x)$ and root-mean-square deviation of the instantaneous boundaries of region $\sigma(x)$ from the mean in this case will be different. The average width of the layer (wake, stream) is determined by the average velocity of displacement of the surface of the superlayer through the nonturbulent medium. The value of root-mean-square deviations of the surface of the superlayer is determined mainly by turbulent diffusion (transfer) of large eddies, which distort this surface. On the basis of dimensional considerations, it is possible to derive a formula which determines the value of average rate of increase of the quantity a with accuracy up to an empirical constant, and also to obtain a relation for $\sigma(x)$ analogous to Taylor's formula (4.13). However, within the scope of the present work, it is most convenient to give simply a final empirical expression for these values according to the above cited authors.

For the boundary layer of a rough wall (data of Corrsin [21] in the region of measurements $0 \leq x = 3000$ mm, $x_0 = -508$ mm), we have an average thickness of the turbulent layer $a = 0.404 (x - x_0)^{0.67}$ mm, $\sigma = 0.0641 (x - x_0)^{0.47}$ mm; thickness of

the boundary layer $\delta = 0.671 \times (x - x_0)^{0.61}$ mm; displacement thickness of $\delta^* = 0.459 (x - x_0)^{0.61}$ mm.

For a round stream (data of Corrsin [21] in the region of measurements $20 \leq x/d \leq 80$), we have

$$2r_{1/2}/d = 0.193 (x/d - 3).$$

Here $r_{1/2}$ is the radius of the stream, where $v = 0.5 v_{\max}$;

$$2a/d = 0.326 (x/d - 3)^{0.93};$$

$$2\sigma/d = 0.0845 (x/d - 3).$$

For determination of the turbulent wake (data of Townsend [12] in the region of measurements $500 \leq x/d \leq 1000$), we have

$$a/d = 0.35 (x/d - 90)^{0.5};$$

$$y_{1/2}/d = 0.217 (x/d - 90)^{0.5},$$

where $y_{1/2}$ is the ordinate at $v_{\omega} - \bar{v} = 1/2 (v_{\omega} - v_{\min})$, $\sigma/d = 0.133 (x/d - 90)^{0.5}$.

In Fig. 4.13, 4.16 and 4.17 there are given typical distributions of intensity and scale of turbulence over x and y in the boundary layer, in a wake and in a stream.

Turbulence during deformation of the flow. If the rate of deformation is sufficiently great: i.e., the time of passage of the flow through the section of deformation (Vitashinskiy nozzle, diffuser, and so forth) is less than the time of existence of eddies, then change of turbulence during deformation is sufficiently accurately described by a simple physical model, which was given for the first time by Prandtl. An arbitrary spherical volume in a flow before a nozzle with equiprobable (isotropic) orientation of eddies in all directions in the nozzle is deformed into an ellipsoid, extended along the central stream filament of the current. With such deformation, the average radius of twist of eddies along a stream filament of the current, and this means the average longitudinal scale of turbulence, l_{Eu} increases, and in the transverse direction decreases. Thus, in virtue of the law of conservation of momentum, the momentum of the longitudinal pulsations of velocity (along the average flow) decrease, and transverse fluctuations increase. A solution of such a problem in the linear formulation was given for the first time by Batchelor [1]. In Fig. 4.18 there are given numerical results of this solution. For contraction coefficients $v_2/v_1 = F_1/F_2$ greater than unity, Batchelor gives, in particular the simple working formulas

$$\frac{\overline{u_2'^2}}{\overline{u_1'^2}} = \frac{3}{4} \left(\frac{a_1}{a_2} \right)^2 \left[\ln 4 \left(\frac{a_1}{a_2} \right)^2 - 1 \right]; \quad \frac{\overline{v_2'^2} + \overline{w_2'^2}}{\overline{v_1'^2} + \overline{w_1'^2}} = \frac{3}{4} \frac{a_1}{a_2}. \quad (4.24)$$

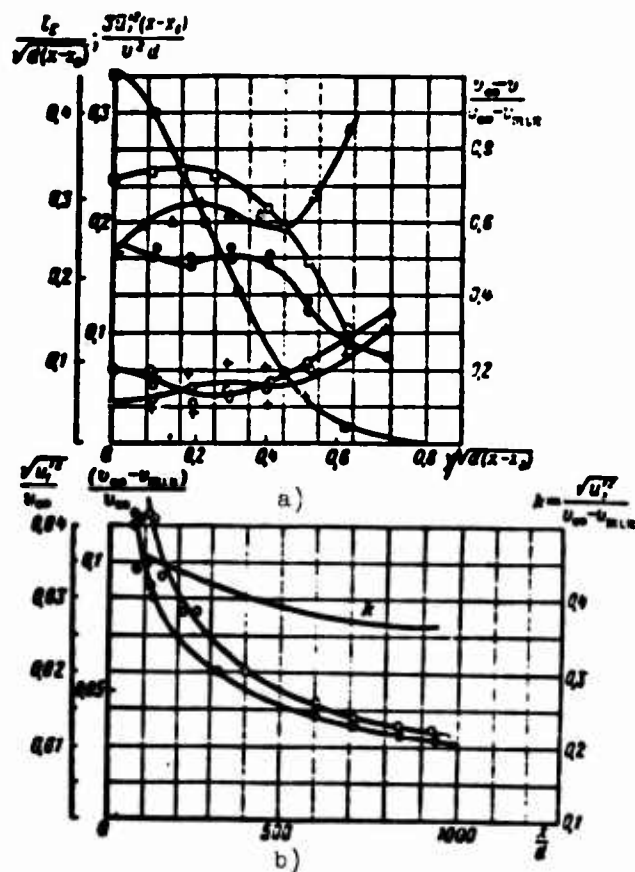


Fig. 4.16. Change of turbulent characteristics over the cross section and the axis of the wake.

- a) change of turbulent energy and scales of turbulence over the cross section of a wake (data of Townsend), $Re_d = 8400$, $\frac{x}{d} = 160$.

$$\square - \frac{u'_{max} - u'_{min}}{u'_{max}};$$

$$\square - \frac{(\overline{u'^2} + \overline{v'^2} + \overline{w'^2})(x-x_0)}{2\overline{u'^2}d} = \frac{3\overline{u'^2}(x-x_0)}{u'^2d};$$

$\Delta - l_E$ - calculation; $\bullet - l_{Eu}$;

$+ - l_{Ev}$; $\circ - l_{Ew}$;

- b) change of turbulent velocity along the axis of the wake

$$\bullet - \frac{u'_{max} - u'_{min}}{u'_{max}}; \circ - \frac{\sqrt{\overline{u'^2}}}{u'_{max}}$$

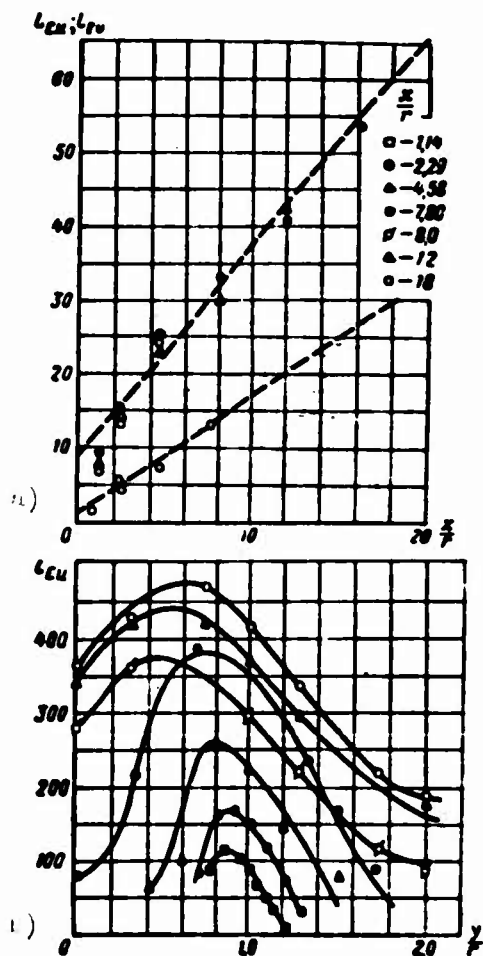


Fig. 4.17. Distribution of scales of turbulence along the axis of a stream (a) and over cross sections of a stream (b) data of Laurence; $d_{TP} = 89$ mm).

Along the axis of the stream:

- — hot-wire anemometer with one filament;
- — hot-wire anemometer with two filaments;
- △ — calculation according to the spectrum.

Over cross sections of the stream:

- — $x/2 = 1.14$,
- — $x/2 = 2.29$,
- ▲ — $x/2 = 4.58$,
- — $x/2 = 7.80$,
- ◊ — $x/2 = 8.0$,
- △ — $x/2 = 12$,
- — $x/2 = 18$.

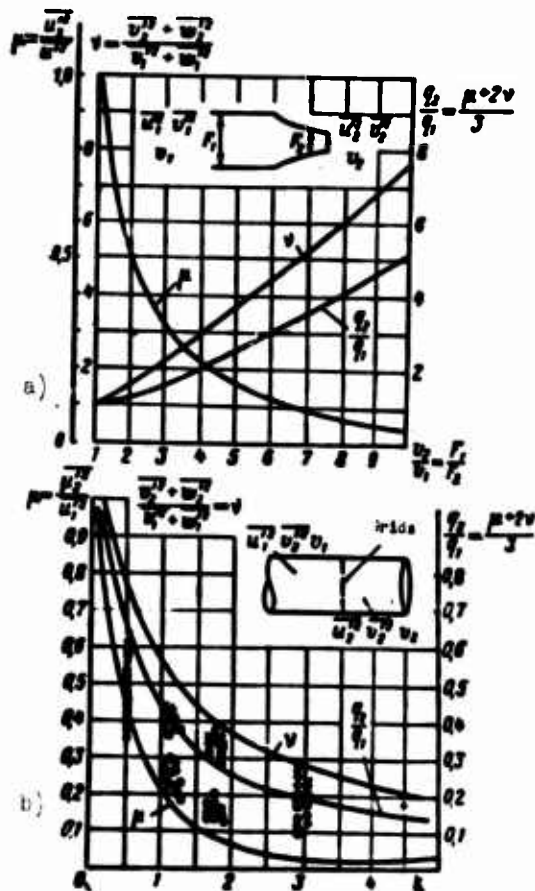


Fig. 4.18. Behavior of turbulence during symmetric deformation of a flow (a) and during passage through an attenuating grid (b).

- — $M = 5.08$ cm } μ
- — $M = 2.54$ cm } μ
- + — $M = 5.08$ cm } ν
- — $M = 2.54$ cm } ν

Such a solution does not take into account the actions of forces of inertia, pressure, viscosity and the finite rate of deformation. The action of these forces leads to a situation in which transverse pulsations increase less than is shown in Fig. 4.18a, since they succeed in transmitting part of their energy to longitudinal pulsations; but part of their energy will be converted

by viscosity into heat (transverse scales decrease during compression, so that the action of viscosity on them increases). Longitudinal pulsations, obtaining energy from transverse pulsations, decrease less than is shown in Fig. 4.18a. The influence of forces of inertia, pressure and viscosity will be more noticeable, the less the rate of deformation is. Therefore, the degree of anisotropy of turbulence after the nozzle turns out to be less than follows from the theory. The behavior of the total magnitude of turbulent energy ($\overline{u'^2} + \overline{v'^2} + \overline{w'^2}$) is prescribed by the theory much more exactly.

In spite of the growth of the absolute value of transverse pulsations, their relative magnitude (intensity of turbulence) decreases in inverse proportion to the square root of contraction coefficient, and intensity of the longitudinal pulsations decreases to a still greater degree [see expression (3.43)]. This peculiarity is utilized in practice with the use of a nozzle for the extinguishing of turbulence. The behavior of turbulence in a diffuser with small opening angles of the diffuser is approximately the reverse (the above mentioned results are reversible). At large opening angles, flow in the diffuser turns out to be unstable: there occurs separation of flow, with formation of intense, large eddies. Both these effects (deformation and flow separation) lead to a case in which the intensity of turbulence strongly increases along the diffuser.

Turbulence after grids. Characteristic scales of grids (dimensions of rods and mesh) are usually much smaller than scales of turbulence of the incident flow; therefore, they do not have essential significance. Controlling parameters of the grids are the hydraulic loss coefficient $\xi = \Delta p / \frac{1}{2} \rho v^2$ and the deviation ratio, which is defined as $\varphi = k(\alpha)$ (α and φ are angles between the normal to the grid and the directions of flow before and after passage through the grid). According to data of Schubauer and Klebanov [2], for grids of different constructions and small values of initial angle of inclination α there exists the approximate empirical equality

$$k = \frac{1.1}{\sqrt{1+\xi}}, \quad (4.9)$$

so that the one parameter ξ is essentially initial.

In Fig. 4.18b there are given results of Batchelor's solution of the problem of extinguishing turbulence by a grid and experimental data of Townsend on extinguishing turbulence by a grid after two turbulizing grids. It is clear that longitudinal pulsations of velocity are extinguished by the grid more strongly than

transverse pulsations. The theory, as in the preceding case, does not take into account the effect of forces of inertia and pressure; therefore, in reality transverse pulsations are obtained to be somewhat smaller, but longitudinal pulsations are obtained to be somewhat larger (due to the effect of pressure forces); change of total turbulent energy, as can be seen from the results given in Fig. 4.18b, is sufficiently accurately described by the theory.

Dependence of turbulence on pressure. This dependence is necessary to the designer for correct estimation of the influence of turbulence during the operation of combustion chambers at various altitudes. Nevertheless, the total number of works dedicated to this question at present is relatively small, which is apparently explained by the great methodological difficulties of measurement of parameters of turbulence in pressure chambers.

The first measurements showed that the rate of turbulent combustion decreases with fall of pressure. In the work of Khramtsov [45], considerable attention was paid to detailed measurement of parameters of turbulence at various pressures. With the help of the optical-diffusion method, there were measured turbulent velocity $\sqrt{\overline{v^2}}$, diffusion coefficient D and the scale of turbulence derived from them l_L in the range of pressures from 0.6-0.1 atm (abs.). Diffusion parameters of turbulence are of the greatest interest for appraisal of burning in combustion chambers; their measurement, furthermore, depends to a lesser degree on methodological errors depending on pressure; therefore, it is expedient to give the basic results of these measurements (Fig. 4.19). From Fig. 4.19 it is clear that turbulent velocity and diffusion coefficient change proportionally to pressure taken to an identical power, equal to 0.34. This is more strongly than according to hot-wire anemometric measurements.

The scale of turbulence, according to experiments of Khramtsov [45], remained practically constant; the same result is obtained in the work of Laurence [23] by variation of the average flow velocity, but within the same range of change of Reynolds number Re ($1.9 \cdot 10^5$ to $7.3 \cdot 10^5$). This result can be treated so that increase of viscosity with fall of pressure does not affect dimensions of eddies of the macrostructure, which give the main contribution to the integral scale of turbulence. Scales of microstructure and, in particular the Kolmogorov scale, according to (4.9) strongly increase; the fraction of turbulent energy in a fixed interval of length (width of the burning zone) also decreases with fall of pressure, but this leads to

the case in which the rate of turbulent combustion decreases, according to experiments of Khramtsov, with fall of pressure (although u_H increases), even if the level of macrostructure turbulence is held constant [45].

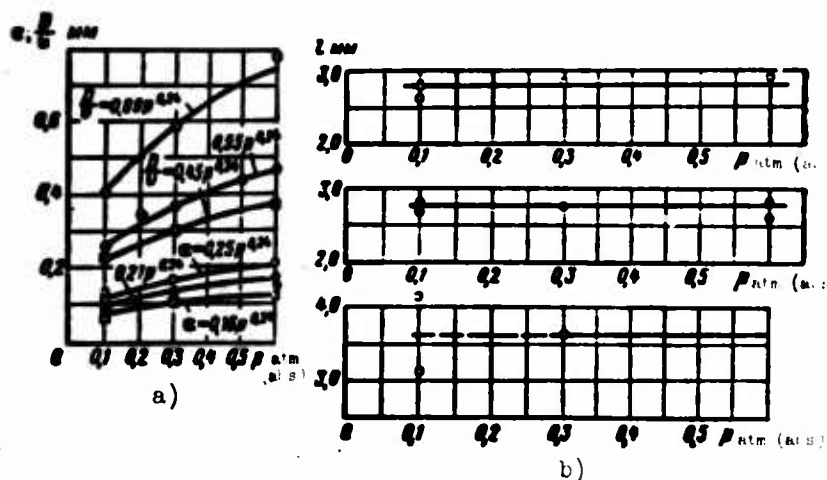


Fig. 4.19. Experimental dependence of intensity of turbulence ε , coefficient of turbulent diffusion D (a) and scale of turbulence (b) on pressure p .

Pipe $\varnothing 45$ mm, $v = 40$ m/sec, $x = 55$ mm

Grids	M mm	b mm
□	10.8	2.2
●	13	3.01
●	16	5.0

Turbulence in a flame. A number of authors (Landau [34], Markstein [42], Karlovitz [39], Scurlock [37] and others) have expressed the idea of the possibility of appearance (or increase) of turbulence in a flame. The question has arisen about so-called "auto-turbulence of a flame" and about the possibility of influence of the latter on the process of burning. It has for a long time been attempted to coordinate the differences between existing theories of turbulent burning and results of experiments with this unknown characteristic of a turbulent flame. The few measurements of turbulence in a flame which have been conducted [44], [47], [48], showed that the process of burning can change turbulence first of all by change of the hydrodynamics of the flow during burning. For instance, turbulence in the wake after a stabilizer during burning will be absolutely different from turbulence after the same stabilizer without burning (due to change of the field of average velocities after the stabilizer during burning); it can be greater or less than turbulence without burning, and depend on conditions of burning (mixture, ratio whether the combustion is

in a pipe or in an open flow, and so forth). But these peculiarities do not explain or remove the existing disagreement between theory and experiment, inasmuch as these differences are caused not by auto-turbulence, but by inaccurate experimental determination of the rate of turbulent combustion (see the following paragraph). With correct measurement, there are obtained values of the rate of turbulent combustion which are completely explainable by turbulence of the incident flow alone. Existing data on auto-turbulence are still absolutely insufficient to make a final conclusion concerning its influence on the rate of turbulent combustion, or to give recommendations and empirical formulas for their practical use. It is possible, however, to assert on the basis of data given in Chapter V, that for strongly developed turbulence of the incident flow the influence of auto-turbulization by the flame on the width and speed of the zone of turbulent burning will not be so great as was assumed initially.

LITERATURE

1. G. K. Batchelor. Theory of Homogeneous Turbulence, Camb. Univ. Press, 1952.
2. G. K. Batchelor. Theory of homogeneous turbulence, II, 1955.
3. G. K. Batchelor. The Application of the Similarity Theory of Turbulence to Atmospheric Diffusion, Quart., Journ. Meteorol. Soc., Vol. 76, No. 328, pp. 135-146.
4. G. K. Batchelor. Diffusion in a Field of Homogeneous, Turbulence, I Eulerian Analysis. Aust. J. Sci. Res., 1949, Vol. 2, No. 4.
5. G. K. Batchelor. "Diffusion in Turbulence Flow," Appl. Mech. Rev., 1950, No. 3.
6. G. K. Batchelor. Pressure Fluctuations in Isotropic Turbulence, Proc. Camb. Phil. Soc., 1951, Vol. 47.
7. G. K. Batchelor. Diffusion in a Field of Homogeneous Turbulence, Proc. Camb. Phil. Soc., Vol. 48, 345.
8. A. N. Kolmogorov. Breaking up of drops in a turbulent flow, Reports of the Academy of Sciences of the USSR, 1949, No. 5.
9. A. N. Kolmogorov. Local structure of turbulence in an incompressible viscous liquid at very large Reynolds numbers, Reports of the Academy of Sciences, 1941, Vol. 30, No. 4.
10. L. D. Landau and Ye. M. Lifshits. Mechanics of continuous media, State Technical and Theoretical Press, 1954.
11. A. A. Townsend. The Diffusion behind a Line Source in Homogeneous Turbulence, Proc. Roy. Soc., 1954, Vol. 224, No. 1159.
12. A. A. Townsend. The Fully Developed Turbulent Wake of a Circular Cylinder, Aust. J. Sci., Res., Vol. 2, 1949, No. 4.
13. A. A. Townsend. Structure of a turbulent flow with transverse shift, II, Moscow, 1959.

14. A. M. Obukhov and A. M. Yaglom. Microstructure of turbulent flow, "Applied Mathematics and Mechanic," Academy of Sciences of USSR, 1941, Vol. XV, Issue 1.
15. A. M. Obukhov. On the distribution of energy in the spectrum of turbulent flow, News of the Academy of Sciences of the USSR, 1941, Issue 4-5.
16. Ye. M. Minskiy. Turbulence of channel flow, Gidrometeoizdat, 1952.
17. H. L. Dryden, G. B. Shubauer, W. C. Mock, and H. K. Skramstad. Measurements of Intensity and Scale of Wind-tunnel Turbulence, Rep. NACA, 1937, No. 581.
18. G. B. Shubauer. A Turbulence Indicator Utilizing the Diffusion of Heat, Rep. NACA, 1935, No. 524.
19. M. S. Uberoi and S. Corrsin. Techn Notes NACA, 1952, Wash, No. 2710.
20. M. S. Uberoi and S. Corrsin. Diffusion of Heat from a Line Source in Isotropic Turbulence, Rep. NACA, 1953, No. 1142.
21. S. Corrsin and M. S. Uberoi. Further Experiments on the Flow and Heat Transfer in a heated Turbulent Air Jet, Report NACA, 1950, No. 998.
22. S. Corrsin and A. L. Kistler. Free-Stream Boundaries of Turbulent Flows, Report NACA, 1955, No. 1244.
23. C. L. Laurence. Intensity, Scale and Spectra of Turbulence in mixing Region of Free Subsonic Jet. By. James Report NACA, 1950, No. 1292.
24. W. D. Baines and E. G. Peterson. An Investigation of Flow Through Screens, Transactions of the ASME, 1951, Vol. 73, No. 5, pp. 467-480.
25. A. G. Prudnikov. Measurement of turbulence of air flows and flames by the optical-diffusion method, Collection of articles, "Burning in a Turbulent Flow," Publishing House of the Academy of Sciences of the USSR, 1959.
26. A. G. Prudnikov. Determination of average parameters of a turbulent flame. Publishing House of the Academy of Sciences of the USSR, Department of Technical Sciences (CTN), 1960, No. 1.
27. S. A. Gol'denberg. Certain experimental facts concerning turbulent diffusion. News of the Academy of Sciences of the USSR, OTN, 1950, No. 4.
28. G. J. Taylor. Statistical Theory of Turbulence, Proc. of the Royal Soc., London, 1935, Vol. 151.
29. G. J. Taylor. The Dispersion of Matter in Turbulent Flow through a Pipe Proc. Royal Soc. A 223, No. 1155.
30. A. G. Loytsyanskiy. Homogeneous isotropic turbulence, Transactions of the Central Aero-Hydrodynamic Institute, No. 440, 1939.
31. Chuang Feng-Can. On the Decay of Turbulence. Acta Sci Sinica, 1955, Vol. 2, No. 3, pp. 187-200.
32. P. S. Klebanoff. Characteristics of Turbulence in a Boundary Layer with zero Pressure Gradient. Report NACA N 1247, 1955, No. 4.
33. W. Paul Jensen. Flame Generated Turbulence, Jet Propulsion, 1946, No. 6.
34. L. D. Landau. On the theory of slow burning, Journal of Experimental and Theoretical Physics, 1944, 14, 240.
35. A. E. Scurlock. Meteor. Report N 19, Fuels Research Laboratory M. J. T., July, 1948.
36. G. C. Williams, H. C. Hottel, and A. C. Scurlock. Flame Stabilization and Propagation in High Velocity Streams, Third Symposium on Combustion, Flame and Explosion Phenomena, Baltimore, 1949, p. 21.

37. A. C. Seurlock and I. H. Grover. Propagation of Turbulent Flames, Fourth Symposium on Combustion, Baltimore, 1958, p. 649.
38. B. Karlovitz, D. Denniston, Wyr, and F. E. Wells. Studies on Turbulent Flames, I. Chem. Phys., 1951, Vol. 19, No. 5.
39. B. Karlovitz. Open Turbulent Flames, Fourth Symposium on Combustion, Baltimore, 1953, p. 60.
40. B. Karlovitz, I. B. Denniston, D. H. Knapshafer, and F. E. Wells. Studies on Turbulent Flames. A. Flame Propagation Across Velocity Gradients. B. Turbulence Measurement in Flames. Fourth Symposium on Combustion, 1958.
41. G. N. Markshteyn. Experimental and theoretical study of flame-front stability. "Problems in rocket engineering," No. 4, 1951.
42. G. H. Markstein. Instability Phenomena in Combustion Waves, Fourth Symposium on Combustion, 1953.
43. G. N. Markstein. Interaction between flame propagation and flow perturbations, "Problems in Combustion," 1953, No. 1, pp. 103-109.
44. A. Westenberg. Measurement of flame turbulence by the method of helium diffusion, "Problems of Rocket Technology," 1955, 2 (26).
45. V. A. Khramtsov. Investigation of Pressure Effect on the Parameters of Turbulence and on Turbulent Burning. Seventh Symposium (international) on Combustion (Combustion and Detonation Waves), Baltimore, Williams and Wilkins Co, 1959.
46. T. A. Bowina. Studies of Exchange between the Recirculation Zone behind the Flame Holder and the outer flow. Seventh Symposium (international) on Combustion (Combustion and Detonation Waves), Baltimore, Williams and Wilkins Co, 1959.
47. A. G. Prudnikov. Flame turbulence, Seventh Symposium (international) on Combustion (Combustion and Detonation Waves), Baltimore, Williams and Wilkins Co, 1959.
48. A. Robert, and Gross. Flame Generated Turbulence, Jet Propulsion, 1951, Vol. 25m, No. 12.

CHAPTER V

BURNING OF HOMOGENEOUS FUEL-AIR MIXTURES IN A TURBULENT FLOW

§ 1. PROBABILITY CHARACTERISTICS OF A TURBULENT FLAME

Turbulent burning is on the disordered, non-stationary process of turbulent displacement of volumes of combustion products and fresh mixture, and reaction of the latter due to increase of its temperature. Therefore, in distinction from a laminar flame front, in a turbulent combustion zone parameters of the flow will be random functions of space and time coordinates. In particular, the instantaneous value of a flow parameter, let us say temperature, at an arbitrary point of the turbulent flame is not equal to the time average of temperature at this point.

The random character of oscillations of flow parameters indicates the necessity of application of probability theory (statistics) to the considered phenomenon. Inasmuch as below there are used probability characteristics of a turbulent flame, it will be useful to recall basic concepts and definitions necessary for the following presentation which are known from probability theory, but in application to turbulent burning.

In probability theory there is introduced the idea of a random function. This may be, for instance, the value of temperature as a function of time at a fixed point of a zone, or the value of temperature at a fixed moment of time as a function of space coordinates. In concept, the word "random" implies that the value of temperature at a fixed point of the zone can not be predicted beforehand. It is possible only to determine relative duration of some temperature at the considered point of the zone. Thus, there arises the idea of the probability of appearance of a given temperature to the total time of observation as the time of observation tends to infinity; i.e.,

$$P_1 = \lim_{t \rightarrow \infty} \frac{\sum_{i=1}^n t_i}{t} \quad (5.1)$$

where $P_1(T_1)$ — probability of appearance of temperature (T_1) at the given point of the zone;

t_i — one of the elementary time intervals of observation during which the temperature at the given point of the zone is equal to T_1 ;

t — total time of observation (Fig. 5.1).

If random function $T(t)$ can take any values from T_1 — the temperature of the fresh mixture, to T_2 — the temperature of the combustion products, then we introduce the idea of the integral of probabilities of temperatures: $P(T)$ is the probability that at the considered point of the zone, temperature will take a value not less than T . It is obvious that at any point of the zone

$$P(T_1 - 0) = 0 \text{ and } P(T_2 + 0) = 1.$$

For the interval of values $T_1 \leq T \leq T_2$ it is possible to introduce the idea of the probability density function:

$$p(T) = \frac{dP(T)}{dT} \quad (5.2)$$

where $P(T)dT$ is the probability of appearance of values of temperature in the interval from T to $T + dT$.

We will designate functions of probability and of the integral of probabilities by P with corresponding subscripts ("1", "2", and so forth), and the probability density functions by p . The appearance of a given temperature at a given point of a zone is the result of turbulent displacements of volumes of gas. It is possible to introduce the probability density function of turbulent displacements of volumes of gas. (For a one-dimensional zone $p(x - x_0; t)$ is the probability that a unit volume from point x_0 will arrive at point x at moment t .)

The probability that volumes of gas will arrive at point x from an interval of finite length $(x_2 - x_1)$ can be determined accordingly by the formula

$$P_{1,2} = \int_{x_1}^{x_2} p(x - x_0) dx_0 \quad (5.3)$$

Since temperature at the considered point changes in some random manner, then not its instantaneous values are of interest to us, but its mean-statistical values. The mean value of temperature (in statistics it is frequently called mathematical expectation) is defined in our case as

$$\bar{T} = \int_{-\infty}^{\infty} T dP(T) = T_1 P_1 + T_2 P_2 + \int_{T_1+0}^{T_2-0} T \cdot p(T) dT. \quad (5.4)$$

" $T_1 + 0$ " or " $T_1 - 0$ " denotes the region of integration respectively from the right of point T_1 and from the left of point T_2 . Inasmuch as the magnitude of temperature fluctuations relative to the mean value is equal to zero, then as the characteristic of the fluctuations we take the mean square value of the fluctuations:

$$\sqrt{\overline{T^2}} = \sqrt{\overline{(T - \bar{T})^2}} = \sqrt{\int_{-\infty}^{\infty} (T - \bar{T})^2 dP(T)}. \quad (5.5)$$

Equality of the mean value of fluctuations of the random variable to zero indicates the fact that probabilities of both positive and negative values of fluctuations are identical, so that on the average in time they add up to zero.

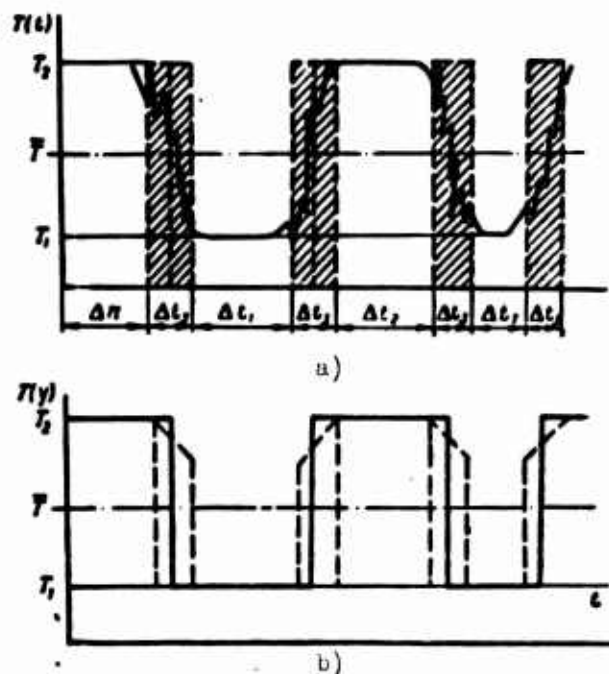


Fig. 5.1. Determination of average temperatures (model of surface combustion).

a) example of a graph of true temperature fluctuations with respect to time ($P_2 \approx 0.2$),

$$P_1 = \lim_{t \rightarrow \infty} \frac{\sum \Delta t_1}{t}; \quad P_2 = \lim_{t \rightarrow \infty} \frac{\sum \Delta t_2}{t}; \quad P_3 = \lim_{t \rightarrow \infty} \frac{\sum \Delta t_3}{t};$$

b) graph of temperature fluctuations with respect to time for the model of "surface combustion."

Let us imagine that in the zone of turbulent displacement there is no molecular exchange. Then in the zone of turbulent displacement there will exist only two initial temperatures T_1 and T_2 , inasmuch as turbulent displacement is purely mechanical displacement (turbulent transfer of "cold" and "hot" volumes by continuous eddy motions). In this case relation (5.4) and (5.5) will be written in the simple form

$$\begin{aligned} \bar{T} &= T_1 P_1 + T_2 P_2, \quad \overline{T^2} = (T_1 - \bar{T})^2 P_1 + (T_2 - \bar{T})^2 P_2 = \\ &= (T_2 - T_1)^2 P_1 P_2, \quad \overline{T'u'} = (T_2 - T_1)(\bar{u}_2 - \bar{u}_1) P \end{aligned} \quad (5.6)$$

where P_1 and P_2 are probabilities of the appearance respectively of "cold" and "hot" volumes of gas; it is obvious that $P_1 + P_2 = 1$.

The profile of temperatures formed as a result of turbulent displacement is shown in Fig. 5.1.

The maximum value of the mean square value of fluctuations, which is equal to $(T_2 - T_1)^2/4$, is attained at the point where $P_1 = P_2 = 0.5$. In this case mean values of density $\bar{\rho}$ and temperature \bar{T} turn out to be related with each other by the linear dependence

$$P_1 = \frac{\bar{\rho} - \bar{\rho}_1}{\bar{\rho}_2 - \bar{\rho}_1} = \frac{\bar{T} - T_1}{T_2 - T_1}. \quad (5.7)$$

If at the initial moment the two gases are separated by a plane partition passing through point $x = 0$ ("cold" gas is located on the left of point $x = 0$, and "hot" gas is located on the right), then the probability of appearance of "hot" gas at point x at the time t will be determined according to (5.3):

$$P_2(x) = \int_0^x p(x-x_0) dx_0. \quad (5.8)$$

In statistics it is assumed as a working hypothesis (ergodic hypothesis) that probability averaging of form (5.4) and (5.6) is equivalent to averaging over time or over the space coordinates along which the properties of the random variables do not change on the average; i.e.,

$$\bar{T} = \int_{-\infty}^{\infty} T dP(T) = \lim_{t \rightarrow \infty} \frac{1}{t} \int_0^t T(t') dt' = \lim_{y \rightarrow \infty} \frac{1}{y} \int_0^y T(y') dy' \text{ etc.} \quad (5.9)$$

If the averaged values of the random function do not depend on time or space coordinates, then such a function is called respectively a stationary random function or a homogeneous random function. For a stationary (homogeneous) random function naturally, the following condition is satisfied:

$$\frac{\partial \bar{T}}{\partial x} = \frac{\partial \bar{T}}{\partial y} = \frac{\partial \bar{T}^2}{\partial x} = \frac{\partial \bar{T}^2}{\partial y} = 0 \text{ etc.} \quad (1.10)$$

The process of averaging is usually designated by a long line drawn above the symbol of the random function. It is useful to recall a number of properties of averaging which directly ensue from the essential nature of averaging as a limiting operation of summation:

$\overline{(a+b)} = \bar{a} + \bar{b}$, where a and b are arbitrary random functions;

$$\overline{(a+b)^2} = \bar{a}^2 + 2\bar{a}\bar{b} + \bar{b}^2; \quad \overline{\rho T} = \bar{\rho}\bar{T} + \overline{\rho'T'}; \quad \overline{(\partial T/\partial x)} = \partial \bar{T}/\partial x;$$

$$\int_0^L T(x) dx = \int_0^L \bar{T}(x) dx; \quad \overline{(T-\bar{T})^2} = \overline{T^2} - (\bar{T})^2; \quad \bar{T} + \overline{\rho T/\rho} = \bar{\rho} \bar{T} + \overline{\rho'T'}$$

§ 2. EQUATIONS OF HYDRODYNAMICS FOR A TURBULENT FLAME

Parameters of the medium in the zone of turbulent burning are random functions of space and time coordinates. On the other hand, these parameters are continuous and differentiable functions of these coordinates, so that the equations of hydrodynamics are fully applicable to them. Continuity and differentiability are explained by the fact that molecular viscosity completely suppresses components of turbulent motion whose scales are comparable with the mean free path of the molecules, so that the smallest scales of turbulent pulsations of any of the indicated parameters always turn out to be much larger than this length. Therefore, it is possible to always disregard molecular structure of the fluid, and to consider the latter as a continuous medium. The applicability of equations of hydrodynamics for a turbulent front is confirmed also by their successful use in the theory of the laminar flame front and in the theory of turbulent motion.

Chemical reaction occurring in the turbulent zone does not affect the form of the continuity equations or the equations of motion if they are written in the most general form, taking into account the fact that density and kinematic viscosity of the medium ν are functions of temperature and pressure. Since turbulent burning usually occurs at speeds much less than the speed of sound, it is possible, with accuracy up to Mach number M^2 , to consider that the density of the medium is a function only of temperature, i.e., to consider that up to the front, the liquid is incompressible and nonisothermal. Then, at any point of the front and at any time

$$\rho T = \rho_1 T_1 = \text{const.} \quad (1.11)$$

Molecular weight is assumed to be constant; ρ and T are respectively density and temperature of the mixture. Subsequently, in all cases, all physical parameters with subscript "1" will pertain to the fresh mixture, and all with subscript "2" will pertain to the burned mixture.

For problems of turbulent burning in a pipe, the constant in condition (5.11) can be considered to be a weakly changing function of the coordinate along the pipe (due to fall of pressure).

Equations of hydrodynamics are conveniently written with the help of "dummy" indices, which permit us to represent the equations in more compact form. The continuity equation has the form

$$\frac{\partial \rho}{\partial t} + \frac{\partial \rho u_i}{\partial x_i} = 0, \quad (5.12)$$

where u_i - i -th component of instantaneous flow velocity at the considered point x_i at the time t .

Subscripts i, j , and k everywhere pass through the values 1, 2, 3, corresponding to components of vectors respectively along the axes x, y, z . In the remainder of this text, by all repeated indices there is implied summation over the values 1, 2, 3, and the summation sign for brevity is not written. For a one-dimensional burning zone, the averaged parameters of which change only along one of the coordinates (through the depth of the zone), the continuity equation after averaging can be written as

$$\frac{\partial \bar{\rho}}{\partial t} + \frac{\partial \bar{\rho} \bar{u}}{\partial x} = 0. \quad (5.13)$$

Subscript "1" is omitted, since it is not needed for further operations.

During investigation of turbulent burning, of most interest are the equations of conservation of energy and mass (fuel, oxidizer).

In the most general form, under the condition of constancy of pressure, it is possible to write them as [13]

$$c_p \rho \frac{DT}{Dt} = c_p \rho \left(\frac{\partial T}{\partial t} + u_i \frac{\partial T}{\partial x_i} \right) = \sigma'_{ik} \frac{\partial u_i}{\partial x_k} + \frac{\partial}{\partial x_i} \lambda \frac{\partial T}{\partial x_i} + \Phi(T; c); \quad (5.14a)$$

$$\rho \left(\frac{\partial c}{\partial t} + u_i \frac{\partial c}{\partial x_i} \right) = \frac{\partial}{\partial x_i} \rho D_{ik} \frac{\partial c}{\partial x_i} - W(T; c), \quad (5.14b)$$

$$i = 1, 2, 3,$$

where σ'_{ik} is the tensor of viscous stresses.

The left side of equation (5.14a) constitutes the quantity of heat obtained by a unit volume of gas per unit time at point x_i ($i = 1, 2, 3$) and at the time t .

From equation (5.14a) it is clear that it is composed of heat obtained from dissipation of kinetic energy by viscosity $\sigma_{ik} \frac{\partial u_i}{\partial x_k}$, heat transferred to the considered volume by means of thermal conduction, and heat released per unit time from possible chemical reactions. The physical meaning of the terms of the equation of conservation of mass is analogous. The left side of equation (5.14b) — rate of change of concentration of substance c per unit volume — is equal to the rate of supply of substance by molecular diffusion minus the rate of loss of substance by chemical reaction. In terms for diffusion flows of heat and mass, there will be disregarded the effect of thermal diffusion; i.e., it will be assumed that molecular flow of heat is proportional only to the temperature gradient, and flow of mass is proportional only to the concentration gradient of the given substance. This assumption for usual conditions of burning is immaterial. Just as immaterial will be the fact that heat released during decay of turbulence is disregarded [first term of the right side of equation (5.14a)].

As the concentration c it is possible to take the concentration of substance carrying on the chemical reaction. This can be the concentration of oxygen, the concentration of fuel vapor or the concentration of intermediate reaction products (active centers) and so forth, depending upon the physical conception of the heat emission mechanism which is selected. The quantity ρ_c is the mass of given substance per unit volume. Between the rate of disappearance of the concentration of initial reaction products and the rate of heat release caused by this reaction there exists, obviously, a direct relation:

$$\Phi = H_u W,$$

where H_u is the heat of reaction.

Using this relation, it is possible, by multiplying relationship (5.14b) by H_u and adding it with relationship (5.14a), to obtain under the condition of the equality $\lambda/c_p\rho = D_M$ a relationship for enthalpy of the gas:

$$\rho \frac{\partial H}{\partial t} + \rho \alpha_i \frac{\partial H}{\partial x_i} = \frac{\partial}{\partial x_i} \frac{\lambda}{c_p} \frac{\partial H}{\partial x_i} \quad (i = 1, 2, 3), \quad (5.15)$$

where $H = c_p T + H_u c$ — enthalpy of a unit of mass of gas;

D_M — coefficient of molecular diffusion;

λ — coefficient of thermal conductivity;

$\lambda/c_p\rho = a$ — coefficient of thermal diffusivity.

Equality of the diffusion coefficient D_m to the coefficient of thermal diffusivity α is a well-known result of the classical theory of molecular diffusion; it is widely applied in the thermal theory of laminar burning as one of the assumptions (see Chapter III). For fuel-air mixtures it is satisfied with sufficient accuracy, although there are possible cases when the deviation from a perfect equality turns out to be considerable, for instance, at the rich concentration boundaries of ignition, when distribution curves of the quantity u_{II} with respect to mixture ratio are asymmetric (see Chapter III) and so forth.

By definition, enthalpies in the fresh mixture and in the completely burned mixture are identical, i.e.,

$$H_1(-\infty) = c_p T_1 + H_{s1} = H_2(+\infty) = c_p T_2$$

With such boundary and initial conditions, the solution of equation (5.15) turns out to be the following:

$$H = c_p T + H_{s1} = c_p T_1 + q_0 = c_p T_2 = \text{const.}^* \quad (5.16)$$

Thus, at any point of the zone, two random functions T and c are related by (5.16), the physical meaning of which is that in the case of equality of rates of molecular diffusion of heat and reactant during any turbulent motion, there is established dynamic equilibrium between the internal and chemical energies: their sum remains constant at any point of the burning zone, at any moment of time.

Formula (5.16) was obtained as the solution of equation (5.15) for the first time by Zel'dovich (see Chapter III) in reference to a laminar flame front; from the given reasoning it is clear that it has a wider region of application; in particular, it remains valid in the turbulent burning zone for any mechanism of combustion.

With the help of (5.16), the system of equations (5.14) can be reduced to one equation if there are known functions $\Phi(T; c)$ or $W(T; c)$. Let us consider in greater detail what the form of these functions is.

Let us select an arbitrary "fluid volume" of fresh mixture, which is small enough that at all subsequent moments of time temperature and concentration in it will be constant over the whole volume. In the hydrodynamics of an inviscid fluid, by "fluid volume" there is understood a volume within whose boundaries there are

*The question about the uniqueness of this solution for arbitrary initial conditions remains open. All further considerations of turbulent burning are conducted on the basis of solution (5.16).

contained always the same particles of fluid. In this case we assume that this volume does not exchange particles with its surroundings by means of hydrodynamic motion; but it can change its composition and temperature by means of molecular exchange with its environment; i.e., this volume should be much smaller than the smallest eddies (smallest scales of hydrodynamic motion), but large enough that it is possible to consider it as a continuous medium. The existence of such a volume is possible, since at atmospheric pressure the distance between molecules $\sim 30\text{\AA}$, which is many order of magnitude smaller than the smallest eddies, whose dimensions are measured in tenths, and, in extreme cases, in hundredths of a millimeter (see Chapter IV).

Exchange between such a volume and its surroundings will indeed occur only due to molecular transfer, since any turbulent pulsations will transfer it as a single whole. Therefore, the relationships of molecular exchange and kinetics are completely applicable to such a volume.

With the thermal mechanism, the rate of heat release at an arbitrary point of a turbulent flame at any moment of time is determined by the relationship

$$\Phi(T; t) \sim \sqrt{T} c' \exp\left(-\frac{E}{RT}\right)$$

or, in virtue of condition (5.16) by the expression

$$\Phi(T) \sim (T_s - T) \exp\left(-\frac{E}{RT}\right), \quad (5.17)$$

where ν , E and R are respectively the total reaction order, activation energy and gas constant; these are assumed to be identical for laminar and turbulent flames.

The turbulent burning zone comprises an infinite set of elementary fluid volumes, each of which is in a definite stage of chemical reaction, where this stage, according to (5.16), (5.17), is uniquely determined by the temperature of the volume. Therefore, if at an arbitrary moment of time at an arbitrary point of the zone there is recorded a definite temperature, then it is possible to say definitely what volume is located at the considered point, and, consequently, what the rate of heat release is in the arbitrarily small unit of volume surrounding the given point. Formally (5.17) does not differ from the relationship for rate of heat emission in a homogeneous, thermally insulated mixture, but in the given case rate of heat emission is a random function of a random argument (temperature).

The above considerations, from the point of view of description of the process by the method of dimensional theory, indicate that the physico-chemical parameter

of a fuel-air mixture having the dimension of time (characteristic burning time) remains the same during turbulent burning as during laminar burning.

With help of the continuity equation and relationship (5.17), it is possible to write the energy equation in the form

$$c_p \left(\frac{\partial T}{\partial t} + \frac{\partial T u_i}{\partial x_i} \right) = \frac{\partial}{\partial x_i} \lambda \frac{\partial T}{\partial x_i} + \Phi(T)$$

or (since $\rho T = \text{const}$)

$$\frac{\partial u_i}{\partial x_i} = \frac{\partial}{\partial x_i} a \frac{\partial T}{\partial x_i} + F(T), \quad (5.18)$$

where

$$F(T) = \frac{\Phi(T)}{c_p \rho T_i};$$

$$i = 1, 2, 3.$$

Equation (5.18) is interesting due to the fact that it is almost linear, except for the term $F(T)$; in it there are not contained products of various random functions, so that during averaging there do not appear additional unknowns — correlation moments. In it there evidently are also not contained terms characterizing turbulent exchange and non-stationarity of the process. Such a form turns out to be very convenient for subsequent mathematical transformations of the equations of hydrodynamics of a turbulent flame.

The system of equations of momentum conservation can be simplified analogously, but for a turbulent flame it is not of fundamental interest; therefore, here we will not consider it. Solution of the given system of equations can be obtained only on the basis of definite physical concepts. In the following paragraphs there are presented physical concepts involved in the process of development of turbulent burning in reference to combustion chambers of air-breathing jet engines there are also given definitions of the basic physical parameters characterizing this process.

§ 3. STAGES OF DEVELOPMENT OF THE TURBULENT BURNING ZONE

The question of the vicissitude of turbulent burning was considered for the first time in the works of Sokolik [11] and Sviridov [12]. Here it is expounded in the light of the latest data on turbulence and turbulent burning.

Let us consider the simplest case: development in time of a one-dimensional burning zone from the initial plane separating fresh mixture from combustion products. This case, strictly speaking, is the physical ideal, but to it, with relatively small error, it is possible to reduce all cases of burning in open flows and with a series of additional refinements — also cases of burning in a pipe (see

Section 5, Chapter V). The most exact physical equivalent of a one-dimensional zone is the burning zone on the boundary between two plane flows (fresh mixture and combustion products) moving with identical velocities v (Fig. 5.2a). In this case, with error of the order of $\bar{u}_1'^2/v^2$, variation of parameters of this zone in some transverse cross section of the flow can be considered as variation of parameters through the depth of a one-dimensional zone; and variation of parameters from cross section over the distance x_0 along the flow - as change of the one-dimensional zone in time $t = x_0/v$. This makes it possible to use available experimental material on turbulent burning in high-speed flows.

During the analysis of experimental material, there are first of all noted two experimental facts: stationarity of the rate of turbulent combustion (when turbulence of the incident flow is homogeneous) and non-stationarity of the width of the turbulent burning zone (Fig. 5.3 and 5.4). In an open flow, this distinction is

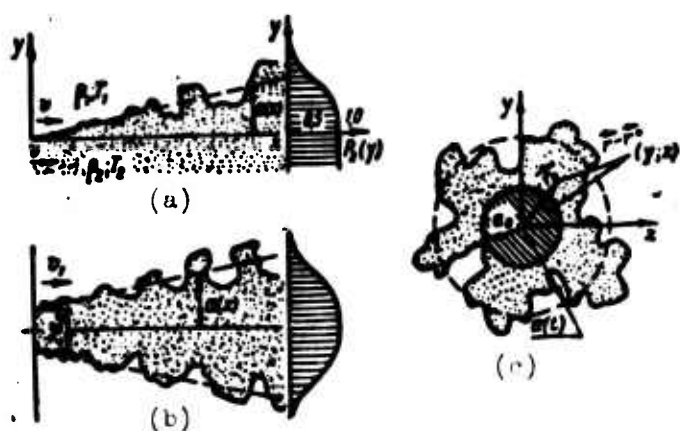


Fig. 5.2. Determination of the profile of average temperatures in a turbulent flame. a) plane case; b) linear case; c) axially symmetric case.

immediately evident from the first visual observation of a plane turbulent flame: the angle of expansion of the flame, which is proportional to the quantity u_T/v , practically does not change over the length of the flame, and the width of the zone of luminosity (along the normal to the main flow) increases along the flame.

Let us dwell on the first fact. The equation of conservation

of energy (5.18) for a one-dimensional zone acquires after averaging the form

$$\frac{d\bar{u}}{dx} = D_s \frac{d^2\bar{T}}{dx^2} + \bar{F}(T). \quad (5.19)$$

Integrating it over x from $-\infty$ to $+\infty$, we will obtain (taking into account the equation of conservation of mass $\rho_1 u_T = \rho_2 u_2$) a relationship which determines the speed of turbulent combustion:

$$u_T = \frac{1}{(n-1)} \int_{-\infty}^{\infty} \bar{F} dx = \frac{1}{(n-1)} \int_{-\infty}^{\infty} \frac{\bar{F}(T)}{c_p \rho_1 T_1} dx, \quad (5.20)$$

where $n = T_2/T_1 = \rho_1/\rho_2$.

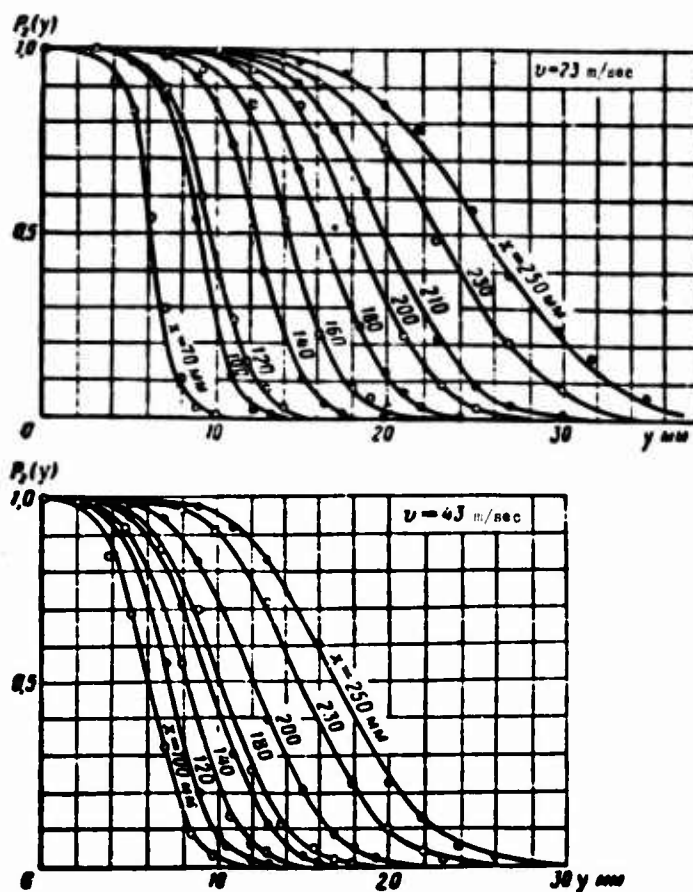


Fig. 5.3. Distribution of the probability of finding combustion products (physical combustion efficiency) at various points over the cross sections of an open flame after a burner.

$\alpha = 1.2$; $t = 150^\circ\text{C}$. $d_{Tp} = 150 \text{ mm}$ — data of Lushpa.

○ ● — experimental points,
----- — theoretical curve,

$$P_{p,y} = \frac{1}{2} \left[1 - \exp\left(-\frac{y}{x}\right) \right].$$

Relationship (5.20) has a simple physical meaning: the velocity of propagation of the flame is equal to the integral burning speed of the mixture in the burning zone. It is possible to consider it as a certain modification of the equation of conservation of mass: the velocity of volumes of fresh mixture moving toward the motionless (on the average) combustion zone is equal to the total burning speed of these volumes in the zone. Equation (5.20) is applicable to any model of burning, including a laminar front. In this sense, it is possible to consider it as an identity. The fundamental distinction between all existing models of burning consists only of the form of the distribution function $P(T; x)$ which is contained

in $\bar{\Phi}(T)$. For instance, for a laminar flame front, the distribution function $P(T)$ is such that the random function of temperature is simply equal to its own mean value (the probability of mean temperature is equal to one). In this case, relationship (5.20) is reduced to the form which was for the first time given by Zel'dovich:

$$u_0 = \frac{1}{c_p \rho_1 (T_0 - T_1)} \int_{-\infty}^{\infty} \Phi(T(x)) dx, \quad (5.20a)$$

whence we will obtain

$$u_1/u_0 = \int \bar{\Phi} dx / \int \Phi dx. \quad (5.20b)$$

Let us note that for a laminar flame front equation (5.19) is reduced to the well-known Zel'dovich-Frank-Kamenetskiy equation by the simple substitution:

$$T = \bar{T}; \quad u = \bar{u} = u_1 T / T_1 \text{ and } \Phi = \bar{\Phi}.$$

Let us consider now what physical meaning function $P(T; x)$ has in the case of turbulent burning.

The process of formation of a one-dimensional burning zone can arbitrarily be divided into three stages. Fundamental peculiarities of these stages are

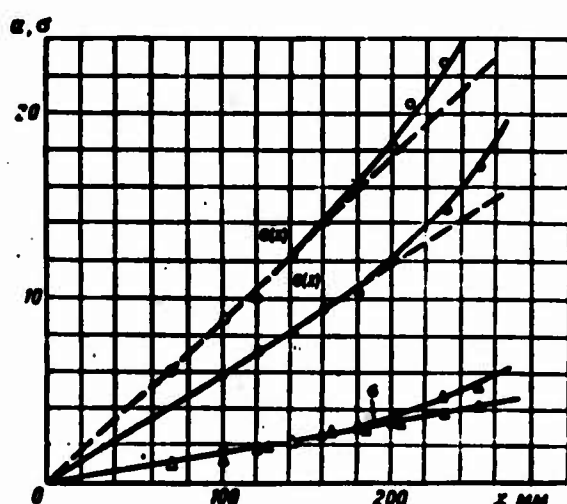


Fig. 5.4. Distribution of functions of average $a(x)$ and dispersion $\sigma(x)$ of an open flame after a "point" burner (data of Lushpa).

○ — $a(x)$, $v = 23$ m/sec;
● — $a(x)$, $v = 43$ m/sec;
△ — $\sigma(x)$, $v = 23$ m/sec;
▲ — $\sigma(x)$, $v = 43$ m/sec;
 $u = 1.2$; $t = 150^\circ\text{C}$.

schematically depicted in Fig. 5.5. In the first moments of the initial stage, formation of the burning zone occurs just as in laminar flow, since the coefficient of turbulent diffusion according to Taylor's equation is equal to zero.

The quantity u_T is determined according to (5.20) by the integral of the average rate of heat release. According to properties of averaging (see § 1, Chapter V), the instantaneous profile of rate of heat emission can first be integrated over x , and then averaged along the y -axis (or z -axis). For convenience of analytic integration, we will replace the instantaneous profile of rate of heat release along the x -axis by the Gaussian curve:

$$\Phi = \Phi_{\text{max}} e^{-\frac{x^2}{2\sigma_0^2}} \quad (5.21)$$

Such an approximation is permissible with great accuracy for a laminar front, as well as for the initial stage of formation of a turbulent front. It is also permissible for the intermediate stage, if by expression (5.21) we understand the instantaneous profile of rate of heat release, but averaged over small-scale fluctuations of rate of heat release. By substituting corresponding expressions (5.21) for laminar and turbulent fronts in (5.20) and carrying out integration over x , and then averaging, we will obtain

$$\frac{u_T}{u_0} = \frac{\bar{\sigma}_0}{\sigma_0} \quad (5.22)$$

where $\bar{\sigma}_0$ is the mean-statistical width (along the x -axis) of the burning front for the turbulent burning zone;

σ_0 is the characteristic width of the burning front for a laminar front. From (5.21) it is determined as the width at which the rate of heat release decreases by \sqrt{e} times from its maximum value.

For Reynolds number of the flow close to critical, in the flow there exist only very large eddies, with dimensions tens and hundreds of times larger than the scale σ_0 . Therefore, in the first approximation, for the initial stage we may assume that widening of scale σ as compared to scale σ_0 occurs mainly due to rotation of the burning surface by an angle to the x -axis, i.e.,

$$\bar{\sigma}_0 = \sigma_0 / \cos(\bar{n}, \bar{x}) = \sigma_0 \overline{(dS/dy \cdot dz)} \quad (5.23)$$

where \bar{n}, \bar{x} — angle between the normal to the instantaneous burning surface and the x -axis;

dS — element of "burning surface" at the moment of time t , projected on an element of initial area $dy \cdot dz$ of the plane yOz .

After substituting (5.23) in (5.22), we will obtain the following relationship, which is well-known in the theory of turbulent burning [1], [2], [14]:

$$\frac{u_T}{u_0} = \left(\frac{\overline{dS}}{dy \cdot dz} \right) \quad (5.24)$$

thus relation has a very limited field of application; and for high-speed flows is not very limited field of application, and for high-speed flows is not useful in practice. The fact is that in high-speed combustion chambers, in the spectrum of turbulent eddies there exist eddies which are tens, and even possibly hundreds of times smaller than the scale σ_0 , so that it is possible to speak about a definite

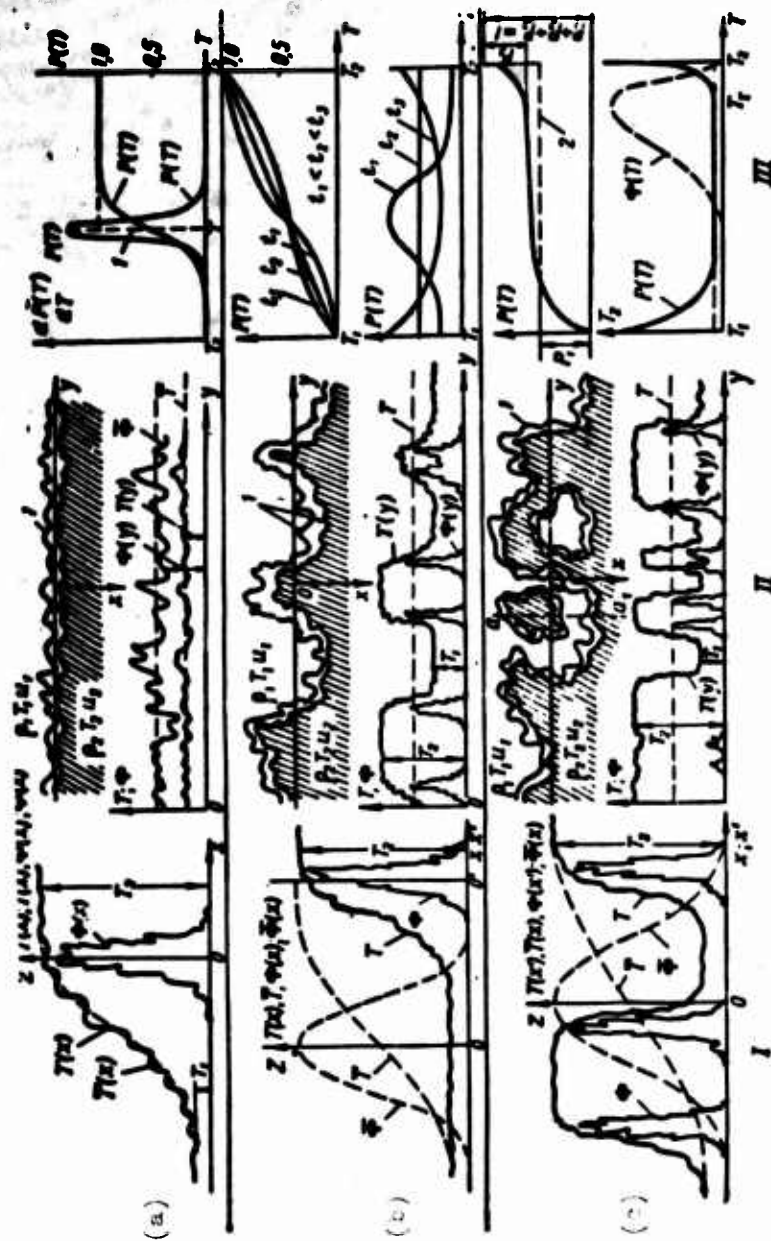


Fig. 5.5. Stages of formation of a one-dimensional of turbulent burning zone of a homogeneous mixture.
a) initial stage; b) intermediate stage, along section a-a₁; c) final stage.
I) plane cross section of zone xOz; II) plane cross section of zone xOy; 1 - line of equal rates of heat emission; III) integral of probability and probability density of temperatures (from the right of the figure): 1 - P(T) of an ideally "volume mechanism" (laminar front); 2 - P(T) of an ideally surface mechanism.

burning surface with constant quantity $u_H(t)$ over the surface only at the first moment of time.

At a certain moment there will begin distortion (deformation) and broadening of isothermal planes (burning front) by the smallest eddies. This moment occurs earlier, the smaller the internal scale of turbulence η is (Kolmogorov scale), i.e., the larger Reynolds number of the flow is. For large Reynolds numbers it occurs practically immediately at the ignition source. Distortion (deformation) and broadening of the burning front in the plane xOy is formally registered as increase of the average integral of heat release in the direction of the x -axis, or, which is the same, of the magnitude of scale $\bar{\sigma}_0$. Thus, in principle it is impossible to distinguish what causes the average integral of rate of heat release to increase - broadening of the burning front by eddies smaller than or equal to the instantaneous width of the front, or distortion of the burning "surface" at an angle to the y -axis by eddies larger than the width of the front. Thus for large Reynolds numbers in the initial and subsequent (intermediate) stage, it is impossible in principle to draw a clear boundary between the effects of "microvolume" and "surface" increase of burning rate. With passage of time, larger and larger eddies will start to act. Large eddies not only distort the burning "surface", but also transfer its elements as a whole in various directions from its average position. For well-developed turbulence ($Re \approx 10^5$) this on the average obeyed the following rule: the larger the scale of the eddy is, the greater is its contribution to the magnitude of turbulent transfer of the burning "surface" and the smaller is its contribution to deformation and broadening of this surface.

Let us note that the actual concept of "surface" is purely arbitrary, since on it there is not obeyed the Gouy-Michelson principle: it is impossible to uniquely determine its exact boundaries and the burning rate normal to this surface, which is constant over the surface. In Fig. 5.5 there are given boundaries of the burning front along points of equal (zero) rate of heat emission; these boundaries are also arbitrary, since inside the front itself there is no homogeneity.

The intermediate stage of development of the one-dimensional burning zone is uniquely characteristic of the burning surface: axis x intersects the burning front (more exact, the larger of increased probability of heat release) on the average one time. Strictly speaking, this stage continues until a moment of time of the order of l_P/u' . In high-speed flows, this time is expressed in distances from

the ignition source: $x_0 = l_L v/u'$. For chambers with diameter of $d_R = 200$ to 400 mm, this distance is not less than 50 to 100 mm.

For the final stage, in principle there is possible a more complicated form of burning "surface": the x-axis can intersect the surface more than once (three, five, etc., times). However, the surface will remain simply connected. The integral of the instantaneous action of rate of heat release in such cross sections over x (section a-a₁ on Fig. 5.5c) can be noticeably larger than on single-valued cross sections. If we disregard the effect of "thinning" of the front in such cross sections due to the fast extension of the burning "surface" by large vortices, the the instantaneous contribution of such cross sections will be three, five, etc., times as great as the contribution from one burning layer (front). The mean-statistical contribution of such triple intersections to the heat release integral will be greater, the higher the probability of encounter of such triple intersections.

Stages of development of a simultaneous burning zone are distinctly evident in the change of character of the statistical distribution of random variables T and ϕ . This distribution can be constructed if we consider the "oscillogram" of change of the given quantity along the one-dimensional zone (along axis y or z). In Fig. 5.5 there are given graphs of the integral of probabilities of temperatures $P(T)$ [$P(T)$ is the probability of appearance of a temperatures less than T] and its derivative $p(T)$ [$p(T)$ is the probability of encounter of the temperature in the interval from T to $T + dT$].

With an ideal "volume" (microvolume) mechanism of burning of the same type as the laminar front, the probability integral will be depicted by a step, and instantaneous values of parameters at a point of the zone (front) will coincide with their mean values. With an ideal "surface" mechanism of turbulent displacement in the zone, the probability integral will be depicted by a double step, since in the mixing zone intermediate temperatures are completely absent.* In the first case, by solving the equations of hydrodynamics, we will obtain the well-known laminar burning. In the second case ($D_M = D_{M,T} = 0$), we will obtain purely mechanical turbulent displacement of "cold" and "hot" volumes, with coefficient of turbulent diffusion D_T , practically complete absence of heat release in the zone, since according to relationships of the first paragraph we have

$$\bar{\phi} = \phi(T_1)P_1 + \phi(T_2)P_2 = \phi(T_1)P_1 \approx 0.$$

*The graphic concepts of "volume" and "surface" burning mechanisms in coordinates $P(T)$ and T were for the first time proposed by V. A. Frost.

It is obvious that neither case corresponds to reality, since in the zone of developed turbulent burning there exist layers of intermediate temperatures, and in these layers themselves there exist deviations of instantaneous temperatures from their mean value (in the layer). In the initial stage, the concepts of burning zone and burning front coincide (or, in other words, the concepts "macro-" and "microzone" of turbulent burning coincide).

In the initial stage, deviations of temperatures from their average value are small, since they are determined by the action of eddies smaller than the instantaneous width of the burning front.

In this case the dispersion of the deviation of fluctuations of temperatures from their average value is small, and the shape of the probability density curve of temperatures is close to that of the Gaussian curve. Dispersion of the fluctuations of temperatures increases in time. At an arbitrary point of the zone in a system of coordinates connected with the initial motionless middle plane of the zone yOz , there appears a finite value of probability density of temperatures T_1 and T_2 . The probability density curve $p(T)$ is transformed from a curve of Gaussian type to curves of absolutely different type. Let us note that in the moving coordinate system connected with the center of the instantaneous position of the burning front, the dispersion of temperature fluctuations will also be changed up to the moment of establishment of the steady state of the front, but the curve of function $p(T)$ will remain, as before of Gaussian type. Finally, in the final stage in the motionless system of coordinates of plane yOz (in the system of coordinates of the macrozone), the greatest probability density turns out to be in the region of temperatures T_1 and T_2 .

All three stages of development of the one-dimensional burning zone encompass, in principle, all possible cases of burning. If turbulence is such that all its scales are equal to or less than the width of the laminar flame front, the process

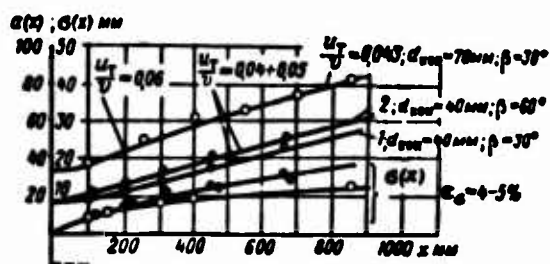


Fig. 5.6. Average boundaries and dispersion of a turbulent flame after a single stabilizer in a pipe (data of V. P. Polntsev).

will not emerge from its initial stage of development: the front will pass through an eddy before the latter has time to essentially deflect the surface of the front from the middle plane. If Reynolds number of the flow is small (close to critical), the microstructure of turbulence is not well-developed and the average scale of turbulence

l_E is much greater than the width of the laminar front, burning will occur on the first stage by the "surface" mechanism in Shchelkin's treatment [2]. Subsequently the process will remain for a long time in the second stage if $u' \ll u_H$, and will rapidly develop to the third stage if $u' \gg u_H$ and decay time of an individual eddy is equal to or larger than the time of passage of the front through the eddy. Thus, the quantity u_T should continuously increase in time from values of the order of u_H in the initial stage to values noticeably larger than u_H .

Experiment shows that for large Reynolds numbers Re ($Re \geq 10^5$), the quantity u_T becomes much larger than u_H , even in the first stage, and further, on all lengths of the flame interesting in practice, remains constant (see Fig. 5.4, 5.6 and 5.7). This indicates that the main contribution to the heat release integral is obtained

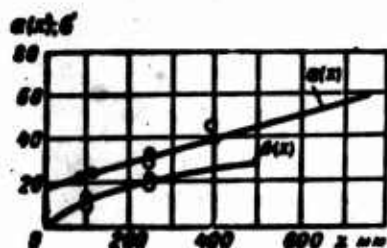
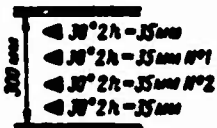


Fig. 5.7. Average boundary and dispersion of a turbulent flame after a group of stabilizers in a pipe (data of V. P. Solntsev).

$T_1 = 100^\circ\text{C}$, $T_2 = 1360^\circ\text{C}$, $\alpha = 1.5$, $v = 50$ m/sec

$\frac{u_T}{v} = 0.055$, $\epsilon_0 \sim 5\%$.



on the average from one burning layer; in other words, although the probability of cross sections similar to cross section a-a₁ in Fig. 5.5 increases with increase of the total width of the zone, it remains relatively small for all lengths of chambers interesting in practice; more exactly, the contribution of such sections to the heat release integral is small.

In Fig. 5.8 there are given experimental curves of the instantaneous burning surface of a turbulent flame jet, determined by Kokushkin [9] with the help of a battery of quick-response resistance thermometers. According to data of work [9], the probability of encounter of triple intersections on lengths of flames interesting in

practice does not exceed 0.1 to 0.2. The high probability of encounter of a single-valued burning surface can be explained by the finite lifetimes of the eddies; after turning on the average by a quarter of a turn, the eddy disintegrates, transmitting energy to smaller eddies and leaving the burning surface, on the average, single values (Fig. 5.9).

The influence of small scales of turbulence on the quantity u_T can be examined by solving the closed system of equations of hydrodynamics. The fundamental scheme of derivation of the closed system of equations is as follows [50]: We

consider a one-dimensional, stationary turbulent flame front, inside of which there act turbulent pulsations with scales much smaller than scales of average parameters: the scale of eddies is less than the thickness of the front $\sim \sigma_{0x}$; the scale of turbulent velocity is less than u_T ; the scale of temperature pulsations is less than the average temperature; and so forth. Transition from such a model to an actual turbulent flame zone with elements of the burning fronts dispersed by large eddies is carried out with the help of relationships of Kolmogorov's theory of local turbulence. For instance, the characteristic scale of turbulent velocity in the considered problem is determined by the contribution of all eddies smaller than or equal to the scale of width of the burning front $(\sim \sigma_T)^*$ according to the well-known Kolmogorov-Obukhov relationship (see Chapter IV). During averaging, in the continuity equation and the thermal conduction equation of the one-dimensional front there will be contained unknown correlation moments of the type $\overline{T^2}$, \overline{uT} and others. For determination of such unknown moments, it is possible to write the linearized system of differential equations of hydrodynamics with respect to turbulent pulsations of the hydrodynamic parameters, using for this the well-known method of small perturbations, which is applicable in this case in virtue of the assumed relative smallness of these pulsations.

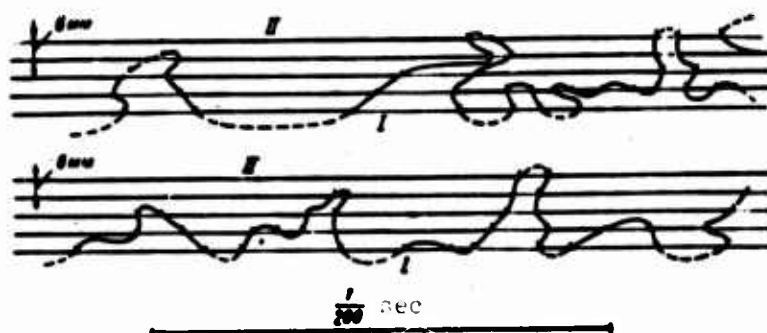


Fig. 5.8. Experimental curves of instantaneous burning surface (change of temperature of the mixture).
I) zone of burned mixture; II) zone of unburned mixture,
 $d_{TP} = 300 \text{ mm}$, $v = 30 \text{ m/sec}$.

Using further on the correlation method, developed in the statistical theory of turbulence, (Friedman-Keller method), we can reduce this system to a system of equations for correlation moments of different forms. Using elements of tensor

*Scale σ_T is determined according to the beginning and end of the rise of the profile of average temperatures in the front.

analysis and conditions of axial symmetry of tensors, we can relate all correlation moments of the second order with each other, expressing them in terms of the correlation moment of temperature pulsations at two neighboring points (or in terms of the moment of longitudinal velocity pulsations connected with it). If the two neighboring points are shrunk into one, we will obtain a system of equations which is closed with accuracy up to moments of higher order of smallness. The main controlling turbulent parameters of a system closed in this manner are: scale of velocity of all eddies smaller than or equal to the width of the front v_0 , and the scale of eddies of dissipation λ_0 , which is equal to

$$\lambda_0^2 = \nu / \left(\overline{\left(\frac{\partial u}{\partial x} \right)^2} \right),$$

where $\left(\overline{\frac{\partial u}{\partial x}} \right)^2$ is the mean-square of the gradient of turbulent velocities.

The complete analytic solution of such a problem is quite complicated and cumbersome; however, the main results of solution can be obtained on the basis of certain physical concepts and dimensional considerations.

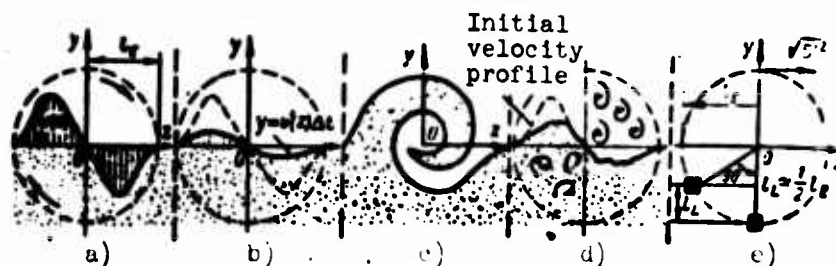


Fig. 5.9. Change of the boundary between two gases in time. a) position of the boundary between two gases at the initial moment; $v'(z)$ is the velocity profile of an eddy; b) position of boundary after an infinitesimal interval of time; c) position of boundary after a finite (large) interval of time; time of existence of the eddy $T_E = \infty$; d) position of boundary after a finite (large) interval of time; time of existence of eddy $T_E < 1/\sqrt{\nu}$; e) model of an eddy (concerning the equation of the relationship between scales).

If a weakly distorted (simple) burning surface is replaced by the conditional scheme of Shchelkin [2] of conical surfaces with average height $\sim \sigma$ and width of base $\sim L_0$, then the order of magnitude of the ratio u_T/u_H will then be determined by the expression (for a laminar burning surface; Fig. 5.10a)

$$\frac{u_T}{u_H} \sim \sqrt{1 + \frac{\sigma^2}{L_0^2}} \sim 1 + \frac{\sigma^2}{L_0^2}. \quad (5.25)$$

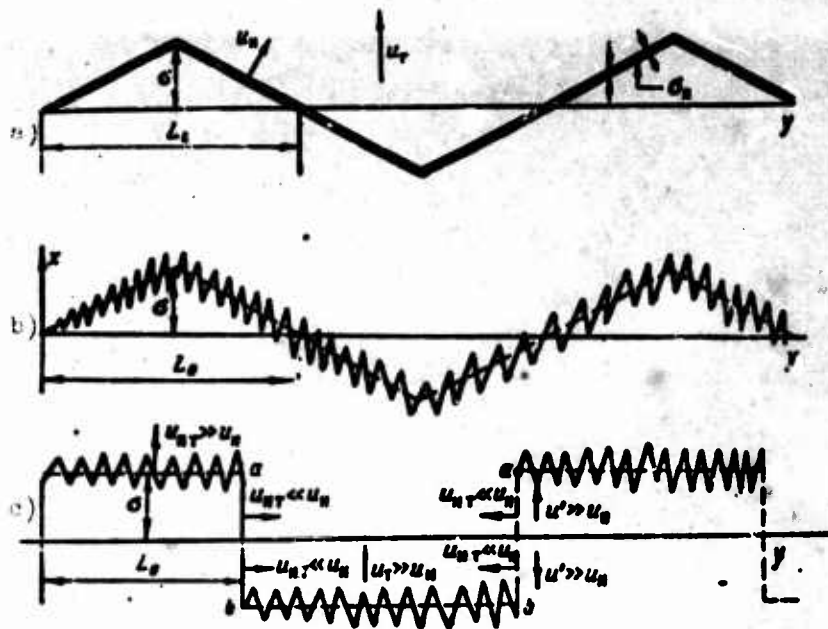


Fig. 5.10. Schematic diagram turbulent burning. a) diagram of the surface of a laminar front during "weak turbulence" (according to data of Shchelkin); b) the same diagram, taking into account small-scale turbulence; c) diagram of dispersed "microvolume" burning fronts.

where $L_0 \sim l_E$ — scale of the temperature nonuniformities in the center of the burning zone;

$\sigma \sim u'$ — scale of width of burning zone (exact definitions of scales σ and L_0 are given in §§ 4 and 5 of the present chapter).

From this relationship it is clear that increase of burning rate is determined not simply by the magnitude of turbulent velocity u' , but by its gradient u'/l_E (other kinetic factors being equal). However, if this is so, it is necessary to remember immediately that the main contribution to the magnitude of the mean-square gradient of turbulent velocities is given not by eddies of the macrostructure, but by eddies of the microstructure (see Chapter IV). Therefore, Shchelkin's scheme should be supplemented by local distortions of the burning surface (Fig. 5.10b). For local hydrodynamic distortions of isotherms of the burning front, the ideas of Shchelkin about balancing of these distortions by molecular diffusion and kinetics remain valid. Therefore, it is possible to write the following, using geometric considerations of dimensional considerations:

$$\frac{u_0}{u'} \sim \sqrt{1 + \frac{\sigma^2}{L_0^2} + \frac{\sigma^2 \cdot \frac{u_0^2}{L_0^2}}{L_0^2}} \sim 1 + \frac{\sigma}{L_0} + \sqrt{\left(\frac{u_0}{u'}\right)^2}. \quad (5.26)$$

where $\tau_T = \frac{\sigma_T}{u_T}$ - characteristic time scale of burning:

σ_T - characteristic width of burning front.

Behavior of the scale σ_T , which is determined by the width of the profile of average temperatures, is quite complicated, since it is determined by the sum of two scales: a scale of the same type as that of the preheating zone for a laminar front $\sigma_H \sim \sqrt{(D_H + v_0 \lambda_0) \tau_x}$, and of the scale of the burning zone $\sigma_{Ox} \sim u_T$. For a turbulent front which is close to laminar ($u_T \sim u_H$), scale σ_T can change proportionally to λ_0 . Thus, relationship (5.26) is reduced to the relationship given for the first time by Shchelkin [3]:

$$\frac{u_T}{u_H} \sim \sqrt{1 + \sigma_H^2 / u_H^2}. \quad (5.26a)$$

For a developed fine structure of turbulence (for large values of u_T), scale $\sigma_T \sim (\sigma_H + \sigma_{Ox})$ remains approximately constant. Relationship (5.26) will then be written in the approximate form

$$u_T \sim \sqrt{\frac{\sigma_T \cdot u_H \cdot u_H}{\lambda_0}} \sim \frac{u_H^{0.75} \cdot u_H^{0.5}}{v^{0.25} \cdot \lambda_0^{0.25}}, \quad (5.26b)$$

since

$$\lambda_0 \approx \frac{v}{\sigma} \cdot \sqrt{\frac{v \cdot l_E}{\sigma}} \quad \text{and} \quad v \sim u'.$$

The diagram shown in Fig. 5.10b also specifies a certain role played by small-scale turbulence in the ratio u_T/u_H , whose value increases in time. Complete negation of this role on the basis of the experimental fact of constancy of the quantity u_T for times larger than σ_T/u_T logically leads to another extreme diagram, which is given in Fig. 5.10c. According to this diagram, large-scale turbulence freely carries elements of the burning surface in various directions with velocity much higher than the speed of forming of the burning front on lateral surfaces of the type b-a (the quantity u_T on elements of b-a is practically equal to zero), and determines mainly the rate of increase of the scale of the burning zone σ , and the turbulent burning front is formed on elements of the type b-l, which determine the magnitude of the mean-statistical scale σ_{Ox} .

Inside of the front, the character of burning can be conditionally represented according to the diagram of Shchetinkov (Fig. 5.11b), if on the characteristic scale of the reacting volume we take not the scale of the macrostructure l_E , but the characteristic scale of the microstructure λ_0 , and instead of "volume burning" use

the idea of "microvolume burning." Analysis of the obtained system of equations shows that the condition for existence of a stationary turbulent front has the form $\lambda_0 \geq \sigma_{\pi}$. Its physical meaning is analogous to the physical meaning of the condition for ignition of a fresh mixture by a hot volume of dimension λ_0 (see Chapter III). If formation of the burning front occurs in the vortex sheet on the boundary between the incident flow and the recirculation zone after the stabilizer (flame holder), then this condition turns out to be the criterion of stabilization, which was given for the first time in works of DeZubay and Khitrin-Gol'denberg:

$$\lambda_0 \sim \sqrt{\frac{v \cdot d_{cr}}{v}} > \sigma_{\pi} \text{ or } \frac{v \cdot d_{cr} \cdot \sigma_{\pi}^2}{v \cdot D_{cr}^2} > \text{const.}$$

If we apply this condition to the scale $\lambda_0 \sim \sqrt{\frac{v \cdot l_g}{v}} \sim \sqrt{\frac{v \cdot d_{cr}}{v}}$ for

turbulence of the incident flow, we will obtain the limit of existence for the rate of turbulent combustion for increase of turbulence of the flow without limit.

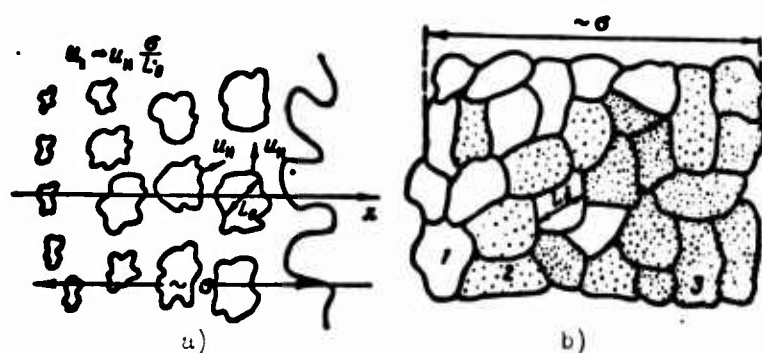


Fig. 5.11. Models of burning. a) model of surface burning for strong turbulence (according to data of Shchelkin); b) model of volume burning (according to Shchetinkov). 1 - fresh mixture, 2 - intermediate products, 3 - combustion products.

Large-scale distortions of the burning surface play a fundamental role in the magnitude of u_T in the absence of a microstructure of turbulence for very small Reynolds numbers and partially for large Reynolds numbers. In the latter case, this influence can be considered as a correction to the main influence of the microstructure of turbulence. At very small Reynolds numbers it is possible to use the concepts: burning surfaces and normal velocity of propagation of an element of the surface through the fresh mixture $u_{h,T}$, disregarding thus the influence of scales of turbulence which are smaller than or equal to the instantaneous width of the burning front. Relationship (5.24), which is correct with regard to its formal, mathematical

basis, turns out to be nonapplicable to a real turbulent flame, first of all because it is impossible to consider the value of $u_{H,T}$ to be constant over the burning surface and equal to the quantity u_H (due to the effect of fast extensions of the burning surface by large-scale eddies).

Simple calculations show that the mean value of $u_{H,T}$ over the burning surface for undeveloped turbulence can be noticeably less than the value of u_H . For instance, if we take experimental values of u_T measured for a very weak intensity of turbulence, then they turn out to be close to corresponding values of u_H (see Table 5.1). Estimation of the average relative burning surface for these experiments (according to direct measurements of the burning surface with a resistance thermometer [9], by Toepler photography, etc.) gives value noticeably larger than unity, so that the quotient obtained from division of the real quantity u_T by the real quantity $(ds/dy \cdot dz)$ gives values of $u_{H,T}$ which are noticeably smaller than the quantity u_H . Thus, the more accurately we measure this surface, taking into account its smaller and smaller distortions, the smaller the value of $u_{H,T}$ which will be obtained. If in the consideration of small distortions we further include local distortions of the surface by the microstructure, we will arrive mathematically at an infinitely large burning surface with infinitesimal value of $u_{H,T}$ on it.

From the given simple reasoning, it is clear that application of relationship (5.24) to a real turbulent flame at best gives instead of one unknown quantity u_T , two unknown quantities: $(ds/dy \cdot dz)$ and $u_{H,T}$; neither of these has by itself an exact physical determination without determination of the other parameter, although mathematically it is possible to construct, with various degrees of accuracy, an infinite set of surfaces and an infinite set of corresponding values of $u_{H,T}$. The limitations of relationship (5.24) indicate the necessity of application in practice of the more general relationship (5.20), and of introduction of better defined concepts in practice.

If local fluctuations of temperature inside a single burning front are much less than the characteristic interval of temperatures of the reaction zone, or are completely absent for the limiting mechanism of surface burning, then for description of the influence of large-scale turbulence on the quantity u_T , it is possible to use the spectrum of values of scales σ_{0x} . Scale σ_{0x} can be determined as the instantaneous value of width of a single front along the x-axis, occurring on the

characteristic temperature interval, where practically the entire rate of heat release is concentrated. For a laminar front $\sigma_{0x} \approx \sigma_n$. The instantaneous value of σ_{0x} can be not only larger than the value of σ_n due to deflection of the normal of the instantaneous element of the burning surface from axis x , but less than the value of σ_n due to rapid extensions of the burning surface. Investigation of statistics of the spectrum of values of σ_{0x} in various regimes of burning, for instance with the help of an ion-sensitive element, would be very useful for deeper study of the nature of turbulent burning. For practical calculations, it is possible to use the mean-statistical value $\bar{\sigma}_{0x}$.

Calculations show that the mean value $\bar{\sigma}_{0x}$ remains constant throughout the depth of the burning zone. An example of such a calculation for a laminar model is given in work [9], where there is shown the constancy of values of $\sigma_n/\sigma_{0x} = \cos(\vec{n}; \vec{x})$ throughout the depth of the zone, when the laminar burning surface is represented in a simplified manner only in the form of two random sine curves. For a continuous spectrum of distortions of the burning surface, taking into account all its local distortions, the constancy of the average scale $\bar{\sigma}_{0x}$ throughout the depth of the zone will be fulfilled with still higher accuracy.

Besides by the average scale $\bar{\sigma}_{0x}$, the quantity u_T is also determined by the average number of fronts intersected by the x -axis through the depth of the burning zone. This number may be called the degree of non-single-valuedness of the burning surface and designated by the letter a . The relation between the mean-statistical integral scale σ_0 in formula (5.22) and scales σ_{0x} will be determined, obviously, by

$$\sigma_0 \approx a \sigma_{0x} \quad (5.23a)$$

The value of u_T will then be determined from (5.22) in the form

$$u_T \approx u_n a \sigma_{0x} / \sigma_n \quad (5.22a)$$

In the limiting case of a strongly distorted, but laminar burning surface ($\sigma_{0x} \approx \sigma_n$) (Fig. 5.11a) the quantity u_T will depend on turbulence practically only from the quantity a , i.e., it will be proportional to the degree of non-single-valuedness of the burning surface:

$$u_T \approx a \cdot u_n \quad (5.22b)$$

According to (5.22b), the quantity u_T will be as many times greater than u_n , as the average number of intersections of the burning surface by the x -axis is greater than unity.

The mean value of \bar{a} when it does not considerably exceed unity (more exactly, when it is less than three) can be determined by the simple relationship

$$\bar{a} = 1(1 - P_a) + 3 \cdot P_a = 1 + 2 \cdot P_a,$$

where P_a - probability of encounter of triple intersections of the x-axis with the burning surface.

Relationship (5.22a) will be written in the form

$$\frac{u_T}{u_a} = (1 + 2P_a) \frac{u_{aT}}{u_a}. \quad (5.22c)$$

The parameter u_{aT} introduced above can now be given a clearer physical definition:

$$u_{aT}/u_a \approx \bar{a}_{aT}/a_a. \quad (5.23b)$$

Formula (5.22a) can now be written as:

$$u_T = (1 + 2P_a) u_{aT} = \bar{a} \cdot u_{aT}. \quad (5.24a)$$

When \bar{a} has a large value, it is possible, when necessary, to express it in terms of the average number of rotations of an eddy during the time of its passage through the burning zone, and in terms of the average number of eddies of the macrostructure per unit area of the average area of the burning surface. However, as before, the quantity σ_{Ox} , which during large and fast increase of the burning surface and in the absence of eddies of the microstructure may be considerably less than the value of σ_a , remains unknown. However, there is possible another, more convenient, practical approach to determination of u_T when macro- and micro-structures have identical value, or when the predominant influence on u_T remains after the macro-structure of turbulence. In such a case it does not make special practical sense to separate the parameters a and σ_{Ox} from each other (in certain cases this may be impossible in practice). It is much more convenient to use the initial integral scale σ_0 , which may be determined by relationship (5.20b) and σ_a for the laminar front. Analogous scales $Y_{M,T}$ and Y_M were introduced in Chapter IV for the case of diffusion without burning, and there is defined the coefficient of accelerated molecular diffusion $D_{M,T}$ according to the relationship

$$(Y_a + Y_{M,T})/Y_a = \sqrt{1 + \frac{D_{M,T}(t)}{D_a}}, \quad (5.27)$$

where $D_{M,T} + D_M$ - effective coefficient of molecular diffusion in a turbulent flow.

The influence of large-scale turbulence on scales σ_0 and $(Y_M + Y_{M,T})$ will be to a great degree analogous, with accuracy up to the time factor of burning τ_x . In development of the burning surface by large-scale turbulence (in the statistics of scales σ_{0x} and σ_0), the factor τ_x plays an unimportant role (§ 4, Chapter V). Therefore, applying for a turbulent flame the well-known considerations of dimensional theory, which are analogous to those for a laminar flame, we can write

$$\sigma_0 \sim \sqrt{(D_m + D_{m,T}(\tau))\tau} \quad \text{and} \quad \sigma_x \sim \sqrt{D_m \tau}$$

or

$$\sigma_0/\sigma_x = \sqrt{1 + \frac{D_{m,T}(\tau)}{D_m}}, \quad (5.27a)$$

where $\tau_x = \rho_1 T_1 c_p / \Phi_{\max}$ - dimensional parameter of burning time, which is identical in both turbulent and laminar flow.

By substituting (5.27) in (5.22), we will obtain a relationship which in form is analogous to the well-known relationship of Damköhler, Shchelkin and Zel'dovich [2], [14]:

$$\frac{u_T}{u_m} \approx \sqrt{1 + \frac{D_{m,T}(\tau)}{D_m}}. \quad (5.28)$$

However, in the given expression there stands not the general coefficient of turbulent transfer D_T , but the coefficient of accelerated molecular diffusion $D_{m,T}$. Formula (5.28) relates the value of u_T to the unique parameter of turbulence $D_{m,T}$, which can be determined experimentally (see Chapter IV).

Relationship (5.28), in light of its derivation, should always be valid: for large- and small-scale turbulence, and for large and small Reynolds numbers. However, it is most well-founded physically to apply it to the case of only large-scale increase of burning rate, or for the case of sluggish (not frontal) burning, when the turbulent factor, expressed in terms of parameter $D_{m,T}$, will be dominant in determination of scale σ_0 , and not the kinetic factor, determined by parameter τ_x , so that the influence of factor τ_x on the form of function $D_{m,T}$ can be disregarded. Let us note that, in general, parameter $D_{m,T}(\tau_x)$ is a function of burning time τ_x . This means that stationarity of burning can occur before the value of $D_{m,T}(t)$ becomes constant in the process of turbulent diffusion. In other words, in the process of turbulent diffusion without burning, the quantity $D_{m,T}(t)$ is determined in time by all eddies of the flow, whereas the value of $D_{m,T}(\tau_x)$ and u_T are determined by the small-scale part of turbulence, which is comparable in scale with the average width of a single burning front σ_T .

§ 4. PARAMETERS OF A TURBULENT FLAME

Let us consider again the simple case of a one-dimensional zone of turbulent burning with plane (at the initial moment) interface between fresh mixture and combustion products. At the first moment, formation of the burning zone (front) occurs just as in a laminar front. At a certain moment there will start distortion, deformation and widening of the instantaneous burning front by the smallest eddies.

With passage of time there will start to act larger and larger eddies. Eddies with scales larger than the instantaneous width of the burning front not only deform the burning "surface", but also transfer its elements as a whole in both directions from its average position. Thus, it is always possible to distinguish two scales of linear dimension of the turbulent burning zone: the average width of the entire zone of turbulent burning — scale σ , which determines the average amplitude of oscillations of the instantaneous burning layers (fronts) at the moment of time t , and the total average width of the burning front — scale σ_0 . By scale σ_0 we may understand the integral scale through the depth of the one-dimensional zone, which is occupied by a characteristic interval of temperatures where practically all of the heat release is concentrated.

In the given examination it is not important what is concealed in the scale σ_0 : several laminar fronts or one widened (by the microstructure) turbulent front.

In virtue of the well-known experimental fact of stationarity of the rate of turbulent combustion (for times greater than σ_0/u_T , under the condition of homogeneous turbulence), scale σ_0 , according to condition (5.22), will also be stationary. On the other hand, at present the experimental fact of non-stationarity of the width of the turbulent burning zone is well-known (non-stationarity of scale σ). Due to its continuous increase, scale σ will in time become much larger than scale σ_0 . Estimation of scale σ_0 according to relationship (5.22) (even if we use greatly exaggerated values of u_T , measured at the extreme boundaries of the flame) gives values measured in millimeters, whereas values of the scale σ for times $> \sigma_0/u'$ (u' is the scale of turbulent velocity) are measured for large-scale combustion chambers (≥ 100 mm) in tens of millimeters. Therefore, in a certain sense, if we consider only the condition $\sigma_0/\sigma \ll 1$, we can speak of a burning "surface." Subsequently, the non-stationarity of width of the turbulent burning zone (scale σ) will be important.

Let us show that the width of the zone will always be a non-stationary quantity in principle, even in the limiting case $u_T \approx u_H \gg u'$, if only, of course, $l_E > \sigma_0$ (l_E ; l_L will be respectively the integral scales of turbulence of Euler and Lagrange; see Chapter IV). Let us quantitatively define the scale of the zone σ as the root-mean-square deflection of an element of the "surface" from its mean position.* Let us multiply the instantaneous deflection of an element of the "surface" $\sigma = \int u(t') dt'$ by the speed of its deflection from its average position $u(t)$ at the time t by a turbulent eddy, through which the given element of the burning surface passes; we will obtain after averaging an equation analogous to Taylor's equation (see Chapter IV):

$$\frac{1}{2} \frac{d\sigma^2}{dt} = \int u(t) u(t') dt. \quad (5.29)$$

It is possible, when necessary, to connect the correlation function standing under the integral sign in (5.29) with correlation functions of Euler and Lagrange [6], [23] by a series of hypotheses; however, only the considered limiting case is of practical interest (for estimation of the smallest of the possible values of σ). If the time of passage of the burning surface through the eddy $\sim l_E/u_T$ is sufficiently small, the field of turbulent velocities will practically not change during that time, so that equation (5.29) can be written approximately as

$$\frac{1}{2} \frac{d\sigma^2}{dt} = \overline{u_{(0)}^2} t \text{ for } t < l_E/u_T \quad (5.29a)$$

and

$$\frac{1}{2} \frac{d\sigma^2}{dt} \approx \frac{\overline{u_{(0)}^2} l_E}{u_T} \approx \frac{2D_T \sqrt{\overline{u_{(0)}^2}}}{u_T} \text{ for } t > l_E/u_T. \quad (5.29b)$$

After integration of (5.29b) we will obtain

$$\sigma^2 \approx 4 \frac{D_T u'}{u_T} t \left(\text{we assume that } u' = \sqrt{\overline{u_{(0)}^2}} \right).$$

*This definition is understandable for the given particular case ($u_T \approx u_H \gg u'$), when the burning surface is known to be single-valued. In the general case of a many-valued surface, scale σ can be given a more general definition, by defining scale σ as the root-mean-square deflection (in a given direction) of an element of volume of gas in the zone, including those volumes in which elements of the burning "surface" are located.

if we consider that (according to the data of Taylor and Townsend, see Chapter IV) $l_E \approx 2l_L$. According to our estimates in technical pipes, the coefficient at l_L is still larger.

What conclusions follow from these relationships?

1. No matter how large the ratio u_T/u' is the width of the zone will always be a non-stationary quantity.
2. For values of $u_T < 2u'$, the turbulent burning zone expands practically just as the zone of turbulent displacement.

In high-speed flows at usual levels of intensity of turbulence (~ 5 to 20%), the quantity u_T (if it is measured correctly) never exceeds the value of $2u'$ (for hydrocarbon-air mixtures), so that it is possible to disregard the effect of motion of the zone with average velocity u_T through the fresh mixture, considering that expansion of the zone occurs just as during turbulent diffusion of two neutral gases: a "cold" gas and a "hot" gas.

At the initial moment of time, the field of turbulent velocities is continuous and uniformly over all of space, and the field of pulsational velocities induced by motion of the burning "surface" (autoturbulence) is obviously equal to zero.* Therefore, at first diffusion of the zone will occur with the coefficient of diffusion D_T of the fresh mixture which is assigned at the initial moment. During intense burning, for calculation of fields of temperatures, this value of D_T will be fully sufficient (experiment confirms this), since the flame will be joined with the flame proceeding toward it or with the wall of the pipe before the width of the zone becomes so great that it affects the magnitude of D_T . During unlimited propagation of the flame in unbounded space, the extent of the burning zone can become so great that it will become necessary to consider the change of magnitude of $ld\sigma^2/dt \approx D_T$ over the depth of the zone: first, due to the possible space heterogeneity of turbulence of the incident flow of fresh mixture, and, secondly, due to the possible additional pulsations of velocity induced in the burning zone by the strongly distorted burning surface (autoturbulence). Therefore, in general, the value of D_T should be considered to be a continuous function of space coordinates, and there should be taken into account possible anisotropy of turbulence, by considering the matrix of values D_{ij} ($ij = 1, 2, 3$), possible changes of u_T under the condition $u_T \gg u'$, etc.

*Even if it is considered that the field of turbulent velocities has a discontinuity at the initial boundary, in this case the value of D_T in formula (5.29) corresponds to the field of turbulent velocities of the fresh mixture, since deflections of elements of the burning surface from their average positions are specified by turbulent displacements of the fresh mixture.

However, in the overwhelming majority of cases of burning in high-speed flows, the problem is reduced to turbulent transfer in one direction (transverse to the main flow), and, as experiment shows, and also analysis of relationships (5.29), is practically completely determined within the limits of existing chamber lengths (observation times) by the transverse component of the coefficient of turbulent transfer D_T of the incident flow (taking into account its heterogeneity transverse to the flow).

We will dwell in greater detail on experimental confirmation of the obtained conclusions. In Fig. 5.4 and 5.12 there are given the average boundaries and scales (variance) of a flame after a "point" burner in an open flow, which were

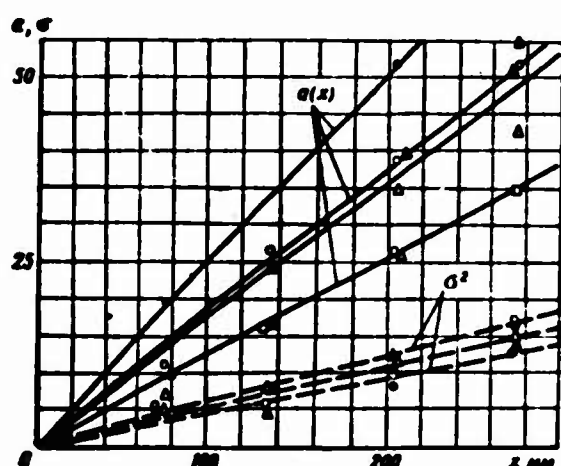


Fig. 5.12. Distribution of average $a(x)$ and variance σ^2 of a flame after a "point" burner:

According to data of Vlasov, $v = 45$ m/sec.

Δ $\alpha = 1.1$,

\blacktriangle $\alpha = 0.9$.

According to data of Lushpa, at $v = 28$ m/sec.

\bullet $\alpha = 1.3$,

\circ $\alpha = 1.1$,

\square $\alpha = 0.9$.

calculated according to fields of impact pressures by Lushpa and Vlasov. It is clear that the average boundaries change with change of velocity and mixture ratio, but scale σ does not depend on velocity and mixture ratio. According to data of Lushpa obtained with the help of a hot-wire anemometer, the intensity of turbulence of the cold flow in the region of the flame was equal to $u' \cdot 100/v = 1$ to 2%. Values from calculation of $\sigma(x)$ according to the relationship (5.29a) also lie in the same range.

Data of Lushpa indicate that σ^2 is a purely hydrodynamic parameter, not depending on the burning parameter u_T , but determined only by parameters of turbulence of the incident flow, even at $u_T \sim u_H$ noticeably larger than $2u'$.

Data of Vlasov were obtained in a flow after a turbulence-generating grid with intensity of turbulence $\sim 5\%$ (the same value is obtained from calculation according to $\sigma(x)$). Comparison of the function \bar{Y}^2 (variance in the cold flow) measured such a grid with function $\bar{\sigma}^2$ shows that within the limits of accuracy of measurements,

these functions coincide. Vlasov processed data on the scale of width of the zone δ_T , which were obtained by him with the help of an ion-sensitive element. Due to the method of their measurement, these data are less exact, but are interesting because of the fact that they cover a much wider range of velocity, mixture ratio, distance from the burner and pipe diameter. In all cases, a flow with natural level of pipe turbulence was incident on the pipe (see Chapter IV):

$$\alpha' \cdot 100/\sigma \approx 5\%; D_v/\sigma \cdot d_p \approx 0.001.$$

If we consider the approximate relationship existing between scales δ_T and σ [1],

$$\delta_T \approx 4.6\sigma,$$

we can plot all data in dimensionless coordinates on one graph, which practically completely coincides with the dimensionless function \bar{Y}^2 for pipe turbulence (Fig. 5.13), i.e., on all lengths of the flame scale σ interesting in practice is completely determined by turbulence of the incident flow.

We will briefly summarize the essence of the above presented ideas, emphasizing what their fundamental distinctions from the first ideas of Shchelkin [3] and subsequent ideas of Karlovitz, Scurlock, Wohl, and others [6], [17], [18], [23], consist of.

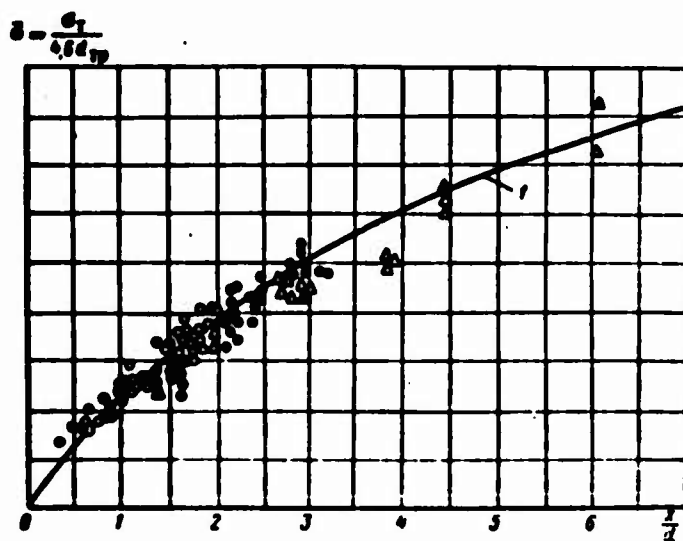


Fig. 5.13. Dependence of width of burning zone on the distance from the ignition source (data of Vlasov on σ):

$v = 35-75$ m/sec, $\alpha = 0.5-1.3$, $d_{TF} = 150-200$ mm.

1 - Calculated data of Prudnikov on $\sqrt{\frac{\sigma}{\sigma_{TF}}}$.

The process of turbulent burning in combustion chambers of air-breathing jet engines is first of all a process of turbulent (mechanical) mixing of volumes of fresh mixture and combustion products, and then of burning. In development of the width of the burning zone, the turbulent side of the process dominates over the kinetic side, and is the controlling factor. Shchelkin [2], [3] initially assumed that the kinetic side of the process and the diffusion (side turbulent) were in equilibrium. Due to this, the width of the turbulent burning zone σ is a stationary magnitude, determined by the equality between the time of turbulent motion of a mole and the time of existence (combustion) of a fresh mole ejected by the turbulent motion into the burning mixture:

$$\frac{\sigma}{s} \approx \frac{L}{u_n}. \quad (5.30)$$

The ideas developed for the first time by Shchelkin, as was noted in § 3, Chapter V, to a certain extent are applicable to the process occurring in a burning microzone.

Our ideas to a certain degree coincide with ideas of Scurlock, Wohl, Grover, Karlovitz and others, but there are fundamental differences. Scurlock and Wohl start with a specific conditional picture of the burning surface, which has constant burning velocity u_H over the surface,* and give on the basis of this picture a complete list of all conceivable a priori effects determining the width and average velocity of the turbulent burning zone. In view of the great schematism and conditionality of their concepts of the burning "surface", the "accuracy" of their quantitative estimates of all effects is not justified, and in a number of questions causes serious objections (consideration of autoturbulence, mechanical addition of all effects, and so forth). As a result of their analysis there are obtained a large number of effects, and all of them turn out to be equivalent; but this is incorrect. As experiment shows, there is only one decisive effect: turbulent diffusion, which is assigned by the turbulence of the incident flow.

The main physical error of these authors is apparently the following. The velocity of an element of the burning "surface" relative to the fresh mixture is not given by the quantity u_H , but is obtained to be whatever turbulent diffusion

*Normal velocity with respect to the burning "surface" is known not to be constant, both due to the existence of eddies of the microstructure smaller than the width of the stationary laminar front, and due to the presence of local extensions of the burning "surface" by eddies of the macrostructure, with speed much higher than the speed of formation of the stationary flame front.

causes it to be: at some points, it may be much less than u_H ; at other points, much larger than u_H . For a well-developed microstructure of turbulence, when the internal scale of turbulence is less than scale σ_0 , it makes no sense in practice to talk about some definite element of the burning surface having a definite velocity of the type of u_H (§ 3, Chapter V). As a result, the mathematically accurate reasoning of the authors, based on erroneous physical concepts, led to practically unjustified results.

How do we correctly measure burning velocity (Fig. 5.14), taking into account the non-stationarity of the turbulent burning zone? This question, obviously, does not occur for the stationary zone: in this case, starting at that moment when

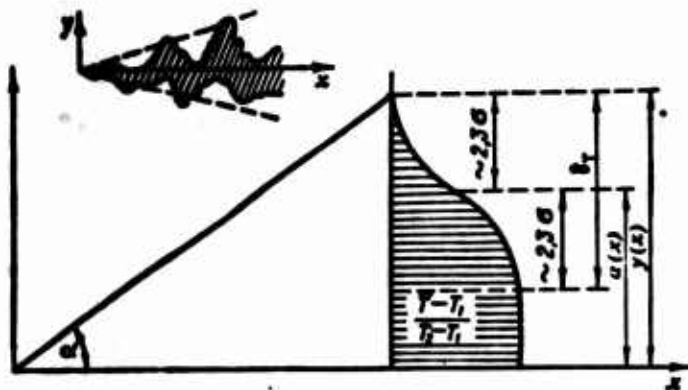


Fig. 5.14. Determination of the velocity of turbulent propagation of a flame u_T and width of the burning zone δ_T .

$$u_T = v \sin \alpha.$$

scales of the burning zone σ_0 and σ become stationary, the speed of all statistically averaged isotherms will be identical, and equal to the speed of turbulent combustion.

In the case of the non-stationary zone, every isotherm has its own speed; therefore, there appears the question — which isotherm speed should be taken as the speed of turbulent combustion?

The speed of turbulent (laminar) combustion is the mean-statistical volume of fresh mixture burning per unit time, and referred to a unit area of the average position of the burning surface.* The last stipulation is not essential for the laminar front, inasmuch as average and instantaneous positions of the burning front coincide. In the turbulent burning zone, the "burning surface" has the mean-statistical (average) position and the distribution of probabilities of the instantaneous positions of the burning fronts (with variance σ^2) relative to the average position. Thus there exist two characteristic rates: the rate of increase of average and the rate of increase of the scale of width of the zone σ . The rate of

*In virtue of relationship (5.20), this definition is identical to the following: the speed of turbulent combustion is the average speed (at infinity) of the fresh mixture incident on the motionless, on the average, zone of turbulent combustion.

increase of the average exactly corresponds in its definition to the speed of turbulent combustion. In order to find the average position in practice at the time t , it is necessary to mentally collect all mixture burned by this moment at boundaries assigned by the initial conditions. If the initial boundary is a plane, then — on one side of a plane parallel to the initial plane; if the initial boundary is a sphere (point), then — on one side of a sphere equidistant from the initial, etc.

The rate with which the characteristic dimension (normal — for a plane, radius — for sphere, etc.) of the average surface increases exactly determines the rate of decrease of the volume of fresh mixture (in the coordinates of the motionless fresh mixture), referred to the entire average burning surface at the time t ; i.e., it is by definition the rate of turbulent combustion. Such a practical operation can be given a quite simple mathematical expression, if it is considered that the distribution of probabilities of the turbulent displacements of volumes in the zone of turbulent burning obeys the law of Gauss. This assumption is first of all confirmed by experiment (see § 6, Chapter V). It also finds its explanation logically. For diffusion without burning, the law of Gauss is well-known. If in the burning zone it would essentially differ, then this, in the first place, would be noticed by the deviation of the magnitude of variance σ^2 from the magnitude of \bar{Y}^2 , and also by the appearance of asymmetry or excess of the actual probability density curve. It follows directly from this that for a one-dimensional burning zone, the rate of turbulent combustion is determined by the speed of the isotherm, where the combustion efficiency is equal to 0.5. The one-dimensional zone is the only case when the average surface is determined sufficiently strictly by an isotherm with combustion efficiency 0.5. In other cases, the average surface is determined strictly by integration all the entire profile of temperatures, taking into account change of average speed, mixing in the submerged stream, and so forth (see § 5, Chapter V).

The rate of increase of the scale of width of the zone σ determines the speed of turbulent diffusion of "cold" and "hot" gas, which, according to what has been said above, remains practically the same as in the zone of mixing without burning. In the mixing zone the speed of "isotherm 0.5" is equal to zero; all remaining isotherms move with different speeds relative to this isotherm. The further from

isotherm 0.5 an isotherm is advanced into the fresh mixture, the higher the speed with which it moves toward the fresh mixture. An isotherm located from "isotherm 0.5" at a distance equal to scale σ first moves with speed u' ; an isotherm located a distance equal to two scales σ away - with speed $2u'$, etc., to infinity, and more exactly the more closely the extreme branches of the true distribution curve of turbulent velocities correspond to the Gaussian distribution.

In the practice of experimental investigation, there is applied the method of measurement of burning rate according to the "extreme" boundaries of the turbulent flame, which essentially reduces to measurement of the speed of some "extreme" isotherm. By measuring the speed of turbulent combustion according to "extreme" isotherms, experimenters often arrive at practically complete distortion of the physical essence of the studied process.

For instance, by measuring according to data of Lushpa the true value of u_T , it is simple to show that u_T close to u_H and does not depend within the range of operating conditions on u' (see Fig. 5.4). If, however, we measure the burning rate "along the extreme boundaries of the flame" adding thereby the large value $\sim 3u'$ to the constant of relatively small magnitude $u_T \approx u_H$, we will arrive at the conclusion of the existence of direct proportionality between burning speed and the magnitude of turbulent speed u' . In distinction from the value of u_T , speed determined according to the extreme isotherm will be called the speed of propagation of the turbulent flame and will be designated u'_T .

If we admit the possibility of coexistence of these different concepts in the practice of experimental investigation and engineering estimates of lengths of combustion chambers of air-breathing jet engines - speed of propagation of the turbulent flame u'_T and the speed of turbulent combustion u_T - we should consider the following: the speed of propagation u'_T formally includes the physico-chemical parameter, speed of turbulent combustion u_T , and the purely hydrodynamic parameter, speed of expansion of the zone of turbulent combustion.

The magnitude and properties of speed of propagation are determined basically by the magnitude and properties of speed of expansion of the zone, including here the numerous systematic errors connected with different methods of its measurement (thermocouple, Pitot-static head, ion-sensitive element, photography).

The speed of turbulent combustion u_T is usually many times less than the speed of turbulent propagation u'_T . There is not eliminated the possibility that in

pre-separation regimes (with respect to mixture ratio or pressure) it may be less than u_H . The magnitude of turbulent velocity of the incident stream turns out to be more than sufficient for explanation of the measured values of u_T without utilizing the concept of autoturbulence. Indeed, if autoturbulence does not noticeably influence the speed of expansion of the zone, then it must not be high for the average speed of expansion.

§ 5. DISTRIBUTION OF AVERAGE PARAMETERS IN THE TURBULENT BURNING ZONE

Equations of Hydrodynamics for the "Surface" Model of Turbulent Burning

Analysis of experimental data shows that the scale of width of the burning zone σ increases in time, and the scale of width of the burning front σ_0 , determined by u_T , remains practically constant. Due to this, at a certain moment of time ($> \sigma_0/u'$) the value of σ will become much larger than σ_0 .

Direct observation of oscillograms of temperature fluctuations in a turbulent flame which were conducted by Kokushkin [9] with the help of a quick-response resistance thermometer experimentally confirm this conclusion. In this case, during determination of distributions of average parameters in a turbulent burning zone, it is possible with great accuracy to disregard the probability of appearance of intermediate values, and to write average parameters in the form

$$T = T_1 P_1 + T_2 P_2; \quad \bar{u} = \bar{u}_1 P_1 + \bar{u}_2 P_2 \quad \text{or, since } P_1 + P_2 = 1,$$

$$\frac{T - T_1}{T_2 - T_1} = \frac{\bar{u} - \bar{u}_1}{\bar{u}_2 - \bar{u}_1} = P_2 \quad (5.31)$$

where P_1, P_2 are probabilities of appearance of volumes of fresh and burned mixture respectively. In physical meaning, P_2 is nothing else but the physical combustion efficiency at a given point of the combustion chamber;

T_1 is the temperature of the fresh mixture;

$T_2 = \eta_{XHM} \cdot T_{\max}$ is the temperature of the combustion products.

Temperature of combustion products T_2 can be considered as the product of maximum adiabatic temperature of the burned mixture by chemical combustion efficiency η_{XHM} . It is known that even in a laminar flame front the temperature after the front does not attain its limiting value at once for many reasons. In Fig. 5.15 there are given data from the book of L. N. Khitrin converted to values of η_{XHM} along a turbulent flame in a high-speed flow (for $u_T = 0.5$ m/sec and

$v = 40$ m/sec). Along the turbulent flame chemical combustion efficiency $\eta_{\text{chem}}(x)$ changes slightly. For actual lengths and flow velocities of a homogeneous flame, its values oscillate from 0.85 at the beginning of the flame to 0.98 at the end of the flame at atmospheric pressure (see Fig. 5.15).

Thus, the problem of calculation of average temperatures in the turbulent burning zone is reduced to determination of the probability of appearance of "cold" or "hot" volumes of mixture at a given point of the zone.

The system of averaged equations of hydrodynamics (see § 2, Chapter V) for the "surface" model of turbulent burning in a high-speed flow will be written in the form

$$-\frac{\partial \bar{p}}{\partial x} + \frac{\partial \bar{p} u_1}{\partial x_1} = 0; \quad (5.32a)$$

$$\frac{\partial \bar{u}_1}{\partial x_1} = \bar{F}. \quad (5.32b)$$

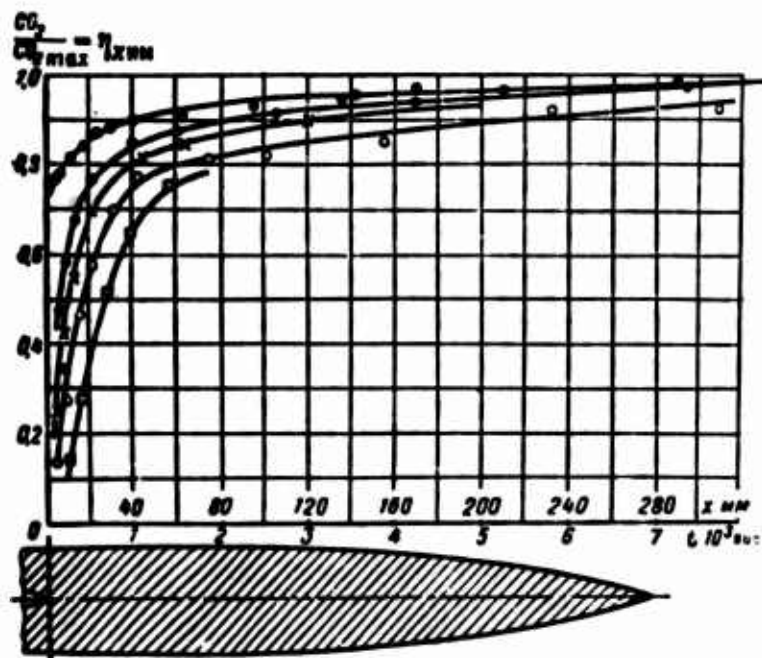


Fig. 5.15. Distribution of chemical combustion efficiency along the flow axis of a Bunsen burner (laminar flame). Mixture of air +29.6% CO, pre-heating 370°C . $v_{\text{fl}} = 0.5$ m/sec, $x = 40$ m/sec; ● — pressure 760 mm; ● — pressure 402 mm; ○ — pressure 308 mm; □ — pressure 162 mm.

The influence of viscosity appears only in the flame front (in the discontinuity); therefore, the viscosity term in (5.32b) is discarded. Let us expand the terms of equations (5.32a) and (5.32b). Using relationship (5.6) and Prandtl's Hypothesis for determination of turbulent, diffusion mass flow, we will obtain

$$\overline{\rho u_i} = \bar{\rho} \cdot \bar{u}_i - (\rho_1 - \rho_2)(\bar{u}_{2i} - \bar{u}_{1i}) P_1 \cdot P_2 - D_T \frac{\partial \bar{\rho}}{\partial x_i}, \quad (5.33a)$$

where $D_T = \frac{1}{2} \frac{d\sigma^2}{dt}$ - coefficient of turbulent diffusion;

\bar{u}_{1i} ; \bar{u}_{2i} - components of average speed, averaged selectively only with respect to the fresh mixture or only with respect to combustion products.

During mixing without burning, these components do not undergo a discontinuity on the instantaneous interface between the two media, so that it is possible to write

$$\overline{\rho u_i} = \bar{u}_i \bar{\rho} - D_T \frac{\partial \bar{\rho}}{\partial x_i}. \quad (5.33b)$$

The physical meaning of parameter $D_T = \frac{1}{2} \frac{d\sigma^2}{dt}$ was considered in § 4, Chapter V for the case of a one-dimensional turbulent burning zone. As was shown in § 4, variance σ^2 of turbulent displacement of the burning front is determined by the variance of turbulent displacements of cold volume of the incident flow.

The following system turns out to be equivalent to the system of equations (5.31), (5.32a and b):

$$\frac{\partial P_1}{\partial t} + \bar{u}_{1i} \frac{\partial P_1}{\partial x_i} = D_T \frac{\partial^2 P_1}{\partial x_i^2} + \frac{dV_1}{Sdt} P_S; \quad (5.34a)$$

$$\frac{\partial P_2}{\partial t} + \bar{u}_{2i} \frac{\partial P_2}{\partial x_i} = D_T \frac{\partial^2 P_2}{\partial x_i^2} - \frac{P_1 dV_1}{P_2 Sdt} P_S. \quad (5.34b)$$

where $\frac{dV_1}{Sdt} = -u_T$ - rate of decrease of the volume of fresh mixture V_1 per unit surface of the average burning surface S (rate of turbulent combustion);

P_S - probability density of appearance of the burning surface at a given point.

The last term in equations (5.34a) and (5.34b) are written only for a single ignition source (single flame). Both equations constitute the mathematical formulation of the law of conservation of the assemblies of "cold" and "hot" volumes, taking into account the source (sink), turbulent diffusion and the discontinuity of selectively averaged speeds, and are a generalization of the Kolmogorov equations known in the theory of stochastic processes.

Above there was introduced the term "selective averaging," in which time averaging at an arbitrary point of space is carried out selectively: only in those time intervals when at the given point of space there is only fresh mixture or only combustion products. At these moments of time there are satisfied the usual equations of hydrodynamics for an isothermal, incompressible gas. In particular,

the continuity equations averaged selectively will take the form

$$\frac{\partial \bar{u}_1}{\partial x_1} = 0; \quad \frac{\partial \bar{u}_2}{\partial x_1} = 0. \quad (5.35)$$

The equation of conservation of energy (5.32b) averaged selectively will give the same relationship, since $\bar{F}_1 = \bar{F}_2 = 0$.

We will show the identity of systems (5.32) and (5.34). Multiplying the first of equations (5.34) by ρ_1 and the second by ρ_2 , and adding both equations, we will obtain with the help of relationships (5.35) the continuity equation (5.32a). If we simply add equations (5.34), we will obtain with help of relationships (5.31) the equation of conservation of energy (5.32b):

$$\partial \bar{u}_1 / \partial x_1 = + (n-1) u_1 p_2,$$

where

$$(n-1) u_1 p_2 = \bar{F}; \quad n = T_2/T_1 = \rho_1/\rho_2$$

Solution of system (5.34) turns out to be in most cases more convenient than solution of the system of the averaged equations of conservation of mass and energy (5.32).

Let us consider a series of simple problems whose solutions we may obtain with the help of analytic integration of the initial system of equations (5.32) or (5.34).

One-Dimensional Burning Zone

The average boundary between the fresh mixture and combustion products is motionless, and is taken as the coordinate plane yOz .

The initial system of equations for a burning one-dimensional zone will be written in the form

$$\left. \begin{aligned} \frac{\partial \bar{p}}{\partial t} + \frac{\partial \bar{p} u}{\partial x} &= 0, \\ \frac{\partial \bar{u}}{\partial x} &= u_1 \left(\frac{T_2}{T_1} - 1 \right) p(x), \end{aligned} \right\} \quad (5.36)$$

where $p(x - x_0)$ is the probability density of displacements of a unit volume from point x_0 to point x in the time t .

The value of average density will be determined according to (5.8) as

$$(\bar{p} - \rho_2)/(\rho_1 - \rho_2) = P_1 = \int_{-\infty}^{\infty} p(x - x_0) dx_0 = \int_{-\infty}^{\infty} p(\xi) d\xi. \quad (5.37)$$

From (5.37) it follows that $p(x) = -\partial P_1 / \partial x$. Substituting this value in the second equation (5.36) and integrating the latter over x from $-\infty$ to x , we will obtain the distribution of average speed:

$$\bar{u} = u_T P_1 + \frac{T_2}{T_1} u_T P_2 \quad (5.38)$$

From (5.38) and (5.31) it is clear that average speed, averaged selectively only with respect to the fresh mixture, gives the value u_T , and with respect to the burned mixture - the value $u_T T_2 / T_1$. Thus $\bar{p}u$ turns out to be equal to

$$\bar{p}u = p_1 u_T - D \frac{\partial \bar{p}}{\partial x}, \quad (5.39)$$

the continuity equation will take the form

$$\frac{\partial \bar{p}}{\partial x} = D \frac{\partial^2 \bar{p}}{\partial x^2} \quad \text{or} \quad \frac{\partial P_1}{\partial x} = D \frac{\partial^2 P_1}{\partial x^2}.$$

Its solution gives the distribution of average densities (temperatures) over the depth of the zone:

$$(\bar{p} - p_1)(p_1 - p_2) = (T_2 - T_1)(T_2 - T_1) = \frac{1}{2} \left[1 - \Phi\left(\frac{x}{\sigma}\right) \right],$$

where $\Phi\left(\frac{x}{\sigma}\right)$ is the tabulated function of the integral of probability:

$$\Phi(\xi) = \frac{2}{\sqrt{\pi}} \int_0^\xi \exp\left(-\frac{t^2}{2}\right) dt. \quad (5.40)$$

Distribution of Turbulent Fluctuations of Speed in the Macrozone of Turbulent Burning

In the macrozone of turbulent burning, it is possible to distinguish between turbulent root-mean square velocity, obtained by selective averaging only with respect to the fresh mixture $\sqrt{u_1^2}$, and the corresponding velocity for combustion products $\sqrt{u_2^2}$. In general, these values may be different due to the abrupt change in the flame front (on the instantaneous of burning surface) or due to the continuous change through the depth of the macrozone (for very large diffusion time).

Besides this velocity, there further exists the profile of "virtual turbulent velocity," which is obtained due to the fact that at a given point of the zone there appears first fresh, then burned mixture (each of them has different selectively averaged, average speeds). Indeed, for the surface model of burning, the total mean square value of velocity fluctuations can be written (under the condition of constancy of values of \bar{u}_{11}^2 ; \bar{u}_{21}^2 throughout the depth of the zone) in the form

$$\begin{aligned}\overline{u_i^2} &= \overline{u_i^2} - (\overline{u_i})^2 = \overline{u_{1i}^2} P_1 + \overline{u_{2i}^2} P_2 - (\overline{u_{1i}} P_1 + \overline{u_{2i}} P_2)^2 = \\ &= \overline{u_{1i}^2} P_1 + \overline{u_{2i}^2} P_2 + (\overline{u_{2i}} - \overline{u_{1i}})^2 \cdot P_1 \cdot P_2\end{aligned}\quad (5.41)$$

or for a one-dimensional zone, if $\overline{u_1^2} = \overline{u_2^2}$, in the form

$$\overline{u^2} = \overline{u^2}(-\infty) + u_*^2(n-1)P_1P_2 \text{ and } \overline{v^2} = \overline{v^2}(-\infty). \quad (5.41a)$$

Thus, even if the field of turbulent velocities of the incident stream is homogeneous and isotropic, the field of pulsational velocities will be nonhomogeneous and anisotropic throughout the depth of the zone. The same relationship can be obtained directly from the equations of hydrodynamics. By multiplying the equation of conservation of energy by the velocity component u_j and averaging, we will obtain

$$u_j \frac{\partial \overline{u_i}}{\partial x_i} = \overline{F \cdot u_j}$$

or for a one-dimensional zone, assuming satisfaction of the conditions

$$\begin{aligned}\overline{u_1 \frac{\partial u_1}{\partial x_1}} &= \overline{u_2 \frac{\partial u_1}{\partial x_1}} = 0; \quad \overline{F \cdot u_1} = \overline{F \cdot u_2} = 0, \\ \frac{1}{2} \frac{\partial \overline{u^2}}{\partial x} &= \overline{F \cdot u}\end{aligned}\quad (5.42)$$

(superfluous indices are omitted). We will find the form of the correlation moment \overline{Fu} . Since the value of the random function F is equal to zero everywhere except on the discontinuity surface, then

$$\overline{Fu} = \overline{F_S \cdot \overline{u_S}} = u_*^2(n-1) \left(\frac{\overline{u_1} + \overline{u_2}}{2} \right) p_S(x) = \frac{u_*^2(n-1)}{2} p_S(x).$$

(where $\overline{u_S}$ is the value of average velocity at the point of discontinuity).

By substituting the obtained expression of the moment in (5.42), we will obtain after integration from $-\infty$ to x , taking into account the boundary condition and relationship (5.37),

$$\overline{u^2} - u_*^2 - \overline{u^2}(-\infty) = u_*^2(n^2 - 1)P_1P_2. \quad (5.43)$$

It is simple to see that relationships (5.41) and (5.43) are identical. Analogous relationships can be considered for more complicated cases.

Analysis of existing experimental data on the distribution of fluctuating values of velocity in a turbulent flame on the basis of the given equations indicates the fact that the observed distributions of fluctuating velocities in a turbulent flame and in combustion products can be explained by only two effects: 1) the

varying selectively averaged average flow velocity in the burning zone and by the effect of deformation of eddies during acceleration of the flow.

A Turbulent Flame in an Open Flow

For a flame in an open flow it is possible to disregard diffusion along the flow and change of the longitudinal component of average velocity (due to the absence of a drop of static pressure along the flow).

The solution of system (5.34) for a flame in an open flow proceeds as follows: after placing the value of average velocity along the flame $\bar{u}_1 = \bar{u}_2 = v = \text{const}$ in the continuity equations (5.35), we will obtain (taking into account boundary conditions $\bar{v}_1(0) = 0$ — for a right flame cone, and $\bar{v}_2(0) = 0$ — for an inverted flat cone of flame),

$$\frac{\partial \bar{v}_1}{\partial y} = 0 \text{ or } \bar{v}_1 = 0 \text{ (for a right cone in all of space)}$$

and

$$\frac{\partial \bar{v}_2}{\partial y} = 0 \text{ or } \bar{v}_2 = 0 \text{ (for an inverted flat cone in all of space).}$$

Since $\frac{\partial p_1}{\partial t} = \frac{\partial p_2}{\partial t} = 0$ and $\frac{\partial v_1}{\partial t} = -u_T$ for each half of the flame, the system of equations (5.34) for the right and inverted cones of flame will be written in the form

$$v \frac{\partial p_1}{\partial x} = D_1 \frac{\partial^2 p_1}{\partial y^2} - u_T p_1; \quad \frac{\partial \bar{v}}{\partial y} = u_T (n-1) \frac{\partial p_1}{\partial y} - u_T p_1 (n-1)$$

or for a right cone

$$v \frac{\partial p_1}{\partial x} + u_T \frac{\partial p_1}{\partial y} = D_1 \frac{\partial^2 p_1}{\partial y^2}. \quad (5.43a)$$

Analogously,

$$v \frac{\partial p_1}{\partial x} = D_1 \frac{\partial^2 p_1}{\partial y^2} + n \cdot u_T p_1;$$

$$\frac{\partial \bar{v}}{\partial y} = (n-1) u_T p_1 = - (n-1) u_T \frac{\partial p_1}{\partial y}$$

or for an inverted cone,

$$v \frac{\partial p_1}{\partial x} + n u_T \frac{\partial p_1}{\partial y} = D_1 \frac{\partial^2 p_1}{\partial y^2}. \quad (5.43b)$$

Let us note that the equations of conservation of energy are written only for one of the halves of the flame.

The general solution of equations (5.34a) and (5.34b) has the form

and

$$\left. \begin{aligned} P_1 &= \int_{-\infty}^{\infty} p(y - y_0) dy_0 \\ P_2 &= \int_{-\infty}^{\infty} p(y - y_0) dy_0 \end{aligned} \right\} \quad (5.44)$$

where $p(y - y_0)$ - Gaussian probabilities distribution;

$y_1(x)$ - average boundary of the flame, which is determined in the first

case by the equation $y_1 = y_0 + \int_0^x \frac{u_r}{v} dx$, and in the second - by

the equation $y_2 = y_0 + n \int_0^x \frac{u_r}{v} dx$.

I.e., P_1 and P_2 are determined in every specific case directly as the total probability of appearance at the considered point of volumes of fresh and burned mixture respectively, which occupy in the initial section of the flame $x_0 = 0$ some definite volume, the boundaries of which change along the flame.

Let us give without derivation formulas for a number of the most widely occurring cases of a turbulent flame in an open flow.

Turbulent Flame After a Plane Precombustion Chamber
(see Fig. 5.2b)

$$P_2(x, y) = \frac{T - T_1}{T_2 - T_1} = \frac{1}{2} \left[\Phi\left(\frac{y+a}{\sigma}\right) - \Phi\left(\frac{y-a}{\sigma}\right) \right], \quad (5.44a)$$

where

$$a = \frac{T_1}{T_2} \int_0^x \frac{u_r(x)}{v} dx + a_0;$$

a_0 - half-width of the precombustion chamber (burner);

$$2a(x) = \int_{-\infty}^{\infty} P_2 dy \text{ for } a > 3\sigma; \quad \sigma = -\frac{1}{\sqrt{2\pi}} / \left(\frac{\partial P_2}{\partial y} \right)_{\max}.$$

In particular, on the axis of the flame we will obtain

$$P(x, a) = \Phi\left[\frac{a(x)}{\sigma(x)}\right].$$

Turbulent Torch After an Axially Symmetric Burner
(Inverted Cone) (see Fig. 5.2c)

$$P_2(x, r) = \frac{T - T_1}{T_2 - T_1} = \frac{1}{\sigma^2} \int_0^{\infty} \exp\left(-\frac{r^2 + r_1^2}{2\sigma^2}\right) I_0\left(i \frac{rr_1}{\sigma^2}\right) r_1 dr_1, \quad (5.44b)$$

where I_0 - Bessel function of zeroth order;

$$a = a_0 + \frac{T_2}{T_1} \int_0^r \frac{u}{v} dx - \text{average radius of the flame};$$

a_0 - radius of precombustion chamber (burner);

$$e^2 = 2 \int_0^r P_2 \cdot dr.$$

In particular, on the axis of the flame

$$P_2(x, 0) = \left(1 - e^{-\frac{e^2}{2x^2}}\right).$$

Formulas (5.44a) and (5.44b) are applicable to the case when temperature and exit velocity of hot gases are close respectively to values of T_2 and v , or when initial dimensions of the burners are relatively small.

Turbulent Flame After a Plane Bunsen Burner

Boundary conditions are as follows: width of the initial flow of homogeneous mixture is equal to $2a_0$; width of the burners, which are located on the edges of the flow (at the end of the pipe), is equal to $2b_0$; axis x coincides with the flow axis (Fig. 5.16 and 5.17):

$$P_2(x, y) = \frac{1}{2} \left\{ \Phi \left[\frac{y + (a_0 + b_1)}{\sigma} \right] - \Phi \left[\frac{y - (a_0 + b_1)}{\sigma} \right] + \right. \\ \left. + \Phi \left[\frac{y - (a_0 - b_1)}{\sigma} \right] - \Phi \left[\frac{y + (a_0 - b_1)}{\sigma} \right] \right\}, \quad (5.44c)$$

where

$$b_1 = b_0 + \int_0^r \frac{u}{v} dx; \quad b_2 = b_0 + \left(\frac{T_2}{T_1} - 1 \right) \int_0^r \frac{u}{v} dx; \\ 2(b_1 + b_2) = \int_{-\infty}^{\infty} P_2 \cdot dy \quad \text{for } b_1 > 3\sigma; \quad \sigma = \frac{1}{\sqrt{2\pi}} / \left(\frac{\partial P_2}{\partial y} \right)_{\max}.$$

In this formula the value of σ can be taken as variable over the entire volume of the flame, if we take into account change of the coefficient of turbulent diffusion over space, and also the change of average velocity. For the majority of practical calculations, it is possible to consider, apparently, that the whole flame is in the core of average velocities, so that the average longitudinal velocity is constant and equal to the initial average flow velocity, but it is known to be impossible to take parameters of turbulence to be constant. Formula (5.44c) allows a series of simplifications in certain particular cases. For instance, if flames

from both burners are far removed from each other, then in the system of coordinates whose x-axis coincides with the axis of one of the burners, relationship (5.44c) will be written in the form

$$P_2(x, y) = \frac{1}{2} \left[\Phi \left(\frac{y+b_1}{\sigma} \right) + \Phi \left(\frac{b_1-y}{\sigma} \right) \right].$$

As one of the relatively simple and sufficiently accurate methods of consideration of heterogeneity of turbulence, it is possible to take the value of σ in the first term equal to the value of $\sqrt{V_1}$, which can be determined according to parameters of turbulence of the incident flow and the value $\sigma \approx 0.1x$ in the second term, which can be determined according to the average parameters of turbulence in the zone of mixing of the submerged (hot) stream with its surrounding motionless space.

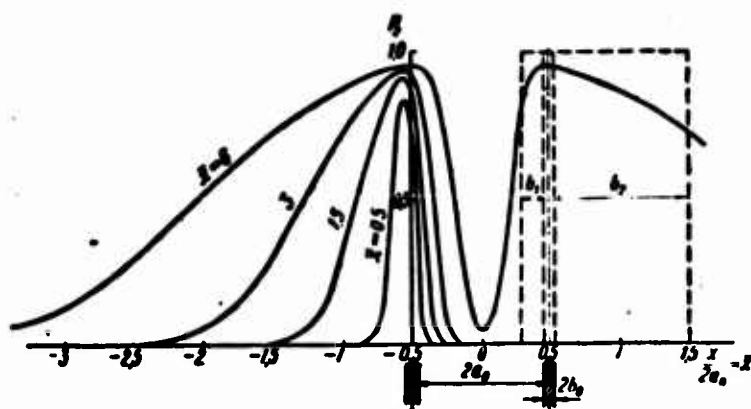


Fig. 5.16. Physical combustion efficiency over cross sections of a flame from a plane Bunsen burner.

$$\frac{b_1}{\sigma} = 0.01.$$

From relationship (5.44c) it follows that along the flow axis change of combustion efficiency is determined by the relationship ($y = 0$)

$$P_2(x, 0) = \Phi \left(\frac{a_0+b_1}{\sigma} \right) - \Phi \left(\frac{a_0-b_1}{\sigma} \right).$$

A graph of this function is shown in Fig. 5.17. Combustion efficiency on the flow axis increases with increase of distance from the end of the burner until that moment when b_1 attains a value equal to a_0 . At this instant flames proceeding toward each other from the two burners join in the middle, so that burning speed will abruptly fall to zero (there will be nothing to burn). From this moment on, the process will be basically only a diffusion process, and combustion efficiency on the axis will begin to decrease due to diffusion of the flame into the surrounding medium. In reality, on the final stage of combustion there exist a number of other factors:

increase of chemical combustion efficiency, simultaneous appearance of burning zones in the same volume, and so forth. If in the initial mixture there is contained a surplus of fuel, then in the zone of mixing combustion products with the surrounding air there will also be observed a secondary effect — diffusion burning. In Fig. 5.17 there is also given a curve calculated taking into account the beforehand assumed coincidence of events, but without taking into account diffusion into the surrounding space (solid curve). Analysis of experimental data indicates the absence of the effect of coincidence of events.

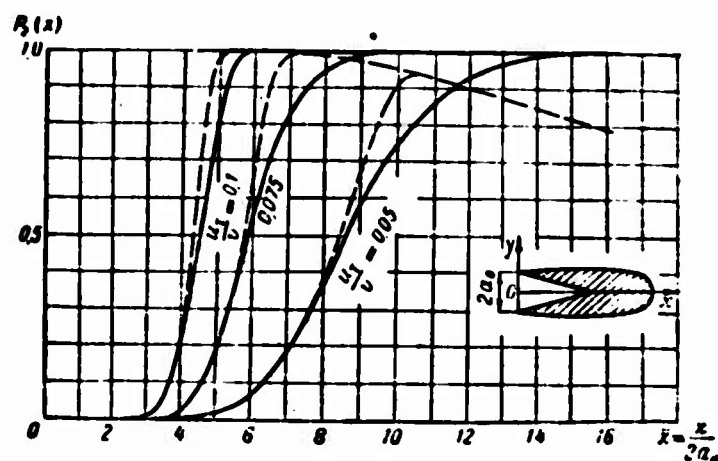


Fig. 5.17. Determination of average temperatures in a turbulent flame from a plane Bunsen burner. Physical combustion efficiency along the axis of the turbulent flame from a plane Bunsen burner:

- taking into account coincidence of events,
 - - - - taking into account stirring of the surrounding medium.

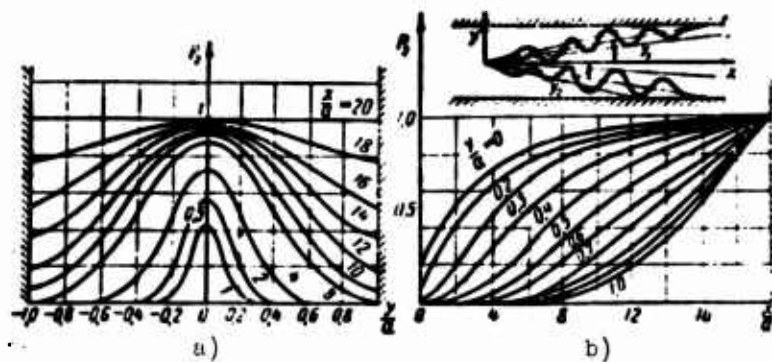


Fig. 5.18. Distribution of average temperatures of a flame in a pipe.

- a) transverse to the flow $\frac{u_T}{v} = 0.05$; $\frac{D_T}{v \cdot a_0} = 0.002$;
 $\frac{x}{a} = 1; 2; 4; 6; 8; 10; 12; 14; 16; 18; 20$;
 b) along the flow $\frac{u_T}{v} = 0.05$; $\frac{D_l}{v \cdot a_0} = 0.002$;
 $\frac{y}{a} = 0; 0.1; 0.2; 0.3; 0.4; 0.5; 0.6; 0.7; 0.8; 0.9; 1.0$.

A Turbulent Flame After an Annular Bunsen Burner (Without
Taking Into Account Mixing With the Surrounding
Motionless Air)

The relationship for $P_1(x)$; r inside the flame is analogous to relationship (5.44b) for $P_2(x; r)$, but $a = a_0 - \int_0^x \frac{u_T}{v} dx$ (a_0 is the radius of the igniting ring of the burner). In particular, on the axis of the flame

$$P_1(x; 0) = e^{-\frac{x^2}{4a_0^2}}. \quad (5.45)$$

Relationships for determination of burning speed u_T according to experimental temperature profiles, and relationships relating values of u_T to the velocity of propagation of the flame u_T are given in work [28].

Turbulent Flame in a Pipe

Let us consider the case of a turbulent flame after a linear ignition source located in a plane pipe. Solution of such a problem was given in works of Zel'dovich, Tszyan, and Scurlock and was developed further in the works of Talantov and Khrantsov.

Let us note what the fundamental difference is between these solutions and those considered below. In the above mentioned works, a real flame was replaced by a hypothetical surface of zero or finite thickness, before and after which the authors apply equations of flow rate, momentum and energy averaged over the cross section of the pipe. The system of equations turns out not to be closed, and is closed by assignment of the width of the burning zone (or burning time), burning speed satisfying Mickelsen's law and the law of change of average velocities (or average temperatures). The form of the burning "surface" (discontinuity) is unknown. In such a formulation, the problem is a long way from the real physical picture of burning in a high-speed turbulent flow. If such a surface really existed at the initial moment of time, then in virtue of its characteristic instability, and mainly under the action of turbulent diffusion of the incident flow, at subsequent moments of time it would turn into a complicated burning surface with a certain probability distribution of appearance at any point over the cross section of the chamber. This distribution, as experiment shows, is assigned by turbulence of the incident flow.

Let us place the origin of coordinates at the source (see Fig. 5.18); the x -axis will be directed along the flow axis; axis y will be directed perpendicularly; and axis z (parallel to which all properties are assumed to be uniform) — along the linear source. We will designate the width of the pipe by $2a$, the average boundary

of the upper half of the flame by $y_1(x)$ and the average boundary of the lower half of the flame by $y_2(x)$. In virtue of the axial symmetry, absolute values of y_1 and y_2 are obviously equal. In the given problem there are assumed to be given: the average incident stream velocity $u_1(0) = v$, the coefficient of turbulent transfer of the incident flow D_T (constant over the cross section of the pipe) and the rate of turbulent combustion u_T . The quantity u_T is uniquely determined by the turbulent structure of the incident flow, independently of where the burning occurs (in the pipe or in an open flow) and whether or not the secondary field of turbulent velocities induced by the flame is large (§ 6, Chapter V). Solution of the problem is more conveniently begun with solution of the equations for the cold component of the flow, since for it there are known the initial and boundary conditions. Let us disregard change of the transverse component of average velocity of the cold part of the flow \bar{v}_1 , i.e., let us consider that $\bar{v}_1 = 0$ not only in the initial section and on the walls of the pipe, but also in all of the remaining cold part of the flow.

At high turbulent velocity transverse to the flow (much higher than average transverse velocity \bar{v}_1), this assumption is sufficiently obvious. Let us note that in the above mentioned works it would also have been possible to safely disregard the transverse component of average velocity before the flame front, but in that case this component to a certain extent replaced the transverse turbulent velocity, which was not taken into account.

From the continuity equation (5.35) written, taking into account change of density along the pipe, we will obtain, using condition ($\bar{v}_1 = 0$); that

$$\rho_1(0) \cdot v = \rho_1(x) \bar{u}_1(x). \quad (5.46)$$

We will now disregard the value of \bar{v}_2 ; this is a rough approximation, and is sufficiently accurate only for high transverse turbulent velocities ($\sqrt{\bar{v}_1^2}; \sqrt{\bar{v}_2^2}$).

The equation for the probability density function of the appearance of cold volumes p_1 can be written in the form

$$\frac{\partial p_1}{\partial x} = \frac{D_T}{a_1} \frac{\partial^2 p_1}{\partial y^2}. \quad (5.47)$$

The boundary condition on the wall is the condition of zero flow of cold volumes through the wall:

$$\left(\bar{v}_1 p_1 + D_T \frac{\partial p_1}{\partial y} \right)_{y=\pm a} = 0. \quad (5.48)$$

Solution of equation (5.47) with the boundary condition (5.48) has the following form for the upper half of the flame:

$$p_1(y_0) = \frac{1}{\sqrt{2\pi} \sigma} \left[e^{-\frac{1}{2} \frac{(y-y_1)^2}{\sigma^2}} + e^{-\frac{1}{2} \frac{(2\sigma-y-y_1)^2}{\sigma^2}} \right] \quad (5.49a)$$

and for the lower half of the flame

$$p_1(y_0) = \frac{1}{\sqrt{2\pi} \sigma} \left[e^{-\frac{1}{2} \frac{(y-y_1)^2}{\sigma^2}} + e^{-\frac{1}{2} \frac{(2\sigma+y+y_1)^2}{\sigma^2}} \right]. \quad (5.49b)$$

Let us note that these solutions are, strictly speaking, approximate: they take into account only the influence of the nearest wall; in practice the influence of the opposite wall turns out to be insignificant. The probability of finding fresh mixture and products of combustion at an arbitrary point of the pipe is determined by the relationships

$$\left. \begin{aligned} P_1 &= \int_{-a}^{y_1} p_1 dy_0 + \int_{y_1}^a p_1 dy_0 \\ \text{and} \\ P_2 &= 1 - P_1 = \int_{y_1}^{y_2} p_1 dy_0, \\ \text{since} \\ \int_{-a}^a p_1 dy_0 &= 1. \end{aligned} \right\} \quad (5.50)$$

By substituting in the first term of function P_1 the value of p_1 for the lower half of the flame, and in the second term the value of p_1 for the upper half of the flame and considering that $y_2 = -y_1$, we will obtain after a series of transformations

$$\left. \begin{aligned} P_1 &= \frac{1}{2} \Phi\left(\frac{y-y_1}{\sigma}\right) - \frac{1}{2} \Phi\left(\frac{y+y_1}{\sigma}\right) + \frac{1}{2} \Phi\left(\frac{2\sigma-y-y_1}{\sigma}\right) + \\ &\quad + \frac{1}{2} \Phi\left(\frac{2\sigma+y-y_1}{\sigma}\right), \\ P_2 &= 1 - \frac{1}{2} \left[\Phi\left(\frac{y-y_1}{\sigma}\right) + \Phi\left(\frac{2\sigma-y-y_1}{\sigma}\right) - \right. \\ &\quad \left. - \Phi\left(\frac{y+y_1}{\sigma}\right) + \Phi\left(\frac{2\sigma+y-y_1}{\sigma}\right) \right]. \end{aligned} \right\} \quad (5.50a)$$

where $\Phi(\xi) = \frac{2}{\sqrt{\pi}} \int_0^\xi e^{-\frac{t^2}{2}} dt$ is the probability integral function.

Graphs of function P_2 versus x and y for values of $D_T/v_1 a_0 = 0.002$ and $u_T/v_1 = 0.05$ are shown in Fig. 5.19.

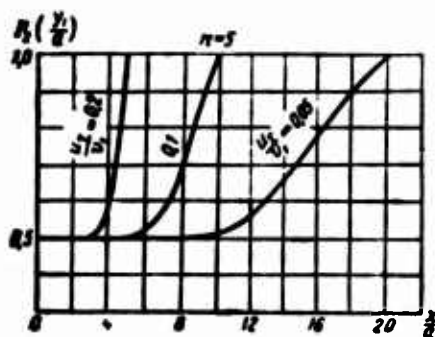


Fig. 5.19. Experimental determination of the average boundary of the flame.

$$\frac{D_T}{v \cdot a_0} = 0.002; \quad \frac{h}{n} = 1.$$

$$-\bar{u}_1 \frac{dy_1}{dx} [p_1(y_1) + p_2(y_2)] = -u_T [p_1(y_1) + p_2(y_2)]$$

or

$$\frac{dy_1}{dx} = \frac{u_T}{\bar{u}_1},$$

i.e., the average boundary of the turbulent flame for $v_1 \approx 0$ is determined by the relationship

$$y_1(x) = \int \frac{u_T}{\bar{u}_1} dx = \frac{1}{v} \int \frac{p_1(x) u_T(x)}{p_1(0)} dx. \quad (5.52)$$

The value of y_1 according to the experimental profile of average temperatures is determined according to (5.50a) by the equation

$$P_2(y_1) = 1 - \frac{1}{2} \left[\Phi \left(\frac{2s - 2y_1}{\sigma} \right) - \Phi \left(\frac{2y_1}{\sigma} \right) + \Phi \left(\frac{2s}{\sigma} \right) \right].$$

A graph of this function for various values of u_T/v and $D_T/v \cdot a_0 = 0.02$ is shown in Fig. 5.19. From Fig. 5.19 it is seen that at $y_1 \approx 3\sigma$ the average boundary passes through combustion efficiency 0.5, just as in an open flow, and rapidly increases to unity only in cross sections close to the cross section of complete burnup.

For determination of \bar{u}_2 and \bar{v}_2 we use the equation of conservation of energy written in the form

$$-(\bar{u}_2 - \bar{u}_1) \frac{\partial P_1}{\partial x} - \bar{v}_2 \frac{\partial P_1}{\partial y} = u_T (n - 1) [p_1(y_1) + p_2(y_2)]. \quad (5.53)$$

Substituting in this equation the value of $\partial P_1 / \partial x$ from (5.50), we will obtain after a series of transformations

$$\left(\frac{\bar{u}_2}{\bar{u}_1} - 1 \right) = \frac{u_T (n - 1) [p_1(y_1) + p_2(y_2)] - \bar{v}_2 \frac{\partial P_1}{\partial y}}{u_T [p_1(y_1) + p_2(y_2)] - D_T \frac{\partial^2 P_1}{\partial y^2}}. \quad (5.54)$$

Substituting the values of derivatives of functions P_i in (5.54), we will find our final formula for calculation:

$$\frac{\bar{u}_2 - \bar{u}_1}{\bar{u}_1 (n-1)} = \frac{2y_1 \left\{ \left[1 + \frac{\bar{v}_2}{u_1 (n-1)} \right] p(y-y_1) + \left[1 - \frac{\bar{v}_2}{u_1 (n-1)} \right] p(2a-y-y_1) + \left[1 - \frac{\bar{v}_2}{u_1 (n-1)} \right] p(y+y_1) + \left[1 + \frac{\bar{v}_2}{u_1 (n-1)} \right] p(2a+y+y_1) \right\}}{(y+y_1)p(y-y_1) + (2a-y+y_1)p(2a-y-y_1) + (y_1-y)p(y+y_1) + (2a+y+y_1)p(2a+y-y_1)}, \quad (5.54a)$$

where

$$n = \frac{P_1(0)}{P_1(x)} = \frac{P_1(x)}{P_1(x)}; \quad p(t) = \frac{1}{\sqrt{2\pi} \sigma} \exp\left(-\frac{t^2}{2}\right);$$

$$\bar{v}_2 = -\frac{\partial}{\partial x} \int \bar{u}_1 dy \quad - \text{according to the continuity equation (5.35).}$$

Formula (5.54) acquires a simple expression on the axis of the flame ($y = 0$) and on the wall of the pipe ($y = a$).

On the axis of the flame ($y = 0$; $\bar{v}_2 = 0$)

$$\frac{\bar{u}_2 - \bar{u}_1}{\bar{u}_1 (n-1)} = \frac{2 \left[1 + \exp\left(-\frac{2a(a-y_1)}{\sigma^2}\right) \right]}{\left[1 + \exp\left(-\frac{2a(a-y_1)}{\sigma^2}\right) \right] + \frac{2a}{y_1} \exp\left(-\frac{2a(a-y_1)}{\sigma^2}\right)}, \quad (5.54b)$$

In particular, at

$$y_1 \rightarrow 0 \quad \frac{\bar{u}_2 - \bar{u}_1}{\bar{u}_1 (n-1)} \approx 2$$

and at

$$y_1 \rightarrow a \quad \frac{\bar{u}_2 - \bar{u}_1}{\bar{u}_1 (n-1)} \rightarrow 1.$$

On the wall of the pipe ($y = a$), discarding terms for the influence of the opposite half of the flame, we will obtain

$$\frac{\bar{u}_2 - \bar{u}_1}{\bar{u}_1 (n-1)} = \frac{2y_1}{(a+y_1)} \quad \text{for } y_1 \rightarrow a \quad \frac{\bar{u}_2 - \bar{u}_1}{\bar{u}_1 (n-1)} \rightarrow 1.$$

For calculation of the profile of velocity \bar{u}_2 by the formula (5.54), it is possible to use the method of successive approximations. Considering in (5.54) that $\bar{v}_2 = 0$, we will find the profile of \bar{u}_2 in the first approximation. From the

continuity equation according to the profile of \bar{u}_2 which has been found, we will determine the first approximation of the profile of \bar{v}_2 and substitute it in (5.54),

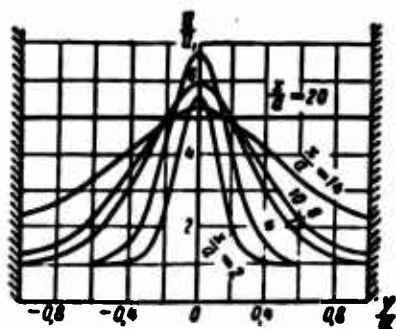


Fig. 5.20. Distribution of average flame speeds in a pipe.

$$\frac{D_T}{u \cdot a_0} = 0.002; \frac{u_T}{u} = 0.05; n = 5.$$

etc. For quite large values of D_T , \bar{v}_2 is practically equal to zero, so that it is possible to be limited to calculation of the profile in the first approximation. At very small values of D_T , it is necessary to consider \bar{v}_2 . In the limit, $D_T \approx 0$, the value of \bar{v}_2 at separate points of the pipe can attain values $\sim u_T(n-1)$. The value of \bar{v}_2 can be different from zero on the wall, since the probability of appearance of a flame front on the wall has finite value.*

The profile of average velocities \bar{u} is determined by the formula

$$\bar{u} = \bar{u}_1 P_1 + \bar{u}_2 P_2 = \bar{u}_1 + (\bar{u}_2 - \bar{u}_1) P_2 \quad (5.55)$$

Graphs of the profile of u transversely across the pipe for $u_T/v = 0.05$ are shown in Fig. 5.20.

For practical calculations, sometimes it is more convenient to use equations averaged over the cross section of the pipe. Equations of conservation of mass, energy and momentum averaged over the cross section of the pipe will be written respectively in the form

$$\frac{\partial \bar{u}_{cp} \bar{u}_{cp}}{\partial x} = 0 \text{ or } \rho_1 \bar{u}_1 = \bar{u}_{cp} \rho_{cp},$$

$$\frac{\partial \bar{u}_{cp}}{\partial x} = \frac{u_T(n-1)}{a} \text{ or } \bar{u}_{cp} - \bar{u}_1 = u_T(n-1) \frac{x}{a}$$

and

$$\frac{\partial \bar{u}_{cp} \bar{u}_{cp}^2}{\partial x} = \frac{-\partial P_{cp}}{\partial x} \text{ or } \rho_1 \bar{u}_1 \cdot u_T(n-1) \frac{x}{a} = P(x) - P_1,$$

$$\rho_1 \bar{u}_1^2(n-1) = \Delta P_{max}.$$

The momentum equation can be used for estimation of the value of u_T according to the drop of static pressure along the pipe. Let us note that during solution of

*The term "wall" in the given problem naturally is understood to mean the external limit of the boundary layer, beyond which the influence of walls of the pipe begins.

the problem there were not used momentum equations selectively averaged, but the general equation. These equations are satisfied under the simple assumptions that:

$$\bar{v} = \overline{u'v'} = \frac{\partial p}{\partial y} = 0 \text{ and } \bar{v}^2 = \text{const.}$$

However, if we use more exact assumptions ($\bar{v}_2 \neq 0$ and so forth), we can obtain the distribution of turbulent velocities in the combustion products $\bar{v}_2'^2$ satisfying the condition of zero pressure drop transverse to the flow, which is different from the distribution of $\bar{v}_1'^2$. Besides this velocity, there also exists the profile of "virtual turbulent velocity," which is obtained during measurement of total fluctuations of velocity in the burning zone (see p. 285). All of this indicates the possibility of measurement of values of fluctuating velocity in the zone and in combustion products of a flame in a pipe which essentially differ from the turbulent velocity of the incident stream, although, as was seen from the solution, basic parameters of the flame - dispersion σ and mean y_1 - are determined by turbulence of the incident flow.

The given solution is applied to burning after flame-holder and after small-dimension precombustion chambers, if the temperature of the stream of the precombustion chamber does not strongly differ from the temperature of the combustion products. In this case, the origin of coordinates is placed at the edge of the flame-holder (precombustion chamber); distance a is the width of the opening between the edge of the flame-holder and the wall. The value of D_T , which is given in the flow before the flame-holder in the form of the ratio D_T/v_0 , practically does not change in a narrow place; there is increased only the value of velocity from v_0 to v_1 , so that in place of the given value of D_T/v_0 , we should substitute in calculations the value of D_T/v_1 (v_1 - average longitudinal velocity in a narrow place).

In a number of cases (burning after several ignition sources in the presence of average transverse velocities), during large change of longitudinal average velocities, and so forth, for technical calculations it is apparently more correct to use the average (over the cross section of the pipe) value of dispersion, determined by the formula

$$\sigma^2 = 2 \int_{x_0}^x \frac{D_T dx}{\bar{u}_{cp}} = 2 \frac{D_T x}{u_1 \left[1 + \frac{u_T}{u_1} (n-1) \frac{x}{a} \right]} = \frac{2 D_T x}{(\bar{u}_{cp} - u_1)} \ln \left(\frac{\bar{u}_{cp}}{u_1} \right)$$

for

$$x > 2x_0 \left(\text{where } x_0 \approx \frac{l_1 u_1}{2u_T} \right). \quad (1.56)$$

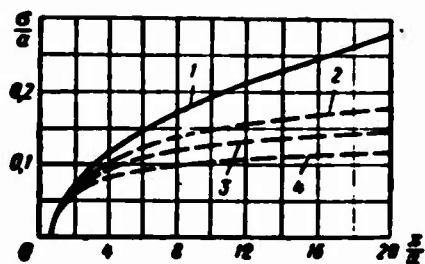


Fig. 5.21. Dispersion of a turbulent flame in a pipe and in an open flow.

1 - in an open flow $\frac{a}{a_0} = \sqrt{\frac{2D_T(x-x_0)}{u_T \cdot a_0}}$;

$$\frac{D_T}{a_0} = 0.002; \quad \frac{u_T}{a_0} = 0;$$

2 - in a pipe at $\frac{u_T}{a_0} = 0.05$;

3 - in a pipe at $\frac{u_T}{a_0} = 0.1$;

4 - in a pipe at $\frac{u_T}{a_0} = 0.2$.

Graphs of this function for different \bar{u}_T/v_1 are given in Fig. 5.21. The quantity u_T is given according to experimental data obtained with the help of any of the above mentioned methods of measurement in an open flow. The solution given in the present article can also serve as the basis for measurement of u_T .

Statistical Distribution of Scales of Temperature Heterogeneities in the Macrozone of Turbulent Burning

In a number of technical problems on turbulent burning, it is important to clarify not only the basic parameters of the turbulent flame - dispersion $\sigma^2(x)$ and mean $a(x)$, but also the structure of the burning zone of the turbulent flame. In other words, it is interesting to know not only burning rate and width of the burning zone, but also dimensions of the "cold" and "hot" volumes filling this zone. For instance, during heterogeneous burning, the basic flame is obtained from homogeneous burning of the vapor phase of the fuel. This flame is penetrated by a swarm of unevaporated droplet. It is interesting to investigate the behavior of the droplets (their evaporation, ignition, and so forth) during their passage through the macrozone of the turbulent flame. As far as it is known, such investigations, even if they have been conducted, have been conducted without taking into account physical peculiarities of the structure of the turbulent burning zone (there has simply been considered the behavior of a droplet in a field of variable average temperatures without taking into account its statistical oscillations). Consideration of these peculiarities can considerably change the results of investigations. It would also be interesting to investigate the reverse action of the swarm of droplets on the turbulent flame; for instance, conditions of ignition of cold material in the burning zone by burning drops, and so forth.

Let us consider peculiarities of the macrostructure of a turbulent flame in the example of a one-dimensional turbulent burning zone. Obtained regularities can, when necessary, be extended to a real flame in a high-speed flow, since the distribution of statistical parameters through the depth of the one-dimensional zone

can be considered with practical accuracy as the distribution through the depth of a flame along the basic flow, compressed in the ratio u_T/v .

The statistics of scales of temperature heterogeneities of the one-dimensional zone can be studied, by considering at an arbitrary depth of the zone x an "oscillogram" of temperature fluctuations along one of the coordinates y or z , along which statistical properties of the parameters of the zone are homogeneous. For moments of time when the linear scales of "cold" and "hot" moles l_1 and l_2 become noticeable larger than the integral scale of the burning front σ_0 (for $t > \sigma_0 \sqrt{a_1^2}$), if it possible to speak definitely of the probability of appearance of "cold" or "hot" scales, and of the probability of appearance of a burning front (a layer of intermediate temperatures). Let us consider at first the statistics of "cold" scales l_1 (where l_1 is a random function) along the y -axis. Let us determine over a sufficiently large segment of the y -axis the absolute number of scales whose values fall within the interval from l_1 to $l_1 + d\bar{l}_1$. Let us designate this number as $n(l_1)d\bar{l}_1$; it is obvious that it increases with increase of the selected segment of the y -axis. The total number of all "cold" scales on the given segment will probably also depend on the length of the segment y , and be equal to

$$n_1 = \int_0^y n(l_1) dl_1.$$

We will define the value of the mean-statistical scale of "cold" moles L as the limit of the relation

$$L_1 = \lim_{y \rightarrow \infty} \frac{\int_0^y l_1 n(l_1) dl_1}{\int_0^y n(l_1) dl_1}. \quad (5.57a)$$

The value of L_1 obviously no longer depends on the coordinate y , but is only a function of depth of the zone x .

An analogous definition can be given for the statistical scale of hot moles L_2 :

$$L_2 = \lim_{y \rightarrow \infty} \frac{\int_0^y l_2 n(l_2) dl_2}{\int_0^y n(l_2) dl_2}. \quad (5.57b)$$

We will find the relation between scales L_1 , L_2 and functions P_1 , P_2 . Let us note that values of

$$\int_0^y l_1 n(l_1) dl_1 \text{ and } \int_0^y l_2 n(l_2) dl_2$$

constitute the total extent respectively of the cold and hot mixtures on the considered segment of the y-axis, and the value of

$$\int_0^{\bar{y}} l_1 n(l_1) dl_1 + \int_0^{\bar{y}} l_2 n(l_2) dl_2$$

constitutes the total extent of the considered segment of the y-axis. Then, according to the definition of functions P_1 and P_2 (see § 1, Chapter V), we have

$$P_1 = \lim_{\bar{y} \rightarrow \infty} \frac{\int_0^{\bar{y}} l_2 n(l_2) dl_2}{\int_0^{\bar{y}} l_1 n(l_1) dl_1 + \int_0^{\bar{y}} l_2 n(l_2) dl_2}; \quad (5.58a)$$

$$P_2 = \lim_{\bar{y} \rightarrow \infty} \frac{\int_0^{\bar{y}} l_1 n(l_1) dl_1}{\int_0^{\bar{y}} l_1 n(l_1) dl_1 + \int_0^{\bar{y}} l_2 n(l_2) dl_2}. \quad (5.58b)$$

Dividing relationships (5.58a and 5.58b) by

$$n_1 = n_2 = \int_0^{\bar{y}} n(l_1) dl_1 = \int_0^{\bar{y}} n(l_2) dl_2 = n, \quad (5.58c)$$

we will obtain

$$P_1 = \frac{L_1}{L_1 + L_2}; \quad P_2 = \frac{L_2}{L_1 + L_2}. \quad (5.59)$$

During derivation of these equations, we disregarded the average dimension of the burning front σ_{0y} along the y-axis, i.e., we considered $2\sigma_{0y} \ll L_1 + L_2$. By analogous reasoning, but with more cumbersome transformations, it is possible to consider the dimension of the burning front σ_{0y} in relationships (5.59) and to determine additionally the function of probability of its appearance P_3 . During derivation of the relationship for P_3 it is necessary only to consider that the total number of fronts on segment y is equal to

$$n_3 = 2n_1 = 2n_2 = n_1 + n_2; \\ P_1 = \frac{L_1}{L_1 + L_2 + 2\sigma_{0y}}; \quad P_2 = \frac{L_2}{L_1 + L_2 + 2\sigma_{0y}}; \quad P_3 = \frac{2\sigma_{0y}}{L_1 + L_2 + 2\sigma_{0y}}. \quad (5.60)$$

Inasmuch as in all cases interesting in practice the inequality $2\sigma_{0y} \ll L_1 + L_2$ is satisfied, then equations (5.60) can be written in the simpler form:

$$\left. \begin{aligned} P_1 &= \frac{L_1}{L_1 + L_2}, \\ P_2 &= \frac{L_2}{L_1 + L_2}, \\ P_3 &= \frac{\sigma_{0y}}{L_1 + L_2} = \frac{\sigma_{0y} \cdot P_1}{L_1} = \frac{\sigma_{0y} P_1}{L_1}. \end{aligned} \right\} \quad (5.61)$$

The same relationships could have been obtained in examining of the statistics along the time axis, so that they obviously remain in valid for any point of a three-dimensional, inhomogeneous burning zone. In particular, at the point where $P_1 = P_2 = 0.5$, according to (5.61), we have $L_1 = L_2 = L_0$ and $P_3 = \sigma_{0y}/L_0$.

Function $P_3(x)$, just as function $P_1(P_2)$, can be determined not only according to the statistics of events along the y-axis, but also according to the statistics of events along the x-axis (for a one-dimensional burning zone). The probability of appearance at point x of a one-dimensional burning zone of intermediate temperatures (burning front) is equal (see § 1, Chapter V) to

$$P_3(x) \approx k_{0x} \cdot p_3(x), \quad (5.62)$$

where $p_3(x)$ — probability of appearance of a discontinuity (burning front) in a unit interval of length at depth of the zone x;

σ_{0x} — mean-statistical width of the burning front along the x-axis;

k — approximately constant form factor of the order of unity, which takes into account small inaccuracies of determination of the width of the front with scale σ_{0x} .

With the microvolume mechanism of combustion, in virtue of the high probability of single-valuedness of the burning surface existing in this case and isotropy of local distortions of the burning surface, scales σ_{0y} and σ_{0x} will be practically equal to

$$\sigma_{0x} = \sigma_{0y} = \sigma_0. \quad (5.63)$$

In the general case of a non-single-valued burning surface the value of scale σ_{0x} will be equal to the value of σ_{0y} multiplied by the average number of burning fronts intersected by the x-axis (during averaging, naturally, of this number along the y- or z-axes. This number (we will designate it by a) was called above the degree of non-single-valuedness of the burning surface.

The probability density function $p_3(x)$ in formula (5.62) satisfies Gauss's law with high accuracy; the accuracy of its coincidence with Gauss's function will

apparently be higher, the nearer the burning surface is to a single-valued surface. Equating the two independent definitions of function P_3 , (5.61), (5.62), and substituting in them the specific forms of functions P_1 and $p_S(x)$, we will obtain the distribution of scales L_1 , L_2 over the depth of the burning zone:

$$L_1 = \frac{\sqrt{2\pi}}{a} \left[1 - \Phi\left(\frac{x}{\sigma}\right) \right] e^{\frac{x^2}{2\sigma^2}} = L_0 \left[1 - \Phi\left(\frac{x}{\sigma}\right) \right] e^{\frac{x^2}{2\sigma^2}} \quad (5.64)$$

and

$$L_2 = \frac{\sigma \sqrt{2\pi}}{k \cdot a}, \quad (5.65)$$

where L_0 is the scale of temperature heterogeneities at the center of the zone.

From formula (5.65) it is clear that scale L_0 increases in time approximately proportionally to σ , with accuracy up to increase of the quantity a from unity to

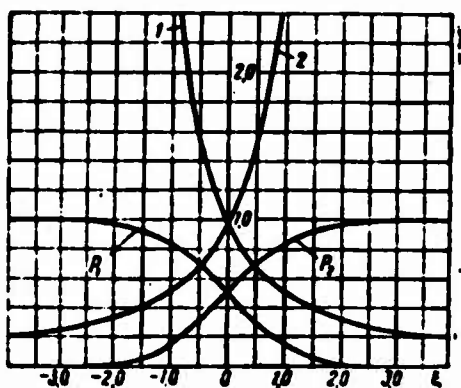


Fig. 5.22. Distribution of scale L_1 and L_2 over the depth of the burning zone.

$$1 - \frac{L_1}{L_0} = \left[1 - \Phi\left(\frac{x}{\sigma}\right) \right] e^{\frac{x^2}{2\sigma^2}};$$

$$2 - \frac{L_2}{L_0} = \left[1 + \Phi\left(\frac{x}{\sigma}\right) \right] e^{\frac{x^2}{2\sigma^2}}.$$

values somewhat larger than unity (for the microvolume mechanism of burning). Function a determines the behavior of scale L_0 from the relationship between turbulent and physico-chemical factors of the turbulent flame.

The value of a has a tendency to increase with decrease of Reynolds number Re of the flow, to decrease with increase of the quantity u_T or (for constant turbulence) with increase of the quantity u_H , etc. In accordance with this, scale L_0 changes. The obtained relationships

will agree well with results of the experimental investigations of Kokushkin [9] of distributions of L_1 and L_2 with respect to flow velocity, length and depth of the flame, mixture ratio, etc.

In Fig. 5.22 there is shown a universal curve of L_2/L_0 versus x/σ . In Fig. 5.23 and 5.24 there are plotted theoretical and experimental curves of L_1 and L_2 versus P_1 , according to data of Kokushkin [32] after burners.

Estimation of values of k from the condition $\frac{k}{\sqrt{2\pi}} \approx \frac{1}{L_0}$ (at $a \approx 1$)

according to experimental values of L_0 and σ gives the value $k = 0.8$ to 1.3 .

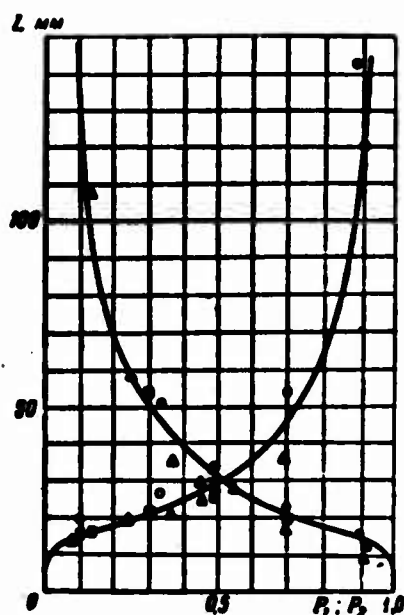


Fig. 5.23. Dependence of scales L_1 and L_2 on combustion efficiency for various flow velocities.
—— theory.

L_1	L_2	η	m/sec
○	●	1.893	30
□	■	1.80	30
△	▲	1.61	20

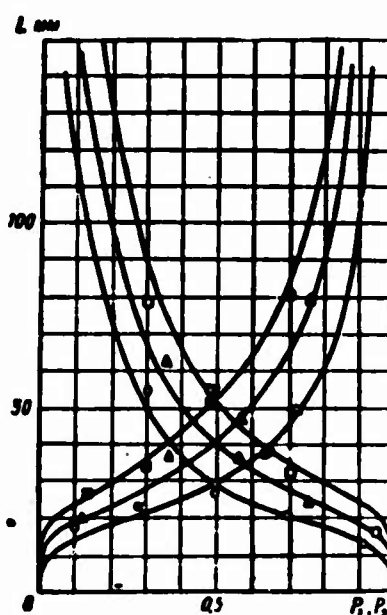


Fig. 5.24. Dependence of scales L_1 and L_2 on combustion efficiency for various values of air-fuel ratio (according to data of [32]).*

L_1	L_2	η	m/sec
○	●	1.6	30.0
△	▲	1.36	32.5
□	■	1.13	31.8

* Distance from the burner is 500 mm.

As can be seen from the comparison of theory with experiment shown in Fig. 5.23 and 5.24, the dependence of scales L_1 and L_2 on average flow velocity, on η , etc, is completely described by the given theoretical relationships.

If we consider that $a \approx 1$ and $k \approx 1$, then during detailed analysis of experimental values of L_0 with the help of (5.60) and (5.62), we can perceive in the experiments of Kokushkin a certain anisotropy of local distortions of the fronts. The quantity σ_{Oy} (along the flow) according to his data is always obtained to be somewhat higher than the quantity σ_{Ox} (transverse to the flow); this indicates the still insufficiently developed local (small-scale) distortions of the burning surface for the given conditions of turbulent burning ($u'/v \approx 0.05\%$; $v \approx 30$ m/sec, $l_L = 10$ mm).

§ 6. HYDRODYNAMIC PECULIARITIES OF TURBULENT BURNING AFTER BLUFF BODIES (FLAME-HOLDERS)

Peculiarities of the structure of turbulence in the wakes after bluff bodies were noted in Chapter IV. Let us consider these peculiarities in reference to the wake after flame-holders in a combustion chamber. For this we will use detailed measurements of the distributions of intensity of turbulence over different cross sections of the wake after flame-holders (without combustion) which were conducted in the work of Solntsev [34]. Complete description of the distribution of $\epsilon(x; y)$ can be obtained if there are known the following parameters of the turbulent wake: distribution of intensity of turbulence along the axis of the wake $\epsilon(x; 0)$, functions of the mean $a(x)$ and dispersions $\sigma(x)$ (for the turbulent wake). The distribution of $\epsilon(y)$ is shown in Fig. 5.25.

The distribution of $\epsilon(x)$ along the axis of the wake after three different flame-holders used in the work of Solntsev is shown in Fig. 5.26. All measurements were conducted in pipes of rectangular cross section (300×175 or 200×175 mm) after trough-shaped flame-holders with angles of 30° or 60° at the vertex. Width of the base of the cone of the stabilizer $2h$ was equal to 35 or 70 mm. In one of the flame-holders, on the lateral walls along the generatrices of the cone there were cut strips, and part of these strips (every other one) were bent perpendicularly to the flow, so that the inside width of such a flame-holder was equal to 70 mm along the bent part of the strips and 35 mm along the unbent part (Fig. 5.27). Values of $\epsilon(x)$ for each of the flame-holders are shown in the figures. From Fig. 5.26 it is clear that the maximum intensity of turbulence over the cross section of the wake rapidly attenuates along the axis of the wake, and at distances of $\sim 40h$ attains the level of turbulence of the external flow. The value of $\epsilon(x)$ in the external flow weakly increases from values ~ 3 to 4% , which are somewhat smaller than the level of pipe turbulence (5%) (due to the small contraction of the flow in experiments [34]), to values somewhat larger than 6% , if the turbulent wake joins with the external flow in layers adjacent to the walls (as this occurs for a pipe of 200×175 mm), where the value of turbulent intensity becomes noticeably larger than 5% of the level in the flow core.

A flame-holder with protrusions in the form of strips with the largest width of the center section equal to 70 mm gives a somewhat larger value of $\epsilon(x)$ than a "smooth" flame-holder with the same center section. Decay of the intensity of

turbulence after the bent flame-holder occurs, however, somewhat more rapidly, apparently due to the smaller scales of eddies formed after such a flame-holder.

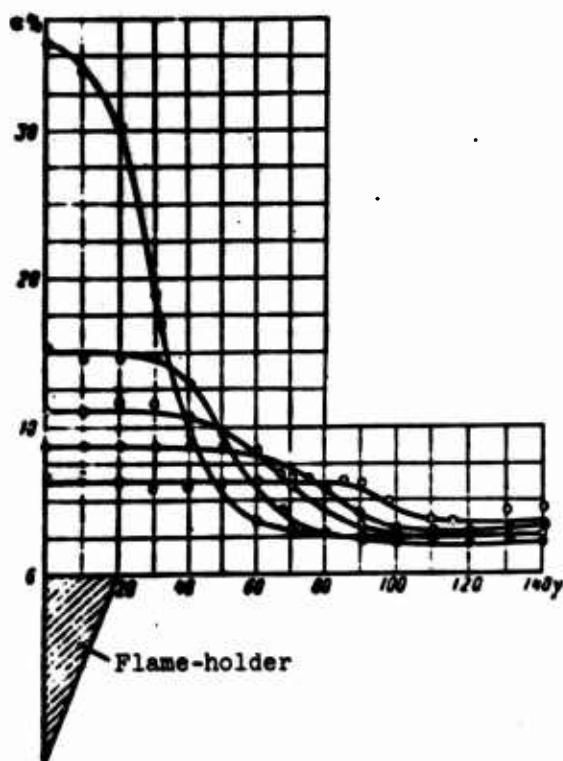


Fig. 5.25. Distribution of intensity of turbulence in the wake after a flame-holder (without combustion) according to data of V. P. Solntsev.

Values of $\epsilon(x)$ along the axis of the wake can be determined with sufficient technical accuracy without conducting direct measurements of $\epsilon(x)$, but by measuring only the magnitude of the dip of average velocities on the axis of wake: $(v_{\max} - v_{\min})$. According to calculations given in Chapter IV, $\epsilon(x) \approx 0.4 \text{ to } 0.34 (v_{\max} - v_{\min})$.

According to experimental distributions of $\epsilon(x; y)$, there were constructed functions of the mean $a(x)$ and dispersion $\sigma(x)$ which define them; these are shown in Fig. 5.28. From Fig. 5.28 it is clear that the average speed of expansion of the turbulent wake practically does not depend on the shape and size of the stabilizer, is constant over the length of the wake and is determined for a pipe of

300 × 175 mm at $v = 50$ m/sec by the ratio $u^*/v \approx 0.1$. According to the single measurement in a narrower pipe (200 × 175 mm) and at lower speed ($v = 35$ m/sec), the ratio u^*/v is obtained to be somewhat smaller (0.065).

It is still not clear how such divergence appears: due to large blockage of the pipe or due to deviation of the flow pattern from self-similar at the indicated average speeds.

From Fig. 5.28 one may also see that the average boundary for a flame-holder with protrusions passes somewhere between those of flame-holders with widths of 70 and 35 mm. The dispersion function $\sigma(x)$ in this case characterizes the root-mean-square deviation of the instantaneous boundary of the region of increased turbulence from its average position. Oscillations of boundaries of the region of increased

turbulence occur under the action of the biggest vortices shed after the edges of the flame-holder. These vortices are quite rare; their shedding frequency is

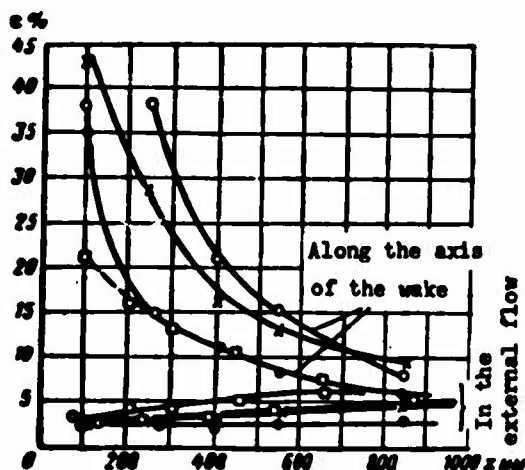


Fig. 5.26. Distribution of intensity of turbulence along the axis of the wake after flame-holders (without combustion) and in the external flow (according to Solntsev).

● — $\beta 30^\circ$; $2h=35$
 x — $\beta 30^\circ$; $2h=70$ mm } Pipe 300x175 mm, $v=30$ m/sec
 ○ — $\beta 35^\circ$; 70; flame-
 holder with protrusions
 □ — $\beta 30^\circ$; $2h=35$ } Pipe 200x175, $v=35$ m/sec

apparently determined in most cases by the Strouhal frequency. Dimensions of these vortices transverse to the flow do not exceed the half-width of the flame-holder h ; their dimensions along the flow may be considerably larger, especially for flame-holders in sufficiently narrow pipes.

The magnitude of intensity u'/v calculated according to $\sigma(x)$ characterizes the velocity of large eddies transverse to the flow. In spite of the most sharply pronounced anisotropic character of the large eddies, such turbulent velocity can to a certain degree characterize the fraction of turbulent energy contained in these eddies. By values of ϵ_0 calculated according to the magnitude of σ and total values of ϵ_{yTa} measured by a hot-wire

anemometer and shown in Fig. 5.26, it is possible to see that the energy of large eddies does not exceed 14% of the total energy of turbulence in the wake. Scales of turbulence l_L calculated according to $\sigma(x)$ determine in this case the average displacement length of an element of volume of the medium by the largest eddies in their average lifetime. The order of the lifetime of these eddies is determined by the equality $l_L/u' = D/v \cdot \epsilon_0$, and the quantity $x_0 \approx D/v \cdot \epsilon_0^2$ determines the order of magnitude of distances from the edge of the flame-holder along the flow at which it is possible to observe separate large eddies shed from the edges of the flame-holder.

However, the considered picture of the turbulent wake after a flame-holder will exist only in the absence of burning after the flame-holder. The main purpose of the flame-holder is to give the simplest and most convenient constant ignition source of (stagnant wake), which ensures a stable regime of burning in a high-speed flow within quite wide limits (with respect to speed, mixture ratio, and so forth).

At first glance it may seem that the flame-holder, being a source of high turbulence in a flow without burning, serves during burning not only as a source of stable ignition, but also as an intensifier of the process of burning in the flame after the given flame-holder.

Analysis of existing experimental data shows, however, that this is not so. The sources of high turbulence after a flame-holder without burning are the large

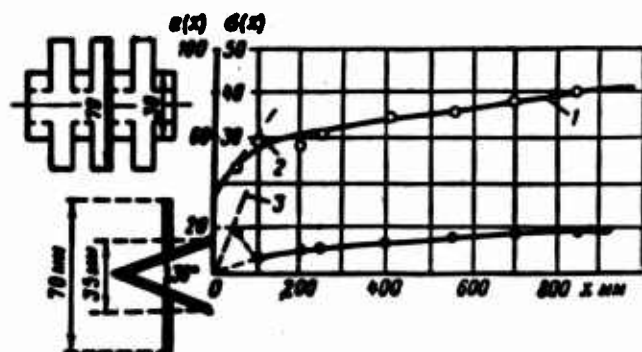


Fig. 5.27. The influence of local increases of intensity of turbulence in the region of a flame-holder on parameters of a turbulent flame.

$$1 - \frac{u}{u_0} = 0.04; 2 - \frac{u}{u_0} = 0.3; 3 - \frac{u}{u_0} = 30\%$$

be absolutely different from the hydrodynamics of flow without burning; the hydrodynamics will considerably change due to the conditions of burning (in a pipe or in an open flow), due to mixture ratio, and so forth. Turbulent parameters of flow in

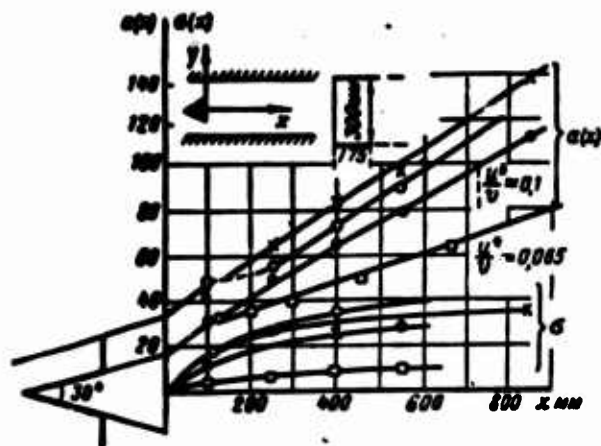


Fig. 5.28. Average boundaries and dispersion of the wake after trough-shaped stabilizers without combustion (according to data of Sclintsev).

gradients of average velocities - the dip in the profile of average velocity. During acceleration of the flow in a flame after a flame-holder, the magnitude of these gradients can greatly decrease, reach zero, and further change sign, so that instead of a dip in profile of average velocity, on the axis of the wake there will be a projection. In other words, hydrodynamics of the flow after a flame-holder during burning will

a flame, as a result of hydrodynamics of the average flow, will obviously be different from turbulent parameters after a flame-holder without burning.

Let us now go over to analysis of experimental data. If the turbulent wake after a flame-holder without burning and with burning would remain constant, then the burning rate in such a wake would be very high because of the high values of intensity of turbulence in the wake, so that according

estimates of corresponding values of u_T , the whole wake would be filled with burned mixture. In other words, the average boundaries of the turbulent wake without burning should under such an assumption coincide with the average boundaries of a turbulent flame, if turbulence outside of the instantaneous boundaries of the wake (in the incident flow) is equal to zero.

For a sufficiently high level of turbulence of the incident flow ($\approx 5\%$), boundaries of the flame at the value of u_T corresponding to it can even be noticeably wider than the average boundaries of the wake. In reality, experimental data of Solntsev [35], Bupalov (Chapter VIII) and Shcherbina [24] show that average boundaries of the turbulent flame after a flame-holder are always much narrower than the average boundaries of a turbulent wake after the same flame-holder (compare Fig. 5.28 and 5.6). This indicates that the concept of invariability of a turbulent wake after a flame-holder with burning and without burning should be rejected: in a turbulent flame after a stabilizer there does not exist the turbulent wake which exists after the same stabilizer without burning. There appear the questions: what parameters of turbulence exist directly before the flame and assign values of its parameters? Will these parameters be uniquely determined by the structure of turbulence of the incident flow, or will they depend on hydrodynamics of the flow after the flame-holder, on its dimensions, mixture ratio, conditions of burning and so forth? Analysis of experimental data shows that parameters of a turbulent flame after a flame-holder are determined practically completely by turbulence of the incident flow (we consider not flow before the flame-holder, but the flow of fresh mixture directly before the boundaries of the flame).

From the data of Solntsev, Shcherbina and Bupalov given below (see § 1, Chapter VIII), one may see (Fig. 5.29-5.32) that dispersion of a flame after flame-holders is determined by the turbulence of the incident flow, while turbulence of the combustion products (on the axis of the flame) greatly differs from the latter, and depends on the regime of burning [36], [37], [24], [33]. Measurements of distributions of scales of temperature heterogeneities conducted by Kokushkin [32], showed that values of scales in the burning zone of a flame after a flame-holder completely coincide with corresponding scales of a flame after a point burner, the scales of which are assigned by turbulence of the incident flow (see § 5, Chapter V).

Finally, quantity u_T measured in a flame after a flame-holder completely correlates with turbulence of the incident flow and does not depend on dimensions

of the flame-holder (whereas the magnitude of intensity of the turbulence in the wake after a flame-holder without combustion and in combustion products on the axis of a flame greatly depends on dimensions of flame-holder), where values of u_T after flame-holders and burners coincide. During a survey of values of u_T found after flame-holders and their comparison with values of u_T obtained in flames after ignition sources with "zero" dimensions (burners) (see § 7, Chapter V), there is composed the idea that boundaries of a flame after a flame-holder move through the fresh mixture with a velocity, determined by the structure of turbulence of the incident flow; thus, directly after the burning zone, turbulence can be considerably different from turbulence of the incident flow and turbulence in the wake after a flame-holder without burning. In § 5 it was shown that this is fully possible in virtue of the discontinuity of average and fluctuating values of hydrodynamic parameters (selectively averaged over the fresh mixture and combustion products) which exists during burning.

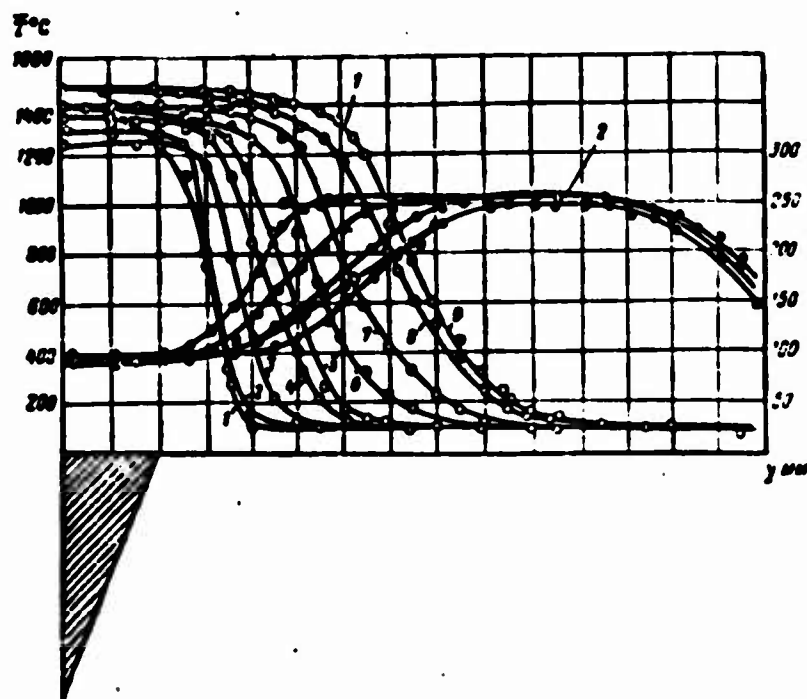


Fig. 5.29. Temperatures profiles (curve 1) and total head profiles (curve 2) after a flame-holder in a pipe (data of Solntsev). 1) 50 mm, 2) 100, 3) 150, 4) 250, 5) 400 mm, 6) 550, 7) 700, 8) 850.

We will now consider peculiarities of measurement of the speed of turbulent combustion u_T along average boundaries of a turbulent flame after a flame-holder, first for a flame in an open flow. In the absence of a pressure drop along the open

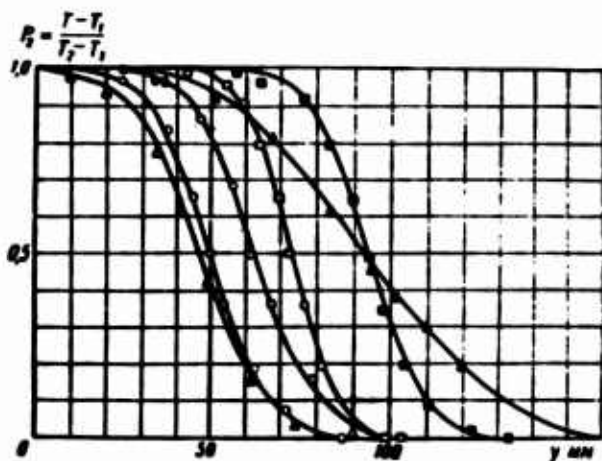


Fig. 9.30. Probability distribution of finding combustion products (physical combustion efficiency) over cross sections of flames after flame-holder in a pipe and in an open flow.

○, ● — data of Solntsev,
□, ■ — data of Bessalov,
Δ, ▲ — data of Shcherbina.

the open flame, combustion products in it expand not longitudinally along the basic flow, but transverse to it. Thus the average boundaries of combustion products after the flame-holder may be expanded not only toward the fresh mixture, but toward the flame-holder axis, filling the space formed behind the flame-holder.

The lower average boundary, which is arbitrarily called the line of constant consumption starts at the edge of the flame-holder, and further, passing around the recirculation zone, approaches the axis of the flame-holder, coinciding with the latter at infinity.

The component of average flow velocity which is normal to this line is by definition equal to zero. For a flame after an ignition source of zero dimension, this boundary coincides with the axis of the flame, and therefore is not specially distinguished in examining of the latter.

The upper average boundary starts at the edge of the flame-holder and extends toward the fresh mixture. In the region, located above the lower average boundary at a certain distance from the flame-holder, the longitudinal component of average velocity remains approximately constant longitudinally along, as well as transverse to the open flame, and is approximately equal to the average longitudinal flow velocity v , so that the pattern of development of the turbulent flame will be practically identical to the earlier considered case of an open flame after a burner, with only the difference that average increase of volumes of combustion products must be calculated taking into account change of the two average-boundaries — the upper and lower.

Determination of the lower average boundary is the most complicated. For sufficiently large distances (> 3 to $4d_{CT}$), when this boundary practically coincides with the axis of the flame-holder, burning rate can be found by the expression

$$\frac{u_1 T_1}{u T_1} \approx \frac{y(x)}{x},$$

where $y(x)$ is the ordinate of the upper average boundary, measured from the flame-holder axis;

v is the average longitudinal component of velocity.

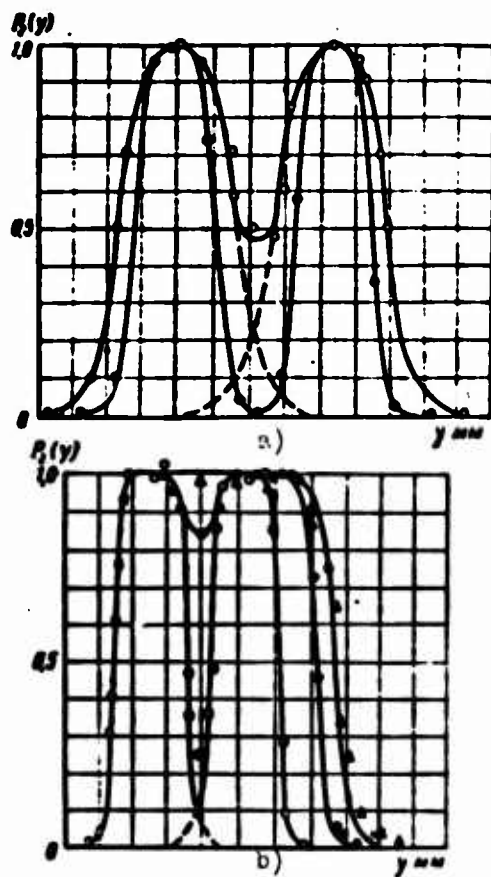


Fig. 5.31. Combination of two flames. Comparison of theory with experiment (turbulent flame between two flame-holders).

- a) data of Bespalov, $2a_0 = 40$ mm, $v = 90$ m/sec, $\alpha = 1.4$ (homogeneous mixture),
 ● — $x = 200$,
 ○ — $x = 400$ } experiment, — theory,
 b) data of Bespalov: $2a_0 = 20$ mm, $v = 70$ m/sec, $\alpha = 1.4$ (heterogeneous mixture),
 ○ — $x = 80$,
 ● — $x = 100$,
 Δ — $x = 300$.

At very large distances from the flame-holder, when the dimension of the flame-holder does not play a role in the value of $y(x)$, determination of the quantity u_T/v can be performed just as in the case of burners, according to the slope of the upper average boundary of the flame. Values of u_T determined taking into account the noted systematic peculiarities for a turbulent flame after a flame-holder in an open flow coincide with corresponding values of u_T measured in flames after burners (see § 7).

In Fig. 5.6 there are given average boundaries and dispersion of a turbulent flame after a single flame-holder in a pipe, calculated according to [34]. From Fig. 5.6 it is clear that average boundaries of the flame after flame-holders of

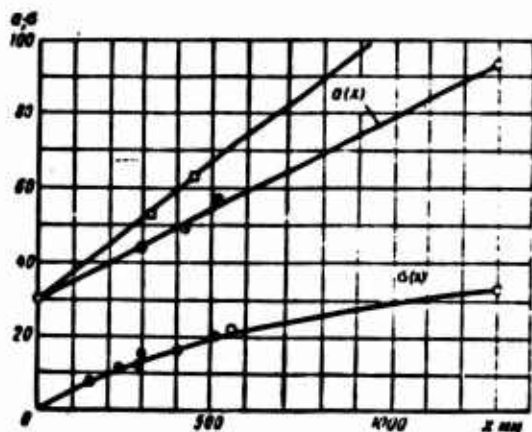


Fig. 5.32. Distribution of the mean $a(x)$ and dispersion σ^2 of a flame after a flame-holder. Data of Fisherbina: $v = 26$ m/sec, $\alpha = 1.48$, $\alpha = 1.80$, $\sigma = \sqrt{\sigma^2}$.

various dimensions and various angles at the vertex occur practically in parallel with each other, with the same slope to the direction of the incident flow. The intensities of turbulence of the incident flow, according to measurements by hot-wire anemometer, were in all cases identical and equal approximately to the steady-state level of pipe turbulence (4 to 5%). From Fig. 5.6 it is clear that the same values of intensity of the turbulence are obtained from calculations with the dispersion function. For decrease of the influence of averaging errors of the thermocouple, function $\sigma(x)$ was calculated over the lower

half of the profile of average temperatures. Dispersion functions $\sigma(x)$ for all three flame-holders are practically identical, and coincide with the dispersion of turbulent diffusion of the incident flow. The understating of the value of $\sigma(x)$ at large lengths of the flame after a flame-holder with diameter of 70 mm can be explained by the contraction of the flow of fresh mixture during approach of boundaries of the flame to walls of the pipe (by increase of average velocity of the incident flow along the pipe).

Possibly for this reason, for function $a(x)$ of this flame there is noticed a weak inflection [weak decrease of the slope of function $a(x)$]. Let us note that

"such an understatement" is also fully possible due to errors in the calculation of points. The straight lines of the average boundaries $a(x)$, as one may see from Fig. 5.6, converge not to the edge of the flame-holder, but in the region of the stagnant wake after the flame-holder. For flame-holders with diameter $d = 35$ mm and angle at the vertex of the cone of 30° , the distance from the edge of the flame-holder to the point of intersection of the average boundary with the stagnant wake is approximately equal to 150 mm. For a stabilizer with diameter of 35 mm and angle of 60° , and for a stabilizer with a diameter of 70 mm and angle of 30° , this distance is noticeably shorter, and is equal approximately to 100 mm. At this distance, according to our concept, there is formed a turbulent flame front. Conditions for the existence of a burning front in the vortex sheet on the boundary between the stagnant wake and the incident flow of fresh mixture, which is continuously maintained by heat from the combustion products of the stagnant wake, and which is motionless relative to the incident flow, are replaced by conditions for existence of a burning front moving independently toward the incident flow of fresh mixture. At this distance there is answered the question about independent existence of a turbulent flame after a given flame-holder. Therefore, the magnitude of this distance will depend on the mixture ratio, dimension and shape of the flame-holder, but will never exceed the length of the recirculation zone (stagnant wake) after the flame-holder.

Values of u_T/v calculated according to the average slope of the average boundaries will agree with values of the intensity of turbulence of the incident flow, with corresponding values of u_T/v measured behind flame-holders in an open flow and behind burners (§ 7). This indicates the fact that the flow pattern of fresh mixture in the flame after a flame-holder turns out to be practically the same as in the case of a flame after a linear burner (in a pipe) (see § 5), but both halves of the flame are spaced at the edges of the flame-holder. Mathematically this means that the transverse component of average velocity, averaged selectively only over the fresh mixture, is practically equal to zero at any point of the flame, since by imposing this condition on either of the halves of the flame after the flame-holder, it is possible to arrive, just as in the case of a flame after a linear burner (§ 5), at the formula

$$\frac{da(x)}{dx} = \frac{u_T}{v}.$$

Physically this means that an arbitrary elementary volume of fresh mixture, for instance, passing along the edge of a flame-holder, moves practically parallel to the axis of the pipe without experiencing average deflections to the axis of the turbulent flame until fresh mixture in this volume starts to burn. Elementary volumes of the formed combustion products can then expand and move longitudinally, as well as transversely across the basic flow, thus filling the space after the flame-holder. In practice such a picture of the flow is apparently obtained, because in the process of formation the hydrodynamics of a turbulent flame after a flame-holder, it is easier for forces of pressure and inertia to form a new flow of the light, hot gas which is formed than to change the existing motion of the heavier (with greater inertia) flow of fresh mixture.

With such a consideration another experimental fact becomes more understandable: why dispersion of the turbulent flame after a flame-holder turns out to be practically equal to the root-mean-square turbulent displacements of volumes of fresh mixture.

If the turbulent flame is located after a single flame-holder in the pipe, then there always appears the doubt: is such a flame compressed by the walls of the pipe enough that flow in it can be considered to be the same as in a closed flame. For instance, in the experiments of Shcherbina [24], the turbulent flame is actually open, although it stands in a pipe, but the average boundaries of the flame do not

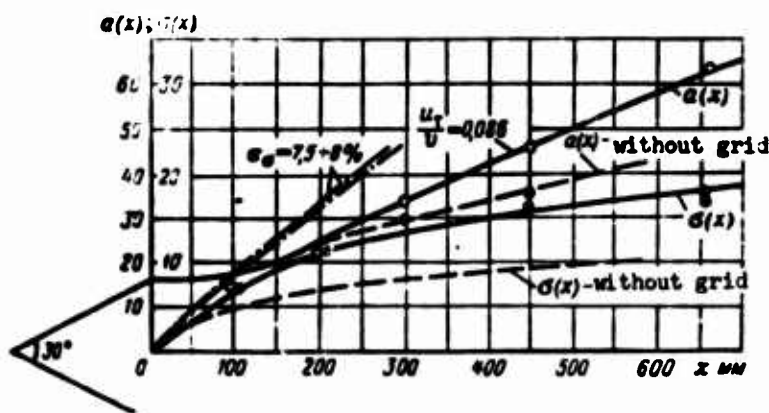


Fig. 1.53. The influence of a turbulence-generating grid before a flame-holder on parameters of the turbulent flame.

Grid $b=10$ mm, $\gamma_{TA}=13\pm 5\%$, $\alpha=1.5$, $T_1=80^\circ\text{C}$, $T_2=1160^\circ\text{C}$, $v=30$ m/sec, $2A=35$ mm.

cover the entire cross section of the pipe. Therefore, it is expediently to consider parameters of turbulent flames after a group of stabilizers in a pipe, when it is surely possible to speak about a closed flame. In Fig. 5.7 there are given graphs of functions of the mean $a(x)$ and dispersion $\sigma(x)$, which were calculated over fields of average temperatures with

group placement of flame-holders according to data of Solntsev. Comparing these data with the same data, but after a single flame-holders (presented in Fig. 5.7),

it is possible to see that values of u_T/v and u'/v calculated according to the mean and the dispersion practically coincide; i.e., the given data after a single stabilizer indeed pertain to the case of burning of a flame in a pipe.

Till now there have been presented cases when turbulence of the incident flow was practically equal to pipe turbulence: the intensity of turbulence of the incident flow oscillated moreover in dependence on the accuracy of calculation and measurements, and also on small local contraction of the flow within the range of values ~ 3 to 5% . In Fig. 5.33 and 5.34 there are given graphs of functions of the mean and the dispersion of a flame in that case when before the flame-holder there is installed a turbulence-generating grid. The largest value of intensity of turbulence after the grids, shown in Fig. 5.33 and 5.34, were equal to 13 and 20% . In the plane of location of the flame-holders, values of intensity of turbulence were essentially smaller; at the end of the flame they decreased to values of pipe turbulence $\sim 5\%$. Effective values of intensity of turbulence of the incident flow at the beginning of the flame can most accurately be judged by values of u'/v calculated according to dispersion of the flame.

From Fig. 5.33 and 5.34, it is seen that average values of u_T/v at the beginning of the flame correspond to values of the intensity of turbulence of the incident flow at the beginning of the flame (according to data of Solntsev at $\epsilon \approx 7$ to 12% , $u_T/v \approx 0.07$ to 0.1). With decrease of the value of ϵ along the flame, the quantity u_T/v also decreases. This is especially noticeable for a stronger turbulizing grid, for which the difference between values of intensity of turbulence at the beginning and at the end of the flame is greater. In Fig. 5.33 and 5.34 there is also seen a large difference between values of the mean and the dispersion of the flame after a flame-holder with grid and without grid. However, this difference, as can be seen, is fully explained by the difference between levels of turbulence of the incident flow.

Thus, parameters of a turbulent flame after a flame-holder are completely determined by turbulence of the incident flow. It is possible once again to be convinced of this by considering two other specific forms of the influence of turbulence of the incident flow. This is the influence of local increases and decreases of turbulence of the fresh mixture on parameters of a turbulent flame after a flame-holder. In Fig. 5.27 there are given graphs of functions $a(x)$ and $\sigma(x)$ after a flame-holder with protrusions. This flame-holder can be considered as a flame-holder with diameter of 35 mm on which there is set a small turbulizing

grid with a height of 70 mm, which gives in the region of the flame-holder a local increase of turbulence of the incident flow. What is obtained after such a flame-holder may be seen from Fig. 5.27. In the region of the flame-holder there is observed a noticeable increase of magnitude u_T corresponding to the local raised value of intensity of turbulence, calculated according to the dispersion. After the

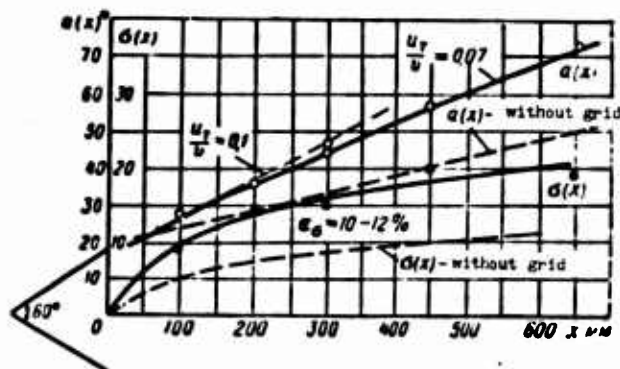


Fig. 5.34. The influence of a turbulizing grid before the flame-holder on parameters of a turbulent flame. Grid $b = 15$ (mm), $\epsilon_{YTA} = 20\%$ to 5% , $\alpha = 1.5$, $T_1 = 100^\circ\text{C}$, $T_2 = 1320^\circ\text{C}$, $v = 50$ m/sec, $2h = 35$ (mm).

average boundary of the flame passes beyond the bounds of the region of the local raised value of intensity of turbulence, the magnitude of u_T/v takes a value corresponding to turbulence of the incident, undisturbed flow. The average boundary of the flame is obtained to be in the form of a broken line.

In Fig. 5.35 there are given contours of the average boundaries of flames when there is considerable

blockage of the section of the chamber by flame-holders. With such blockage, average flow velocities of the fresh mixture between flame-holders turn out to be much larger

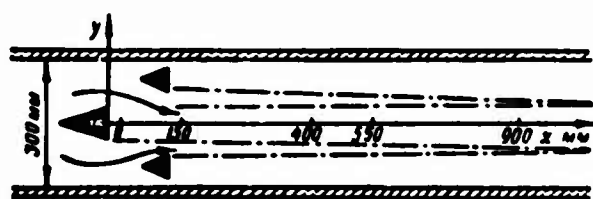


Fig. 5.35. Influence of blockage of the section of a chamber by flame-holders (flow contraction) on parameters of a turbulent flame.

$$\frac{u_T}{v} = 0.03$$

turn out to be noticeably lower. Values of $\sigma(x)$ also turn out to be lower. The effect of bringing the two flame-holders closer together was investigated in detail by Bespalov (see Chapter VII). According to his data, the dependence of decrease of the value of u_T with decrease of the gap between flame-holders is still more noticeable. However, this dependence may also be explained by deflection of the aerodynamic axes of the flame during their approach which was possible in the experiments of Bespalov.

than the average velocity before the flame-holders. Due to contraction of the flow, the intensity of turbulence between the flame-holders considerably decreases (approximately in the ratio of the average velocities in the narrow place and before it). Values of u_T/v , as can be seen from Fig. 5.35, then

The two given examples suggest the possibility of obtaining much shorter chambers, with larger mean values of u_T , if we alternate grids of flame-holders with combustion and without combustion. The grid of flame-holders without combustion must be set at a distance upstream somewhat larger than the length of zone of counter currents so that the flame will not jump into the recirculation zones of these flame-holders, in such a manner that the wake of increased turbulence after the flame-holder without combustion falls exactly within the space between the flame-holders without burning will be used to the full extent for the intensification of the burning process. All necessary rough engineering calculations can be performed using data given in this paragraph and in § 7.

We will consider one more hydrodynamic peculiarity of burning after a flame-holder. The profile of average temperatures along the axis of a flame, as is known from many experimental data, including those data of Solntsev analyzed here,

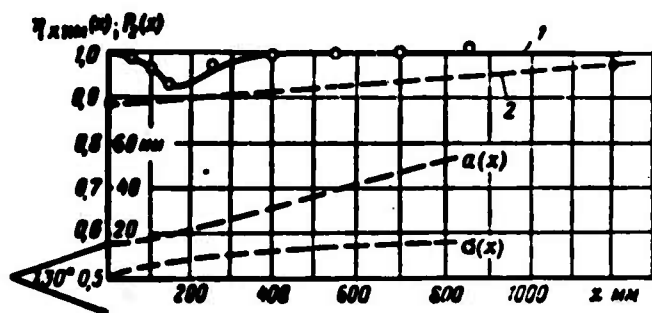


Fig. 5.36. Physical and chemical combustion efficiencies along the axis of a flame after a single flame-holder in a pipe.

1) theory; 2) $\frac{a}{\sigma} = 1.9$; $\varepsilon \approx 6\%$ $\rho_{r-} \left(1 - \frac{\sigma^2}{2\beta^2}\right)$.

undergoes unique dip in values of temperatures somewhere in region of the recirculation zone. There appears the question: is it possible to explain this dip by a simple relationship between values of $a(x)$ and $\sigma(x)$ calculated according to turbulence of the incident flow, or is this dip explained by some specific

peculiarities of the hydrodynamics

of large eddies in the recirculation zone inherent only to the flame-holder? In Fig. 5.36 there is given an example of calculation of physical combustion efficiency along the axis of a flame $P_2(x)$ and comparison of it with the theoretically calculated function $P_2(x)$ according to assigned values of $a(x)$ and $\sigma(x)$. Chemical combustion efficiency was determined by the ratio of temperature at the end of the flame to the adiabatic temperature for the given mixture ratio. In experiments of Solntsev, this efficiency oscillated within the interval of values $\eta_{XVM}(\infty) = 0.95$ to 0.96 . Likewise, according to values of temperatures on the axis of the flame near the flame-holder (practically in the stagnant wake), there was determined chemical combustion efficiency in the beginning of the flame. It, as should have

been expected, was somewhat lower (~ 0.885). Through these two points it is possible to draw a graph of the monostonic function $\eta_{xMM}(x)$, which is shown on Fig. 5.36 by the dotted line. According to the graph of average temperatures $\bar{T}(x)$ and the graph of $\eta_{xMM}(x)$ there was calculated the function of physical combustion efficiency $P_2(x)$; the maximum dip of this function at $x = 150$ mm can be explained if we substitute values of $a(x)$ and $\sigma(x)$ determined earlier by an independent method for the given value of x .

In Fig. 5.36, through experimental points of the function $P_2(x)$, there is drawn a theoretical curve with parameters $a(x)$ and $\sigma(x)$ of the theoretical value of $P_2(x)$ which were given earlier. It is possible to explain the dip by existing values of functions $a(x)$ and $\sigma(x)$. The value of the "dip" given in Fig. 5.36 was the largest in the experiments of Solntsev. All other values were less. In general, the magnitude of this dip can be noticeably larger, especially in pre-separation regimes of burning, when the average boundaries of the flame converge at the end of the recirculation zone [the magnitude of $a(x)$ in these cases may be noticeably less than the half-width of the flame-holder, and comparable with the magnitude of the dispersion $\sigma(s)$].

§ 7. EMPIRICAL DEPENDENCES OF THE SPEED OF TURBULENT COMBUSTION ON PARAMETERS OF TURBULENCE; COMPOSITION OF THE MIXTURE AND PRESSURE

Earlier it was noted that the overwhelming majority of Soviet investigators of turbulent combustion determined not the speed of turbulent combustion measured according to the speed of growth of the mean-statistical boundary of the turbulent flame, but the speed of turbulent propagation of the flame measured according to the speed of growth of the "front" boundary of the flame. This error was a logical result of the erroneous opinion that width of the macrozone of a turbulent flame is stationary since with stationary width of the zone it makes no difference which boundary is used to measure the velocity of propagation of the flame into the fresh mixture: any of these speeds will determine the burning speed of the fresh mixture.

With such a definition of burning speed, experimenters did not note a series of other remarkable properties of the speed of turbulent combustion u_T : its relatively small magnitude, which is fully explainable by turbulence of the incident flow; its stationarity for uniform turbulence when width of the macrozone is non-stationary; the "rapid response" of the magnitude u_T during fast changes of turbulence (see § 6, Chapter V); the possible decrease of the value of u_T by large-scale

turbulence to values, noticeably smaller than the speed of laminar burning u_H ; the universality of parameter u_T ; and, finally, the existence of limits of propagation of a stationary turbulent flame front for a strongly developed local structure of turbulence. Let us note, however, that the last fact recently was reflected in a number of experimental works [38], [39]. For determination of parameters of a turbulent flame there were used experimental materials of Besspalov, Vlasov, Lushp, Solntsev, Talantov and Khramtsova.* According to experimental functions $\sigma(x)$ there were determined values of intensity of turbulence and diffusion coefficient; in all cases they appeared to be equal to corresponding parameters of the incident flow measured directly. Therefore, in all those cases when independent measurements of turbulence were not conducted, parameters of turbulence calculated according to function $\sigma(x)$ were taken as parameters of turbulence of the incident flow. Values of u'/v and D_T/v calculated according to profiles of average temperatures measured by thermocouple may be somewhat understated due to errors from averaging by the thermocouple [41].** This error will be minimum during calculation of $\sigma(x)$ according to the lower half of the profile of average temperatures. Values of D_T/v calculated according to $\sigma(x)$ of a flame in a pipe may be somewhat understated due to possible decrease of growth of $\sigma(x)$ during acceleration of flow in the pipe (see § 5). Values of D_T/v calculated according to $\sigma(x)$ of the flame of a Funsen burner may be somewhat exaggerated due to increase of the level of turbulence at the end of the flame, when the latter goes beyond the limits of the core of constant turbulent velocities. However, comparisons of values of u'/v and D_T/v calculated according to $\sigma(x)$ with values given by direct measurements of u'/v and D_T/v under these conditions indicate that the magnitudes of the above mentioned errors are small in practice, so that these values, with the indicated reservations, can be taken as parameters of turbulence of the incident flow in the case when direct measurements are absent, or the accuracy of these measurements is less reliable.

The value of u_T/v was determined according to the function of the mean $a(x)$. In all cases, without exception, when it was possible to guarantee homogeneity of turbulence across (transverse to) the flow, the value of u_T/v remained constant along

*K. P. Vlasov and Yu. A. Sncherbina participated in selection and analysis of the gathered material.

**The highest accuracy is given by calculation of $\sigma(x)$ according to fields of velocity head of the flame in an open flow.

the flame [functions $a(x)$ were straight lines]. Error in determination of u_T/v and $u_T T_2/vT_1$ according to function $a(x)$, and determination of function $a(x)$ according to profiles of average parameters turns out to be much smaller than corresponding errors during calculation of u'/v ; D_T/v and $a(x)$ by any methods of measurement of the distribution of average parameters. The largest error in determination of u_T/v from $u_T T_2/vT_1$ for the inverted cone of flame turns out to be during calculation of the magnitude T_2/T_1 . For a flame in a pipe, corrections for expansion do not have to be introduced, but it is necessary to be sure that the flame is indeed located within the pipe.

In Table 5.1 there are given results of processing of the data of Vlasov, Lushp, Inozemtsev and Scherbina. Values of intensity of turbulence $\epsilon\%$ calculated according to ϵ , measured by a hot-wire anemometer [HWA] (YTA) and by the optical-diffusion method [ODM] (ODM) are designated accordingly by ϵ_0 ; ϵ_{YTA} ; ϵ_{ODM} . Values of measured temperatures T_1 and T_2 are also entered in the table with indication of their method of measurement. Values of u_T/v turn out to be of the same order for burners and for flame-holders; they, as a rule, are somewhat lower than or equal to corresponding values of the intensity of turbulence of the incident flow (at $u_T > u_H$). Obtained values of u_T/v turn out to be two or three times smaller than corresponding values for velocity of propagation u'/v , since, according to § 5, we have $\frac{u'}{v} \approx \frac{u}{v} + (2 \text{ to } 3) \frac{u'}{v}$, and so forth.

The value of u_T noticeably increases with growth of turbulent velocity of the incident stream u' , and apparently by the same law for any method of change of magnitude u' (by increase of average speed, installation of turbulizing grid or contraction, and so forth). During strong extinguishing of turbulence by a contraction (data of Lushp), the values of u_T turn out to be of the order of u_H or even less than u_H . Let us note that going only the data of Lushp, it is impossible to assert that u_T is less than u_H , inasmuch as it is possible to have doubt about the true value of u_H due to the fact that the regime of burning indicated by the author with respect to α and T_1 was inaccurate, and also due to the noticeable disagreement between absolute values of u_H in the data of various authors. In Table 5.1 there are given data on u_H according to Inozemtsev, which for the regime indicated by Lushp with respect to α and T_1 are larger than values of u_T measured according to the magnitude $da/dx = u_T T_2/T_1 v$ at the minimum possible values of T_2/T_1 . If, however, for determination of u_H we take the data of other authors (Dagger, etc),

then u_T turns out to be somewhat larger than u_H . It is possible, however, to be sure that for a still higher degree of extinguishing of small-scale turbulence, values of u_T will become less than the corresponding speed of laminar burning u_H . If we divide the experimental value of u_T in the experiments of Lushp by the average relative magnitude of the burning surface, then we will obtain a value of the average normal velocity with respect to the burning surface $u_{H.T}$ much smaller u_H , which once again indicates the inconstancy of the magnitude $u_{H.T}$ with respect to the burning surface.

Frequently in the literature there are given curves of combustion efficiency (temperature) along the flow axis between two flames (axis of the flame of a Bunsen burner, axis of flow between edges of two flame-holders, and so forth). By such experimental data it is also possible, with accuracy sufficient for practice, to estimate all necessary parameters of turbulence and the magnitude u_T/v . Really, from geometric considerations and the scheme of statistical addition of turbulent flames between two ignition sources (Fig. 5.37), it is possible to write

$$\frac{u_T}{v} L_0 + 2.5\delta_r(x_0) = a_0 \text{ and } 2.5\delta_r = \delta_r \sin \epsilon \approx \delta_r \lg \epsilon \approx \delta_r \frac{u_T}{v}, \quad (5.66)$$

where a_0 - half of the distance (transverse to the flow) between ignition sources;

L_0 - distance along the flow axis from ignition sources to the beginning of the rise of the profile of average temperatures (height of the inner cone of a Bunsen burner);

δ_T - distance along the flow axis from the point of beginning of the temperature rise to the point of ending of the temperature rise.

The value of coefficient 2.5 corresponds to a 5% deviation of the "beginning point" and "end point" of rise of the profile of average temperatures from the temperatures T_1 and T_2 respectively.

Substituting the second equation in the first, we will obtain

$$\left. \begin{aligned} \frac{u_T}{v} L_0 + \delta_r \frac{u_T}{v} &= a_0; \\ \frac{u_T}{v} &= \frac{a_0}{L_0 + \delta_r} \\ \text{and} \\ \epsilon &\approx \frac{\delta_r \cdot a_0}{2.5(L_0 + \delta_r)} = \frac{\delta_r u_T}{2.5 \cdot v} \end{aligned} \right\} \quad (5.67)$$

Table 5.1. Materials on Turbulent Burning Speed (Data of Vlasov, Lushp, Shcherbina and Solntsev)

λ	T	u_H	v	λ_{mm}	T_{2T}	T_{2mm}	$(\frac{T_2}{T_1})$	$\frac{T_{2T}}{T_1}$	$(\frac{u_T}{v})$	ϵ	ϵ_{YTA}	ϵ_{ODM}	u_T	u'	Ignition source	Author	Note
1.1	200	95	30	0.9		2000	4.2	0.187	0.045	5	5	5	1.3	1.5	Burner in an open flow $d_{TP} \approx 200$ mm	Vlasov	
1.2	200	100	30	0.9		2140	5.0	0.25	0.045	5	5	5	1.54	1.5			
1.1	200	95	45	0.9		2000	4.2	0.165	0.0394	5	5	5	1.78	2.3			
1.2	200	100	45	0.9		2140	5.0	0.187	0.042	5	5	5	1.9	2.3			
1.2	150	70	23	0.95	1780		4.25	0.09	0.021	1.5 to 1.8	1 to 2%		0.5	0.25	Burner in an open flow $d_{TP} \approx 150$ mm	Lushpa	
1.2	150	70	43	0.95	1780		4.25	0.06	0.014	1.5 to 1.8	1 to 2%		0.6	0.64			
1.4	200	70	26	0.86	1530	1650	3.2	0.12	0.038	5		5-6%	1.0	1.3	Flame-holder with $\phi 60$ mm in a pipe with $\phi 400$ mm, axisymmetric	Shcherbina	open flow
1.5	200	48	26	0.8	1420	1960	3.0	0.08	0.027 to 0.03	5		5-6%	0.6	1.3			
1.1	125	42	50	0.95	1780	1860			0.04 to 0.038	6-7	3-6%		3 to 3.5	3 to 3.5	Flame-holder $2h = 75$ mm	Solntsev	Three flame-holders in a pipe. YTA is taken over the contraction section between the flame-holders (grid $b = 10$ and $b = 1$ mm)
1.1	125	42	77	0.95	1780	1860			0.038	4-4.7	2-4%		3.0	3.1 to 3.6			
1.1	125	42	94	0.95	1780	1860			0.03	3.3-3.8			2.8 to 2.6	3.1 to 3.6			
1.1	125	48	50	0.90	1680	1860			0.04	4-5.0	~1%		2.0	2.5			
1.1	125	48	50	0.9	1680	1860			0.086	7-8.0	~20%		3.3	4.0			
1.1	125	48	50	0.9	1680	1860			0.09 to 0.07	10-12			4.0	5.0			

The first equation gives a certain average value of u_T/v over the length of the flame. Let us note that velocity of propagation then is determined by the quantity $u_T/v \approx a_0/\bar{L}_\phi$. The accuracy of determination of u_T/v by this equation turns out to be higher, the less the influence of mixing of the flame with the surrounding air. During strong mixing (for instance, at low pressures in the stream), the measured value of δ_T can be noticeably understated, and the value of u_T due to this can be noticeably exaggerated. The second equation gives the value of σ for a certain average value of x_{op} between values of \bar{L}_ϕ and $\bar{L}_\phi + \delta_T$. For very short flames (u_T/v is large, δ_T is small), according to the value of σ it is possible to give an estimate of the magnitude of intensity of turbulence of the incident flow, after writing according to Taylor's equation:

$$\frac{\sigma'}{\sigma} \approx \frac{\sigma}{L_\phi} \approx \frac{\delta_T \cdot u_T}{2.5 \bar{L}_\phi \cdot v}. \quad (5.68)$$

and for sufficiently long flames (u_T/v is small; and δ_T is large), it is possible to estimate the coefficient of turbulent diffusion, using the other limiting solution of Taylors equation:

$$\frac{D_T}{v} \approx \frac{\sigma^2}{2(L_\phi + \frac{\sigma_T}{2})} = \frac{1}{2(L_\phi + \frac{\delta_T}{2})} \left(\frac{\delta_T \cdot u_T}{2.5 \cdot v} \right)^2. \quad (5.69)$$

Data of Talantov and Bepalov processed with the help of the given relations are given in Tables 5.2 and 5.3.

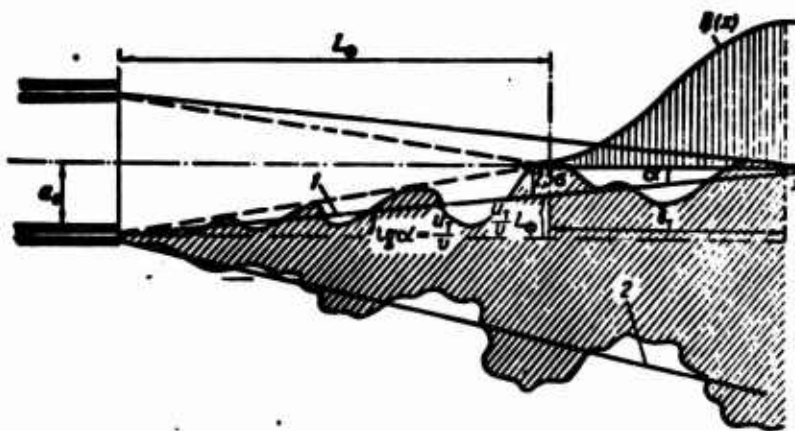


Fig. 5.37. Determination of parameters of a flame according to the profile of combustion efficiency along the axis of a Bunsen burner.

$$\frac{u_T}{v} = \frac{a_0}{L_\phi + l_T}; \quad \sigma = \frac{l_T \cdot a_0}{2.5(L_\phi + l_T)}.$$

1) flame front; 2) average external boundary of combustion products.

From the given tables it is clear that values of u'/v calculated according to σ practically coincide with values of u'/v measured by hot-wire anemometers. The certain insignificant understating of values of ε_0 as compared to values of ε_{TA} can be explained by the above mentioned systematic errors in the determination of quantity ε_0 (by the large value of x). The value of $D_T/2a_0v$ calculated according to σ from data of Talantov coincides with the corresponding value for pipe turbulence measured directly by the optical-diffusion method (see Chapter IV).

Values of u_T/v for corresponding values of average speeds and mixture ratio coincide with the data of Flazov and Solntsev given earlier. In Table 5.2 for comparison there are given values of u_T'/v and of \bar{L}_ϕ and δ_T , according to which the ratios u_T/v and u_T'/v were determined.

From the given data one may also see that u_T/v practically does not depend on the shape of the flame-holder (see Table 5.3), decreases with increase of average flow velocity and increases with increase of the magnitude u_H . The dependence of u_T/v on average flow velocity is represented in Fig. 5.38. The character of the dependence of u_T/v on average velocity v for $\varepsilon = 3$ to 5% according to data of all authors is identical; for strictly identical values of parameters of turbulence and identical properties of the mixture, all data can apparently be plotted on one curve. From the curves shown in Fig. 5.38, it is clear that the exponent of average flow velocity in the dependence of u_T on average flow velocity increases continuously from 0.6 to 0.7 and higher in accordance with the theory. The character of the dependence of u_T/v on u_H according to data of all authors is qualitatively identical, but the quantitative disagreement between data of Talantov and that of the other authors is quite pronounced. According to data of Besaplov, Vlasov and Khramtsov (see Table 5.4), the value of u_T/v increases with increase of u_H taken to a much smaller power than according to Talantov (see Table 5.2). Disagreement between the data of Talantov and that of other authors can first of all be explained, in our opinion, by the understated values of u_H indicated in the work of Talantov. For all of the other authors, there were used data of Inozemtsev of u_H measured approximately under the same conditions; if, however, these data have a certain absolute error, then the relative error arising during comparison of data of all of the authors turns out to be small. The stronger dependence of u_T/v on u_H and higher values of u_T/v according to Talantov can be partially explained by two other circumstances: by considerably smaller values of average velocities and considerably smaller scales of turbulence. For instance, at an average flow velocity of 5 m/sec, the value of

Table 5.2. Materials on Turbulent Burning Speed (Data of Talantov)

u_H cm/sec	v m/sec	L_ϕ mm	δ_T mm	$\frac{u_T}{v} = \frac{d_0}{L_\phi + \delta_T}$	u_T cm/sec	$\epsilon_\sigma \sim \frac{\delta_T + u_T}{2.5L_\phi v}$ %	ϵ_{YTA} %	$\frac{D}{2vd_0}$ according to σ	u' cm/sec	$\frac{u_T}{u_H}$	$\frac{u_T}{v}$	Note
20	5	111	140	0.06	40	~4.1	5	-	25	2.0	0.18	Smooth pipe, 40 x 40 mm, $a_0 = 20$ mm. Right cone of flame, $\alpha = 1.0$ to 1.5. There are given, apparently, greatly understated values of u_H
20	10	133	193	0.06	60	~4.1	5	-	50	3.0	0.15	
20	20	174	250	0.047	94	~4.1	5	-	100	4.7	0.115	
20	30	177	300	0.042	126	~4.1	5	-	150	6.3	0.113	
20	40	200	330	0.038	150	~4.1	5	-	200	7.5	0.1	
20	50	200	356	0.036	180	~4.1	5	0.001	250	9.0	0.1	
30	5	105	110	0.093	46	~4.0	5	0.001	25	1.55	0.29	
30	10	125	160	0.07	70	~4.0	5	0.001	50	2.3	0.16	
30	20	130	210	0.06	120	~4.0	5	0.001	100	4.0	0.15	
30	30	150	250	0.05	150	~4.0	5	0.001	150	5.0	0.133	
30	40	160	280	0.0455	180	~4.0	5	0.001	200	6.0	0.125	
30	50	170	312	0.042	210	~4.0	5	0.001	250	7.0	0.118	
40	5	100	90	0.105	52	~4.0	5	0.001	25	1.3	0.2	
40	10	100	120	0.091	91	~4.0	5	0.001	50	2.3	0.2	
40	20	121	180	0.067	135	~4.0	5	0.001	100	3.4	0.165	
40	30	136	212	0.058	174	~4.0	5	0.001	150	4.3	0.147	
40	40	146	240	0.052	210	~4.0	5	0.001	200	5.2	0.137	
40	50	154	260	0.048	240	~4.0	5	0.001	250	6.0	0.13	
40	20	50.5	140	0.105	210	12.0	15	0.003	300	5.2	0.37	There is installed a turbulizing grid, $K =$ $= 8$ mm in the pipe
40	30	59.1	170	0.087	260	12.0	15	0.003	450	6.5	0.32	
40	40	64	198	0.076	305	12.0	15	0.003	600	7.6	0.30	
40	50	72	225	0.068	337	12.0	15	0.003	750	8.5	0.27	

u_H/v changes according to Talantov within the interval of values 0.04 to 0.08, which comprises the overwhelmingly larger part of the quantity u_T/v . If we subtract from all values of u_T/v the values of u_H/v corresponding to them, then the data of Talantov will lie practically on the same curve of $(u_T - u_H)/v$ versus u_H , but this curve will nevertheless pass above the one given by the other authors. Let us note that due to the large magnitude of u_H/v at small average velocities, curves of u_T/v versus v (see Fig. 5.38) go steeply upwards with decrease of average velocity. Scales of turbulence in the experiments of Talantov were approximately five times less than the corresponding scales in experiments of the other authors. Although the dependence of u_T/v on scale is relatively weak, this could also lead to a certain noticeable increase of values of u_T/v in the experiments of Talantov.

Data of Besspalov are interesting because of the wider indicated range of change of properties of the fresh mixture. If we consider the possible causes of disagreement of data of various authors, including here the considerable errors of the given approximate calculation of u_T/v , then it is possible to plot the most probable curve of absolute values of u_T/v versus v and u_H ; this curve will pass somewhere in range of values of Solntsev, Vlasov and Khramtsov.


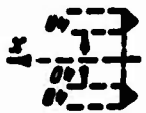
The given graphic dependences can be transformed to an analytic dependence which is more convenient for engineering calculation:

$$u_T \sim A \cdot u^{0.7} \cdot u_H^{0.3}. \quad (5.70)$$

where $A \approx 1$ (minimum value of A , according to data of Besspalov, equal to 0.7).

Values of u_H are taken according to data of Inozemtsev for gasoline-air mixtures. Let us note that the given dependence is useful only for technical calculations of burning of lean mixtures, inasmuch as it reflects the physical content of turbulent combustion only in approximate form. For instance, all of the complicated dependences on T_1 and T_2 in terms of the parameters T_2/T_1 ; D_M ; u_H , etc., are expressed in this relationship only in terms of the parameter u_H . Formally this can be done only because the given parameters are physically related with each other, consequently they are analytically related. Change of the value of T_2 with mixture ratio turns out to be similar to the change of u_H , so that it is still not exactly known why the value of u_T changes with mixture ratio similarly to u_H : due to change of the actual value of u_H or the value of T_2 , besides change of u_H . To this question there was dedicated a special experimental investigation by Sokolik and Karpov [39]. For technical calculations all these fine points turn out to be

Table 5.3. Materials on Turbulent Burning Rate (Data of Bespalov)

α	T_1 °C	u_H cm/sec	v cm/sec	$\frac{u_T}{u_H}$	$\left(\frac{u_T}{v}\right)$	ε_σ %	ε_{TA} and ε_{DM} %	u_T m/sec	u' m/sec	Source of ignition	Notes
1.3	300	120	90	2.3	0.31	3 to 4		2.77	3.6		Form of stabilizer has practically no effect
1.35	600	270	90	1.35	0.04	3 to 4		3.6	3.6		
1.3	300	120	90	2.7	0.036	3 to 4		3.3	3.6		
1.42	300	115	90	2.3	0.0294	3 to 4		2.64	3.6		
1.4	200	75	92	2.80	0.0235	3 - 4	Not measured	2.1	3.7		The dependence of u_T on T_1 and u_H is evident
1.4	300	117	92	2.14	0.0276	3 - 4		2.5	3.7		
1.4	400	160	92	1.81	0.0323	3 - 4		2.9	3.7		
1.4	500	215	92	1.53	0.0367	3 - 4		3.3	3.7		
1.4	600	272	92	1.32	0.040	3 - 4		3.6	3.7		
1.4	200	75	65	2.48	0.0274	3 - 4		1.78	2.0		Dependence on T_1 is evident. It is also evident that with a growth in v the value of u_T/v drops somewhat
1.4	300	117	65	1.660	0.0299	3 - 4		1.945	2.0		
1.4	400	160	65	1.4	0.0364	3 - 4		2.37	2.0		
1.5	400	185	96	1.7	0.345	3 - 4		3.31	3.8		Dependence on α is evident
1.4	400	160	96	1.91	0.0317	3 - 4		3.05	3.8		
1.69	400	133	96	2.1	0.0285	3 - 4		2.74	3.8		
2.0	400	100	96	2.5	0.026	3 - 4		2.5	3.8		
1.4	400	160	64	1.4	0.0357			2.28	2.5		Dependence on v is evident
1.4	400	160	65	1.4.	0.0364			2.37	2.6		
1.4	400	160	96	1.9	0.0317			3.05	3.8		
1.4	400	160	92	1.81	0.0323			2.9	3.7		
1.4	400	160	138	2.46	0.0286			3.94	5.5		

immaterial as long as it is possible to express them formally mathematically by a dependence on any one parameter T_1 ; T_2 or u_H . The difference between empirical coefficients in relations of such type can appear only with considerable change of the physico-chemical side of the process: with essential change of type of fuel, value of D_M , a , ν , and so forth.

Likewise with the help of the above obtained relationships, there were processed the data of Khramtsov [40]. According to values of \bar{T}_ϕ and δ_T given in work [40] we can determine the speed of turbulent burning u_T which is of interesting and estimate by the calculated value of σ the average values of the parameters of turbulence along the length of the flame. From the systematic errors of such calculation, in our opinion only one error will be important in the determination of value of δ_T . The fact is that due to strong agitation of the submerged stream in the limited volume of the pressure chamber, temperature along the axis of the flame in experiments of Khramtsov attained the greatest value (much smaller than the value of the temperature of combustion products) and further began to drop along the axis of the flame due to mixing with the surrounding air. Thus, values of δ_T measured by Khramtsov from point of beginning of rise to the point of end of rise of the profile of average temperatures turn out to be too low as compared to the values of δ_T contained in relationships (5.66) and (5.67), which were derived taking into account mixing. This gives a certain exaggeration of the value of u_T/ν , which does not exceed, however, according to our estimates 5 to 15%. This error will show up more in the determination of σ_{cp} . Results of calculations of corresponding parameters according to data of Khramtsov are given in Table 5.4.

Intensity of turbulence calculated according to σ_{cp} is not given, since it is obtained to be greatly understated for two reasons: from large values of $x_{cp} \approx \bar{T}_\phi$ at which the first limiting equation of Taylor is inapplicable, and due to understated values of δ_T . For those values of \bar{T}_ϕ which were observed in the experiments of Khramtsova, it is possible to estimate only the ratio D/ν , which is the average over the length of the flame (see Table 5.4). For comparison, in the same place there are given values of D/ν measured after the grid in the beginning of the flame. From their comparison it is clear that D/ν measured directly behind the grid at distances smaller than 100 mm from the beginning of the flame turn out to be much larger than D/ν measured at the end of the flame according to σ ; so much larger that this difference cannot be explained by the understated values of δ_T , obtained due to agitation at the end of the flame. This can be explained only by the

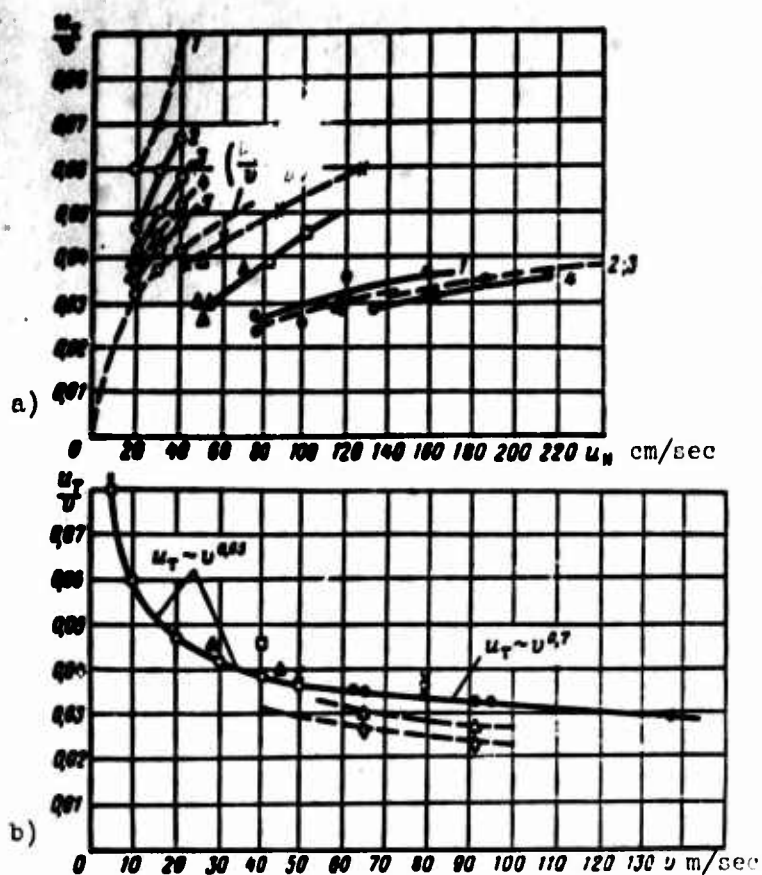


Fig. 5.38. Dependence of $\frac{u_T}{v}$ on average flow velocity.

a) dependence of u_T/v on $u_H(T_1)$ Data of Talantov
 $\epsilon \approx 5\%$

Data of Bespalov:

$$\bullet - \begin{cases} 1 - v = 65 \text{ m/sec} \\ 2 - v = 90 \text{ m/sec} \\ 3 - v = 92 \text{ m/sec} \\ 4 - v = 96 \text{ m/sec} \end{cases} \quad \circ - \begin{cases} 1 - v = 10 \text{ m/sec} \\ 2 - v = 20 \text{ m/sec} \\ 3 - v = 30 \text{ m/sec} \\ 4 - v = 40 \text{ m/sec} \\ 5 - v = 50 \text{ m/sec} \end{cases}$$

$\Delta \epsilon \approx 3 \text{ to } 4\%$

$v = 50 \text{ m/sec}$ $\alpha = 1.5$ (Solntsev) $\square - \epsilon = 5\%$: $v = 45 \text{ m/sec}$; $\alpha = 0.9 - 1.1$ (Vlasov); $X - \epsilon = 13-15\%$; $p = 0.6$; $v = 40 \text{ m/sec}$; $\alpha = 1.4$ - data of Khramtsov; $\blacktriangle - \epsilon = 5\%$: $v = 26 \text{ m/sec}$; $\alpha = 1.48$; $\alpha = 1.8$ - data of Shcherbina;

b) dependence of u_T/v on average flow velocity;

$\circ -$ (Talantov) $\alpha = 1.5$, $t = 30^\circ\text{C}$;
 $\bullet -$ (Bespalov) $\alpha = 1.4$, $t = 400^\circ\text{C}$;
 $X -$ (Solntsev) $\alpha = 1.5$, $t = 100^\circ\text{C}$;
 $\blacktriangle -$ (Vlasov) $\alpha = 1.1$, $t = 200^\circ\text{C}$;
 $\diamond -$ (Bespalov) $\alpha = 1.4$, $t = 200^\circ\text{C}$;
 $\Delta -$ (Bespalov) $\alpha = 1.4$, $t = 300^\circ\text{C}$;
 $\square -$ (Khramtsov) $\alpha = 1.4$, $t = 100^\circ\text{C}$.

fact that at the end of the flame, parameters of turbulence turn out to be much smaller than directly after the grid; they apparently are equal to, or even less than the limiting level of pipe turbulence. The value of D/v calculated according to the value of δ_T coincides with the magnitude of pipe turbulence if we only consider δ_T is understated by 1.5 to 2 times due to agitation (mixing). According to our estimates, understatement of δ_T in the experiments of Khramtsov is obtained to be of such an order of magnitude.

On the basis of these data, we can make the conclusion that effective (average over the length of the flame) parameters of turbulence are not equal to the arithmetic mean between the largest values at the beginning of the flame (directly after the grid) and the lowest limiting values at the end of the flame, but are located nearer to the limiting least values. The same result is also seen from comparison of values of u_T/v and limiting values of the intensity of turbulence given in Table 5.4 with experimental data for turbulence homogeneous along the flame which are given in the preceding tables. The same result was noted according to the data of Solntsev (see § 6, and Table 5.1): with fast decay of turbulence after the grid, the value of u_T/v is very regular with certain averaging, but without any delay follows after the intensity of turbulence along the flow and rapidly after the intensity takes the limiting least value corresponding the steady-state value of u'/c . Thus the average value of u_T/v along the length of the flame will apparently be described well by u'/v_1 , which is defined as the average over the length of the flame by the relationship

$$u' = \frac{1}{L} \int_0^L u'(x) dx. \quad (5.71)$$

In Table 5.4 there are presented also u_T/v and u'/v for atmospheric pressure, which were obtained by extrapolation of data given in work [40]. As follows from Table 5.4, u_T at low pressures can be noticeably less than u_H . The dependence of parameter u_T on pressure can be expressed very approximately by the working formula

$$u_T \sim p^{0.4}. \quad (5.72)$$

(Strictly speaking, the exponent noticeably changes with change of initial temperature of the mixture). It coincides with the power dependence given by himself for speed of propagation u_T .

Table 2.4. Turbulent Characteristics of Flow During Burning (Data of Khrantsov)

T_1 , °C	u_H , cm/sec	L_Φ , mm	δ_T	ϵ_{0PM} , %	$\left(\frac{D}{v}\right)_{0PM}$	$\left(\frac{D}{v}\right)_\sigma$	$\frac{u_T}{v}$	u_T	$\frac{u_T}{v}$	$\frac{u_T}{u_H}$	u_{cp} , p	p atm	$\left(\frac{u_T}{v}\right)_{p=1}$	$(u_T)_{p=1}$	$\epsilon_{p=1}$	$u_{cp}(p=1)$, m/sec
27	43	276	190	13 to 5	0.38	0.0189	0.0391	1.56	0.066	3.6	3.6	0.6	0.048	1.9	5 to 15% obtained by extrapolation	4.0
100	60	240	155	13 to 5	0.38	0.0195	0.0455	1.82	0.075	3.0	3.6	0.6	0.056	2.24		4.0
200	89	215	126	13 to 5	0.38	0.0199	0.0527	2.1	0.084	2.36	3.6	0.6	0.064	2.5		4.0
300	128	195	105	13 to 5	0.38	0.02	0.060	2.4	0.092	1.9	3.6	0.6	0.073	2.9		4.0
27	48	385	250	11 to 5	0.33	0.0125	0.0284	1.1	0.047	2.4	3.0	0.4	0.073			4.0
100	67	303	190	11 to 5	0.33	0.0151	0.0365	1.46	0.059	2.2	3.0	0.4	0.073			4.0
200	97	250	145	11 to 5	0.33	0.0169	0.0455	1.8	0.072	1.9	3.0	0.4	0.073			4.0
300	140	222	110	11 to 5	0.33	0.0161	0.0542	2.17	0.081	1.56	3.0	0.4	0.073			4.0
27	77	535	410	7 to 5	0.2	0.0104	0.019	0.76	0.034	0.99	2.4	0.1	0.073			4.0
100	1.08	395	280	7 to 5	0.2	0.0132	0.0267	1.07	0.046	0.99	2.4	0.1	0.073			4.0
200	1.54	330	174	7 to 5	0.2	0.0116	0.0357	1.43	0.055	0.93	2.4	0.1	0.073			4.0
300	2.24	260	130	7 to 5	0.2	0.01385	0.0461	1.84	0.069	0.82	2.4	0.1	0.073			4.0

From relationships given in § 3, Chapter V, it is clear that the basic dependence of u_T on pressure is determined by the dependence of u' on pressure. Substituting the experimental dependence $u' \sim p^{0.34}$ (see Chapter IV) in formulas for u_T , we will obtain a dependence which is close to the experimental dependence, but with somewhat smaller value of the exponent: $u_T \sim p^{0.28}$. This indicates that u_T decreases with fall of pressure not only due to decrease of turbulent velocity u' .

In order to eliminate the influence of parameter u' on u_T , there were applied grids [40], which gave approximately identical values of u' at various pressures. (Let us remember that this parameter is determined basically by the macrostructure of turbulence). If the influence of turbulence on u_T reduced only to the influence of u' and u_H , then the value of u_T would in this case only increase with fall of pressure, since u_H grows with fall of pressure. In reality, u_T , in spite of increase of u_H , decreased proportionally to $p^{0.12}$. Decrease of u_T can be explained only by the increase of viscosity ν . Increase of viscosity leads to decrease of the importance of the role of the microstructure of turbulence (scale η increases with increase of viscosity). This effect, as experiment shows, turns out to be stronger, than the positive effect of increase of D_M and τ . The sum of the exponents in the dependence of u_T on u' and the microstructure function λ exactly gives the total experimental dependence of parameter u_T on pressure ($0.28 + 0.12 = 0.4$). Let us note that when turbulence influences the burning front, increase of parameter τ with fall of pressure must also be considered as a positive factor: the more slowly the burning front passes through the vortices, the larger the deformation of the burning front by these vortices, the larger the scale σ_T (see § 3) and the larger the quantity u_T .

The obtained empirical relationships permit us in the first approximation to estimate the length of a straight-through-flow combustion chamber.

Let us give an example of such a calculation. The distance between the nearest edges of two neighboring flame-holders is equal: $2a_0 = 40$ mm. The length of the chamber according to (5.67) is equal to

$$L_x \approx \frac{a_0 v}{u_T}. \quad (5.73)$$

In the most general case, in this relationship it is necessary to consider:

1) increase of average flow velocity according to the relationship $v(x) = v_1 \frac{f_1(0)}{f_1(x)}$ (v_1 and ρ_1 are velocity and density of the flow before the combustion

chamber) due to fall of pressure along the chamber;

2) decrease of u_T due to fall of pressure along the chamber.

3) variation of parameters of turbulence along the chamber due to decay of turbulence (after the grid), contraction (diffusivity) of the flow in the conical chamber, contraction of flow between the flame-holders, and so forth.

However, usually these factors turn out to be not so essential, so that the value of L_R can with sufficient accuracy be determined according to the mean values of v and u_T of the incident (on the flame) flow.

At $p_R = 1$ atm (abs.), $\varepsilon = 5$ to 6% ; $\alpha = 1$ to 1.4 $v > 30$ m/sec, we have according to Fig. 5.38 $u_T/v = 0.03$ to 0.04 ;

so that

$$L_R = \frac{20}{0.03 + 0.04} = 700 \text{ to } 500 \text{ mm}$$

For a homogeneous mixture, combustion efficiency at the end of a chamber of length L_R will not be below 0.95 to 0.98 according to the determination of experimental values of u_T/v in Fig. 5.38. For a two-phase mixture the given expressions remain valid if the composition of the homogeneous mixture is determined according to the vapor phase of the fuel. The total combustion efficiency will be thus determined by combustion efficiency of the vapor phase ($\eta \approx 0.9-0.95$) and the combustion efficiency of the liquid droplets which do not have time to be vaporized before the flame front. Calculation of physical incomplete burning due to unevaporated drops in the turbulent burning zone can be performed by the method given in Chapter II.

LITERATURE

1. G. Damköhler. Der Einfluss des Turbulenz auf die Flammgeschwindigkeit in Gasgemischen, Jahrbuch, 1939, D. L. F. S. 113, 17.

2. K. I. Shchelkin. On combustion in a turbulent flow, ZHTF (Journal of Theoretical Physics), 1943, Vol. XIII, Issue 9-10, p. 520.

3. K. I. Shchelkin. Concerning the question of turbulent burning and phases of combustion in an engine, News of the Academy of Sciences of the USSR, 1953, OTN (Department of Technical Sciences), Issue 3, pp. 463-471.

4. W. Mickelsen and N. Ernstein. Propagation of a Free Flame in a Turbulent Gas Stream, Report NACA, 1956, No. 1286, p. 26.

5. Ye. S. Shchetinkov. On calculation of propagation of a flame in a turbulent flow, Collection of articles "Burning in a Turbulent Flow," Publishing House of the Academy of Sciences of the USSR, 1959.

6. A. C. Scurlock and I. Grover. Propagation of Turbulent Flames, Fourth Symposium on Combustion, Baltimore, 1953, p. 645.

7. G. Richardson. Mathematical Theory of Turbulent Flames, Proc. Aero-thermochemistry Gas Dynamics, Symposium, 1956.
8. M. Tucker. Interaction of a Free Flame Front with a Turbulence Field Report NACA, 1956, No. 1277.
9. N. V. Kokushkin. Investigation of burning of a homogeneous mixture in a turbulent flow by means of recording of temperature fluctuations, News of the Academy of Sciences of the USSR, OTN, 1958, No. 8.
10. M. A. Summerfield and oth. The Physical Structure of Turbulent Flames, Jet Propulsion, July-Aug. 1954, Vol. 24, and Jet Propulsion, 1955, Vol. 25, No. 8.
11. A. S. Sokolik, A. N. Voinov and Yu. B. Sviridov. The influence of chemical and turbulent factors on the combustion process in an engine, News of the Academy of Sciences of the USSR, OTN, 1949, No. 12.
12. Yu. B. Sviridov. On the nature of turbulent burning, News of the AS USSR, OTN, 1953, No. 11.
13. L. D. Landau and Ye. M. Lifshits. Mechanics of continuous media, State Technical and Theoretical Press, 1954.
14. Ya. B. Zel'dovich and D. A. Frank-Kamenetskiy. Turbulent and heterogeneous burning, Publishing House of the Moscow Mechanics Institute, 1947.
15. K. P. Vlasov and N. N. Inozemtsev. The influence of initial parameters of a flow on speed of propagation of flame in uniform fuel-air mixtures, "Aviation Materiel," 1959, No. 5.
16. A. V. Talantov. Evaluation of the operation of a simple straight flow-through combustion chamber, News of the AS USSR, OTN, 1959, No. 2.
17. K. Wohe. Burning Velocity of Unconfined Turbulent Flames, Ind. Eng. Chem., 1955, Vol. 47, No. 4.
18. Karlovitz, Béla, D. N. Denniston Jr. and F. E. Walls. Investigation of Turbulent Flames, Journ. Chem. Phys.
19. H. C. Hottel, G. C. Williams and R. S. Levine. The Influence of Isotropic Turbulence on Flame Propagation, Fourth Symposium (International) on Combustion, The Williams and Wilkins Co. (Baltimore), 1953, pp. 636-644.
20. D. B. Leason. Turbulence and Flame Propagation in Premixed Gases, Fuel, Vol. XXX, No. 10, Oct. 1951, pp. 233-238; discussion, pp. 238-239.
21. Mickelsen and R. William. The Propagation of a Free Flame Through a Turbulent Gas Stream. M. S. Thesis, Case Inst. of Tech., 1953.
22. A. C. Scurlock. Flame Stabilization and Propagation in High-Velocity Gas Streams Meteor Rep. 19, Fuels Res. M. I. T., May 1948 (contract Nord 9661).
23. K. Wohl, L. Shore, H. von Rosenberg and C. W. Weil. The Burning Velocity of Turbulent Flames, Fourth Symposium (International) on Combustion, The Williams and Wilkins Co. (Baltimore), 1953, pp. 620-635.
24. Yu. A. Shcherbina. Calculation of temperature profiles in the wake after a bluff body during burning, Collection on mechanics and applied mathematics, Transactions of the MFTI (Moscow Physicochemical Institute), No. 3, Oborongiz, 1958.
25. H. Hahnemann and Z. Ehret. Effect of Intense Sound Waves on a Stationary Gas Flame. NACA TM 12H, 1950.
26. G. H. Markstein. Interaction of Flame Propagation and Flow Disturbances, Third Symposium on Combustion and Flame and Explosion Phenomena, The Williams and Wilkins Co. (Baltimore), 1949, pp. 162-167.

27. Sam Ioshaek, R. S. Fein and H. L. Olsen. The Effect of Sound on the Normal Velocity and Stability Limits of Laminar Propane-Air Flames, Rep. CM-553, Dept. Chem., Naval Res. Lab., Univ Wisconsin, July 9, 1949 (Navy Bu Ord Contract Nord 9938).

28. A. G. Prudnikov. On the determination of average parameters of a turbulent flame, News of the AS USSR, OTN, Power engineering, 1960, No. 1.

29. B. Lewis, N. Pease and H. S. Taylor. Combustion processes, Fizmatgiz, 1961.

30. A. G. Prudnikov. On the influence of small-scale turbulence on burning velocity and limits of the existence of a stationary turbulent flame front, News of the AS USSR, 1963.

31. A. G. Prudnikov. Equations of a turbulent flame, Third All-Union Conference on the Theory of Combustion, Volume 1, Publishing House of the Academy of Sciences of the USSR, 1960.

32. N. V. Kokushkin. Investigation of the macrostructure of a turbulent flame in homogeneous gasoline-air mixtures, Dissertation, MAI (Moscow Aviation Institute), 1960.

33. V. A. Frost. Homogeneous rapid deformation of turbulence in a gas. Reports of the AS USSR, 1960, Vol. 133, No. 4.

34. V. P. Solntsev. The influence of parameters of turbulence on the process of combustion of a homogeneous gasoline-air mixture after a flame-holder in a closed flow. Collection of articles, "Stabilization of Flame and Development of the Process of Combustion in a Turbulent Flow," Oborongiz, 1961.

35. V. P. Solntsev and V. A. Golubev. Combustion of a gasoline-air mixture after systems of flame-holders (in the same collection).

36. A. G. Prudnikov. Measurements of turbulence in air flows and flames by the optical-diffusion method. Dissertation, MFTI, 1957. Collection of articles, "Burning in a Turbulent Flow," Publishing House of the Academy of Sciences of the USSR, 1959.

37. A. G. Prudnikov. Flame Turbulence, Seventh Symposium (international) on Combustion, Baltimore, Williams and Wilkins Co, 1959.

38. V. P. Karpov, Ye. S. Semenov and A. S. Sokolik. Turbulent burning in a closed volume, Reports of the AS USSR, 1959, 128, No. 6, 1220.

39. A. S. Sokolik and V. P. Karpov. Dependence of the speed of turbulent burning on laminar speed and burning temperature, Reports of the AS USSR, 1959, 129, No. 1, 168.

40. V. A. Khramtsov. Experimental investigation of burning of a homogeneous fuel-air mixture in a turbulent flow at low pressures, Collection of articles, "Burning in a Turbulent Flow," Publishing House of the Academy of Sciences of the USSR, 1960.

41. K. P. Vlasov and N. V. Kokushkin. On errors in thermocouple during burning, temperature measurement, News of the AS USSR, 1957, OTN, No. 8.

CHAPTER VI

VIBRATIONAL BURNING REGIMES

§ 1. GENERAL CHARACTERISTIC OF VIBRATIONAL BURNING

Not infrequently in the development of combustion chambers, burning ceases to be stable, as a consequence of which there are observed knocking, flameout and other similar phenomena which must be overcome to improve organization of the process of burning in accordance with the principles presented in the other chapters. Sometimes instability acquires another character - burning enters the regime of steady-state oscillation. We do not refer to those random oscillations of pressure which always accompany the process of fuel combustion, but to oscillations with large amplitude and a pronounced frequency. Not infrequently such oscillations damage elements of the combustion chamber. They are always characterized by a sharp increase of noise and, as a rule, are impermissible. In certain chemical industrial apparatus in furnaces of boilers and similar devices there are being made attempts to use such burning as a normal operating regime.

Burning characterized by clearly expressed periodicity will be called vibrational burning. This phenomenon has been the subject of many investigations (see for instance work [3]). Vibrational burning can be characterized by different frequencies. In the huge majority of cases, the frequency of oscillations is determined by acoustical properties of the combustion chamber, air conduits and the channel through which combustion products move. This is due to the fact that the material whose vibrations are observed is made up of elastic gas masses, and vibrations of an elastic gas are described by the equations of acoustics.

Depending upon how the masses of gas vibrate, it is possible to speak of "zero-dimensional" or "one-dimensional" oscillations. The first are characterized by the

fact that pressure in the whole volume is changed simultaneously and identically. Such oscillations are observed, in particular, in combustion chambers of liquid-fuel rocket engines and are described in detail in the literature [1]. These oscillations usually have relatively low frequency and not infrequently are called therefore "low-frequency" oscillations. In combustion chambers considered in the present book as a rule there are realized "one-dimensional" oscillations, in which gas masses oscillate in the direction along the flow axis; i.e., there occur longitudinal oscillations. Moreover, in different sections along the flow axis, amplitudes of the oscillations are different, although they occur with the same frequency (standing waves). The frequency of these oscillations depends on the extent of the gas flow and on boundary conditions. Inasmuch as masses of gas oscillate not only in the region directly adjacent to the burning zone, but also, for instance, in feed pipes, we will consider the following idealized process: gas moves through a sufficiently long pipe of constant cross section, and in a certain region of this pipe there occurs burning. As it is known from acoustics, the period of oscillation of the gas in such a pipe τ_1 (if both its ends are open or closed) is equal to the transit time of the acoustical pulse through the pipe along the flow and back again:

$$\tau_1 = \int_0^L \frac{dx}{u+a} + \int_L^0 \frac{dx}{u-a} = 2 \int_0^L \frac{adx}{a^2 - u^2}, \quad (0.1)$$

where x — coordinate along the flow axis;

L — length of pipe;

u — local velocity of (one-dimensional) flow;

a — local speed of sound.

If one end of the pipe is open and the other is closed, then the period is doubled:

$$\tau_1 = 4 \int_0^L \frac{a}{a^2 - u^2} dx. \quad (0.2)$$

It is necessary to say that frequencies ω found by these formulas,

$$\omega = \frac{2\pi}{\tau_1}, \quad (0.3)$$

will characterize the fundamental tone, or first harmonic of the oscillations.

However, there can be excited higher harmonics, having higher frequencies. For the first case these frequencies can be obtained from the frequency of the first harmonic

by multiplication by 2, 3, 4, etc., and for the second case - by multiplication by 3, 5, 7, etc.

It is necessary to say that frequencies calculated in this way will give only orders of magnitudes of the actually observed frequencies, since the elementary acoustic calculation given above does not take into account certain properties of the burning process. However, usually such a rough estimate is sufficient.

The boundary conditions mentioned above require a certain explanation. The end is considered to be "open" in the case when flow in it is subsonic and the end section is not blocked by structural elements, but it is "closed" in the case when total flow areas are very small as compared to the cross section of the flow in the pipe or are absent altogether, or if flow in the end section attains the speed of sound (critical contraction at the entrance to the pipe or initial section of the Laval nozzle at the exit from the pipe). When at either one or both ends of the pipe there exist transonic velocities, the length of the pipe L is defined as the distance between the sections in which the speed of sound is attained, or between such a section and the other end of the pipe.

Along with longitudinal oscillations there can also exist transverse oscillations. In this case masses of gas oscillate not along the flow axis, but in directions normal to this axis. Here there can be realized tangential oscillations, in which the characteristic dimension will not be the length of the pipe L , but its diameter D , or radial oscillations, possessing axial symmetry and characterized by the radius $D/2$. Inasmuch as usually $L \gg D$, tangential oscillations will be characterized by higher frequencies than longitudinal oscillations, and radial - by higher frequencies than tangential. This explains the fact that transverse oscillations sometimes are called "high-frequency" oscillations.

Upon the appearance of vibrational burning, it is necessary first of all to determine with what type of oscillations we are dealing. As a rule, this is determined by an oscillogram. Knowing the characteristic dimensions of the combustion chamber, it is easy to estimate the orders of magnitude of the expected frequencies of longitudinal acoustic oscillations and "high-frequency" oscillations. If the observed frequencies are noticeably lower than those which are determined by formulas (6.1), (6.2) and (6.3), then we have "low-frequency" oscillations. In the huge majority of cases there appear longitudinal oscillations, which are considered below.

§ 2. GENERATION OF ACOUSTIC ENERGY BY THE BURNING PROCESS

During the analysis of vibrational burning it is necessary to imagine clearly the physical essence of this phenomenon. It is obvious that vibrational burning is a self-oscillatory process, inasmuch as in combustion chambers there are absent devices capable of serving as a source of forced oscillations. In those rare cases when there nevertheless appear forced oscillations (for instance, in the case of a nonuniform, fluctuating supply of fuel by the pump), their suppression is absolutely elementary.

As already was indicated, during vibrational burning elastic masses of gas oscillate. These oscillations are associated with energy losses; therefore, it is most important to discover the source of energy supporting the oscillation, and the mechanism ("value") which periodically communicates this energy to the masses of gas.

Let us consider at first the energy side of the process of vibrational burning. In Fig. 6.1 there is depicted a cylindrical pipe with length of L , through which



Fig. 6.1. Schematic diagram of a pipe with burning zone σ located inside it.

there flows a gas in the positive direction of the x -axis. In a certain region σ heat is supplied to the gas. The region σ , with volume equal to V , is the burning zone. On the left and the right of σ there are located passive masses of flowing gas which oscillate. These oscillations

are accompanied by radiation losses of acoustic energy from the ends of the pipe into the external space. Oscillations are supported by processes occurring inside the burning zone, where there is generated acoustic energy, which then flows to the left and to the right from σ and replenishes the losses.

We will designate the total magnitude of acoustic energy flux "radiated" by region σ by A_{Σ} , and by A' and A'' we will designate energy fluxes intersecting the left and right boundaries of the region σ .

Then

$$A_{\Sigma} = A'' - A'. \quad (6.4)$$

Signs of A' and A'' are selected in such a manner that flux A_{Σ} is positive if the acoustic energy flows from zone σ toward the ends of the pipe; then it is considered that A' and A'' are positive, if energy flows in the positive direction of the x -axis.

It is obvious that the condition $A_{\Sigma} > 0$ signifies transmission of acoustic energy from the burning zone σ to masses of gas located in neighboring sections of

the pipe. In case of the ideal process, when losses are absent, the condition for excitation of the system (condition of instability) can be written in the form of inequality

$$A_{\Sigma} > 0. \quad (6.5)$$

Actually, since in the absence of losses (including radiation losses into the external space) acoustic energy will remain in the pipe, then in accordance with inequality $A_{\Sigma} > 0$ the quantity of it will constantly increase, and, as a result, the amplitude of the oscillations will increase. This increase of amplitudes we will call excitation of the system, and we will call the system itself unstable.

If there is realized the condition

$$A_{\Sigma} < 0, \quad (6.6)$$

then the oscillations will alternate. It is possible to imagine this in the following way: Let us assume that the system builds up with the help of some external influence. Then the oscillating gas masses will contain a certain reserve of acoustic energy. Condition $A_{\Sigma} < 0$ shows that this acoustic energy will flow toward the zone σ and be absorbed in it. In this case the burning process in region σ appears not as a generator of acoustic energy, but as an absorber of it. Such oscillations characterize a stable system.

The process differentiating the two considered processes will be characterized by constancy of the amplitudes of oscillations and be called the boundary of stability (neutral oscillations), and the condition of its existence can be written in the form of the equality

$$A_{\Sigma} = 0. \quad (6.7)$$

If there exist losses and if they are equal to $R > 0$, then instead of conditions (6.5)-(6.7) it is natural to write

$$\begin{aligned} A_{\Sigma} &> R - \text{instability,} \\ A_{\Sigma} &< R - \text{stability} \\ A_{\Sigma} &= 0 - \text{boundary of stability} \end{aligned} \quad (6.8)$$

The found expressions can serve as a basis for further investigation, if we give expressions for calculation of fluxes of acoustic energy A . As it is known, the total flux of energy of the gas flow is equal to

$$\mathcal{E} = \rho u \left(\frac{u^2}{2} + c_p T \right) + p u. \quad (6.9)$$

where ρ - density of gas;
 u - velocity of flow;
 p - pressure;
 T - temperature of gas;
 c_v - its heat capacity at constant volume.

The first term (flux of kinetic and internal energy) is not of interest, since it is connected with mass transfer, whereas the acoustic energy is the energy transmitted by pressure. Therefore, we will be limited to consideration of only the last term of formula (6.9). Let us assume that in the gas flow are established harmonic oscillations

$$\left. \begin{aligned} p &= p_0 + \delta p, \quad \delta p = |\delta p| \sin \omega \tau, \\ u &= u_0 + \delta u, \quad \delta u = |\delta u| \sin(\omega \tau + \varphi). \end{aligned} \right\} \quad (6.10)$$

The sign \parallel here and below denotes amplitudes of the corresponding oscillations. The term pu in formula (6.9) can be represented in the form

$$pu = p_0 u_0 + p_0 \delta u + u_0 \delta p + \delta u \delta p.$$

By integrating this equality over the period of oscillation $2\pi/\omega$ and referring the obtained quantities to the period, we will find the mean value of energy flux

$$(pu)_{\text{av}} = p_0 u_0 + \frac{\omega}{2\pi} \int_0^{\frac{2\pi}{\omega}} \delta u \delta p d\tau. \quad (6.11)$$

Flux $p_0 u_0$ is in no way connected with the oscillations, and therefore will not be considered below. The second term on the right side, however, is the flux of acoustic energy. Simple calculations give

$$A = \frac{\omega}{2\pi} \int_0^{\frac{2\pi}{\omega}} \delta u \delta p d\tau = \frac{1}{2} |\delta p| |\delta u| \cos \varphi. \quad (6.12)$$

Thus, the flux of acoustic energy A depends on amplitudes of oscillation of pressure and velocity and on the phase shift φ between them.

Let us return to Fig. 6.1. We will consider the flow on the left and on the right of zone σ to be one-dimensional. Subscript "1" will denote values on the left boundary of the burning zone, and subscript "2" will denote values on its right boundary. Then formulas (6.4) and (6.12) will take the form

$$A_2 = \frac{\omega}{2\pi} \int_0^{\frac{2\pi}{\omega}} (\delta u_2 \delta p_1 - \delta u_1 \delta p_2) d\tau. \quad (6.13)$$

Quantities δu_2 , δu_1 , δp_2 and δp_1 can have various amplitudes of oscillation and can be shifted relative to one another by certain phase angles [similar to the shift φ in formulas (6.6)]. However, their main property is that they will oscillate with the same period (identical frequency), since all four of these quantities are connected with oscillations of the mass of gas in the pipe, which oscillates as a single elastic medium.

Let us introduce the designations

$$\left. \begin{aligned} \delta p_2 - \delta p_1 &= X, \\ \delta u_2 - \delta u_1 &= E. \end{aligned} \right\} \quad (6.14)$$

As it is known, the sums or differences between sine curves having identical period are also sine curves of the same period and have amplitudes and phases which depend on the amplitudes and phases of the sine curves which were added or subtracted. Based on what has been said, it is possible to state that quantities X and E change in time sinusoidally with the frequency ω .

The quantities X and E formally here introduced have a simple physical meaning. X indicates oscillation of the resistance of zone σ . Actually, the static pressure drop $p_2 - p_1$ appears due to thermal resistance and hydraulic resistance (flow friction) of zone σ . If pressures p_2 and p_1 have harmonic components δp_2 and δp_1 , then oscillation of resistance $p_2 - p_1$ in time will be equal to $\delta p_2 - \delta p_1$, i.e., to X .

Regarding the quantity E , it indicates oscillation of the velocity of expansion of the volume of gas inside σ . Actually, due to heating of the gas inside σ it is expanded, and this expansion is characterized by the difference $u_2 - u_1$. Therefore, $\delta u_2 - \delta u_1$ characterizes oscillation of this velocity of expansion.

E and X describe certain general properties of the burning zone σ : during oscillatory burning it is possible to expect oscillations of both the resistance of zone σ and the velocity of expansion of gas within this zone.

By expressing δp_2 and δu_2 in terms of δp_1 , δu_1 , X and E , and placing these expressions in (6.13), we will obtain

$$A_2 = \frac{\omega}{2\pi} \int_0^{\frac{2\pi}{\omega}} (E\delta p_1 + X\delta u_1 + EX)d\tau. \quad (6.15)$$

Inasmuch as X and E are generalized characteristics of the process of oscillatory burning, it is possible to state that the obtained formula gives the value of the flux of acoustic energy "radiated" by region σ in the form of a function of the oscillation of pressure and velocity before the burning zone and properties of the actual burning process (X and E). It is interesting to note that of the great number of possible characteristics of burning, for finding A_Σ it is sufficient to know only two — X and E .

If we agree to designate phase shifts between E and δp_1 by ψ_1 , between X and δu_1 by ψ_2 , and between E and X by ψ_3 , then by analogy with expression (6.12) it is possible to write

$$A_\Sigma = \frac{1}{2} (|E| |\delta p_1| \cos \psi_1 + |X| |\delta u_1| \cos \psi_2 + |X| |E| \cos \psi_3). \quad (6.16)$$

Let us consider two particular cases. Let us assume that, for instance, $X = 0$. Then

$$A_\Sigma = \frac{1}{2} |E| |\delta p_1| \cos \psi_1.$$

The condition for excitation $A_\Sigma > 0$ will be satisfied only for $-\frac{\pi}{2} < \psi_1 < \frac{\pi}{2}$. For slow flows it is possible in the first approximation to consider that the oscillatory component of velocity of expansion E is near in phase to the oscillatory component of heat addition. Then the most favorable condition for excitation of the system ($\psi_1 = 0$) will be the condition that the phase of pressure oscillation coincide with the phase of heat addition (the maximum of heat addition should occur at the moment of the highest compression).

Another particular case will be the condition $E = 0$. Then

$$A_\Sigma = \frac{1}{2} |X| |\delta u_1| \cos \psi_2.$$

Considerations analogous to those mentioned above will give the condition which is the most favorable for excitation of the system $\psi_2 = 0$. It is necessary only to consider that increase of heat addition corresponds, due to increase of thermal resistance, to decrease of p_2 (and not to increase of u_2 as in the preceding example), and therefore the maximum of heat addition (minimum of X) should be attained at the moment when velocity u_1 has its minimum value (δu_1 has its maximum negative value).

The two elementary cases considered here correspond to borrowing of energy from two different sources — the thermal and kinetic energy of the flow. This can be shown by means of simple reasoning.

1. When oscillation of heat addition is in phase with oscillation of pressure, then moments of increased pressure correspond to increased heat addition, and moments of lowered pressure correspond to a decreased quantity of added heat. If we consider this process relative to a certain average level of heat addition, then it is possible to say that during compression of the gas there occurs extra heat addition, and during rarefaction of the gas there occurs heat removal. As it is known from thermodynamics, such a cycle gives positive work, i.e., converts thermal energy into mechanical energy, where this occurs periodically. Consequently, into the oscillatory system there will periodically enter mechanical energy, building up oscillations of the system.

2. Oscillating heat addition will give rise to oscillating thermal resistance. Just as any other oscillating resistance, it can transform part of the kinetic energy of a flow of gas incident on it to oscillatory form.

Thus, an oscillatory system can acquire energy from the two indicated sources.

Under actual conditions, E and X are different from zero, and the oscillatory system simultaneously interacts with the two sources of energy. Inasmuch as heat addition cannot simultaneously be in phase with pressure and in antiphase with velocity, in general the conditions for excitation are more complicated, and will not be described here. Formally they are expressed by formulas (6.16) and (6.8). Thus, for analysis of the process of excitation of vibrational burning, it is sufficient to know only two characteristics of the burning zone — E and X . The elementary considerations given here concerning the relationship of E and X with oscillation of heat addition are insufficient, and their determination requires special investigations.

§ 3. IDEALIZATION OF A PERTURBED COMBUSTION PROCESS

In order to give a method for actual determination of E and X , we will consider the process occurring in the burning zone in more detail. Let us make the assumption that the extent of the intense burning zone σ is small as compared to the total length of the combustion chamber L (see Fig. 6.1). Speaking of smallness of σ as compared to L , let us agree to understand by the region of perturbed heat addition only that part of the burning zone in which there occurs noticeable oscillation of heat addition. As a rule, this zone corresponds to the initial section of the region of burning. This is quite natural, inasmuch as initial sections of the region of burning, where burning still has not completely developed, are especially sensitive to perturbations

of velocity, pressure, temperature and other parameters of the gas incident on the burning zone. With regard to sections located at a sufficient distance from the flame front, although there may be considerable heat release here, oscillation of heat addition is less probable.

We will define the boundaries of the region σ . We will call the volume V contained between two fixed planes normal to the axis of the pipe inside which the process of perturbed burning occurs the zone of perturbed burning. Thus the surfaces of the flame and of the region of perturbed burning must not intersect the boundaries of volume V when they are in their extreme forward and extreme rear positions, which they can take as a result of the oscillatory motion of the mass of gas in the burning zone.

The burning zone σ is schematically depicted in Fig. 6.2. It is bounded by sections F_1 and F_2 . Inasmuch as sections F_1 and F_2 are removed from the surface of the flame S , we will consider flow in them to be one-dimensional. For relation of the parameters of flow in sections F_1 and F_2 , we will write the laws of conservation of mass, momentum and energy:



Fig. 6.2. Burning zone (S is the flame front).

$$\left. \begin{aligned} \rho_2 u_2 &= \rho_1 u_1 - \frac{1}{F} \frac{\partial}{\partial t} \int \rho dV, \\ \rho_2 u_2^2 + p_2 &= \rho_1 u_1^2 + p_1 - \frac{1}{F} \frac{\partial}{\partial t} \int \rho u_1 dV, \\ \rho_2 u_2 \left(\frac{u_2^2}{2} + c_p T_2 + q_2 \right) &= \rho_1 u_1 \left(\frac{u_1^2}{2} + c_p T_1 + q_1 \right) - \\ &\quad - \frac{1}{F} \frac{\partial}{\partial t} \int \rho \left(\frac{u^2}{2} + c_p T + q \right) dV, \end{aligned} \right\} \quad (6.17)$$

where

F - area of cross section of the flow;

u_x - projection of instantaneous value of velocity of the element on the axis of the flow (x -axis in Fig. 6.1);

c_p and c_v - heat capacities at constant pressure and constant volume;

q - latent chemical energy of a unit mass of the fuel mixture (the change of the flux of q at intersection of zone σ indicates that part of this energy was converted to thermal energy as a result of the process of combustion).

In virtue of the incompleteness of the process of combustion, $q_2 \neq 0$. Introducing the concept of instantaneous net combustion efficiency

$$\eta_c = \frac{q - q_2}{q_1}, \quad (6.18)$$

it is possible to eliminate q_2 from the equations.

Equations (6.17) relate parameters of flow in sections F_1 and F_2 . From the preceding paragraph it is known that excitation of acoustic oscillations is connected with differences between pressures in sections F_1 and F_2 and with differences of velocities in the same sections. In order to understand why these differences can oscillate, we will for simplicity consider that p_1 and u_1 (section F_1) are constant and examine what might cause oscillation of p_2 and u_2 (section F_2).

First, this can be a result of oscillating heat addition. Actually, if heat addition oscillates, then this means that $(\rho_1 u_1 q_1 - \rho_2 u_2 q_2)$ has an oscillatory component. Furthermore, partial derivatives of the integrals will also have such a component. Let us show this in the example of the first equation (6.17). Due to oscillating heat addition, density ρ behind the flame front S will oscillate, and therefore the total amount of mass in the volume V will have an oscillatory component. Consequently, in the right sides along with the constants (p_1 , u_1 , ρ_1 , etc.) there will be terms with oscillatory components; this means that p_2 , u_2 , ρ_2 , etc., will oscillate.

Secondly, even with constant heat addition, oscillation of p_2 and u_2 can be caused by mobility of the flame front. Let us assume, for instance, that the flame front oscillates between positions S and S_1 in Fig. 6.2. Then, in spite of the constancy of the density of combustion products, the mass in volume V will fluctuate. Analogous considerations can also be given for the two other integrals. This leads to the appearance of oscillatory components of p_2 and u_2 .

Consequently, the appearance of oscillatory components of the differences $p_2 - p_1$ and $u_2 - u_1$, which were designated as X and E , is connected with the oscillation of heat addition or oscillation of the position of the flame front, or with both simultaneously. It is possible to show that these two processes cannot be reduced to the same process (i.e., that they are equivalent), and therefore each of them has an independent value.

Oscillation of the flame front can be associated with two causes. First, it can be a result of oscillation of flow velocity bu_1 ; the flow will, as it were, "drag" the flame front after itself. This cause, from the point of view of analysis of vibrational burning, is only secondary, since it is not connected with the burning process. Secondly, the flame front can be displaced due to change of the local velocity of propagation of the flame due to the influence of local eddy zones on the configuration of the flame front, or other similar causes, which are very significant for this analysis. In order to characterize them by one quantity, we will talk about

change of the effective velocity of flame propagation δu_{cr} . This velocity can be defined as

$$\delta u_{cr} = \delta u_1 + \frac{1}{F} \frac{\partial}{\partial \tau} V_T(\tau). \quad (6.19)$$

Here $V_T(\tau)$ is the volume of hot gases after the flame front S in zone σ in Fig. 6.2 (positive direction of u_{cr} is taken to be opposite to the positive direction of the flow velocity u_1 , since the flame moves toward the cold gas). For a plane flame front normal to the axis of the pipe, this formula will coincide with the usual definition of perturbation of the velocity of propagation of a flame. If, for instance, such a flame front is motionless with respect to an observer, then $V_T(\tau) = \text{const}$ and $\delta u_{cr} = \delta u_1$, i.e., the velocity of propagation of the plane flame front strictly follows the flow velocity in magnitude. For a flame front of arbitrary configuration, δu_{cr} is a certain effective averaged quantity, which is analogous to the perturbation of velocity of propagation of the plane flame front. Below we will everywhere use this averaged characteristic.

Let us define the time rate of heat addition to the gas per unit cross sectional area:

$$Q' = \rho_1 u_1 q_1 - \rho_2 u_2 q_2$$

Then, using the first and last equalities (6.17) and also (6.18), it is possible to write

$$Q' = \rho_1 u_1 \eta_{cr} q_1 + (1 - \eta_{cr}) q_1 \frac{1}{F} \frac{\partial}{\partial \tau} \int_V \rho dV.$$

By taking the variation of the written expression with respect to q_1 and η_{cr} , i.e., with respect to quantities determining the combustion process, and eliminating terms of higher order of smallness relative to the perturbations δ , we will find

$$\delta Q' = \rho_1 u_1 q_1 \delta \eta_{cr} + \rho_1 u_1 \eta_{cr} \delta q_1 + (1 - \eta_{cr}) q_1 \frac{1}{F} \frac{\partial}{\partial \tau} \int_V \rho dV.$$

The last term is retained without change, since it from the very beginning had the same order as δ . Actually, differentiation with respect to time eliminated the constant term and left only perturbations of the written integral.

Let us assume that density before the flame front is equal to ρ_1 , and after it ρ_2 . Then in virtue of the fact that the fraction of change of volume of cold gases V_x is equal and opposite in sign to the fraction of change of the volume of hot gases

V_r , we will obtain

$$\frac{\partial}{\partial \tau} \int \rho dV = \frac{\partial}{\partial \tau} \int \rho_1 dV + \frac{\partial}{\partial \tau} \int \rho_2 dV = (\rho_2 - \rho_1) \frac{\partial}{\partial \tau} \int dV.$$

Taking into account equality (6.19), we will have

$$\delta Q' = \rho_1 u_1 q_1 \delta \eta_{cr} + \rho_1 u_1 \eta_{cr} \delta q_1 + (1 - \eta_{cr}) q_1 (\rho_2 - \rho_1) (\delta u_{cr} - \delta u_1).$$

Thus, the last term is connected with the perturbation δu_{cr} , and consequently has already been taken into account above. Perturbation of heat addition, which is not connected with displacement of the flame front, will be expressed as:

$$\delta Q = \rho_1 u_1 q_1 \delta \eta_{cr} + \rho_1 u_1 \eta_{cr} \delta q_1. \quad (6.20)$$

If we linearize system (6.17), then in the final result we can obtain δp_2 , δu_2 and, for instance, δp_2 in terms of values of δp_1 , δu_1 , δp_1 , δu_{cr} , and δQ . Inasmuch as for the considered question, the differences $\delta p_2 - \delta p_1$ and $\delta u_2 - \delta u_1$ are of main interest, then it is better to write immediately

$$\left. \begin{aligned} E = \delta u_2 - \delta u_1 &= a_{11} \delta p_1 + a_{12} \delta u_1 + a_{13} \delta p_1 + a_{14} \delta u_{cr} + a_{15} \delta Q, \\ X = \delta p_2 - \delta p_1 &= a_{21} \delta p_1 + a_{22} \delta u_1 + a_{23} \delta p_1 + a_{24} \delta u_{cr} + a_{25} \delta Q. \end{aligned} \right\} \quad (6.21)$$

It is inexpedient here to give methods of numerical determination of coefficients a_{11} , ..., a_{25} [2], inasmuch as they will not be needed in our calculations. It is important only to note that all these coefficients are constants, depending only on the parameters of the steady-state flow.

In certain cases coefficients in formulas (6.21) turn out to be simple. Let us use this fact to point out certain important aspects of the process of excitation of vibrational burning in an elementary example. Let us consider, for instance, a very slow flow, and assume that δu_{cr} is equal to zero. Then it is simple to show that

$$\begin{aligned} E &\approx \frac{k-1}{k p_1} \delta Q; \\ X &\approx 0, \end{aligned}$$

where k is the adiabatic exponent.

This will give according to formula (6.16) the following expression for A_2 :

$$A_2 = \frac{k-1}{2k p_1} |\delta p_1| |\delta Q| \cos \psi. \quad (6.22)$$

If losses of acoustic energy are equal to $R > 0$, then in accordance with the first inequality (6.8) the condition for excitation of the system will be

$$\frac{k-1}{2\rho_1} |\delta p_1| |\delta Q| \cos \psi_1 > R. \quad (6.23)$$

Analysis of this inequality leads to the following conclusions:

1. Inasmuch as from acoustics it is known that the quantity R is proportional to squares of the amplitudes of the oscillations, i.e., to $|\delta p_1|^2$, and for the given $|\delta p_1|$ can be considered to be a constant, then excitation is impossible if the amplitude of oscillation of heat addition δQ is insufficiently large.

Here it is necessary to explain that we are speaking of the ratio of $|\delta Q|$ to $|\delta p_1|$. This becomes evident, if we divide both sides of the inequality by $|\delta p_1|^2$.

2. For a given sufficiently large value of relative amplitude $|\delta Q|$, excitation is possible only in the case when phase angle ψ_1 lies within the interval $-\frac{\pi}{2} < \psi_1 < \frac{\pi}{2}$, where the region of permissible phase shifts ψ_1 is smaller, the smaller $|\delta Q|$ is.

Thus, for realization of conditions of self-excitation of the system, it is necessary that perturbation of the burning process be sufficiently strong compared to amplitudes of oscillation of the medium, and that the phase of this perturbation be properly coordinated with the phase of oscillation of the medium. In order to introduce definiteness to the idea of amplitude and phase of oscillation of the medium, we will take, for instance, oscillation δp_1 as the base and will compare all quantities with δp_1 .

We will use expression (6.20) and assume that mixture entering the zone ϕ burns completely ($\eta_{cr} = 1$). Then $\delta Q = \rho_1 u_1 \delta q_1$. Calorific value of the mixture is related to the air-fuel α , so that $|\delta Q| = \rho_1 u_1 \frac{\partial q_1}{\partial \alpha} |\delta \alpha|$. Consequently, instead of (6.23) it is possible to write

$$c \cos \psi_1 \cdot \frac{|\delta \alpha|}{|\delta p_1|} > \frac{R}{|\delta p_1|^2} = \text{const} > 0,$$

where c is same constant.

The left side of the inequality shows that for excitation of oscillations the quantity $\frac{|\delta \alpha|}{|\delta p_1|}$ should be sufficiently large; i.e., the air-fuel ratio should sufficiently strongly depend on pressure of the medium. In principle, such a dependence is possible, since pressure oscillation of the medium theoretically changes the flow rate (due to oscillation of counterpressure) through the fuel injectors. Usually, however, for high-pressure injectors this dependence is too weak, and such phenomenon

cannot lead to the excitation of oscillations. This is a typical example of non-satisfaction of condition (6.23) due to violation of the necessary amplitude relationships.

Let us assume, however, that the injectors are low-pressure, and therefore $|\frac{\delta q}{\delta p_1}|$ turns out to be a sufficiently large quantity. It is easy to comprehend that in this case, with increase of pressure of the medium, the mixture will become leaner; i.e., at moments when δp_1 attains its maximum, δQ will be at its minimum. Consequently, phase shift ψ_1 between δp_1 and δQ will be about π . For excitation, however, it is necessary that it be less than $\pi/2$. Consequently, excitation also turns out to be impossible in this case. However, actually excitation of such a system has been observed. The fact is that heat addition does not instantly follow change of mixture ratio, since combustion requires a certain time. This leads to a certain delay of heat release. If this delay is close to half of the period of oscillation, then phases of δp and δQ will coincide ($\psi_1 = 0$), and self-excitation will become possible.

The given elementary example has shown that during excitation of vibrational burning, a decisive role is played by the relative amplitudes of perturbation of the burning process and phase shifts of this perturbation relative to the phase of oscillation of the medium, where these phase shifts must be considered taking into account the time lags peculiar to the process of burning. These conclusions are accurate not only for the considered simple example, but also for the most general cases.

§ 4. FEEDBACK MECHANISMS

Above it has already been said that during the study of a self-oscillatory system it is necessary to analyze the question concerning the source of energy supporting the oscillation and the question concerning the mechanism which regulates entry of this energy into the oscillatory system. The first of these questions already has been considered. It turned out that if heat addition δQ and velocity of propagation of the flame δu_{cr} oscillate with acoustic frequency, then this leads to the appearance of values of E and X different from zero. The latter, if they have the necessary value and proper phase shifts relative to, for instance, δp_1 , will lead to generation of acoustic energy in the burning zone σ , where this energy A_Σ will continuously be expended in build-up of oscillations of gas masses flowing on the left and on the right of σ .

If we ponder this conclusion, then we can definitely assert that in the case

when perturbations of heat addition or velocity of propagation of the flame are different from zero and oscillate with acoustic frequency, then they are able to support mechanical oscillations of the medium (acoustic oscillations). But so that such oscillations will be self-excited, there is necessary one more link — acoustic oscillations must in turn cause perturbation of the burning process (give δQ and δu_{cr} different from zero), where these perturbations must follow acoustic oscillations, be perturbed in the same rhythm, and have the required phases and amplitudes. In the presence of such "feedback" the system will be able to undergo self-excitation. Physical phenomena leading to this will for brevity be called "feedback mechanisms." In the given example there was considered the following mechanism: the dependence of flow rate of fuel through the injectors, and consequently also the calorific value of the mixture, i.e., in the final result δQ , on oscillation of pressure δp_1 . Before we proceed to systematic consideration of specific feedback mechanisms, we will turn to a simple example which will allow us to clarify the role of feedback.

Let us assume that organization of the burning process is such that δQ and δu_{cr} are functions of oscillatory the component of the gas flow velocity before the burning zone δu_1 . This can turn out to be connected with the fact for instance, that with change of flow velocity there is changed combustion efficiency, and there occurs deformation of the flame front. Let us assume that corresponding theoretical or experimental dependences already have been found and can be represented in the form of the equalities

$$\left. \begin{aligned} \delta u_{cr} &= k_1 \delta u_1, \\ \delta Q &= k_2 \delta u_1, \end{aligned} \right\} \quad (6.24)$$

where k_1 and k_2 are certain constants.

Equalities (6.24) can be considered as an analytic representation of the fact of existence of feedback in the system. Actually, the given representation indicates that δu_{cr} and δQ "generated" by δu_1 ; i.e., by acoustic oscillations. Inasmuch as k_1 and k_2 are constant, then the frequencies of oscillations δu_{cr} and δQ will be the same as the frequency of oscillations δu_1 (acoustic frequency).

If in the system there appears feedback, then by using equality (6.21) and assuming that flow before the burning zone is isoentropic (i.e., δp_1 can be expressed in terms of δp_1), we will write

$$\left. \begin{aligned} E &= b_{11} \delta p_1 + b_{12} \delta u_1, \\ X &= b_{21} \delta p_1 + b_{22} \delta u_1, \end{aligned} \right\} \quad (6.25)$$

where

$$\begin{aligned} b_{12} &= a_{12} + k_1 a_{11} + k_2 a_{13}; \\ b_{22} &= a_{22} + k_1 a_{21} + k_2 a_{23}. \end{aligned}$$

Thus E and X essentially depend on feedback factors k_1 and k_2 . Substitution of E and X in formula (6.15) permits us to find the flux of acoustic energy generated by region σ :

$$A_z = \frac{\omega}{2\pi} \int_0^{2\pi} (B_1 \delta p_1^2 + B_2 \delta p_1 \delta u_1 + B_3 \delta u_1^2) d\tau. \quad (6.26)$$

Numerical constants B_1 , B_2 and B_3 depend on b_{11} , b_{12} , b_{21} , b_{22} , i.e., in the final result on feedback factors k_1 and k_2 .

Let us assume that in the pipe there appear acoustic oscillations, for instance, at the first harmonic. Then in the region of the pipe in which the burning zone is located, there will occur oscillations of flow velocity and pressure. Amplitudes of these oscillations can change in time, but ratio of $|\delta u_1|$ to $|\delta p_1|$ in the considered section will remain constant; this is a well-known property of standing waves.

By analogy with formula (6.12), we will give the last expression the following form:

$$A_z = \frac{1}{2} |\delta p_1|^2 \left(B_1 + B_2 \cos \psi \frac{|\delta u_1|}{|\delta p_1|} + B_3 \frac{|\delta u_1|^2}{|\delta p_1|^2} \right), \quad (6.27)$$

where ψ — phase shift between δp_1 and δu_1 .

It is easy to see that the expression in parentheses is constant. Its sign depends, other things being equal, on k_1 and k_2 . Let us assume that k_1 and k_2 are such that the expression in parentheses is larger than zero; then $A_z > 0$ and acoustic energy generated in zone σ will be transmitted to the mass of gas. If losses are absent, then this will lead to increase of amplitudes of oscillations, i.e., to increase of $|\delta p_1|^2$ in formula (6.27), which in turn will increase $A_z > 0$, and as a result there will appear a process of theoretically infinite increase of amplitudes of the oscillations, no matter how small the initial perturbation was. Certainly an infinite increase of amplitudes will not occur, since then at some moment of time the burning processes will be disturbed, acoustic laws will cease to be valid, and so forth, but amplitudes of the oscillations can attain great magnitude.

At other values of k_1 and k_2 , the expression standing in parentheses in formula (6.27) could be negative. Then we would have $A_\Sigma < 0$, and the initial perturbation with passage of time would tend to zero.

The considered example indicates the essential role of feedback in self-excitation of vibrational burning. Namely, feedback realizes the phase and amplitude relationships necessary for self-excitation which were considered in more detail in the preceding paragraph. Therefore, feedback can strongly affect vibrational characteristics of a combustion chamber.

There exist many different feedback mechanisms, which in the final result lead to fluctuating heat release or to oscillations of the flame front (or to both simultaneously), and through them in turn lead to excitation and supporting of acoustic oscillations. Below there will be briefly discussed the characteristics of basic feedback mechanisms. Certainly the mechanisms enumerated below by no means exhaust all probable causes of support of vibrational burning. Here we will discuss only those phenomena which are sufficiently frequently observed and apparently play a fundamental role in the considered type of natural oscillations. Inasmuch as the process of combustion in combustion chambers is connected with the process of carburetion, eddy formation and the actual burning, then the group of all mechanisms of feedback can be divided into mechanisms connected with carburetion, hydromechanics of flow and actual burning. This classification, just as other conceivable classifications, is of course very arbitrary.

During the analysis of possible feedback mechanisms, we will everywhere assume that oscillations have already appeared, and will describe the chain of phenomena leading to the supporting of these oscillations.

Feedback Mechanisms Based on Carburetion

Carburetion, which occurs in the engine duct, can be characterized by spatial nonuniformity in the distribution of fuel. If this spatial nonuniformity moreover has a periodic character, then into the burning zone there will arrive a mixture with periodically varying air-fuel ratio or with periodically varying ratio of liquid fuel to vaporized fuel, and so forth. This can lead to both the appearance of fluctuating heat release and mobility of the flame front.

The general considerations given here can be made more concrete in the following feedback mechanisms.

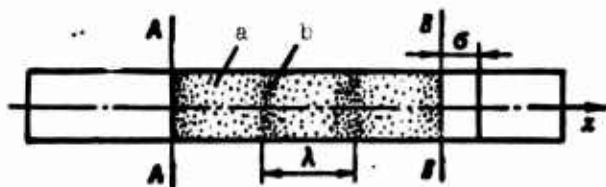


Fig. 6.3. Formation of lean (a) and rich (b) sections of fuel mixture as a result of oscillation of the flow rate of air in the region where the injectors are located (section A - A).

1. Periodic change of air-fuel ratio is possible if in the zone where the ideally operating fuel manifold is located, which gives a constant flow rate of fuel uniformly mixed with air, the flow rate of air oscillates. As a result, flow after the manifold will alternately carry

first a lean mixture and then rich mixture into the burning zone. It is obvious that in the burning zone the frequency of oscillations of air-fuel ratio α will coincide with the frequency of oscillations of the entire gas column in the combustion chamber and air-fuel line; i.e., it will occur with acoustic frequency. This may be seen from the following simple calculation (Fig. 6.3).

Let us assume that in the section A - A there is located a fuel manifold with injectors. Due to acoustic oscillations of the medium, velocity in section A - A is not constant, but has a harmonic component. As a result, in this section there will be formed first rich, then lean mixture alternately. This mixture will be carried to the right with average velocity u_1 ; therefore the "wavelength" of the perturbation α , which is designated in Fig. 6.3 by λ , will be equal to $\lambda = u_1 \tau_1$, where τ_1 is the period of acoustic oscillations. If we assume that in section B - B, which corresponds to the beginning of the burning zone σ , the average flow of velocity the mixture is also u_1 , then the period of oscillations α in this section will be λ/u_1 ; i.e., it will also be τ_1 . The mixture ratio, oscillating at the entrance into the burning zone with acoustic frequency, will cause in zone σ an oscillating combustion process, which is a result of both the oscillatory change of calorific value of the mixture and of combustion efficiency.

2. Oscillations of flight trajectories of droplets of fuel (which are visible as oscillations of the "mushroom" of the working injector) can occur as a result of oscillation of the velocity head in the region of location of the injectors, which occurs due to oscillation of the mass of gas. Then after the injector and further downstream there will be formed periodically varying local concentrations of fuel, and possible there will appear other periodic changes in the quality of the mixture (different coarseness of droplets, different degree of vaporization, and so forth). This phenomenon can give to burning an oscillatory character, which is coordinated with oscillations of the medium inside the combustion chamber. But inasmuch as

oscillations of medium in the region of the injectors which lead to nonuniformity of the quality of carburetion occur with acoustic frequency, then, when it enters zone σ , the fuel mixture carrying these nonuniformities will also, just as in the preceding example, disturb the process of combustion with acoustic frequency.

Thus, the mechanism of excitation in both of the considered cases can be conditionally described by the following: acoustic oscillations of the medium lead to disturbance of carburetion; such carburetion leads to oscillatory burning; the latter leads to acoustic oscillations.

3. During the use of low-pressure fuel-injection systems the flow rate of fuel may oscillate due to the oscillation of counterpressure. This feedback mechanism was described in the preceding paragraph.

4. Too close location of injectors to walls of the chamber sometimes leads to the appearance of vibrational burning. In all probability, oscillations in this case are supported due to the fact that fuel periodically (with acoustic frequency) hits the walls of the combustion chamber due to oscillation of the air mass, for instance, due to oscillations of the "mushroom" of the working injector. As a result the process of combustion also becomes periodic.

Feedback Mechanisms Based on Hydromechanical Phenomena

The possibility of excitation of acoustic oscillations during burning of pre-mixed, homogeneous fuel-air mixtures indicates that carburetion is not the only process which makes it possible for the mechanism of feedback between acoustic phenomena and burning to appear. This completion of the feedback loop can be caused by hydromechanical phenomena in the engine direct.

1. Eddy formation in a combustion chamber, which always has periodic character, can be amplified and returned to the frequency of acoustic oscillations of the gas column in the combustion chamber. If eddy formation has a similar character, then vortices which are shed will be carried into the burning zone and will periodically disturb both the process of heat release and the stationary position of the flame front in it. To overcome this phenomenon, it is possible to take a number of measures. For instance, to improve the aerodynamic contour of entrance sections of the combustion chamber, turning special attention to places where it is possible to expect a diffuser effect, to bluff structural elements, and so forth. Sometimes it is useful to place before the burning zone straightening grids and other devices which destroy large eddies. It is not difficult to see that these measures for

combatting vibrational burning essentially lead to disruption of feedback.



Fig. 6.4. Formation of eddies, which are carried into the burning zone, as a result of the existence of a bluff element A. In the lower part of figure we see breaking up of eddies into smaller vortices by a wind-straightener B.

In Fig. 6.4 there is schematically depicted such a process. In the upper part there is shown a chain of eddies following at a distance of λ from each other in the burning zone, where $\lambda = u_1 \tau_1$. In the lower part there is given an example of destruction of these eddies by a wind-straightening grid.

2. Eddy formation after flame-holders should especially strongly affect the burning process. As it is known, the

shedding frequency of vortices from a flame-holder is determined under usual conditions by a series of hydromechanical rules. Experiments have shown that if the flame-holder is located in a pipe in which there are excited acoustic oscillations, then the process of eddy formation is "retuned." In particular, vortex shedding starts to occur with the frequency of acoustic oscillations. Apparently, oscillation of

the gas column in the pipe, which leads to pulsating flow around the flame-holder, to a strong degree alter the whole process of flow.

Matching of acoustic frequencies with shedding frequencies of burning vortices from the flame holder permits us to assert that in certain cases this matching can lead to the appearance of effective feedback. Actually, powerful eddy formation after a flame-holder, which makes the burning process pulsate, is equivalent to the appearance of a large perturbation of the effective flame propagation velocity δu_{cr} , as follows from formula (6.19), which contains in this case a strongly fluctuating quantity $V_r(\tau)$.

This type of burning after a conical flame-holder (during excitation of acoustic oscillations in the pipe) is represented in Fig. 6.5.

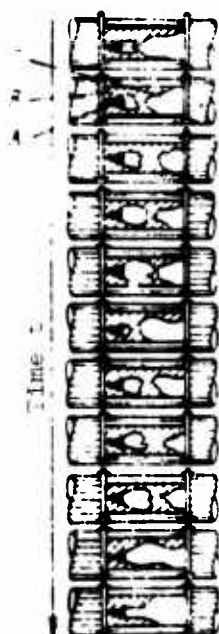


Fig. 6.5. Eddy formation after a flame-holder A during vibrational burning; F is cold mixture; C is the region of combustion.

Feedback Mechanisms Based on Characteristics of the Burning Process

Hydromechanical phenomena and carburetion considered here have led to an indirect influence of acoustic oscillations on the process of combustion. There exists, however, a direct influence of oscillations of the gas column on burning, which can play the role of feedback.

1. It is known that the velocity of normal propagation of a flame depends on temperature and pressure of the mixture; turbulent velocity of propagation is able, furthermore, to change in dependence upon flow velocity.

During oscillations of the gas column in an engine, all three parameters of flow have a periodic component. Consequently, velocity of propagation of the flame will change periodically; this can serve as a cause of vibrational burning. Furthermore, combustion efficiency also can depend on the enumerated flow parameters; in particular, it can be a function of flow velocity.

2. In the presence of an ignition source (flame-holder, precombustion chamber, and so forth), the process of ignition of the mixture can be periodically disturbed when average flow velocity is added to an oscillatory component of velocity caused by acoustic processes.

Actually, every ignition source after which the flame is "held" is characterized, in particular, by a critical flow velocity, at which burning of the mixture incident on the ignition source is still possible. In those cases when the instantaneous value of flow velocity becomes greater than this critical velocity, the flame is "detached" from the ignition source. When the instantaneous flow velocity again becomes comparatively low, the ignition source begins ignition of the mixture again.

The feedback mechanism described here plays an important role. As a rule, this mechanism in a certain degree of development is observed during burning of a mixture after a flame-holder in the regime of strongly developed oscillations, which is characterized by throwing of the flame upstream. This phenomenon can be overcome by means of increase of the power the "pilot flame" in the precombustion chamber and by other measures.

3. The process of combustion is influenced by acceleration of the flame surface. During oscillations of the gas column in an engine and displacements of the flame surface connected with it, this surface is subjected to the influence of very large accelerations.

Considering the flame surface as the boundary between two media of different density, and considering that the position of the flame front is normal to the pipe

axis, the changing accelerations will also be normal to the interface between the media, it is possible to consider "gravity" waves on such a surface, similar to waves on the interface between a heavy liquid and a gas (wave formation on the sea).

From the general theory of gravity waves it is known that they can be either stable or unstable, depending upon the direction of the action of the acceleration: if acceleration acts toward the more dense region (ordinary surface of the sea), the interface is stable; if it acts toward the less dense region, the interface is unstable. Instability of the interface leads to intense growth of the waves on it.

Inasmuch as in the burning zone acceleration periodically changes sign, the interface will periodically be first stable, then unstable. This will lead to periodic change of size of the surface of the flame front due to periodic increase and decrease of the wave formation on it; and this, in turn, will lead to perturbation of the effective velocity propagation of the flame in the rhythm of acoustic oscillations.

§ 5. CERTAIN RECOMMENDATIONS FOR OVERCOMING VIBRATIONAL BURNING

For self-excitation of oscillations there is necessary not just any feedback, but a feedback mechanism which ensures proper amplitude and phase relationships. Above there was presented a theoretical result [for instance, formula (6.23)] according to which an oscillatory system is able to undergo self-excitation only when the perturbation δQ is properly shifted in phase relative to δp_1 and has a sufficiently large relative magnitude. Absolutely analogous laws are peculiar to the process for self-excitation due to the perturbation δu_{cr} . Thus, vibrational burning can, in general, be countered in two ways - by changing the phase of the oscillation δQ and δu_{cr} or their relative amplitudes.

The first way reduces to influencing the phase of the oscillation. If, for instance, the "feedback loop" was completed as a result of oscillation of the air-fuel ratio α , then change of the phase of arrival of riched mixture into the burning zone could be obtained by means of displacement of the fuel manifold along the flow axis (displacement of section A - A in Fig. 6.3). In other cases there should be applied other measures, sometimes just as simple. However, as operational experience with combustion chambers shows, such methods do not give perceptible results. Attempts to influence the period of induction (delay), of the ignition process or "retuning" of the flame front also do not give a noticeable effect. In general, the influencing of processes connected with the phase of the oscillation

extremely rarely gives a positive effect.

An alternate path is the influencing of relative amplitudes of δQ and δu_{cr} . If we would somehow reduce $|\delta Q|$ and $|\delta u_{cr}|$ to very small magnitudes, then vibrational burning would be ceased independently of the realized phase relationships. Consequently, counteraction of vibrational burning is more preferable conducted by means of decrease of relative amplitudes of the perturbations of effective heat addition and effective velocity of propagation of the flame, and not by means of influencing phase relationships. This experimental result (the theoretical explanation is given in work [2]) indicates the most rational methods of counteracting vibrational burning. It is necessary to influence the process of burning in such a manner that relative amplitudes δQ and δu_{cr} are decreased as much as possible, independently of the acting feedback mechanism, which is frequently unknown. Practice shows that the best methods of decrease of $|\delta Q|$ and δu_{cr} which have a sufficiently universal character are measures which lead to dispersed burning. We will explain what has been said by a simple example.

Let us assume that the feedback mechanism is the same as that shown in Fig. 6.3. The wavelength of the perturbation α (distance between neighboring regions of rich mixture) is equal to λ . In the section

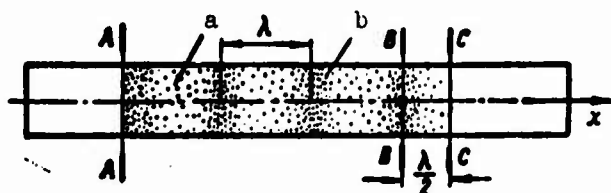


Fig. 6.6. Diagram of dispersed burning; B - B and C - C are regions of location of flame-holders (a - lean mixture; b - rich mixture).

B - B burning begins. If we create two focuses of burning (for instance, by means of location of flame-holders in two different sections), where these focuses are located at a distance of $\lambda/2$ apart, as shown in Fig. 6.6, then the process of burning will be distinguished by the

following characteristic. Let us assume that the two focuses are located in sections B - B and C - C. At that moment when the rich mixture is located in the first of them, in the second there will be lean mixture. As a result, if mixture having $\alpha > 1$ burns, the total heat release will be close to undisturbed heat release, since excess heat obtained in section B - B will be compensated by the deficiency of heat in section C - C. After a time equal to half of a period of oscillation, the lean mixture will be located in B - B, and in C - C there will be mixture; i.e., the process of smoothing out of amplitudes of the perturbation of heat release will continue. Thus, this simple measure can considerably decrease $|\delta Q|$.

The given example has a specialized character; however, even for a number of other feedback mechanisms it is possible to give analogous considerations. Experiments confirm that organization of dispersed burning is a sufficiently universal measure for counteraction of vibrational burning.

LITERATURE

1. L. Krokko and Chzhen Sin'-i. Theory of combustion instability in liquid-fuel rocket engines, IL, 1958.
2. B. V. Kaushenbakh. Vibrational burning, Fizmatgiz, 1961.
3. G. G. Roginskiy. Vibrational burning, Journal of Acoustics, 1961, Vol. VII, Issue 2, p.132-154.

CHAPTER VII

FLAME STABILIZATION IN A FLOW OF FUEL MIXTURE

In combustion chambers of ramjet engines and afterburners of turbojet engines, the flow of fuel mixture moves with high velocities (of the order of 100 m/sec), many times exceeding the velocity of propagation of a flame in a laminar flow. In order that under these conditions the flame will not be carried away by the flow, it is necessary to stabilize it, i.e., to ensure continuous ignition of fuel mixture at fixed points of the combustion chamber. Usually this is done with help of a so-called "pilot" flame (burner, precombustion chamber, etc.) and a system of bluff bodies of different geometric forms.

§ 1. STRUCTURE OF THE FLOW AND MECHANISM OF FLAME STABILIZATION IN THE WAKE AFTER A BLUFF BODY

Investigation of real viscous flows around bodies shows [1] that at moderate incident flow velocity, after the body there are formed two symmetric stable eddies, which with increase of velocity start to be carried off by the flow, forming a "path" of eddies. With further increase of velocity the eddies are so rapidly dispersed after their formation that, for instance, after a cylinder at $Re = 2.5 \cdot 10^3$ the vortex paths are no longer observed. However, sufficiently large eddies continue to be shed, up to $Re = 5 \cdot 10^5$ [2]. Beyond this limit, the boundary layer on the surface of the body becomes turbulent, and the wake becomes a continuous region of purely turbulent flow, retaining, however, two stable (with respect to averaged velocities) symmetric regions of circulating motion of the liquid directly after the stern.

Appearance of circulatory motion of the liquid in the wake after a bluff body is caused by the "ejecting" action of the turbulent streams flowing around the body.

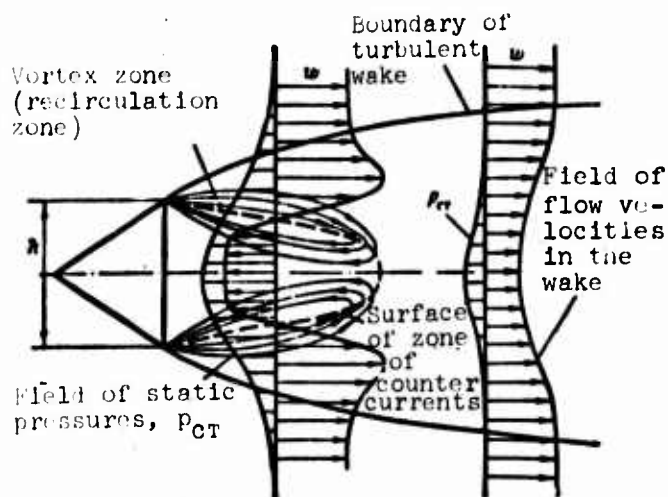


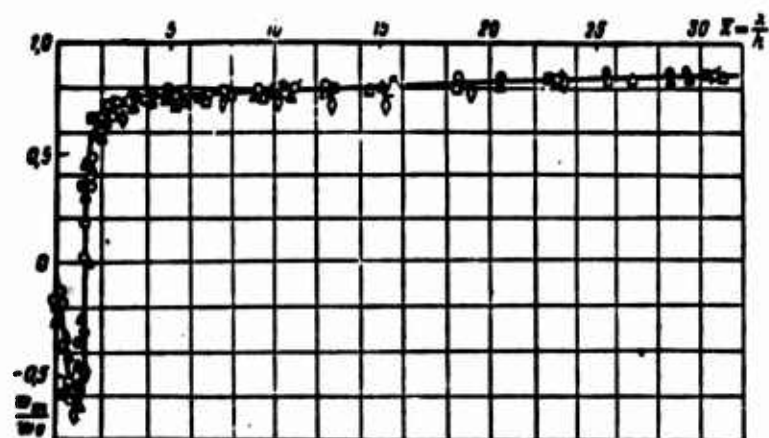
Fig. 7.1. Diagram of flow in the wake after a bluff body.

The flow in the section of the wake directly adjacent to the flame-holder is represented in the following form (Fig. 7.1). Flowing around the obstacle, the viscous flow ejects gasses from the region behind the stern. Up to a certain moment of time, the mass of gas in this zone is not replenished, since the zone is "isolated" from surrounding space by the ejecting flow and the walls of the flame-holder, and in the region of the wake behind

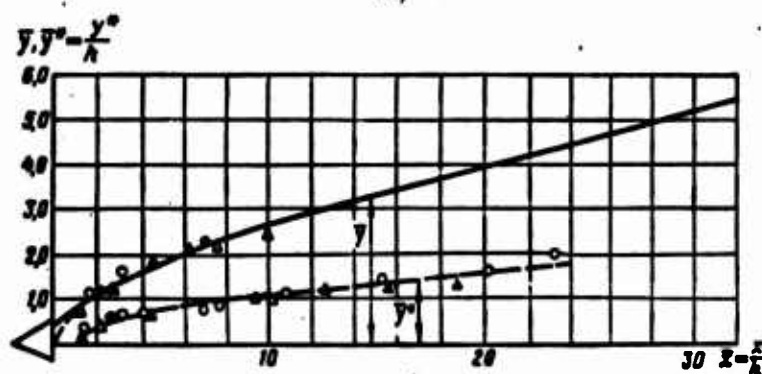
the stern there is created decreased pressure with longitudinal and transverse gradients. Under the action of the transverse gradient of static pressures stream filaments of the flow around the flame-holder are deflected toward the axis of the wake; under the action of the longitudinal gradient of static pressures, along the axis of the wake there appears flow directed toward the body. Simultaneously under the action of forces of friction caused by the difference of velocities, in the boundary layer there appear eddies, twisting toward the axis of the wake, which replenish the mass of gas ejected from the region behind the stern.

As a result in this region there appears a recirculation zone. Inside the recirculation zone there is distinguished a zone of counter currents bounded by a surface of zero flow velocities in projection on the axis of the wake. After a certain time (in absolute value very small), there is established dynamic equilibrium, in which there occurs continuous exchange of masses of gas between the turbulent boundary layer and the zone of counter currents. This equilibrium corresponds to definite dimensions of the zone of counter currents, and also to the distribution of velocities and pressures in the wake.

During isothermal flow around bodies of given geometric form (with fixed point of flow separation), flow in the wake is self-similar: dimensionless profiles of velocity and pressure and also the width of the wake and dimensions of the zone of counter currents do not depend on characteristic dimensions of the bluff body or the velocity of the incident flow (Fig. 7.2). The profile of dimensionless velocities is universal for all cross sections of the main section of the wake. Similarity of flow is also preserved for the boundary layer in the initial section of the wake.



a)



b)

Fig. 7.2. Parameters of the wake behind a bluff body in a half-open flow. a) dimensionless profile of velocity along the axis of the wake; b) width of the wake.

Designations	u_∞ m/sec	λ mm	Designations	u_∞ m/sec	λ mm
●	50	13	○	50-60	13
□	60	13	●	50-60	20
◻	50	20	▲	50-60	32
▲	70	20	△	50-60	
■	50	32			
△	70	32			
○	50	40			
◇	70	40			

The geometric form of the head part of the body determines the direction of the velocity vectors at points of flow separation; the more the velocity vector deviates from the axial direction (consecutively - cylinder, wedge, plate; Fig. 7.3), the greater the width of the wake, the dimensions of the zone of counter currents and, as a rule, the rarefaction in the region behind the stern.

Flow after a body of given geometric form can be changed by means of change of rarefaction in the region of the wake behind the stern, for instance, by removal from or addition to the zone of a definite quantity of gas. In the first case, due to the

increase of rarefaction, there will be increased the transverse and longitudinal gradients of static pressure after the stern of the body, as a consequence of which stream filaments of the current upon separation from the flame-holder will be deflected more toward the axis of the wake, and the length of the zone of counter current will decrease; in the second case, conversely, the transverse gradient of static pressures will decrease, and the zone of counter currents will increase. This is confirmed by experiment (Fig. 7.4).

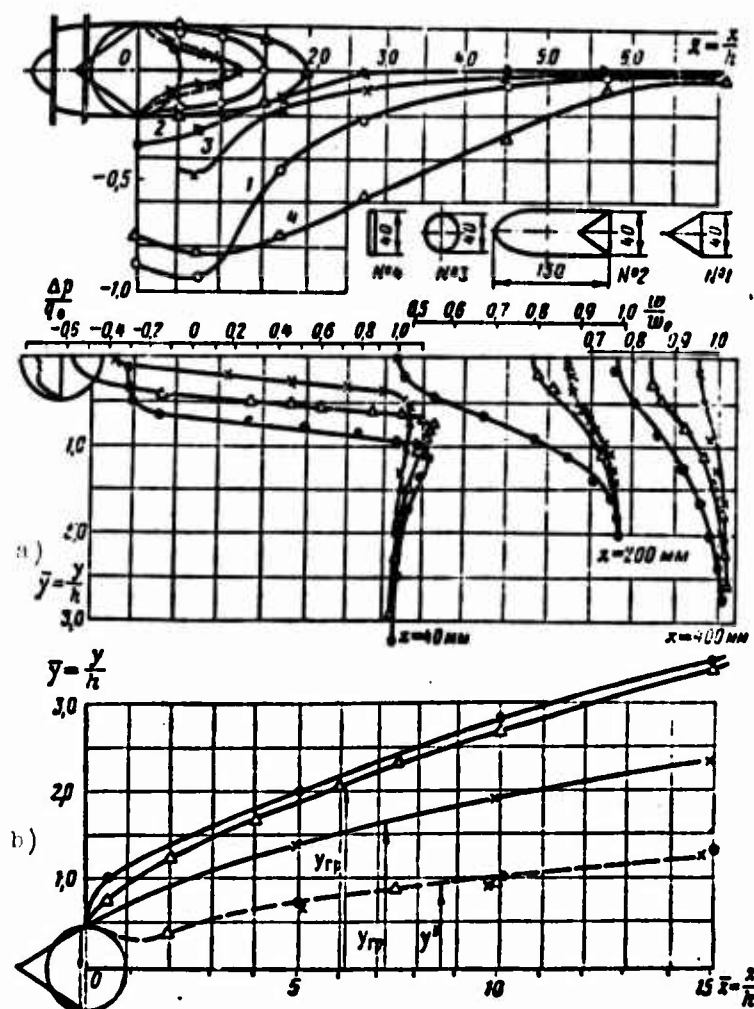


Fig. 7.3. The influence of geometric shape of bluff bodies on parameters of their wakes. a - velocity profile; ● - plate, $h = 40\text{ mm}$; × - cylinder, $d = 40\text{ mm}$; Δ - V-shaped flame-holder, $h = 40\text{ mm}$; b - boundary of wake; designations are the same.

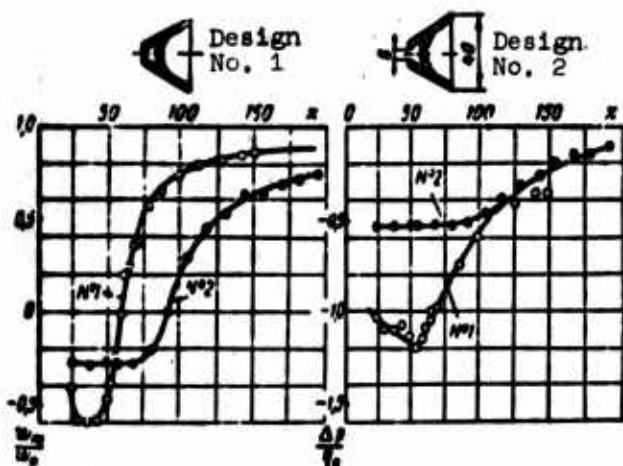


Fig. 7.4. Change of pressures and velocities along the axis of a wake during blowing of air into the zone of counter currents (flow without burning; $q_0 = 220$ mm Hg).

Flow in the zone of counter currents is not steady in time. This can be seen by the strong pulsations of static pressure. These pulsations do not have strict periodicity; they are a result of shedding of vortices in the recirculation zone, and probably play an essential role in the mechanism of blowoff.

In work [3] there are given interesting experimental data showing that the degree of rarefaction after the flame-holder (and consequently

parameters of the entire wake) greatly depends on shedding frequency of vortices in the recirculation zone. Decrease of shedding frequency of vortices by means of installation of a plate along the axis of the wake in the region behind the stern leads to large decrease of rarefaction and increase of the dimensions (length) of the zone of the counter currents.

Parameters of the wake during combustion greatly differ from parameters of the isothermal wake: during burning in a half-open flow, rarefaction in the region behind the stern strongly decreases,

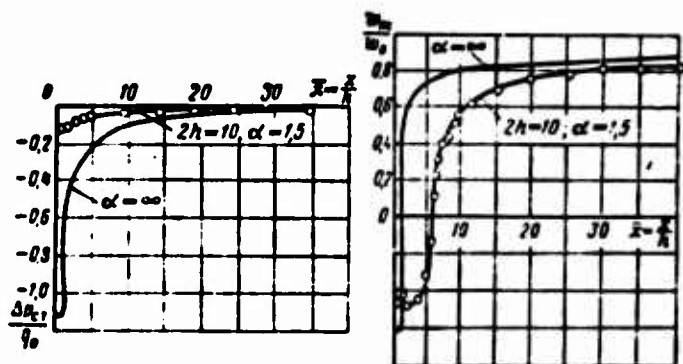


Fig. 7.5. Change of pressures and flow velocities along the axis of the wake after a V-shaped flame-holder both with a cold flow and during combustion ($\beta = 60^\circ$; $q_0 = 300$ mm Hg).

and due to this the dimensions of the zone of counter currents are increased by 3-4 times. For instance, during flow around a V-shaped flame-holder with vertex angle of $\beta = 60^\circ$ in a half-open flow without burning, the length of the zone of counter currents is equal to ~ 1.5 times the height of the flame-holder; with burning,

however, the length of the zone of counter currents increases up to six-seven times the height of the flame-holder (Fig. 7.5).

Increase of static pressure in the region of the wake behind the stern and the increase of dimensions of the zone of counter currents connected with this are the

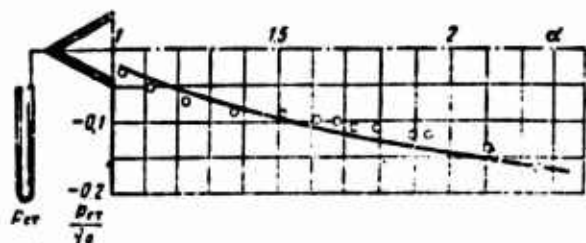


Fig. 7.6. Change of static pressure after a flame-holder during combustion in dependence upon x/d .

the fuel mixture becomes leaner, there is increases the rarefaction after the flame-holder (Fig. 7.6), and accordingly dimensions of the zone of counter currents decrease. However, within quite a wide range of change of mixture ratio, static pressure in the zone of counter currents changes little.

During burning in a pipe, parameters of the wake after the flame-holder to a strong degree depend on the degree of blockage of the useful cross section of the pipe. With considerable blockage (with installation of flame-holders in the same plane with small distance between them), rarefaction in the wake during burning can be even greater than without burning. This is explained by the fact that due to thermal expansion of gases in the flame there is increases the flow velocity of the fresh mixture in the space between the flame-holders, q_0 there is increased rarefaction after the flame-holder proportionally to increase of impact pressure, and, accordingly, there are decreased the dimensions of the zone of counter currents. With echeloned location of flame-holders in the pipe, flow becomes more similar to a half-open flow.

For establishment of the mechanism of flame stabilization, and also for obtaining quantitative theoretical dependences, it is necessary to have correct ideas concerning mass and heat exchange between the zone of counter currents and the turbulent boundary layer surrounding it. For the first time these measurements were made quite thoroughly in a cold flow and during combustion by Kovina [4]. In the indicated work, there was measured the average stay time of particles of gas in the zone of counter currents τ_{Π} :

$$\tau_{\Pi} = \frac{V_{\Pi}}{S \cdot \bar{u}_{\Pi}}, \quad (7.1)$$

where V_{Π} — volume of the zone of counter currents in m^3 ;

S — surface of zone of counter currents in m^2 ;

\bar{u}_{Π} — average escape velocity of gas through the surface of the zone of counter currents in m/sec.

Measurements have shown that during flow around flame-holders of given geometric

shape under conditions close to those of an open flow:

1) the average stay time of particles of gas in the zone of counter currents is proportional to dimensions of the flame-holder and inversely proportional to the average approach flow velocity;

2) during combustion, stay time is approximately 2.8 times longer than during cold flow around the flame holder, and practically does not depend on change of mixture ratio α ;

3) time of stay decreases with increase of the intensity of turbulence of the incident flow.

For calculation of stay time there is obtained the following empirical formula:

$$\tau_n = k \frac{h}{w} \text{ sec}, \quad (7.2)$$

where h — characteristic dimension of the flame-holder, i.e., its height;

w — approach flow velocity;

k — proportionality factor, depending on geometric shape of the flame-holder.

For instance, for V-shaped flame-holders with angle $\beta = 30^\circ$ during cold flow and with combustion, k is respectively equal to 37 and 104. Knowing the average stay time τ_n and the volume of the zone of counter currents V_3 , by formula (7.1), we can determine mass transfer between the zone of the counter currents and the boundary layer surrounding it:

$$G_{\text{обмена}} = \bar{u}_{\text{mix}} S \gamma = \frac{V_3}{\tau_n} \gamma \text{ kg/sec.}$$

For known composition of the fuel mixture α (taking into account almost complete combustion of the fuel in the zone of counter currents), it is also easy to determine heat transfer:

$$Q = G_{\text{обмена}} c_p T_r = \frac{V_3}{\tau_n} \gamma \cdot c_p T_r \text{ kcal/sec,}$$

where γ and T_r are specific gravity and temperature of gases in the zone of counter currents.

Numerous experimental data show that in the whole range of stable combustion with respect to flow velocity and mixture ratio, even under conditions close to critical (flowoff), temperature and chemical composition of gases in the zone of counter currents remain practically constant and correspond either to complete combustion at $\alpha \geq 1.0$, or to full depletion of oxygen at $\alpha \leq 1.0$. However, with approach to critical conditions of burning, for instance, by means of increase of

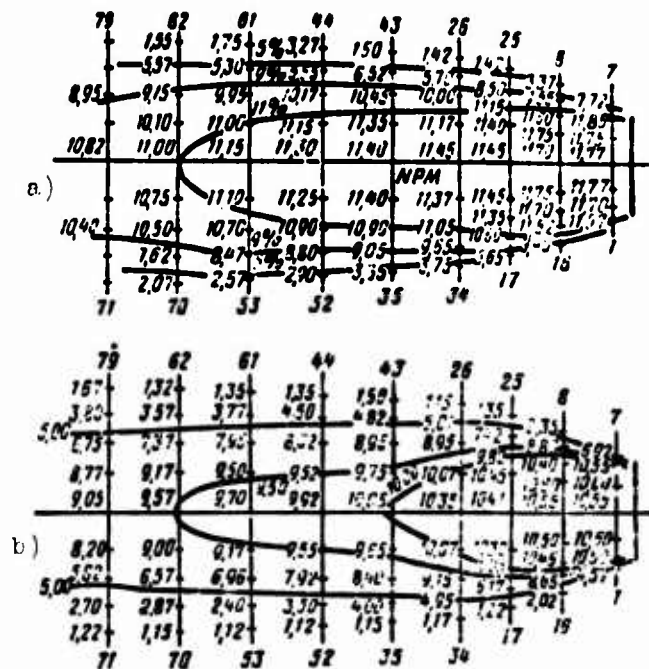


Fig. 7.7. Distribution of concentrations of CO_2 in the recirculation zone. Flame-holder is a disk, $d = 25$ mm; $\alpha = 1.3$: a) flow velocity $w = 85$ m/sec; b) flow velocity $w = 150$ m/sec.

flow velocity, the region of constant temperatures corresponding to complete combustion of fuel is noticeably reduced: the width and length of this zone decrease (compare Fig. 7.7a and 7.7b).

On the basis of what has been said above concerning the structure of flow in a wake, it is possible to formulate the physical essence (model) of flame stabilization by a bluff body in the following way. During burning in the wake after a bluff body, there will be formed a circulation zone consisting of a zone of counter currents filled with combustion products and a turbulent

vortex boundary layer surrounding it, in which gas from the zone of counter currents mixes with the fresh mixture and ignites it. Flame stability is ensured by its continuous ignition at a definite point. A peculiarity of burning after a bluff body is that the stay time of fuel mixture is increased due to circulation of gas in the zone of counter currents, which leads to almost complete combustion of gas entering this zone, and the intensity of ignition is increased due to intense heat addition to the fresh mixture through the inner boundary of the turbulent boundary layer, which creates favorable conditions for ignition of the mixture at high velocities of the incident flow.

§ 2. EXPERIMENTAL DATA ON FLAME STABILIZATION BY BLUFF BODIES

Combustion stability after a bluff body depends on many variables — dimensions and geometric form of the flame-holder, temperature, velocity, pressure and intensity of turbulence of the flow, air-fuel ratio α and chemical nature of the fuel, conditions of burning — in a free flow or in a pipe, etc.

Blowoff from flame-holders can have a double character. During burning in a long pipe, especially in rich mixtures, when the flame touches the walls there frequently appears vibrational burning accompanied by pulsations of pressure and

velocity of the gases and pulsations of the flame front. Blowoff under these conditions is determined mainly by the intensity of pulsations, and can occur at the most diverse values of velocity and mixture ratio. By changing the total length of the pipe and the length of its hot part in the appropriate way, it is possible to observe blowoff at a given average flow velocity at the most diverse values of α . If, however, burning occurs in the absence of sharp oscillations of velocity and pressure of the gases, which is the case during burning in an open flow, in short pipes or in long pipes in lean mixtures, then the blowoff mechanism is different. It is possible to arbitrarily call it kinetic blowoff.

The majority of research in flame stabilization by bluff bodies was conducted in free flows or in short pipes.

During calm, non-fluctuating combustion, enrichment of fuel mixtures to the limits which are of practical interest (to $\alpha \approx 1.0$ to 1.1) usually leads to expansion of the range of stable combustion with respect to flow velocity. Therefore, blowoff in lean mixtures is of practical interest. But, under these conditions, blowoff characteristics of flame-holders, even in long pipes, practically do not differ from characteristics of blowoff in an open flow. Therefore, we may assume that characteristics of the process of flame stabilization during burning in an open flow can also be extended to burning in a pipe - the simplest combustion chamber of straight-flow-through type.

The limits of stable combustion in the wake behind a bluff body are usually characterized by the flow velocity at which blowoff occurs at a given mixture ratio. Maximum flow velocities at which blowoff occurs from a flame-holder of given dimension and geometric shape correspond to a region close to the stoichiometric mixture ratio. As the mixture is made richer or leaner, the blowoff velocity decreases. Extreme values of α (at them there is possible stable combustion after the bluff body at flow velocity $w \rightarrow 0$) correspond to the concentration limits of ignition of hot mixtures under stationary conditions (motionless mixture). Thus, the region of stable combustion (Fig. 7.8) lies inside the curve $w_{cp} = f(\alpha)$ dimensions of which depend on a number of factors.

Influence of dimension of the flame-holder. The limits of stable burning with respect to flow velocity and mixture ratio are widened with increase of the dimension of the stabilizer (see Fig. 7.8). It has been experimentally established that, other conditions being equal, the following relationship holds:

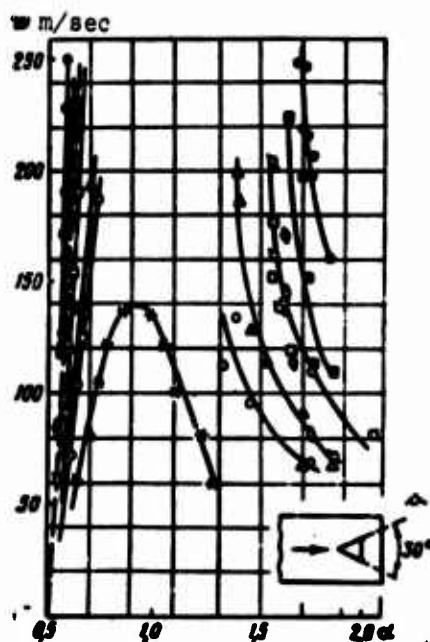


Fig. 7.8. Blowoff characteristics of conical flame-holders (experiments of Khramtsov); w - flow velocity in the radial clearance at the flame-holder exit.

Designations	○	△	□	◇	◇	■	●	*
d in mm	25	40	51.5	60	70	80	90	10

$$\frac{w_{cr}}{h^a} = f(\alpha), \quad (7.3)$$

where h is the characteristic dimension of the flame-holder (diameter or width) in m.

For flame-holders of relatively large dimension (at $Re \geq 5 \cdot 10^4$), the exponent $a \approx 1.0$; at $Re < 5 \cdot 10^4$, the best agreement with experimental data is obtained at $a = 0.45$. During burning of petroleum fuels (gasoline, kerosene, and so forth) behind V-shaped flame-holders with height $h > 10$ mm the influence of dimension of the flame-holder is satisfactorily taken into account by the formula (7.3) at $a = 1.0$ (Fig. 7.9).

Influence of geometric form of the flame-holder. Well streamlined bodies (drop-shaped, and so forth) do not stabilize a flame in high-velocity flows. The flame is stabilized only after bodies with blunt rear edge, during flow around which there occurs flow separation. It was determined that for an identical characteristic dimension of a flame-holder (its middle section), the range of stable

combustion is wider, the larger the drag coefficient of the streamlined body during burning c_x (for axially symmetric bodies, successively - disk, cone, sphere; for flat bodies - plate, wedge, cylinder). Quantitative relations for calculation of the influence of geometric form of the flame-holder (Fig. 7.10) on the limits of flame stabilization with respect to flow velocity and mixture ratio have not been established. In the first, very rough approximation, the influence of geometric form of the flame-holder can be estimated (other conditions being identical) by the relationship [5]

$$\frac{w_{cr}}{d \cdot c_x} = f(\alpha). \quad (7.4)$$

The influence of the chemical nature of the fuel. The limits of stable combustion depend on the chemical nature of the fuel: the higher the velocity of normal propagation of the flame u_H , the wider the range of stable combustion with respect to α and flow velocity. However, the value of u_H does not determine the range of stable combustion uniquely: thus, at $\alpha = 1.3$, temperature of the mixture $293^\circ K$ and pressure of 1 atm (abs), the velocity of normal propagation of the flame in an acetylene air

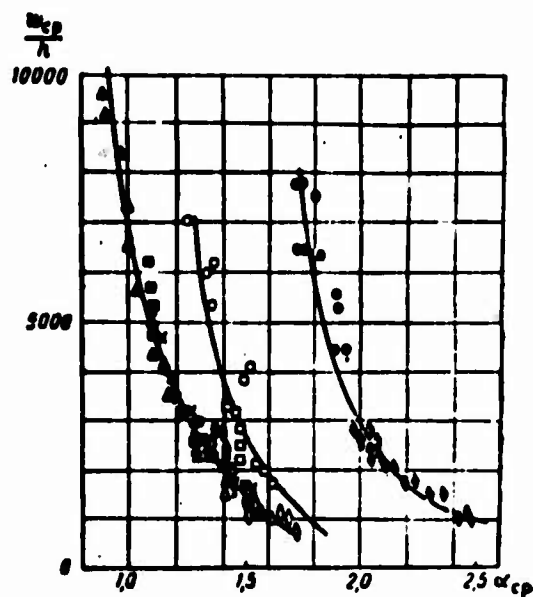


Fig. 7.9. $d_{CT} = f(\frac{w_{cp}}{h})$ for flame-holders of different geometric form.

Design	h mm	d_{CT}	Designations
Conical flame-holder with $\beta = 30^\circ$ in a pipe with $\phi = 100$ mm	11.5	100	▲
	17.9		■
	25		×
	40		△
	51.5		◇
V-shaped flat flame-holder with $\beta = 30^\circ$ in a half-open flow	20	100	○
	50		□
Flat V-shaped flame-holders with $\beta = 60^\circ$ in a pipe 135 x 350 mm, $L = 800$ mm; 11 flame-holders with $h = 10$ mm and 5 with $h = 40$ mm	10	200	●
	40		◆

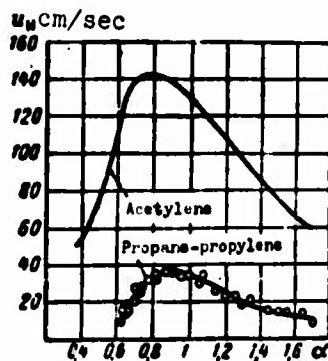


Fig. 7.11. Dependence of normal velocity of propagation of a flame on mixture ratio at $t_{CM} = 20^\circ C$.

mixture exceeds the velocity of normal propagation of the flame in a propane-propylene-air mixture by approximately five times, but the blowoff velocity of the flame-holder (flameout) during burning of acetylene air mixtures turns out to be 15 times higher than during burning of propane-propylene-air mixtures (Figs. 7.11 and 7.12).

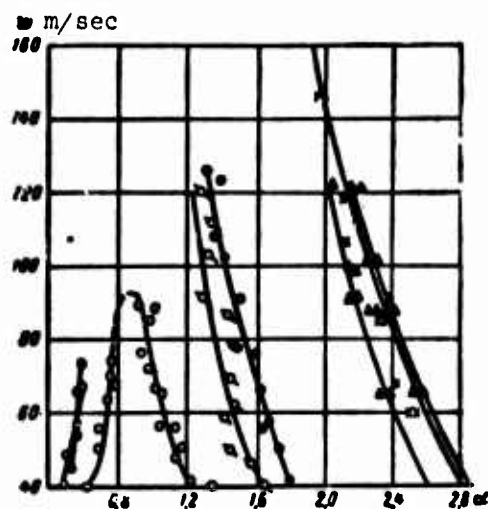


Fig. 7.10. Characteristics of stable combustion after flame-holders of different geometric form. Homogeneous gasoline-air mixture, $t_{CM} = 20^\circ C$. □ - cone, $d = 40$ mm; ● - disk, $d = 40$ mm; ○ - sphere, $d = 40$ mm; ▲ - cylinder, $\phi = 40$ mm; △ - plate, $h = 40$ mm; × - V-shaped flame-holder, $h = 40$ mm.

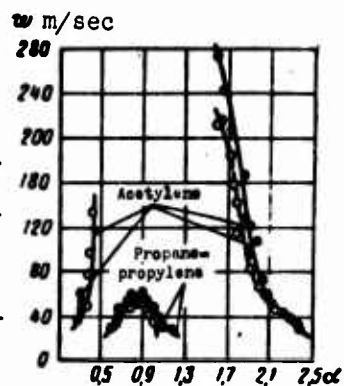


Fig. 7.12. Dependence of limits of stable combustion after a conical flame-holders on chemical nature of the fuel at atmospheric pressure and $t_{CM} = 20^\circ C$.

● - $d_{CT} = 5.7$; ○ - $d_{CT} = 4.5$.

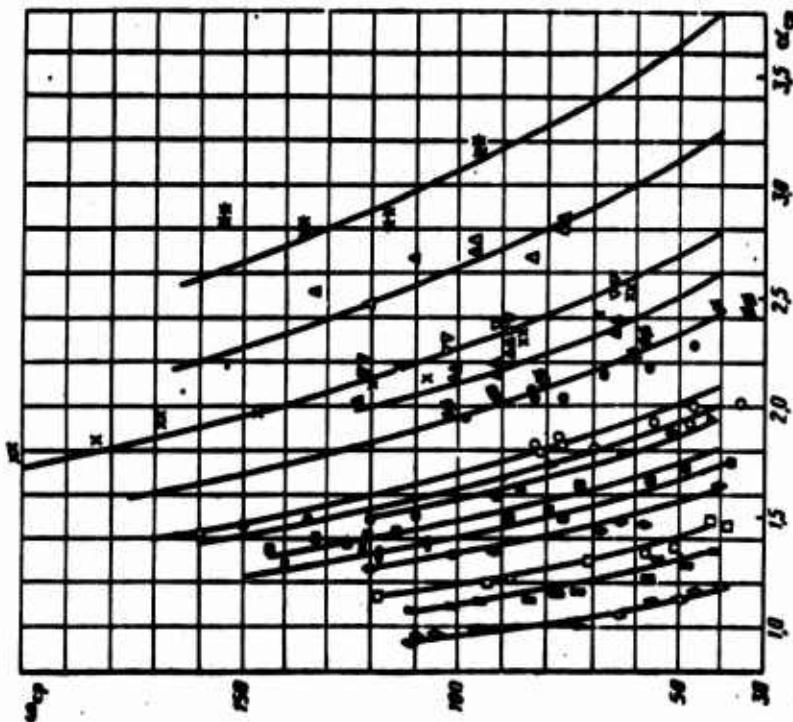







Fig. 7.13. Change of the range of stable combustion after flame-holders depending upon temperature of the mixture at atmospheric pressure.

Design	Δ mm	ϵ %	Designations
Circular conical flame-holder in a pipe with ϕ 100, $\beta = 30^\circ$	11.5 17.5 25 40 51.5	100 100 100 100 100	\circ \square \triangle \diamond \bullet
Wedge-shaped flat flame-holder $\beta = 30^\circ$ 	20 30	100 100	\square \bullet
Wedge-shaped flat flame-holder in a pipe of 135 x 350 mm (2) $h = 40$ mm, $S = 40$ mm, $\beta = 60^\circ$ 	40	100 200 300 400 500	\circ \bullet \times \triangle \square
Two cylinders with ϕ 40 mm, $S = 40$ mm, $\beta = 0^\circ$ 	40	300	\triangle
2 plates $\beta = 180^\circ$ $h = 40$ mm, $S = 40$ mm 	40	300	∇
Four flame-holders $h = 10$, $S = 20$ mm, $\beta = 60^\circ$; $a = 20$ (echeloned). 5 flame-holders with $h = 40$ mm, $S = 20$ mm, $\beta = 60^\circ$; $a = 60$  (echeloned)	40 40	300 300	∇ \diamond

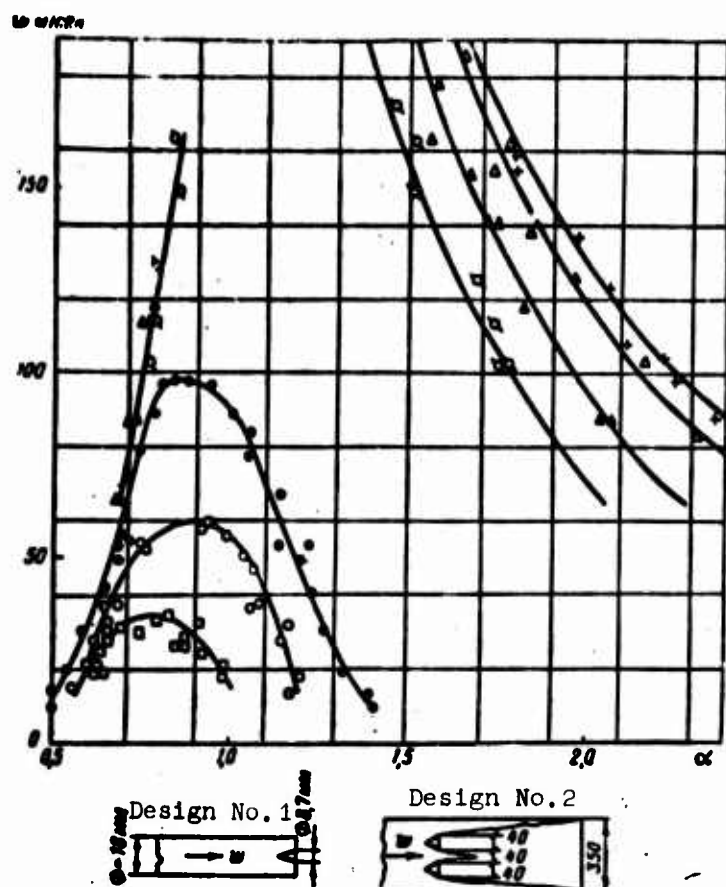


Fig. 7.14. Change of the range of stable combustion after a flame-holder depending upon pressure in the flow.

Designations	p, atm (abs)	t ₀ , °C	Design, dimensions, flame-holder, fuel
○	0.004	20	Design No. 1, Conical flame-holder, d = 8.7 mm, propane-propylene [6]
●	0.02	20	
□	0.335	20	
◻	0.31	210	Design No. 2, V-shaped flame-holder, h = 40 mm, gasoline
▲	0.4	210	
△	0.6	210	
+	0.8	210	

Influence of chemical nature of the fuel on the range of stable burning in the wake after a bluff body has been insufficiently studied, and reliable quantitative relations have not been established.

Influence of temperature of the mixture. With increase of temperature of the mixture, the boundaries of stable combustion are widened (Fig. 7.13). This is partially explained by the increase of u_H with increase of temperature of the mixture. However, the relative increase of flow velocity up to blowoff with increase of u_H by means of heating of the mixture is

considerably less than in the case of increase of u_H means of changing the chemical nature of the fuel. This is explained, apparently, by the fact that fuels with high u_H have, as a rule, lower activation energy and lower ignition temperature. The dependence of blowoff

velocity on the initial tempera-

ture of the fuel mixture during burning of hydrocarbon fuels (gasoline, kerosene, and so forth) is satisfactorily approximated by the relationship

$$\frac{w_{cp}}{w_{0cp}} \sim \left(\frac{T}{T_0} \right)^n, \quad (7.5)$$

where T_0 , °K is the value of temperature of the mixture at which the value of flow velocity w_{0cp} at blow off from a flame-holder of given dimensions at given value of

α is known. The exponent m , according to various authors, should be 1.5 to 1.65 [6].

Influence of pressure in the flow. With decrease of pressure, the limits of stable combustion in the wake after a bluff body are narrowed (Fig. 7.14). The influence of pressure on the limits of stable combustion is different depending upon dimensions of the flame-holder: it is stronger for small dimensions of the flame-holders and less for larger dimensions. This question has been studied insufficiently, but the majority of researchers [8] arrive at the conclusion that the limits of stable combustion in dependence upon pressure changed according to the expression

$$\frac{u_p}{u} \sim \frac{1}{p^n}, \quad (7.6)$$

where $n = 0.95$ to 0.6 and depends on dimension of the flame-holder: the higher values of n correspond to flame-holders of small dimensions, and conversely (for V-shaped flame-holders with height of $h > 30$ mm, the value of n is close to 0.6).

The influence of turbulence of the incident flow. With increase of intensity of turbulence of the incident flow, the limits of stable combustion decrease. Turbulence of given scale and intensity affects stability limits less when flame-holder dimensions are large. Quantitative relations have not been established.

The influence of thermal losses. Experimental data on the influence of thermal losses from a flame on combustion stability in the wake after a bluff body are contradictory. In works [9], [15] it is indicated that preheating of the flame-holder (a tube with diameter of 0.8 mm fixed normal to the flow) to 925°C expanded the range; and cooling to 30°C narrowed the range of stable combustion as compared to the equilibrium temperature of the flame-holder (which had a rod without additional cooling or heating). At the same time it was noticed that cooling of walls of the flame-holder by running water practically did not change the range of stable combustion as compared that of an uncooled flame-holder.

On the whole, one may assume that the influence of temperature of the flame-holder on the range of stable combustion is noticeable only for small dimensions of the flame-holder. At pressures close to or higher than atmospheric, thermal losses from the flame by means of radiation and through the walls of the flame-holder during its cooling practically do not affect the range of stable combustion in the wake after the flame-holder. At low pressures (of the order of tenths to hundredths of an atmosphere), the influence of thermal losses can be considerable; it depends on temperature and composition of the fuel mixture and, as calculations show [8] for burning of propane with air ($t_{\text{cm}} = 16^\circ\text{C}$), only radiative thermal losses lead to the

impossibility of flame stabilization by a bluff body: for stoichiometric composition, at $p \approx 5 \cdot 10^{-3}$ atm (abs); for a mixture with $\alpha \approx 0.5$ and 1.8 – at a pressure of $p \approx 0.1$ atm (abs).

Influence of phase composition of the fuel mixture. Above there was considered the influence of different factors on flame stabilization in a flow of homogeneous fuel mixtures. In combustors of ramjet and turbojet engines, fuel is usually injected

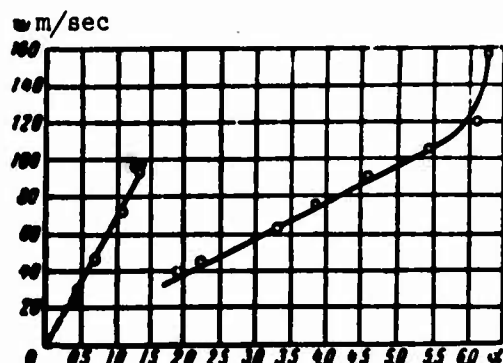


Fig. 7.15. Limits of stable combustion of a two-phase gasoline-air mixture at $t_{CM} = 150^\circ\text{C}$ after a flame-holder.

in liquid-droplet state, and it is necessary to deal with the burning of two-phase mixtures. Experiments have shown that during burning of two-phase mixtures, blowoff from the flame-holders occurs at greater average leanness as compared to burning of a homogeneous mixture. Moreover, stable combustion of two-phase mixtures after a flame-holder is possible with very lean mixtures, beyond the ignition limits of homogeneous mixtures of hydrocarbon vapors with air. The rich blowoff limits are

actually on the lean side of stoichiometric composition [14]. This is explained by the fact that in a moving two-phase mixture, a considerable part of the fuel droplets do not pass around the flame-holder along the flow lines of air, but settle on its surface. Depending upon the temperature of the walls of the flame-holder, the settled fuel is partially evaporated, and partially flows from the trailing edges of the flame-holder in the form of a liquid sheet is broken up by the flow into droplets and is evaporated in the recirculation zone. As a result, the fuel mixture in the blockage zone of the wake turns out to be richer than α_{cp} along the whole combustion chamber. With increase of flow velocity, the fraction of drops settling on the flame-holder increases; therefore, in a two-phase mixture, lean blowoff occurs at large average coefficients of air-fuel ratio, the larger the flow velocity is (Fig. 7.15).

Measurements have shown that during burning of two-phase mixtures, the actual mixture ratio at the trailing edges of the flame-holder at blowoff is in all cases close to values of α of blowoff of homogeneous mixtures, independently of average α calculated according to the total flow rate of air and fuel through the chamber. The difference in the limits of stable combustion of homogeneous and two-phase mixtures becomes smaller, the further from the flame-holder the injectors are installed, and

the finer the fuel droplets in the atomization spectrum. Blowoff characteristics in lean homogeneous mixtures can be taken as the lower limit of stable combustion of two-phase fuel mixtures.

Influence of the ignition source. For primary ignition of the mixture, into the region of the wake behind the stern there should be introduced an ignition source -

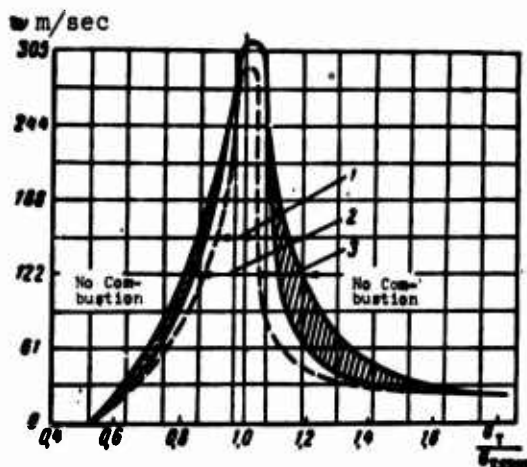


Fig. 7.16. Ignition limits and limits of stable combustion after a flame-holder in the combustor of a ramjet engine: Homogeneous mixture of propane and air. Flame-holder of plate type [9]. 1 - ignition limits; 2 - stable combustion; 3 - unstable combustion.

an electrical spark, a burner with independent feed, and so forth. Experiment shows that during ignition from an outside source, the ignition limits after a flame-holder with respect to flow velocity and air-fuel ratio lie within the limits of stable combustion of the already ignited mixture (Fig. 7.16). In accordance with what has been presented in § 5, Chapter IV, ignition limits are widened with increase of thermal power of the ignition source. If after ignition the ignition source is not turned off, but executes the function of a "pilot flame," then limits of stable combustion are widened more, the

greater the thermal power of the ignition source is.

Peculiarities of flame stabilization by bluff bodies in a combustion chamber.

Above it was indicated that blowoff characteristics of flame-holders during burning

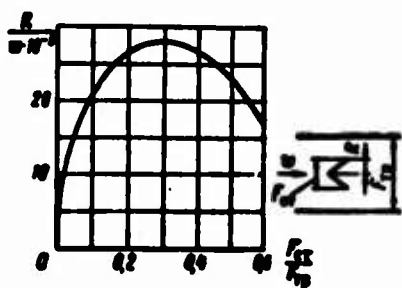


Fig. 7.17. Influence of degree of blockage of the pipe on combustion stability after the flame-holder. $D_{TP} = 150$ mm, $\alpha = 1.0$ [9].

of lean mixtures in a pipe practically do not differ from characteristics of flame-holders during burning in a free flow. However, this is true only in the case of small blockage of the pipe by the flame-holders (for instance, with echeloned location of the flame-holders). In the case of large blockage of the cross section of the flow by flame-holders or considerable increase of the area of a single flame-holder, local flow velocities strongly increase, and there occurs interaction between the turbulent

wakes appearing after each flame-holder. This leads to decrease of the range of stable combustion with respect to approach flow velocity (referred to the cross section

at the rear edge of the flame-holder). Experiments show [13] that in the case of a single flame-holder, maximum blowoff velocities correspond approximately to 30% blockage of the pipe by the flame-holder (Fig. 7.17).

Comparison of numerous experimental data shows that the obtained results to a great degree depend on the conditions under which the experiment was carried out, and, as a rule, are not reproducible by different authors. Therefore, the above-stated results of experiments in the investigation of the influence of different factors on flame stabilization should be considered mainly from the qualitative side.

§ 3. THEORY OF FLAME STABILIZATION BY A BLUFF BODY

A general theory of flame stabilization should take into account the structure of the flow and all of the above-mentioned factors which influence the limits of stable combustion in the wake after a bluff body. In examining this question, we start with the following basic assumption: the flame in the flow is stationary if at one or several points of its front there is ensured continuous ignition of the fuel mixture. From the point of view of the thermal theory of ignition, continuous ignition of the mixture is possible only when to a unit volume of entering mixture there is supplied per unit time from the ignition source the necessary quantity of heat. This is the general condition of stationarity of a flame in a flow.

The difficulty of solution of the problem consists of determination of the amount of this necessary heat. The quantity of heat supplied from the zone of counter currents to an element of volume of fuel mixture depends on the hydrodynamic and thermal state of the recirculation zone. Above it was shown that dimensions of the zone, composition and temperature of the gas in it, and also the average stay time of particles of gas (and consequently mass transfer between the zone of counter currents and the turbulent boundary layer surrounding it) depend on flow velocity, mixture ratio and geometric form and dimensions of the flame-holder.

In turn, the quantity of heat necessary for ignition of the fresh mixture depends on temperature and initial intensity of turbulence of the flow, chemical nature of the fuel, and so forth. Due to the extraordinary complexity of the phenomenon, rigorous analytic or direct experimental determination of the heat actually supplied to the fresh mixture which is necessary for ignition in the critical (near blowoff) regime of burning still turns out to be impossible in practice. Therefore, in examining of flame stabilization of a bluff body in a flow, it is inevitably necessary to resort to one or another simplifying assumption. It is natural that the validity of such assumptions.

The theory of flame stabilization at present has been insufficiently developed, and there is no unified system of views concerning this question. Let us consider briefly the most well-known works.

Williams [9] assumes that the quantity of heat required per unit time for ignition of the fresh mixture is equal to

$$q_1 \sim w (\delta_t (\rho \cdot c_p) (T_1 - T_0)), \quad (7.7)$$

where w - flow velocity in m/sec;

δ_t - thickness of preparation zone in m;

$T_1 - T_0$ - difference between ignition temperature and temperature of the flow;

$\rho \cdot c_p$ - heat capacity of a unit of volume of the fuel mixture.

From dimensional considerations it is taken that

$$\delta_t \sim \frac{a}{u_H}, \quad (7.8)$$

where a - coefficient of thermal diffusivity in m^2/sec ;

u_H - normal velocity of propagation of the flame in m/sec.

Since $a = \frac{\lambda}{c_p \gamma_g}$, then

$$q_1 \sim w \frac{\lambda}{u_H} (T_1 - T_0). \quad (7.9)$$

The quantity of heat transferred from the vortex zone to the cold gas

$$q_2 \sim \left(\text{Re}^{\epsilon} \frac{\lambda}{d} \right) d (T_b - T_0) = \left(\left(\frac{dw}{\nu} \right)^{\epsilon} \frac{\lambda}{d} \right) d (T_b - T_0), \quad (7.10)$$

where $T_b - T_0$ - difference of temperature between the burned gas and the flow of fresh mixture;

d - characteristic dimension of flame-holder (its diameter);

ν - coefficient of kinematic viscosity in m^2/sec .

The combustion process is stable if $q_2 \geq q_1$; for $q_2 < q_1$ there occurs blowoff; critical conditions occur at $q_2 = q_1$. In this case

$$\frac{u_H}{w} \sim \frac{1}{\nu^{\epsilon}} \left(\frac{a (T_b - T_0)}{(T_1 - T_0)} \right)^{1+\epsilon}, \quad (7.11)$$

where

$$\epsilon = \frac{1}{1-\epsilon}.$$

This equation takes into account the influence of the dimension of the flame-holder, pressure in the flow (in terms of ν) and initial temperature of the mixture, but does not consider the influence of geometric form of the flame-holder. In the

solution there is not considered change of the thermal state of the recirculation zone: it is assumed that temperature of gases in the recirculation zone at a given value of α of the mixture does not change up to the moment of blowoff of the flame, and does not depend on dimension of the flame-holder or flow velocity.

At constant pressure and temperature in the flow, type of fuel and geometric form of the flame-holder, the right side of equation (7.11) is only a function of mixture ratio; then this equation will be written as:

$$\frac{q_2}{\rho^2} = \Phi(\alpha). \quad (7.12)$$

In the derivation of these relations, two basic assumptions are quite well-founded:

- 1) proportionality of thickness of the preparation zone to the ratio a/u_H ;
- 2) proportionality of the quantity of heat transferred from the vortex zone q_2 to the heat transfer coefficient $\alpha = Re \frac{\lambda}{d}$. This relationship is valid for the case of heat exchange between a solid body and a gas flow, but it is not clear whether it is possible to extend it to the case of heat exchange between two gas flows under the conditions of turbulent flow.

During burning of homogeneous mixtures of petroleum fuels with air after flame-holders of given geometric form, experimental data will agree well with data calculated by formula (7.12) for $a = 1.0$, if temperature of the mixture remains constant (see Fig. 7.9). Formula (7.12), as experiment shows, takes into account the influence of pressure quite well if we take $a = 1$. Calculated data strongly disagree with experimental data if temperature of the fuel mixture is changed.

The idea of another approach to theoretical consideration of flame stabilization by a bluff body consists of the following. The process of ignition of a fresh mixture by combustion products essentially does not differ from propagation of a flame in it if the conditions of cooling of combustion products are identical in both cases. Therefore, it may be concluded that if propagation of a flame is possible in the fresh mixture, i.e., if the process occurs within the concentration limits of flame propagation, then there is ensured continuous ignition of the mixture by the combustion products.

Consequently, while the zone of counter currents is filled with burned gas, there is provided continuous ignition of the mixture, i.e., flame stability. The process of continuous ignition will be disturbed in the case when the zone of counter currents is with insufficiently filled hot, i.e., with incompletely burned or

completely unburned gas. Consequently, the question concerning the mechanism of blowoff of a flame in the wake after a bluff body is reduced to clarification of the conditions under which the zone of counter currents is filled with incompletely burned or completely unburned gas.

Based on these qualitative physical concepts, it is possible to proceed to quantitative relations in the following way: Boundaries of the region of stable combustion can be characterized in general form by an inequality relating a certain effective value of "stay time" in the reaction zone τ_{np} and "turbulent combustion time" τ_{cr} the flame is stable if $\tau_{cr} \leq \tau_{np}$. Quantitative relations between these quantities are determined with help of similarity theory. According to this theory, for a definite family of similar systems there should be fulfilled constancy of the ratios of the dimensional quantities. The author considers that in particular there should be satisfied the condition

$$\frac{\tau_{np}}{\tau_{cr}} = \text{const.} \quad (7.13)$$

It is assumed that the stay time

$$\tau_{np} \approx \frac{d}{w}, \quad (7.14)$$

where d — characteristic dimension of the flame-holder;

w — flow velocity.

Burn-up time of the mixture in the zone of counter currents is taken to be proportional to the burn-up time in a laminar flame-front

$$\tau_{cr} \sim \tau_{np} \approx \frac{d}{u_H}, \quad (7.15)$$

where a — coefficient of thermal diffusivity;

u_H — speed of propagation of a flame in a laminar flow, whence we will obtain

$$\frac{\tau_{np}}{\tau_{cr}} \sim \frac{d u_H}{d^2} = M_1 = \text{const} \quad (7.16)$$

As numerous comparisons have shown, satisfactory agreement of calculated with experimental data at $M_1 = 0.45$ is obtained only for conical flame-holders with diameter from 3 to 11 mm in the case of burning in an open flow (at the pipe exit) of homogeneous mixtures with $\alpha > 1.0$. Calculated and experimental curves of $w_{cp} = f(\alpha)$ diverge with increase of the dimension of the flame-holder, with change of its geometric form and with change of temperature of the fuel mixture.

The authors of work [10] consider that flame stabilization by a bluff body is provided until there exist certain mass transfer and heat release conditions in the

recirculation zone, i.e., while the chemical reaction occurs with a definite rate, and combustion efficiency of fuel in the recirculation zone does not lie below a definite value. Thus, qualitatively they also relate conditions of stable combustion with a definite thermal state of the recirculation zone. However, derivation of quantitative relations is approached differently. Proceeding from the fact that the recirculation zone is a zone of intense mixing, the volume of the zone is represented as a homogeneous reactor, and peculiarities of flame stabilization by a bluff body are explained from considerations of combustion in this zone as a chemical reaction of the second order. From the equation of material balance for steady-state process in volume V at mass flow rate of air A and ratio of fuel mass to air mass f/a , there is obtained the relationship

$$\frac{A}{Vp^2} = \frac{B' \cdot e^{-\frac{E}{RT}}}{T^2} \cdot \frac{(1-\epsilon)(1-y)}{\epsilon} \cdot \frac{1}{R^2 \left(\frac{1}{p} + \frac{1}{29} \right)^2}, \quad (7.17)$$

where ϵ — fraction of fuel burning in the recirculation zone;

p — static pressure;

μ — molecular weight of the fuel;

E — activation energy;

B' — molecular collision coefficient in the kinetic equation;

T — flame temperature during combustion of a fraction ϵ of fuel;

y — equivalence relationship for lean mixtures;

$$y = \frac{\text{actual ratio } f/a}{\text{stoichiometric ratio } f/a}.$$

For rich mixtures, in equation (7.17) it is assumed that $y = 1.0$.

In Fig. 7.18, equation (7.17) is represented graphically for various equivalence coefficients y . From the graph it is clear that for every curve there exist three values of ranges of ϵ at which the reactor can operate. The low range at $\epsilon = 0$ does not have practical significance, since in this case no flame is observed, and substance passes through the reactor at extremely low reaction rate. Intermediate values (shown by the dotted line) do not have physical meaning because shortening of the stay time of gases in the zone, i.e., increase of A/Vp^2 , must not cause increase of ϵ .

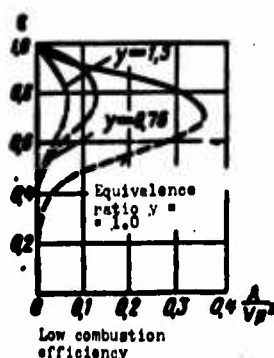


Fig. 7.18. Region of action of a homogeneous reactor. Calculated for $E = 40,000$ cal/mole, $B' = 4 \cdot 10^{12}$ cm³·sec; fuel is heptane, temperature of entering mixture is 366°K [10].

Of practical interest is only one curve – the upper curve. According to this curve, with increase of air velocity (increase of A) ϵ slowly decreases, until there is attained the maximum abscissa of this curve. With further increase of mass flow rate of air, there occurs blowoff. For mixtures differing from stoichiometric, blowoff always appears at mass flow rates progressively decreasing with increase of deviation from stoichiometric proportion.

Equation (7.17) explains peculiarities of flame stabilization by bluff bodies well qualitatively: instantaneous blowout of the flame with increase of flow velocity or change of α , influence of mixture ratio, pressure in the flow, etc. However, its application for analysis of flame stabilization is still not possible. The use of the quantities V and A for calculation, measured during stationary burning or for cold flows, is impossible, since the first case corresponds to stable combustion, and the second corresponds to the impossibility of burning in the zone of counter currents. At the time of blowoff, ratio A/V should be larger than during a stationary burning process, but less than in the absence of burning. Determination of change of quantities V and A in the interval between these extreme values and finding of their dependence at the time of flame blowoff on temperature, mixture ratio, etc., is a very difficult problem in view of non-stationarity and short duration of the blowoff process. Furthermore, the kinetic constants of the combustion reaction E and B' are unknown for the majority of fuel mixtures.

Recently, in a number of works, for instance in [4], there was expressed the assumption that during stabilization of a flame in a flow with the help of bluff bodies, a controlling factor in the ignition process of fresh mixture is the time necessary for preparation of the mixture for burning. This time, arbitrarily called the induction time, includes both the time necessary for heating of an element of volume of fuel mixture to the ignition temperature by means of mixing and the time necessary for development of the reaction, which depends on kinetics of the reaction.

These considerations, which are based on clear physical premises, are confirmed by experimental data on flame stabilization in the boundary layers of heated plates. For instance, it has been experimentally shown that the distance from the leading

edge of a heated plate to the stabilized flame front at constant flow velocity depends on mixture ratio and the temperature of the plate: the less the temperature of the plate, the bigger this distance. It is also obvious that at constant wall temperature and mixture ratio α the distance to the stabilized flame front will increase with increase of flow velocity.

Thus, the time of contact of the combustible mixture with the ignition source is one of the controlling factors of flame stabilization. However, for the case of ignition of fresh mixture during its contact with heated gasses (or combustion products) in the recirculation zone after a bluff body, as this is considered in work [4], theoretical concepts are insufficiently developed, and cause serious objections to a number of points.

Analysis of the well-known theoretical works on flame stabilization leads to the conclusion that this complicated process can qualitatively be explained with the help of the thermal theory of ignition. However, attempts to find a quantitative relation for the heat balance equation in the chemical reaction zone have still not been crowned with success under these complicated conditions.

§ 4. ANALYSIS OF FLAME STABILIZATION BY A BLUFF BODY

In order to obtain empirical dependences, which would be useful for approximate engineering calculations of the dimension of a flame-holder which ensures reliable flame stabilization at known parameters of the fuel mixture, we processed experimental data known to us on "lean" blowoff during burning of homogeneous gasoline-air and kerosene air mixtures after bluff bodies: cones, through-shaped flame-holders with different heights and vertex angles β , plates and cylinders.

From the graph shown in Fig. 7.9, it is clear that for flame-holders of given geometric form at constants temperature and mixture ratio, the flow velocity* at which blowoff occurs is proportional to the dimension of the flame-holder. At constant ratio w_{cp}/h , the range of stable combustion with respect to mixture ratio is wider, the higher the temperature of the flow and the larger the flow friction coefficient of the flame-holder.

In Fig. 7.19 there are plotted blowoff characteristics in "lean" mixtures in dimensionless coordinates $w_{cp}/w_{0\ cp} = f(\alpha_{0\ cp}/\alpha_{cp})$ for single flame-holders and grids

*Flow velocity was determined in the narrowest section of the pipe, in the exit plane of the flame-holder.

of flame-holders of various geometric forms and dimensions, for different relative locations of the flame-holders, various mixture temperatures and pressure close to atmospheric. For all of the considered cases, experimental points are satisfactorily grouped around one straight line, which is approximated by the dependence

$$\frac{w_{cp}}{w_{0cp}} = 0.844 + 0.156 \frac{\alpha_{cp}}{\alpha_{0cp}}, \quad (7.18)$$

where $w_{0cp} = 40$ m/sec - constant value of flow velocity at which there occurs blowoff from flame-holders at some value of α_{0cp} depending on the dimension and geometric form of the streamlined body, temperature of the combustible mixture, etc.;

α_{0cp} - mixture ratio at which there occurs blowoff from a flame-holder at $w_{0cp} = 40$ m/sec;

w_{cp} and α_{cp} - respectively the flow velocity mixture ratio at which blowoff occurs, if $w_{cp} > 40$ m/sec.

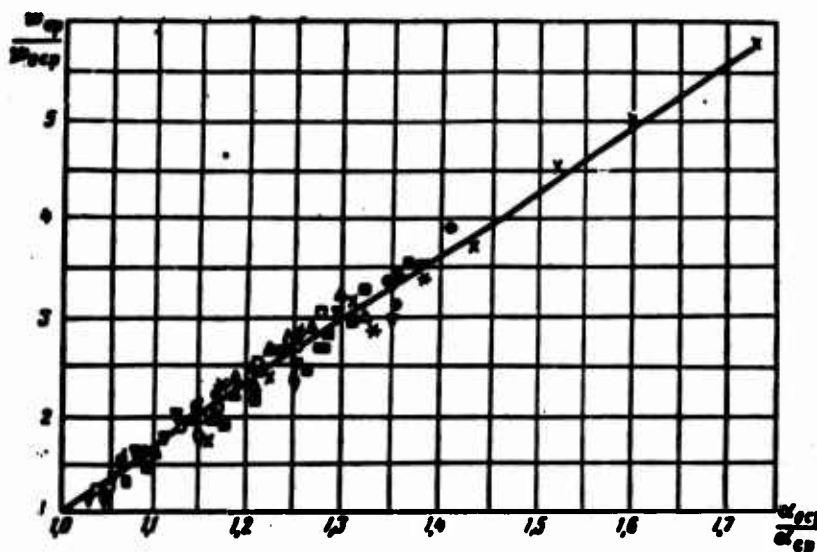


Fig. 7.19. The dependence $w_{cp}/w_{0cp} = f(\alpha_{cp}/\alpha_{0cp})$ in lean homogeneous mixtures after single flame-holders and after grids of flame-holders of different geometric form. (Designations are the same as in Fig. 7.13).

As can be seen from the graph, in the range of ratios $w_{cp}/w_{0cp} = 1-6$, the maximum spread of experimental points with respect to the ratio α_{cp}/α_{0cp} (at a given constant ratio w_{cp}/w_{0cp}) does not exceed $\pm 5\%$. At constant value of α_{cp}/α_{0cp} , the spread with respect to flow velocity is somewhat higher, and reaches to $\pm 12\%$, which from the technical point of view can be recognized as fully satisfactory.

*The quantity w_{0cp} , equal to 40 m/sec, is selected as the limiting minimum flow velocity possible in combustors of straight-flow-through type. It would be possible to select another value of w_{0cp} , equal, for instance, to 50 or 60 m/sec, etc.; the structure of relationship (7.18) then would remain the same; only the coefficients would be changed.

Relationship (7.18) can be used for analysis of flame stabilization if there is known the dependence of $\alpha_{0\text{cp}}$ on various factors which determine blowoff during burning of "lean" mixtures — geometric form and dimension of flame-holders, temperature of the flow, etc.

Analysis of available experimental data shows that there can be found satisfactory empirical dependences, relating $\alpha_{0\text{cp}}$ with the dimension and geometric form of the flame-holder and the temperature of the fuel mixture at pressure close to atmospheric.

From Fig. 7.20a, it is clear that for flame-holders of the given geometric form and dimensions, experimental points of the dependence $\lg \alpha_{0\text{cp}} = f(t_{\text{CM}})$ in the range to $t_{\text{CM}} = 500^\circ\text{C}$ are fully satisfactorily grouped about the straight lines approximated by the equation

$$\lg \alpha_{0\text{cp}} = A + B t_{\text{CM}} \quad (7.19)$$

where t_{CM} is the initial temperature of the fuel mixture.

Coefficient A in this relationship depends on the geometric form and dimension of the flame-holder, but coefficient B is identical for grooved and conical flame-holder and is equal to $6.4 \cdot 10^{-4}$.

At constant temperature of the fuel mixture in the same given geometric form of flame-holder, experi-

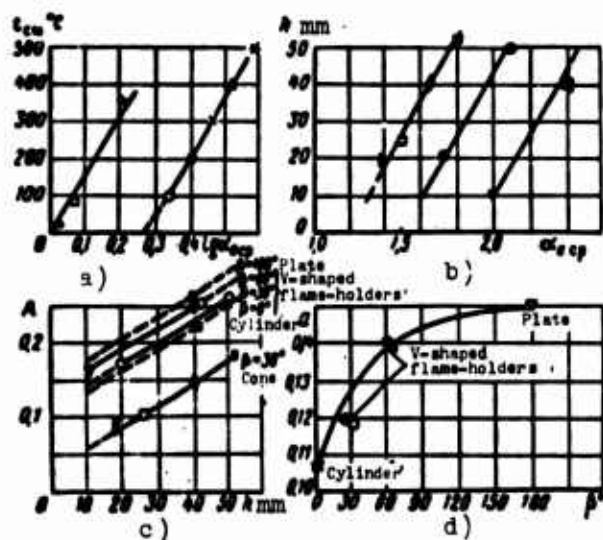


Fig. 7.20. Dependence of $\alpha_{0\text{cp}}$ on t , dimensions and geometric form of flame-holders. Homogeneous mixture $w_0 = 40$ m/sec. (Designations are the same as in Fig. 7.13).

mental points of dependence $\alpha_{0\text{cp}} = \varphi(h)$ are also satisfactorily grouped about the straight lines (Fig. 7.20b) approximated by the dependence

$$\alpha_{0\text{cp}} = M + N \cdot 2h \quad (7.20)$$

Where, as in the first case, coefficient M depends on the geometric form of the flame-holder, and coefficient N is identical for flame-holders of all of the considered geometric forms.

By substituting in equation (7.19) the values of $\alpha_{0\text{cp}}$ calculated according to equation (7.20) (or taken from Fig. 7.20b), we can find the dependence of coefficient A on dimension of a flame-holder of given geometric form. In Fig. 7.20c, there are

given such dependences for grooved flame-holders with vertex angles $\beta = 30^\circ$ and 60° , and for a plate, a cylinder and cones with vertex angle $\beta = 30^\circ$. From the graph it is clear that dependence of A on dimension of the flame-holder is approximated by the linear relationship

$$A = a + c \cdot 2h \quad (7.21)$$

Coefficient a depends on the geometric form of the flame-holder, but coefficient c is identical for flame-holders of all of the considered geometric forms, and is equal to $28.3 \cdot 10^{-4}$.

For grooved flame-holders, the dependence $a = a(\beta)$ is given in Fig. 7.20d (it is arbitrarily accepted that a grooved flame-holder with $\beta = 0$ is equivalent to a cylinder with $d = h$); for cones with diameter of base $d > 20$ mm and $\beta = 30^\circ$ $a \approx 0.05$.

The influence of pressure on the limits of stable combustion with respect to flow velocity (other conditions being equal) can be approximately taken into account by the relationship

$$\frac{w_{cp1}}{w_{cp2}} = \left(\frac{p_1}{p_2}\right)^n, \quad (7.22)$$

where w_{cp1} — a certain flow velocity at which blowoff from the flame-holder occurs at pressure p_1 ;

w_{cp2} — the unknown flow velocity at which blowoff occurs from the flame-holder at pressure in the flow p_2 .

During selection of the exponent n , one should be guided by considerations presented in § 2 of the present chapter.

According to formulas (7.18)-(7.22), with the use of Fig. 7.20d, it is possible to calculate the dimension of the flame-holder which will ensure stable combustion of the fuel at the given parameters of the homogeneous fuel mixture. Results of calculation will agree satisfactorily with experiment (see Fig. 7.13).

The empirical relationships given above for calculation of flame stabilization were obtained as a result of processing of much experimental material. They do not contradict contemporary conceptions of the mechanism of flame stabilization by bluff bodies, which are based on the thermal theory of ignition. But, just as any empirical relationships, there are accurate only in the investigated range of change of controlling parameters. It is obvious, for instance, that the linear dependence of a_{0cp} on the dimension of the flame-holder is accurate within a limited range of change of dimensions h . This limitation is connected with the concentration limits of ignition of a fuel mixture: with approach to this limit and increase of the dimension of the flame-holder, the relative increase of the range of stable combustion

with respect to α will tend to zero. It is also probable that in the case when temperature of the mixture is close to the ignition temperature, its influence on $\lg \alpha_0$ op will be different than in the cases considered by us at t_{cm} lower than the ignition temperature.

LITERATURE

1. L. G. Loytsyanskiy. Aerodynamics of a boundary layer, State United Publishing Houses, 1941.
2. S. Gol'dshteyn. Contemporary state of hydrodynamics of a viscous fluid, IL, 1948.
3. A. Rozhko. On the vortex wake and drag of bluff bodies, "Mechanics," 1956, No. 4 (35).
4. T. A. Bowina. Studies of exchange between the recirculation zone behind the flame-holder and the outer flow, Seventh symposium (international) of combustion (combustion and detonation waves), 1959.
5. Office National d'Etudes et de Recherches Aeronautiques, 1957, No. 41 (article by Repenot and Grossen).
6. De Zubey. Character of disk controlled flames, Aero Digest, 61, 1950.
7. S. A. Gol'denberg and L. N. Khitrin. The influence of preheating of a fuel mixture and ambient pressure on its stabilization limits, News of the AS USSR, OTN (Department of Technical Sciences), 1957, No. 2.
8. D. Spaulding and V. Toll.* Flame stabilization in high-speed gas flows and the influence of thermal losses at low pressures, VRT, 1955, No. 4.
9. G. Williams. Concerning the question of flame stabilization, VRT, 1951, No. 3.
10. D. Longwell, E. Frost and M. Veys.* Flame stabilization in the recirculation zones of bluff bodies, VRT No. 4, 1954.
11. R. Tsimer* and A. Kolebel.* Flame stabilization in boundary layers of heated bodies, VRT, 1959, No. 3.
12. S. S. Penner and F. Williams. Recent studies on flame stabilization of premixed turbulent gases, applied mechanics reviews, 1957, Vol. 10, No. 6.
13. I. P. Longwell. Combustion problems in ramjet design, Journal of the Aeronautical Sciences, XII, 1949, No. 12.
14. Kh. Khottel'* and V. Mey.* Flame stabilization in two-phase fuel-air mixtures. Questions concerning combustion and detonation waves (Fourth symposium), Oborongiz, 1958.
15. M. Russi, N. Cornett and R. Kornog.* The influence of temperature of the flame-holder on flame stabilization. Questions concerning combustion and detonation waves (Fourth symposium), Oborongiz, 1958.

*The non-Russian names marked with an asterisk have been directly transliterated from the cyrillic alphabet, since the correct foreign spellings could not be found.
[Trans. Ed. Note]

CHAPTER VIII

BURNING OF FUEL-AIR MIXTURES IN THE WAKE AFTER A BLUFF BODY

§ 1. BURNING OF A HOMOGENEOUS MIXTURE IN THE WAKE AFTER A SINGLE STABILIZER IN A HALF-OPEN FLOW

In combustors of ramjet engines (ПБПД) and afterburners of gas-turbine engines (ГТД), burning of fuel occurs mainly in wakes after bluff bodies - flame holders. The process of turbulent burning depends on physicochemical and hydrodynamic parameters of the flow of hot mixture. The influence of these factors, at least qualitatively, appears to be identical in the cases of burning in flows with homogeneous and isotropic turbulence and burning in combustion chambers of straight-flow-through type.

Specific peculiarities of burning in the wakes after bluff bodies consist of the following. As measurements have shown, the intensity of turbulence in an isothermal

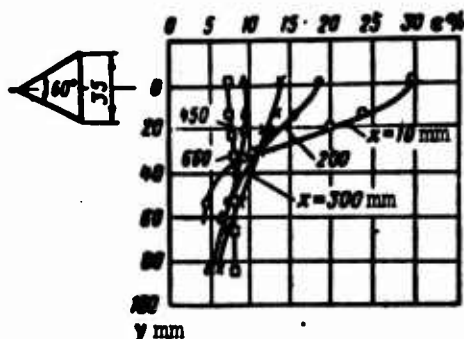


Fig. 8.1. Intensity of turbulence in the wake after a flame-holder in a pipe during cold flow around it (experiments of Solntsev).

flow sharply changes over the length and in the cross sections of the wake, attaining 30% and more on the axis near the flame-holder, and decreasing to the intensity of turbulence in the incident flow with increase of distance from the flame-holder and on the boundaries of the wake (Fig. 8.1). Turbulent characteristics of the wake depend on dimensions and geometric form of the bluff bodies. For a grid of flame-holders, the intensity and scale of turbulence along the combustion chamber and over its cross sections

will depend also on the number and relative location of the flame-holders. During flow of gas through the grids, homogeneous and isotropic turbulence appears at a distance of 20 to 30 times the caliber of the cross piece of the grid downstream

(see Chapter III). Consequently, homogeneous and isotropic turbulence can be expected only at the end of the combustion chamber, where the process of burning of the fuel should be practically completed. It is also known that parameters of turbulence in the wakes after bluff bodies in a pipe are different during burning and in cold flows, and depend on the degree of preheating of the gases (see Chapter IV).

Another peculiarity of burning after a bluff body is that combustion products with high temperatures, which fill the recirculation zone, not only stabilize the burning process, but also, while being continuously mixed in the turbulent boundary layer, apparently render an essential influence on burning velocity.

Below there are expounded some results of experimental investigation of burning of homogeneous and two-phase mixtures in the wakes after single flame-holders and after grids of flame-holders fixed in a half-open flow and in a pipe.

A typical distribution of time-averaged temperatures in a flame during burning of gas mixtures in a wake after a bluff body is shown in Fig. 8.2. The temperature of the gases has a maximum on the axis of the wake and decreases to the temperature of the initial fresh mixture on the boundaries of the flame. During stable burning, the maximum temperature depends on composition and initial temperature of the mixture, but does not depend on dimension and geometric form of the flame-holder, or on flow velocity. With approach to the boundaries of "lean" blowoff (by any means - increase of flow velocity, making the mixture leaner or decrease of flame-holder dimension), the temperature of gases along the axis of the wake changes: in the zone of counter currents it is close to maximum; in the transition section it drops considerably (magnitude of this decrease depends on the degree of approach to the blowoff regime of the flame), and then again increases in the main section of the wake, attaining a maximum at a considerable distance from the flame-holder.

Width of the flame in a fixed cross section depends on the dimension and geometric form of the flame-holder: the greater the "bluffness" of the bodies, i.e., the greater their flow friction is, the wider the flame is. Width of the flame decreases with increase of flow velocity and leanness of the mixture (see Fig. 8.2), and also depends on conditions of burning - whether in an open flow or in a pipe, with different degrees of blockage by flame-holders (Fig. 8.3).

Curves of temperature change of gases over cross sections of the flame from temperature of the fresh mixture t_0 on the boundary of the flame to maximum temperature at the axis t_m are universal: independently of flow velocity, composition and temperature of the mixture, temperature profiles in dimensionless coordinates reduce to one symmetric curve (Fig. 8.4).

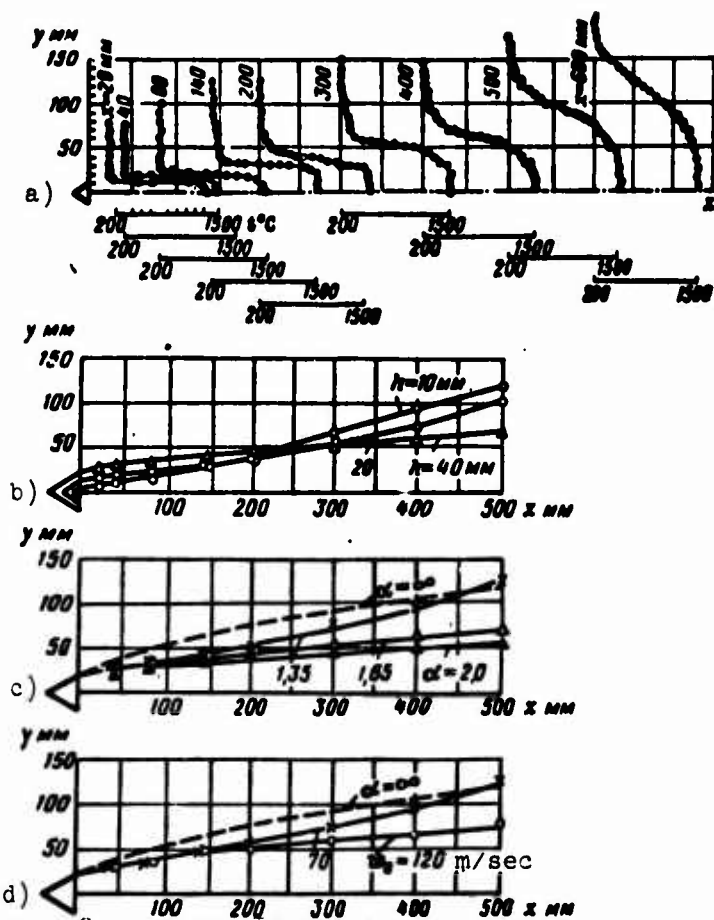


Fig. 8.2. Temperature fields and flame widths during burning of a homogeneous mixture in the wake after a flame-holder in a half-open flow depending upon various factors. a) field of temperatures after a flame-holder, $w_0 = 70$ m/sec, $\alpha = 1.4$, $h = 20$ mm, $t_{CM} = 200^\circ\text{C}$; b) influence of dimension of the flame-holder, $w_0 = 70$ m/sec, $\alpha \approx 1.6$, $t_{CM} = 200^\circ\text{C}$; c) influence of mixture ratio, $w = 70$ m/sec, $t_{CM} = 200^\circ\text{C}$, $h = 40$ mm; d) influence of flow velocity, $t_{CM} = 200^\circ\text{C}$, $\alpha = 1.35$, $h = 40$ mm.

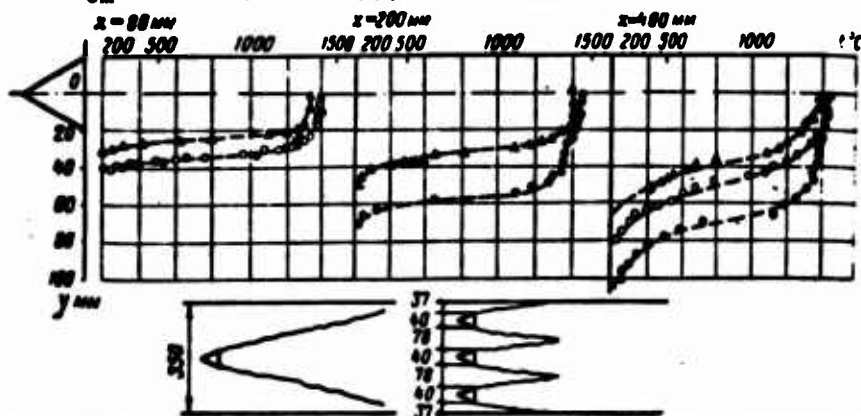


Fig. 8.3. Temperature fields in various cross sections of a wake during burning in a half-open flow and in a pipe after a single flame-holder and after a grid of flame-holders: ● - burning after a single flame-holder in a half-open flow; ○ - burning after a single flame-holder in a pipe $135 \times 350 \times 800$ mm; Δ - burning after three flame-holders in a pipe $135 \times 350 \times 800$ mm (distance between flame-holders is 78 mm); $w = 80-90$ m/sec; $\alpha = 1.6$; $t_{CM} = 200^\circ\text{C}$; $h = 40$ mm.

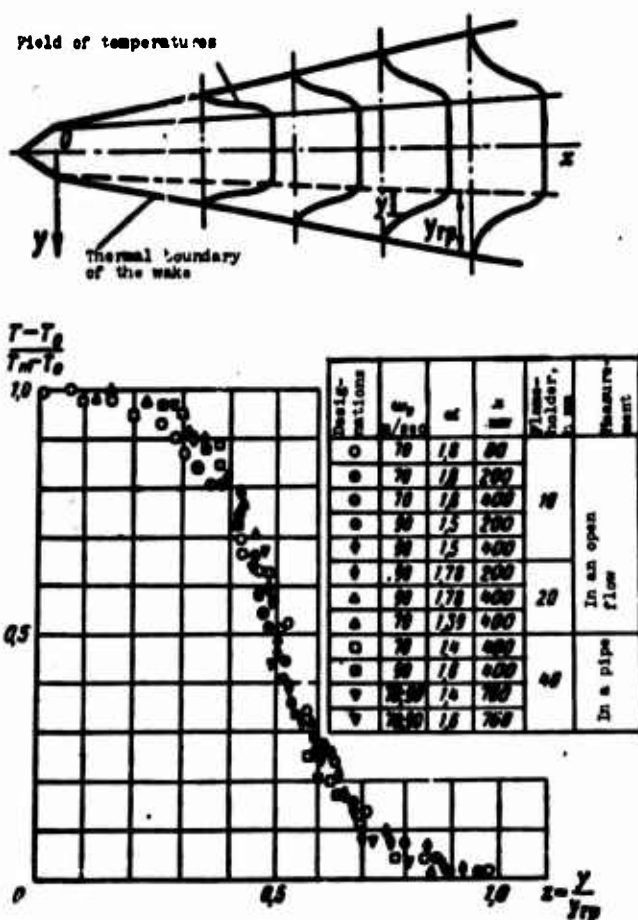


Fig. 8.4. Dimensionless temperature fields in cross sections of the flame after a single flame-holder.

Heat release in the wake does not depend on flame-holder dimension either during burning after a single flame-holder in a half-open flow or during burning in a pipe after a grid of flame-holders. In Fig. 8.6 there are given temperature fields in various cross sections of a pipe during burning of a homogeneous gasoline-air mixture after three V-shaped flame-holders of dimension $h = 40$ mm and after four flame-holders of dimension $h = 10$ mm. In both cases, distances between the wall of the pipe and edges of the flame-holders adjacent to it, and also between edges of adjacent flame-holders were identical (parameters of the flow were also identical). In spite of the fact that the degree of blockage of the cross section of the pipe by flame-holders in the first case was 34%, and in the second — altogether 11%, the combustion efficiency of fuel in the chamber with four flame-holders $h = 10$ mm was even somewhat higher than in the chamber with three flame-holders $h = 40$ mm (at the end of the pipe, at $x = 760$ mm, in the first case $\eta_z = 0.95$; in the second — $\eta_z = 0.92$).

Thus, for the purpose of intensification of the burning process with the same (or even smaller) hydraulic losses in the combustion chamber, it is expedient to

On the basis of a large number of experimental data, it has been established that during burning of homogeneous mixtures in a wake after a bluff body, the quantity of heat released in the flame, other things being equal, practically does not depend on the dimension of the flame-holders (Fig. 8.5).

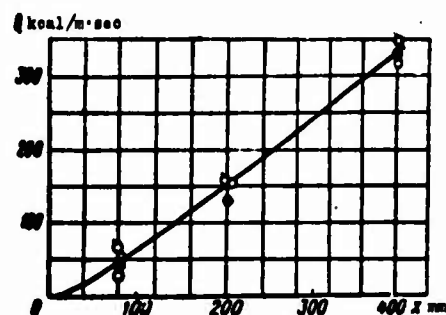


Fig. 8.5. Heat release in the flame after flame-holders of various dimensions. Burning of a homogeneous mixture in a half-open flow. $w_0 = 90$ m/sec, $\alpha = 1.8$. ● — $h = 10$ mm; ■ — $h = 20$ mm; ○ — $h = 40$ mm.

increase the number of flame-holders with small dimensions, but not their dimension. The minimum dimension of a flame-holder thus should be chosen from the condition of guarantee of stable combustion within a given range of variation of parameters of the flow of fuel mixture.

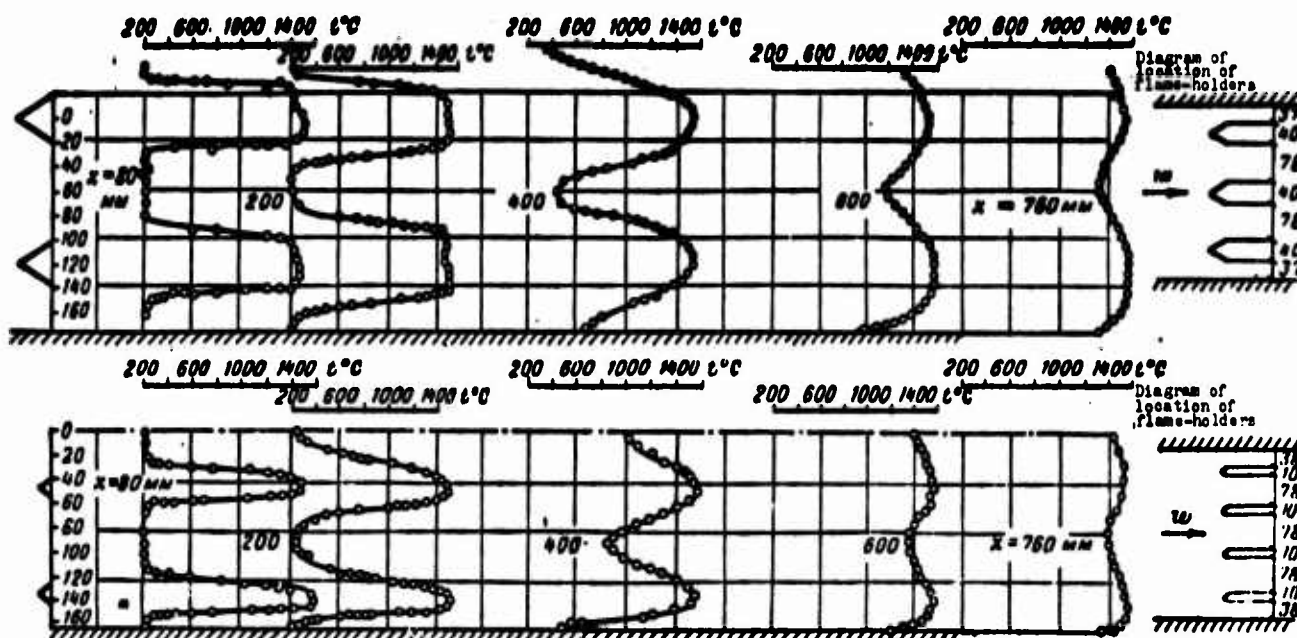


Fig. 8.6. Temperature fields over cross sections of a pipe during burning after grids of 3 flame-holders with $h = 40$ mm and 4 flame-holders with $h = 10$ mm. Homogeneous mixture, $\alpha = 1.4$, $t_{CM} = 200^\circ\text{C}$, $w_0 = 70$ m/sec.

§ 2. CERTAIN PECULIARITIES OF BURNING OF HOMOGENEOUS GAS MIXTURES AFTER A GRID OF FLAME-HOLDERS IN A PIPE

In combustors of ramjet engines and afterburners of gas-turbine engines, the process of burning of fuel occurs after a grid (group) of flame-holders. In this case, dimensions and configuration of flames after each flame-holder depend on the number of flame-holders and their relative location in the combustion chamber. With uniform location of the flame-holders in the same plane (when the distances S between edges of adjacent flame-holders are identical, and the distances between pipe walls and edges of the flame-holders adjacent to it are equal to $S/2$), axes of the flames are parallel to the axis of the pipe, and after every flame-holder of identical dimensions and geometric form the flames have identical dimensions. In the case when flame-holders over the cross section of the combustion chamber are located in an echeloned manner, or nonuniformly, with different distances S , under the action of aerodynamic forces and thermal expansion, the dimensions, gas-dynamic and thermal characteristics of flames after each flame-holder turn out to be different (Fig. 8.7).

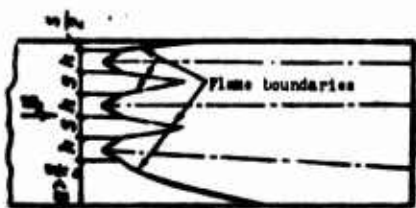


Fig. 8.7. The influence of relative location of flame-holders on flame geometry during burning in a pipe.

Especially strongly changed are the gas-dynamic and thermal parameters of flames after each flame-holder when there is applied echeloned location of them in the combustion chamber. Characteristic in this case is the sharp decrease of temperature of the gas along the axis of the flame at a certain distance from the flame-holder (see below, § 5 and Fig. 8.17).

The mutual influence of the flames shows up not only in the fact that conditions of thermal expansion are changed and their shape is deformed by the flow, but also in the fact that turbulence characteristics of the flow are changed along the length and over the cross sections of the combustion chamber. It is obvious that the less the distance is between flame-holders, the higher will be (at the same length) the general level of intensity of turbulence in the interval between the flame-holders, and the higher will be the burning rate of fuel in this interval. During burning after a grid of flame-holders, gradients of flow velocity increase over cross sections of the pipe. This causes additional turbulization of the flow, and this also leads to increase of burning rate.

At present it is not possible to consider in advance the influence of each of the enumerated factors on development of the burning process in combustion chambers. At the same time, the accumulation of empirical data and their statistical reduction for the purpose of obtaining dependences characterizing the burning process on the whole in the wake after a single flame-holder, are unsuitable for use in examining of the process of burning of fuel after a grid of flame-holders.

For study of processes of burning, it is apparently more expedient to use experimental data obtained during the investigation of burning not after one, but after a group of flame-holders, considering thereby the total effect of their mutual influence on the process of burning.

Above it was indicated that combustion efficiency of fuel along the axis of the flame after a flame-holder remains practically constant over the whole length of the wake. In the interval between flame-holders, combustion efficiency is increased from zero to the given value in a distance which is dependent on many factors — physicochemical parameters of the flow of fuel mixture, dimensions and geometric form of flame-holders, distance between them, etc.

If we consider a design of a combustion chamber inside which there are installed flame-holders of identical shape and dimension in the same plane, then it will become

evident that independently of the diameter of the chamber and the number of flame-holders installed in it, the entire process of burning of fuel is essentially determined only by characteristics of burning in the plane of symmetry between the two adjacent flame-holders and between the wall and the flame-holders adjacent to it. Consequently, a group of two flame-holders can be considered as a basic element of the combustion chamber, and characteristics of burning in the interval between these flame-holders can be extended to a combustion chamber of any dimensions with any number of flame-holders.

This consideration, of course, is valid only in the case when burning in the interval between two adjacent flame-holders indeed does not depend on the total number of flame-holders installed in the chamber, or their mutual influence can be disregarded. The characteristic change of intensity of turbulence after each flame-holder, with maximum of intensity on the axis of the wake, creates as it were two barriers, which hinder the penetration of velocity pulsations generated after the other flame-holders into the space between the two considered adjacent flame-holders, and consequently the influence of the other flame-holders in this relation should be insignificant. But increase of the number of flame-holders will lead to growth of heat release, and at the same flow rate of air there will be increased the average flow velocity along the length of the combustion chamber; furthermore, there will be changed conditions of thermal expansion of the flames. This can influence the combustion process in the interval between two adjacent flame-holders with change of the total number of flame-holders in the combustion chamber.

For clarification of this question there were conducted special experiments. In a rectangular tube with the dimensions 350×135 mm, there were consecutively installed in the same plane two, and then four identical flame-holders with the dimension $h = 40$ mm, with distance between adjacent edges $S = 40$ mm. At identical flow rate, temperature and mixture ratio, there were measured temperature profiles in various cross sections of the combustion chamber; there were determined boundaries of the flames and with the help of chemical analysis, there was measured the depletion of fuel along the length of the chamber in the plane of symmetry between the flame-holders. Results of measurements showed that flame boundaries and fuel depletion in the plane of symmetry (along the axis of the chamber) between flame-holders in both cases turned out to be practically identical (Fig. 8.8). These experiments convincingly confirmed the above consideration about the fact that a group of two flame-holders can be considered as a basic element of a combustion chamber, and

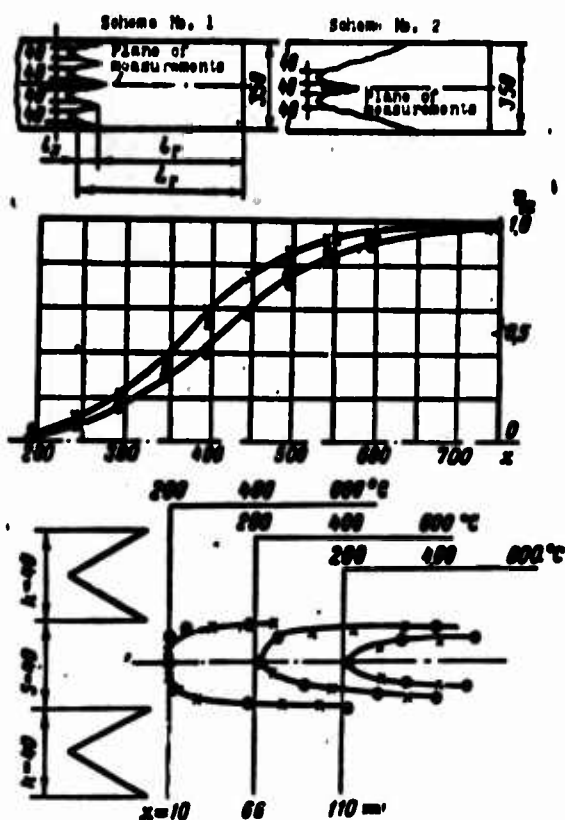


Fig. 8.8. Change of gas temperature and η_2 in the plane of symmetry between two adjacent flame-holders. Uniform fuel mixture; $\alpha = 1.4$, $t_{0M} = 200^\circ\text{C}$, $w_0 = 70$ m/sec, \bullet - scheme No. 1, \times - scheme No. 2.

characteristics of burning in the interval between these flame-holders can be extended to a combustion chamber of any dimensions with any number of flame-holders.

The section of the length of the combustion chamber from the flame-holders to the nozzle, which we will subsequently call the "hot" part of the chamber L_r , can be considered to consist of two parts: the initial part l_x , in which flames between the flame-holders intersect each other, and the section l_r , in which combustion efficiency of the fuel in the plane of symmetry between the flame-holders is changed from zero to the given value.

The initial section l_x is conveniently estimated by the mean angle of expansion of the flames φ :

$$\overline{\lg \varphi} = \frac{S}{2l_x}.$$

§ 3. DEPENDENCE OF ANGLE OF EXPANSION OF FLAMES ON VARIOUS FACTORS

The length of the initial section of the hot part of the combustion chamber depends on many factors - temperature and air-fuel ratio, velocity and initial turbulence of the flow, geometric form of the flame-holders and the distance between them, etc. Change of some of these enumerated factors strongly affects the magnitude φ ; the influence of others affects it insignificantly. In Fig. 8.9 there are given experimental data on the influence of different factors on the magnitude φ .

The angle of expansion of the flame greatly depends on flow velocity, temperature and mixture ratio, but depends little on the distance between flame-holders (at $S \geq 10$ mm) and practically does not depend on dimensions of the flame-holders h . Over the length of the initial section, the geometric form of the bluff body has an influence: the greater the "bluffness" of the bodies, the shorter the length l_x is, other things being equal. Increase of intensity of turbulence of the incident flow of fuel mixture also leads to reduction of the length of the initial section.

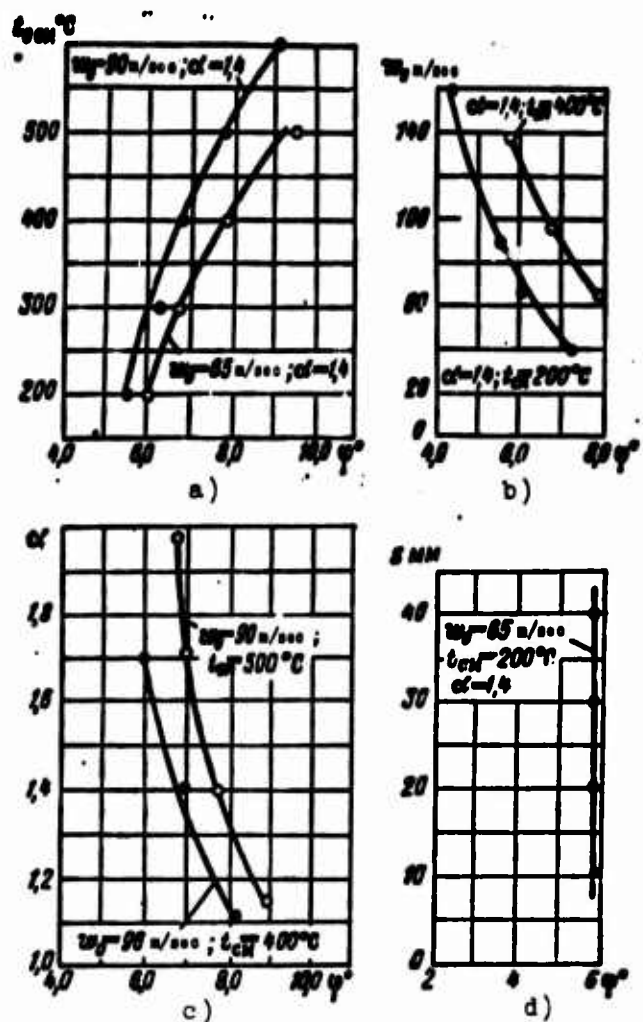


Fig. 8.9. Change of angle of expansion of flames φ in the interval between two flame-holders depending upon various factors. Homogeneous fuel mixture; V-shaped flame-holders with $\beta = 60^\circ$. a) influence of temperature of the mixture t_{CM} ; b) influence of flow velocity rate w_0 ; c) influence of mixture ratio α ; d) influence of distance S between flame-holders.

determination of the length of the burning zone, one can with satisfactory accuracy determine points corresponding to $\eta_z \approx 0.0$ and $\eta_z \approx 0.9$. As numerous experiments have shown, for increase of η_z from 0.9 to 0.95, it is necessary to increase length of the combustion chamber by an amount approximately equal to $0.5 l_r$. Length of the burning zone l_r depends on many factors.

The influence of geometric form of the flame-holders. The length of the hot part of the combustion chamber L_r , other things being equal, depends on geometric form of the flame-holders. In Fig. 8.10 there are given curves of change of combustion efficiency of fuel over the length of the pipe during burning of a homogeneous mixture after flame-holders of various geometric forms. Parameters of the flow, characteristic

On the whole, in the range of change of flow velocity of the fuel mixture ($w_0 = 40-160$ m/sec, $t_{CM} = 200-600^\circ\text{C}$ and $\alpha = 1.1-2.0$) at the usual pipe intensity of flow turbulence, the angle φ changes within the limits $5-10^\circ$. In rough approximate calculations, it is possible to assume that on the average $\bar{\varphi} = 7^\circ$; for a more accurate estimate of length of the initial section l_x , it is possible to use the graphs given in Fig. 8.9.

§ 4. INFLUENCE OF VARIOUS FACTORS ON FUEL DEPLETION IN THE PLANE OF SYMMETRY BETWEEN THE FLAME-HOLDERS

Combustion efficiency of fuel over the length of the combustion chamber in the plane of symmetry between flame-holders changes according to the characteristic curves shown in Fig. 8.10. Curves of $\eta_z = f(x)$ sharply, almost by a linear law, increase over the segment $\eta_z = 0.2$ to 0.9, and then there occurs very slow burning. During experimental

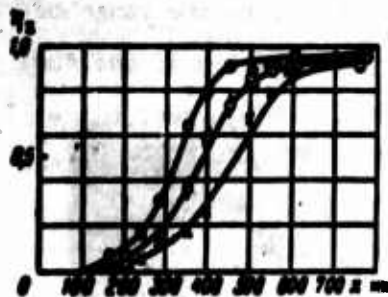


Fig. 8.10. Change of η_z in the plane of symmetry between flame-holders depending upon their geometric form. Homogeneous combustible mixture, $\alpha = 1.4$, $t_{CM} = 300^\circ\text{C}$, $w_0 = 70$ m/sec, $S = 40$ mm. \circ - two plates, $h = 40$ mm; \square - two V-shaped flame-holders, $\beta = 60^\circ$, $h = 40$; \times - two cylinders with ϕ 40 mm.

dimensions of flame-holders and distances between them were identical, but the length L_r , as can be seen from the graph, turned out to be different; it was least during burning after plates fixed perpendicularly to the flow, and largest during burning after cylinders. Change of L_r occurs with change of both l_x and l_r . This is explained by the fact that with increase of drag of the bluff body, the width of the turbulent wake after it increases, and intensity of the turbulent wake somewhat increases, which leads to increase of burning velocity, which corresponds to increase of angle of expansion of the flame ϕ and to decrease of the length of the burning zone l_r .

Influence of temperature of the fuel mixture t_{CM} . Change of temperature of the fuel mixture renders a very strong influence on length of the burning zone. Thus, for

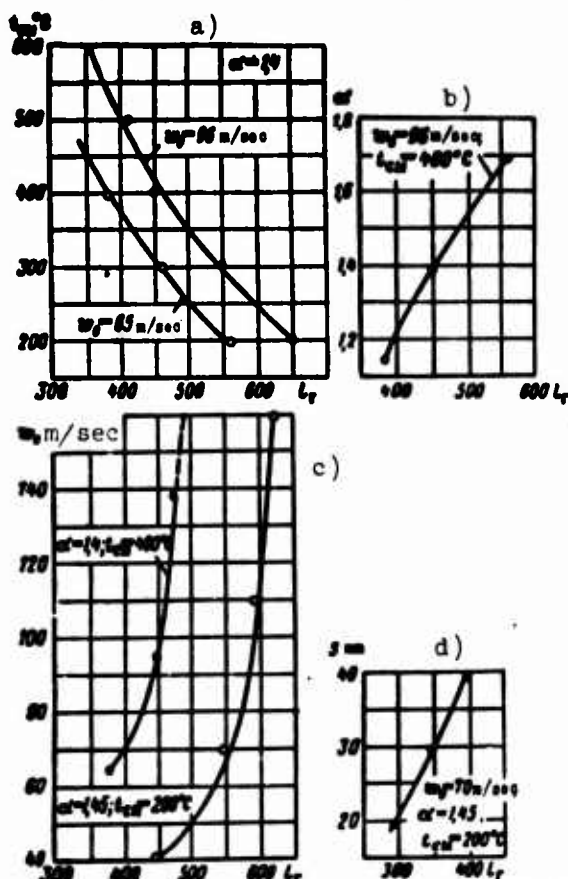


Fig. 8.11. Dependence of length of the burning zone l_r in the plane of symmetry between flame-holders on various factors. Homogeneous fuel mixture. $h = 40$ mm, $S = 40$ mm.

instance, at a flow velocity of $w_0 = 90$ m/sec, $\alpha = 1.4$ and $S = 40$ mm, change of t_{CM} from 200° to 600°C led to decrease of l_r by almost twice (Fig. 8.11a).

Influence of mixture ratio α . The length of the burning zone greatly depends also on mixture ratio α . Other things being equal, with increase of α as compared to stoichiometric composition, length of the burning zone increases (Fig. 8.11b). The least value of l_r corresponds to a composition of the fuel mixture which is close to stoichiometric.

The influence of flow velocity w_0 . In Fig. 8.11c there are experimental data on the influence of flow velocity on length of the burning zone. From the graph it is clear that change of velocity of the incident flow within

the range $w_0 \leq 60-70$ m/sec noticeably affects length l_T , and this influence is greater the smaller the value of w_0 . For w_0 higher than 70 m/sec, length of the burning zone very weakly depends on flux velocity.

The influence of distance S between flame-holders. From Fig. 8.11d one may see that the length of the burning zone greatly depends on distance between flame-holders: l_T increases almost linearly with increase of S . This is explained by the fact that with increase of distance between flame-holders, average level of intensity of turbulence of the flow in the space between them decreases, and this leads to decrease of burning velocity and increase of size of the zone of heat release l_T .

The influence of dimension of the flame-holder. Other things being equal, length of the burning zone practically does not depend on the dimension of a flame-holder h of given geometric form (see Fig. 8.6 and 8.12).

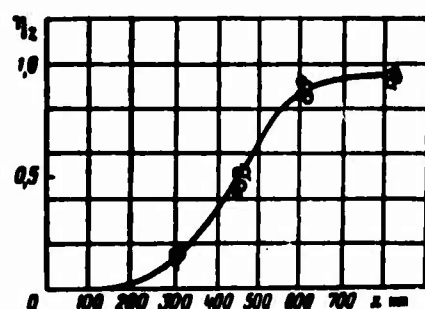


Fig. 8.12. Change of η_z in the plane of symmetry between flame-holders of various dimensions. Homogeneous mixture, $\alpha = 1.4$, $t_{CM} = 200^\circ\text{C}$, $w_0 = 70$ m/sec, $S = 40$ mm. ● — $h = 10$ mm, ● — $h = 20$ mm, ○ — $h = 30$ mm, □ — $h = 40$ mm.

Influence of initial flow turbulence. The influence of intensity of turbulence of the incident flow ϵ_0 on length of the hot part of the combustion chamber is different depending upon the dimension of the flame-holder: the greater the dimension of the flame-holder, the less this influence is. This means that the process of burning in the wake after a flame-holder is influenced not only by the intensity, but also by the scale of turbulence. On the whole we may assume that increase of initial intensity, as a rule, leads to decrease of L_T . However, if ϵ_0 is

considerably less than the intensity of turbulence generated by the flame-holder itself, then it has little effect on a change of L_T . However, if ϵ_0 is comparable with the intensity of turbulence generated by the flame-holders, then L_T decreases considerably. This is graphically illustrated by Fig. 8.13, where there are given experimental curves of burn-up in the plane of symmetry between two flame-holders at various intensities of turbulence of the incident flow, which is generated by grids fixed at a distance of 185 mm in front of the flame-holders. The grids had identical dimensions of their openings, but different widths of their crosspieces. Consequently, it was possible to expect that the scale of turbulence of the flow after them would be approximately identical, and that the intensity of turbulence would be different, increasing from grid No. 1 to grid No. 3. In accordance with change of ϵ_0 , there was changed the length of the burning zone L_T .

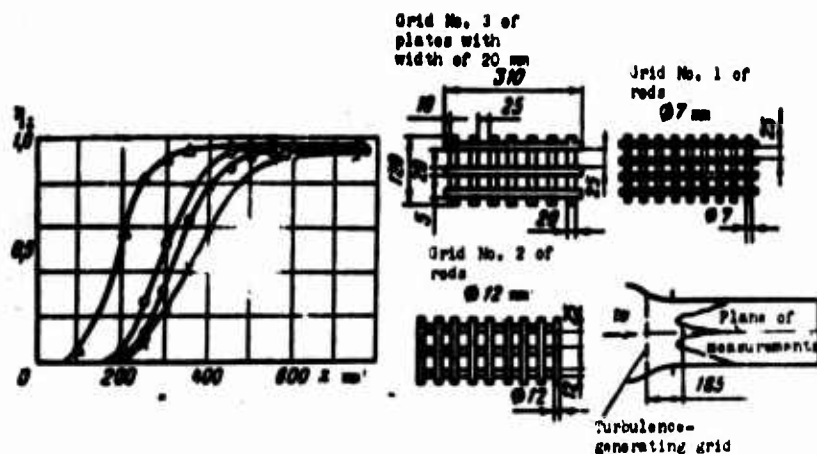


Fig. 8.13. Influence of intensity of turbulence of the incident flow ε_0 on burn-up in the plane of symmetry between the flame-holders. Homogeneous mixture, $\alpha = 1.3$, $t_{CM} = 400^\circ\text{C}$, $w = 70$ m/sec, \times without a grid, \bullet - grid No. 1, \circ - grid No. 2, Δ - grid No. 3.

Influence of pressure in the flow. Decrease of pressure in the below atmospheric leads to deceleration of burning, and, as a result of this, to increase of total length of the burning zone L_T in the plane of symmetry between the flame-holders (Fig. 8.14). Burning velocity drops mainly due to decrease of the intensity of turbulence because of increase of the viscosity of the flow with decrease of pressure. But, furthermore, as it was shown by Khramtsov, even at constant intensity of turbulence of the flow, the decrease of pressure by itself leads to a certain deceleration of burning.

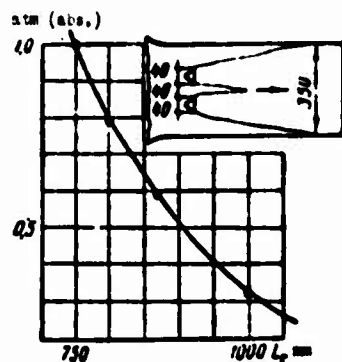


Fig. 8.14. Influence of pressure in the flow on the length L_T . Homogeneous gasoline-air mixture, $\alpha = 1.35$, $t_{CM} = 225^\circ\text{C}$, $w_0 = 90$ m/sec.

The universality of burning curves. Curves of change of combustion efficiency of fuel versus dimensionless length of the burning zone l_T in the plane of symmetry between flame-holders are universal. At different flow parameters of the fuel mixture, different dimensions and geometric forms of the flame-holders, different distances between them, etc., experimental points of the dependence $\eta_z = f(l_T)$ fall on one curve (Fig. 8.15). From the graph it is clear that for increase of η_z from 0.9 to 0.94-0.95, it is necessary to increase length of the burning zone l_T by about one and a half times.

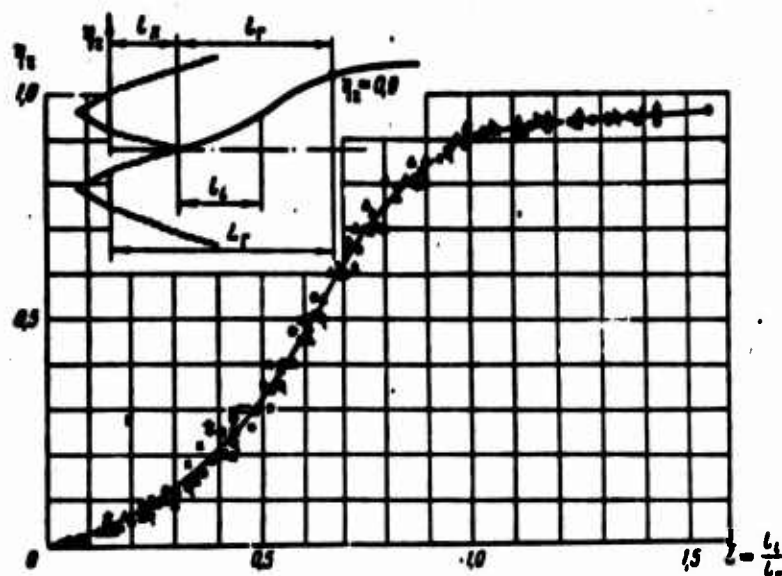


Fig. 8.15. Change of η_z in the plane of symmetry between flame-holders.

Number and geometric form of flame-holders	Designations	u_0 m/sec	α	t_{cu} °C	Fuel mixture
Two flame-holders $A=40$ mm; $S=40$ mm	●	91	1.38	400	Homogeneous gasoline-air mixture
	■	90	1.41	300	
	○	120	1.4	400	
	○	92	1.3	400	
Four flame-holders $A=40$ mm; $S=40$ mm	▲	120	1.42	300	
Two plates $A=40$ mm; $S=40$ mm	△	90	1.4	300	Two-phase kerosene-air mixture
Two cylinders $\varnothing 40$ mm	⊗	88	1.4	300	
Two flame-holders $A=40$ mm; $S=40$ mm	⊗	90	—	300	
	×	89	—	300	

§ 5. BURNING AFTER A GRID OF FLAME-HOLDERS, LOCATED IN THE SAME PLANE AND ECHELONED ALONG THE LENGTH OF THE COMBUSTION CHAMBER

Above it was indicated that during stable burning, the temperature of gases on the axis along the entire length of the wake after each flame-holder remains practically constant. Strictly speaking, this is true during burning after a single flame-holder in open and half-open flows, and also during burning in a pipe after a grid of flame-holders located in the same plane, under the condition that distances between them are sufficiently large (not less than 40 mm).

During burning after a grid with a large number of flame-holders located close to one another, change of hydrodynamic and thermal parameters in the wake after each flame-holder becomes more complicated. In Fig. 8.16 there are given curves of the

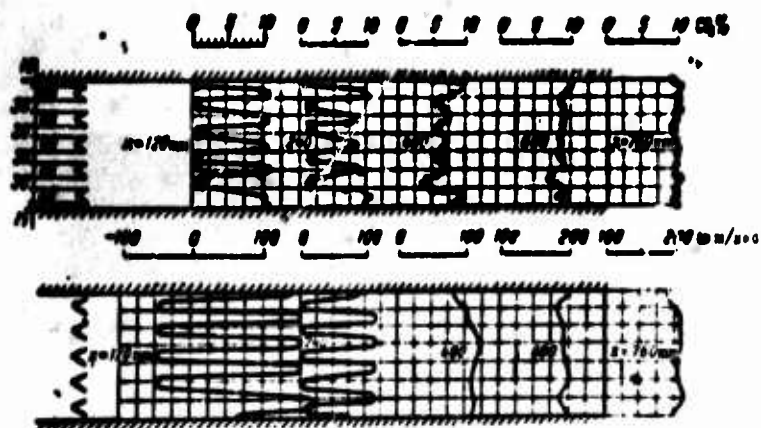


Fig. 8.16. Change of composition and velocity of gas over the length of the pipe during burning after a grid of flame-holders installed in the same plane. Homogeneous mixture, $\alpha = 1.5$, $t_{CM} = 200^\circ\text{C}$, $w_0 = 10\text{ m/sec}$.

composition and velocity of gas over cross sections of the pipe during burning of a homogeneous mixture after a grid of five flame-holders fixed in the same plane at a distance from each other of $S = 30\text{ mm}$. Characteristic for this case is the decrease of content of CO_2 (or, which is the same, of temperature of the gases) along the axis of the

wake at a certain distance from the flame-holder. For instance, over a distance of $x = 400\text{ mm}$ the content of CO_2 on axes of the wakes fell to $\sim 7\%$ (as compared to 19% in the cross section $x = 120\text{ mm}$) and became approximately identical with the content of CO_2 in the plane of symmetry between flame-holders. Thus, over the entire cross section of the combustion chamber, velocity profiles of the flow were smoothed.

With further increase of the distance from the stabilizers, over the entire cross section of the pipe there is uniformly increased combustion efficiency of the fuel; the velocity profile of the flow also remains uniform. Such a change of gas temperature on the axis of the wake is caused by the fact that with decrease of distance between flame-holders there is increased the intensity of mixing of fresh mixture with combustion products. Fresh mixture penetrates into the axial region of the wake after each flame-holder, and combustion products from the axial region penetrate into the plane of symmetry between the flame-holders. Thus, the time average gas temperatures are equalized over the entire cross section of the pipe, but do not reach the theoretical burning temperature, since a considerable part of the fuel still does not enter into the combustion reaction. At the same time, as comparison of experimental data shows, even in this case the extent of the burning zone and change of combustion efficiency of fuel in the plane of symmetry between flame-holders along the length of the burning zone α_T remain practically the same as starting burning after two flame-holders, other conditions being identical.

Gas-dynamics and thermal structure of the flow in the hot part of the combustion chamber becomes still more complicated for non-lens location of the flame-holders, when they are located not in the same plane, but are displaced relative to each other

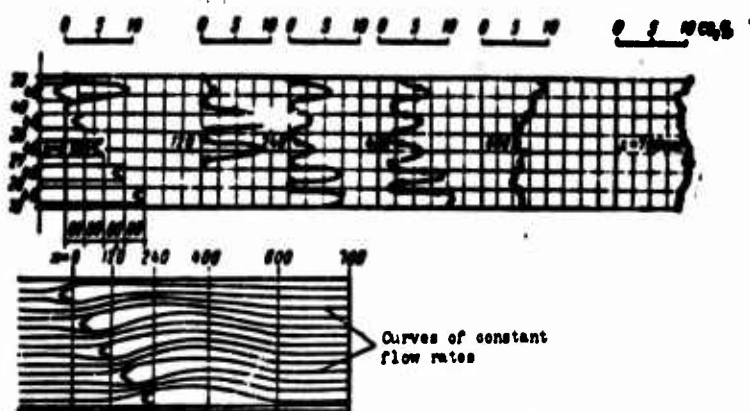


Fig. 8.17. Composition of gas and "flow lines" (curves of constant flow rates) over the length of a pipe during burning after a grid of flame-holders located in an echeloned manner. Homogeneous mixture, $\alpha = 1.5$, $t_{CM} = 200^\circ\text{C}$, $w_0 = 60 \text{ m/sec}$.

along the length of the chamber. The flow incident on the flame-holders is deflected in the direction of least resistance, flow lines are distorted, and there occurs redistribution of gas flow velocities over cross sections of the combustion chamber, accompanied by intense mixing of fresh mixture with combustion products and a sharp fall of maximum temperature (time average) in the wake after

the flame-holders located further forward. Thus, for instance, in the flame after the first upper flame-holder, the content of CO_2 in one of the combustion regimes fell from $\sim 9\%$ in the recirculation zone to $\sim 1.0\%$ at a distance of 120 mm from the flame-holder, and only at a distance of 600 mm again increased to 10% (Fig. 8.17). An analogous picture is observed in wakes after other flame-holders. Strong distortion of flow lines along the length and change of the field of velocities over cross sections of the combustion chamber is apparently accompanied by intense turbulization of the flow.

The above mentioned experimental data show how difficult it is to calculate flow characteristics in the space behind a flame-holder ahead of time, and to give an exact analytic solution of the problem of burn-up along the length and over cross sections of a full-scale combustion chamber of straight-flow-through type.

With echeloned location of flame-holders, the character of burn-up in the intervals between them will be different from the case of burning with location of flame-holders in the same plane. However, experiments show that, in spite of such a complicated gas-dynamic and thermal structure of the flow, on the whole, the length of the burning zone in the plane of symmetry between two flame-holders located in an echeloned manner turns out to be practically the same as and during burning between two flame-holders installed in the same plane, if the clearance between them and other conditions remain identical.

In order that with echeloned location of flame-holders, combustion of fuel to a given combustion efficiency be finished in one cross section of the combustion chamber,

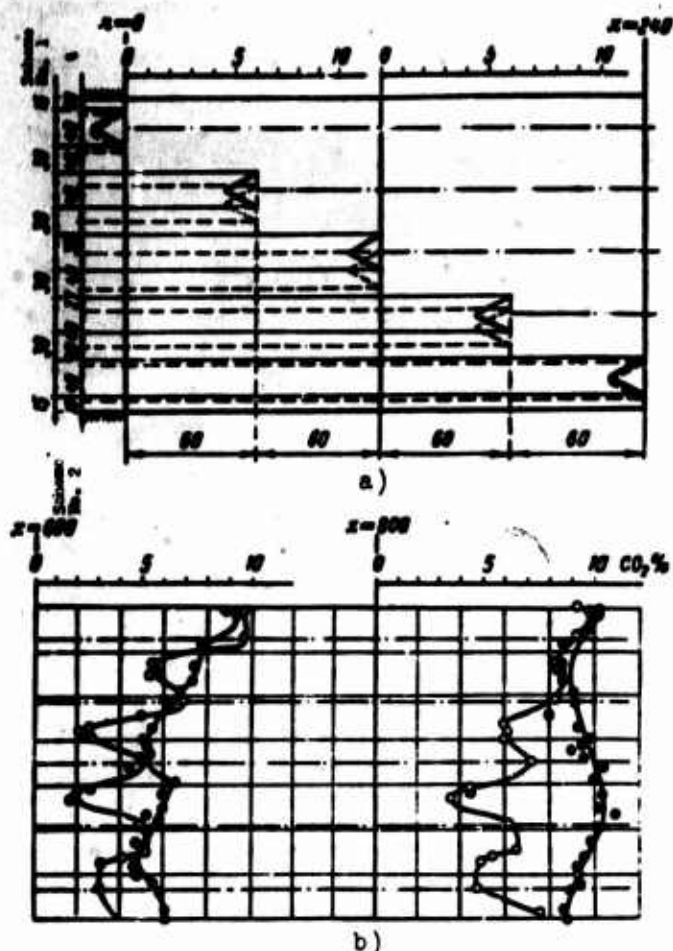


Fig. 8.18. Burn-up over the length of a pipe. a) for uniform distance between flame-holders $S = \text{var}$; b) for nonuniform distance between flame-holders $S = \text{const}$. Homogeneous mixture, $\alpha = 1.5$, $w_0 = 60 \text{ m/sec}$, $t_{\text{CM}} = 200^\circ\text{C}$. \circ - scheme No. 1. \bullet - scheme No. 2.

radial distances between flame-holders have to be variable. In Fig. 8.18 there are given experimental data which show change of composition of combustion products over the length of the combustion chamber with echeloned location of flame-holders. In the first case, the distance between flame-holders was identical and was equal to 30 mm. Burn-up over the length of the combustion chamber was nonuniform, and at the end of the pipe average combustion efficiency was low. In the second case, the distance between flame-holders was variable; it was changed from 40 to 20 mm. In this case burn-up over the length of the combustion chamber was more uniform, and was finished in the same cross section and with higher average combustion efficiency for the same combustion chamber length.

With echeloned location of flame-holders, the radial distance between them S is chosen from simple geometric

considerations in such a manner that for a given length of the hot part of the combustion chamber, and given number and dimensions of flame-holders, burn-up in the interval between all flame-holders to the assigned combustion efficiency is finished in the same section of the combustion chamber.

§ 6. CHARACTERISTICS OF BURNING OF TWO-PHASE MIXTURES IN A TURBULENT FLOW

In combustion chambers of straight-flow-through type, fuel is usually injected in the liquid state into a flow of air; thus the process of burning itself precedes the process of carburetion - atomization of the fuel, motion of liquid droplet in the flow and evaporation and mixing of the vapor with air. As a result, a fuel mixture with some relative concentration of liquid-droplet phase to vapor phase of the

fuel approaches the flame front. The process of carburation also continues after the flame front, in the burning zone, where large droplets of fuel are evaporated which were not able to vaporize in the preparation zone of the fuel mixture - in the space between the fuel manifold and the flame holders.

The two-phase fuel mixture is characterized by the total weight ratio of vapor phase to liquid phase of the fuel, the spectrum of coarseness of droplets of the liquid phase and the distribution of concentrations of liquid and vapor phases over the cross section of the chamber (see Chapter III).

In contrast to homogeneous mixtures, in two-phase mixtures the local concentrations of fuel differ to a greater or lesser degree from the average total values: the flow of fuel mixture possesses macro- and microheterogeneities in the content of both vapor and liquid phases of the fuel. The mass ratio of evaporated fuel to liquid phase, the spectrum of coarseness of droplets and micro- and macroheterogeneities of concentrations depend on the type and geometric parameters of injectors, distance between them on the fuel manifold, feed pressure and direction of injection of the fuel (along the flow, against the flow, etc.), distance from the place of injection, physical constants of the fuel, pressure, speed and temperature of the air flow, etc.

Characteristics of a two-phase mixture continuously change along the length of the combustion chamber. With increase of distance from the manifold, there is increased the quantity of evaporated fuel, and due to turbulent and molecular diffusion its concentrations over the cross section of the pipe are equalized. During flow around obstacles - the precombustion chamber and flame-holders - flow of fuel mixture changes direction; thus the droplets are not completely entrained in the flow, and part of them settle on the surface of the obstacles, and as they accumulate are carried away by the flow into the zone after the flame-holder. A considerable part of the fuel can settle on the walls of the chamber. Further on, behavior of fuel which has settled on the solid surfaces depends on the temperatures of these surfaces. On heated surfaces fuel to a considerable degree is evaporated; from cold surfaces it flows off in the form of a sheet, which is broken up in the flow of air into droplets of larger dimension than droplets produced during atomization by swirl injectors.

Nonuniform distribution of total concentrations of fuel over the cross section of the combustion chamber can lead to overenrichment of the mixture in individual zones. In these zones, combustion efficiency of fuel decreases due to the deficiency of oxygen. This explains the fact that, as a rule, the maximum combustion efficiency of the fuel in combustors of ramjet engines corresponds not to stoichiometric air-fuel

ratio, but lies in region of leaner mixtures, corresponding to $\alpha \approx 1.2$ to 1.3 .

The more uniformly the fuel spray nozzles are located over the cross section of the burning path, the smaller the diameters of droplets of atomized fuel, and the greater the distance from the fuel manifold to the flame-holder, then the more fuel is evaporated on approach to the flame front, the more uniformly its concentration is distributed over the cross section of the combustion chamber and the more homogeneous the fuel mixture is. And, conversely, with location of the fuel manifold close to the flame-holders, large dimensions of fuel droplets and low temperature of air, a large quantity of the fuel in the liquid-droplet state will pass through the flame front and burn according to laws which are different from those for burning of a homogeneous mixture.

The process of burning of liquid atomized fuel in a turbulent flow approaches the actual process of burning of fuel in a combustion chamber to the highest degree. However, this question up to now has been little investigated. Results of a large number of theoretical and experimental works on the study of burning of single droplets of fuel in a motionless medium or at small relative velocities (falling droplets) are not very applicable to real conditions of burning of two-phase mixtures in a turbulent flow. Thus, for instance, the "classical" diffusion theory of burning of a motionless drop is based on the assumption that the liquid drop is surrounded by a vapor shell of uniform thickness with gradients of temperature and concentration of fuel vapor and atmospheric oxygen identical in all radial directions. Fuel instantly burns in an infinitely thin layer on the spherical surface, where the concentrations of oxygen and fuel vapor correspond to $\alpha = 1.0$.

It is obvious that in a combustion chamber such a model of burning of droplets is not realized. Due to heat release, flow velocity over the length of the chamber increases. Thus acceleration reaches hundreds and even thousands of m/sec^2 . With such accelerations, drops will lag behind the flow and, depending upon their dimension, will have larger or smaller blowing velocities. Depending upon the magnitude of relative velocity, the vapor shell around the drop is deformed (stretched out along the flow, blown off from the drop), and under certain conditions the flame breaks off from the drop.

Experiments in the study of burning of drops of fuel with an air blast show that flame breaks off from the drop at blowing velocity of the order to 0.5 to 5.0 m/sec . Its value depends on dimensions of the drop and temperature of the medium: with increase of dimensions of the drop and temperature of the medium, there is increased the flow velocity at which blowoff occurs from the burning drop (Fig. 3.19).

Furthermore, there has been experimentally established a considerable mutual influence of burning drops on the stability of their burning: a group of drops burns more stably than a single drop; blowoff from a group of burning drops occurs at higher relative blowing velocities than during burning of a single drop (Fig. 8.20). This is explained by the fact that during burning of a group of drops, there occurs mutual transmission of heat to the drops by means of thermal conduction and radiation; thereby, there are increased the speed of their evaporation, the temperature of the medium after the burning drops, and, consequently, there appear favorable conditions for stabler burning of each drop.

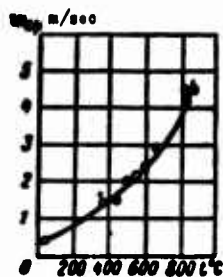


Fig. 8.19. Blow-off velocity of flame from a drop depending upon temperature of the flow. Fuel - gasoline; diameter of drop $d_0 = 1.5$ to 1.7 mm.

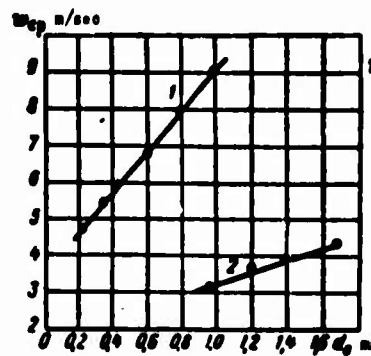


Fig. 8.20. Blowoff velocity of flame from a drop depending upon diameter of the drop. Fuel - gasoline; temperature of medium $t_{cp} = 870^{\circ}\text{C}$. 1 - falling drops in a ceramic pipe; 2 - suspended drops in an open flow.

According to contemporary ideas (see Chapter VI), turbulent flame has a complicated structure, which is nonuniform in temperature. At a given point of space with temperature fixed on the average with respect to time, at different moments of time there actually penetrate either products of almost complete combustion, with temperature close to the burning temperature at the given value of α , or fresh mixture with initial temperature t_{cm} .

Consequently, during burning of a two-phase mixture in a combustion chamber, droplets of fuel will lag behind the gas flow, alternately be blown with high relative velocity by gases with different temperatures, the flame will be blown off from them, and evaporation will occur under essentially non-steady conditions. Vapor removed from the fuel drop, depending upon temperature of the medium and concentration of oxygen, will be either preliminarily mixed with air, and then burn as an approximately homogeneous mixture, or immediately enter into the burning reaction according to the diffusion scheme.

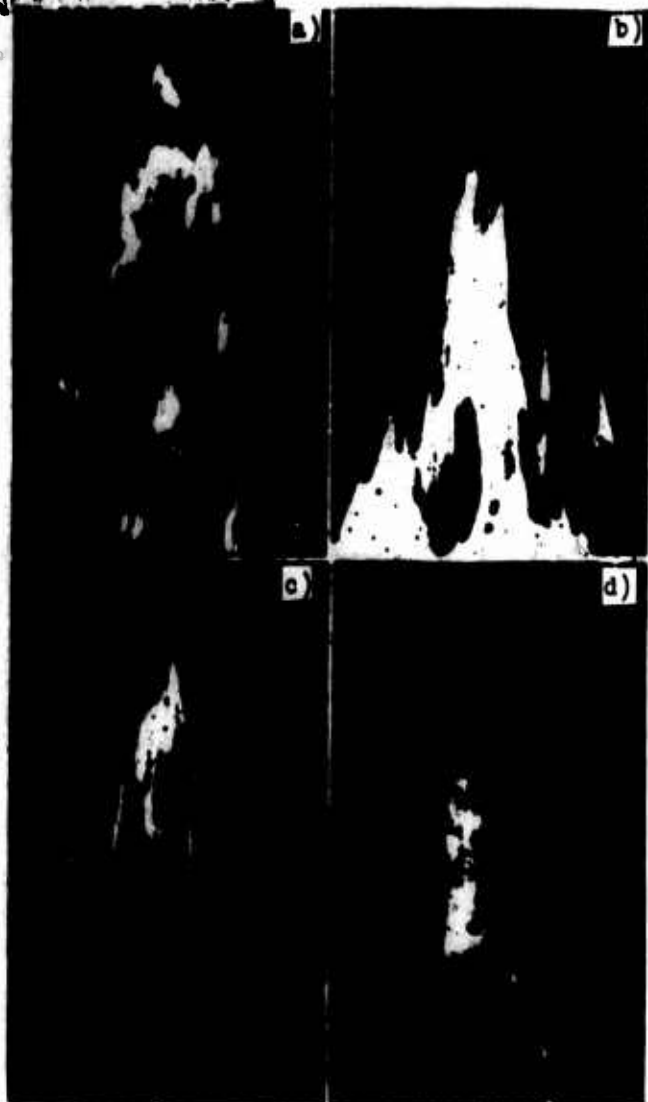


Fig. 8.21. Photographs of a flame in a turbulent flow of fuel mixture $w_0 = 20.5$ m/sec; exposure is $1/1250$ sec (experiments of Tikhomirov). a) homogeneous mixture, $z = 100\%$, $t_0 = 305^\circ\text{C}$, $\alpha_\Sigma = 1.1$. b) two-phase mixture, $z = 50\%$, $t_0 = 310^\circ\text{C}$, $\alpha_\Sigma = 2.54$, c) two-phase mixture, $z = 30\%$, $t_0 = 200^\circ\text{C}$, $\alpha_\Sigma = 2.38$, d) two-phase mixture, $z = 10\%$, $t_0 = 100^\circ\text{C}$, $\alpha_\Sigma = 4.08$.

flame front is absent, and separate drops and clusters of drops of fuel burn. At high temperatures of the mixture and high contents of evaporated fuel, there is observed a continuous flame front, and also focuses of burning of separate drops of fuel after this front (Fig. 8.21). Based on these data and certain calculations, the author arrives at the following qualitative conclusions. In two-phase mixtures, drops can ignite due to transmission of heat from burning drops or clusters of drops to the non-burning drops. Thus it is not necessary (at low content of fuel in the vapor

Thus, the total burning time of a two-phase mixture is composed of the "life time" of the largest drops (to their full evaporation) and the burning time of vapor after full evaporation of the drops. Reliable relationships for quantitative determination of these times have as yet not been obtained.

Above it was indicated that the question of burning of two-phase mixtures in a flow has been little investigated. There are known only a small number of experimental works. The authors of work [5] came to the conclusion that in a laminar flow monodisperse fogs (with diameter of drops $< 10 \mu$) behave during burning as homogeneous mixtures; in large-disperse fogs (with diameter of drops $> 40 \mu$) during burning of stationary or slowly moving mixtures the individual droplets burn.

Tikhomirov [9], investigating burning of two-phase kerosene air mixtures in a turbulent flow, established that at low temperatures of the mixture and low content of evaporated fuel in it, a continuous

phase) that in the space between drops there be realized chemical reaction. In the conducted experiments, the mean value of α with respect to the vapor phase reach values of 20 and more, and with such compositions a homogeneous mixture is not at all combustible, which indirectly confirms the accuracy of the presented scheme of burning of two-phase mixtures.

During burning of homogeneous mixtures, the length of the burning zone, other things being equal, increases with increase of α . In the case of burning of a "lean"

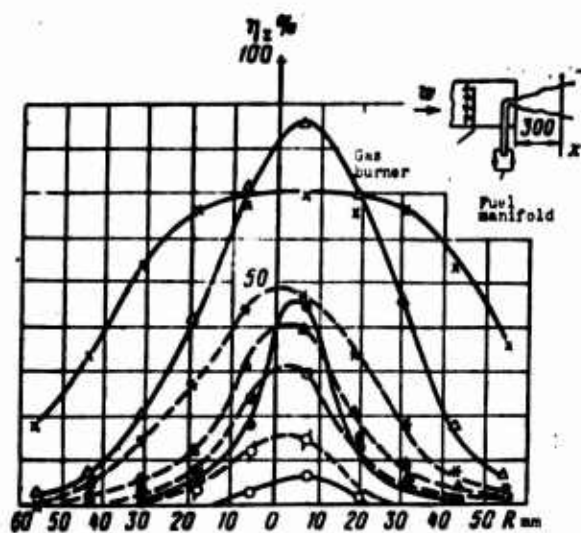


Fig. 8.22. Combustion efficiency of fuel in fixed section of flame during burning of homogeneous and two-phase mixture of gasoline with air, $t_{CM} = 100^\circ\text{C}$, $w_0 = 60$ m/sec. — uniform gasoline-air mixture, --- two-phase kerosene-air mixture $z_{cp} = 50\%$. \circ — $\alpha = 2.0$, Δ — $\alpha = 1.0$, \bullet — $\alpha = 1.4$, $*x$ — $\alpha = 0.7$.

of the fuel is less, and at $\alpha_{cp} > 2.0$ it is larger than for homogeneous mixtures of the same composition (Fig. 8.22).

It is necessary to note that for the purpose of decrease of length of the chamber, the process of burning of fuel is organized in such a way that in the burning zones the true value of the air-fuel ratio does not exceed 1.5-1.7. At such values α , the burning time of two-phase mixtures will be longer than the burning time of homogeneous mixtures. It is also obvious that the greater the diameter of the drops in the atomization spectrum of the liquid, the longer will be the burning time of the two-phase mixture, and the longer should be the length of the combustion chamber for the given combustion efficiency of the fuel.

In combustion chambers of ramjet engines and afterburners of turbojet engines, burning of fuel usually occurs at high temperatures of air; fuel spray nozzles of

two-phase mixture, during evaporation of drops there are created macrovolumes with concentrations of fuel vapor which are more favorable for burning than in a homogeneous mixture with the same mean value of α . Therefore, the limits of flame propagation with respect to α for a two-phase mixture are wider than for a homogeneous mixture. For the same reason, the burning rate of "lean" two-phase mixtures can be greater than the burning rate of a homogeneous mixture, but the length of the burning zone is accordingly less. This is confirmed by experimental data, which show that in a fixed section of a turbulent flame during burning of polydisperse kerosene air mixtures with $\alpha_{cp} \leq 1.4$, the combustion efficiency

centrifugal type are directed upstream and provide good atomization of fuel. Under these conditions, fuel mixture approaches flame holders with large content of vapor; large drops, however, which do not have time to be evaporated in "cold" part of chamber, succeed to be evaporated for the most part after the flame front. Therefore, process of burning of such mixtures is apparently closer to regularities of burning of uniform mixtures. At the same time, it should be borne in mind that in atomization spectrum there are drops of quite large dimensions (to 200 μ and larger), and part of them can not be evaporated in the whole extent of the combustion chamber. In this case, for estimation of physical incompleteness of combustion, it is necessary to calculate volatility of drops over the length of the combustion chamber. Method of calculation is discussed in Chapter III.

§ 7. EXPERIMENTAL DATA ON BURNING OF TWO-PHASE MIXTURES AFTER AN ARRAY OF FLAME-HOLDERS IN A PIPE

In combustion chambers of air-breathing jet engines, liquid fuel is usually injected through a manifold of swirlers.

In a number of cases, along the trajectory of flight, fuel flow rate through chamber can be changed by 5-8 times, which it is impossible to attain by changing only fuel feed pressure. Therefore, fuel manifold is frequently made to be multistage (more frequently - two-stage), and during transition of fuel feed from two to one stage, the step between injectors is considerably increased. Thus distribution of concentrations of fuel over cross section of burning loop can be impaired, and due to appearance of local zones of overenrichment of mixture fullness of combustion of fuel decreases. For a more precise answer to this question, there was experimentally checked influence of feed pressure of fuel and change of step (distance) between injectors on burn-up over the length of the pipe.

In Fig. 8.23 there are given curves of change of fullness of combustion of fuel in plane of symmetry between two flame holders during burning of two-phase kerosene air mixtures, depending upon feed pressure of fuel and number (step) of injectors on the manifold. From graph it is clear that with decrease of feed pressure of fuel to 6 atm (gage), length of zone of burnup starts to increase somewhat. Increase of distance between injectors by twice (from 60 to 120 mm) with feed pressure of fuel constant in both cases $\Delta p_T = 19$ atm (gage) practically did not influence length of burnup zone. Obtained results, naturally, have a specific character, and are accurate in a limited range of change of the indicated magnitudes.

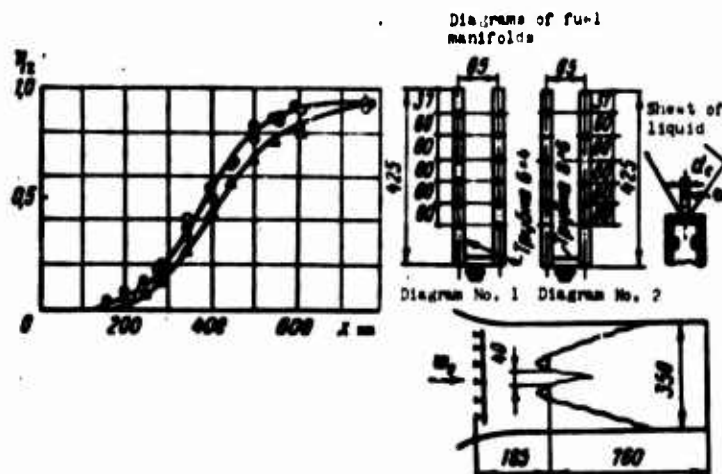


Fig. 8.23. Influence of number of injectors (step) and fuel feed pressure on change of η_2 in plane of symmetry between flame holders. $w_0 = 75$ m/sec, $t_g = 300^\circ\text{C}$, $t_T = 15^\circ\text{C}$.

Legend	No. of manifold	No. of diagram	α	P_T atm (abs.)	Injector characteristics		
					Number of injectors	d_c mm	θ deg
○	1	1	1.16	10	12	0.6	50
△	2	1	1.05	6	12	1.0	60
●	3	2	1.07	10	6	1.0	60

Comparison of experimental data obtained under identical conditions shows that at a temperature of air at entrance to combustion chamber which is variable within limits 300-800°C, speed of combustion and length of burnup zone in interval between flame-holders differ from the same magnitudes during burning of uniform mixtures. If, however, feed pressure of fuel is sufficiently high (more than 10 atm (gage)), then, as can be seen from Fig. 8.24, at identical values of flow velocity, temperature and mixture, ratio, burnup curves in plane of symmetry between flame-holders during burning of uniform and two-phase mixtures turn out to be practically identical.

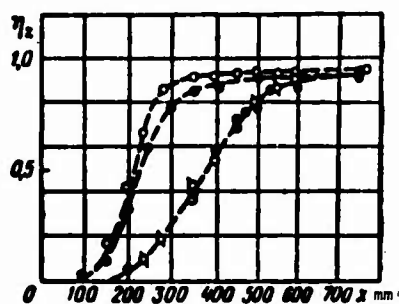


Fig. 8.24. Burnup in plane of symmetry between two flame-holders during burning of homogeneous and two-phase mixtures.

Legend	w m/sec	α	t °C	Mixture
●	91	1.3	500	Homogeneous gasoline-air
●	90	1.27	300	
○	90	1.15	500	Heterogeneous kerosene-air, manifold No. 1
○	90	1.2	300	

This result is not expected. Calculations show (see § 18, Chapter II) that for the parameters of flow and geometric characteristics of injectors shown in Fig. 8.23, the fuel mixture with approach to flame-holders (at distance of 200-300 mm from the manifold downstream) has 75-90% fuel in vapor phase, but at distance of 200-300 mm after flame front, degree of evaporation is increased to 97-98%. At

atmospheric pressure in flow, average median diameter of drops $d_m = 30-50 \mu$ and air-fuel ratio $\alpha = 1.1$, number of drops in 1 cm^3 of mixture $n = 11,000-4000$, and average distance between them does not exceed 1 mm. With such small distance between drops and high intensity of turbulence of flow fuel vapors are well mixed with air, and with approach to flame-holders form a fuel mixture close to homogeneous. It is natural that in considered cases, burning of such "two-phase" mixtures practically does not differ from burning of a technically uniform mixture.

In case of lower temperatures of flow and worse atomization of liquid, fuel mixture will have considerable amount of fuel in liquid-droplet phase, and necessary length of hot part of combustion chamber will be determined by time of evaporation of drops plus time of burning of vapor after full evaporation of drops. Length of burnup zone thus will be larger than during burning of uniform mixtures with the same mean values of α .

At a temperature of flow of air exceeding $950-1000^\circ\text{C}$, fuel in combustion chamber ignites itself practically immediately after leaving injector, and burning occurs not in flame front, as occurs at lower temperatures, but in all volumes where there are combustible concentrations of fuel vapor and oxygen. In this case, it is possible to estimate approximately the necessary minimum length of hot part of combustion chamber according to time of evaporation (burning) of drops, assuming that fuel evaporated from burns instantly.

§ 8. BURNING IN TURBULENT FLOW NEAR WALL OF PIPE

During investigation of working process in combustion chambers of air-breathing jet engine, of practical interest is burning of fuel-air mixture near metallic wall. However, for systematic investigations of turbulent burning at the wall under conditions close to those of burning in chambers of a ramjet engine have been conducted.

A number of experimentors have expressed the assumption that burning at wall of chamber of ramjet engine is impaired as compared to burning in flow core, and total decrease of fullness of combustion of fuel to a considerable degree is a result of low combustion efficiency layers of flow near the wall. Such assumptions are mainly based on the following considerations. First, it is assumed that due to intense heat exchange, temperature in zone of burning in layer near wall can sharply drop, and, as a result of this, effective rate of combustion in this layer is decreased. Secondly, directly at the wall intensity of turbulence drops, and this also should lead to decrease of effective burning rate in layer near the wall.

These assumptions to some degree find experimental confirmation. In a number of

cases, measurements of temperature and chemical composition of combustion products in various sections of chamber show that in layers at the wall temperature of gases and fullness of combustion of fuel are lower than in flow core. Compositive test of certain models of combustion chambers of ramjet engine during cooling of walls by water and air showed that, other things being equal, mean values of combustion efficiencies of fuel in first case were 10-12% lower than during cooling of walls of chamber by air.

However, in most cases, lower values of temperature of gases and fullness of combustion of fuel in layers at the wall can be explained not by impairment of combustion itself at the wall, but by other causes - loss of heat from gas flow to cooling water, nonuniform distribution of concentrations of fuel over cross section of combustion chamber with impoverishment of mixture at the wall, etc. Lower combustion efficiency of fuel at the wall as compared to its value in the flow core may also be a result of incorrect (nonuniform) location of flame-holders in combustion chamber: if distance between wall and the nearest flame-holder to it is considerably larger than half of distance between adjacent flame-holders, burnup at the wall will be finished later (at larger distance from flame-holders) than in the interval between flame-holders. Conversely, by decreasing distance between flame-holder and wall and increasing it between neighboring flame-holders, we obviously can obtain in fixed section of combustion chamber high combustion efficiency at the wall and low efficiency in interval between flame-holders. For the purpose of more detailed clarification of this question, there was conducted experimental investigation of burning of uniform fuel-air mixtures near a metallic wall.

In Fig. 8.25 there are given diagrams of experiment and curves of change of chemical composition of gases (CO_2) over length of flame in layer at the wall. Burning of uniform kerosene-air mixture occurred after flame-holder in an open flow, bounded above by a metallic wall made of steel. In one case the wall on the outside was heat-insulated by a layer of asbestos, and temperature of surface along the length changed from temperature of fresh mixture at root of flame to $1000-1200^\circ\text{C}$ at the end; in the other case, being cooled by running water, temperature of its surface did not exceed $60-80^\circ\text{C}$. As seen from Fig. 8.25, under the same conditions of burning, in both cases chemical composition of combustion products, and consequently also combustion efficiency of fuel in corresponding sections of torch were practically identical. Consequently, even much different losses of heat from gases into wall did not noticeably influence burning in the layer of homogeneous mixture at the wall.

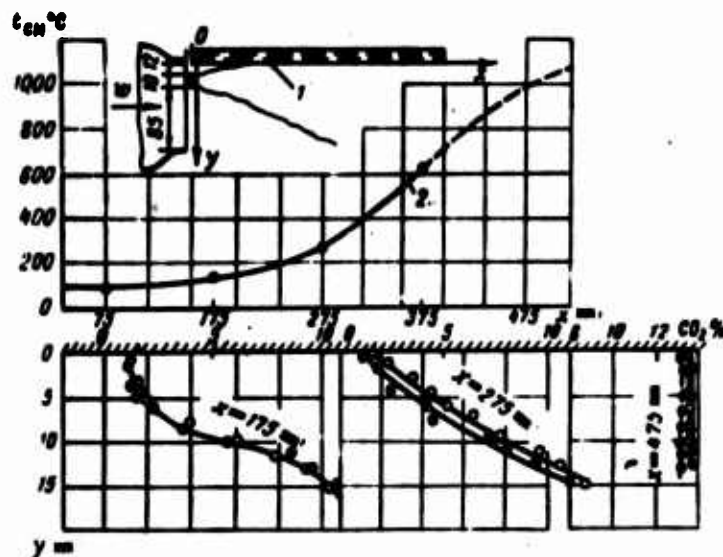


Fig. 8.25. Change of composition of combustion products during burning of uniform mixture at cooled and heat-insulated walls. $w_0 = 70$ m/sec, $\alpha = 1.06$, $t_{CM} = 200^\circ\text{C}$. 1 - heat-insulated or water-cooled wall. 2 - temperature of heat-insulated wall. \bullet - heat-insulated wall, \circ - water-cooled wall.

Given experimental data show that in the combustion chamber, wall practically does not render any essential influence on combustion efficiency of uniform mixtures.

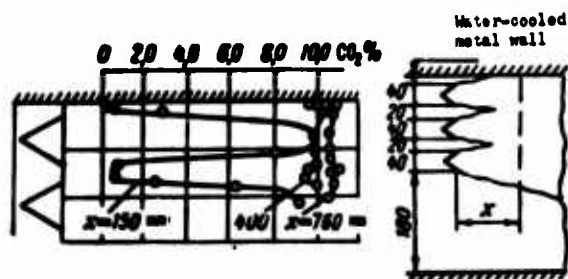


Fig. 8.26. Change of composition of combustion products at the wall and in the interval between flame-holders during burning in a pipe. Uniform mixture; $w_0 = 70$ m/sec, $\alpha = 1.385$, $t_{CM} = 300^\circ\text{C}$.

wall also will practically not noticeably affect combustion efficiency of usual two-phase fuel mixtures.

During low temperatures of flow of air, when large quantity of fuel will be in liquid-droplet state, drops of fuel can settle on cold surface of wall and flow in

In Fig. 8.26 there are given experimental data on chemical composition of combustion products in various sections of chamber during burning of uniform mixtures after an array of flame-holders in a rectangular pipe, walls of which were cooled with water. Flame-holders were established in one section of the pipe. Distance between wall and edge of the nearest flame-holder to it was two times less than distance between edges of adjacent flame-holders. Burnups directly at wall and in plane of symmetry between flame-holders in this case were also practically identical.

In combustion chambers, burning occurs either at the walls of heat jackets (during air cooling of walls of combustion chamber), or at the strongly heated, uncooled (covered with heat-protecting insulation) wall of a short-term working motor. At high temperatures of flow, as was shown above, fuel mixture approaches flame front with almost completely evaporated fuel. Therefore, it is possible to assume that influence of

the form of a liquid sheet, which will not have time to be evaporated during its time of stay in the chamber. This can lead, on the one hand, to impairment of stability of burning (appearance of vibration, pulsational burning), and on the other hand, to lowering of overall combustion efficiency due to incomplete burning caused by removal of liquid fuel.

§ 9. GENERALIZATION OF EXPERIMENTAL DATA ON INVESTIGATION OF BURNING IN THE WAKE AFTER BLUFF BODIES

The above experimental data show that burning rate of a uniform mixture in the wake after flame-holders depends on physicochemical and gas-dynamic characteristics of the mixture: air-fuel ratio α , temperature t , pressure p , speed w and intensity of turbulence of flow ϵ , and also on geometric parameters of combustion chamber: dimensions h , geometric form Φ and distance between flame-holders S , coordinates of considered point x, y, z .

Burning rate u_{τ} on the basis of thermal theory, should in principle depend also on kind of fuel, its calorific value H_u , time of induction $\tau_{\text{инд}}$, activation energy E , reaction rate constant k , coefficient of molecular diffusion and other quantities determining kinetics of chemical reaction of process of burning. However, for hydrocarbon fuels of the type of gasoline - kerosene, which are usually applied in combustion chambers of air-breathing jet engines, quantities determining kinetics of process of burning turn out to be approximately identical; moreover, experience shows that the role of chemical kinetics in process of burning in a turbulent flow is small as compared to influence of physical factors (in the first place, mixing processes) and in the first approximation it is possible to disregard it.

Thus, for a given fuel it is possible to write

$$u_{\tau} = u_{\tau}(\alpha, t, p, w, \epsilon, h, \Phi, S, x, y, z). \quad (8.1)$$

It is easy to note that part of these parameters characterize intensity of turbulence of flow of fuel mixture in the space after the flame-holders, which depends on $\epsilon_0, p, h, \Phi, S$ and changes along the length and over cross sections of the combustion chamber:

$$\epsilon = \epsilon(\epsilon_0, p, h, \Phi, S, x, y, z). \quad (8.2)$$

where ϵ_0 - intensity of turbulence of flow of fuel mixture before flame-holders (in incident flow).

Other parameters determine normal (fundamental) speed of propagation of flame in laminar flow

$$u_n = u_n(\alpha, t, p). \quad (8.3)$$

Fundamental experimental results were obtained in work of Kokushkin [6], who, by using low-inertia methods of measurement of temperature in flame, showed that at flow velocities up to 100 m/sec and intensity of turbulence $\epsilon = 6-7\%$ in a turbulent flame jet of uniform fuel mixture, separate volumes of gas chiefly have temperatures close to adiabatic temperature of burning T_r , or temperature equal to temperature of the initial, cold mixture T_{om} . Temperature changes from T_{om} to T_r over a depth not exceeding 1-2 mm, i.e., comparable with width of laminar flame front. In this layer most of the fuel burns. Thereby, there were experimentally confirmed the basic physical ideas expressed by Shchelkin [7] and Damkohler [8] about the fact that in a turbulent flame burning occurs chiefly in a thin flame front by a mechanism close to that of burning in a laminar flow, speed of which is determined by the magnitude u_H , and mass rate of burning is increased in comparison with burning in a laminar flow mainly due to increase of the burning surface caused by turbulent pulsations of velocity.

Thus, it is possible to consider that in the first rough approximation for fuel of given kind, burning speed

$$u_T = u_T(u_H, \epsilon, w) \quad (8.4)$$

or

$$u_T = u_T(u_H, u'), \quad (8.5)$$

where $u' = \epsilon \cdot w$ — normal component of pulsational velocity flow.

According to the π -theorem of the theory of similarity, from three physical quantities of identical dimension, which determine the flow of the considered process of burning, it is possible to compose two simplexes u_T/u_H and u'/u_H , and by experimental data find a functional relation between them:

$$\frac{u_T}{u_H} = f\left(\frac{u'}{u_H}\right). \quad (8.6)$$

Experimental magnitude u_T , by analogy with u_H , can be determined by using the known principle of Michelson:

$$u_T = w \cdot \sin \alpha, \quad (8.7)$$

where w — flow velocity of fuel mixture before flame front;

α — angle between velocity vector of flow \bar{w} and a certain burning surface.

As is known, Michelson's principle will apply to burning of gas mixtures in a laminar flow, when thickness of flame front can be disregarded and relationship (8.7) in physical meaning expresses the volume rate of burning of the mixture. The time average width of burning zone in turbulent flame attains tens and hundreds of

millimeters; therefore, during use of the principle of Michelson for determination of u_T , it is necessary to take angle α not according to the visible, time average boundary of the flame, but between \bar{w} and the surface passing through points corresponding to $\eta_z = 0.5$ in every cross section of the flame (detailed proof is seen in Chapter V).

During burning after a grid or a single flame-holder, magnitude u_T is changed along length and over cross sections of pipe, since intensity of turbulence of flow continuously changes (see Fig. 8.1). To determine true value of u_T at every point of

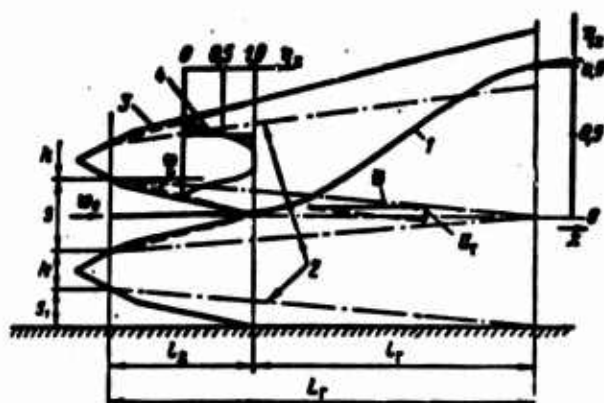


Fig. 8.27. Diagram and time-averaged parameters of a flame in the wake after two flame-holders. 1 - change of η_z in plane of symmetry between flame-holders, 2 - averaged burning surface, 3 - visually observed boundaries of flame, 4 - change of η_z over cross section of flame.

chamber is practically impossible; therefore, it is expedient to consider some average value of \bar{u}_T over the whole length of the burning zone. This magnitude is calculated in the following manner. As the average burning surface is taken the surface lying on a straight line drawn from edge of flame-holder to point in plane of symmetry between flame-holders, where time average combustion efficiency of fuel $\eta_z = 0.9$ (Fig. 8.27). Then, using Michelson's principle, we will obtain

$$\bar{u}_T = \bar{w} \frac{S}{2L_T}, \quad (8.8)$$

where \bar{w} - average flow velocity over the length L_T (taking into account change of speed due to heat emission);

S - distance between adjacent edges of flame-holders;

L_T - length of section of burning from edge of flame-holder to point in plane of symmetry between flame-holders, where combustion efficiency of fuel is increased to $\eta_z = 0.90$.

In Fig. 8.28 there is given a graph of the dependence $\bar{u}_T/u_H = f(\bar{u}'/u_H)$. During construction of this graph there were used known values of u_H (see § 2, Chapter V) and mean values of intensity of turbulence of flow along averaged burning surface.

In a wide range of change of flow velocity, temperature and mixture ratio, and dimensions and geometric form of flame-holders, at various distances between them, experimental points fit satisfactorily on one curve. This indicates the fact that burning speed of a homogeneous mixture in the wake after bluff bodies depends basically on normal velocity of propagation of flame u_H and intensity of turbulence of

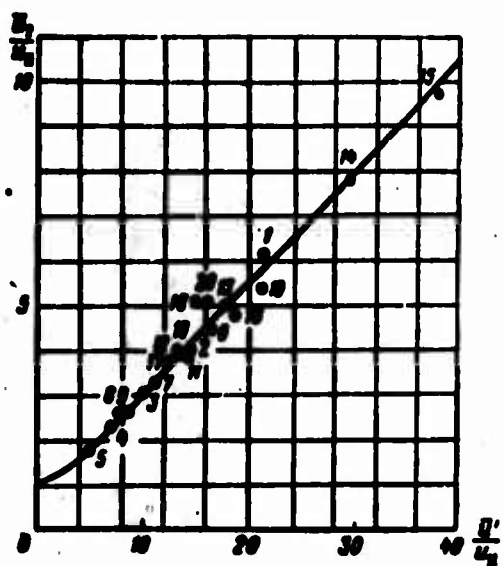


Fig. 8.28. The dependence $\frac{\bar{u}_T}{u_H} = f \frac{\bar{u}'}{u_H}$ during burning of homogeneous mixture in the wake after flame-holders.

No. of position	$\frac{u_T}{u_H}$	$\frac{\bar{u}'}{u_H}$	ϵ	Scheme
1	90	300	1.41	Two flame-holders of V-shaped form, $h=40$ mm; $S=40$ mm; $\beta=60^\circ$
2	92	300	1.36	
3	95	300	1.4	
4	91	300	1.41	
5	90	300	1.36	
6	92.5	300	1.41	
7	94	300	1.39	
8	94	300	1.41	
9	95	300	1.43	
10	97.5	300	1.18	
11	130	400	1.4	
12	41	300	1.4	
13	70	300	1.4	
14	110	300	1.4	
15	150	300	1.4	
16	70	300	1.4	Two flame-holders $h=40$ mm; $S=30$ mm; $\beta=60^\circ$
17	80	300	1.4	Two cylinders $d=40$ mm
18	90	300	1.4	Two plates $h=40$ mm
19	221	300	1.36	Four flame-holders $h=40$ mm; $S=40$ mm; $\beta=60^\circ$
20	130	300	1.42	

flow in burning zone $\bar{\epsilon}$: the higher the level $\bar{\epsilon}$ and the larger the magnitude u_H , the higher the burning rate u_T and the less the necessary length of the combustion chamber will be.

However, the great influence of u_H on burning rate in a turbulent flow appears only at relatively low intensity of turbulence of flow (at $\epsilon \approx 4$ to 5%). During burning in the wake after bluff bodies under the conditions of a straight-through-flow combustion chamber, burning speed u_T depends mainly on pulsational component of flow velocity \bar{u}' , i.e., on intensity of turbulence $\bar{\epsilon}$. Average level of intensity of turbulence along averaged burning surface (see Fig. 8.27) little depends on geometric form of bluff body, and practically does not depend on dimension of flame-holders h (in investigated range of change, $h = 10$ -40 mm), but very strongly depends on distance to the flame-holders: at distance $l \approx 200$ mm downstream, $\bar{\epsilon} = 18$ -20%, and at distance $l = 700$ -800 mm ϵ decreases to 8-9%. Consequently, the shorter the distance between flame-holders S , the less will be the length L_T and the higher will be the burning speed \bar{u}_T .

LITERATURE

1. M. Gol'dsmidt and S. Penner. Burning of individual drops in an oxidizing atmosphere, VRT; 1955, No. 2.
2. D. Spalding. Experimental investigation of burning and extinguishing of liquid fuel on a spherical surface, VRT, 1954, No. 3.
3. D. Spalding. Burning of liquid particles in a gas flow, VRT, 1952, No. 2.
4. M. Gol'dsmidt. Experiments on burning of separate drops of fuel, VRT, 1957, No. 2.

5. I. H. Burgoune and L. Coher. The effect of drop size on flame propagation in light aerosols, Proc. or Roy. Soc., 1954.
6. N. V. Kokushkin. Investigation of combustion of a homogeneous mixture in a turbulent flow by means of recording of pulsations of temperature, News of AS USSR, 1958, No. 8.
7. K. I. Shchelkin. Burning in a turbulent flow, ZhTF (Journal of Theoretical Physics), Volume XIII, Issue 9-10, 1943.
8. G. Damkohler. Der Einfluss der Turbulenz auf die Flammgeschwindigkeit Gasgemischen, Jahrbuch, 1939.
9. Burning of two-phase mixtures, Collection ENIN (Power Engineering Inst. im. G. M. Krzhizhanovskiy), Academy of Sciences of USSR, 1958.

CHAPTER IX

COOLING OF WALLS OF THE COMBUSTION CHAMBER AND THE NOZZLE

§ 1. DIFFERENT METHODS OF AIR COOLING OF A RAMJET ENGINE

Due to high temperatures of combustion products in ramjet engines and high stagnation temperatures of the incident flow at supersonic speeds of flight, the problem of cooling and heat protection of engines is one of the basic problems of jet engineering. Combustion chambers and nozzle prepared from usual heat-resistant materials need intense cooling at present-day speeds of flight. The design of a ramjet engine, its characteristics and performance considerably depend on the simplicity, reliability and economy of the cooling system. The selected cooling system should ensure reliable operation of the engine with minimum cooling losses of specific impulse.

The necessary high-temperature strength and thermal stability of the structure of a ramjet engine can be obtained either by means of cooling, or by means of use of special heat-resistant materials and heat-shielding coatings. For engines with maximum economy, designed for comparatively prolonged operation, depending upon the speed of flight there can be used air or liquid methods of cooling. For engines with maximum thrust, designed for short-term operation, for protection of the chamber and nozzle from the action of the high temperatures of the combustion products it is expedient, apparently, to use special heat-shielding coatings and platings.

For increase of thermal stability, in the contemporary state of the technology of heat-resistant materials it is most expedient to use cooling in combustion with the new structural materials.

Of possible methods of cooling of a ramjet engine, the simplest is air cooling, which does not require a supply of special coolant and does not limit thereby the

duration of flight. Therefore main attention has been turned to development of methods of calculation and investigation of different schemes of air cooling, taking into account data concerning certain new structural materials. There exist four basic methods of air cooling of the combustion chamber and nozzle of a ramjet engine:

1. External cooling, when the wall of the engine is cooled by the external incident flow without application of special cooling devices.

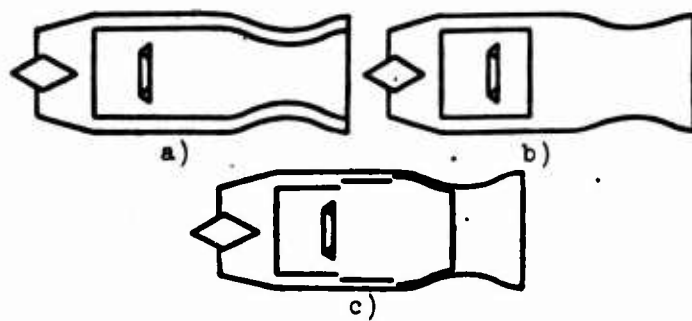


Fig. 9.1. Different schemes of air cooling of a ramjet engine.

2. Convection cooling

(Fig. 9.1a), when air coolant passes from the diffuser into a special annular opening formed by the wall of the engine and a special housing.

3. Boundary cooling (Fig.

9.1b), when air coolant passes from the diffuser through a

special annular slot onto the inner wall of the combustion chamber and the nozzle.

4. Combined cooling (Fig. 9.1c), when the air coolant passes through several echeloned annular openings. Combined cooling includes elements of convection and boundary cooling.

If the stagnation temperature of the incident flow approaches maximum permissible temperature for the selected structural material, then air cooling of a ramjet engine can be carried out with preliminary injection of liquid into the cooling flow.

Liquid cooling presents practically unlimited possibilities from the point of view of heat withdrawal from the construction. It is possible to present two basic methods of liquid cooling:

1. Film cooling (Fig. 9.2a), when liquid coolant passes through a series of annular slots to the inner wall of the combustion chamber and nozzle.

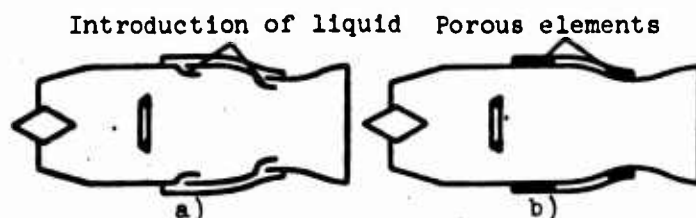


Fig. 9.2. Different schemes of liquid cooling of a ramjet engine.

2. Transpiration cooling

(Fig. 9.2b), when the combustion chamber and nozzle (or separate elements of them) are made of porous material, and liquid coolant is forced through the porous wall onto the inner surface of the combustion chamber and nozzle.

The problems of air cooling of a maximum-economy engine and of a maximum-thrust engine are formulated and solved differently. A maximum-economy engine works at an air-fuel ratio considerably larger than unity, so that a considerable part of the flow rate of air through the engine (up to 40 to 50%) does not participate in burning, and can be used for cooling. In this case the problem is not only organization of reliable cooling, but also creation of good mixing of hot and cold flows in such a manner that losses in thrust and specific impulse caused by cooling and mixing are minimum. A maximum-thrust engine works at $\alpha = 1.0$, so that in the process of burning there participates practically the whole flow rate of air through the engine. In this case, the flow rate of air used in cooling should be minimum. It is important to organize reliable cooling with minimum flow rate of air coolant, and to create good mixing of hot and cold flows, so that losses in thrust caused by cooling and mixing will be minimum.

The least flow rate of air coolant is obtained in that case when temperature of the wall of the engine preserves a constant value, equal to the maximum permissible temperature for the given material. Then it is possible to show that the cooling channel should be convergent. Consequently, in engines working in the regime of maximum thrust, the height of the cooling channel should decrease along the engine.

The simplest from the structural point of view are cooling channels of constant height. In this case the temperature of the wall along the engine changes, attaining maximum value either in the throat, or at the exit of the nozzle. Overcooling of walls of the engine when the height of the channel is constant leads to additional expenditures of air in cooling as compared to the case when $T_w = \text{const}$. In the maximum-economy engine, flow rate of air coolant does not restrict the cooling system; therefore, there can be used cooling channels with constant height.

In this work there is proposed a method of calculation of different schemes of air cooling. Calculation of air cooling of a ramjet engine for given conditions of its operation consists of determination of dimensions of the channel and necessary flow rates of air coolant, at which there is ensured satisfactory heat resistance of the structure, determined by maximum temperature of the engine wall. Along with calculation of the cooling system, there have to be determined losses of thrust and specific impulse caused by cooling of the motor. If dimensions of the cooling channel have already been selected, for instance from structural considerations, then there is performed a control calculation of the cooling system, as a result of which there is determined the flow rate of air coolant and temperature of the wall

of the motor.

Conditions of heat exchange in the combustion chamber and nozzle are essentially different; therefore, in certain cases, cooling of these elements is considered separately. The presence of bluff bodies (precombustion chamber, flame holders, manifold), increased turbulence of the incident flow and heat emission (burning) complicate the process of heat exchange in the motor so much that up to now there are lacking sufficiently reliable data on heat flux from the hot flow to the wall. Therefore, for calculation of the coefficient of convection heat transfer from the gas to the wall of the combustion chamber of the motor, there are usually applied criterial formulas (9.8) and (9.9). We should consider that due to nonuniformity of temperature fields, calculated heat flows from gas to wall can differ from the true heat flows.

§ 2. BASIC INFORMATION FROM HEAT EXCHANGE

Theoretical investigation of heat transfer under turbulent conditions of flow runs into considerable difficulties, which are connected with the absence of a closed system of differential equations [2]. Therefore, along with the use of the analogy of Reynolds and Prandtl, experimental investigation and processing of experimental data in criterial form is one of the basic trends in the investigation of heat exchange for turbulent conditions of flow. For a compressible liquid ($M \neq 0$) with large temperature gradients between the flow and the body ($\bar{T}_w = \frac{T_w}{T_e} \neq 1$), the criterial formula has quite complicated form:

$$Nu = f(\bar{Re}, Pr, \frac{s}{D}, M, \bar{T}_w). \quad (9.1)$$

Here $\bar{T}_w = T_w/T_e$ denotes the temperature factor, which is equal to the ratio of the wall temperature to equilibrium temperature.

On the basis of experimental investigation of local and average coefficients of heat transfer in pipes, it has been established that the local value of the Nusselt number Nu changes approximately as $x^{-0.1}$ [1]:

$$Nu \sim \left(\frac{s}{D}\right)^{-0.1} \quad (9.2)$$

The form of the criterial formulas essentially depends on selection of the determining temperature, i.e., that temperature at which physical parameters of the liquid contained in the numbers Re and Pr (Reynolds and Prandtl) are taken. As the determining temperature there is chosen either the thermodynamic temperature on the boundary of the thermal boundary layer (T_0), the temperature of the wall (T_w), or

the temperature of the boundary layer, which is conditionally equal to $(T_0 + T_w)/2$.

In many cases the expediency of selection of the determining temperature depends on the formulation of the heat engineering problem. If, for instance, the wall temperature is specified (from considerations of strength), then it is necessary to take as the determining temperature T_w . If the temperature of the flow is known (for instance, during calculation of cooling), then it is expedient to choose as the determining temperature T_0 . Eckert showed that there can be found a determining temperature T^* such that when physical parameters are refined to this temperature, the influence of Mach number on coefficient of friction disappears, and for calculation of c_f there can formally be used the formulas of an incompressible fluid. For instance, under turbulent conditions of flow, such a temperature is determined by formula [3].

$$T^* = T_0 + 0.5(T_w - T_0) + 0.22(T_w - T_0). \quad (9.3)$$

where T_0 - thermodynamic temperature on the boundary of the boundary layer;

T_w - wall temperature;

T_e - equilibrium temperature, i.e., temperature of the thermally insulated wall.

Equilibrium temperature is determined by the known formula

$$T_e = T_0 \left(1 + \frac{k-1}{2} r M^2 \right). \quad (9.4)$$

where k - adiabatic exponent;

M - Mach number on the boundary of the boundary layer;

r - coefficient of restitution, which depends on the flow regime (laminar or turbulent), Prandtl number Pr (see below) and Reynolds number Re . During turbulent flow around a flat plate with sufficiently large Reynolds numbers ($Re_L > 10^6$), the recovery factor has the value $r \approx 0.9$.

Thus, calculation of local or average coefficient of friction on a flat plate surrounded by a turbulent flow of compressible fluid in the presence of heat exchange, can be carried out according to the formulas for an incompressible fluid under the condition that density and viscosity μ , which are included in the corresponding Reynolds number, are determined at the characteristic temperature T^* [see formula (9.3)]. The result of calculation of the coefficient of friction in dependence upon Mach number by the method of Eckert is represented in Fig. 9.3 by the solid curve [3]. For calculation of the coefficient of friction on a flat plate for a turbulent flow regime without heat exchange ($T_w/T_e = 1$), it is possible to use the approximate formula

$$\frac{c_{f, \text{cm}}}{c_f} \approx \frac{1}{\sqrt{1 + \frac{k-1}{2} r M^2}}. \quad (9.5)$$

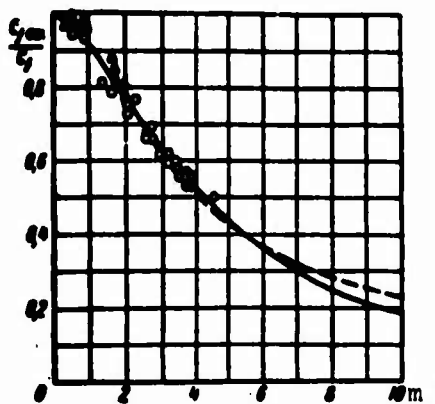


Fig. 9.3. Dependence of coefficient of friction on a flat plate in the turbulent flow regime on Mach number. Δ — according to data of Wilson, \circ — according to data of Chapman and Kester; — according to the formula of Eckert, --- according to formula (9.5).

which agrees satisfactorily with the dependence of Eckert and approximates the experimental points well (dotted curve in Fig. 9.3 at $k = 1.4$ and $r = 0.9$).

If we take as the determining temperature the temperature T^* [see formula (9.3)], then the coefficient of heat transfer during turbulent flow of compressible fluid around a flat plate can be calculated just as for an incompressible fluid [3]. Thus, for instance, for the local Nusselt number we have

$$Nu = 0.029 \cdot Re^{0.8}. \quad (9.6)$$

For the mean value of Nu on a plate of length L , taking into account Prandtl number Pr , we will obtain

$$\bar{Nu} = 0.036 \cdot Re_L^{0.8} \cdot Pr^{1/4}. \quad (9.7)$$

For comparatively small temperature gradients ($T_w/T_0 \approx 1.0$) and large change of Prandtl number ($0.6 \leq Pr \leq 100$), the mean value of Nusselt number Nu for pipes (in the turbulent flow regime) is satisfactorily approximated by the empirical dependence [4]

$$\bar{Nu} = 0.023 \cdot \bar{Pr}^{0.4} \cdot Re^{0.8}, \quad (9.8)$$

where physical parameters of the liquid are determined at the average thermodynamic temperature of the flow:

$$\bar{Nu} = \frac{\bar{\alpha} \cdot D}{\lambda} - \text{Nusselt number, referred to diameter of the pipe;}$$

$$\bar{Pr} = \frac{\bar{\mu} \cdot g \cdot \bar{c}_p}{\lambda} - \text{Prandtl number, calculated according to the average thermodynamic temperature of the flow;}$$

$$\bar{Re} = \frac{\rho U D}{\mu} - \text{Reynolds number, calculated according to the average thermodynamic temperature of the flow.}$$

For these conditions of flow, Mikheyev recommends the following formula [5]:

$$\bar{Nu} = 0.021 \cdot \bar{Pr}^{0.43} \cdot Re^{0.8}. \quad (9.9)$$

Results of calculation of coefficients of heat transfer by formulas (9.8) and (9.9) practically coincide.

In Fig. 9.4 there are compared calculated [see formula (9.8)] and experimental values of Nusselt number \bar{Nu} during turbulent motion of different gases in smooth cylindrical pipes. Calculated values of Nu in the whole investigated range of Re

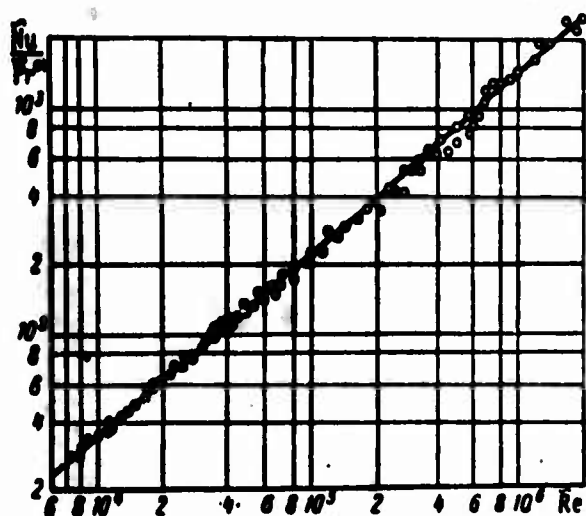


Fig. 9.4. Heat transfer during turbulent flow of different gases in round cylindrical pipes [4].

numbers ($10^4 \leq Re \leq 2 \cdot 10^6$) agree well with experimental data, and the spread of the experimental points lies within the limits of possible error.

For large temperature gradients between the gas and the pipe wall, we should consider the influence of the temperature factor ($\bar{T}_w = T_w/T_0$) on the coefficient of heat transfer. On the basis of theoretical considerations, in work [4] there are obtained approximate formulas for calculation of the coefficient of heat transfer in a pipe,

taking into account the temperature factor. These formulas are well approximated by the following dependences:

for $0.5 < \frac{T_g}{T_0} < 1.0 \quad \frac{\bar{\alpha}_T}{\bar{\alpha}} = 1.27 - 0.27 \left(\frac{T_g}{T_0} \right), \quad (9.10)$

for $1.0 < \frac{T_g}{T_0} < 3.5 \quad \frac{\bar{\alpha}_T}{\bar{\alpha}} = \left(\frac{T_g}{T_0} \right)^{-0.55}. \quad (9.11)$

where $\bar{\alpha}_T$ — average coefficient of heat transfer, with consideration of the temperature factor.

In Fig. 9.5 results of calculation by the formulas (9.10) and (9.11) are compared with experimental data of Il'yin [6]. Calculated and experimental values of $\bar{\alpha}_T/\bar{\alpha}$ satisfactorily agree with each other.

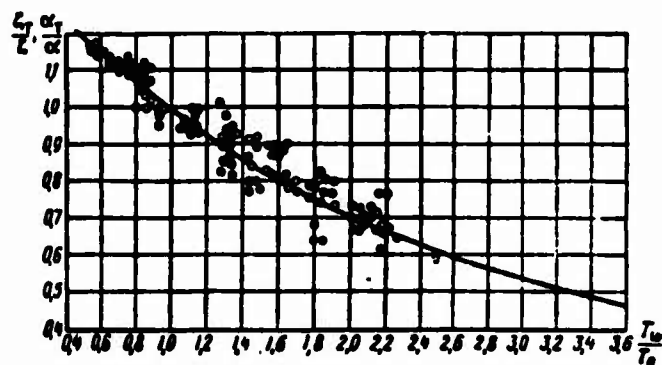


Fig. 9.5. The influence of temperature factor on heat exchange in a round cylindrical pipe [4].

Experiment shows that formulas (9.8) and (9.9) are valid for pipes of sufficient length ($l/D > 50$). When $l/D < 50$ these formulas give values of average coefficient of heat transfer along the length which are too low [5]. The true magnitude of the average coefficient of heat transfer at $l/D < 50$ is determined by the relationships (9.8) or (9.9), taking into account correction ϵ_l ,

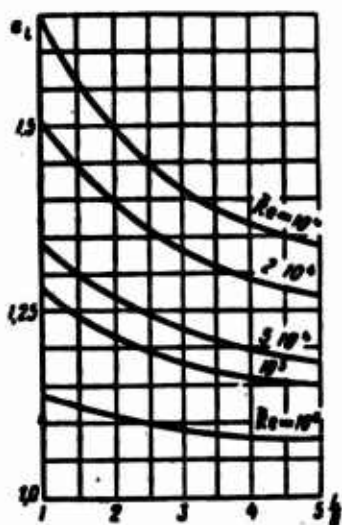


Fig. 8.6. Correction ϵ_1 to the coefficient of heat transfer of short pipes [5].

which depends on Reynolds number Re (\tilde{Re}) and the ratio l/D [4], [5]. The dependence

$$\epsilon_1 = f\left(\tilde{Re}; \frac{l}{D}\right), \quad (9.12)$$

which is determined by experimental means, is represented graphically in Fig. 9.6.

If we take into account the temperature factor and correction ϵ_1 , formula (9.8) for calculation of average coefficient of heat transfer takes the following form:

for

$$0.5 < \bar{T}_0 < 1.0 \quad \bar{Nu} = 0.023 \cdot \bar{Pr}^{0.4} \times \bar{Re}^{0.8} (1.27 - 0.27 \bar{T}_0) \epsilon_1, \quad (9.13)$$

for

$$1.0 < \bar{T}_0 < 3.5 \quad \bar{Nu} = 0.023 \cdot \bar{Pr}^{0.4} \cdot \bar{Re}^{0.8} (\bar{T}_0)^{-0.35} \epsilon_1. \quad (9.14)$$

Using the relation between the local and mean values of the Nusselt number, on the basis of (9.2), (9.13) and (9.14) we will obtain the local coefficients of heat transfer in a round pipe for the turbulent flow regime

for

$$0.5 < T_0 < 1.0 \quad Nu = \frac{\epsilon D}{\lambda} = 0.021 \cdot Pr^{0.4} \cdot Re^{0.8} (1.27 - 0.27 T_0) \epsilon_1 \left(\frac{l}{x}\right)^{0.1}, \quad (9.15)$$

for

$$1.0 < T_0 < 3.5 \quad Nu = \frac{\epsilon D}{\lambda} = 0.021 \cdot Pr^{0.4} \cdot Re^{0.8} \times (\bar{T}_0)^{-0.35} \epsilon_1 \left(\frac{l}{x}\right)^{0.1}, \quad (9.16)$$

where physical parameters of the fluid are determined according to the local thermodynamic temperature of the flow $T_0 = T_0(x)$, and Nusselt number Nu and Reynolds number Re are calculated according to the diameter of the pipe.

In order to take into account the influence of compressibility on the coefficient of heat transfer approximately for a flat plate, we use a formula obtained on the basis of the analogy of Reynolds and Prandtl at $Pr = 1.0$:

$$Nu = \frac{\epsilon x}{\lambda} = \frac{1}{2} c_f \cdot Re, \quad (9.17)$$

where the local coefficient of friction is equal to

$$c_f = 0.0575/Re^{0.2}.$$

The average coefficient of friction on a plate of length L is equal to

$$c_{fL} = 0.072/Re_L^{0.5}.$$

Replacing in this formula c_f on c_{fcm} (9.5) and using values of c_f and c_{fL} , we will obtain formulas for the local and average Nu on a flat plate for the turbulent flow regime [16]:

$$Nu = 0.029 \cdot Re^{0.8} \frac{1}{\sqrt{1 + \frac{k-1}{2} r M^2}}; \quad (9.18)$$

$$\bar{Nu} = 0.036 \cdot Re_L^{0.8} \frac{1}{\sqrt{1 + \frac{k-1}{2} r M^2}}, \quad (9.19)$$

where r denotes the recovery factor.

At high subsonic speeds of flow ($M = 1.0$), compressibility practically does not render an influence on heat exchange in the pipe. In this case, for calculation of coefficients of heat transfer it is possible to use the usual relationships (9.13) to (9.16) under the condition that the temperature factor is determined by the formula

$$\bar{T}_w = \frac{T_w}{T_e},$$

where T_e denotes the equilibrium temperature [see expression (9.4)].

On the basis of generalization of a sufficiently large number of experimental data on heat exchange in pipes with irregular or complicated cross section, it has

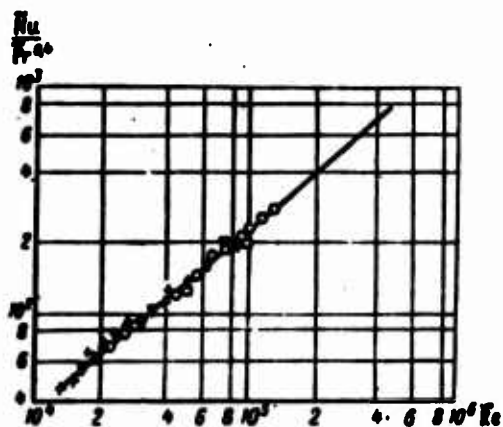


Fig. 9.7. Heat transfer during turbulent flow of fluid in smooth pipes with cross sections of different form [5]. \square - square, ∇ - triangle, Δ - trapezoid, $+$ - rectangle, \circ - circle.

been established that in criterial formulas of the form of (9.8), in place of diameter of the pipe D it is expedient to introduce the equivalent diameter $D_{\text{ЭКВ}}$. Thus formulas (9.8), (9.9), (9.15) and (9.16) will be retained for the case of heat exchange in pipes with irregular or complicated cross section. The dependence of the coefficient of heat transfer on Reynolds number Re in the turbulent flow regime in smooth pipes with cross sections of different shapes is represented in Fig. 9.7. From this graph it is clear that processing of experimental data in dimensionless criteria

$$\frac{\tilde{Nu}}{Pr^{0.4}} \text{ and } \tilde{Re} = \frac{\rho \cdot U D_{np}}{\mu}$$

where

$$\tilde{Nu} = \frac{\alpha \cdot D_{np}}{\lambda}$$

gives a universal law of heat transfer [see expression (9.8) or (9.9)] for pipes with cross sections of different shape.

During determination of local and average coefficients of heat transfer in a supersonic nozzle, there are encountered considerable difficulties, which are explained, on the one hand, by the absence of a rigorous theory of heat exchange in turbulent flows, and, on the other, by the very limited number of experimental data on heat transfer in a supersonic nozzle. Available methods of calculation for determination of coefficients of heat transfer in a nozzle, which are based on boundary layer theory [7], [9], essentially depend on the initial assumptions. In work [8], experimental data on coefficients of heat transfer in a supersonic nozzle are used to obtain a criterial dependence. In the work of Bartz [9] there is given a method of calculation of the coefficient of heat transfer along the nozzle which is based on turbulent boundary layer theory. The formula of Bratz has the form for calculation of local coefficients of heat transfer in supersonic nozzles

$$\alpha = 493.5 \frac{c_p}{Pr^{0.6}} \left(\frac{\mu}{D_{np}} \right)^{0.2} \left(\frac{G}{F_{np}} \right)^{0.2} \left(\frac{D_{np}}{r_c} \right)^{0.1} \left(\frac{F_{np}}{F} \right)^{0.9} \sigma, \quad (9.20)$$

where α — local coefficient of heat transfer in kcal/m²·hr·degree;

c_p — heat capacity of gas flow in kcal/kg·degree;

Pr — Prandtl number;

μ — viscosity of gas flow in kg·sec/m²;

g — acceleration due to gravity in m/sec²;

D_{np} — throat diameter of nozzle in m;

G — flow rate of gas through the nozzle in kg/sec;

F — area of cross section of nozzle at a given x in m²;

F_{np} — throat area of nozzle in m²;

r_c — radius of curvature in the nozzle throat in m;

σ — dimensionless parameter, which takes into account the influence of Mach number and temperature factor on the coefficient of heat transfer:

$$\sigma = \frac{1}{\left[0.5 \cdot T_\infty \left(1 + \frac{k-1}{2} M^2 \right) + 0.5 \right]^{0.65} \cdot \left(1 + \frac{k-1}{2} M^2 \right)^{0.15}}$$

Physical parameters of the gas flow which are contained in formula (9.20) are calculated according to the stagnation temperature T_{00} . Change of Mach number is simply related to the geometry of the nozzle F_{KP}/F [10].

The distribution of local coefficients of heat transfer along a supersonic nozzle calculated by formula (9.20) is represented in Fig. 9.8. The local coefficient of

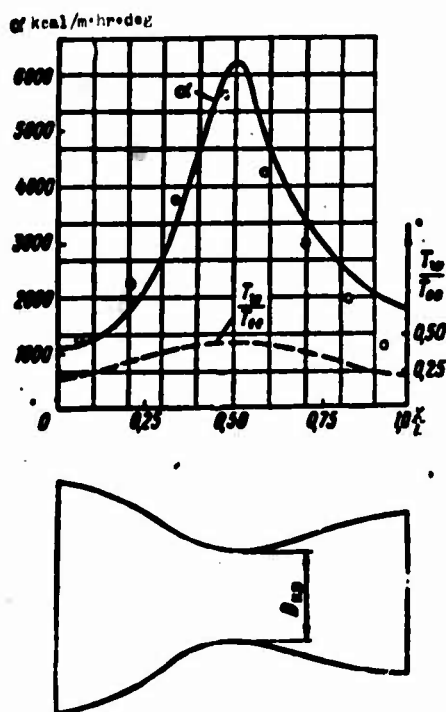


Fig. 9.8. Distribution of local coefficients of heat transfer along a supersonic nozzle [9].

$$\frac{q}{F_{KP}} = 0.135 \cdot 10^6 \text{ kg/m}^2 \cdot \text{sec} \quad D_{KP} = 45 \text{ mm};$$

$$T_0 = 2500^\circ \text{K}; \quad \frac{p_1}{D_{KP}} = 1380 \cdot 10^{-6} \text{ kg/m}^2 \cdot \text{sec}$$

$$K = 1.2; \quad \frac{n_{vp}}{r_c} = 1.0;$$

$$c_p = 0.567 \text{ kcal/kg-deg}; \quad \text{--- calculation according to formula (9.20);}$$

$$Pr = 0.83; \quad \text{O---experiment.}$$

heat transfer attains the largest value in the nozzle throat (at $F = F_{KP}$). This is explained by the fact that when $F = F_{KP}$ the density of the flow (ρu) has a maximum. In Fig. 9.8 experimental values of local coefficients of heat transfer in a supersonic nozzle are compared with the theoretical dependence (9.20) [9]. Considering the complexity of heat exchange in a supersonic nozzle and the difficulty of experimental determination of local coefficients of heat transfer, we should recognize that theoretical and experimental data agree satisfactorily with each other.

§ 3. EXTERNAL COOLING

Let us assume that walls of the combustion chamber of a ramjet engine are washed on the inside by combustion products, but on the outside -- by an air flow with specified parameters. The problem consists of determination of the wall temperature of the combustion chamber of a ramjet engine

$T_w = T_w(x)$ for given conditions of flight and fixed operating conditions of the engine. The method of calculation of external cooling of a combustion chamber of a ramjet engine was developed under a whole series of assumptions, for a considerable number of which there is given corresponding substantiation:

1. It is assumed that the cooling system practically does not affect the temperature of combustion products. Corresponding calculations show that decrease of temperature in the combustion chamber caused by the cooling is insignificantly small. For specified conditions of operation of the ramjet engine, equilibrium temperature

in the hot part of the combustion chamber is a composite function of the coordinates of a point:

$$T_{el} = T_{el}(x, y).$$

In Fig. 9.9 there is schematically represented the change of equilibrium temperature of combustion products near the wall (dotted curve) and change of average-

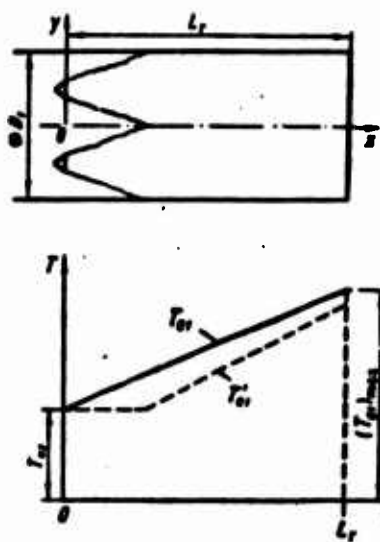


Fig. 9.9. Change of temperature of combustion products along the chamber.

mass equilibrium temperature along the combustion chamber (solid curve). Since the field of temperatures in the combustion chamber has considerable irregularity, then convection heat flow from the combustion products to the wall is determined by the temperature drop between the layer of gas next to the wall and the wall (see Fig. 9.9):

$$q_c \sim T_{el}'' - T_w.$$

Since the radiant heat flux depends on the average-mass thermodynamic temperature of the combustion products, then

$$q_r \sim T_1^4 - T_w^4.$$

The use of different temperatures of combustion products (T_{el}' and T_1) complicates calculation of heat exchange; furthermore, at present there are no sufficiently complete and reliable data on the temperature fields in combustion chambers of different types. Therefore, in calculation of cooling there is used a single curve of burn-up of fuel ($T_{el}' \approx T_1$). Thus, convection heat flows are obtained to be somewhat too high. We will assume that the burn-up curve is approximately determined by a linear function

$$T_{el} = T_{e2} + [(T_{el})_{\max} - T_{e2}] \frac{x}{L_r}, \quad (9.21)$$

where T_{e2} - equilibrium temperature of the incident flow;

$(T_{el})_{\max}$ - maximum combustion temperature of fuel for a given air-fuel ratio α and given combustion completeness φ ;

x - instantaneous coordinate, measured from the beginning of the hot part of the chamber;

L_r - length of the hot part of the combustion chamber.

2. It is assumed that the flow regime in cold and hot flows is everywhere turbulent. The accuracy of this assumption is supported by the comparatively large Reynolds numbers for the considered flows, and also by the relatively high level of

turbulence and the presence of bluff bodies in the combustion chamber.

3. The combustion chamber is made of heat-resistant material, for which the maximum permissible wall temperature for specified mechanical strength is T_{wm} .

4. It is assumed that flow of heat along the wall is practically absent. Elementary calculations show that heat flow along the wall is proportional to the parameter $\sqrt{\lambda_w \delta_w}$, where λ_w is the coefficient of thermal conductivity of the wall and δ_w is the wall thickness [11]. Consequently, the smaller the thickness of the wall of the combustion chamber, made of the given material, the less the longitudinal flow of heat is.

5. It is assumed that the thermal resistance of the wall of the combustion chamber, made of the given material is small, $\frac{\delta_w}{\lambda_w} \rightarrow 0$.

6. Local coefficients of convection heat transfer are considered to be known functions of the longitudinal coordinate x , and the influence of the temperature factor in the first approximation is not considered. During construction of the second approximation, coefficients of convection heat transfer are determined by more exact formulas - taking into account the temperature factor.

7. Viscosity of air as a function of temperature is calculated by the formula of Saterland. The function $\mu = \mu(T)$ is represented graphically in Fig. 9.10. The

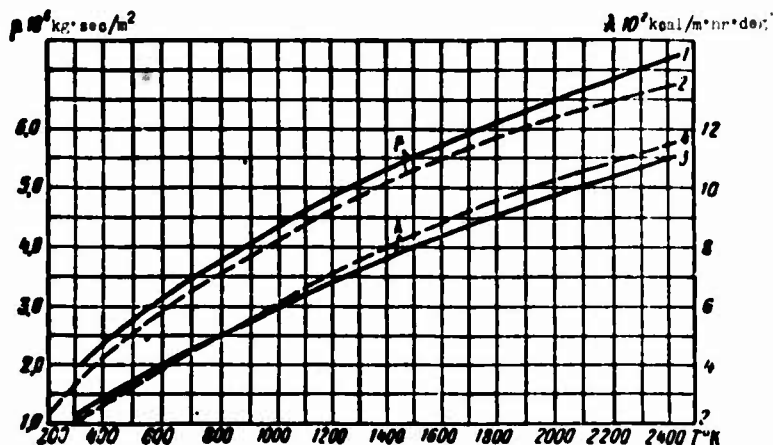


Fig. 9.10. Coefficients of viscosity and thermal conductivity as functions of temperature. 1 and 3 - air; 2 and 4 - combustion products.

change of heat capacity of combustion products as a function of temperature is shown in Fig. 1.7.

During change of temperature within quite a wide range, Prandtl number for air retains practically a constant value [5].

Assuming that for air $Pr = 0.7$, we will obtain a formula for calculation of the coefficient of thermal conductivity of air

$$\lambda = \frac{\mu \cdot c_p}{0.7}.$$

The dependence of λ on temperature for air is represented graphically in Fig. 9.10 by a solid line, and the dotted line shows the dependences $\mu = \mu(T)$ and $\lambda = \lambda(T)$ for combustion products at $\alpha > 1$. From comparison of the dotted and solid curves, it

follows that coefficients of viscosity and thermal conductivity of combustion products at $\alpha > 1$ insignificantly differ from the corresponding magnitudes for air. Therefore, the dependence of physical parameters of combustion products on temperature are taken to be approximately the same as for air.

Local temperature of the wall is determined on the basis of the equations of heat balance composed for an element of the surface. According to these equations, for stationary conditions of heat exchange, the heat flux from the gas to the wall is equal to the heat flux, passing through the wall and the heat flux, passing from the wall to air coolant:

$$\begin{aligned} \alpha_1(T_{e1} - T_{w1}) + \epsilon_r' \cdot \epsilon_w' \cdot c_0 \left[\left(\frac{T_1}{100} \right)^4 - \left(\frac{T_{w1}}{100} \right)^4 \right] = \\ = \frac{\lambda_w}{\delta_w} (T_{w1} - T_{w2}) = \alpha_2(T_{w1} - T_a), \end{aligned} \quad (9.22)$$

where α_1 - local coefficient of convection heat transfer from the gas to the inner surface of the wall;

T_{e1} - equilibrium temperature of the hot flow;

T_{w1} - temperature of inner surface of the wall;

ϵ_r' - effective degree of blackness of combustion products;

ϵ_w' - effective degree of blackness of the wall;

T_1 - thermodynamic temperature of the hot flow;

T_{w2} - temperature of the outer surface of the wall;

α_2 - local coefficient of convection heat transfer from wall to air coolant.

When thermal resistance of the wall is small (assumption 5), we have

$$T_{w1} = T_{w2} = T_w.$$

In this case the system of equations (9.22) takes the form

$$\alpha_1(T_{e1} - T_w) + \epsilon_r' \cdot \epsilon_w' \cdot c_0 \left[\left(\frac{T_1}{100} \right)^4 - \left(\frac{T_w}{100} \right)^4 \right] = \alpha_2(T_w - T_a). \quad (9.23)$$

Disregarding in the first approximation the influence of the temperature factor on coefficients of heat transfer α_1 , α_2 and on the effective degree of blackness of the combustion products ϵ_r' (assumption 6), we will obtain for determination of wall temperature an algebraic equation of fourth order. If, furthermore, radiant heat flow is small as compared to convection heat flow, then solution of equation (9.23) is given by the formula

$$T_w = \frac{T_a + \frac{\alpha_1}{\alpha_2} T_{e1}}{1 + \frac{\alpha_1}{\alpha_2}} \quad (9.24)$$

or

$$\left. \frac{T_w - T_a}{T_a - T_a} = \frac{1}{1 + \frac{\alpha_1}{\alpha_2}} \right\}$$

Usually Mach number in the combustion chamber is small as compared to the Mach number of the external flow. Thus, on the basis of (9.6) and (9.18), local coefficients of heat transfer α_1 and α_2 in the turbulent flow regime are determined by the formulas

$$\alpha_1 = 0.029 \frac{Re_1^{0.8}}{x} \lambda_1; \quad (9.25)$$

$$\alpha_2 = 0.029 \frac{Re_2^{0.8}}{x} \lambda_2 \frac{1}{\sqrt{1 + \frac{k-1}{2} \cdot M_2^2}}, \quad (9.26)$$

where physical constants of the hot and cold flows are taken at corresponding local thermodynamic temperatures, since local conditions of heat exchange are determined by local parameters. On the basis of (9.25) and (9.26) we will obtain

$$\frac{\alpha_2}{\alpha_1} = \left(\frac{Re_2}{Re_1} \right)^{0.8} \frac{\lambda_2}{\lambda_1} \frac{1}{\sqrt{1 + \frac{k-1}{2} \cdot M_2^2}}. \quad (9.27)$$

Of the greatest interest is the dependence of maximum temperature of the wall on speed of flight (on Mach number M_2). Using the equation of state and the definition of Mach number, we will obtain

$$\frac{Re_2}{Re_1} = \frac{\mu_1}{\mu_2} \frac{T_1}{T_2} \frac{p_1}{p_2} \cdot M_2 \frac{\sqrt{k \cdot g \cdot R \cdot T_1}}{U_1}, \quad (9.28)$$

where the ratio of static pressure of the incident flow to static pressure in the combustion chamber ($p_1 \approx p_{01}$) is determined by the known formula

$$\frac{p_1}{p_2} \approx \frac{1}{\sigma_d} \cdot \frac{1}{\left(1 + \frac{k-1}{2} \cdot M_2^2\right)^{\frac{k}{k-1}}}. \quad (9.29)$$

Here σ_d denotes the pressure recovery factor in the diffuser. An approximate dependence of pressure recovery factor on flight Mach number for supersonic diffusers is given in Fig. 9.11. Equilibrium temperature of a cold flow in a turbulent flow regime is given by formula (9.4):

$$T_a = T_2 \left(1 + 0.9 \frac{k-1}{2} M_2^2\right). \quad (9.30)$$

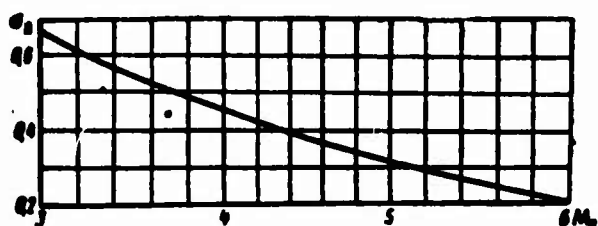


Fig. 9.11. Pressure recovery factor as a function of Mach number.

flying at a height of $H = 30,000$ m ($T_2 = 231.3^\circ\text{K}$, $p_2 = 120$ kg/m²) with flow velocity in the combustion chamber $U_1 = 100$ m/sec. Change of wall temperature along the

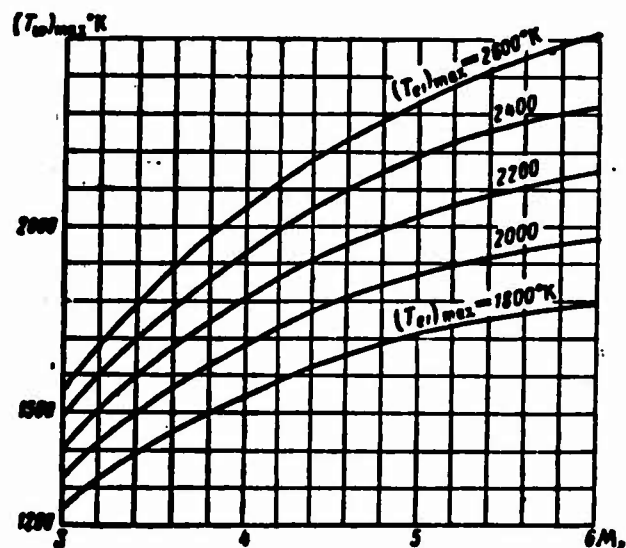


Fig. 9.12. Dependence of maximum wall temperature of a combustion chamber on speed of flight with external cooling.

increases with increase of flight Mach number. Even without taking into account

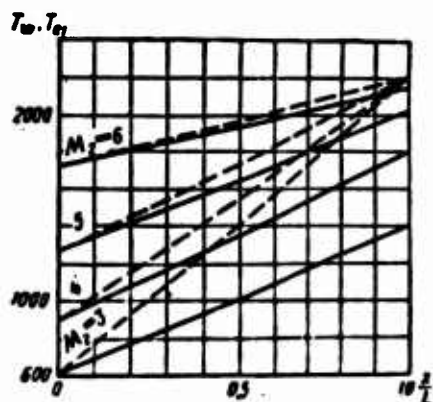


Fig. 9.13. Change of temperature of the wall along a combustion chamber during external cooling [(T_{e1})_{max} = 2200°K].
— T_w , ---- T_e .

In Fig. 9.12 there is represented the dependence of maximum wall temperature ($T_{w \text{ max}}$) of the combustion chamber on Mach number of the incident flow (M_2) for different maximum temperatures of the combustion products ($T_{e1 \text{ max}}$). Calculations are carried out for an engine

combustion chamber while maximum temperature of the combustion products are fixed, at different speeds of flight, is represented in Fig. 9.13 (by the solid lines). Here the dotted straight lines represent laws of burn-up [see formula (9.21)] at different values of M_2 . With increase of M_2 , the average temperature level of the wall increases, and the temperature gradient along the wall decreases.

From Fig. 9.12 it follows that the maximum wall temperature at the end of the chamber ($x/L_T = 1$) considerably

increases with increase of flight Mach number. Even without taking into account radiation from the flame, external cooling turns out to be not very effective.

In Fig. 9.14 there is given the dependence of maximum flight Mach number on maximum temperature of combustion products for different maximum permissible wall temperatures. From this graph one may see, for instance, that for a metal wall having a maximum permissible temperature of about 1300°K , the limiting velocity of flight at an altitude of 30 km corresponds to $M_2 \approx 3.0$ when the temperature of the combustion products is about 1950°K .

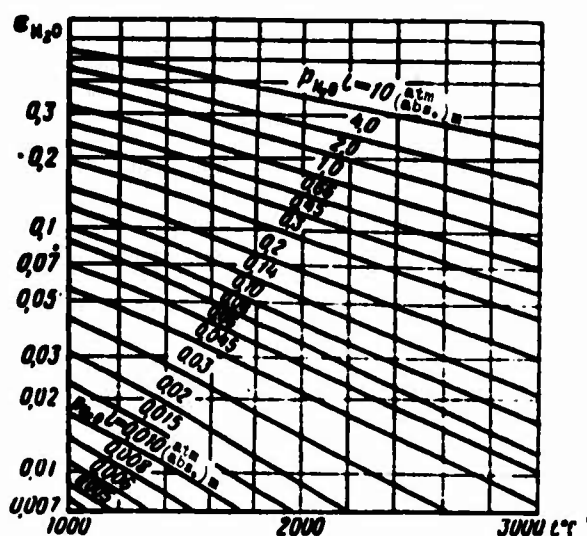


Fig. 9.17. Degree of blackness of water vapor as a function of t and p_{H_2O} [5].

Since gases absorb selectively, then for them emissivity ϵ_T (degree of blackness) is not equal to the absorptivity A_T ; thus the absorptivity of the gas is calculated by the formula

$$A_T = A_{CO_2} + A_{H_2O}.$$

where

$$A_{CO_2} = \epsilon_{CO_2} \left(\frac{T}{T_g} \right)^{0.85};$$

$$A_{H_2O} = \epsilon_{H_2O}.$$

The degree of blackness of the wall also depends on p_l and the composition of the gas. In order to take this circumstance

into account, there is usually introduced the effective degree of blackness of the shell ϵ'_w , which is related with the degree of blackness of the wall by formula [5]:

$$\epsilon'_w \approx 0.5(1 + \epsilon_w). \quad (9.31)$$

If we take into account the relationship (9.31), the final formula for calculation of the radiant heat flux from gas to wall takes the form [5]

$$q = \epsilon'_w \cdot \epsilon'_g \cdot c_0 \left[\left(\frac{T}{100} \right)^4 - \left(\frac{T_g}{100} \right)^4 \right] \text{ kcal/m}^2 \cdot \text{hr},$$

where effective degree of blackness of gas is determined by formula

$$\epsilon'_g = \frac{\epsilon_g - A_g \left(\frac{T_g}{T} \right)^4}{1 - \left(\frac{T_g}{T} \right)^4}$$

Here T denotes the thermodynamic temperature of the gas flow.

We will determine the partial pressures of CO_2 and H_2O in the combustion products. For simplicity we will assume the following weight composition of the fuel (gasoline): $C = 0.85$; $H = 0.15$. Considering that water is not contained in either the air or the gasoline, we will find the volume of the combustion products [12].

$$\left. \begin{aligned} V_{H_2O} &= 1,244 \cdot 9 \cdot H = 1,68 \text{ m}^3/\text{kg}, \\ V_{CO_2} &= 1,855 \cdot C = 1,578 \text{ m}^3/\text{kg}. \end{aligned} \right\}$$

The volume of dry gas is determined by the formula [12]

$$V_{c, \text{ gas}} = 8,879 \cdot C + 20,903 \left(H - \frac{O}{8} \right). \quad (9.32)$$

The total volume of dry gases is given by the relationship

$$V_{\text{total}} = V_{\text{H}_2\text{O}} + V_{\text{c.r.m.}} + (\alpha - 1)L_{\text{min}}, \quad (9.33)$$

where

$$L_{\text{min}} = 8,890 \cdot C + 26,456 \left(H - \frac{O}{8} \right) = 11,52 \cdot w^3 / \kappa \Gamma; \quad (9.34)$$

α — air-fuel ratio.

Then for a given air-fuel ratio α , the relative partial pressures of the combustion products will have the values

$$\left. \begin{aligned} \bar{p}_{\text{CO}_2} &= \frac{V_{\text{CO}_2}}{V_{\text{total}}} = \frac{1,578}{V_{\text{total}}} \\ \bar{p}_{\text{H}_2\text{O}} &= \frac{V_{\text{H}_2\text{O}}}{V_{\text{total}}} = \frac{1,680}{V_{\text{total}}} \end{aligned} \right\} \quad (9.35)$$

The effective degree of blackness ϵ'_T is determined as a function of thermodynamic temperature in the motor T_1 . Thus the air-fuel ratio α , static pressure in the combustion chamber p_1 and average length of a ray l are taken to be constant. The average length of a ray is related to the diameter of the combustion chamber by the approximate dependence [5]

$$l \approx 0,5 \cdot D_1. \quad (9.36)$$

From calculation of partial pressures of carbon dioxide and water vapor, it follows that the ratios

$$\left. \begin{aligned} a_{\text{CO}_2} &= \frac{\bar{p}_{\text{CO}_2}(\alpha)}{\bar{p}_{\text{CO}_2}(1)} \\ a_{\text{H}_2\text{O}} &= \frac{\bar{p}_{\text{H}_2\text{O}}(\alpha)}{\bar{p}_{\text{H}_2\text{O}}(1)} \end{aligned} \right\} \quad (9.37)$$

are practically identical for given α ; i.e., $a_{\text{CO}_2} = a_{\text{H}_2\text{O}} = a$ (Fig. 9.18). Thus, a change of the air-fuel ratio α which is exactly the same as the change of pressure,

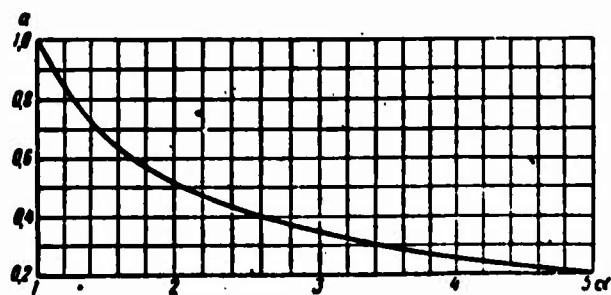


Fig. 9.18. Coefficient a as a function of α .

in the motor p_1 is accompanied by a proportional change of partial pressures. Consequently, the influence of α on degree of blackness ϵ'_T can be taken into account through pressure p_1 , if we introduce in its place the quantity $p_1 a$. In Fig. 9.19 there is represented the dependence of ϵ'_T on temperature in the

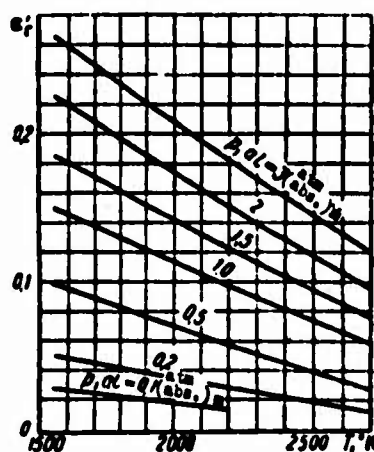


Fig. 9.19. Effective degree of blackness of combustion products at $T_w = 1300^\circ\text{K}$.

combustion chamber for different values of parameter $p_1 \alpha$, at a temperature of the wall equal to $T_w = 1300^\circ\text{K}$.

The fundamental equation (9.23) will be represented in the form

$$C - BT_w = 4.9 \cdot 10^{-8} \cdot T_w^4, \quad (9.38)$$

where there are introduced the designations

$$B = \frac{\alpha_1}{\epsilon_r \cdot \epsilon_w} \left(1 + \frac{T_1}{T_w} \right); \quad (9.39)$$

$$C = \frac{\alpha_1}{\epsilon_r \cdot \epsilon_w} \left(T_{r1} + \frac{T_1}{\alpha_1} T_{r2} \right) + 4.9 \cdot 10^{-8} \cdot T_{r1}^4. \quad (9.40)$$

Here α_1 , determined by formula (9.25), is an explicit function of longitudinal coordinate x . Strictly speaking, every element of the wall exchanges radiant energy with the whole volume of gas located in the combustion chamber. In this case, during calculation of radiant heat flow, it was necessary to use local thermodynamic temperature of combustion products and variable value of length of the path of the ray. However, if we consider that gas with higher temperature radiates more intensely, then it is possible to consider approximately that radiant heat exchange is carried out only between a shell of gas with maximum temperature $(T_1)_{\max}$ and the wall with temperature $T_w(x)$. With the assumptions which have been made, formula (9.40) takes the form

$$C = \frac{\alpha_1}{\epsilon_r \cdot \epsilon_w} \left(T_{r1} + \frac{T_1}{\alpha_1} T_{r2} \right) + 4.9 \cdot 10^{-8} (T_1)_{\max}^4. \quad (9.41)$$

where the effective degree of blackness of combustion products (ϵ'_r) is determined according to the maximum thermodynamic temperature in the combustion chamber $(T_1)_{\max}$, static pressure in the chamber p_1 and composition of the combustion products α (Fig. 9.19). With the use of Fig. 9.19, it is assumed that $(T_w)_{\max} = 1300^\circ\text{K}$. If the true wall temperature is different from 1300°K , then for determination of ϵ'_r we should use graphs analogous to those in Fig. 9.19, but for other values of T_w .*

*It has been established that ϵ'_r is a weak function of T_w ; therefore, for approximate calculations it is possible to be limited to Fig. 9.19.

Equation (9.38) is solved graphically with the help of the nomograph in (Fig. 9.20). The scale of graduated line B is found in the following way: we compare segment b with graduated line C and obtain

$$10^7 = b \cdot T_w = b \cdot 2000.$$

$$b = \frac{10^7}{2000} = 5000.$$

Consequently, to a segment equal to 10^7 on graduated line C there corresponds on graduated line B the segment 5000.

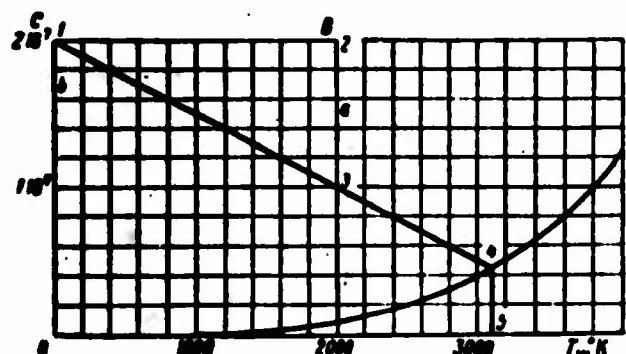


Fig. 9.20. Graphical solution of the heat transfer equation. Scale of graduated line B: 1 cm = 1000.

Assuming that on line C, to the segment 10^7 there corresponds 5 cm, we find that on line B every centimeter corresponds to 1000 units. The graph shown in Fig. 9.20 should be used in the following way: Let us assume that by formulas (9.39) and (9.41) we have found $C = 2 \cdot 10^7$ and $B = 5000$. We plot on scale C the value $2 \cdot 10^7$ — point 1.

This point is taken parallel to the axes

of T_w to scale B — point 2. From point 2 we measured downwards the segment $B = 5000$ and obtain point 3. Connecting points 1 and 3 by a straight line, we will continue the straight line up to intersection with the curve at point 4. Along the horizontal scale we find the corresponding value of T_w — point 5.

Change of wall temperature along the combustion chamber, taking into account radiation during external cooling, is represented on Fig. 9.21. Calculation is

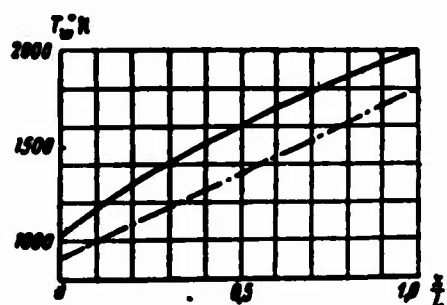


Fig. 9.21. Distribution of temperature of the wall along the combustion chamber, taking into account radiation during external cooling. — temperature of the wall at $\epsilon_r \neq 0$. ---- temperature of the wall at $\epsilon_r = 0$.

carried out for an engine flying at an altitude of 30 km with speed corresponding to $M_2 = 4.0$, with maximum temperature of combustion products $(T_{el})_{\max} = 2200^\circ\text{K}$. From Fig. 9.21 it follows that consideration of radiation from the flame leads to a considerable temperature increase of the wall of the combustion chamber (by approximately 20%) as compared to the case when $\epsilon_r' = 0$. Thus, even without that, the low effectiveness of external cooling (see Fig. 9.12) is lowered still more in the presence of radiation (see Fig. 9.21).

§ 4. CONVECTION COOLING

The problem consists of determination of the wall temperature of a ramjet engine $T_w = T_w(x)$ and the flow rate of air coolant G_2 flowing through an annular channel of

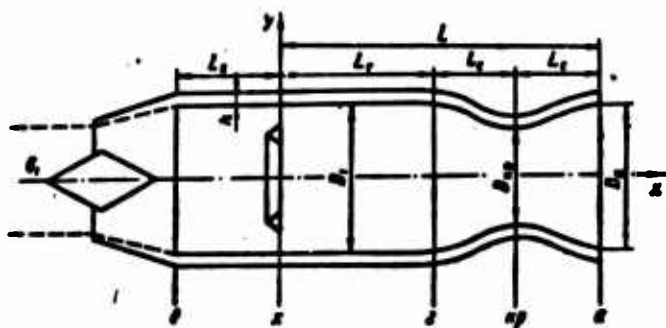


Fig. 9.22. Schematic diagram of convection cooling.

given height h . There are given the total pressure of the flow at the inlet to the cooling channel, the geometry of the internal path, gas-dynamic parameters and flow rate of the hot flow G_1 . The hot part of the motor, which is made of heat-resistant material with maximum permissible wall temperature

T_{wm} , will be subject to cooling. Air coolant is withdrawn from the diffuser and flows in an external annular channel with height h (Fig. 9.22).

Calculation of convection cooling of a ramjet engine is performed under a whole series of assumptions, a considerable number of which are given above (see § 3 of the present chapter). Furthermore, it is possible to make the following statements:

1. Air for cooling is withdrawn at the end of the diffuser. Such a diagram is the simplest structurally. Furthermore, the higher density of the flow of air during external cooling increases the efficiency of convection heat transfer.

2. At the outlet from the cooling channel there is established the stalling speed of outflow

$$\lambda_{a2} = 1.0.$$

This assumption is justified by the fact that in operating regimes of a ramjet engine there practically always exists a supersonic pressure drop. If the pressure drop is nevertheless subcritical, then should be given the static outlet pressure from the cooling channel.

3. For intensification of heat exchange, the cooling channel has longitudinal fins. There is given the fin coefficient ψ (in most cases ψ is chosen from structural considerations), which is equal to the ratio of the area of the heat-emitting surface to the area of heat-absorbing surface.

4. The wall of the housing is thermally insulated on the outside; thus, all heat flowing from the wall of the motor toward the cooling flow increases the enthalpy of this flow. Such an assumption corresponds to more difficult operating regimes of the wall of the motor and the housing.

*Subscript "a" indicates the cross section of the motor (Fig. 9.22), and subscript "2" pertains to the cooling channel.

During solution of the problem of convection cooling, there are used differential equations of heat transfer and heat balance written for an element of length dx , and also continuity equations and momentum equations for the flow in the cooling channel. As a result of solution of the system of equations, it is required to find the change of wall temperature T_w and the temperature of the air coolant T_{e2} as a function of x , and also the reduced velocity of flow at the inlet into the cooling channel λ_{g2} and the flow rate of air coolant G_2 .

The formulated problem will be broken up into two parts. At first, using equations of heat exchange and heat balance, we will solve the thermal problem. Thus the flow rate of the air coolant G_2 is considered to be a parameter, and calculation of temperature of the wall T_w and temperature of the cooling flow T_{e2} is carried out for several values of G_2 . Then, using the equations of flow rate and momentum, we will solve the hydraulic problem. As a result of this solution there is determined the true value of G_2 , at which there is realized flow in a cooling channel of given height h at a fixed value of stagnation pressure at the outlet. From the family of curves $T_w = T_w(x; G_2)$ and $T_{e2} = T_{e2}(x; G_2)$ there are chosen those which correspond to the true flow rate G_2 .

Let us turn to solution of the thermal problem. Let us assume that the quantity of heat transferred from the hot flow to an element of surface of the motor ($dF = \pi D_1 dx$) is equal to the quantity of heat transferred from the element of surface of the motor to the cooling flow. Then the differential equation of heat transfer for element dx will take the form

$$dF \left\{ \alpha_1 (T_{e1} - T_w) + \frac{\alpha_1 \cdot \alpha_2 \cdot c_p}{\psi \cdot \alpha_2} \left[\left(\frac{T_{e1 \max}}{100} \right)^4 - \left(\frac{T_w}{100} \right)^4 \right] \right\} = dF \psi \alpha_2 (T_w - T_{e2}). \quad (9.42)$$

Hence we will obtain a formula for the equilibrium temperature of the cooling flow

$$T_{e2} = T_w - \frac{\alpha_1}{\psi \alpha_2} (T_{e1} - T_w) - \frac{\alpha_1 \cdot \alpha_2 \cdot c_p}{\psi \cdot \alpha_2} \left[\left(\frac{T_{e1 \max}}{100} \right)^4 - \left(\frac{T_w}{100} \right)^4 \right]. \quad (9.43)$$

The quantity of heat transferred from an element of surface of the motor to the cooling flow increases the enthalpy of this flow:

$$\pi D_1 dx \psi \alpha_2 (T_w - T_{e2}) = 3600 \cdot c_{p2} \cdot G_2 \cdot dT_{e2} \quad (9.44)$$

where c_{p2} is the heat capacity of the air coolant.

Thus, for determination of T_w and T_{e2} as a function of x , there are obtained two equations, (9.43) and (9.44), in which G_2 is a parameter. In general, the diameter of the motor (D_1), coefficient of heat transfer from combustion products to the wall (α_1) and the equilibrium temperature of the combustion products are known functions of the longitudinal coordinate x . If the heating of air in the cooling channel is comparatively small, then the coefficient of heat transfer from wall to cooling flow (α_2) can also be considered to be a known function of x in the first approximation.

If radiant heat flow is small as compared to convection heat flow, then on the basis of (9.43) and (9.44) we will obtain a linear differential equation for determination of T_{e2} :

$$\frac{dT_{e2}}{dx} + k(\bar{x}) T_{e2} = k(\bar{x}) T_{e1}, \quad (9.45)$$

where there are introduced the symbols

$$k(\bar{x}) = \frac{\pi \cdot D_1 \cdot \psi \cdot \alpha_1 \cdot L_r}{3600 \cdot c_{p1} \cdot G_2} \cdot \frac{1}{1 + \psi \frac{\alpha_2}{\alpha_1}}, \quad (9.46)$$

$$\bar{x} = \frac{x}{L_r}.$$

Considering that when $x = 0$, $T_{e2} = T_{e2\bar{0}}$, we will represent the solution of equation (9.45) in the form

$$T_{e2} = e^{-\int_0^{\bar{x}} k(\bar{x}) d\bar{x}} \left[\int_0^{\bar{x}} k(\bar{x}) T_{e1}(\bar{x}) e^{\int_0^{\bar{x}} k(\bar{x}) d\bar{x}} d\bar{x} + T_{e2\bar{0}} \right]. \quad (9.47)$$

thus the wall temperature is determined by the formula

$$T_w = \frac{T_{e1} + \psi \frac{\alpha_1}{\alpha_2} T_{e2}}{1 + \psi \frac{\alpha_1}{\alpha_2}}. \quad (9.48)$$

If the gas flows through a cylindrical pipe (combustion chamber), then $D_1 = \text{const}$, and coefficients of heat transfer α_1 and α_2 are determined by formulas (9.15) and (9.16). Disregarding the influence of temperature factor in the first approximation and taking Prandtl number Pr for the combustion products to be equal to 0.625, and for air - 0.70, we will represent local coefficients of heat transfer (9.15) and (9.16) in the form

$$\epsilon_1 = 0,0174 \frac{\lambda_1}{D_1} \text{Re}_1^{0.8} \epsilon_L(\bar{x})^{-0.1}; \quad (9.49)$$

$$\epsilon_2 = 0,0182 \frac{\lambda_2}{D_{2\text{экв}}} \text{Re}_2^{0.8} \epsilon_L(\bar{x})^{-0.1}, \quad (9.50)$$

where equivalent diameter $D_{2\text{экв}}$ will be determined by the formula

$$D_{2\text{экв}} = 4h \frac{1 + \frac{h}{D_1}}{1 + \psi + 2 \frac{h}{D_1}}. \quad (9.51)$$

Reynolds numbers Re_1 and Re_2 , if we take into account the equations of flow rate, will be represented in the form

$$\text{Re}_1 = \frac{\rho_1 \cdot u_1 \cdot D_1}{\mu_1} = 0,13 \frac{G_1}{D_1 \cdot \mu_1}; \quad (9.52)$$

$$\text{Re}_2 = \frac{\rho_2 u_2 D_{2\text{экв}}}{\mu_2} = 0,13 \frac{G_2}{D_1 \cdot \mu_2} \frac{1}{1 + \psi + 2 \frac{h}{D_1}}. \quad (9.53)$$

Using relationships (9.49), (9.50), (9.51), (9.52) and (9.53), we will obtain final formulas for calculation of local coefficients of heat transfer in the cylindrical pipe and in the annular space

$$\epsilon_1 = 0,00340 \left(\frac{\lambda_1}{\mu_1^{0.8}} \right) \left(\frac{G_1}{D_1} \right)^{0.8} \frac{1}{D_1} \cdot \epsilon_L(\bar{x})^{-0.1}; \quad (9.54)$$

$$\epsilon_2 = 0,00356 \left(\frac{\lambda_2}{\mu_2^{0.8}} \right) \left(\frac{G_2}{D_1} \right)^{0.8} \frac{\left(1 + \psi + 2 \frac{h}{D_1} \right)^{0.2}}{4h \left(1 + \frac{h}{D_1} \right)} \cdot \epsilon_L(\bar{x})^{-0.1}. \quad (9.55)$$

In these formulas, only the complex $\lambda/\mu^{0.8}$ depends on local thermodynamic temperature (Fig. 9.23).

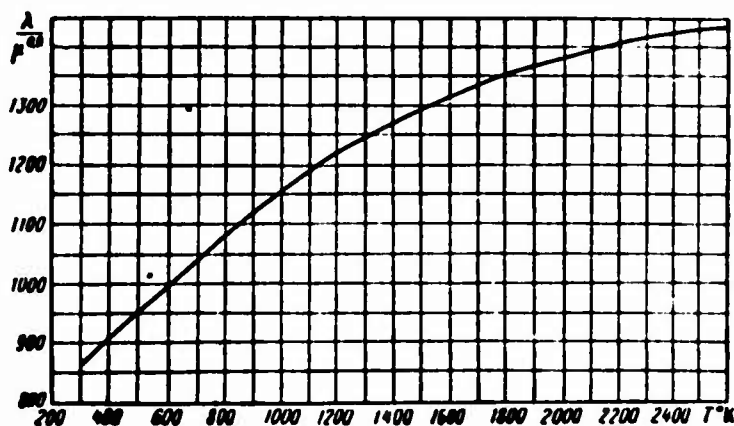


Fig. 9.23. The parameter $\lambda/\mu^{0.8}$ as a function of temperature.

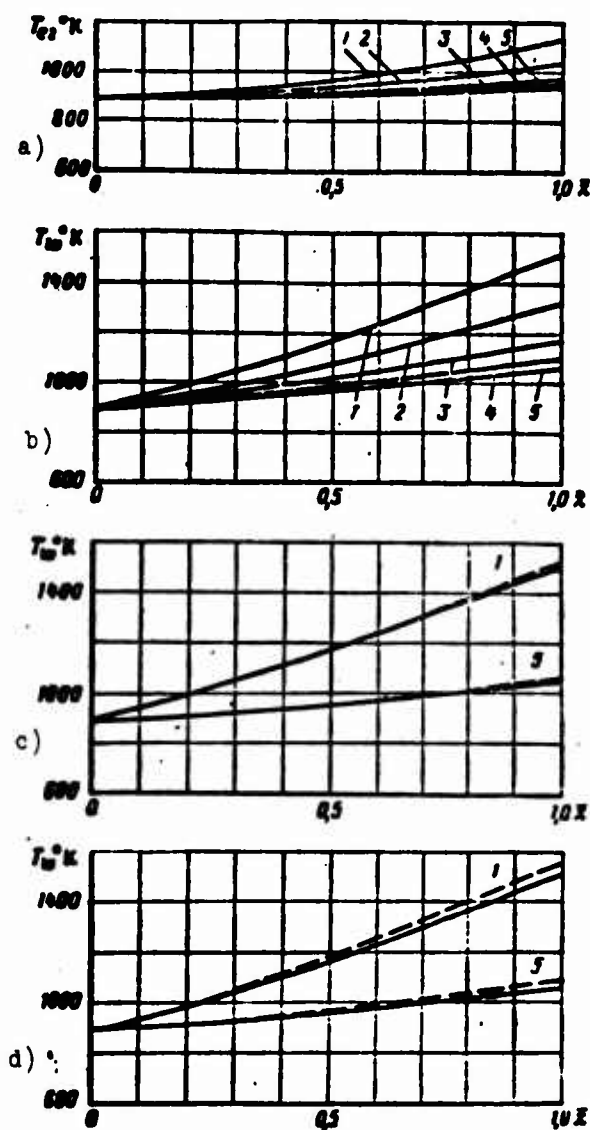


Fig. 9.24. Change of temperature of air (a) and wall (b, c, d) along the cooling channel of a motor during convection cooling. c) — first approximation; ---- second approximation. d) — with respect to average α ; ---- with respect to the local α .

$$(T_{a1})_{\text{max}} = 2200^{\circ}\text{K}; H = 30 \text{ km}; M_2 = 4.0; h = 20 \text{ mm}; D_1 = 1.0 \text{ m}; L_1 = 1.5 \text{ m.}$$

$$1 - \frac{q_1}{q_2} = 0.022; 2 - \frac{q_1}{q_2} = 0.050; 3 - \frac{q_1}{q_2} = 0.1; 4 - \frac{q_1}{q_2} = 0.15; 5 - \frac{q_1}{q_2} = 0.20.$$

Using formulas (9.46), (9.47), (9.48), (9.54) and (9.55), we will calculate change of temperature of the air coolant and temperature of the wall along the combustion chamber. In Fig. 9.24a, there is shown the change of air temperature along a cooling channel with height $h = 20 \text{ mm}$ for different relative flow rates of air coolant G_2/G_1 . Wall temperature of the combustion chamber as a function of longitudinal coordinate \bar{x} is shown in Fig. 9.24b. An example of calculation is given for a hypothetical engine with diameter of the internal circuit of the

combustion chamber $D_1 = 1.0$ m, flying at an altitude of $H = 30,000$ m ($T_2 = 231.3^\circ\text{K}$, $p_2 = 120$ kg/m²) with a speed corresponding to $M_2 = 4.0$ ($T_{e2} = 897^\circ\text{K}$), with maximum temperature in the combustion chamber $(T_{e1})_{\max} = 2200^\circ\text{K}$. Thus the burn-up curve according to formula (9.21) has the form

$$T_{e1} = 897 + (2200 - 897) \bar{x} \quad (9.56)$$

From Fig. 9.24a and b, it follows that along the combustion chamber temperature of the air coolant and wall temperature increase practically linearly. Increase of relative flow rate of air coolant (G_2/G_1) (at a fixed value of \bar{x}) is accompanied by decrease of wall temperature and temperature of the air coolant. Consequently, with increase of G_2/G_1 , the efficiency of convection cooling increases. On the basis of Fig. 9.24b, we conclude that increase of relative flow rate of air coolant over a certain limiting value becomes disadvantageous, since even with considerable increase of G_2/G_1 , the wall temperature is lowered insignificantly.

Dependences represented in Fig. 9.24a and b, are approximate, since there is not considered in them the influence of the temperature factor on local coefficients of heat transfer and the influence of variable thermodynamic temperature of the air coolant. If we take into account the temperature factor, formulas (9.54) and (9.55) for calculation of local heat transfer coefficients take the form (see § 2, Chapter IX)

$$\begin{aligned} \alpha_1 = & 0.00340 \left(\frac{\lambda_1}{\mu_1^{0.8}} \right) \left(\frac{G_1}{D_1} \right)^{0.8} \cdot \frac{1}{D_1} \cdot e_L(\bar{x})^{-1.0} \times \\ & \times \left(1.27 - 0.27 \frac{T_w}{T_{e1}} \right); \end{aligned} \quad (9.57)$$

$$\begin{aligned} \alpha_2 = & 0.00356 \left(\frac{\lambda_1}{\mu_1^{0.8}} \right) \cdot \left(\frac{G_1}{D_1} \right)^{0.8} \frac{\left(1 + \phi + 2 \frac{h}{D_1} \right)^{0.2}}{4h \left(1 + \frac{h}{D_1} \right)} e_L(\bar{x})^{-0.1} \times \\ & \times \left(\frac{T_w}{T_{e1}} \right)^{-0.55}. \end{aligned} \quad (9.58)$$

Calculation of temperature of the air coolant and temperature of the wall of the combustion chamber is carried out in the second approximation according to formulas (9.46), (9.47), (9.48), (9.57) and (9.58). Thus, local values of temperature factors T_w/T_{e1} and T_w/T_{e2} are determined by the first approximation (Fig. 9.24c). Strictly speaking, parameter $\lambda_2/\mu_2^{0.3}$, which is contained in formula (9.58), should be determined by local values of thermodynamic temperature. However, in the cooling

channel flow is subsonic ($\lambda_2 \leq 1.0$), and the difference between thermodynamic temperature and stagnation temperature is not so great. Therefore, for determination of this parameter, it is possible to use stagnation temperature T_{e2} found in the first approximation.

In Fig. 9.24c there are compared the first (solid curves) and second (dotted curves) approximations for wall temperature of the combustion chamber during convection cooling. From this graph it follows that consideration of temperature factors T_w/T_{e1} and T_w/T_{e2} leads to a certain temperature increase of the wall. However, this increase in the majority of practical cases is very insignificant. Still less is the influence of temperature factors on temperature of the air coolant. Therefore, in calculations it is possible to disregard the influence of temperature factor, and to be limited to only the first approximation.

Local coefficients of heat transfer in the pipe α (9.54) and in the annular channel α_2 (9.55) are weak functions of the longitudinal coordinate. This is explained by the fact that the complex $\lambda/\mu^{0.8}$ increases with increase of \bar{x} , and the parameter $(\bar{x})^{-0.1}$ decreases. Considering this circumstance, we will replace the local coefficients of heat transfer in formulas (9.42) and (9.44) by averaged coefficients (9.13) and (9.14):

$$\bar{\alpha}_1 = 0.00372 \left(\frac{\bar{\lambda}_1}{\bar{\mu}_1^{0.8}} \right) \left(\frac{q_1}{D_1} \right)^{0.8} \frac{1}{D_1} \cdot \epsilon_L; \quad (9.59)$$

$$\bar{\alpha}_2 = 0.00390 \left(\frac{\bar{\lambda}_2}{\bar{\mu}_2^{0.8}} \right) \left(\frac{q_2}{D_2} \right)^{0.8} \frac{(1 + \phi + 2 \frac{h}{D_2})^{0.2}}{4h(1 + \frac{h}{D_2})} \cdot \epsilon_L. \quad (9.60)$$

Let us calculate temperatures T_w and T_{e2} according to the average coefficients of heat transfer (9.59) and (9.60). For mean values $\bar{\alpha}_1$ and $\bar{\alpha}_2$, dimensionless parameter k (9.46) takes the constant value

$$\bar{k} = \frac{\pi \cdot D_1 \cdot \phi \cdot \bar{\alpha}_1 L}{2000 \cdot \bar{c}_p \cdot G_1} \frac{1}{1 + \phi \frac{\bar{\alpha}_2}{\bar{\alpha}_1}}. \quad (9.61)$$

In the case when $\bar{k} = \text{const}$, and with linear change of the burn-up curve (9.21),

$$T_{e1} = T_{e2} + [(T_{e1})_{\max} - T_{e2}] \bar{x} \quad (9.62)$$

formula (9.47) takes the form

$$T_{\text{a}} = T_{\text{a}} + \frac{(T_{\text{a}})_{\text{max}} - T_{\text{a}}}{\bar{h}} \left[(\bar{h}x - 1) + e^{-\bar{h}x} \right] \quad (9.63)$$

or

$$\frac{(T_{\text{a}})_{\text{max}} - T_{\text{a}}}{(T_{\text{a}})_{\text{max}} - T_{\text{a}}} = \frac{\bar{h}(1+x) - 1 + e^{-\bar{h}x}}{\bar{h}} \quad (9.64)$$

Calculation of the temperature of the air coolant and temperature of the wall of the combustion chamber for averaged heat transfer coefficients is performed according to formulas (9.48), (9.59), (9.60), (9.61) and (9.63). In this case, calculation turns out to be the simplest. Comparison of wall temperatures of the combustion chamber calculated according to local (dotted curves) and averaged (solid curves) coefficients of heat transfer is presented in Fig. 9.24d. From this graph it follows that results of calculation of convection cooling of combustion chambers according to local and averaged coefficients of heat transfer are practically identical. Therefore, for approximate calculation of convection cooling of combustion chambers, it is possible to use the simpler formulas obtained for the case of the averaged coefficients of heat transfer.

Let us turn to a checking calculation of convection cooling in the presence of radiation from the flame in a ramjet engine. Replacing local coefficients of heat transfer by the averaged coefficients, on the basis of expressions (9.42) and (9.44) we will obtain

$$L_r \bar{D} dx \left\{ \bar{\alpha}_1 (T_{\text{a}1} - T_{\text{w}}) + \epsilon_r \epsilon_w c_0 \left[\left(\frac{T_{\text{a}1}}{100} \right)^4 - \left(\frac{T_{\text{w}}}{100} \right)^4 \right] \right\} = 3600 \bar{c}_p G_d dT_{\text{a}} \quad (9.65)$$

Differentiating (9.43) for constant values of coefficients $\bar{\alpha}_1$ and $\bar{\alpha}_2$, we will find

$$\begin{aligned} dT_{\text{a}} = dT_{\text{w}} - \frac{\bar{\alpha}_1}{\bar{\alpha}_2} (dT_{\text{a}1} - dT_{\text{w}}) + \\ + \frac{\epsilon_r \epsilon_w c_0}{\bar{\alpha}_2} \frac{4}{100} \left(\frac{T_{\text{w}}}{100} \right)^3 dT_{\text{w}} \end{aligned} \quad (9.66)$$

Eliminating $dT_{\text{e}2}$ from equations (9.65) and (9.66), we will obtain a differential equation for determination of wall temperature $T_{\text{w}} = T_{\text{w}}(\bar{x})$ in the presence of radiation

$$\begin{aligned}
& \left[1 + \frac{\bar{a}_1}{\bar{\psi} \bar{a}_2} + \frac{\bar{c}_r \cdot \bar{c}_w \cdot \bar{c}_0}{\bar{\psi} \bar{a}_2} \frac{4}{100} \left(\frac{T_w}{100} \right)^3 \right] \frac{dT_w}{d\bar{x}} + \bar{k} \left(1 + \bar{\psi} \frac{\bar{a}_1}{\bar{a}_1} \right) \times \\
& \times \frac{\bar{a}_1}{\bar{\psi} \bar{a}_2} T_w + \bar{k} \left(1 + \bar{\psi} \frac{\bar{a}_1}{\bar{a}_1} \right) \frac{\bar{c}_r \cdot \bar{c}_w \cdot \bar{c}_0}{\bar{\psi} \bar{a}_2} \left(\frac{T_w}{100} \right)^4 = \\
& = \frac{\bar{a}_1}{\bar{\psi} \bar{a}_2} \frac{dT_{cl}}{d\bar{x}} + \bar{k} \left(1 + \bar{\psi} \frac{\bar{a}_1}{\bar{a}_1} \right) \frac{\bar{a}_1}{\bar{\psi} \bar{a}_2} T_{cl} + \\
& + \bar{k} \left(1 + \bar{\psi} \frac{\bar{a}_1}{\bar{a}_1} \right) \frac{\bar{c}_r \cdot \bar{c}_w \cdot \bar{c}_0}{\bar{\psi} \bar{a}_2} \left(\frac{T_{cl, \max}}{100} \right)^4.
\end{aligned} \tag{9.67}$$

Thus, for determination of wall temperature of the combustion chamber during convection cooling, taking into account radiation, we obtain a nonlinear first order differential equation. Initial wall temperature at $\bar{x} = 0$, $(T_w)_{\text{HAY}}$, is determined from the nomograph in (Fig. 9.20) with the help of coefficients B (9.39) and C (9.41):

$$B = \frac{\bar{a}_1}{\bar{c}_r \cdot \bar{c}_w} \left(1 + \bar{\psi} \frac{\bar{a}_1}{\bar{a}_1} \right); \tag{9.68}$$

$$C = \frac{\bar{a}_1}{\bar{c}_r \cdot \bar{c}_w} \left(T_{cl} + \bar{\psi} \frac{\bar{a}_1}{\bar{a}_1} T_{cl} \right) + 4.9 \cdot 10^{-4} (T_{cl})_{\max}^4. \tag{9.69}$$

Solution of equation (9.67) in general encounters large difficulties. Therefore, it is usually solved approximately. Partitioning the length L_r into a series of equal intervals $\Delta \bar{x}$, we will assume that in every such interval the wall temperature changes linearly. Then T_w at the end of the n -th interval will be determined, obviously, by the formula

$$T_w^n = T_w^{(n-1)} + \left(\frac{dT_w}{d\bar{x}} \right)^{(n-1)} \cdot \Delta \bar{x}, \tag{9.70}$$

where on the basis of (9.67) we have

$$\left(\frac{dT_w}{d\bar{x}} \right)^{(n-1)} = \frac{\frac{\bar{a}_1}{\bar{\psi} \bar{a}_2} \frac{dT_{cl}}{d\bar{x}} + \frac{\bar{k}}{\bar{\psi} \bar{a}_2} \left(1 + \bar{\psi} \frac{\bar{a}_1}{\bar{a}_1} \right) A}{1 + \frac{\bar{a}_1}{\bar{\psi} \bar{a}_2} + \frac{\bar{c}_r \cdot \bar{c}_w \cdot \bar{c}_0}{\bar{\psi} \bar{a}_2} \frac{4}{100} \left(\frac{T_w^{(n-1)}}{100} \right)^3}. \tag{9.71}$$

where

$$A = \left\{ \bar{a}_1 (T_{cl} - T_w^{(n-1)}) + \bar{c}_r \cdot \bar{c}_w \cdot \bar{c}_0 \left[\left(\frac{T_{cl, \max}}{100} \right)^4 - \left(\frac{T_w^{(n-1)}}{100} \right)^4 \right] \right\}.$$

The corresponding value of temperature of the cooling flow is determined by the formula (9.43).

In Fig. 9.25a and b there are given values of the equilibrium temperature of the air coolant and the temperature of the wall of the combustion chamber calculated

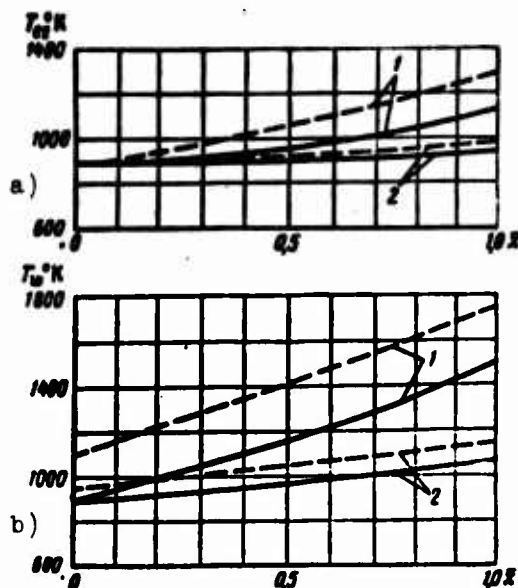


Fig. 9.25. The influence of radiation on the temperature of the air (a) and the wall (b) along the cooling channel of an engine during convection cooling.

$(T_{air})_{max} = 2200^\circ K$; $H = 30$ mm; $M_2 = 4.0$; $\epsilon = 1.2$;

$D_1 = 1.0$ m; $A = 20$ mm; $L_r = 1.5$ m.

$1 - \frac{q_1}{q_2} = 0.025$; $2 - \frac{q_1}{q_2} = 0.02$;

— $\epsilon_r = 0$;

--- $\epsilon_r = 0.04$.

taking into account radiation (dotted curves) and without taking into account radiation (solid curves). From these graphs it follows that consideration of radiation leads to a considerable increase of wall temperature of the combustion chamber (by approximately 10 to 20%, depending upon the relative flow rate of air coolant). Thus, during calculation of cooling of the combustion chamber of a ramjet engine, we should consider not only convection, but also radiant heat flow.

The above discussed examples pertain to the case of convection cooling of cylindrical combustion chambers. For convection cooling of the entire ramjet engine, we should consider heat exchange between the combustion products and the wall not only in the section L_r (hot part of the combustion chamber), but also in the section $l_c + L_c$ (nozzle). Above it was shown that calculation of convection

cooling of the combustion chamber can be carried out with a sufficient degree of accuracy according to the averaged coefficients of heat transfer $\bar{\alpha}_1$ (9.59) and $\bar{\alpha}_2$ (9.60). Then in the section of the combustion chamber (for $0 \leq \bar{x} \leq 1$), equilibrium temperature of the air coolant is determined by relationships (9.61) and (9.63). Due to the considerable change of the coefficient of heat transfer α_1 along the nozzle (see Fig. 9.8), calculation formulas (9.46) and (9.47) under the condition that

$$1 < \frac{x}{L_r} < 1 + \frac{l_c + L_c}{L_r} \quad (9.72)$$

take the form

$$h(\bar{x}) = \frac{\pi \cdot D_1(\bar{x}) \cdot \phi \cdot \alpha_2(\bar{x}) \cdot L_r}{3000 \cdot \epsilon_r \cdot q_2} \cdot \frac{1}{1 + \phi \cdot \frac{\alpha_1(\bar{x})}{\alpha_2(\bar{x})}}, \quad (9.73)$$

$$T_{e2} = e^{-\int_0^{\bar{x}} k(\bar{x}) d\bar{x}} \left[\int_0^{\bar{x}} k(\bar{x}) T_{e1}(\bar{x}) e^{\int_0^{\bar{x}} k(\bar{x}) d\bar{x}} d\bar{x} + (T_{e1})_{\bar{x}=0} \right]. \quad (9.74)$$

where $\alpha_1(\bar{x})$ is given by formula (9.20).^{*} Thus the temperature of the wall is determined by relationship (9.48). Formulas (9.48), (9.73) and (9.74) can be used for calculation of convection cooling under the condition that radiant heat transfer is small as compared to convection heat transfer ($\epsilon_r' \approx 0$).

Change of equilibrium temperature of combustion products along a ramjet engine and a simplified schematic diagram of the flow area are presented in Fig. 9.26. The solid lines in Fig. 9.27a, shows change of equilibrium temperature of air along a cooling channel with height $h = 20$ mm at two values of relative flow rate of air coolant G_2/G_1 . Temperature of the wall of a ramjet engine as a function of longitudinal coordinate \bar{x} is given for $\epsilon_r' \approx 0$ in Fig. 9.27b (solid lines). An example of calculation is given for an engine with diameter of the internal circuit of the combustion chamber $D_1 = 1.0$ m, with $f_{kp} = 0.8$ and $f_a = 2$, flying at an altitude of $H = 30,000$ m ($T_2 = 231.3^\circ\text{K}$, $p_2 = 120$ kg/m²) with speed corresponding to $M_2 = 4.0$ ($T_{e2} = 897^\circ\text{K}$), and maximum temperature in the combustion chamber $(T_{e1})_{\max} = 2200^\circ\text{K}$.

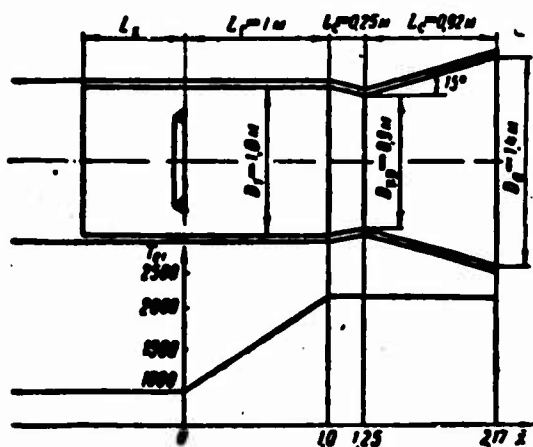


Fig. 9.26. Change of equilibrium temperature of combustion products along the engine and geometry of the nozzle.

From Fig. 9.27 it follows that for the considered example, equilibrium temperature of the cooling flow (T_{e2}) increases along the entire cooling channel, whereas temperature of the wall of the ramjet engine, starting at the nozzle throat, practically does not change. Such shapes of the curves are explained by the fact that along the nozzle, the equilibrium temperature of combustion products T_{e1} and function $k(\bar{x})$, which is determined by formulas (9.20) and (9.73), weakly depend on coordinate \bar{x} , and the local

^{*}With increase of equilibrium temperature in the combustion chamber, adiabatic exponent $k = k_p$ decreases. Therefore, the dimensionless parameter σ [see equation (9.20)], which takes into account the influence of Mach number and temperature factor on the coefficient of heat transfer α_1 , changes very weakly along the nozzle. In the example considered below, it is possible to assume approximately that $\sigma = 0.9$ to 1.0 .

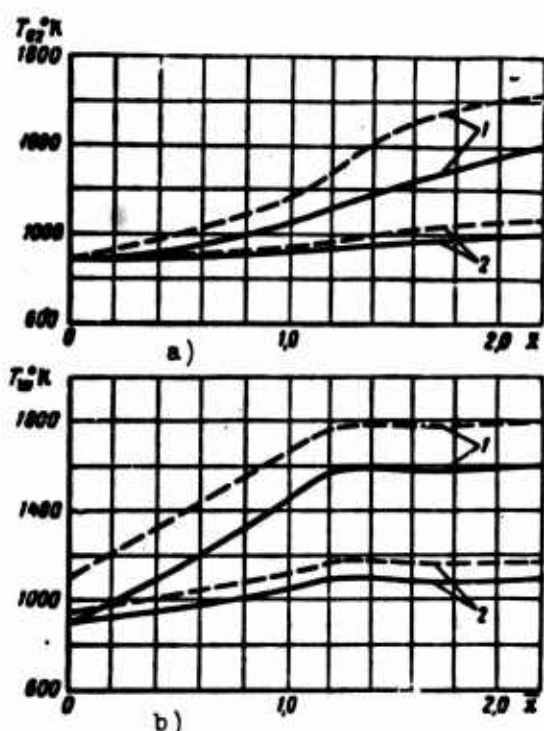


Fig. 9.27. Change of air temperature (a) and wall temperature (b) along the cooling channel of an engine during convection cooling.

$(T_{a1})_{\max} = 2200^\circ\text{K}$; $H = 30 \text{ km}$; $M_p = 4.0$; $A = 20 \text{ mm}$;
 $D_1 = 1.0 \text{ m}$; $L_T = 1.0 \text{ m}$.

$$1 - \frac{G_2}{G_1} = 0.025; \quad 2 - \frac{G_2}{G_1} = 0.20;$$

$$\text{---} \rightarrow i'_r = 0;$$

$$\text{---} \rightarrow i'_r = 0.04.$$

coefficient of heat transfer $\alpha_1(\bar{x})$ changes considerably in the divergent section of the nozzle. Thus, for a rough estimate of wall temperature of a ramjet engine during convection cooling, it is possible to be limited to thermal calculation only for the combustion chamber and the convergent part of the nozzle.

Let us consider calculation of convection of the entire engine in the presence of radiation for the combustion products. Above it was assumed that radiant heat exchange in the combustion chamber is determined mainly by radiation from a layer of gas with characteristic temperature $T_{1 \max} = T_{e1 \max}$. This assumption, with good grounds, can be extended to the convergent part of the nozzle, since in this case on the wall there falls mainly radiant energy from the layer of gas located in the wider part of the channel. In the divergent section of the nozzle, the process of radiation is determined mainly by the average thermodynamic temperature

$$T_{cp1} = \frac{T_{kp1} + T_{a1}}{2}. \quad (9.75)$$

This is explained by two facts: 1) the layer of gas in the nozzle throat has maximum thermodynamic temperature, and therefore radiates the most intensely; 2) onto the walls of the divergent section of the nozzle there falls mainly radiant energy from the layer of gas located in the wider part of the channel (cross section a) and having thermodynamic temperature T_{a1} .

In accordance with the assumed scheme of radiant heat exchange in a ramjet engine, we will divide the entire length of the engine into three characteristic sections:

1. Combustion chamber ($0 \leq x \leq L_T$), where radiation is calculated according to the characteristic temperature $(T_{e1})_{\max}$, and coefficients $\tilde{\alpha}_1$, $\tilde{\alpha}_2$ are practically constant, and equal to their averaged values.

2. The convergent part of the nozzle ($L_T \leq x \leq L_T + l_C$), where radiation is determined as before according to the characteristic temperature

$$(T_{c1})_{\text{max}} \text{ and } \alpha_1 = \alpha_1(\bar{x}), \alpha_2 = \alpha_2(\bar{x}).$$

3. The divergent section of the nozzle ($L_T + l_C \leq x \leq L_T + l_C + L_C$), where radiant heat exchange is approximately characterized by thermodynamic temperature T_{cp1} , and $\alpha_1 = \alpha_1(\bar{x})$ and $\alpha_2 = \alpha_2(\bar{x})$.

In the section of the combustion chamber ($0 \leq x \leq L_T$), calculation of convection cooling of the ramjet engine in the presence of radiation ($\epsilon_T \neq 0$) is carried out with the formulas (9.70) and (9.71). In the section of the convergent part of the nozzle ($L_T \leq x \leq L_T + l_C$), if we take into account the dependence (9.20), approximate formulas for calculation of wall temperature and equilibrium temperature of the air coolant take the form

$$T_w^{(n)} = T_w^{(n-1)} + \left(\frac{dT_w}{dx} \right)^{(n-1)} \Delta \bar{x}, \quad (9.76)$$

$$\left(\frac{dT_w}{dx} \right)^{(n-1)} = \frac{\frac{\alpha_1}{\psi_{a1}} \frac{dT_{c1}}{dx} + \frac{1}{\psi_{a1}} \frac{dz_1}{dx} (T_{c1} - T_w^{(n-1)}) + \frac{k}{\psi_{a1}} \left(1 + \psi \frac{\alpha_1}{\alpha_2} \right) B}{1 + \frac{\alpha_1}{\psi_{a1}} + \frac{\epsilon_T \epsilon_w c_1}{\psi_{a1}} \frac{4}{100} \left(\frac{T_w^{(n-1)}}{100} \right)^3}, \quad (9.77)$$

where

$$B = \left\{ \alpha_1 (T_{c1} - T_w^{(n-1)}) + \epsilon_T \epsilon_w c_1 \left[\left(\frac{T_{c1 \text{ max}}}{100} \right)^4 - \left(\frac{T_w}{100} \right)^4 \right] \right\},$$

$$T_{c1} = T_w - \frac{\alpha_1}{\psi_{a1}} (T_{c1} - T_w) - \frac{\epsilon_T \epsilon_w c_1}{\psi_{a1}} \left[\left(\frac{T_{c1 \text{ max}}}{100} \right)^4 - \left(\frac{T_w}{100} \right)^4 \right]. \quad (9.78)$$

It is not difficult to see that analogous relationships for the divergent section of the nozzle ($L_T + l_C \leq x \leq L_T + l_C + L_C$) can be written in the following way:

$$\left(\frac{dT_w}{dx} \right)^{(n-1)} = \frac{\frac{\alpha_1}{\psi_{a1}} \frac{dT_{c1}}{dx} + \frac{1}{\psi_{a1}} \frac{dz_1}{dx} (T_{c1} - T_w^{(n-1)}) + \frac{k}{\psi_{a1}} \left(1 + \psi \frac{\alpha_1}{\alpha_2} \right) C}{1 + \frac{\alpha_1}{\psi_{a1}} + \frac{\epsilon_T \epsilon_w c_1}{\psi_{a1}} \frac{4}{100} \left(\frac{T_w^{(n-1)}}{100} \right)^3}, \quad (9.79)$$

where

$$C = \left\{ \alpha_1 (T_{c1} - T_w^{(n-1)}) + \epsilon_T \epsilon_w c_1 \left[\left(\frac{T_{cp1}}{100} \right)^4 - \left(\frac{T_w}{100} \right)^4 \right] \right\},$$

$$T_{c1} = T_w - \frac{\alpha_1}{\psi_{a1}} (T_{c1} - T_w) - \frac{\epsilon_T \epsilon_w c_1}{\psi_{a1}} \left[\left(\frac{T_{cp1}}{100} \right)^4 - \left(\frac{T_w}{100} \right)^4 \right]. \quad (9.80)$$

On the basis of (9.20), the derivative $d\alpha_1/dx$ is given by the relationship

$$\frac{ds_1}{dx} = 93,5 \frac{c_{p1}}{Pr_1^{0,5}} \left(\frac{\nu_1 g}{D_{sp1}} \right)^{0,2} \left(\frac{G_1}{F_{sp1}} \right)^{0,8} \times \\ \times \left(\frac{D_{sp1}}{r_c} \right)^{0,1} \left[-1,8 \left(\frac{D_{sp1}}{D_1} \right)^{2,8} \frac{d}{dx} \left(\frac{D_1}{D_{sp1}} \right) + \left(\frac{D_{sp1}}{D_1} \right)^{1,8} \frac{ds}{dx} \right]. \quad (9.81)$$

Usually parameter σ is a weak function of coordinate x (see note on p. 451); therefore, it is possible to consider approximately that

$$\frac{d\sigma}{dx} \approx 0.$$

Temperature T_{a1} , which is contained in relationship (9.75), is calculated according to the evident formula

$$T_{a1} = \frac{T_n}{1 + \frac{k_1 - 1}{2} M_{a1}^2}, \quad (9.82)$$

and M_{a1} denotes Mach number at the nozzle exit.

The obtained relationships make it possible to completely calculate convection cooling the entire engine in the presence of radiation from the flame. Results of such a calculation for the considered example at two values of flow rate of air coolant are represented by the dotted lines ($\epsilon_r' \neq 0$) in Fig. 9.27. From Fig. 9.27b, it follows that consideration of radiation from the flame leads to a noticeable increase of wall temperature of a ramjet engine. For the considered example, this increase is 10 to 15%, depending upon the relative flow rate of the air coolant.

Let us turn to solution of the second part of the problem of convection cooling of a ramjet engine. Using the equations of flow rate and momentum, we will find true value of G_2 at which there is realized flow in a cooling channel of given height h at a fixed value of stagnation pressure at the end of the diffuser (p_{0d}). The equation of flow rate written for cross section d has the form

$$G_2 = \frac{p_{0d} F_d}{a_2^*} \frac{2k_2}{k_2 + 1} \cdot \lambda_{d2} \left(1 - \frac{k_2 - 1}{k_2 + 1} \cdot \lambda_{d2}^2 \right)^{\frac{1}{k_2 - 1}}, \quad (9.83)$$

where k_2 - adiabatic exponent for air in the cooling channel;

λ_{d2} - reduced velocity at the inlet to the cooling channel;

p_{0d} - stagnation pressure after the diffuser;

a_2^* - stalling speed, determined by the formula

$$\zeta_2 = \sqrt{\frac{2k_2}{k_2 + 1} gRT_{a2}}. \quad (9.84)$$

Formula (9.83) contains two unknown quantities G_2 and λ_{a2} . The second relationship relating these quantities is the momentum equation. If we take into account the varying area of the annular channel, heat supply and friction, this equation has the form [13]

$$(1 - \lambda_2^2) \frac{d\lambda_2^2}{\lambda_2^2} = -2 \left(1 - \frac{k_2 - 1}{k_2 + 1} \cdot \lambda_2^2 \right) \frac{dF_2}{F_2} + \\ + (1 + \lambda_2^2) \frac{dT_{a2}}{T_{a2}} + \frac{2k_2}{k_2 + 1} \lambda_2^2 \zeta_2 \frac{dx}{D_{ann}}. \quad (9.85)$$

where ζ_2 denotes the drag coefficient of the annular channel.

For each of the selected values of G_2 , equation (9.85) is solved by the method of successive approximations. In the first approximation we will assume that air flows through a cylindrical ($dF_2 = 0$) thermally insulated ($dT_{a2} = 0$) annular channel; then equation (9.85) is considerably simplified. After separating variables, we will obtain

$$(1 - \lambda_2^2) \frac{d\lambda_2^2}{\lambda_2^2} = \frac{2k_2}{k_2 + 1} \zeta_2 \frac{dx}{D_{ann}}. \quad (9.86)$$

Let us note that when x changes from $L = L_T + l_c + L_c$ to $-L_x$ (see Fig. 9.26), reduced velocity in the cooling channel (λ_2) changes from $\lambda_{a2} = 1.0$ to λ_{x2} .

Integrating equation (9.86) from cross section a to an arbitrary cross section with coordinate x , we find the value of $\lambda_2^{(1)}(x)$ in the first approximation

$$\chi_2(\lambda_2^{(1)}) = \ln \lambda_2^{(1)^2} + \frac{1}{\lambda_2^{(1)^2}} = \\ = 1 - \int_L^x \frac{2k_2}{k_2 + 1} \zeta_2 \frac{dx}{D_{ann}}. \quad (9.87)$$

The dependence of function χ_2 on λ_2 is represented in Fig. 9.28.

During approximate calculation of convection cooling, it is possible to consider that the local drag

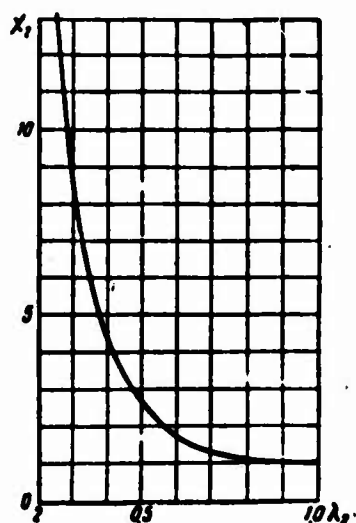


Fig. 9.28. The parameter χ_2 as a function of reduced velocity λ_2 .

coefficient depends only on Reynolds number Re:

$$\zeta_2 = f(\text{Re}_2).$$

We will replace ζ_2 by its mean value; then formula (9.87) takes the form

$$\ln \lambda_2^{(1)} + \frac{1}{\lambda_2^{(1)}} = 1 + \frac{2k_2}{k_2 + 1} \frac{L - x}{D_{\text{max}}} \cdot \zeta_2, \quad (9.88)$$

where ζ_2 , in dependence upon the range of change of Reynolds number Re, is determined by the formulas

$$\left. \begin{aligned} \zeta &= \frac{0.316}{\text{Re}^{0.25}} \text{ for } \text{Re} < 10^4; \\ \frac{1}{\sqrt{\zeta}} &= 2 \cdot \lg \text{Re} \sqrt{\zeta} - 0.8; \text{ Re} < 3.4 \cdot 10^6. \end{aligned} \right\} \quad (8.89)$$

When $x = -L_x$, on the basis of (9.88) we will obtain the reduced velocity at the inlet to the cooling channel

$$\ln \lambda_{22}^{(1)} + \frac{1}{\lambda_{22}^{(1)}} = 1.0 + \frac{2k_2}{k_2 + 1} \frac{L + L_x}{D_{\text{max}}} \cdot \zeta_2 \quad (9.90)$$

Taking several values of x in the interval $(-L_x; L)$, we will obtain, on the basis of formula (9.88), the change of reduced velocity along the cooling channel. Integrating differential equation (9.85) and substituting in the right side in place of λ_2 the first approximation of this variable, we will obtain a formula for calculation of the second approximation $\lambda_2^{(2)}$

$$\begin{aligned} \lambda_2^{(2)} &= 1 + \frac{2k_2}{k_2 + 1} \frac{L - x}{D_{\text{max}}} \zeta_2 + \\ &+ 2 \int_L^x \frac{\left(1 - \frac{k_2 - 1}{k_2 + 1} \cdot \lambda_2^{(1)}\right) dF_2}{\lambda_2^{(1)} F_2} - \int_L^x \frac{(1 + \lambda_2^{(1)}) dT_{e2}}{\lambda_2^{(1)} T_{e2}}. \end{aligned} \quad (9.91)$$

During calculation of the first integral contained in formula (9.91), we should consider the dependence $F_2 = F_2(x)$, and during calculation of the second integral — the dependence $T_{e2} = T_{e2}(x)$, which is found during thermal calculation of the cooling system.

Substituting the second approximation $\lambda_2^{(2)}(x)$ into the integrals standing in the right side of equation (9.91), we will obtain the third approximation $\lambda_2^{(3)}$. This process is continued until the dependence $\lambda_2 = \lambda_2(x)$ does not depend on the number of the approximation. Calculations show that for practical purposes, it is sufficient to be limited to the second approximation. Using (9.91), we will obtain the

reduced velocity at the inlet to the cooling channel

$$\lambda_2(\lambda_{\infty}) = 1 + \frac{2h_1}{h_2 + 1} \frac{L + L_r}{D_{\text{кан}}} \cdot \lambda_2 +$$

$$+ 2 \int_0^{\lambda_2} \frac{1 - \frac{h_1 - 1}{h_2 + 1} \cdot \lambda_2^2}{\lambda_2^3} \cdot \frac{dF_1}{F_1} - \int_0^{\lambda_2} \frac{1 + \lambda_2^2}{\lambda_2^3} \frac{dT_{\text{ст}}}{T_{\text{ст}}} \quad (9.92)$$

After reduced velocity $\lambda_{\text{д2}}$ is found for a given value of $G_2 = (G_2)_3$ on the basis of equation (9.83) we will obtain the flow rate of air.

assigning a series of values of $G_2 = (G_2)_3$, we will find a corresponding series of values $G_2 = (G_2)_n$, and construct a dependence between obtained and given flow rates:

$$(G_2)_n = f(G_2)_3 \quad (9.93)$$

The true flow rate of the cooling flow is realized when

$$(G_2)_n = (G_2)_3 \quad (9.94)$$

Consequently, the true flow rate $G_2 = (G_2)_{\text{нст}}$ is determined by the point of intersection of the curve (9.93) with the bisector of the right angle (Fig. 9.29).

After the true value of flow rate of air coolant $(G_2)_{\text{нст}}$ is graphically found, there is performed calculation of convection cooling at $G_2 = (G_2)_{\text{нст}}$. Results of such a calculation for the considered example are presented in Fig. 9.30. From Fig. 9.30b, it follows that for the considered example the maximum value of wall temperature, even in the presence of radiation, is $(T_w)_{\text{max}} = 1130^\circ\text{K}$.

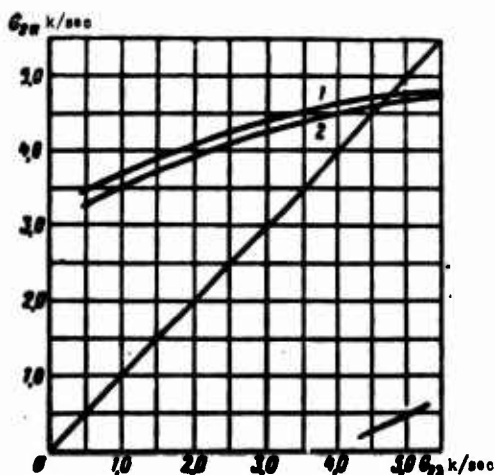


Fig. 9.29. Graphic determination of the true flow rate of air coolant. 1 - $\epsilon_r = 0.04$, 2 - $\epsilon_r = 0$.

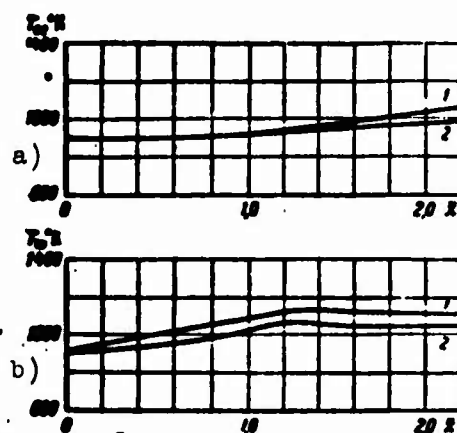


Fig. 9.30. Change of air temperature (a) and wall temperature (b) along the cooling channel of an engine during convection cooling. 1 - $\epsilon_r = 0.04$; 2 - $\epsilon_r = 0$;

$(T_{\text{ст}})_{\text{вх}} = 3200^\circ\text{K}$; $H = 30 \text{ мм}$; $M_1 = 4.0$; $h = 20 \text{ мм}$;
 $D_1 = 1.0 \text{ м}$; $L_r = 1.0 \text{ м}$.

§ 5. CALCULATION OF FLOW IN A TWO-LOOP CYLINDRICAL COMBUSTION CHAMBER WITH CONSIDERATION OF HEAT RELEASE AND HEAT TRANSFER THROUGH THE WALL OF THE FLAME TUBE

In a ramjet engine there are used two-circuit combustion chambers (Fig. 9.31). In these chambers the optimum air-fuel ratio at which there is realized the regime of maximum economy is larger than the air-fuel ratio at which the process of burning occurs the most intensely, i.e., with the greatest completeness. In order to ensure in the combustion chamber itself a highly efficient working process and to maintain the given total air-fuel ratio, part of the air directly from the diffuser is passed through a secondary (annular) circuit. Starting from the cross section k (Fig. 9.31), secondary air is mixed with combustion products.

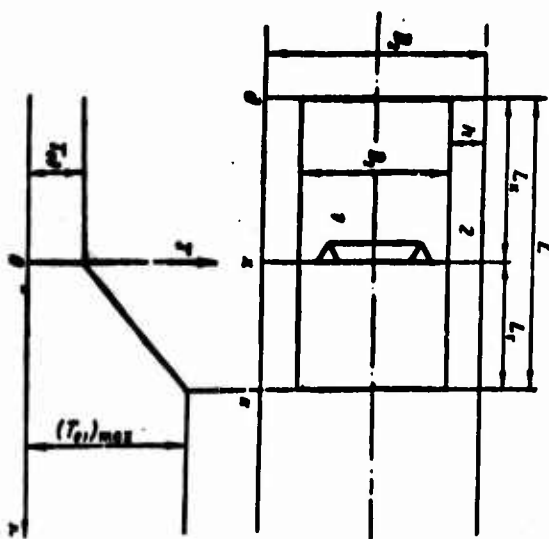


Fig. 9.31. Diagram of a two-loop combustion chamber and change of temperature of the combustion products depending upon x .

During calculation of characteristics of a two-circuit ramjet engine and the cooling system of the engine, it is necessary

to know the distribution of total flow rate of air through the circuits. It is obvious that the given total flow rate of air through the motor is redistributed with respect to the circuits of the combustion chamber depending upon hydraulic and thermal losses.

Let us assume that for a two-circuit engine with air cooling there are given: 1) conditions of flight (speed and altitude); 2) regime of operation (overall air-fuel ratio α_{Σ} , fuel burn-up curve and air-fuel ratio through the inner circuit α_r); 3) mid-section of the combustion chamber. Using the given parameters, we are required to determine: 1) diameter of the actual combustion chamber D_1 ; 2) all gas-dynamic parameters along the combustion chamber and along the annular channel; 3) wall temperature of the flame tube.

The considered problem is reduced to simultaneous solution of the equations of heat transfer and the gas-dynamic equations for a two-circuit combustion chamber. The method of calculation of flow in a two-circuit combustion chamber is based on a series of assumptions. Let us enumerate the basic assumptions:

1. The fuel burn-up curve is determined by a linear function (Fig. 9.31).

This assumption does not limit the generality of the solution of the problem, since any function $T_{e1} = f(\bar{x})$ can be taken as the fuel burn-up curve.

2. The flow regime in cold and hot flows is everywhere turbulent.

3. Calculation of heat exchange is performed with average heat transfer coefficients. The correctness of this assumption is substantiated in the preceding paragraph.

4. In accordance with the method of calculation of characteristics of a ramjet engine, it is assumed that local hydraulic losses in the inner circuit are concentrated in the section $\Delta 1-X1$ and thermal losses are realized in the hot part of the combustion chamber in the section $X1-K1$ (9.31). In the annular channel in section $\Delta 2-X2$ there occur only hydraulic frictional losses, and in the section $X2-K2$, besides hydraulic frictional losses there also appear thermal losses, caused by heat flow through the flame tube.

5. Static pressures p_{K1} and p_{K2} at the end of the flame tube (section K) are equal to each other:

$$p_{K1} = p_{K2}. \quad (9.95)$$

This assumption is confirmed by experimental data.

Let us turn to solution of the problem at hand. The main losses in the annular channel are frictional losses. Then the momentum equation during flow of gas in a cylindrical annular channel with friction and heat supply has the form [12], [13], [14]

$$(1 - \lambda^2) \frac{d\lambda^2}{\lambda^2} = (1 + \lambda^2) \frac{dT_0}{T_0} + \frac{2k}{k+1} \lambda \zeta_2 \frac{dx}{D_{\text{экв}}}, \quad (9.96)$$

where λ — reduced velocity;
 T_0 — stagnation temperature;
 ζ_2 — coefficient of frictional resistance;
 $D_{\text{экв}}$ — equivalent diameter of the annular channel;
 k — adiabatic exponent.

The coefficient of frictional resistance ζ_2 is calculated by the empirical formula (9.89). In the particular case of a flow without hydraulic losses ($\zeta_2 = 0$), equation (9.96) is integrated and takes the form [14]

$$Z(\lambda_{\text{max}}) = \sqrt{\frac{T_0}{T_{0\text{max}}}} \cdot Z(\lambda), \quad (9.97)$$

where $Z(\lambda) = \lambda + \frac{1}{\lambda}$;

λ_{HAY} - reduced velocity in initial section;

$T_{0 \text{ HAY}}$ - stagnation temperature in initial section.

In the absence of heat supply ($dT_0 = 0$), equation (9.96) is integrated and takes the form [14]

$$\chi(\lambda) = \chi(\lambda_{\text{HAY}}) - \frac{2k}{k+1} \int_{\lambda_{\text{HAY}}}^{\lambda} \zeta_2 \frac{dx}{D_{\text{HAY}}} \quad (9.98)$$

where

$$\chi(\lambda) = \frac{1}{\lambda^2} + \ln \lambda^2. \quad (9.99)$$

Since the coefficient of frictional resistance ζ_2 practically does not depend on the longitudinal coordinate x , then equation (9.98) will be simplified still more:

$$\chi(\lambda) = \chi(\lambda_{\text{HAY}}) - \frac{2k}{k+1} \cdot \frac{x - x_{\text{HAY}}}{D_{\text{HAY}}} \cdot \zeta_2. \quad (9.100)$$

The main losses in the inner channel are local losses. Hydraulic frictional losses can be disregarded during calculation of flow in the burning circuit. Local flow friction are usually related to velocity head in the initial section. Then the resisting force is determined in the following way:

$$f = \zeta_{\Sigma} q_{\text{HAY}} F. \quad (9.101)$$

where ζ_{Σ} - local drag coefficient referred to velocity head in the initial cross section;

q_{HAY} - velocity head in the initial cross section;

F - cross sectional area of the combustion chamber.

Applying the momentum equation to the mass of gas contained between the initial and current sections, and considering the resisting force f , we will obtain [14]

$$p + \rho w^2 = p_{\text{HAY}} + \left(1 - \frac{\zeta_{\Sigma}}{2}\right) \rho_{\text{HAY}} w_{\text{HAY}}^2. \quad (9.102)$$

Using the usual gas-dynamic relationships, we represent the momentum equation for the inner channel in the form

$$Z(\lambda) = \frac{1}{\sqrt{\frac{T_0}{T_{0 \text{ HAY}}}}} \left[Z(\lambda_{\text{HAY}}) - \frac{k}{k+1} \zeta_{\Sigma} \lambda_{\text{HAY}} \right]. \quad (9.103)$$

Let us assume that there is given the total flow rate of air through the motor G , the overall air-fuel ratio α and the air-fuel ratio for the actual combustion chamber α_1 . Then the flow rate of air through the inner shell and the annular

channel will be determined by the evident formulas

$$G_1 = G \frac{\tau}{\alpha_1}; \quad (9.104)$$

$$G_2 = G - G_1. \quad (9.105)$$

Taking a series of values of reduced velocity at the inlet to the annular channel ($\lambda_{\pi 2}$), we will calculate by the relative diameter of the shell flow rate equation:

$$\frac{D_1}{D_2} = \sqrt{1 - \frac{G_1}{G_2} \frac{1}{q_{\pi 2}}}. \quad (9.106)$$

where $q_{\pi 2}$ - reduced flow rate in cross section $\pi 2$;

$$G_2 = \sqrt{\frac{2k_2}{k_2 + 1} \frac{p_{0\pi}}{\sqrt{T_{0\pi}}} \frac{\pi}{4} D_2^3}. \quad (9.107)$$

In formula (9.107) $p_{0\pi}$ denotes the total pressure at the end of the diffuser.

From the flow rate equation for the inner circuit, there is found the reduced flow rate $q_{\pi 1}$ in cross section $\pi 1$:

$$q_{\pi 1} = \frac{G_1}{G_2} \left(\frac{D_1}{D_2} \right)^3. \quad (9.108)$$

Using the momentum equation (9.103) for the cold part of the actual combustion chamber, we will obtain

$$Z_{\pi 1} = Z_{\pi 2} - \frac{k_2}{k_2 + 1} \zeta_{\pi 2} \lambda_{\pi 2}. \quad (9.109)$$

The momentum equation (9.97) for the hot part of the combustion chamber, taking into account addition of fuel, takes the form

$$Z_{\pi 1} = \frac{Z_{\pi 2}}{k_2 \sqrt{\tau_1}}. \quad (9.110)$$

where relative preheating τ_1 is determined by the formula

$$\tau_1 = \frac{(T_{01})_{\max}}{T_{0\pi}}. \quad (9.111)$$

On the basis of the definition of function Z , reduced velocity in cross section k is given by the relationship

$$\lambda_{\pi 1} = \frac{Z_{\pi 1}}{2} \pm \sqrt{\left(\frac{Z_{\pi 1}}{2} \right)^2 - 1}. \quad (9.112)$$

For each of the selected values of $\lambda_{\pi 2}$, the momentum equation for the cooling channel (9.96) is solved by the method of successive approximations. In the first

approximation we will assume that cooling (secondary) air flows through a thermally insulated channel ($dT_{e2} = 0$). Then equation (9.96) is considerably simplified, and as a result of integration is reduced to the form (9.98). Applying this equation to the annular channel and considering that when $x_{\text{Hau}} = -L_x$, $\lambda_{\text{Hau}} = \lambda_{\text{d2}}$, we will obtain

$$\chi(\lambda_{\text{d2}}^{(II)}) = \chi(\lambda_{\text{d2}}) - \frac{2k_2}{k_2 + 1} \frac{s + L_1}{D_{\text{ann}}} \zeta_2. \quad (9.113)$$

At the end of the shell, for the cross section κ_2 , relationship (9.113) takes the form

$$\chi(\lambda_{\text{d2}}^{(II)}) = \chi(\lambda_{\text{d2}}) - \frac{2k_2}{k_2 + 1} \frac{L_r + L_1}{D_{\text{ann}}} \zeta_2. \quad (9.114)$$

Reynolds number Re , contained in formula (9.89) for the coefficient of frictional resistance is equal to

$$Re_2 = 0.13 \frac{G_2}{D_2 v_2} \frac{1}{2 + 2 \frac{h}{D_1}}, \quad (9.115)$$

where h is the height of the cooling channel;

$$h = \frac{D_2 - D_1}{2}. \quad (9.116)$$

According to the definition of equivalent diameter we have

$$D_{\text{ann}} = 2h. \quad (9.117)$$

If radiant heat flow from the combustion products to the wall of the flame chamber is small as compared to the convection heat flow, then change of equilibrium temperature of the air along the annular channel is determined by relationships (9.59), (9.60), (9.61) and (9.63).

Incidentally there can be calculated the temperature of the flame chamber:

$$T_g = \frac{T_{g1} + \frac{\frac{q_1}{\epsilon_1}}{\frac{q_1}{\epsilon_1} + 1} T_{g1}}{1 + \frac{\frac{q_1}{\epsilon_1}}{\frac{q_1}{\epsilon_1} + 1}}. \quad (9.118)$$

Calculation of radiant heat exchange between combustion products and the wall of the flame chamber does not present difficulties, and leads only to a certain complication of the formulas for calculation.

By integrating the differential equation (9.96) for the annular channel and substituting in the right side in place of λ_2 the first approximation of this variable, we will obtain a formula for calculation of the second approximation λ_2^2 :

$$\chi(\lambda_2^{(2)}) = \chi(\lambda_{22}) - \frac{2k_2}{k_2 + 1} \frac{x + L_1}{D_{\text{max}}} \zeta_2 - \int_{-L_2}^x \frac{1 + \lambda_2^{(1)2}}{\lambda_2^{(1)2}} \cdot \frac{dT_{\text{ex}}}{T_{\text{ex}}}. \quad (9.119)$$

During calculation of the integral contained in formula (9.119), it is necessary to consider the dependence $T_{\text{ex}} = T_{\text{ex}}(x)$, which is found from relationship (9.63).

Substituting the second approximation $\lambda_2^{(2)}(x)$ in the integral standing in the right side of equation (9.119), we will obtain the third approximation $\lambda_2^{(3)}$. This process is continued until the dependence $\lambda_2 = \lambda_2(x)$ does not depend on the number of the approximation. Calculations show that for practical purposes it is sufficient to be limited to the second approximation. Using (9.119), we will obtain the reduced velocity at the exit section of the flame chamber taking into account heat addition to the air coolant:

$$\chi_{22} = \chi(\lambda_{22}) = \chi(\lambda_{22}) - \frac{2k_2}{k_2 + 1} \frac{L_1 + L_2}{D_{\text{max}}} \zeta_2 - \int_{-L_2}^{L_1} \frac{1 + \lambda_2^2}{\lambda_2^2} \cdot \frac{dT_{\text{ex}}}{T_{\text{ex}}}. \quad (9.120)$$

Using the condition of equality of static pressures in section K, we will obtain

$$p_{21} \left(1 - \frac{k_2 - 1}{k_2 + 1} \lambda_{21}^2 \right)^{\frac{k_2}{k_2 - 1}} = p_{22} \left(1 - \frac{k_2 - 1}{k_2 + 1} \lambda_{22}^2 \right)^{\frac{k_2}{k_2 - 1}}. \quad (9.121)$$

Applying the flow rate equation to cross sections M1 and K1, we will obtain

$$\frac{p_{21}}{p_{22}} = \frac{q_{21}}{q_{22}} \sqrt{\tau_1}. \quad (9.122)$$

From the flow rate equation for the annular channel on section M2 to K2, we will find

$$\frac{p_{21}}{p_{22}} \approx \frac{q_{22}}{q_{21}} \sqrt{\tau_2} \quad (9.123)$$

where τ_2 is the relative preheating of air in the cooling channel;

$$\tau_2 = \frac{(T_{\text{ex}})_{\text{max}}}{T_{\text{ex}}}. \quad (9.124)$$

Using the formula for reduced flow rate

$$q = \lambda \left(1 - \frac{k_2 - 1}{k_2 + 1} \lambda^2 \right)^{\frac{1}{k_2 - 1}} \quad (9.125)$$

and considering the relationships (9.121), (9.122) and (9.123), we will obtain

$$q_{A2} = q_{A1} \frac{\tau_1 \sqrt{\tau_1}}{\sqrt{\tau_2}} \cdot \frac{\frac{1}{\lambda_1} - \frac{k_1 - 1}{k_1 + 1} \lambda_{*1}}{\frac{1}{\lambda_{*2}} - \frac{k_2 - 1}{k_2 + 1} \lambda_{*2}}. \quad (9.126)$$

The true values of λ_{*2} and q_{A2} at which the considered flow is realized are found by means of graphical solution of the equations

$$q_{A2} = \lambda_{*2} \left(1 - \frac{k_2 - 1}{k_2 + 1} \lambda_{*2}^2 \right)^{\frac{1}{k_2 - 1}};$$

$$q_{A2} = f(\lambda_{*2}).$$

After the true value of λ_{*2} is found, determination of true values of the remaining parameters (λ_{*1} , λ_{*2} , h and others) can be carried out either graphically or analytically.

§ 6. BOUNDARY COOLING

The problem consists of determination of the wall temperature of a ramjet engine $T_w = T_w(x)$ and the flow rate of air coolant G_2 flowing through an annular channel of given height h which is formed by the outer wall of the motor and the cylindrical shell. There are considered to be given the following: total pressure of the flow at the inlet to the annular channel, geometry of the engine, gas-dynamic parameters and total flow rate of air passing through the engine:

$$G = G_1 + G_2, \quad (9.127)$$

where G_1 is the flow rate of the hot flow.

The hot part of the motor of length L , made of heat resistant material with maximum permissible wall temperature of T_{wm} will be subject to cooling. Air coolant is withdrawn from the diffuser and flows in an annular channel with height h (Fig. 9.32).

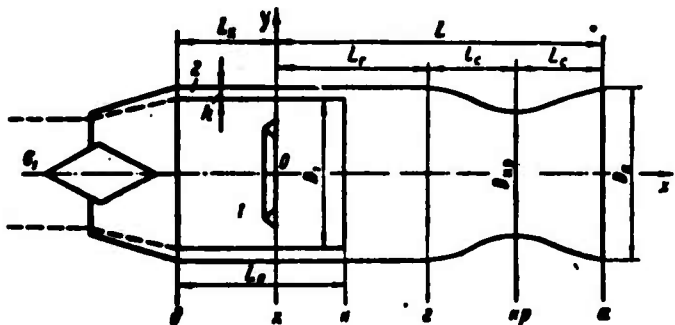


Fig. 9.32. Schematic diagram of boundary cooling.

Calculation of boundary cooling of the engine is based on a series of assumptions, part of which are substantiated above (see assumptions given in § 3, Chapter IX, except for Paragraph 6). Let us enumerate

a series of additional assumptions with their corresponding substantiations:

1. Static pressures p_{K1} and p_{K2} in the beginning of the mixing region (section K in Fig. 9.32) are equal to each other:

$$p_{K1} = p_{K2}$$

This assumption is confirmed with a sufficient degree of accuracy by experimental data.

2. It is considered that regularities established for temperature profiles at moderate flow velocities are approximately satisfied for stagnation temperature profiles at elevated flow velocities.

3. The problem of air-boundary cooling is solved for a flat thermally insulated wall without taking into account radiation. Therefore, in the present investigation it is assumed that all heat transmitted from the gas to the wall by radiation is removed by a convective cooling flow.

4. The cooled part of the engine of length L during calculation of temperature of the wall and the external boundary of the mixing region is taken to be approximately cylindrical. Below there are given experimental data on air-boundary cooling of a supersonic nozzle.

5. Heat transfer through the internal shell is absent; moreover in the annular channel in the section $\mu 2-K2$ there occur only hydraulic losses. Such an assumption is strictly fulfilled for a thermally insulated shell, and approximately for a shell for which section $\mu 2-K2$ is considerably less than section $\mu 2-X2$ (Fig. 9.32).

During solution of the problem about boundary cooling there is used the equation of heat balance, and also the continuity and momentum equations for flow in an annular channel. As a result of solution of the system of equations it is required to find change of temperature of the wall T_w depending upon x, the reduced velocity of the cooling flow at the inlet to the annular channel $\lambda_{\mu 2}$ and the flow rate of air coolant G_2 .

We will break the formulated problem up into the thermal problem and the hydraulic problem. In distinction from convection cooling, the hydraulic problem under the assumptions which have been made (see Paragraph 5) is solved independently of the thermal problem. Therefore during solution of the thermal problem, flow rate of the air coolant G_2 (or velocity of the cooling flow at the outlet from the annular $u_{K2} \equiv u_2$) is considered to be known. During solution of the hydraulic problem, on the basis of the momentum equation and the flow rate equation there is determined the true value of G_2 (or u_{K2}) at which flow in an annular channel of given height h is realized.

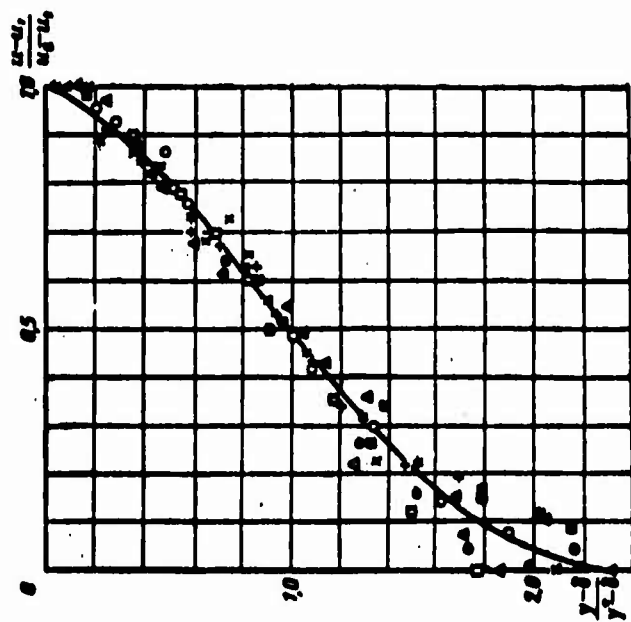


Fig. 9.33. Dimensionless velocity profile during air-boundary cooling.

Cross section	II	III	IV	V	VI	VII	VIII	IX	X
Symbols	□	△	×	+	■	●	○	*	▲
u_s , in m/sec	154	135	141	140	139.8	140	139.7	138	135
u_s , in m/sec	226	202.7	193.4	199.2	187.9	176.9	176.9	172	169.4
K , in mm	2.75	3.25	3.35	4.025	3.55	3.05	4.72	6.03	6.0
$(K-y_s)$, in mm	3.09	4.44	5.5	4.06	5.27	9.11	7.43	8.35	11.25

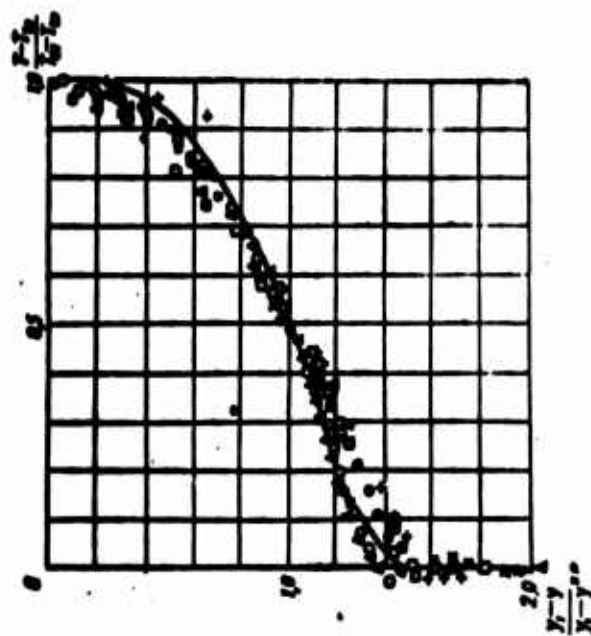


Fig. 9.34. Dimensionless temperature profile during air-boundary cooling.

Cross section	II	III	IV	V	VI	VII	VIII	IX	X
Symbols	□	△	×	+	■	●	○	*	▲
(T_s) , °K	953	903	1003	1008	1003	1006	1006	1017	1023
T_s , in °K	340.7	313	308	329	427.3	462	482	521.3	535.3
K , in mm	9.2	11.8	14.4	17.2	19.8	22.8	25.8	28.8	31.90
$(K-y_s)$, in mm	2.6	4.6	6.3	9.6	11.8	12.7	17.2	19.6	22.45

Holding to the accepted sequence of account, let us turn to solution of the thermal problem. On the basis of the equation of the heat balance and regularities of turbulent mixing of nonisothermal flows near a solid wall, we will find the law of temperature rise of the wall along the engine. Let us give the basic results of investigation of boundary cooling of a flat wall. For the purpose of simplification, boundary cooling is considered at constant temperature of the hot flow: $T_1 \equiv T_{e1} = \text{const}$. This assumption is not too strong, and later it will be possible to disregard it.

Theoretical and experimental investigation of boundary cooling has been carried out for any ratio of velocities of boundary ($u_{x2} \equiv u_2$) and main ($u_{x1} \equiv u_1$) flows and for sufficiently large distances from the nozzle exit $\frac{x}{h} < 150$. Theoretical conclusions are based on the use of the integral relationship of momentum and the integral relationship of enthalpy. All reasonings are based mainly on the experimental fact of self-similarity of velocity profiles and temperature profiles (Figs. 9.33 and 9.34).

On the basis of experimental data there has been established the physical picture of mixing of nonisothermal flows (Fig. 9.35). With accuracy sufficient for

practical purposes we may assume that the boundaries of dynamic and thermal boundary layers coincide.

The entire region of flow can be divided into two characteristic sections: initial and basic. The initial section (Fig. 9.35) directly adjoins the dividing wall and is characterized by the presence of a core of constant velocity u_2 and constant temperature T_{e2} . In the initial section the boundary layer adjacent to the wall practically does not interact with the free turbulent boundary layer. With increase of distance from the dividing wall, the transverse dimension of the core of constant parameters gradually decreases, and in the transition section

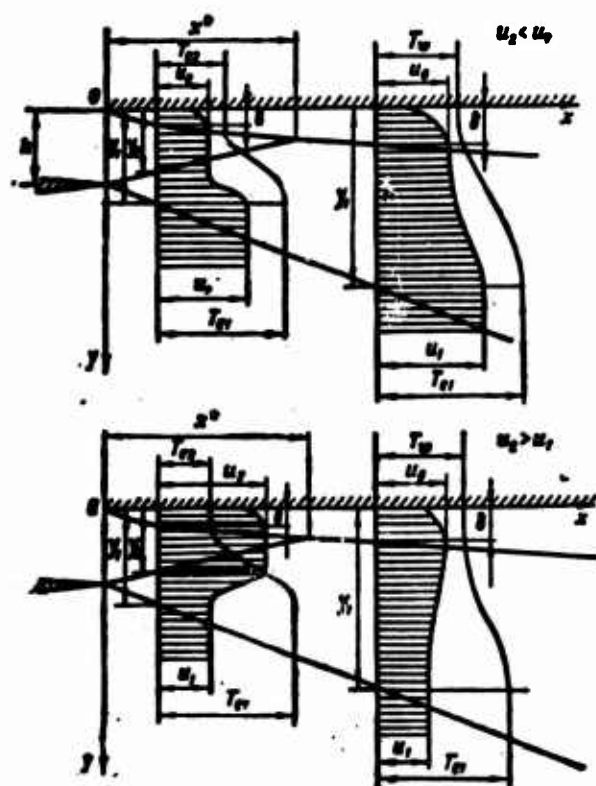


Fig. 9.35. Diagram of mixing of non-isothermal flows.

($x = x^*$) becomes zero. It is assumed that directly after the transition section

there follows the main section, in which the boundary layer adjacent to the wall interacts with the free turbulent boundary layer ($x > x^*$).

Velocity profiles consist of two characteristic sections (Fig. 9.35). Near the wall the velocity profile has the usual form of a turbulent profile during flowing around a flat plate. Directly to this section of the velocity profile there adjoins a second section, which corresponds to the region of jet mixing of flows (see Fig. 9.33).

Geometry of the flow in the initial section ($x < x^*$) is completely determined by the thickness of the boundary layer δ and boundaries y_1 and y_2 of the region of turbulent mixing. The transition section is characterized by the following evident condition: when $x = x^*$, $y_2 = \delta$. The geometry of the main section is determined by the thickness of the boundary layer δ and the external boundary y_1 of the region of jet mixing.

In the main section there occurs transformation of velocity and temperature profiles. Velocity u_0 (at $y = \delta$) within the limits of the main section is a variable magnitude: with increase of x from x^* to ∞ , velocity u_0 changes from u_2 to u_1 . Furthermore, with change of x from x^* to ∞ , wall temperature increases from T_{e2} to T_{e1} .

Use of boundary conditions of the fourth kind along with the condition of thermal insulation of the wall

$$\left(\frac{\partial T}{\partial y}\right)_{y=0} = 0 \quad (9.128)$$

gives us grounds to consider that the wall temperature is equal to the temperature of the flow at $y = 0$:

$$T_w = T(y)_{y=0}. \quad (9.129)$$

Characteristic temperatures in each section are the temperature of the hot flow T_{e1} and the wall temperature T_w (see Fig. 9.35). At any velocities of the boundary flow, velocity and temperature profiles are self-similar, and are satisfactorily approximated by simple analytic dependences.

Let us give a brief account of the theoretical results. The problem of boundary cooling of a flat wall is formulated in the following way: there are given velocity and temperature of the main (u_1 , T_{e1}) and boundary (u_2 , T_{e2}) flows in the initial cross section ($x = 0$). Furthermore, there is given the length L of the cooled wall (for unit width) and height h of the cooling slot.

It is required to determine the maximum wall temperature T_{wm} at $x = L$.

$$T_w(L) = T_{wm} \quad (9.130)$$

on the assumption that for any x there is satisfied the condition of thermal insulation of the wall $\left(\frac{dT}{dy}\right)_{y=0} = 0$. The proposed formulation of the thermal problem is not unique. Thus, for instance, if there is given the maximum permissible wall temperature T_{wm} and the height of the slot, then solution of the problem consists of determination of the cooled length L .

Along with the method of determination of the temperature of a thermally insulated wall depending upon coordinate x :

$$T_w = T_w(x), \quad (9.131)$$

below there are given formulas for calculation of fields of velocity and temperature. True fields of velocity and temperature in the engine must be known for determination of the economy of a ramjet engine with air-boundary cooling and for detailed study of the working process.

Basic dimensionless parameters determining the temperature of the thermally insulated wall, and also the fields of velocities and temperatures are:

1) the ratio of outflow velocity of the boundary flow (u_2) to the velocity of the main flow (u_1)

$$m = \frac{u_2}{u_1}; \quad (9.132)$$

2) the ratio of temperature of the boundary flow at the outlet from the slot (T_{e2}) to the temperature of the main flow (T_{e1})

$$T_a = \frac{T_{e2}}{T_{e1}}; \quad (9.133)$$

3) turbulence constant c^2 (at $m \neq 1$) or turbulent diffusion coefficient $D_T m^2/\text{sec}$ (at $m \approx 1.0$);

4) Reynolds number Re calculated according to parameters of the hot flow and according to the height of the slot h (or the length of the hot wall L):

$$Re_1 = \frac{u_1 h}{\nu_1} \quad \left(\text{or } Re = \frac{u_1 L}{\nu_1} \right). \quad (9.134)$$

For determination of external (y_1) and internal (y_2) boundaries of the region of jet mixing ($m \neq 1$ and $x < x^*$), there is used the integral momentum relationship, applied once for the entire region of free turbulence and a second time only for half of it. Thus, there are obtained two equations, with solution of which turbulent friction is determined according to the known formula of Prandtl [15]. It has been experimentally established that during boundary and combined cooling of a ramjet

engine the velocity of the cold flow is less than the velocity of the main flow or, in the limiting case, is equal to it. Therefore, subsequently there are given results pertaining only to the most interesting case from the practical point of view, $m \leq 1.0$.

In Fig. 9.36 there are presented results of calculation of boundaries of the region of turbulent mixing of nonisothermal flows at $m < 1$ and at values of $\bar{T}_{c2} = 0.2, 0.6$ and 1.0 . Ordinates \tilde{y}_1, \tilde{y}_2 and q are thus measured from the edge separating main and boundary flows. From the presented graph it follows that the positions of the boundaries of the mixing flows essentially depends on the parameter m .

During derivation of the working formulas there are used the basic regularities of the theory of free streams [15]. These regularities have received experimental

confirmation only when there exists a considerable difference in the speeds u_1 and u_2 of the mixing flows. Theoretical boundaries of the region of turbulent mixing (Fig. 9.36) will satisfactorily agree with experimental data only at $m < 0.6$. Divergence of theoretical and experimental data during change of parameter m in the interval $(0.6, 1.0)$ is apparently explained by the fact that in this region of the ratio of speeds, there exists a more complicated mechanism of mass transfer, which is determined not only by the difference of speeds of the mixing flows, but also by turbulent diffusion. It is not excluded that with accumulation of experimental data, the field of application of the obtained solution will be more precisely defined.

On the basis of theoretical and experimental data, it is possible to show that the formula for calculation of thickness of the boundary layer adjacent to the wall during mixing of nonisothermal flows has the form

$$\delta = 0.37 \left(\frac{v_1}{u_1} \right)^{1/2} \left[\frac{x}{\bar{p}_w + 0.3(1 - \bar{p}_w)} \right]^{1/2}. \quad (9.135)$$

where parameter $\bar{\rho}_w$ is determined by the formula

$$\bar{\rho}_w = \frac{\rho_w}{\rho_1} = \frac{T_1}{T_w}. \quad (9.136)$$

Thus, during mixing of nonisothermal flows, the thickness δ depends on the ratio of temperatures on the boundary δ and on the wall. It has been experimentally established that along the wall temperatures T_δ and T_w are changed practically proportionally, so that with an accuracy to 10%, the quantity $\bar{\rho}_w$ preserves a constant value. Thus, for instance, when $\bar{T}_{e2} = 0.3$ to 0.4 , the numerical value of parameter $\bar{\rho}_w$ is 1.2-1.3.

Subsequently all linear dimensions will be referred to the height of the slot h . Let us introduce parameter K , which characterizes the boundary layer adjacent to the wall:

$$K = \frac{0.37}{Re_1^{1/4}} \left\{ \frac{1}{c^2 [\bar{\rho}_w + 0.3(1 - \bar{\rho}_w)]} \right\}^{1/4}. \quad (9.137)$$

On the basis of (9.135) and (9.137), we will obtain

$$\bar{\delta} = K(c^2 \bar{x})^{0.8}, \quad (9.138)$$

where c^2 — turbulence constant,

$$\bar{\delta} = \frac{\delta}{h} \text{ and } \bar{x} = \frac{x}{h},$$

Re_1 — Reynolds number, calculated by the formula (9.134).

From the flow diagram (see Fig. 9.35), it follows that the internal boundary of the mixing zone is determined by the relationship

$$\bar{y}_2 = 1 + \left(\frac{\bar{y}_1}{c^2 \bar{x}} \right) (c^2 \bar{x}). \quad (9.139)$$

The quantity $\bar{y}_2/c^2 \bar{x}$ characterizes the slope of the inner boundary y_2 , and at given m and \bar{T}_{e2} is found by the graph shown in Fig. 9.36.

The length of the initial section is determined by the equation (see Fig. 9.35).

$$\delta(x^*) = y_2(x^*). \quad (9.140)$$

Using (9.138) and (9.139), we will represent relationship (9.140) in the form

$$K(c^2 \bar{x})^{0.8} = 1 + \left(\frac{\bar{y}_1}{c^2 \bar{x}} \right) (c^2 \bar{x}). \quad (9.141)$$

The result of solution of this equation for different values of K and $\bar{y}_2/c^2 \bar{x}$ is presented in Fig. 9.37. Parameter K is changed within quite wide limits and practically encompasses the whole possible range of Reynolds numbers Re_1 and turbulence constants c^2 . From Fig. 9.37 it follows that the thickness of the boundary layer

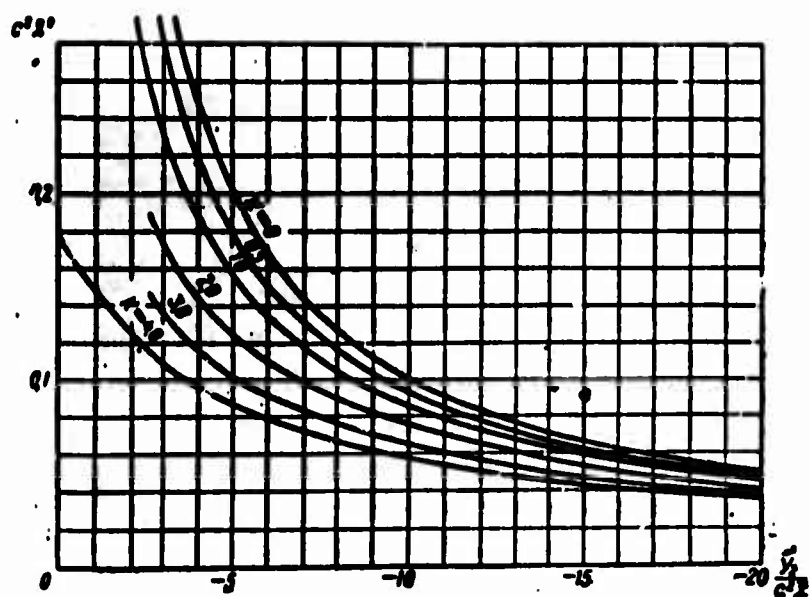


Fig. 9.37. Length of the initial section at $m < 1$.

on the wall greatly affects the length of the initial section (differentiation of the curves according to values of parameter K). With decrease of the difference between speeds of the mixing flows ($m \rightarrow 1$), the length of the initial section considerably increases.

It is not difficult to see that the external boundary of the region of

turbulent mixing (for $m < 1.0$) is calculated by the formula

$$\bar{y}_1 = 1 + \left(\frac{\bar{y}_1}{c^2 x} \right) c^2 \bar{x}, \quad (9.142)$$

where parameter $\bar{y}_1/c^2 x$ is determined by the graph shown in Fig. 9.36, for corresponding values of m and \bar{T}_{e2} . For the transition section relationship (9.142) takes the form

$$\bar{y}_1 = 1 + \left(\frac{\bar{y}_1}{c^2 x^*} \right) (c^2 \bar{x}^*). \quad (9.143)$$

The given formulas completely determine the geometry of the flow in the initial section and are applied for $m < 0.6$.

Referring all velocities to the characteristic velocity u_1 ($\bar{u} = \frac{u}{u_1}$), and all temperatures to the characteristic temperature T_{e1} ($\bar{T} = \frac{T}{T_{e1}}$), we will give a formula for calculation of profiles of \bar{u} and \bar{T} in the initial section ($c^2 \bar{x} \leq c^2 \bar{x}^*$) at $m < 0.6$. The velocity profile in the initial section is determined by relationships

$$\left. \begin{aligned} \bar{u} &= m \left(\frac{\bar{y}}{\delta} \right)^{\frac{1}{5}} & \text{for } 0 < \bar{y} < \delta, \\ \bar{u} &= m & \text{for } \delta < \bar{y} < \bar{y}_2, \\ \bar{u} &= m + (1-m) \left[1 - \left(\frac{\bar{y}_1 - \bar{y}}{\bar{y}_1 - \bar{y}_2} \right)^{\frac{3}{2}} \right]^{\frac{1}{5}} & \text{for } \bar{y}_2 < \bar{y} < \bar{y}_1. \end{aligned} \right\} \quad (9.144)$$

Under these same conditions ($m < 0.6$; $c^2 \bar{x} \leq c^2 \bar{x}^*$), for calculation of the temperature profile there are obtained the following formulas:

$$\left. \begin{aligned} T &= T_n & \text{for } 0 \leq \bar{y} < \bar{y}_1 \\ T &= T_n + (1 - T_n) \left[1 - \left(\frac{\bar{y} - \bar{y}_1}{\bar{y}_1 - \bar{y}_2} \right)^n \right] & \text{for } \bar{y}_1 < \bar{y} < \bar{y}_2 \end{aligned} \right\} \quad (9.145)$$

Let us turn to determination of parameters of the flow in the main section for the case when velocity of the cold flow is less than the velocity of the hot flow ($m < 1$). On the basis of (9.138) and (9.142), we conclude that \bar{v} and \bar{y}_1 are known functions of $c^2 \bar{x}$ also within the limits of the main section ($c^2 \bar{x} > c^2 \bar{x}^*$).

On the basis of the integral relationship of mementum

$$\int_{\bar{y}_1}^{\bar{y}_2} \frac{d}{d\bar{x}} (\bar{\rho} \bar{x}^2) d\bar{y} - \int_{\bar{y}_1}^{\bar{y}_2} \frac{d}{d\bar{x}} (\bar{\rho} \bar{u}) d\bar{y} = 0 \quad (9.146)$$

we will obtain an equation for determination of velocity on the boundary of the boundary layer adjacent to the wall $\omega = u_0/u_1^*$ during mixing of nonisothermal flows

$$F(\omega; \bar{\rho}_{\text{bc}}) = F(m; \bar{\rho}_{\text{bc}}) \left(\frac{\bar{y}_1}{\bar{y}_2} \right). \quad (9.147)$$

The dependence of auxiliary function F on ω for different values of $\bar{\rho}_{\text{bc}}$ is represented in Fig. 9.38. In formula (9.147), $\bar{\rho}_{\text{bc}}$ denotes the average integral (over the length of the cooled section) value of density on the boundary of the boundary layer adjacent to the wall:

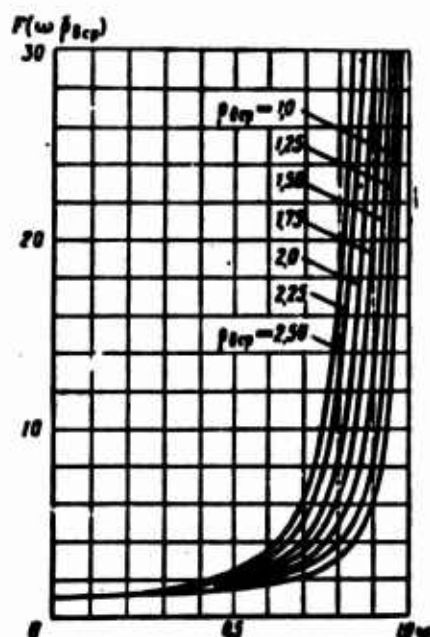


Fig. 9.38. Graph for determination of velocity during air-boundary cooling.

$$\begin{aligned} \bar{\rho}_{\text{bc}} &= \frac{1}{c^2 L} \int_0^{c^2 L} \bar{\rho}_i d(c^2 \bar{x}) = \\ &= \frac{1}{c^2 L} \int_0^{c^2 L} \frac{1}{T_i} d(c^2 \bar{x}). \end{aligned} \quad (9.148)$$

Velocity $\omega = u_0/u_1$ as a function of $c^2 \bar{x}$ is determined by Fig. 9.38 and formula (9.147) by the method of successive approximations. The average magnitude of density $\bar{\rho}_{\text{bc}}$ in the first approximation is taken equal to unity, after which, according to formula (9.147), for every value of \bar{y}_1

*Subsequently, velocity u_0 on the boundary of the boundary layer adjacent to the wall (see Fig. 9.35) will be designated by u_0 .

there is determined $F(\omega; \rho_{0\text{ cp}})$ and from the graph in (Fig. 9.38) there is found the corresponding value of ω . Using the found velocity in calculation of the temperature field (see below), we will obtain the distribution of $\bar{\rho}_0 = 1/\bar{T}_0$ with respect to $e^2 x$. By formula (9.148) there is found the refined value of $\bar{\rho}_{0\text{ cp}}$, after which there is again performed calculation of velocity for $\bar{\rho}_{0\text{ cp}} \neq 1$. It has been established that the third approximation practically coincides with the second. Therefore, during calculations of ω we should be limited only to the first two approximations.

The temperature of the thermally insulated wall in the main section is determined from the integral relationship of enthalpy, which at $T_{e1} = \text{const}$ has the form

$$\int_0^{\bar{y}_1} \bar{\rho} \bar{u} (1 - \bar{T}) d\bar{y} = \text{const.} \quad (9.149)$$

Using the self-similarity of velocity and temperature profiles, we will reduce equation (9.149) to the form

$$\gamma(\omega; z_0; \bar{T}_w) = \gamma(m; z_1^*; \bar{T}_{w1}) \left(\frac{\bar{y}_1}{y_1} \right). \quad (9.150)$$

Determination of temperature of the wall \bar{T}_w by formula (9.150) is performed in the following way: according to \bar{y}_1 there is calculated the magnitude γ , and according to γ , ω and z_0 , from the graphs (Fig. 9.39) there is found the corresponding value of \bar{T}_w .

The dependence of function γ on parameters ω , z_0 and \bar{T}_w is represented in Fig. 9.39. Parameters z_0 and z_0^* are found by the formulas

$$z_0 = \frac{\bar{y}_1 - \delta}{\bar{y}_1}; \quad (9.151)$$

$$z_0^* = \frac{\bar{y}_1^* - \delta^*}{\bar{y}_1}. \quad (9.152)$$

Temperature \bar{T}_0 , which is necessary for calculation of $\bar{\rho}_{0\text{ cp}}$ (9.148), is given by the relationship

$$\bar{T}_0 = \bar{T}_w + (1 - \bar{T}_w)(1 - z_0^*)^2. \quad (9.153)$$

Profiles of velocity and temperature in the main section at $m < 1.0$ are calculated by the formulas

$$\left. \begin{aligned} \bar{u} &= \omega \left(\frac{\bar{y}}{\delta} \right)^{\frac{1}{2}} && \text{for } 0 < \bar{y} < \delta, \\ \bar{u} &= \omega + (1 - \omega) \left[1 - \left(\frac{\bar{y}_1 - \bar{y}}{\bar{y}_1 - \delta} \right)^{\frac{3}{2}} \right]^2 && \text{for } \delta < \bar{y} < \bar{y}_1. \end{aligned} \right\} \quad (9.154)$$

$$T = T_{\infty} + (1 - T_{\infty}) \left[1 - \left(\frac{\bar{y}_1 - \bar{y}}{\bar{y}_1} \right)^{\omega} \right] \quad \text{for } 0 < \bar{y} < \bar{y}_1. \quad (9.155)$$

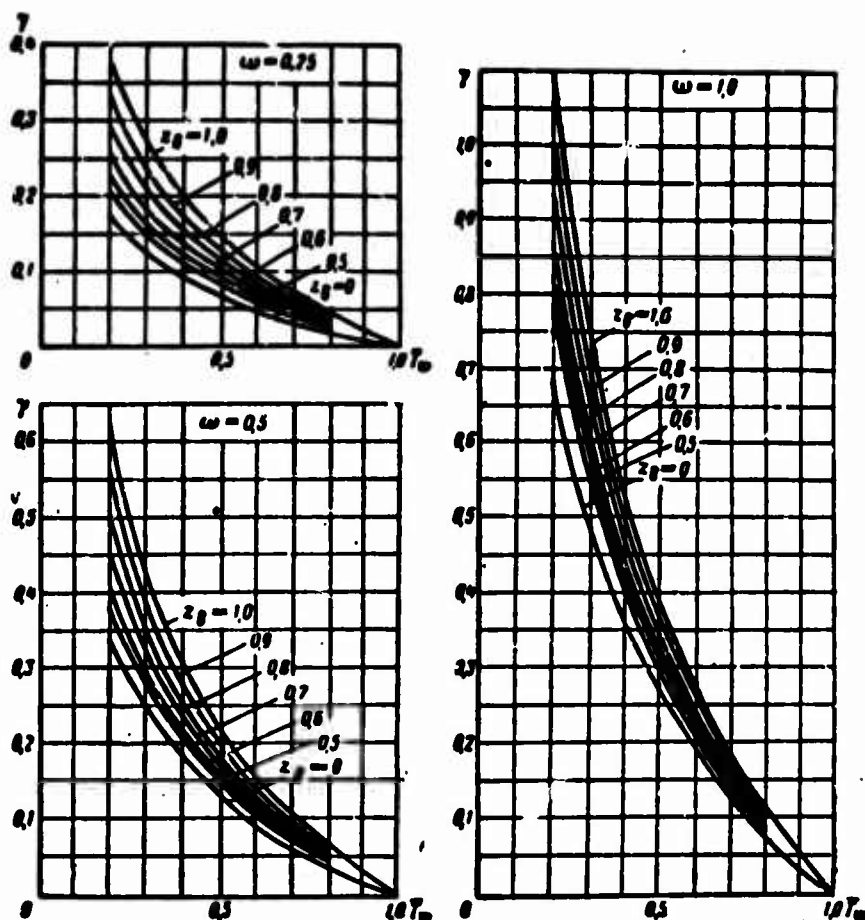


Fig. 9.39. Graph for determination of wall temperature during air-boundary cooling.

We use the above method for determination of temperature of the thermally insulated wall at $m < 1.0$. Analysis of the obtained formulas shows that dimensionless temperature of the wall is a function of the following basic parameters:

$$\bar{T}_w = f(\bar{c}^2 \bar{x}, m, \bar{T}_{\infty}, K). \quad (9.156)$$

Calculations carried out for a quite wide range of changes of these parameters encompass operating regimes of the combustion chamber of a ramjet engine having the highest heat-release rates. Length of the cooled wall is within the limits from $0 \leq \bar{c}^2 \bar{x} \leq 2.0$. During theoretical calculations, the ratio of velocities of the mixing flows changed from 0.2 to 0.9: $0.2 \leq m \leq 0.9$. Let us remember that results of calculation of the boundaries of mixing by the jet method will satisfactorily agree with experimental data at $m \approx 0.6-0.7$. In Fig. 9.40a and b, there are represented results of calculation of wall temperature (\bar{T}_w) at $K = 0$ and at $\bar{T}_{e2} = 0.2$ and 0.6 .

Analogous data for $K = 4$ at the same temperatures \bar{T}_{e2} are shown in Fig. 9.40c and d. Using linear interpolation with respect to parameters K and \bar{T}_{e2} , we will determine the temperature of the thermally insulated wall \bar{T}_w for any specific conditions of cooling at $m < 1.0$.

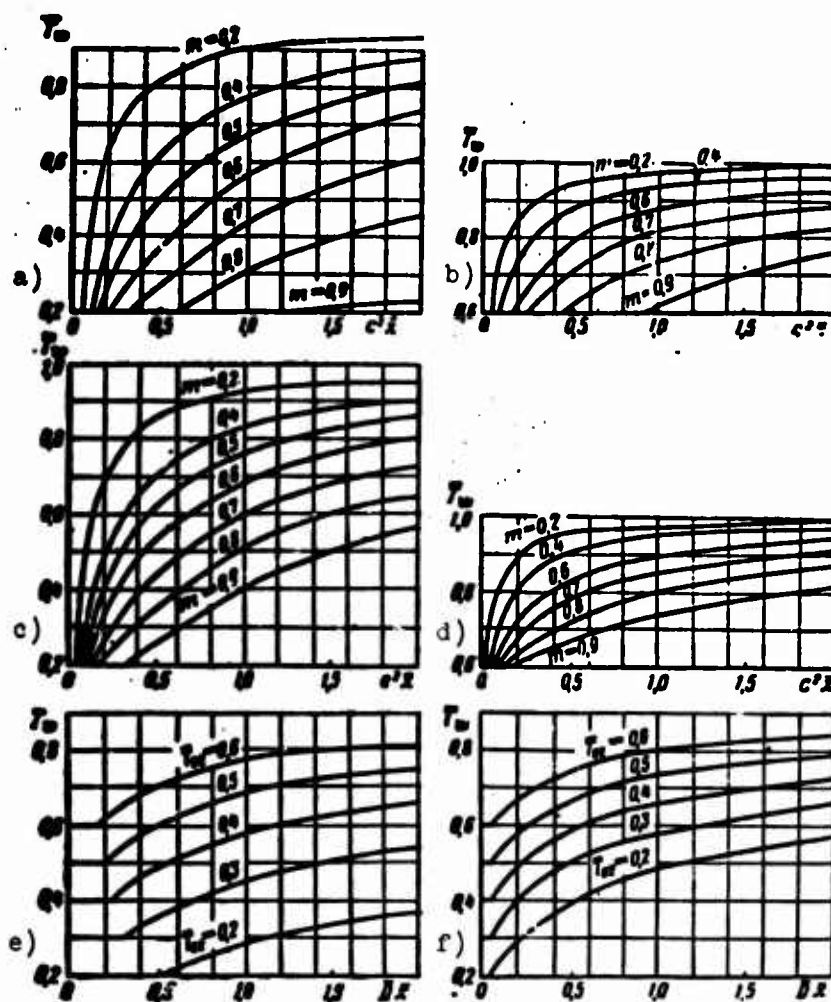


Fig. 9.40. Temperature of the wall during air-boundary cooling.

- a) $m < 1.0$; $\bar{T}_{e2} = 0.2$; $K = 0$;
- b) $m < 1.0$; $\bar{T}_{e2} = 0.6$; $K = 0$;
- c) $m < 1.0$; $\bar{T}_{e2} = 0.2$; $K = 4$;
- d) $m < 1.0$; $\bar{T}_{e2} = 0.6$; $K = 4$;
- e) $m = 1.0$; $K = 0$;
- f) $m = 1.0$; $K = 8$.

The basic mechanism of mass transfer in the transverse direction at $m \approx 1.0$ is the mechanism of turbulent diffusion, which is determined by the turbulent diffusion coefficient

$$D_T = \lambda \alpha_1 = \text{const}, \quad (9.157)$$

where λ — scale of turbulence;

ϵ — degree of turbulence of the incident flow.

This mechanism will also be the basic mechanism for a certain interval of values of m in the neighborhood of unity. At present it is impossible to indicate this interval strictly. Let us assume conditionally that the solution of the problem obtained on the basis of turbulent diffusion at $m = 1.0$, is applicable for values of m in a certain interval $0.9 \leq m \leq 1.1$.

Introducing the nondimensional turbulent diffusion coefficient

$$\bar{D} = \frac{D_t}{\lambda(a_1 + a_2)}, \quad (9.158)$$

we will represent the thickness of the boundary layer adjacent to the wall in the form

$$\delta = K_1 (\bar{D} \bar{x})^{\frac{1}{2}}, \quad (9.159)$$

where

$$K_1 = \frac{0.37}{Re_1^{\frac{1}{2}}} \left\{ \frac{1}{\bar{D}[\bar{p}_w + 0.3(1 - \bar{p}_w)]} \right\}^{\frac{4}{3}}. \quad (9.160)$$

Due to the different temperatures of the cold and hot flows, there appears a thermal boundary layer with boundaries \tilde{y}_1 and \tilde{y}_2 . Use of the integral enthalpy

relationship once for the entire region of the thermal boundary layer and a second time for half of it makes it possible to determine the change of boundaries \tilde{y}_1 and \tilde{y}_2 depending upon coordinate \bar{x} and parameter \bar{T}_{e2} . In the case of turbulent diffusion, boundaries \tilde{y}_1 , \tilde{y}_2 and the width of the thermal boundary layer \tilde{q} are

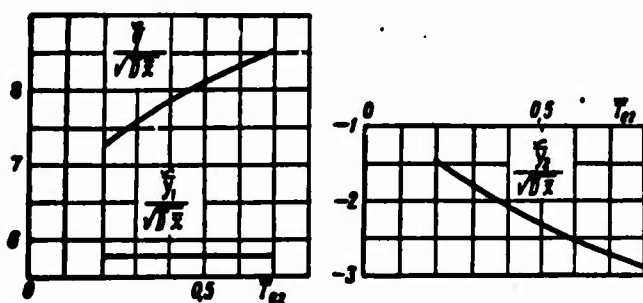


Fig. 9.41. Boundary of the mixing region ($m \approx 1.0$).

changed proportionally to $\sqrt{\bar{x}}$. The dependence of geometric characteristics of flow on the parameter \bar{T}_{e2} (at $m \approx 1.0$) is represented in Fig. 9.41. Thus the inner boundary of the thermal boundary layer is calculated by the formula

$$\bar{y}_2 = 1 + \left(\frac{\bar{y}_1}{\sqrt{\bar{D} \bar{x}}} \right) (\bar{D} \bar{x})^{\frac{1}{2}}. \quad (9.161)$$

Using (9.159) and (9.161), we will obtain an equation for determination of the length of the initial section $\bar{D}x^*$ in the case of turbulent diffusion

$$K_1 \left[(\bar{D} \bar{x}^*)^{\frac{1}{2}} \right]^{1.6} = 1 + \left(\frac{\bar{y}_1}{\sqrt{\bar{D} \bar{x}^*}} \right) (\bar{D} \bar{x}^*)^{\frac{1}{2}}. \quad (9.162)$$

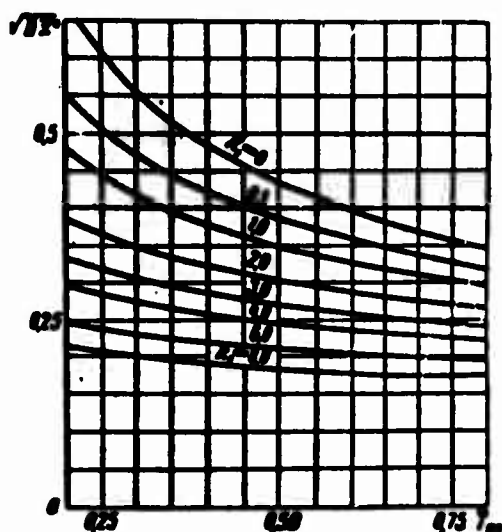


Fig. 9.42. Length of the initial section ($m \approx 1.0$).

In Fig. 9.42 there is given the result of calculation of the length of the initial section \overline{Dx}^* for different values of parameters \overline{T}_{e2} and K_1 . Parameter K_1 is contained within the limits $[0-8]$ and covers practically the whole possible range of change of Reynolds number Re_1 and coefficient \overline{D} . Increase of thickness of the boundary layer adjacent to the wall (growth of K_1) leads to considerable decrease of the length of the initial section (see Fig. 9.42).

The outer boundary of the region of turbulent diffusion is determined by the relationship

$$\overline{y}_1 = 1 + \left(\frac{\overline{y}_1}{\sqrt{\overline{Dx}}} \right) \sqrt{\overline{Dx}}. \quad (9.163)$$

For the transition section this equation gives

$$\overline{y}_1^* = 1 + \left(\frac{\overline{y}_1^*}{\sqrt{\overline{Dx}^*}} \right) \sqrt{\overline{Dx}^*}. \quad (9.164)$$

Let us give formulas for calculation of velocity profiles and temperature profiles in the initial section ($\overline{Dx} \approx \overline{Dx}^*$) in the presence of turbulent diffusion

$$\left. \begin{aligned} \overline{u} &= \left(\frac{\overline{y}}{\delta} \right)^{\frac{1}{5}} & \text{at } 0 < \overline{y} < \delta, \\ \overline{u} &= 1.0 & \text{at } \delta < \overline{y} < \overline{y}_1, \end{aligned} \right\} \quad (9.165)$$

$$\left. \begin{aligned} T &= T_a & \text{at } 0 < \overline{y} < \overline{y}_2, \\ T &= T_a + (1 - T_a) \left[1 - \left(\frac{\overline{y}_1 - \overline{y}}{\overline{y}_1 - \overline{y}_2} \right)^4 \right] & \text{at } \overline{y}_2 < \overline{y} < \overline{y}_1. \end{aligned} \right\} \quad (9.166)$$

Temperature of the thermally insulated wall in the main section is determined from the integral enthalpy relationship (9.149), which when $m \approx 1.0$ is reduced to the form

$$\Phi(z_1; T_a) = \left(\frac{\overline{y}_1}{\overline{h}} \right) \Phi(z_1^*; T_a). \quad (9.167)$$

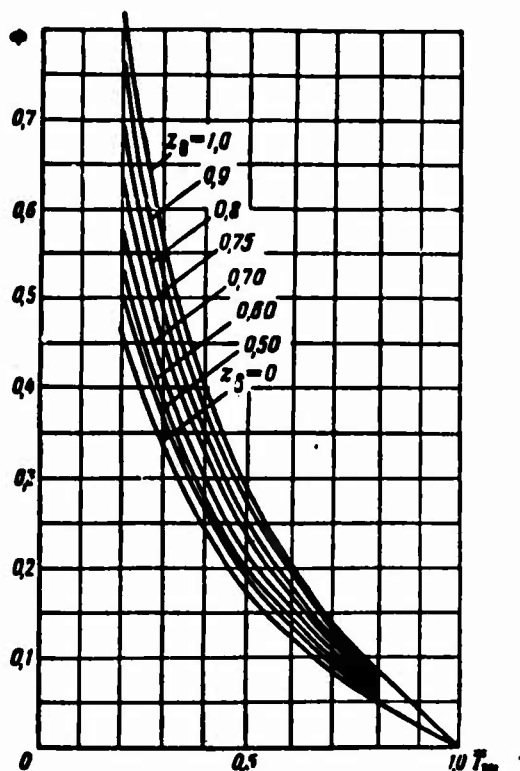


Fig. 9.43. Graph for determination of wall temperature during air-boundary cooling.

The dependence of function Φ on parameters z_0 and \bar{T}_w is represented in Fig. 9.43. For determination of the geometric characteristics z_0 and z_0^* , there are used formulas (9.151) and (9.152). With the help of Fig. 9.43 and relationship (9.167), calculation of temperature of the wall is carried out in the following way: from the known (in the given cross section x) value of \bar{y}_1 , on the basis of (9.167), there is found the magnitude of Φ ; then from the graph (for known z_0) there is determined the corresponding value of \bar{T}_w .

Profiles of velocity and temperature in the main section at $m \approx 1.0$ are determined by the following relationships:

$$\left. \begin{aligned} \bar{u} &= \left(\frac{\bar{y}}{\delta} \right)^{\frac{1}{4}} & \text{for } 0 \leq \bar{y} < \delta, \\ \bar{u} &= 1.0 & \text{for } \delta \leq \bar{y} < \bar{y}_1. \end{aligned} \right\} \quad (9.168)$$

$$\bar{T} = \bar{T}_w + (1 - \bar{T}_w) \left[1 - \left(\frac{\bar{y} - \bar{y}_1}{\bar{y}_1} \right)^4 \right] \quad \text{for } 0 \leq \bar{y} < \bar{y}_1. \quad (9.169)$$

Analyzing the obtained results, we conclude that in the case of turbulent diffusion, dimensionless wall temperature is a function of the following basic parameters:

$$\bar{T}_w = f(\bar{D}x, \bar{T}_{e2}, K_1). \quad (9.170)$$

By the given method there is calculated the wall temperature in the neighborhood of $m \approx 1.0$ for a comparatively large range of change of basic parameters. Thus, for instance, in the calculations it is assumed that the length of the cooled section changes within the limits

$$0 < \bar{D}x < 2.0,$$

and the ratio of temperatures of the mixing flows satisfies the inequality

$$0.2 < \bar{T}_{e2} < 0.6.$$

In Fig. 9.40e, for different values of parameter \bar{T}_{e2} there is given change of dimensionless temperature along the flat wall in the absence of a boundary layer adjacent to the wall ($K_1 = 0$). Analogous dependences in the presence of a boundary

layer ($K_1 = 8$) are shown in Fig. 9.40f. Thus, for $m \approx 1.0$ and given parameters K_1 and \bar{T}_{e2} , temperature of the wall is determined by linear interpolation of the dependences represented in Fig. 9.40e and f.

In Fig. 9.44, the points represent experimental values of temperature of the thermally insulated wall during boundary cooling. In the same place the solid lines represent theoretical dependences obtained by the proposed method. Satisfactory coincidence of theoretical and experimental data with selection of only one experimental constant (c^2 or D) indicates that the obtained theoretical solution correctly reflects the physical essence of the phenomenon.

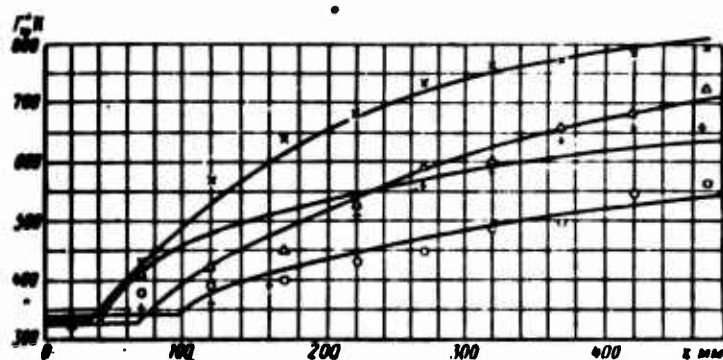


Fig. 9.44. Wall temperature during air-boundary cooling.

Symbols	x	+	Δ	O	
T_w	0.335	0.336	0.345	0.356	— theory
c^2	0.627	~1.0	0.644	1.0	+ Δ + O —
D	0.012	7.5°	0.012	3.2°	experiment

*Large value of D corresponds to smaller height of the plot h (see formula (9.158)).

We will present results of the experimental investigation of air-boundary cooling in a simple model of a supersonic nozzle. Experiments were conducted with an axially symmetric conical nozzle designed for $M = 3.0$. The angles of opening of the supersonic parts of the nozzles were 20 and 30°, and the throat diameter was equal to 6.25 mm.

Air coolant was fed through the annular slot in the subsonic part of the nozzle near the throat.

In the process of experiment there was measured the temperature of the thermally insulated wall of the supersonic nozzle in the presence of boundary cooling.

In Fig. 9.45, for several flow rates of air coolant, there are given experimental values of temperature of the thermally insulated wall of a supersonic nozzle during boundary cooling. As a result of the conducted experimental investigation, it was established that air-boundary cooling of a supersonic nozzle, in spite of a series of

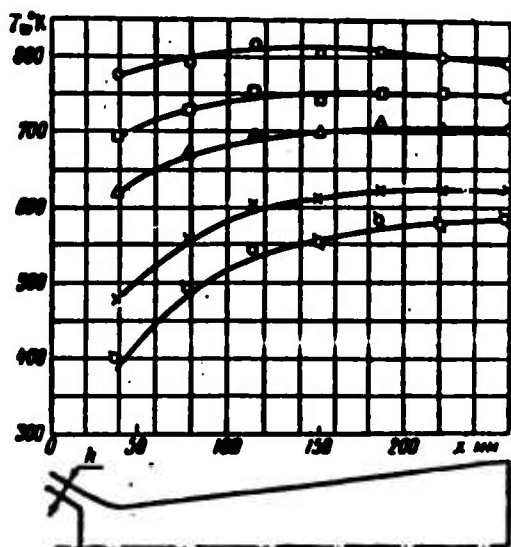


Fig. 9.45. Wall temperature of a supersonic nozzle during boundary cooling ($h = 5.5$ mm, $\alpha = 20^\circ$).

Symbols	○	□	△	×	◇
$\frac{m}{\rho_0 D_0}$	0.0438 0.388 0.03345	0.0643 0.377 0.0499	0.0890 0.364 0.0664	0.1125 0.310 0.100	0.1525 0.342 0.1335
	— theory ○ □ △ × — experiment				

specific peculiarities, has much in common with the process of boundary cooling of a flat plate. For instance, just as in case of cooling of a flat plate, increase of speed of boundary flow leads, other things being equal, to decrease of wall temperature of the nozzle. Increase of height of the slot, with other parameters retained constant, is accompanied by a corresponding lowering of wall temperature of the thermally insulated nozzle. From Fig. 9.45 it follows that at small flow rates of air coolant, the wall temperature of the thermally insulated nozzle has a weakly pronounced maximum. On the basis of experimental investigation, it has been established that with change of the angle of opening of the supersonic part of the nozzle from 20 to 30° , temperature of the wall is changed insignificantly.

After processing experimental data in dimensionless parameters, we will obtain for calculation of the maximum wall temperature of the nozzle (during boundary cooling) the empirical formula

$$\frac{(T_w)_{\max} - T_{\infty}}{T_{\infty} - T_{\infty}} = e^{-0.5m \frac{h}{D_{hp}}} \quad (9.171)$$

In Fig. 9.46 there are compared results of calculation of the maximum temperature of the wall of the nozzle by formula (9.171) with experimental data. From this figure it follows that formula (9.171) can be used for rough estimation of the maximum temperature of the wall of the supersonic nozzle during boundary cooling. It is natural that the region of application of the obtained formula is limited to the range of change of dimensionless parameters in which the experimental investigation is conducted.

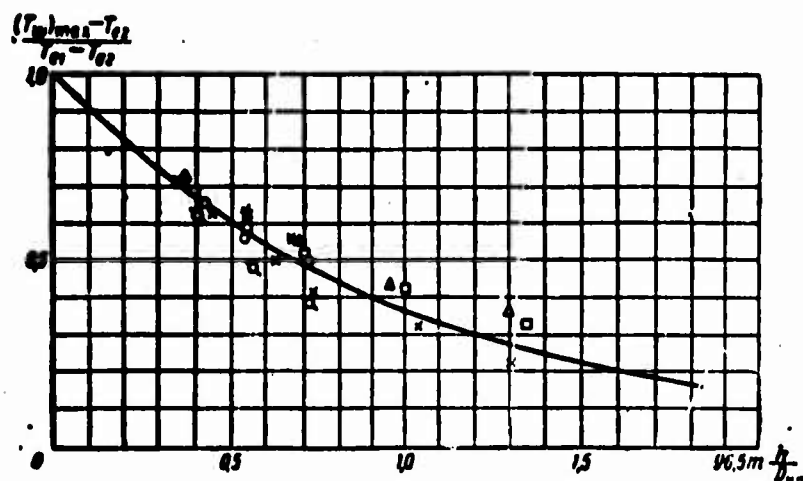


Fig. 9.46. Temperature of the wall during air-boundary cooling.

Symbols	x	□	△	○	*	
$\frac{u}{h}$	0.032	0.056	0.088	0.032	0.056	0.088
	<div style="display: flex; align-items: center;"> <div style="flex: 1; border-bottom: 1px solid black; width: 20px; margin-right: 5px;"></div> theory </div> <div style="display: flex; align-items: center;"> <div style="flex: 1; border-bottom: 1px dashed black; width: 20px; margin-right: 5px;"></div> x □ △ ○ * - </div> <div style="display: flex; align-items: center;"> <div style="flex: 1; border-bottom: 1px dotted black; width: 20px; margin-right: 5px;"></div> experiment </div>					

The method given here makes it possible, with given initial parameters m , \bar{T}_{e2} and K , to determine temperature $\bar{T}_w = T_w/T_{e1}$ of the thermally insulated wall without taking into account radiation. Due to radiation from the flame, the true temperature of the wall will be higher than the found value by same magnitude ΔT_w . In accordance with assumption 3, we will compose the equation of heat balance, assuming that all heat transmitted from the gas to the wall by radiation, is removed by the convective cooling flow

$$\tilde{\alpha}_2(T_w + \Delta T_w - \bar{T}_a) \approx \tilde{\epsilon}_1 \tilde{\epsilon}_2 c_0 \left[\left(\frac{\tilde{T}_1}{100} \right)^4 - \left(\frac{T_w + \Delta T_w}{100} \right)^4 \right], \quad (9.172)$$

hence we will obtain

$$\Delta T_w = \frac{\tilde{\epsilon}_1 \tilde{\epsilon}_2 c_0}{\tilde{\alpha}_2} \left[\left(\frac{\tilde{T}_1}{100} \right)^4 - \left(\frac{T_w + \Delta T_w}{100} \right)^4 \right] - (T_w - \bar{T}_a). \quad (9.173)$$

Disregarding the second term on the right, we will somewhat overstate the correction. Passing over to dimensionless temperatures, we will find the final formula for the increase of wall temperature due to radiation:

$$\Delta \bar{T} = \frac{\tilde{\epsilon}_1 \tilde{\epsilon}_2 c_0}{T_{e1} \tilde{\alpha}_2} \left(\frac{\tilde{T}_1}{100} \right)^4 \left[1 - \left(\frac{T_{e1}}{\tilde{T}_1} \right)^4 (T_w + \Delta T_w) \right]. \quad (9.174)$$

Equation (9.147) is solved for $\Delta \bar{T}_w$ by graphic means or by the method of successive approximations. The coefficient of heat transfer $\tilde{\alpha}_2$, contained in formula (9.174) may be determined approximately by formula (9.60). Then the maximum wall temperature

during boundary cooling, taking into account radiation from the flame, is determined by the evident relationship

$$T_{\text{aw}} = (T_{\text{e}})_{x=L} + \Delta T_{\text{e}} \quad (9.175)$$

The obtained method of calculation of boundary cooling of a flat wall can be used for calculation of boundary cooling of walls of an engine (axially symmetric problem) only in the case when the transverse dimension of the mixing region is small as compared to the diameter of the engine. Otherwise, it is necessary to consider the axial symmetry of the flow.

The above investigation of air-boundary cooling relates to the case when the equilibrium temperature of the hot flow retains a constant value ($T_{\text{e}1} = \text{const}$). In reality, due to burnup of fuel, the temperature $T_{\text{e}1}$ increases along the combustion chamber, and is approximately determined by the dependence (9.21). Let us generalize the method of calculation of air-boundary cooling to the case of variable temperature of the hot flow $T_{\text{e}1} = T_{\text{e}1}(x)$. For this we will divide the whole length of the combustion chamber into several sections and replace function $T_{\text{e}1}(x)$ by a step curve in such a manner that on each of these sections the equilibrium temperature has a constant value. Let us assume that a hot flow of constant temperature and speed flows around each of the obtained sections. As the height of the equivalent slot in the beginning of every section we take the ordinate of the outer boundary y_1 at the end of the preceding section. For the following section, parameters m and $\bar{T}_{\text{e}2}$ are calculated according to averaged profiles of velocity and stagnation temperature at the end of the preceding section.

Using relationships (9.154), (9.155) and (.169), we will obtain a formula for calculation of the averaged parameters:

for $m < 1$,

$$\bar{\alpha}_q = \frac{6}{7} \cdot \frac{\bar{T}}{\bar{h}} + \frac{\bar{h} - \bar{\delta}}{\bar{h}} \left[\alpha + (1 - \alpha) \frac{9}{20} \right]; \quad (9.176)$$

$$\bar{T}_q = \bar{T}_{\text{e}} + (1 - \bar{T}_{\text{e}}) \frac{8}{15} \quad (9.177)$$

and for $m \approx 1.0$,

$$\bar{T}_q = \bar{T}_{\text{e}} + (1 - \bar{T}_{\text{e}}) \frac{9}{14}. \quad (9.178)$$

Let us illustrate the application of the obtained formulas in the following example. Let us assume that it is required to calculate the temperature of the wall of the combustion chamber of a ramjet engine of length $L_{\text{T}} = 1$ m during air-boundary cooling. We will assume that velocities of the cold and hot flows are practically

equal (just such a flow is realized in the majority of cases in practice); then $m \approx 1.0$. The air coolant has a stagnation temperature $T_{e2} = 897^\circ\text{K}$ flows from a slot with height of $h = 20$ mm. Calculation of the wall temperature is carried out with two assumptions: 1) equilibrium temperature of the hot flow is constant over the entire length L and is equal to $(T_{e1})_{\max} = 2200^\circ\text{K}$; 2) equilibrium temperature of the hot flow is changed according to the step curve.

Results of calculation of wall temperature (for $\bar{D} \approx 2$ and $Re_1 = 10^5$) with different laws of change of equilibrium temperature of the hot flow are represented in

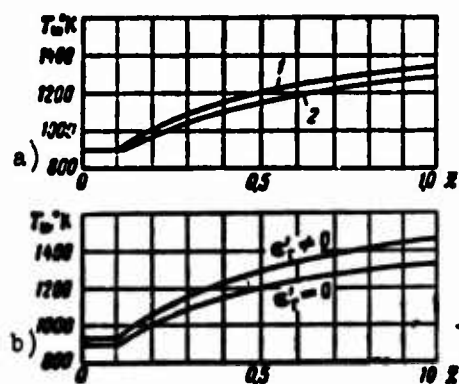


Fig. 9.47. Wall temperature of engine combustion chamber with air-boundary cooling.

a) - $\left\{ \begin{array}{l} 1 - T_{e1} - (T_{e1})_{\max} \\ 2 - \text{step approximation of} \\ \text{burnup curve} \end{array} \right.$
b) - effect of radiation

Fig. 9.47a. From this graph it follows that calculation of air-boundary cooling at constant temperature $T_{e1} = (T_{e1})_{\max}$ gives a somewhat higher value of wall temperature as compared to the case of step approximation of the burnup curve. Averaging of temperatures by the formulas (9.177) or (9.178) leads to increase of the temperature of the cooling flow in the considered section ($\bar{T}_{cp} > \bar{T}_w$); consequently, the true dependence $T_w = T_w(x)$ will fall somewhat lower.

Let us give the solution of the second part of the problem of air-boundary cooling of a ramjet engine. On the basis of the flow rate

equation and the momentum equation, we will find the true value of G_2 (or m) at which there is realized flow in an annular channel of height h for given velocity head at the end of the diffuser (p_{0R}). Using the flow rate equation (9.83) for an annular channel in the section π - κ (see Fig. 9.32) and considering assumption 5, we will obtain

$$\rho_{0\pi} \lambda_{\pi} \left(1 - \frac{k_2 - 1}{k_2 + 1} \cdot \lambda_{\pi}^2 \right)^{\frac{1}{k_2 - 1}} = \rho_{0\kappa} \lambda_{\kappa} \left(1 - \frac{k_2 - 1}{k_2 + 1} \cdot \lambda_{\kappa}^2 \right)^{\frac{1}{k_2 - 1}}. \quad (9.179)$$

The momentum equation (9.78) for an annular channel, in accordance with assumption 1, will take the form

$$\ln \lambda_{\pi}^2 + \frac{1}{\lambda_{\pi}^2} = \ln \lambda_{\kappa}^2 + \frac{1}{\lambda_{\kappa}^2} + \frac{2k_2}{k_2 + 1} \frac{(L - L_x) - x}{D_{\text{ann}}} \zeta_2, \quad (9.180)$$

where drag coefficient ζ_2 in dependence upon the range of change of Reynolds number Re is determined by formulas (9.89). For $x = -L_x$, by formula (9.180) we will obtain the reduced velocity at the inlet to the cooling channel

$$\ln \lambda_{\pi}^2 + \frac{1}{\lambda_{\pi}^2} = \ln \lambda_{\kappa}^2 + \frac{1}{\lambda_{\kappa}^2} + \frac{2k_2}{k_2 + 1} \frac{L}{D_{\text{ann}}} \zeta_2, \quad (9.181)$$

or, introducing function χ (9.87), we will find

$$\chi_2(\lambda_{K2}) = \chi_2(\lambda_{K2}) + \frac{2k_1}{k_1 + 1} \frac{L}{D_{\text{max}}} \cdot \zeta_2 \quad (9.182)$$

Using the condition of equality of static pressures in cross section K , we will find

$$p_{K1} = p_{K2} = p_{K0} \left(1 - \frac{k_1 - 1}{k_1 + 1} \cdot \lambda_{K2}^2 \right)^{\frac{k_1}{k_1 - 1}} \quad (9.183)$$

On the basis of (9.179) and (9.183), we will obtain

$$p_{K1} \cdot \lambda_{K2} \left(1 - \frac{k_1 - 1}{k_1 + 1} \cdot \lambda_{K2}^2 \right)^{\frac{1}{k_1 - 1}} = \frac{p_{K1} \cdot \lambda_{K1}}{1 - \frac{k_1 - 1}{k_1 + 1} \cdot \lambda_{K2}^2} \quad (9.184)$$

Equations (9.182) and (9.184) constitute a system of two equations with two unknowns λ_{K2} and λ_{K1} . Taking a number of values of λ_{K2} , on the basis of (9.182) we find the corresponding values of λ_{K1} . After constructing the right and left sides of equation (9.184) in dependence upon λ_{K2}

$$y_1 = \frac{p_{K1} \cdot \lambda_{K1}}{1 - \frac{k_1 - 1}{k_1 + 1} \cdot \lambda_{K2}^2}; \quad (9.185)$$

$$y_2 = p_{K0} \lambda_{K2} \left(1 - \frac{k_1 - 1}{k_1 + 1} \cdot \lambda_{K2}^2 \right)^{\frac{1}{k_1 - 1}}, \quad (9.186)$$

we will find the true value of reduced velocity λ_{K2} at the point of intersection of these curves

$$y_1(\lambda_{K2}) = y_2(\lambda_{K2}) \quad (9.187)$$

Using the definitions of reduced and critical velocities, we will find the value of parameter m :

$$m = \frac{s_1}{s_2} = \frac{\lambda_{K1}}{\lambda_{K2}} \sqrt{\frac{k_1}{k_1 + 1} \cdot \frac{k_1 + 1}{k_1}} \sqrt{T_{K2}} \quad (9.188)$$

where k_1 - adiabatic exponent for the combustion products;

λ_{K1} - reduced velocity of combustion products in section .

We will apply the method of calculation presented in the present chapter for determination of wall temperature of the combustion chamber of a ramjet engine during air-boundary cooling. Let us assume that it is required to calculate cooling of the combustion chamber of an engine with mid-section $D_1 = 1.0$ m flying at an altitude $H = 30,000$ m ($T_2 = 231.3^\circ\text{K}$), ($p_2 = 120$ kg/m²), with velocity corresponding to $M_2 = 4.0$ ($T_{e\Delta} = 897^\circ\text{K}$), for maximum temperature in the combustion chamber $(T_{e1})_{\text{max}} = 2200^\circ\text{K}$.

In Fig. 9.48 there is given a graphical solution of equation (9.187). From this solution we have $\lambda_{K2} \approx 0.465$. Considering that $\lambda_{K1} \approx 0.30$ and that $\bar{T}_{e2} \approx 0.4$, on the

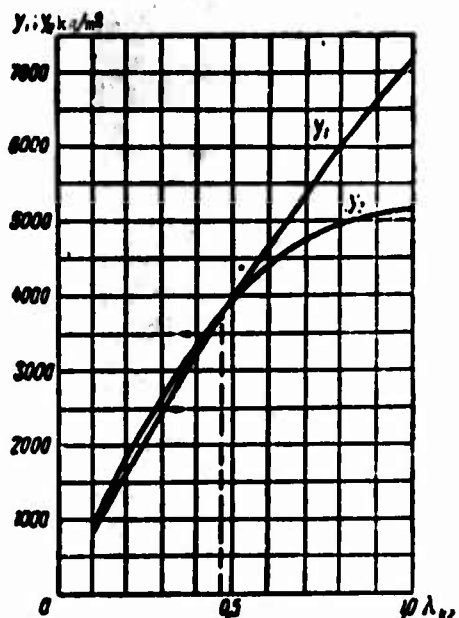


Fig. 9.48. Graphical solution of equation (9.187).

basis of (9.188) we will obtain $m \approx 1.0$. Assuming that $\bar{D} \approx 2$, $Re_1 = 10^5$ and using (9.160), we will find the value of the parameter $K_1 \approx 2.0$, which takes into account the influence of the boundary layer next to the wall. Using the curves presented in Fig. 9.40e and f, we will find for the considered example the change of temperature of the wall along the combustion chamber (Fig. 9.47b). Consideration radiation from the flame by formula (9.174) leads to a certain increase of wall temperature.

In conclusion let us remember that the proposed method of calculation of air-boundary cooling makes it possible to find not only temperature of the wall of a straight-through-flow

combustion chamber, but also all gas-dynamic parameters in the mixing region.

§ 7. COMBINED COOLING

Sometimes it is expedient to carry out cooling of a ramjet engine by a combined method. In this case, air coolant proceeds from the diffuser partially into the annular channel (between the wall of the combustion chamber and the outer shell), and partially onto the inner surface of the wall of the combustion chamber (through a system of annular slots). This form of cooling contains elements of both convection and boundary cooling.

In a rigorous solution of the thermal and hydraulic problems for combined cooling, there appear great mathematical difficulties. This is explained by the fact that distribution of air coolant over the loops depends on the flow friction and thermal resistance of each loop, which are unknown beforehand. Therefore, during calculation of combined cooling we are usually limited to solution only of the thermal problem. Thus we assume that both flow friction and thermal resistances of all loops are approximately identical. Then the flow rate of air through the loops is distributed proportionally to areas of the annular cross sections.

Let us give results of investigation of the wall temperature during combined cooling of a flat plate and expound briefly a simplified method of calculation.

Knowing the parameters m , \bar{T}_{e2} , c^2 and h (or h_{eff})* we find by the method presented in § 6, Chapter IX, the distribution of temperature along the thermally insulated wall during boundary cooling

$$\bar{T}_w = f\left(m, \bar{T}_w, \frac{c^2 x}{h}\right), \quad (9.189)$$

where $\bar{T}_w^* = \frac{T_w^*}{T_{e1}}$ - relative temperature of the system during purely boundary cooling;

x - longitudinal coordinate, measured from the slot along the plate.

During boundary cooling of a thermally insulated wall, the temperature of the flow in the boundary layer adjacent to the wall is very close to the temperature of the wall \bar{T}_w^* . Therefore, as the temperature of the hot flow during calculation of convection cooling, we should take the temperature \bar{T}_w^* .

Let us now consider convection cooling of a plate of length L_p and width l . We assume that around the plate there flows from one direction a hot flow with temperature $T_w^*(x) \equiv T_{e1}^*(x)$, and from the opposite direction there flows a cold flow with temperature $T_{e2}^*(x)$. Introducing average coefficients of heat transfer $\tilde{\alpha}_1$ and $\tilde{\alpha}_2$ and disregarding radiation, on the basis of (9.47) and (9.48) we will obtain a formula for calculation of the equilibrium temperature of the cooling flow and the wall temperature during combined cooling:

$$T_{\text{eq}}(\bar{x}) = e^{-\tilde{k}\bar{x}} \left[\tilde{k} \int_0^{\bar{x}} T_{e1}(\bar{x}) e^{\tilde{k}\bar{x}} d\bar{x} + T_{e2} \right], \quad (9.190)$$

$$T_{\text{eq}}(\bar{x}) = \frac{T_{e1}(\bar{x}) + \frac{\tilde{\alpha}_2}{\tilde{\alpha}_1} T_{e2}(\bar{x})}{1 + \frac{\tilde{\alpha}_2}{\tilde{\alpha}_1}}, \quad (9.191)$$

where

$$\tilde{k} = \frac{l \cdot \tilde{\alpha}_1}{3600 \cdot \tilde{c}_p \cdot G_1} \cdot \frac{1}{1 + \frac{\tilde{\alpha}_2}{\tilde{\alpha}_1}}. \quad (9.192)$$

*If there is considerable nonuniformity of the field of velocities and the field of temperatures at the outlet from the slot ($x = 0$), then instead of h there is usually used the effective height of the slot, which is determined from the following integral condition:

$$\int_{h_1}^{h_2} \frac{u}{T} (T - T_2) dy = \int_{h_1}^{h_2} \frac{u}{T} (T_1 - T) dy,$$

where $u(y)$ and $T(y)$ are experimental profiles of velocity and temperature at $x = 0$, h_1 and h_2 are values of the transverse coordinate y at which there are satisfied the conditions $T_1 = T(h_1)$ and $T_2 = T(h_2)$.

The average coefficient of heat transfer from combustion products to a flat wall on the basis of (9.7) for $Pr = 0.625$ (see § 1) has the form

$$\bar{\alpha}_1 = 0.0308 \frac{\bar{\lambda}_1}{L_r} \left(\frac{\bar{p}_1 \bar{u}_1 L_r}{\bar{\mu}_1} \right)^{0.8} \quad (9.193)$$

Considering the equation of state, we will obtain

$$\bar{\alpha}_1 = 0.0308 \frac{\bar{\lambda}_1}{L_r} \left(\frac{\bar{p}_1 \bar{u}_1 L_r}{\bar{p}_1 \bar{g} R \bar{T}_{e1}} \right)^{0.8} \quad (9.194)$$

where physical parameters of the gas flow ($\bar{\lambda}_1$ and $\bar{\mu}_1$) are determined according to the average thermodynamic temperature

$$\bar{T}_1 = \bar{T}_{e1} = \frac{T_{e1}^*(0) + T_{e1}^*(L_r)}{2} \quad (9.195)$$

where $T_{e1}^*(0) = T_{ed}$.

On the basis of (9.14), for $Pr = 0.7$ (see § 1), the average coefficient of heat transfer from the wall to the cooling flow is determined by the formula

$$\bar{\alpha}_2 = 0.0199 \frac{\bar{\lambda}_2}{D_{\text{can}}} \left(\frac{\bar{p}_2 \bar{u}_2 D_{\text{can}}}{\bar{\mu}_2 \bar{g} R \bar{T}_{e2}} \right)^{0.8} \quad (9.196)$$

Heating of air in the cooling channel is comparatively small; therefore, we can use the thermodynamic temperature $T_d \approx T_{ed}$ as the determining temperature in the first approximation.

On the basis of (9.194) and (9.196), we will obtain

$$\frac{\bar{\alpha}_2}{\bar{\alpha}_1} = 0.65 \frac{\bar{\lambda}_2}{\bar{\lambda}_1} \left(\frac{L_r}{D_{\text{can}}} \right)^{0.2} \left(\frac{\bar{p}_2}{\bar{p}_1} \frac{\bar{\mu}_1}{\bar{\mu}_2} \frac{\bar{T}_{e1}}{\bar{T}_{e2}} \frac{\bar{u}_2}{\bar{u}_1} \right)^{0.8} \quad (9.197)$$

Very frequently in practical calculations, the heating of the air in the cooling channel turns out to be small. In this case the determining temperature of the air coolant is practically equal to the temperature

$$\bar{T}_{e2} = T_{e2}(x) = T_{e2} = \text{const}$$

and the fundamental working formulas (9.191) and (9.197) are considerably simplified:

$$T_{e2}(\bar{x}) = \frac{T_{e1}(\bar{x}) + \frac{\bar{\alpha}_2}{\bar{\alpha}_1} T_{e2}}{1 + \frac{\bar{\alpha}_2}{\bar{\alpha}_1}}; \quad (9.198)$$

$$\frac{\bar{\alpha}_2}{\bar{\alpha}_1} = 0.65 \frac{\bar{\lambda}_2}{\bar{\lambda}_1} \left(\frac{L_r}{D_{\text{can}}} \right)^{0.2} \left(\frac{\bar{p}_2}{\bar{p}_1} \frac{\bar{\mu}_1}{\bar{\mu}_2} \frac{\bar{T}_{e1}}{T_{e2}} \frac{\bar{u}_2}{\bar{u}_1} \right)^{0.8} \quad (9.199)$$

where λ_2 and μ_2 are determined according to the temperature T_{ed} .

The ratio of characteristic velocities of the cold and hot flows is a certain function of the parameter m :

$$\frac{\tilde{u}_1}{\tilde{u}_2} = f(m). \quad (9.200)$$

Let us take for this function the exponential expression

$$\frac{\tilde{u}_1}{\tilde{u}_2} = cm^e. \quad (9.201)$$

Choosing constants c and e from the condition of best agreement between theoretical and experimental values of the wall temperature during combined cooling, we will obtain

$$\frac{\tilde{u}_1}{\tilde{u}_2} = 0.64m^{0.45}. \quad (9.202)$$

On the basis of (9.199) and (9.202), we will find the final formula for the ratio of averaged heat transfer coefficients:

$$\frac{\tilde{\alpha}_2}{\tilde{\alpha}_1} = 0.45 \frac{\lambda_2}{\lambda_1} \left(\frac{L_T}{D_{\text{max}}} \right)^{0.2} \left(\frac{p_1}{p_2} \frac{\tilde{T}_{c1}}{\tilde{T}_{c2}} \right)^{0.8} m^{0.45}. \quad (9.203)$$

Let us give results of comparison of experimental and calculated values of temperature of the plate during combined cooling (Fig. 9.49). From this graph it

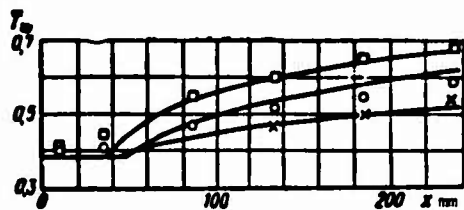


Fig. 9.49. Wall temperature during combined cooling.

— theory
□ ○ × — experiment.

Symbols	□	○	×
m	0.476	0.675	1.052
T_{c1}	0.265	0.391	0.397
\tilde{u}_1	0.018	0.018	—
\tilde{u}_2	—	—	2.5
L_T mm	4.0	4.1	4.5

follows that results of calculation satisfactorily agree with experimental data in the whole investigated range of the parameter m ($0.476 \leq m \leq 1.052$) and during change of longitudinal coordinate x from 0 to 235 mm. Comparison of theoretical and experimental data indicates that the proposed method of calculation of the temperature of the wall during combined cooling can be used for calculations.

§ 8. THE LIMITS OF APPLICABILITY OF AIR COOLING OF COMBUSTION CHAMBER AND NOZZLE

On the basis of the proposed methods of calculation, it has been established that during the use of heat-resistant materials, air cooling ensures the necessary thermal stability and high-temperature strength of straight-through-flow combustion chambers to speeds corresponding to quite large Mach numbers. This result has been confirmed by experimental data on thermal stability of high-temperature combustion chambers.

Further increase of speeds of flight leads to a case in which the stagnation temperature of the incident flow becomes higher than the maximum permissible temperature of present-day structural materials, and air cooling without preliminary lowering of temperature of the air becomes impossible.

The most promising methods of cooling and thermal protection of ramjet engines in this case are considered to be:

- 1) air cooling with preliminary lowering the the air temperature in some thermodynamic cycle;
- 2) liquid cooling;
- 3) thermal-protective coatings;
- 4) various combined methods.

LITERATURE

1. W. McAdams, W. Kennel and J. Addams. Heat transfer to super heated steam at high pressures, Trans. ASME, 1950, Vol. 72, No. 4.
2. L. G. Loytsyanskiy. Aerodynamics of a boundary layer, State United Publishing Houses, 1941.
3. E. Eckert. Engineering methods of calculation of laminar and turbulent heat exchange and friction during high-speed gas flow with constant pressure and temperature around surfaces, "Questions of Rocket Technology," 1957, No. 4.
4. S. S. Kutateladze. Fundamentals of the theory of heat exchange, Mashgiz, 1957.
5. M. A. Mikheyev. Fundamentals of heat transfer, GEI (Gosenergoiedat), 1956.
6. L. N. Il'in. On the influence of temperature on convective heat transfer, Transactions of the UKTI, No. 18, Mashgiz, 1951.
7. D. Bartz. An approximate solution of compressible turbulent boundary layer development and convective heat transfer in convergent-divergent nozzles, Trans. ASME, 1955, No. 8.
8. O. Sounders and P. Colder. Heat transfer and nozzle of supersonic speeds, Engineering, 1952, Vol. 174, No. 4518.
9. D. Bartz. A simple equation for rapid estimation of rocket nozzle convective heat transfer coefficients, Jet propulsion, 1957, No. 1.
10. G. N. Abramovich. Applied gas dynamics, State Technical and Theoretical Press, 1951.
11. E. Eckert. Introduction to the theory of heat- and mass transfer, GEI (State Power Engineering Publishing House); 1957.
12. G. F. Knorre. Furnace processes, State Power Engineering Publishing House, 1951.
13. L. A. Vulis. Thermodynamics of gas flows, GEI, 1950.
14. B. M. Kiselev. Calculation of one-dimensional gas flows, "Applied Mathematics and Mechanics." 1947, Vol. XI, Issue 1.
15. G. N. Abramovich. Turbulent streams of liquids and gases, GEI, 1948.
16. V. S. Avduyevskiy and others. Fundamentals of heat transfer in aeronautical and rocket engineering, Oborongiz, 1960.